LEABHARLANN CHOLÁISTE NA TRÍONÓIDE, BAILE ÁTHA CLIATH | TRINITY COLLEGE LIBRARY DUBLIN
Ollscoil Átha Cliath | The University of Dublin

Terms and Conditions of Use of Digitised Theses from Trinity College Library Dublin

Copyright statement

All material supplied by Trinity College Library is protected by copyright (under the Copyright and Related Rights Act, 2000 as amended) and other relevant Intellectual Property Rights. By accessing and using a Digitised Thesis from Trinity College Library you acknowledge that all Intellectual Property Rights in any Works supplied are the sole and exclusive property of the copyright and/or other IPR holder. Specific copyright holders may not be explicitly identified. Use of materials from other sources within a thesis should not be construed as a claim over them.

A non-exclusive, non-transferable licence is hereby granted to those using or reproducing, in whole or in part, the material for valid purposes, providing the copyright owners are acknowledged using the normal conventions. Where specific permission to use material is required, this is identified and such permission must be sought from the copyright holder or agency cited.

Liability statement

By using a Digitised Thesis, I accept that Trinity College Dublin bears no legal responsibility for the accuracy, legality or comprehensiveness of materials contained within the thesis, and that Trinity College Dublin accepts no liability for indirect, consequential, or incidental, damages or losses arising from use of the thesis for whatever reason. Information located in a thesis may be subject to specific use constraints, details of which may not be explicitly described. It is the responsibility of potential and actual users to be aware of such constraints and to abide by them. By making use of material from a digitised thesis, you accept these copyright and disclaimer provisions. Where it is brought to the attention of Trinity College Library that there may be a breach of copyright or other restraint, it is the policy to withdraw or take down access to a thesis while the issue is being resolved.

Access Agreement

By using a Digitised Thesis from Trinity College Library you are bound by the following Terms & Conditions. Please read them carefully.

I have read and I understand the following statement: All material supplied via a Digitised Thesis from Trinity College Library is protected by copyright and other intellectual property rights, and duplication or sale of all or part of any of a thesis is not permitted, except that material may be duplicated by you for your research use or for educational purposes in electronic or print form providing the copyright owners are acknowledged using the normal conventions. You must obtain permission for any other use. Electronic or print copies may not be offered, whether for sale or otherwise to anyone. This copy has been supplied on the understanding that it is copyright material and that no quotation from the thesis may be published without proper acknowledgement.

The influence of particle size in adjuvant induced innate and adaptive immune responses

Claire Hearnden

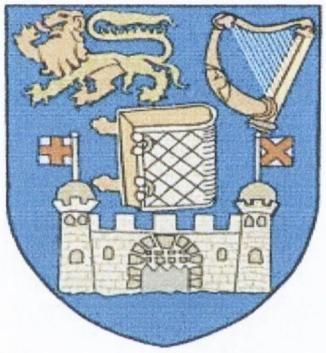

A thesis submitted to Trinity College Dublin

for the degree of Doctor of Philosophy

Supervisor: Dr Ed Lavelle

Adjuvant Research Group

School of Biochemistry and Immunology

Trinity College Dublin

2015

TRINITY COLLEGE
29 JUL 2015
LIBRARY DUBLIN

Declaration of authorship

This report represents the sole work of the author except where stated and has not been submitted in whole or in part to any other university or institution as a part of a degree or other qualification. The author gives permission to the Trinity College Library to lend or copy this thesis upon request.

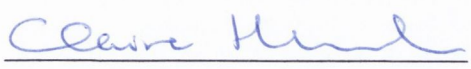

Claire Hearnden

Acknowledgements

Firstly I would like to thank the Health Research Board for allowing me to pursue my interest in research and for funding this work. I want to particularly thank Prof. Paul Moynagh and Dr. Antonio Campos-Torres for organising the programme, as well as the other HRB PhD scholars throughout the years for feedback and discussion at the monthly meetings. To my fellow TCD HRB scholars - Alan, Cáit and Anna. Well done guys and thanks for the chats along the way. I would also like to thank Prof. Celia Holland, School of Natural Sciences for encouraging me to do a PhD and for giving me some very sound advice about research.

I want to sincerely thank my supervisor Dr. Ed Lavelle for giving me the opportunity to work in his lab and for all the advice, guidance, encouragement and enthusiasm he has supplied consistently throughout this project. I have thoroughly enjoyed my PhD and that is mainly due to the environment that Ed has created and which I will miss.

I am very grateful to all those in the Lavelle lab, past and present who have given advice and their valuable time. Isolation days would not be possible without you! A huge thank you to those who have gone before me: Fiona, Marie, Karen, Edel, Corinna, Jim, Andres (the other half of the banter bench), Ewa, Cliona, Aine and Graham, and to those who continue the great work: Liz, Chris, Craig, Lorraine, Ciaran, Filipa, Dulce, Hannah, Stephanie, Sean and Natalia. Ewa and Graham require a special mention for their insight and advice on experiments, particularly at the early stages of the project. Thank you both so much for answering my numerous questions and for your patience in thoroughly going through protocols.

I'd also like to thank Prof. Con Feighery, Dr. Derek Doherty and Prof. Joe Keane for the time I spent in their respective labs as part of my PhD. I gained insight into different types of research and am a better rounded scientist due to the positive experiences I had. Thank you to all the people I met in the labs in James', there was always someone with a friendly face and I really enjoyed my time there.

I am extremely grateful to Dr. Joan Geoghegan for supplying the ClfA and for performing some of the neutralising antibodies assays. I would also like to thank Dr. Tom Barr for his generous gift of the influenza-specific tetramer and his advice on experiments. My sincerest thanks to Rachel McLoughlin and Stephen Lalor for the Staph challenge collaboration. Particular thanks to Stephen for all the work he did behind the scenes and for

his willingness to answer any questions I had. I'd also like to thank Natalia and Sean for help with the challenge experiment so close to the end, I'd never have been able to include it without you.

A big thank you to Barry Moran for all flow cytometry related suggestions and advice. I would also like to thank all members past and present of the School of Biochemistry and Immunology. It is a place of great support and collaboration. Thank you so much for the lend of antibodies/the advice on cell culture/the chats on the balcony. All of it helped me enormously throughout my PhD.

I want to thank Graham for his constant support and encouragement throughout my PhD as a colleague, mentor and friend; you made the tough days easier and the good days better. Amy and Leah deserve a big thank you for being the best housemates I could have asked for during this adventure. Thanks for listening to me ramble about science! Finally thank you to my wonderful family who supported me and slagged me in equal measure for being a student for so long.

It's been an exciting journey and my hope of handing up a piece of work that I am proud of has been fulfilled.

Abstract

Advances in vaccine development have enabled the application of adjuvanted subunit vaccines as opposed to attenuated or killed whole organisms. However the efficacy of this approach is strongly dependent on the optimisation of adjuvant characteristics. Biodegradable particles are potent adjuvants that have the capacity to elicit strong and long-lasting immunity to associated antigens. Although the optimum size of these particles for generating humoral responses has been investigated, how particle size dictates adjuvant induced innate immunity and T cell responses is unclear.

Here it is shown that particle size dramatically influences adjuvant-induced innate and adaptive immune responses. Mice immunised intra-peritoneally with polystyrene particles ranging in size from 50nm-100μm exhibited size-dependent inflammatory profiles. 50nm and 10μm particles were the most inflammatory stimuli, inducing the production of the chemo-attractants IL-1β, CXCL1 and CXCL2 in the peritoneum and subsequently recruiting neutrophils and monocytes into the site of injection. Injection of 50nm particles also induced the production of IL-33 and the recruitment of eosinophils. In contrast, injection of 1μm, 30μm or 100μm particles elicited limited inflammation. The requirement of the IL-1 receptor in neutrophil recruitment has been demonstrated for several adjuvants, however although neutrophil recruitment in response to 50nm particles was IL-1R1 dependent, 10μm PS particle-induced neutrophil recruitment was IL-1R1-independent. Even without cell recruitment to the injection site, 100μm particles were still capable of modulating immune responses as exemplified by increased IL-4 secretion from restimulated PECs and increased IL-9 mRNA expression in splenocytes after injection.

Particle size was also a decisive factor determining the antigen-specific antibody and T cell responses induced. Correlating with the greatest induction of inflammatory mediators, 50nm PS particles co-administered with OVA or the influenza NP_{311} peptide optimally induced the proliferation of antigen-specific $CD8^+$ and $CD4^+$ T cells respectively. No other PS particle size was capable of inducing T cell proliferation as measured by antigen-specific tetramers. Using the *Staphylococcus aureus* antigen Clumping factor A in an adjuvant model, immunisation with 50nm particles enhanced antigen-specific antibody titres to the greatest extent, independent of both route of administration and antigen. The dependence on particle size for the induction of significant antigen-specific antibody titres was less marked using OVA, all sized PS particles capable of enhancing OVA-specific antibodies. Similarly, subcutaneous co-administration of ClfA with all sized PS particles led to greater production of antigen-specific antibodies, indicating that the dependence of antibody induction on particle size is influenced by both the antigen and route of vaccination. Particle size also influenced the type of T cell response induced, however the nature of the response was again dependent on antigen and route of administration. For example, subcutaneous immunisation with all sized particles except those of 1μm in diameter enhanced ClfA-specific IFN-γ secretion from restimulated splenocytes whereas only 50nm PS particles were capable of promoting the same response in PECs after intra-peritoneal immunisation. In contrast, when mice were immunised with 50nm PS particles and OVA, the only detectable antigen-specific T cell response was IL-13 secretion from restimulated PECs. Overall, these results strongly indicate that particle size is crucially important in the induction of innate and antigen-specific cellular and humoral immunity and should be a central consideration in vaccine adjuvant design.

Publications

Meraz IM ¶, **Hearnden CH** ¶, Liu X, Yang M, Williams L, Savage DJ, Gu J, Rhudy JR, Yokoi K, Lavelle EC ¶, Serda RE ¶. (2014). Multivalent Presentation of MPL by Porous Silicon Microparticles Favors T Helper 1 Polarization Enhancing the Anti-Tumor Efficacy of Doxorubicin Nanoliposomes. *PLOS ONE*, 9(4): e94703.
¶ Equal contributors

Tynan GA, **Hearnden CH**, Oleszycka E, Lyons CL, Coutts G, O'Connell J, Corrigan MA, Lynch L, Campbell M, Callanan JJ, Mok KH, Geoghegan J, O'Farrelly C, Allan SM, Roche HM, O'Shea DB, Lavelle EC. (2014). Endogenous oils derived from human adipocytes are potent adjuvants that promote IL-1α-dependent inflammation. *Diabetes*, 63(6):2037-50.

Yang M, **Hearnden CHA**, Oleszycka E and Lavelle EC. (2013). NLRP3 Inflammasome activation and cytotoxicity induced by particulate adjuvants. *Methods in Molecular Biology*, 1040:41-63.

Yang M, Flavin K, Kopf I, Radics G, **Hearnden CHA**, McManus GJ, Moran B, Villalta-Cerdas A, Echegoyen LA, Giordani S, and Lavelle EC. (2013). Functionalization of carbon nanoparticles modulates inflammatory cell recruitment and NLRP3 inflammasome activation. *Small*, 9(24):4194-206.

Peral de Castro C, Jones SA, Ní Cheallaigh C, **Hearnden CA**, Williams L, Winter J, Lavelle EC, Mills KHG and Harris J. (2012). Autophagy regulates IL-23 secretion and innate T cell responses through effects on IL-1 secretion. *Journal of immunology*, 189(8):4144-53.

Book Chapters

Hearnden C and Lavelle EC. (2013). 'The use of adjuvants within the cancer vaccine setting' in Cancer Immunotherapy, 2nd Edition: Immune Suppression and Tumor Growth. Editors: Prendergast and Jaffee. ISBN: 9780123942968.

Abbreviations

AGP	aminoalkyl glucosamimide phosphate
AIM	absent in melanoma
ALR	AIM2-like receptor
Alum	aluminium hydroxide
ANOVA	analysis of variance
APC	antigen presenting cell
AS	adjuvant system
ASC	apoptotic speck-like protein containing a caspase recruitment domain
ATP	adenosine triphosphate
BCA	bicinchoninic acid
BCG	Bacille Calmette-Guérin
Bcl6	B cell lymphoma 6
BCR	B cell receptor
BMDC	bone-marrow derived dendritic cell
Breg	regulatory B cells
BSA	bovine serum albumin
CARD	caspase recruitment domain
CCL	CC chemokine ligand
CCR	CC chemokine receptor
CD	cluster of differentiation
cDC	classical dendritic cell
cDNA	complimentary DNA
CDP	common dendritic cell progenitor
CFA	complete Freund's adjuvant
CFU	colony forming units
ClfA	clumping factor A
CLR	C-type lectin receptor
CpG	cytidine-phosphate-guanosine
CTL	cytotoxic T lymphocyte
CXCL	CXC chemokine ligand
CXCR	CXC chemokine receptor
d	distilled
DAMP	damage associated molecular pattern
DC	dendritic cell
DDX	DEAD box proteins
DHR	Dihydrorhodamine
DHX	DEAH box proteins
DNA	deoxyribonucleic acid
dNTP	deoxyribonucleotide triphosphate
ds	double stranded

EDTA	ethylenediaminetetraacetic acid
ELISA	enzyme-linked immunosorbent assay
ET	extracellular traps
EU	endotoxin units
FACS	fluorescence-activated cell sorting
Fc	fragment crystallisable
FCS	foetal calf serum
FDA	Food and Drugs Administration
FoxP3	forkhead box P3
GATA-3	trans-acting T-cell-specific transcription factor 3
GLA	glucopyranosyl lipid adjuvant
GM-CSF	granulocyte-macrophage colony-stimulating factor
GSK	GlaxoSmithKline
HBsAg	Hepatitis B surface antigen
HBV	Hepatitis B virus
HIV	human immunodeficiency virus
HPV	human papillomavirus
HRP	horseradish-peroxidase
HSV	herpes simplex virus
ICAM	intracellular adhesion molecule
ICOS	inducible costimulator
IFA	incomplete Freund's adjuvant
IFI	interferon-inducible
IFN	interferon
Ig	immunoglobulin
IL	interleukin
IL-1R	IL-1 receptor
ILC	innate lymphoid cell
ION	ionomycin
i.p.	intra-peritoneal
IPS	IFN-β promoter stimulator
IRF	interferon regulatory factor
ISCOM	immuno-stimulating complex
iTreg	inducible regulatory T cell
LAL	*Limulus* Amebocyte Lysate
LB	lysogeny broth
LGP	laboratory of genetics and physiology
LPS	lipopolysaccharide
LT	lymphotoxin
Mal	MyD88-adaptor-like
MARCO	macrophage receptor with collagenous structure
MDA	melanoma differentiated-associated gene

MDR	macrophage disappearance reaction
MGC	multinucleate giant cells
MHC	major histocompatibility complex
MHCc	MHC class
mins	minutes
MMP	matrix metalloproteinase
MPP	multi-potent progenitor
MPL	3-O-desacyl-4'-monophosphoryl lipid A
MSCRAMM	microbial surface components recognizing adhesive matrix molecules
MSU	monosodium urate
MyD88	myeloid differentiation primary response gene (88)
NAIP	neuronal apoptosis inhibitory protein
NETs	neutrophil extracellular nets
NF-κB	nuclear factor kappa-light-chain-enhancer of activated B cells
NK	natural killer
NLR	nucleotide-binding oligomerization domain-like receptor
NLRC	NOD-, LRR- and CARD-containing
NLRP3	NLR family, pyrin domain containing 3
NOD	nucleotide-binding oligomerization domain
NOS	nitric oxide synthase
NP	nucleoprotein
nTreg	natural regulatory T cells
OD	optical density
ODN	oligodeoxynucleotides
OPD	0-phenylenediamine dihydrochloride
OVA	ovalbumin
O/W	oil-in-water
PAMP	pathogen associated molecular pattern
PBS	phosphate buffered saline
PCR	polymerase chain reaction
PD	programmed death
pDC	plasmacytoid dendritic cell
PE	R-phycoerythrin
PECs	peritoneal exudate cells
PFA	paraformaldehyde
PI3K	phosphatidylinositide 3-kinases
PLA	poly (lactic acid)
PLG	poly (D,L-lactide)-co-glycolide
PLGA	poly (lactic-*co*-glycolic acid)
PMA	phorbol 12-myristate 13-acetate
PMMA	polymethylmethacrylate
poly IC	polyinosinic polycytidylic acid

PRR	pattern recognition receptor
PS	polystyrene
qPCR	quantitative PCR
QS21	saponin fraction 21
RIG	retinoic acid-inducible gene
RLR	RIG-I like receptors
RNA	ribonucleic acid
ROI	reactive oxygen intermediates
ROR	retinoic-acid-receptor-related orphan receptor
Rpm	rotations per minute
RPMI	Roswell Park Memorial Institute
RT	reverse transcription
SAR	systemic acquired resistance
SARM	sterile-alpha and Armadillo motif containing protein
s.c.	subcutaneous
SD	standard deviation
SE	stable emulsion
SEM	standard error of the mean
ss	single stranded
SSC	side scatter
STAT	signal transducer and activator of transcription
syk	Spleen tyrosine kinase
TB	tuberculosis
Tc	T cytotoxic
TCD	Trinity College Dublin
TCM	central memory T cells
TCR	T cell receptor
tet	tetramer
TEM	effector memory T cells
Tfh	follicular T helper
TGF-β	transforming growth factor
Th	T helper
TIR	Toll/IL-1R homology
TLR	toll-like receptor
TNF	tumour necrosis factor
TRAM	TRIF-related adaptor molecule
Treg	regulatory T
TRIF	TIR-domain-containing adapter-inducing IFN-β
TRM	tissue-resident memory T cells
TSA	tryptic soy agar
VLP	virus-like particles
W/O	water-in-oil

Contents

Declaration of authorship i

Acknowledgements ii

Abstract iv

Publications v

Abbreviations vi

1. Introduction **1**
1.1 The immune system 2
1.1.1 Anatomical barriers and innate immunity 2
1.1.1.1. PRRs, PAMPs and DAMPs 4
1.1.1.2. Dendritic cells 7
1.1.1.3. Trained immunity 10
1.1.2. Adaptive immunity 11
1.1.2.1. T cells 12
1.1.2.1.1. $CD8^+$ T cells 12
1.1.2.1.2. $CD4^+$ T cells 14
1.1.2.1.3. Memory T cells 17
1.1.2.2. B cells 19
1.2. Vaccines and adjuvants 22
1.2.1. Immuno-stimulatory adjuvants 23
1.2.1.1. Pathogen-derived immuno-stimulatory adjuvants 23
1.2.1.2. QS21 25
1.2.2. Particulate vaccine adjuvants 25
1.2.2.1. Emulsions 26
1.2.2.2. ISCOMs 28
1.2.2.3. Mineral salts 28
1.2.2.4. Biodegradable micro-particles 30
1.2.2.5. Other particulate vaccine adjuvants 30
1.2.3. Combination vaccine adjuvants 32
1.3. Adjuvant size 33
1.4. Hypothesis and Aims 35
2. Materials and Methods **39**
2.1. Materials 40
2.1.1. General cell culture materials 40
2.1.2. Cell culture and animal study treatments 40
2.1.3. Flow cytometry/Fluorescence-activated cell sorting (FACS) materials. 42
2.1.4. Enzyme-linked immunosorbant assay (ELISA) materials 44
2.1.5. Measuring free dsDNA in the peritoneum 47
2.1.6. Real-time polymerase chain reaction (PCR) materials 47
2.1.7. Endotoxin detection and removal materials 49
2.1.8. Materials for protein determination 49

2.2. Methods 49
2.2.1. Mice 49
2.2.2. Cell culture 49
2.2.2.1. Cell viability and counting 49
2.2.2.2. Culture of J558 granulocyte-macrophage colony-stimulating factor (GM-CSF)-expressing cell line 50
2.2.2.3. Isolation and culture of murine BMDCs 50
2.2.2.4. Isolation and culture of splenocytes 51
2.2.2.5. Isolation and culture of peritoneal exudates cells 52
2.2.2.6. Isolation and culture of lymph node cells 52
2.2.3. Flow cytometry/FACS 53
2.2.3.1. Innate immune responses in PECs 53
2.2.3.2. Intracellular cytokine staining 53
2.2.3.3. OVA-specific $CD8^+$ tetramer staining 54
2.2.3.4. Influenza peptide-specific $CD4^+$ tetramer staining 54
2.2.3.5. Cell death 55
2.2.4. ELISA 55
2.2.4.1. Measurement of cytokine and chemokine secretion 55
2.2.4.2. Measurement of serum antibodies 56
2.2.4.2.1. Antigen-specific IgG, IgG1 and IgG2b 56
2.2.4.2.2. Antigen-specific IgG2c 56
2.2.4.2.3. Total IgE and antigen-specific IgE 57
2.2.5. Measuring neutralising antibodies in serum 57
2.2.6. Real time PCR 58
2.2.7. Animal studies 58
2.2.7.1. Peritonitis model 58
2.2.7.2. Adjuvant model 58
2.2.7.3. Challenge model 59
2.2.7.3.1. Preparation of bacterial inoculum for *in vivo* challenge studies 59
2.2.7.3.2. Isolation of tissues 59
2.2.7.3.3. Quantification of bacterial burden 60
2.2.8. Statistical Analysis 60
3. Innate immune responses to particles are dictated by particle size 63
3.1. Introduction 63
3.2. Aims 65
3.3. Results 66
3.3.1. 50nm and 10μm PS particles promote cell recruitment into the injection site 66
3.3.2. Different sized particles elicit distinct inflammatory profiles *in vivo* 68
3.3.3. 0.4mg and 4mg PS particles drive a comparable inflammatory response at the injection site 75
3.3.4. Injection of 50nm PS particles causes an infiltration of neutrophils which precedes that of macrophages 79
3.3.5. IL-1β, IL-33, CXCL1 and CXCL2 levels in the peritoneum correlate with subsequent cell infiltration after injection PS particles 82

3.3.6. PS particles modulate cytokine and chemokine secretion 3 hours after injection 85
3.3.7. Injection of PS particles does not induce detectable cell death 87
3.3.8. DNA is present in the peritoneum of mice injected with 50nm PS particles after 3 hours, but 10μm particles induce the release of local free DNA in the peritoneum at later time points 89
3.3.9. IL-1β is not present in significant levels in the serum of mice injected with PS particles 91
3.3.10. Neutrophil recruitment in response to 50nm, but not 10μm, PS particles is dependent on IL-1R1 93
3.3.11. The neutrophil chemoattractants CXCL1, CXCL2 and IL-1β are induced in *Il1r1*$^{-/-}$ mice immunised with 10μm PS particles 97
3.3.12. PS particle size modulates cytokine production from restimulated PECs 99
3.3.13. PS particle size modulates cytokine production from restimulated splenocytes 104
3.3.14. PS particle size modulates cytokine production from restimulated lymph node cells 107
3.3.15. IL-4 mRNA expression is up-regulated in PECs 3 hours after injection with PS particles 109
3.3.16. IL-4Rα expression is not up-regulated in PECs 24 or 72 hours after injection with PS particles 113
3.3.17. All sizes with the exception of 100μm PS particles can modulate mRNA cytokine expression 3 hours after injection 123
3.3.18. Injection of 100μm PS particles induces the up-regulation of IL-9 mRNA in splenocytes 125
3.4. Discussion 128
4. Adaptive immune responses to particles are dictated by particle size 139
4.1. Introduction 140
4.2. Aims 142
4.3. Results 143
4.3.1. ClfA in combination with 10μm PS particles promotes enhanced antigen-specific serum antibody responses 143
4.3.2. Vaccination with 1μg ClfA in combination with 10μm PS particles induces the production of serum neutralising antibodies against *S. aureus* 145
4.3.3. The candidate antigen ClfA is highly immunogenic *in vivo* and is capable of driving antigen-specific antibody responses alone 147
4.3.4. Removing endotoxin from ClfA preparation significantly reduces the ability of ClfA to stimulate BMDC secretion of IL-6 149
4.3.5. Subcutaneous immunisation with ClfA and PS particles promotes antigen-specific antibody responses with all but 100μm PS particles 152
4.3.6. Vaccination with 1mg PS particles and ClfA does not induce the production of significant antigen-specific antibodies 154
4.3.7. Route of administration influences the antigen-specific antibody response following immunisation with ClfA and 1μm PS particles 156
4.3.8. The type and magnitude of OVA-specific antibody responses induced by PS particles can be dictated by particle size 158

4.3.9. The type and magnitude of ClfA-specific cellular immunity induced by PS particles is dictated by particle size 160
4.3.10. The type and magnitude of ClfA-specific cellular immunity induced by PS particles depends on route of administration 163
4.3.11. Vaccination with ClfA and 50nm PS particles induces the production of intracellular IFN-γ, but not IL-17, in PECs 165
4.3.12. Immunisation with OVA and 50nm PS particles induces OVA-specific IL-13 secretion from PECs 170
4.3.13. 50nm is the optimal particle size for promotion of antigen-specific $CD8^+$ T cell responses 172
4.3.14. 50nm is the optimal particle size for promotion of antigen-specific $CD4^+$ T cell responses 176
4.3.15. Vaccination with ClfA and 50nm PS particles induces the recruitment of activated neutrophils to the site of challenge which does not correlate with protection against *S. aureus* infection 179
4.4. Discussion 185
5. General Discussion **195**
6. References **207**
7. Appendix **245**
7.1. Appendix I – Validation of particle size 246
7.2. Appendix II – Publications 247

Chapter 1

Introduction

1.1. The immune system

The primary role of the vertebrate immune system is to recognise and eliminate microbes that constitute a threat to the host. Microbes that establish an infection in the host are termed pathogens and two arms of immunity have evolved to prevent this occurring. The innate system is the first line of defence against infection and is triggered immediately. Innate immunity is sufficient to eliminate many common infections however pathogens that are not eliminated from the host by the innate immune system require the second arm of the immune system to be engaged, the adaptive immune response. The adaptive immune response requires a 4-5 day priming period, during which the innate system contains the infection until the adaptive response can be unleashed on the invading pathogen.

1.1.1. Anatomical barriers and innate immunity

The innate immune system is an evolutionarily ancient system used by all multi-cellular organisms to prevent the establishment of infection. In vertebrates, pathogens initially encounter significant anatomical and chemical barriers which include epithelial barriers such as the skin, a low pH in the stomach, mucus, anti-microbial peptides and lysozymes in tears and saliva[1]. If pathogens successfully penetrate anatomical barriers, pathogen recognition by innate sensor cells induces the secretion of a range of soluble factors including cytokines and chemokines, resulting in a response termed inflammation. Inflammation is a major component of the innate immune system and is characterised by four cardinal signs; redness, heat, swelling and pain.

Tissues at the site of pathogen invasion release inflammatory proteins such as histamines which increase blood flow to the site and cause capillaries to leak. Innate immune cells that differentiate and mainly reside in the bone marrow are also found circulating in the blood, usually in immature precursor forms. As a result of chemoattractant signalling from resident tissue macrophages, mast cells and dendritic cells (DCs) at the site of insult, immature innate immune cells move into the tissue and differentiate into mature effector cells[1,2].

The first innate immune cells to arrive at the site of inflammation are neutrophils which are the most abundant circulating leukocyte in humans[3]. Since neutrophils are in their mature form in the circulation, they can rapidly respond to injury or inflammation. Through intracellular adhesion molecule (ICAM)-1 expression on endothelial cells at the site of

inflammation, neutrophil β_2-integrin expression mediates attachment and initiates neutrophil transmigration[4]. The cytoplasm of neutrophils is enriched with granules that are formed during maturation. These granules are composed of different pro-inflammatory molecules that act non-specifically and cause local tissue damage[5]. In fact, it is the tissue injury mediated by infiltrating neutrophils that often further propagates the inflammatory cascade[6]. Since neutrophils are the first innate immune cells to arrive in the inflamed tissue, they are directly involved in eliminating any pathogen that they subsequently encounter. They achieve this feat using three well established mechanisms; phagocytosis, degranulation and release of neutrophil extracellular traps (NETs)[7]. Neutrophils are crucial in recruiting other innate immune cell types to sites of inflammation, such as macrophages[8,9].

During inflammation, resident macrophages are activated and monocytes responding to CC chemokine ligand (CCL)2, CCL3 and CCL5 signalling, through their CC chemokine receptor (CCR)2, CCR1 and CCR5 receptor expression are recruited from the circulation, thus leading to an accumulation of inflammatory tissue macrophages[10,11]. Tissue resident macrophages can be defined according to their location, for example Langerhans cells are resident macrophages of the skin while Kupffer cells are resident macrophages of the liver. Acute inflammation leads to 'classical' activation of macrophages, whereby microbial ligands and cytokine signalling (interferon (IFN)-γ) lead to a macrophage phenotype that promotes the secretion of pro-inflammatory cytokines such as tumour necrosis factor (TNF)-α, interleukin (IL)-12 and IL-23 as well as the production of nitric oxide and reactive oxygen intermediates (ROI)[12–14]. These classically activated macrophages are termed M1 macrophages, and are capable of eliminating pathogens following phagocytosis. Conversely, M2 macrophages are 'alternatively' activated macrophages that dampen inflammation and promote tissue remodelling[14,15]. Monocytes can differentiate into inflammatory macrophages and alternatively activated macrophages, as well as activated DCs[11,16].

As well as macrophages and neutrophils, there are a plethora of innate sensor cells involved in recognising pathogens, such as mast cells and eosinophils. Mast cells are located at numerous host-environment interfaces and their ability to rapidly release several pro-inflammatory mediators from intracellular stores is crucial for optimal immune responses during infection. Mast cells are also involved in phagocytosis and subsequently presenting antigen to various cell types in early inflammation[17]. Independent of infection or sterile inflammation, mast cells also respond to passive IL-33 release from necrotic

cells[18,19]. Alternatively activated macrophages are involved in tissue recruitment of eosinophils, which are capable of secreting inflammatory mediators quickly due to pre-translated intracellular stores of inflammatory cytokines[20–22]. Eosinophils have also been implicated in the resolution of inflammation through IL-4 signalling[23].

Hematopoietic cell infiltration into sites of infection or damage also includes innate lymphoid cells (ILCs), natural killer (NK)T cells and γδ T cells. ILCs are innate lymphocytes that lack antigen specificity and have recently been classified into three groups in a similar nomenclature to T helper (Th) cells[24,25]. ILC1s comprises cells such as NK cells that are primarily anti-viral and can produce IFN-γ and TNF[26,27]. In both humans and mice they have been found in mucosal tissues[28]. These cells develop through the transcription factors T-bet and Eomes and have cytotoxic abilities through perforin and granzyme producing granules[24,29]. ILC2s contain a well described subset of cells that require trans-acting T-cell-specific transcription factor (GATA)3, retinoic-acid-receptor-related orphan receptor (ROR)α and Notch for their development and have been associated, in a similar manner to Th2 cells, to immunity to helminths and the development of allergy and asthma[30–32]. Independently termed nuocytes, natural helper cells and innate type 2 helper cells, the ILC2s have been grouped together under an umbrella of cells that secrete IL-5, IL-13 and IL-9[33]. Group 3 ILCs produce IL-22 and IL-17A and like Th17 cells express RORγt[34,35]. Other innate lymphoid cells include NKT cells and γδ T cells. γδ T cells are particularly prevalent at mucosal and epithelial sites where they have been shown to facilitate bacterial clearance via neutrophil, macrophage, and NK cell recruitment[36]. NKT cells are present in the lymph nodes and skin and upon local cytokine signalling can induce innate production of IL-17[37].

All of these innate sensor cells are capable of recognising insult or damage to the body in distinct ways. However, antigen presenting cells (APCs) such as macrophages and DCs are termed 'professional' APCs due to their ability to present antigenic peptides to T cells and activate the adaptive immune system. This is achieved through recognition of foreign antigen and/or damage by pattern recognition receptors (PRRs).

1.1.1.1. PRRs, PAMPs and DAMPs

Microbes have evolved to avoid detection by their host's immune system by limiting their ability to be recognised. However, certain motifs expressed by pathogens are conserved

across species and are referred to as pathogen associated molecular patterns (PAMPs). These evolutionarily conserved motifs are essential for the survival of the pathogen and thus cannot be mutated in an attempt to evade innate immune recognition. Importantly, PRRs are expressed primarily by cells at the front line of the innate immune system and specifically recognise PAMPs and damage associated molecular patterns (DAMPs), which are endogenous molecules released by necrotic host cells. DAMPs include the cytokines IL-1α and IL-33 as well as endogenous deoxyribonucleic acid (DNA) which are all usually sequestered within a cell but are passively released upon the loss of membrane integrity during necrosis[38]. Upon recognition of PAMPs and/or DAMPs, PRRs initiate a signalling cascade that generates an appropriate immune response.

There are four well established members of the PRR family, Toll-like receptors (TLRs), C-type lectin receptors (CLRs), nucleotide-binding oligomerization domain (NOD) like receptors (NLRs) and retinoic acid-inducible gene 1 (RIG-I) like receptors (RLRs), as well as the more recently described nucleic acid sensing PRR members; absent in melanoma (AIM) 2-like receptors (ALRs) and DEAD/DEAH box proteins (DDX/DHX). TLRs are the most well described subset of PRRs. TLRs contain ectodomain leucine rich repeats and signal through a Toll/IL-1 receptor (1R) homology (TIR) domain[39]. Each TLR, or heterodimer of TLRs, recognises particular PAMPs. For example, TLR1:TLR2 heterodimers recognise triacyl lipoproteins, TLR4 recognises lipopolysaccharide (LPS) from Gram-negative bacteria, TLR5 recognises flagellin and TLR2:TLR6 heterodimers recognise diacyl lipoproteins[40,41]. TLR3, TLR7, TLR8 and TLR9 are located in endosomal compartments and recognise nucleic acids derived from viruses and intracellular pathogens (Figure 1.1)[42]. For example, TLR3 recognises double stranded (ds) ribonucleic acid (RNA), TLR7 recognises single stranded (ss) RNA and TLR9 recognises unmethylated cytidine-phosphate-guanosine (CpG) motifs present in bacterial DNA and DNA viruses[43–45]. TLR8 is very closely related to TLR7 and functional studies have shown that human, but not mouse, TLR8 also senses ssRNA[44].

Following recognition of a cognate ligand, TLRs activate distinct TIR domain-dependent signalling cascades through specific adaptor molecules. There are five different adaptor molecules; TIR-domain-containing adapter-inducing IFN-β (TRIF), TRIF-related adaptor molecule (TRAM), myeloid differentiation primary response gene 88 (MyD88), MyD88 adaptor-like (Mal) and sterile-alpha and Armadillo motif containing protein (SARM) which was identified as the first TIR adaptor to negatively regulate the immune system[46].

These signalling cascades induce the transcription of genes involved in inflammation (Figure 1.1).

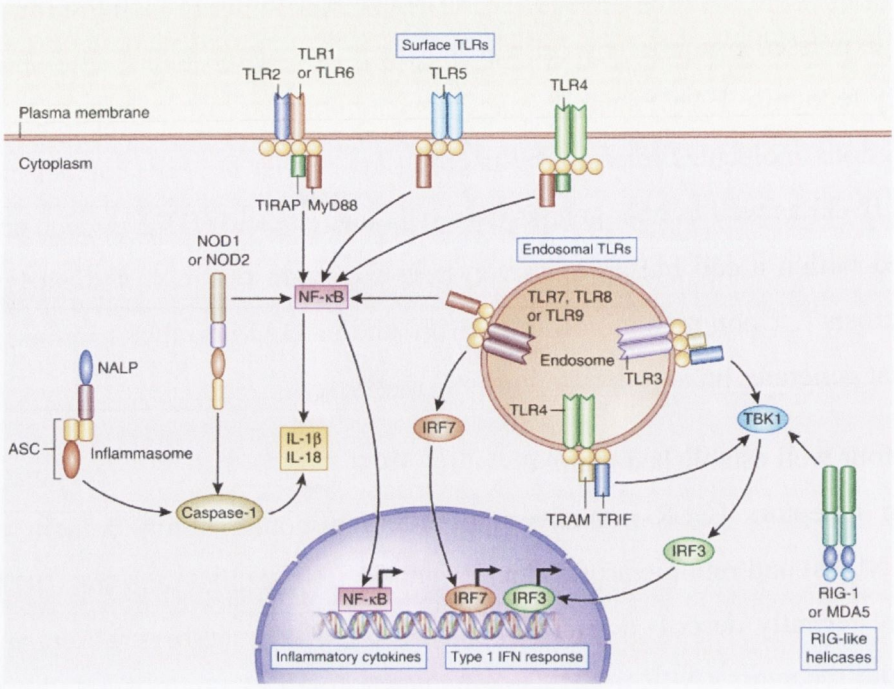

Figure 1.1 – Pattern recognition receptors. PRRs can activate transcription factors nuclear factor kappa-light-chain-enhancer of activated B cells (NF-κB), interferon regulatory factor (IRF)7 and IRF3 in distinct ways to initiate an inflammatory response. TLRs are located at the cell surface (TLR1, TLR2, TLR4, TLR5, TLR6 and TLR11) or the endosome (TLR3, TLR7, TLR8 and TLR9). NLRs (NOD1, NOD2) and RIG-like helicases (RIG-1, MDA5) are found in the cytoplasm[47].

The CLRs, including Dectin-1, Dectin-2 and Mincle, are located on the plasma membrane and recognise carbohydrate moieties[48,49]. RLRs and NLRs are both cytoplasmic receptors. The three members of the RLR family are RIG-I, melanoma differentiated-associated gene (MDA)5 and laboratory of genetics and physiology (LGP)2 (Figure 1.1). RLR family members sense dsRNA either generated by ssRNA viruses during replication or in the genome of dsRNA viruses[50,51]. NLRs are a large group of cytosolic sensors capable of recognising and responding to a range of pathogenic stimuli including bacterial peptidoglycans, bacterial toxins, fungal components and crystalline structures such as aluminium hydroxide (alum) as well as endogenous DAMPs such as adenosine triphosphate (ATP) and monosodium urate (MSU)[52–57]. NLR signalling is tightly regulated since the production of pro-inflammatory cytokines in the wrong context can be

detrimental to the host. When activated, some members of the NLR family form multi-protein complexes, called inflammasomes, which process inactive precursors of the pro-inflammatory cytokines IL-1β and IL-18 into their mature, active forms that are actively secreted from the immune cell (Figure 1.1)[58].

ALRs and DDX/DHXs are purely nucleic acid sensing receptors. The ALRs AIM2 and interferon-inducible (IFI)16 are located in the cytoplasm and both recognise dsDNA[59]. The family of DDXs/DHXs is expanding, with at least seven members all located in the cytoplasm[59]. DDXs/DHXs primarily recognise dsDNA but some, such as DDX60, have been shown to also recognise ss/dsRNA[60]. Like the TLRs, innate immune receptors from other families signal through signalling adaptors that initiate the formation of large multimeric protein complexes. These complexes activate inflammatory responses primarily through NF-κB, type-1 IFNs or caspase 1 (Figure 1.1)[61].

DCs are an important class of APC which possess PRRs and hence are capable of recognising PAMPs and DAMPs and subsequently activating the adaptive immune system. As professional APCs, DCs are sensor cells that represent an important bridge between innate and adaptive immunity[62].

1.1.1.2. Dendritic cells

DCs were first described in 1973 by Steinman and Cohn based on their distinct morphological structure and were eventually acknowledged as the 'critical cell required for the induction of T lymphocyte responses'[63–65]. DCs phagocytose and process antigens into peptides which are transported to the cell surface and presented to T cells in lymphoid organs. Importantly, antigen presentation is restricted by major histocompatibility complex (MHC) molecules[62]. Whether a peptide is displayed on MHC class I (MHCcI) or MHCcII depends to a large degree on its origin. Typically, peptides derived from intracellular pathogens undergo proteasomal degradation and are transported to the endoplasmic reticulum where they are loaded onto MHCcI molecules[66]. Extracellular pathogens are phagocytosed, degraded in lysosomal vesicles by pH-dependent proteases and peptides derived from these antigens are delivered from endosomes to MHCcII complexes[67]. In a distinct third mechanism, pathogens in the extracellular space can be taken up by DCs and through a process termed cross-presentation, exogenous peptides can be transferred to the MHCcI pathway[68,69].

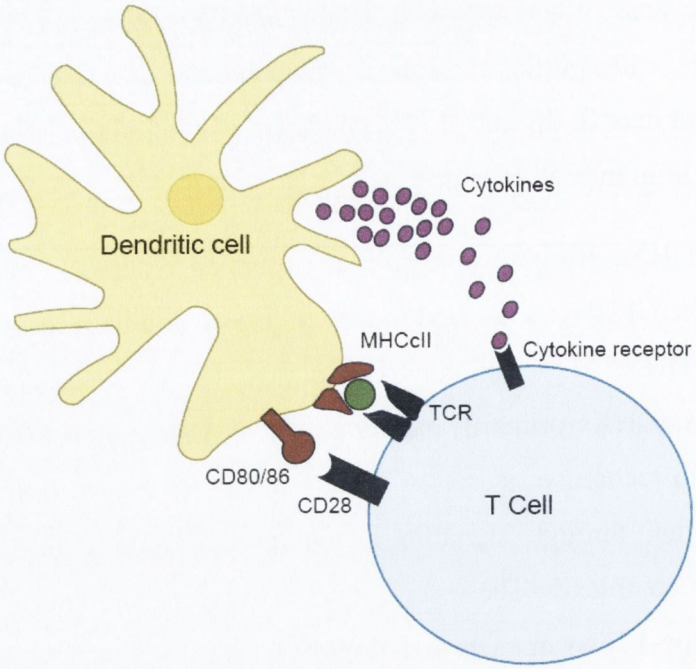

Figure 1.2 – T cell activation requires several signals. DCs activate naive T cells primarily by three signals. Antigen is presented as peptides on MHC, in this case MHCcII to a T cell receptor (TCR) on a naive $CD4^+$ T cell. Costimulatory molecules are a second necessary signal for activation to take place, for example cluster of differentiation (CD)80/86 engagement with CD28. Finally, cytokines secreted from DCs provide the third signal.

A combination of signals is required for T cells to be activated, a process which is tightly regulated. When DCs recognise PAMPs/DAMPs, maturation of the cell is induced, a process characterised by loss of endocytic ability, increased MHC stability and expression on the cell surface, up-regulation of adhesion and costimulatory molecules and the secretion of pro-inflammatory cytokines/chemokines (Figure 1.2)[70]. Once matured, DCs migrate to secondary lymphoid organs where they present antigen on MHC to T cells.

DCs can be distinguished into subtypes based on their location, migration pathway and the infection or inflammatory stimuli to which they are exoposed[71]. There are three main DC groupings; inflammatory DCs, pre-DCs and classical DCs (cDCs) (Figure 1.3)[72]. cDCs undergo terminal differentiation in the peripheral lymphoid organs or tissues and can be divided into two distinct lineages, migratory and lymphoid tissue resident[73,74]. cDCs are short-lived and as immature cells have a high phagocytic ability. Once matured, cDCs exhibit reduced phagocytosis but a significantly increased capacity to secrete high levels of

cytokine. Since cDCs are specialised for antigen processing and presentation they are highly 'migratory' cells, frequently moving from tissues to lymphoid organs, where they engage cells of the adaptive immune system[75]. These non-lymphoid based cDCs can roughly be divided into two groups; $CD103^+$ $CD11b^-$ cDCs and $CD11b^+$ cDCs[76]. The lymphoid resident cDCs collect and present antigens from within the lymphoid tissue itself[77,78]. Lymphoid resident cDCs can be further subtyped based on the expression of CD8α and CD11b[76,79]. Further more specific phenotypic definitions describing the numerous subsets of cDCs can be misleading because they are often based on arbitrary surface markers that can be up-regulated/down-regulated depending on the inflammatory state and environment[74]. More recently, the transcription factor Zbtb46 has been proposed as a unifying feature of both mouse and human cDCs (Figure 1.3)[80,81].

pre-DCs are DC precursors which primarily depend on microbial or inflammatory stimuli to develop into specific types of cDC. For example plasmacytoid DCs (pDCs) are long-lived cells which are usually found in the bone marrow[82,83]. They are effective responders to nucleic acid stimulation, preferentially expressing TLR7 and TLR9 and are capable of secreting significant amounts of IFN-α[83]. However, pDCs have a reduced expression of MHCcII molecules and hence have a reduced capacity to present antigen.

Monocytes can carry antigens to local lymph nodes, where they can either transfer antigens to cDCs or differentiate into monocyte-derived DCs[16,84]. Monocytes contribute to intestinal $CD103^-$ $CD11b^+$ DCs[85,86], splenic $CD11b^+$ $Esam^{low}$ DCs[87] and muscular fragment crystallisable (Fc)γRI^+ DCs in the steady state[88] as well as inflammatory DCs that are only induced when the body is inflamed or infected[76]. For example, following infection with *Listeria monocytogenes* a population of inflammatory DCs named 'Tip DCs' were induced which secreted TNF and produced inducible nitric oxide synthase[89].

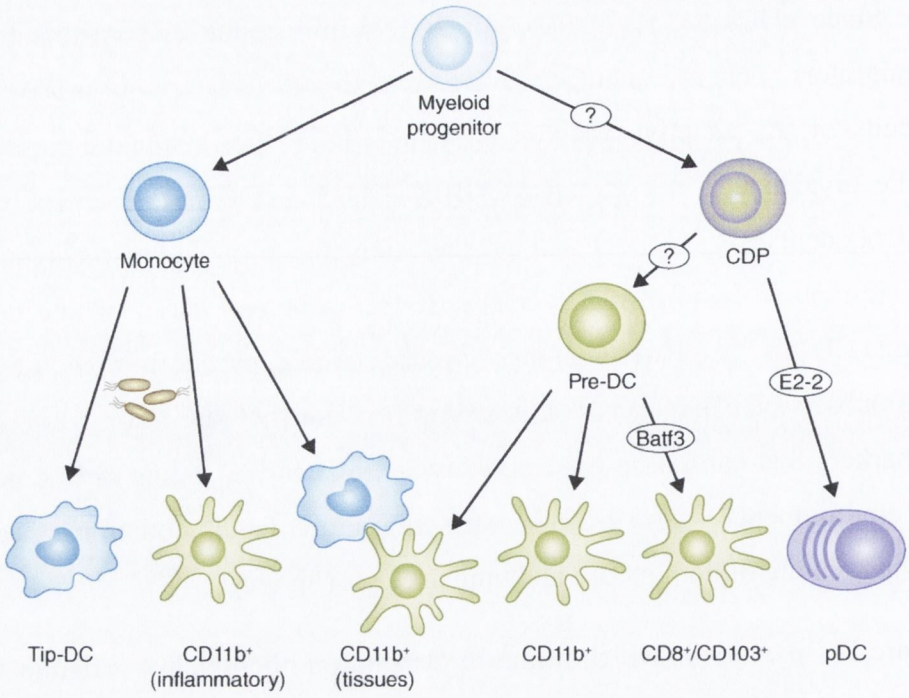

Figure 1.3 - Dendritic cell lineages in the mouse. Myeloid progenitors can give rise to DCs, differentiating through the monocyte or common DC progenitor (CDP) lineage. Progenitors are represented as "conceptual" entities according to cDC-specific gene Zbtb46 expression rather than to the current phenotypic definitions. CDPs can give rise to cDCs and pDCs but no other cell types. cDCs can be classified into two main subsets, the $CD11b^+$ and $CD8^+/CD103^+$ cDCs in mice. Monocyte-derived DCs are often inflammatory, including Tip-DCs. The known and possible (question marks) specific transcriptional regulators of DC development are indicated[74].

1.1.1.3. Trained immunity

The innate immune system, being non-specific and rapid, had also been thought to be short-lived and incapable of developing memory. However, the concept of 'trained immunity' has recently been proposed which describes a subset of innate effector cells that acquire memory characteristics after initial exposure, enabling non-specific protection against re-infection[90]. Innate immune memory is a well accepted arm of plant and invertebrate immunity. Systemic acquired resistance (SAR) in plants enables long term protection against infection, irrespective of the pathogen first encountered and mechanistically involves chromatin remodelling, DNA methylation and epigenetic regulation[91,92]. Invertebrates lack adaptive immunity yet several studies have exhibited

enhanced immune responses upon re-infection as well as transmission of protection to offspring[93–96].

Evidence for the existence of enhanced heterologous innate immune protection in vertebrates was demonstrated as far back as 1969 with the observation that immunisation of mice with the Bacille Calmette-Guérin (BCG) vaccine protected against mycobacteria as well as *Listeria monocytogenes*, *Salmonella typhimurium*, *Staphylococcus aureus, Candida albicans* and *Schistosoma mansoni*[97–100]. Similarly, after injection with a live attenuated strain of *C. albicans,* mice were also protected against *S. aureus* and this protection was also induced in athymic mice indicating a T-cell independent mechanism[101–103]. With regards to the BCG, children immunised with this vaccine have enhanced heterologous protection again other infections and reduced mortality and morbidity[104,105]. The precise mechanism of the non-specific protection mediated by vaccination with the BCG are unclear, however as with plant SAR, epigenetic reprogramming appears to take place, specifically in monocytes by modulation of histone methylation[106]. Similarly, macrophage epigenetic reprogramming occurs after β-glucans of *C. albicans* activate the dectin-1/Raf-1 pathway, leading to specific hypermethylation of histones and innate immune memory[103,107].

Monocytes and macrophages are not the only cells involved in trained immunity. NK cells exhibit functional reprogramming after initial exposure to pathogens and have been shown to deliver non-specific protection against re-infection[102]. In terms of long term responses of NK cells, infection with cytomegalovirus induces virus-specific receptor expression on NK cells that can reside in lymphoid organs for months and upon re-infection rapidly degranulate and produce cytokines[108]. Similarly, Paust *et al.* have shown that adoptive transfer of virus-sensitised NK cells into naive recipient mice enhanced the survival of the mice after lethal challenge, which was virus-specific[109]. This NK cell memory of viruses depends on CXC chemokine receptor (CXCR)6 expression, as does NK cell-mediated antigen-specific contact hypersensitivity in mice with haptens[109]. Further investigation into the ability of the innate immune system to induce memory is clearly required.

1.1.2. Adaptive immunity

Although the innate immune system is rapid and effective it's activation is also non-specific and it's long term ability to protect unclear. Non-specific responses can lead to

tissue damage and chronic inflammation if the source of the insult is not properly eliminated. Hence, adaptive immunity has evolved in vertebrates as a sustained antigen-specific response capable of clearing pathogens completely and initiating memory so that repeat exposure does not lead to infection. The adaptive immune system is mediated by two main types of cells; T cells which differentiate in the thymus and B cells which develop and differentiate in the bone marrow. Much like the innate immune response, adaptive immunity also requires several signals before it is initiated. For T cells, these signals primarily come from DCs.

1.1.2.1. T cells

Once DCs or macrophages recognise PAMPs and/or DAMPs these sentinel cells up-regulate the antigen processing machinery and present peptides on the cell surface on either MHCcI or MHCcII molecules. These MHC:peptide complexes are recognised by TCR on naive T cells, with each T cell expressing a specific TCR capable of recognising a unique peptide conformation. T cells expressing CD4 recognise peptides presented on MHCcII molecules whereas T cells expressing CD8 molecules recognise peptides presented on MHCcI molecules[110]. These mechanisms allow for a $CD8^+$ T cell response to be generated against intracellular infections (and extracellular in the case of cross-presentation), whereas $CD4^+$ T cell responses are generated against extracellular pathogens. As mentioned previously, along with MHC:peptide:TCR engagement, costimulatory molecule engagement as well as polarising cytokine signalling is required for a T cell to become activated (Figure 1.1).

1.1.2.1.1. $CD8^+$ T cells

In the lymph nodes, antigen-specific contact between $CD8^+$ T cells and DCs leads to the activation and expansion of a phenotypically and functionally heterogeneous population[111]. $CD8^+$ T cells are cytotoxic T lymphocytes (CTL) that are capable of killing virally infected cells and tumour cells by forcing them into apoptosis (Figure 1.4). $CD8^+$ T cells recognize MHCcI molecules on the cell surface and can discriminate between healthy and infected or transformed cells via recognition of peptides that the MHCcI presents[112]. Proteins within cells are constantly being degraded and representative peptides displayed on MHCcI molecules[113]. Since MHCcI molecules are present on all nucleated cells, $CD8^+$ T cells

essentially play an immune surveillance role, detecting and eliminating cells that present peptides indicating viral infection or tumorigenesis[112]. Short-lived $CD8^+$ T cells kill infected or transformed cells by a controlled release of perforin and granzymes, whereas long-lived $CD8^+$ T cells survive and contribute to a memory population[114–116]. $CD8^+$ T cells can go through a 500,000 fold expansion but in order to fully achieve this, TCR engagement, costimulation and cytokine signalling are required[117,118]. IL-12 is the key cytokine involved in $CD8^+$ T cell differentiation whereas IFN-γ is the key cytokine involved in effector function[111,118,119].

$CD8^+$ T cells have also been shown to be capable of producing IL-4, and can be subdivided into T cytotoxic-1 (Tc1) cells and T cytotoxic-2 (Tc2) cells based on their cytokine profile[120]. Both Tc1 and Tc2 cells are equally cytotoxic, IL-12 and IL-4 promoting the differentiation of $CD8^+$ T cells into Tc1 and Tc2 cells respectively[121,122]. Tc1 cells produce IL-2 and IFN-γ and support a $CD4^+$ T cell response of the Th1 subset whereas Tc2 cells produce IL-4, IL-5, IL-10 and to a lesser extent IFN-γ, and support a Th2 cell response[122,123]. Suggestions that $CD8^+$ T cells can also be subdivided into Tc17 cells that secrete IL-17, Tc9 cells that secrete IL-9 and Tcreg cells with regulatory functions are still to be shown experimentally but may also have a role within $CD8^+$ T cell biology[124,125].

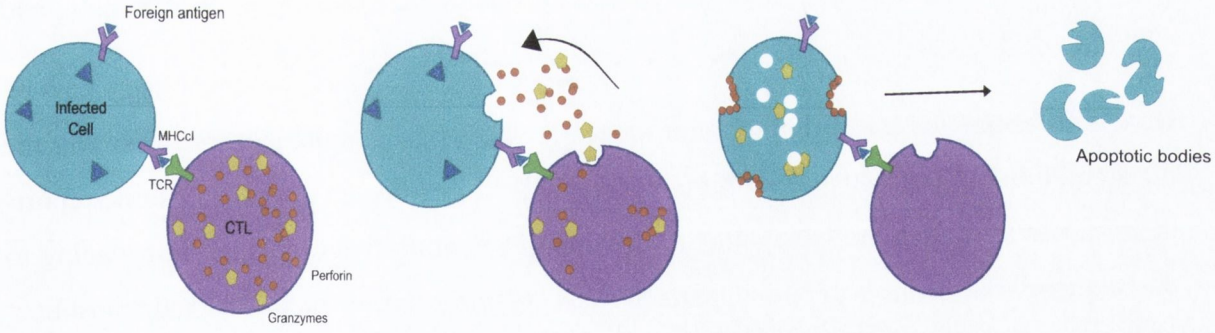

Figure 1.4 – CTL-mediated cytotoxicity. CTL recognise infected cells by peptide presented by MHCcI molecules on the cell surface. CTL activation stimulates the extracellular release of perforin and granzymes from cytotoxic granules which function in a complimentary fashion to induce apoptosis in the target cell.

1.1.2.1.2. $CD4^+$ T cells

Following activation, naive $CD4^+$ T cells can differentiate into several distinct subsets, namely Th1, Th2, Th17, regulatory T (Treg) cells, Th9 and T follicular helper T (Tfh) cells (Figure 1.4). The fate of the naive T cell depends primarily on the nature of the pathogen or insult. Specifically, Th cell subset differentiation is influenced by factors including the dose and form of antigen, the affinity of the antigen-TCR interaction, the TCR interaction with the MHC, the costimulatory interactions between cell surface molecules (signal 2) and polarising cytokines (signal 3) (Figure 1.2)[126,127].

IL-12 secretion from macrophages and DCs encountering intracellular pathogens is responsible for the polarisation of naive T cells into Th1 cells[128–130]. Th1 polarisation is further enhanced by IFN–γ secreted by NK cells, which up-regulates IL-12 production and in turn inhibits the differentiation of other Th cell subsets. The presence of both IL-12 and IL-18, secreted by innate immune sentinel cells following PRR stimulation, serves to maintain the Th1 cell phenotype as IL-18 synergizes with IL-12 to stimulate the production of IFN-γ by Th1 cells[131,132]. The development of the Th1 subset is dependent on activation of the transcription factor T-bet, which simultaneously represses the onset of a Th2 phenotype (Figure 1.5)[133,134]. Th1 cells primarily secrete IFN-γ but can also produce IL-2, TNF-α, TNF-β and lymphotoxin (LT)[135]. These cytokines can orchestrate powerful cell-mediated immunity by recruiting and activating macrophages, neutrophils, NK cells and CTLs[133].

IL-4 is essential for the differentiation of Th2 cells, while simultaneously inhibiting the differentiation of Th1 cells. The initial source of IL-4 remains controversial, some reports have shown that DCs and basophils are capable of secreting this cytokine, thus leading to the sequential activation of the signature Th2 cell transcription factors signal transducer and activator of transcription (STAT)6 and GATA-3 (Figure 1.5)[136–140]. However, ILCs also play an important role in Th2 differentiation, with multi-potent progenitor type 2 (MPP^{type2}) cells capable of differentiating into macrophages, basophils and mast cell populations and collectively promoting the development of Th2 cytokine responses[141]. More recently, IL-10 and IL-33 have been suggested to drive Th2 cell differentiation through IRF4 activation in DCs[142,143].

Th2 cells are generated in response to parasitic infections and secrete IL-4 along with IL-5, IL-9, IL-10 and IL-13[135]. These signature Th2 cytokines promote B cell expansion, antibody production and in particular immunoglobulin (Ig)G1 and IgE isotype switching

which leads to eosinophil recruitment and mast cell degranulation[131,144]. However Th2 cytokines are also critical in the allergic response as an over-exuberant production of IL-4 can lead to pathological changes in the host, contributing to asthma and other allergic inflammatory diseases[133].

Th17 cells produce IL-17 and are implicated in the pathology of autoimmune diseases such as collagen-induced arthritis and multiple sclerosis as well as in host defence against extracellular bacteria such as *Klebsiella pneumoniae, Mycobacterium tuberculosis* and *S. aureus*[145,146]. DCs secrete transforming growth factor β (TGF-β) and IL-6 upon recognition and phagocytosis of infected apoptotic cells which induces the expression of RORγt, the Th17 polarising transcription factor (Figure 1.5)[147–149]. IL-1β and IL-23 can amplify the Th17 phenotype whereas IL-27 (from the IL-12 family) is capable of inhibiting Th17 polarisation[146]. IL-23 plays a role in promoting cell survival, expansion and continual expression of the Th17 specific cytokines, particularly IL-17A. IL-23 is up-regulated by RORγt$^+$ Th17 cells and so appears to function after IL-6/TGF-β signalling has committed a naive T cell to the Th17 lineage[150].

Th17 cells specifically produce IL-17A, IL-17F and IL-22[151,152]. IL-17 promotes inflammation by recruiting cells to peripheral tissues[153]. IL-22 is needed to enhance the expression of anti-microbial peptides associated with host defence and works cooperatively with IL-17A and IL-17F to regulate local tissue inflammation[151,152]. This is achieved by stimulating fibroblasts, endothelial cells, epithelial cells and macrophages to produce chemokines, cytokines and matrix metalloproteinase (MMP) which in turn recruit neutrophils[154].

Treg cells differ from other CD4$^+$ T cell subsets in that their role is in peripheral tolerance and immune homeostasis. The role of the adaptive immune system is to generate huge random variability in antigen-specific lymphocyte receptors so that the host is protected against infectious disease. However, the processes involved in building this variability inherently generate self-reactive receptors. Treg cells are involved in the active suppression of autoreactive lymphocytes, although their precise mechanism of action remains unclear. However, it is clear that Treg cells' functionality is heterogeneous in that they use multiple inhibitory mechanisms which are tissue- and context-dependent[155]. The immunosuppressive activity of Treg cells is dependent on TCR activation and cell contact, and it has been suggested that it is the inhibition of the transcription of IL-2 that causes suppression[156–158]. The signature Treg cell transcription factor forkhead box P3 (FoxP3) is

dependent on TGF-β signalling alone, hence the balance of IL-6 and TGF-β may control the local differentiation of Treg and Th17 cells[148,159].

Treg cells are subdivided into natural Treg (nTreg) cells and adaptive or inducible Treg (iTreg) cells. nTreg cells develop in the thymus during TCR affinity selection where they recognize self-antigens that are presented on MHCcII molecules (altered negative selection) whereas iTreg cells develop in secondary lymphoid organs under the influence of TGF-β or IL-10 and are found in the periphery (Figure 1.5)[158,160–162].

Tfh cells were exclusively identified in B cell follicles in secondary lymphoid organs through expression of CXCR5 and are now also characterised by the expression of inducible costimulator (ICOS) and programmed death(PD)-1[163]. The primary role of Tfh cells is to provide B cell help and regulate antibody isotype class switching[164,165]. Antigen presentation by DCs is necessary and sufficient for Tfh cell differentiation whereas antigen presentation by activated B cells is important for the maintenance of Tfh cell responses[166]. DCs initiate the induction of the transcription factors B cell lymphoma (Bcl)-6 and STAT3 enabling differentiation of Tfh cells by IL-6 and IL-21 signalling (Figure 1.4)[167,168]. CXCR5 expression is promoted by IL-21 and binds CXC chemokine ligand (CXCL)13 which is found in abundance in B cell follicles[169]. Tfh cells secrete the B cell-promoting cytokines IL-10 and IL-21 which promote the generation of high affinity antibodies and memory B cells, thus contributing significantly to antigen-specific humoral immunity[170,171]. However, the possibility that previously established $CD4^+$ T cell lineages adopt a Tfh cell profile by down-regulating CCR7 and up-regulating CXCR5 in the presence of IL-6 and IL-21 cannot be discounted[172].

Th9 cells are a distinct population capable of promoting tissue inflammation and anti-cancer effects and are characterised by secretion of the cytokines IL-9 and IL-21[173]. *In vitro* studies originally exhibited how TGF-β and IL-4 promoted the differentiation of Th9 cells, but could not determine a transcription factor that confirmed Th9 cells were a distinct subset[174–176]. More recently IL-1β has also been shown to play a role in this differentiation, specifically in expressing the transcription factor IRF1 in TGF-β and IL-4 polarized Th9 cells, enhancing the IL-9 and IL-21 secretion from Th9 cells in anti-cancer responses[177]. IRF4 has also been implicated in Th9 development since IL-9 expression is dependent on IRF4 signalling[178].

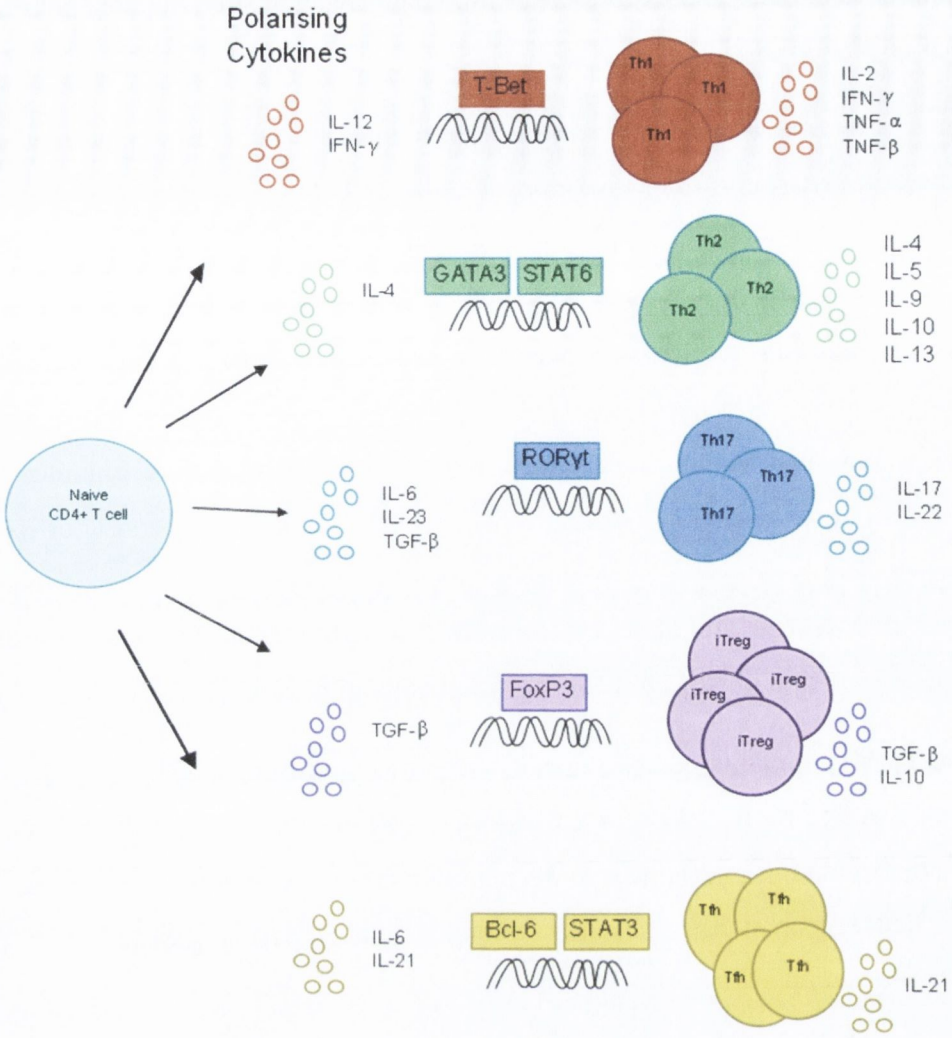

Figure 1.5 - Polarizing and signature cytokines and transcription factors of T helper cell subtypes. Following activation, naive $CD4^+$ T cells can differentiate into a number of distinct lineages. The discrete phenotype obtained is dependent on the cytokines present in the local environment (polarising cytokines) and subsequent expression of transcription factors. Each $CD4^+$ T cell lineage secretes a range of cytokines that are characteristic of that particular lineage.

1.1.2.1.3. Memory T cells

Following pathogen clearance, $CD8^+$ and $CD4^+$ effector T cells are killed by apoptosis in a process termed the contraction phase. T cells that do not initiate apoptosis enter the memory phase and become memory T cells. The memory phase maintains sufficient numbers of memory T cells and stabilises them over long periods of time[179]. This allows

for a more potent, rapid and aggressive recall response against pathogens that the body has previously been exposed to.

Memory T cells can be subdivided into central memory T cells (TCM), effector memory T cells (TEM) and tissue-resident memory T cells (TRM). TCM home to lymphoid tissue and require antigen presentation for activation while TEM circulate through non-lymphoid tissue[180]. The ability of TEM to respond so quickly is enabled by a change in the expression of cell surface markers and gene expression profile reprogramming in the T cells. For example, $CD8^+$ TEM constitutively express genes encoding IFN-γ, perforin and granzymes enabling the rapid secretion of cytokines and cytotoxic granules[181–183]. The more recently described TRM migrate into peripheral tissues and persist for long periods as organ-specific resident non-circulating memory T cells[184,185]. The skin and mucosal lining are often the first site of attack from infectious pathogens, and it is at these sites that TRM appear to reside to help prevent the establishment of infections[186].

TEM and TCM are maintained by signals driven by cytokines such as IL-15, IL-7 and IL-2 leading to a steady proliferation of a memory T cell pool (Figure 1.6)[187–190]. TRM do not re-enter the circulation and appear to be maintained independently[191–194]. These processes enable a T cell response that is sustained over a prolonged period of time.

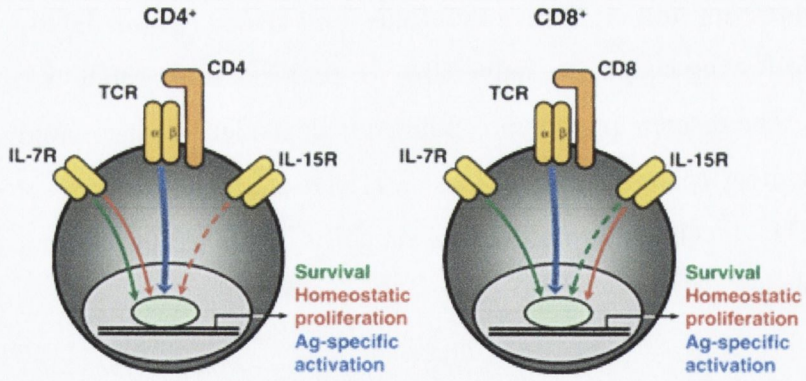

Figure 1.6 - Homeostatic proliferation and survival of memory T cells. Survival (bright green) of memory $CD4^+$ and $CD8^+$ T cells is TCR-independent but requires IL-7 driven signals, while IL-15 may also contribute to memory $CD8^+$ T cell survival. Conversely, homeostatic proliferation (red) of memory $CD8^+$ T cells depends mainly on IL-15, whereas memory $CD4^+$ T cells undergo homeostatic proliferation in response to both IL-7 and IL-15 signals. Adapted from Boyman *et al.*, 2009[195].

1.1.2.2. B cells

The humoral arm of the adaptive immune response is developed within germinal centres where antigen-specific naive B cells proliferate and differentiate into plasma or memory B cells (Figure 1.7)[196,197]. Naive B cells encounter pathogens in the periphery and recognise antigen through the B cell receptor (BCR). Although B cells can up-regulate co-stimulatory molecules and play a role in presenting antigen to T cells, their primary role is in generating antibodies[198]. Following activation, in an early extrafollicular phase, low affinity antibodies, mostly IgM, are produced from short-lived plasma cells[199]. BCR activation also induces B cell proliferation and the formation of germinal centres in lymphoid follicles of secondary lymphoid organs. Here Tfh cell and B cell interactions influence B cell somatic hypermutation, isotype switching and affinity-based selection, thus resulting in the generation of memory B cells or long lived plasma cells[200].

Long lived plasma cells are terminally differentiated, non-dividing cells that are a primary source of antibodies, predominantly generating antibodies that have undergone isotype switching[196,197]. IgM can be expressed without isotype switching and is therefore the first antibody to be produced. However, IgM monomers are of lower affinity for target antigens and so compensate for this by forming pentamers, thus providing high avidity for antigen. IgM and IgD are co-expressed on mature B cells. While both IgM and IgD are involved in activating the complement system, IgM is also involved in binding myeloid cells in order to promote the release of anti-microbial, inflammatory and B cell-stimulating factors[201,202]. Isotype switching following B cell activation and maturation in germinal centres enables the production of IgG, IgA and IgE. IgG is monomeric and the most abundant antibody isotype in the blood. It is involved in the neutralisation and opsonisation of pathogens, as well as activating the complement system. IgG is subdivided into 4 subclasses in both mice and humans although they are not direct homologues. In mice all but IgG4 is capable of complement fixation and opsonisation. In general in mice IgG1 and IgG3 are induced in response to protein antigens whereas IgG2 and IgG4 are associated with polysaccharide antigens[203]. IgG subclasses can also be characterised to a degree based on their dependence on Th1 or Th2 responses with IgG2 associated with Th1 responses and IgG1 with Th2 responses. IgA is synthesised as monomers which can enter the blood and extracellular fluids but primarily forms dimers that are secreted at mucosal sites such as the gastro-intestinal and respiratory tracts where they protect epithelial sites from pathogens. IgE is the least abundant antibody isotype but efficiently sensitises mast cells. Cross linking of

IgE molecules on mast cells leads to their degranulation, a process which initiates the release of pro-inflammatory mediators[201]. Differentiated plasma cells home to bone marrow where stromal cells provide survival signals either by direct contact or secretion of cytokines. However, there is limited space in the bone marrow, with newly differentiated plasma cells displacing older plasma cells[204].

Critically, cytokines secreted by Th cells influence the antibody isotype switching of activated B cells which enables both T cells and B cells to act synergistically. For example in mice, IL-4 induces B cells to switch isotypes to IgE and IgG1, TGF-β and IL-10 regulate IgA and IgG2b switching and IFN-γ controls IgG2a and IgG3 isotype switching[205–207].

Memory B cells are persistent, long-lived, antigen-specific $CD27^+$ B cells that form in germinal centres simultaneously with long-lived plasma cells[208]. Memory B cells are made up of equal amounts of two subsets, IgM^+ memory B cells and isotype switched memory B cells. IgM^+ memory B cells are critical for efficient protection against capsulated bacteria and it has been shown that an expanded population of IgM^+ memory B cells correlates with protection from pneumococcal infections, as measured by both antibody titres and clinical susceptibility[209]. Isotype switched memory B cells enable the generation of high affinity, antigen-specific antibodies as a result of somatic hypermutation[210].

B-1 cells are produced in the foetus and undergo self-renewal in the periphery unlike conventional B cells that are continually produced in the bone marrow[211]. B-1 cells are thought to be involved in innate-like defence through rapid humoral responses, possibly owing to the constitutively active STAT3 which allows for rapid proliferation[212]. B-1 cells express low affinity IgM, the IgG subtype IgG3 and IgA as well as low levels of IgD and in the absence of exogenous stimulation can produce what are termed 'natural antibodies' [212–215]. Natural antibodies do not undergo affinity maturation but can recognise self, altered self and foreign antigens that contain phospholipids, carbohydrate sequences, ssDNA and peptides or surface glycoproteins[216]. B-1 cells constitute a small population in the spleen but are the dominant B cell subset in the peritoneal and pleural cavities[211,217,218].

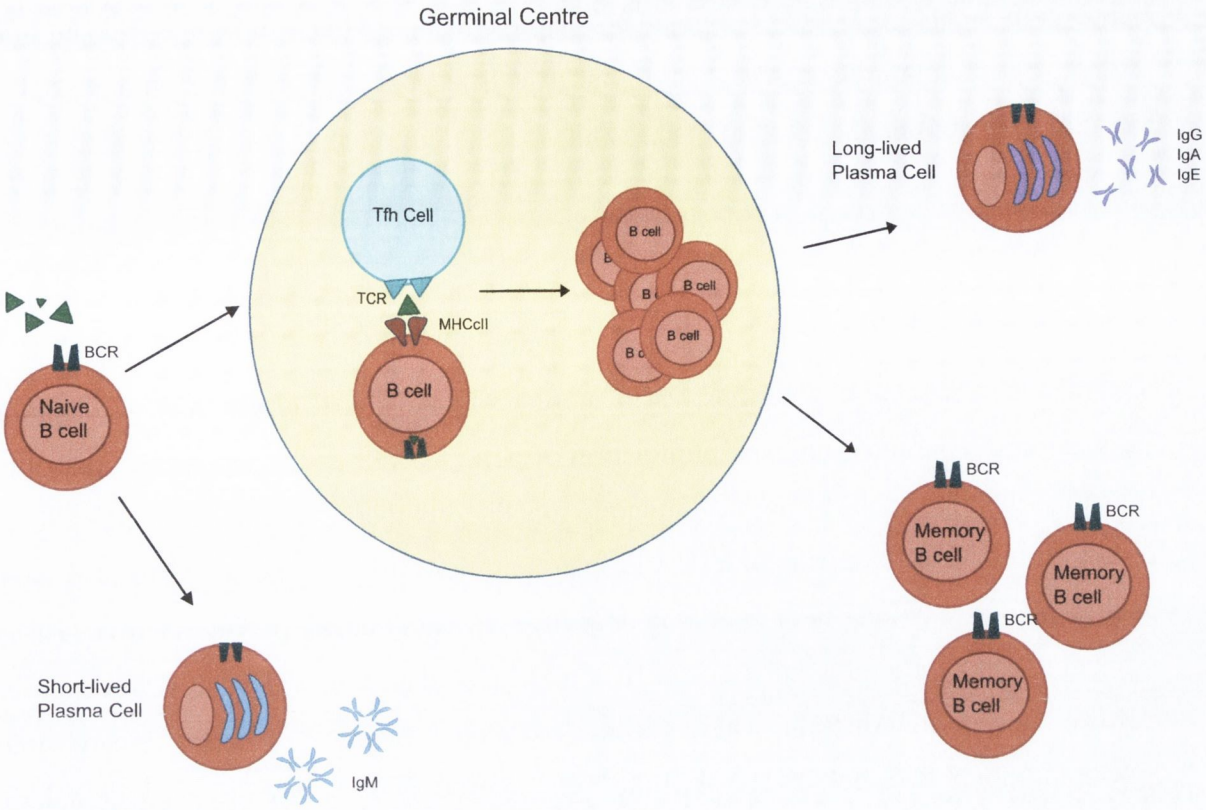

Figure 1.7 - Development of B cell subsets. Short-lived plasma cells that primarily make IgM (but some IgG) are generated during the initial B cell immune response. Upon recognition of antigen, B cells proliferate to form a germinal centre and subsequently differentiate into memory B cells or long-lived plasma cells (predominantly generating isotype switched antibodies). Adapted from Gray, 2002 and Pieper *et al.* 2013[197,219].

Regulatory B (Breg) cells are a distinct B cell subset that can negatively regulate the immune response by producing the anti-inflammatory cytokine IL-10[220–222]. IL-10 signalling from Breg cells dampens the ability of DCs to present antigen and produce pro-inflammatory cytokines and inhibits the development of Th cell subsets while simultaneously inducing the expansion of Treg cells[223]. B cells were not previously known to have any suppressive properties. However, recent studies have demonstrated that an absence of B cells can lead to sustained autoimmune inflammatory responses and that these responses are negated by IL-10 producing B cells[221,224,225]. Although Breg cells have been shown to recruit Treg cells, whether or not this B cell subset is antigen-restricted is unclear[226,227].

Hence both T cells and B cells generate an adaptive response that can be specific and long lasting. In particular, the memory T cell and B cell responses provide the immunological basis for vaccination.

1.2. Vaccines and adjuvants

No other medical intervention has had a more profound global effect than vaccination. Eradication of smallpox, the near elimination of polio as well as the successful control of infectious diseases such as measles, mumps, rubella, diphtheria, tetanus and yellow fever are all largely due to vaccination[228]. Chronic conditions such as cancer have also been tackled by vaccination, with both the Hepatitis B and human papillomavirus (HPV) vaccines significantly reducing cases of liver and cervical cancer respectively, in countries such as Taiwan and Australia where vaccine coverage is high[229,230]. Hence research into developing novel vaccines is crucial in the fight against endemic diseases such as malaria and human immunodeficiency virus (HIV), as well as replacing current vaccines that are reactogenic[231].

Vaccination involves administering an antigen formulation to the host that will generate an appropriate long-term protective immune response without causing disease[232]. Therefore, upon exposure to the corresponding pathogen, memory T and/or B cells will be activated and mount a more rapid and effective immune response, thus preventing infection. This process is dependent on APCs, particularly DCs, which capture foreign antigens, process them and display the resulting peptide epitopes in an immunogenic context to stimulate T cells[233].

Although many vaccines have been developed using attenuated whole organisms (smallpox, polio, adenovirus), there now exist safer approaches such as DNA vaccines and subunit vaccines. DNA vaccines deliver DNA encoding antigens which can be taken up by host cells and expressed as proteins[234]. Once the antigens are expressed in the body the immune system can then mount appropriate responses to them. Recombinant vector vaccines use an attenuated virus or bacterium to introduce microbial DNA into cells of the body. Subunit vaccines do not use whole organisms but instead incorporate specific antigens, which can be protein or peptide in form. However, for both DNA and subunit vaccines, most purified antigens do not induce a protective T cell response when administered by themselves. Adjuvants are substances that can be incorporated into

vaccines to enhance the magnitude, breadth and quality of the immune response to antigens. Adjuvants were first described by Ramon as "substances used in combination with a specific antigen that produce more immunity than the antigen alone"[235]. Despite extensive research, in most cases the precise mechanism of adjuvanticity remains unknown and it is because of this that Charles Janeway once referred to adjuvants as "the dirty little secret of immunologists".

Adjuvants comprise a diverse group of compounds whose proposed roles range from carriers or antigen depots to immuno-stimulatory/immuno-modulatory molecules[236]. There are many advantages of using adjuvants in vaccine formulations including their ability to promote cell-mediated immunity, to serve as an antigen depot and reduce the amount of antigen necessary in vaccines for protection ('dose sparing') and also to reduce the number of vaccinations required to induce an effective immune response[237]. Ultimately, adjuvants are required to activate DCs and promote effective uptake, processing and presentation of antigen to T cells in secondary lymphoid organs, thereby stimulating powerful antigen-specific immune responses[238].

It is critical that the adjuvants administered in vaccines are safe, well tolerated, biodegradable and can promote long lasting protective immunity[239]. For this reason, current adjuvants in development must be very well characterized, both physically and chemically. This has led to the rational design of adjuvants that can target specific receptors and generate adaptive immune responses, as well as adjuvants that are not immuno-stimulatory by themselves, but are capable of modulating the immune system in a particular way. Adjuvants can be roughly divided into immuno-stimulatory adjuvants, those that interact directly with specific receptors on APCs and particulate vaccine adjuvants that are capable of delivering antigen to APCs, particularly DCs[240].

1.2.1. Immuno-stimulatory adjuvants

1.2.1.1. Pathogen-derived immuno-stimulatory adjuvants

A primary aim of vaccines is to induce DC maturation so that antigens can be presented to T cells in order to generate long term immunity[241,242]. DCs that are activated through PRR signalling possess an enhanced capacity to present peptides to T cells and therefore to generate an antigen-specific immune response[243]. For example, CpG can engage TLR9 and

induce DC maturation in a process characterised by increased surface expression of CD80, CD86 and MHCcII and the secretion of a range of pro-inflammatory cytokines[244,245].

Synthetic analogs of dsRNA such as polyinosinic polycytidylic acid (poly IC), poly ICLC (poly IC with Polylysine and Carboxymethylcellulose) and poly $IC_{12}U$ (polyinosinic with polycytidylic$_{12}$ and uridylic) have also been developed as adjuvants[246–248]. These target TLR3, RIG-I and/or MDA5, hence activating DCs and initiating Th1-type responses[43,50]. Flagellin is the main component of the bacterial flagellum and is recognized by the immune system through TLR5 on the cell surface as well as cytosolic NLRs, specifically NOD-, LRR- and caspase recruitment domain (CARD)-containing 4 (NLRC4)[249]. Expression of flagellin within tumor cells ensures recognition of tumor-derived antigen within the inflammatory context of microbial recognition and was shown to be an effective anti-tumor vaccination strategy. This process was mediated through TLR5 activation of macrophages in addition to TLR5 and NLRC4/neuronal apoptosis inhibitory protein (NAIP)5 mediated priming of anti-tumor $CD4^+$ and $CD8^+$ T cells[250].

3-O-desacyl-4'-monophosphoryl lipid A (MPL) is derived from detoxified LPS of the Gram-negative bacterium, *Salmonella minnesota* and is recognised by TLR4. Importantly, MPL is significantly less toxic than LPS and is therefore considered safe for use in humans[251–253]. MPL promotes cell-mediated immunity with a predominantly Th1 profile in addition to a CTL response and is currently the only TLR ligand in licensed human vaccines[237,253]. MPL is used in combination with aluminium salt as Adjuvant System (AS)04 and is included in two licensed vaccines, the HPV vaccine Cervarix® and the Hepatitis B virus (HBV) vaccine Fendrix®. Due to the success of MPL, a new generation of TLR4 agonists are being developed for use in vaccine formulations, including aminoalkyl glucosamimide phosphates (AGPs) and a synthetic LPS mimetic RC-529[254].

Of all PRR subsets TLRs are characterised the best. However they are not the only targets for the development of novel vaccine adjuvants. For example the CLR Mincle acts as a receptor for the mycobacterial cord factor/trehalose dimycolate which can act as a potent adjuvant for Th1/Th17 vaccination[255,256]. In a combination approach, the CLR CD205 has been targeted in combination with poly IC as the adjuvant for the pre-erythrocytic stage of malaria infection. This approach induced antigen-specific antibody and multi-functional $CD4^+$ T cell responses in non human primates[257]. The N-CARD domain of the RLR activator, IFN-β promoter stimulator (IPS)-1 has been shown to promote vaccine immunogenicity by enhancing antigen-specific Th1-type immune responses in an influenza

infection model[258]. Similarly a RIG-I agonist has been explored as an adjuvant as part of an influenza virus DNA vaccine vector, however while it enhanced serum antibody responses, it did not induce the $CD8^+$ T cell responses required[259]. Thus although PRRs such as RLRs are less well characterized than TLRs they may also have important roles in adjuvanticity that are being resolved.

The development of pathogen-derived immuno-stimulatory adjuvants needs to focus on targeting PRRs that are involved in antigen presentation to ensure that antigen processing and stimulation occur simultaneously in the same DC so that T cells are efficiently activated[260,261]. Another important issue in pathogen-derived immuno-stimulatory adjuvant development is that PRR expression can be very different on human DC subsets compared to mouse DC subsets[262]. However, targeting one DC population may neglect the need for collaboration between different DC subsets in generating a sufficient adaptive immune response[260].

1.2.1.2. QS21

Saponins are derived from the bark, stem, roots and flowers of many plant species and are composed of sterol glycosides and triterpenoid glycosides[263]. Saponin fractions from the South American tree *Quillaja saponaria* have been isolated and shown to have potent adjuvant properties[264]. Kensil *et al.* purified numerous fractions and found fraction 21 (QS21), a mixture of soluble triterpene glycosides, to have exceptional adjuvant properties when administered with a range of antigens[263]. QS21 has subsequently been shown to stimulate the production of CTLs and induce Th1 cytokines (IL-2 and IFN-γ) and IgG2a antibodies to protein antigens[263,265]. Studies have shown that although QS21 is effective as an adjuvant when used alone, it is more effective when used in combination with other adjuvants such as CpG, Titermax and MPL in the GlaxoSmithKline (GSK) AS01 and AS02[266,267].

1.2.2. Particulate vaccine adjuvants

Particulate adjuvants do not generally contain specific agonists for PRRs yet they are still capable of promoting innate and adaptive immune responses. How they accomplish this feat is not fully understood, although proposed mechanisms include depot formation,

inducing the release of DAMPs, controlled antigen release and/or inflammasome activation[268,269]. Several types of particulate adjuvants have been described, including emulsions, immuno-stimulating complexes (ISCOMs), mineral salts and biodegradable micro-particles (Table 1.1).

Table 1.1 – Particulate vaccine adjuvants

Adjuvant	Examples	Proposed mechanism of action	Licensed for use in humans
Emulsions	CFA, ISA 51, MF59	Antigen depot	MF59 is used in flu vaccines in the EU
ISCOMs	ISCOMS or ISCOMATRIX	Activate DCs and are phagocytosed leading to both humoral and T cell responses	Phase I clinical trials
Mineral salts	Alum	Humoral response involving IL-4 and possibly depot/IL-1/DNA/uric acid	Yes, used in many vaccines in the EU and US
Biodegradable particles	PLGA, PLA	Dependent on shape and size, can target DCs and release antigen slowly	PLGA licensed as drug delivery system
Liposomes		Can incorporate antigen into surface to target certain cells	Used as components of VLPs, phase I clinical trials (CAF01)
Virosomes		Highly repetitive viral protein surfaces that can target PRRs	Engerix-B® and Recombivax HB® (HBV), Cervarix® and Gardasil® (HPV) and flu vaccines in the EU

1.2.2.1. Emulsions

Emulsions were first used as adjuvants back in 1916 when Le Moignic Pinoy used a water and vaseline emulsion containing inactivated *Salmonella typhimurium*[270]. Since then, emulsion adjuvants have diversified slightly but still remain the same in essence, essentially rendering antigens particulate in nature through aggregate formation[271].

One of the most widely used vaccine adjuvants was developed by Freund in the 1930s. This adjuvant is a paraffin oil based emulsion (incomplete Freund's adjuvant, IFA) that can also contain heat-killed *Mycobacteria* (complete Freund's adjuvant, CFA). Freund's adjuvant is an example of a water-in-oil (W/O) emulsion. W/O emulsions consist of water droplets containing antigen that are surrounded by a continuous oil phase. CFA enhances both T and B cell responses which are MyD88-dependent and inflammasome-independent

respectively[272–274]. However, Freund's adjuvants are not used in a clinical setting due to an unacceptable safety profile.

Alternative W/O emulsions with better safety profiles such as ISA 51 and ISA 720 have been developed using specific surfactants and refined oils. ISA 51 is a mineral-oil based emulsion while ISA 720 contains the animal or vegetable oil squalene[275,276]. Although both ISA 51 and ISA 720 can lead to the development of mild to moderate local reactions, these adjuvants have been used in both therapeutic and prophylactic vaccines when the benefits of their application outweigh the risks involved[276].

Oil-in-water (O/W) emulsions were developed as an alternative to W/O emulsion adjuvants, and are composed of antigen in a water phase containing oil droplets. O/W emulsions have a far superior safety profile than W/O emulsions due to the reduced oil content. MF59® is an O/W emulsion which is composed of squalene with Tween 80 and Span 85 as surfactants. The squalene droplets exist at sizes ranging from 10-200nm. Like most adjuvants its precise mechanism of action is unclear however it has been shown to cause an influx of granulocytes to the site of injection, activate muscle cells as well as an increase in endocytosis and increased expression of markers indicative of DC maturation (MHCcII, CD86, CD83, CCR7)[239,277,278]. Antigen-specific humoral responses have been shown to be NLR family, pyrin domain containing (NLRP)3-independent but apoptotic speck-like protein containing a caspase recruitment domain (ASC)-dependent and more recently transient ATP release has been shown to be required for innate and adaptive immune responses induced by MF59®[279,280]. Importantly, MF59® has been licensed for use as an adjuvant in influenza vaccines and used in clinical trials for vaccines against infectious diseases such as herpes simplex virus (HSV), HBV, and HIV[281].

Due to their success, O/W emulsions have also been used in the generation of what have been termed 'second generation' adjuvants, or particulate adjuvants that have immune potentiators incorporated to enhance immune responses[239]. For example, a synthetic TLR4 agonist glucopyranosyl lipid adjuvant (GLA) has been incorporated into the squalene based emulsion SE (stable emulsion) as SE-GLA[282,283]. Encouragingly, compared with alum-GLA and other alternative adjuvant systems, SE-GLA induced the most potent Th1 responses in mice against ID93, a lead tuberculosis (TB) vaccine antigen[284].

1.2.2.2. ISCOMs

Immuno-stimulating complexes or ISCOMs are spherical, cage-like particles that are approximately 40nm in diameter and were first described in 1984 by Morein *et al.*[285]. They are capable of promoting long-lasting functional antibody responses as well as powerful T cell responses, including enhanced cytokine secretion and $CD8^+$ T cell activation[286,287]. Studies have shown that ISCOMs can be efficiently phagocytosed and activate DCs, leading to the development of an adaptive immune response[288–290]. ISCOMs appear to destabilize the endosomal membrane, inducing more efficient translocation of antigen into the cytosol compared to other forms of antigen delivery[291]. They are primarily being evaluated within the therapeutic vaccine context[292].

ISCOMs can be composed of several different materials and tend to be subdivided into two main types, classical ISCOMs and the ISCOMATRIX®. Classical ISCOMs are made up of saponins from *Quillaia saponaria,* cholesterol, phospholipid and amphipathic protein, and were originally designed to incorporate viral components, thus making them extremely immunogenic[285]. The difference between ISCOMATRIX® and classical ISCOMs is that the protein component and antigen which are incorporated into ISCOMs can be mixed together with ISCOMATRIX®.

1.2.2.3. Mineral salts

Adjuvants containing aluminium have been used in numerous different vaccine formulations for decades. Aluminium potassium phosphate and aluminium hydroxide (commonly called 'alum') are the most common mineral salts currently being used and are licensed for use in several vaccines including Diptheria-Pertussis-Tetanus, *Haemophilus influenza* B and HPV[293]. Alum elicits strong humoral immunity which is primarily mediated by antigen-specific antibodies although the precise mechanism of action of this adjuvant remains elusive. There are several proposed mechanisms (Table 1.2)[273,294–300]. Firstly, it is proposed that alum principally works as an antigen 'depot', thus allowing prolonged exposure of the antigen to the immune system[296,297,301–303]. However, studies removing this 'depot' 2 hours after injection found that this did not alter the capacity of alum to promote antigen-specific antibody responses, therefore suggesting that the depot is not required for its adjuvanticity[298,304]. Secondly, the requirement for the inflammasome NLRP3 and IL-1β in alum-induced adaptive immune responses is also surrounded by

controversy with some groups indicating the requirement for NLRP3 in alum-induced humoral responses and others demonstrating comparable antigen-specific T cell responses in WT and NLRP3$^{-/-}$ mice[273,294,295,300]. Finally, Flach *et al.* suggest that alum is not recognized by any receptor, but rather is sensed by plasma membrane lipids leading to receptor-independent DC activation dependent on the spleen tyrosine kinase (syk) - phosphatidylinositide 3-kinase (PI3K) pathway[305]. Precisely how alum polarizes the adaptive response to a humoral response is still unclear and currently under investigation (Table 1.2).

Table 1.2- Proposed mechanisms of action of alum

Proposed mechanism of action	For	Against	References
NLRP3	• NLRP3-dependent innate response to alum • NLRP3-deficient mice have defects in alum-driven antigen-specific IgG1	• WT and *nlrp3*$^{-/-}$ mice have similar antigen-specific IgG1 titres • WT and *nlrp3*$^{-/-}$ mice have comparable antigen-specific T cell responses	293–295,300
Uric Acid	• Released into the peritoneal cavity 2 hours after intra-peritoneal (i.p.) injection. • Treatment with uricase decreases antigen-specific T cell and humoral response		139
DNA	• Accumulates in the peritoneal cavity 3 hours after i.p. injection • DNase decreased antigen-specific IgG1 and IgE responses • Immunisation with dsDNA mimics alum-induced adaptive immune responses	• IRF3-deficient and WT mice immunized with alum and OVA have similar antigen-specific IgG1 titres	299
Depot	• If nodules at the site of injection are ground up and injected into a naïve animal they induce immune responses against the adsorbed antigen	• Nodules from the site of injection do not only contain alum and antigen but also extracellular chromatin, histones, extracellular myeloperoxidase and neutrophils. • Removal of depot 2 hours after immunisation did not affect the magnitude of the antigen-specific IgG1 responses	296–298,304

1.2.2.4. Biodegradable micro-particles

Several groups have shown that biodegradable micro-particles have the capacity to elicit strong and long lasting antibody and T cell proliferative responses to incorporated antigens[306]. Although particles can be formulated from a wide range of polymers such as poly(lactide-co-glycolide) (PLG), polymethylmethacrylate (PMMA) and poly(lactide) (PLA), PLG is Food and Drugs Administration (FDA)-approved as it is degraded into lactic acid and glycolic acid which are normal metabolites and well tolerated in the human body[307]. PLG micro-particles are prime candidates for vaccine adjuvant development as they are biodegradable *in vivo* and their half-life can range from days to years depending on their composition. Although not currently licensed for use as adjuvants, the processing and manufacturing facilities are already in place for biodegradable micro-particles to make this transition[308]. Antigens, as well as adjuvants, can be encapsulated within PLG particles and directed into the processing pathways for presentation on MHCcI and MHCcII. These systems have been shown to effectively increase antibody titres compared to antigen/adjuvant alone[309–311].

In addition to their desirable safety profile, other advantages of using PLG particles include their ability to target DCs while protecting antigen from degradation and from entering the systemic circulation, as well as the multi-meric presentation of antigen absorbed to their surface which is required for optimal B cell activation[312]. Importantly, PLG particles can also promote cell-mediated adaptive immunity and can facilitate co-delivery of various immune-modulators to DCs[307,313,314].

Interestingly, PLG particles have been shown to drive equal if not superior adaptive immune responses compared to the 'A' standard adjuvants such as alum and Freunds adjuvant. Men *et al.* found that PLG particles 1-80μm in size, encapsulating weakly immunogenic malarial peptides can elicit strong and sustained proliferative T cell responses as well as antigen-specific antibody responses when compared with IFA[315]. The same group have also demonstrated a superiority of PLG particles over alum using a tetanus toxoid model[316].

1.2.2.5. Other particulate vaccine adjuvants

Other particulate vaccine adjuvants include liposomes and virus-like particles (VLP). Liposomes are particulate structures composed of either natural or synthetic phospholipids

and range between 100-400nm in diameter[317]. They were first developed by Alec Bangham who extracted lipids from egg yolk and described the formation of a double layered bubble the size of a cell when these lipids were added to an aqueous solution. Incorporating antigen into liposomes leads to increased antibody titres, hence much work has been conducted into designing liposomes that are stable in the bloodstream and can target specific cells of the immune system to generate an enhanced adaptive immune response[318–320]. However, without the addition of an immune potentiator liposomes alone are not effective adjuvants[292].

Cationic liposomes have been shown to induce pro-inflammatory cytokines, chemokines and a pronounced inflammatory exudate at the injection site consisting of neutrophils, monocytes, macrophages and activated NK cells[321,322]. CAF01 is a cationic liposome composed of dimethyldioctadecylammonium bromide, and the glycolipid trehalose 6,6′-dibehenate[323]. Cholesterol modifications of the bi-layer enabled the development of an adjuvant that remains in the muscle for longer allowing slow release of liposome/antigen from the site of injection hence favoring a strong Th1 response[324]. CAF01 has been shown to enhance the immunogenicity of antigens from a range of pathogens, including those causing TB, HIV, Chlamydia, flu, and malaria[292,325–329].

Based on the ability of viruses to efficiently penetrate cells, VLP and virosomes have been developed as adjuvant vectors to present and deliver antigens to immune cells. These particles range from 20-100nm in size, consist of self-assembling viral envelope proteins and lack the ability to replicate and infect cells as they do not contain any viral nucleic acids[330]. Importantly, both VLP and virosomes are capable of stimulating both cell-mediated and humoral immunity through their highly repetitive surfaces composed of viral proteins[331–333]. VLPs are known to induce receptor-mediated endocytosis on APCs and can escape endosomal degradation allowing for antigen presentation on both MHCcI and MHCcII[334,335]. VLP can be manipulated in such a way that other PAMPs can be incorporated within them, allowing specific targeting of PRRs and hence dictating the type of immune response induced[336]. However, since VLPs and virosomes are not substances 'added' to antigens to improve their immunogenicity but in fact are 'ordered arrays of antigens that are either expressed from cells or self-assembled into particles', their inclusion as adjuvants is debated[292].

1.2.3. Combination vaccine adjuvants

The advances in biotechnology, molecular biology and immunology have enabled the rational development of well-defined, PAMP-based adjuvants. This, along with developments in synthetic chemistry has enabled the advancement of combination vaccine adjuvants.

Combining different adjuvants allows for a tailored immune response to be optimised. The advantages of using this type of strategy include the ability to promote the development of heterologous antibodies that have increased cross-reactivity among strains of pathogens, more effective T cell responses and more potent functional antibodies. Although the process of combining adjuvants with other immuno-stimulatory components is not novel, it is only recently that these types of adjuvants have been licensed[239].

IC31® is composed of a lysine/leucine rich anti-bacterial peptide KLK (KLKLLLLLKLK) derived from sapecin B that interacts with the synthetic oligodeoxynucleotide (ODN)1a[337]. IC31® signals via the TLR9/MyD88-dependent pathway inducing a Th1-type cellular and humoral immune response[338]. KLK appears to stimulate uptake and subsequent cellular internalisation of ODN1a by endocytosis[292,339]. Once inside the cell, ODN1a associates with TLR9 positive compartments including early and late endosomes[339].

GSK has been the front runner in the development of combination adjuvants. Their AS portfolio is composed of various mixtures of classical adjuvants combined with other immuno-modulators (Table 1.3)[340]. AS04 is a combination of MPL and alum and is used in the Fendrix® and Cervarix® vaccines that are currently on the market. ASO4 is known to induce an increase in local cytokine and chemokine signaling leading to cell recruitment (DCs and monocytes) locally as well as an increase in antigen-loaded DCs and monocytes in draining lymph nodes[253]. ASO3 is licensed for the pandemic flu vaccine and works in a similar way to AS04 except it also improves spatio-temporal co-localisation with antigen at the site of injection and primarily recruits granulocytes and monocytes[341]. There are several other AS combinations that are in clinical trials for infectious diseases such as malaria as well as some cancers (Table 1.3)[342,343].

Table 1.3 – GSK combination adjuvant systems

Adjuvant System	Composition	Licensed for use
AS01	liposome formulation with MPL and QS21	As part of ASO1E in GSK's candidate malaria vaccine RTS,S AS01, Phase III clinical trial[222]
AS02	O/W emulsion formulated with MPL and Stimulon® QS21	As part of ASO1E in GSK's candidate malaria vaccine RTS,S AS01, Phase III clinical trial[222]
AS03	squalene, DL-α-tocopherol and polysorbate 80	Pandemic H1N1 vaccine Pandemrix™ and Arepanrix™
AS04	MPL and alum	Cervical cancer vaccine Cervarix™
AS15	CpG 7909, MPL and QS21	MAGE-A3 immunotherapeutic in Phase III trial for melanoma and non-small cell lung cancer[223]

1.3. Adjuvant size

Although many particulate adjuvants have been compared based on their composition, comparing adjuvants based on size is an area that has been somewhat neglected. Adjuvants currently used in licensed vaccines vary in shape and size, with MF59 droplets less than 250nm and Alhydrogel and AdjuPhos aggregates ranging between 0.5-10μm[344] (Figure 1.8).

Interestingly, it has been observed that size has an important role in the type of immune response generated by particulate adjuvants independent of composition. For example, although polystyrene (PS) nano-particles of 40-49nm and 93-123nm in size are both capable of enhancing antigen-specific IgG1 when conjugated to ovalbumin (OVA) and injected intra-dermally, the effects of these particles on T cell responses are distinct, with 40-49nm particles inducing antigen-specific IFN-γ from splenocytes and 93-123nm particles driving IL-4[345]. Interestingly, using nano-particles engineered from lecithin/glyceryl monostearate-in-water emulsions, Li *et al.* also demonstrated that nano-particles elicit size-dependent immune responses, with 230nm OVA-conjugated particles inducing more potent OVA-specific antibody and cellular immune responses than 708nm OVA-conjugated particles following subcutaneous (s.c.) injection[346].

Although there is an ever-increasing obsession with the nano-scale, micro-size particles also have many advantages as adjuvants. Micro-size particles are a similar size to many pathogens that the body encounters (Figure 1.8) and it is their size that enables prolonged

antigen release compared with nano-size particles[347–349]. Importantly, micro-particles are capable of promoting both cellular and humoral responses[306,350]. Katare *et al.* demonstrated that PLA micro-particles in the 2-8μm size range are more effective in generating antigen-specific IgG than particles less than 2μm and greater than 10μm when using tetanus toxoid as an antigen[351]. In another study using PLA particles, this time containing Hepatitis B surface antigen (HBsAg), particles 2-8μm in size induced the most potent antigen-specific antibody response as well as significantly more IL-4 secretion and MHCcII up-regulation than nano-particles (200-600nm)[352].

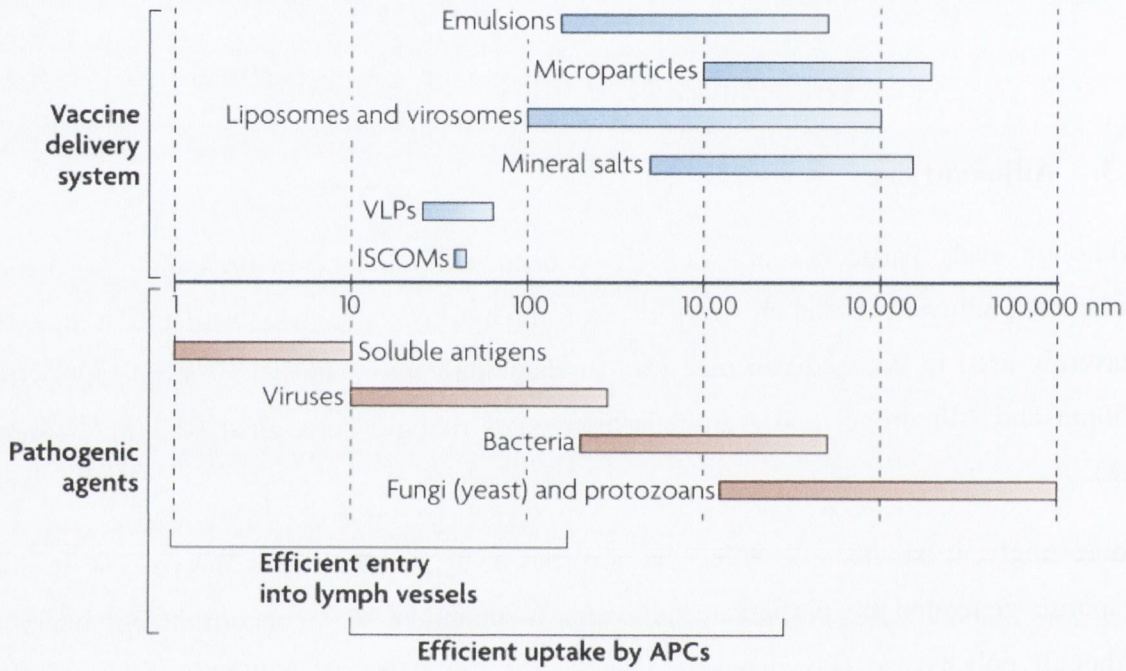

Figure 1.8 – The sizes of adjuvant delivery systems and pathogenic agents. The size range of various adjuvants and pathogenic agents are indicated on a nanometre log scale. The range of particle sizes that allows most efficient uptake by APCs and the size of macromolecules that most efficiently enter the lymphatic vessels are shown[336].

The route of administration has been shown to be important within these studies, with i.p. injection but not s.c. injection revealing size-dependent antibody responses in a study using PLA particles ranging from 3-50μm[353]. This was suggested to be due to the inability of particles to migrate through s.c. tissue and hence their failure to affect the induction of an adaptive immune response[353]. Hence it appears that differences across studies may be due

in part to the differences in the route of administration, the antigen incorporated into the vaccines as well as particle composition, poly-dispersity of particles and immune read-out.

Very few studies have compared particle size across the nano- and micro-scale in terms of their induction of innate and adaptive immunity. Of those studies that have examined a broader spectrum of sizes, there has been inconsistency with regards to particle composition, antigen and route of administration. In a study comparing PLA particles of nano- and micro-size containing HBsAg injected intra-muscularly, Kanchan *et al.* found that although nano-particles 200-800nm in size are capable of inducing antigen specific IFN-γ responses, micro-particles 2-8μm in size can drive antigen specific IL-4 as well as antigen-specific antibody responses[352]. Interestingly, PLG particles administered parenterally exhibit a similar profile, with peptides from *Plasmodium berghei* circumsporozoite protein and influenza A virus nucleoprotein (NP) both inducing greater CTL responses when entrapped within nano-particles (<500nm) compared with micro-particles (>2μm)[314]. However, 40nm PS particles were shown to induce both humoral and cellular immunity, as well as protection/clearance of tumours to the greatest extent when a range of particles 20nm-2μm were compared[354]. Based on these findings, it is clear there are contradictions within the literature as well as an absence of a mechanistic understanding of the effect of particle size on the immune response. Hence there is a need to fully elucidate the immune response to both nano- and micro-particles of the same material and to determine the mechanisms by which particles of different sizes generate distinct immune responses.

1.4. Hypothesis and Aims

The development of adjuvants in the current era is focused on developing tailored systems to specifically control the type of adaptive immune responses elicited by vaccines in order to control cancers and infectious diseases such as malaria and HIV. This approach requires adjuvants that are capable of inducing a $CD8^+$ T cell response coupled with pro-inflammatory cytokines such as IFN-γ, IL-12p70 and TNF-α which can polarize a Th1 type response. However, current adjuvants/vaccines are remarkably poor in generating cell-mediated immunity. Since particle size plays an important role in determining the type of adaptive immune response that is generated, the size of particles in vaccine formulations could be specifically tailored to a size that best facilitates the onset of cellular immunity and effective resolution of the ensuing threat to the host.

Several studies have previously investigated the importance of size in the ability of particles to enhance immune responses[345,346,351,353]. However, although size has been shown to have a major impact on the type of immune response induced, there are no studies providing a detailed account of the effects of particle size on local inflammation, the production of key T cell-associated cytokines and the induction of functional humoral responses. A recent review on next generation adjuvants highlighted how the affect of particle size on T cell responses in particular has not yet 'been clearly demonstrated'[292].

Previous work in the laboratory by Fiona Sharp (PhD thesis, data unpublished) showed interesting histological differences in inflammation in mice immunised subcutaneously with different sized PS particles mixed with OVA. Neither PBS nor OVA induced significant local inflammatory changes 7 days and 21 days after injection. However, injection of different sized PS particles ranging from 200nm to 30μm showed remarkably different inflammatory profiles in histological sections. PS particles of sizes 200nm, 400nm and 1μm all induced significant local necrosis, cell infiltration and granuloma formation whereas 10μm and 30μm PS particles had less inflammation and very little local necrosis. Interestingly, when the antigen-specific antibody responses were determined in serum 21 days after injection, immunisation with all sized PS particles drove significant levels of OVA-specific antibodies when compared with OVA alone.

Based on this work, it was hypothesised that the differential ability of nano-particles and micro-particles to induce and direct adaptive immunity reflects distinct particle size mediated innate immune responses. Further, nano-particles may induce potent inflammation that may be detrimental to the host and induce a regulatory response that negatively influences the ensuing adaptive immune response. Conversely, large particles are recognised by the host and drive limited but sufficient inflammation leading to an adaptive immune response that protects the host. With these factors in mind, and to address the lack of clarity in the field, this project aims to achieve the following objectives:

- To determine the ability of a broad spectrum of different sized PS particles to induce inflammation at the local injection site, specifically identifying infiltrating immune cells and the local production of chemo-attractants.
- To examine the ability of a broad spectrum of different sized particles to induce adaptive immune responses, incorporating both antigen-specific antibody and T cell responses

- Using the candidate *S. aureus* vaccine antigen, Clumping factor A (ClfA), to assess the ability of particles to modulate bacterial induced innate immunity and perform a *S. aureus* challenge with the most promising sized PS particles.

Chapter 2

Materials and Methods

2.1 Materials

Unless stated otherwise, all materials were purchased from Sigma-Aldrich.

2.1.1. General cell culture materials

Complete RPMI 1640 Medium

Roswell Park Memorial Institute (RPMI) 1640 medium (Biosera) was supplemented with 2 millimolar (mM) L-Glutamine (Gibco), 50units/ml penicillin (Gibco), 50μg/ml streptomycin (Gibco) and 8% (v/v) heat-inactivated (56°C for 30 minutes (mins)) and filter sterilised foetal calf serum (FCS) (Biosera).

Complete RPMI 1640 T cell Medium

RPMI 1640 medium (Biosera) was supplemented with 0.04mM β-mercaptoethanol (Gibco), 0.88mM sodium pyruvate (Gibco), 0.88mM L-Glutamine (Gibco), 4.4 units/m penicillin (Gibco), 4.4μg/ml streptomycin (Gibco), 0.88% (v/v) 100X MEM Non-Essential Amino Acids (Gibco), 0.35% (v/v) 100X MEM Vitamins (Gibco) and 10% (v/v) heat-inactivated (56°C for 30 mins) and filter sterilised FCS (Biosera).

0.88% ammonium chloride (NH_4Cl) red blood cell lysis solution

8.8g ammonium chloride was dissolved in 1 litre (L) of endotoxin-free water (H_2O) (Baxter) and filter sterilised with a 0.22μm syringe-driven filter (Millipore).

2.1.2. Cell culture and animal study treatments

Polystyrene micro- and nano-particles

Polystyrene micro-particles and nano-particles were sourced from Phospherex, Inc. (Ma 01748, USA). To determine the size of particles after mixing with OVA, particle sizes were verified using a Malvern Zetasizer Nano ZS (Malvern Instruments Ltd, UK)(Appendix I). Sizes were verified only for particles that fell within the parameters of the instrument (50nm and 1μm). Experiments performed by Dr. Dulce Bento.

Alum adjuvant

Alhydrogel (alum) was sourced from Brenntag Biosector (Frederikssund, Denmark).

PRR agonist

The PRR agonist LPS, from *E. coli* LPS, Serotype R515 (Enzo life Sciences), was used to stimulate bone-marrow DCs (BMDCs).

Antigens for *in vivo* studies (Table 2.1)

Table 2.1 – Antigens used for *in vivo* studies

Reagent	Supplier
Clumping factor A, *Staphylococcus aureus*	Dr. Joan Geoghegan, Department of Microbiology, Trinity College Dublin.
Endotoxin-free ovalbumin (EndoOVA)	Hyglos GmbH
NP311 influenza nucleoprotein peptide (QVYSLIRPNENPAHK)	JPT Peptide Technologies (12489 Berlin, Germany)

Ex vivo restimulation assay reagents (Table 2.2)

Table 2.2 – Reagents used for *ex vivo* restimulation assays

Reagent	Supplier
NA/LE Hamster Anti-Mouse CD3e	BD Pharmingen
Phorbol 12-myristate 13-acetate (PMA)	Sigma-Aldrich
Ionomycin (ION)	Sigma-Aldrich
LPS, Serotype R515	Enzo life Sciences
Heat-killed *E. coli,* BL21 strain	N/A

Heat-killed *E. coli,* BL21 strain

This work was performed by Dr. Eimear Lambe of the Adjuvant Research Group in the School of Biochemistry and Immunology, Trinity College Dublin (TCD). An agar plate containing lysogeny broth (LB) was streaked with BL21 strain *E. coli.* The bacteria were left to grow overnight at 37°C in 10ml of LB. The culture was then transferred into 100ml of LB and was incubated shaking for 2 hours at 37°C. Serial dilutions of the culture were made and a known volume of each of these dilutions was spread onto LB agar plates and

incubated overnight at 37°C. The number of colonies were counted and then multiplied by the dilution factor to determine the number of cells/ml in the original culture. The number of bacteria in the culture was confirmed further using a spectrophotometer to measure the optical density (OD) value of a sample at 600nm. The *E. coli* were killed by heating at 70°C for 15 mins and were then plated onto LB agar to ensure that no growth occurred. The cells were pelleted by centrifugation and resuspended in phosphate buffered saline (PBS) (Biosera) to a final concentration of 1 x 10^9 cells/ml.

2.1.3. Flow cytometry/Fluorescence-activated cell sorting (FACS) materials

FACS buffer

1X PBS was supplemented with 0.1% sodium azide and 2% heat-inactivated (56°C for 30 mins) and filter sterilised FCS (Biosera).

Reagents to measure cell death

Cells were stained with LIVE/DEAD Fixable Aqua Dead Cell Stain (Invitrogen) which binds free amines.

4% Paraformaldehyde (PFA)

40g PFA in 1L sodium phosphate buffer (13.4 g Na_2HPO_4, 6.9 g NaH_2PO_4, 1L dH_2O). Heat with stirring bar for 30 to 45 mins at 60°C to dissolve PFA, pH 7.

0.1% Saponin

0.1g Saponin in 1L PBS.

OVA-specific iTAg MHCcI tetramer

OVA-specific iTAg MHCcI tetramer, H-2 Kb conjugated with R-phycoerythrin (PE), loaded with SIINFEKL peptide (Beckman Coulter) was used to determine OVA-specific $CD8^+$ T cells.

I-A(b)/Influenza $NP_{311-325}$ MHCcII tetramer

I-A(b) restricted Influenza $NP_{311-325}$ MHCcII tetramer conjugated with PE (NIH) was kindly donated by Dr Tom Barr, University of Glasgow. The tetramer was used to determine peptide-specific $CD4^+$ T cells.

FACS antibodies (Table 2.3, 2.4, 2.5)

Table 2.3 – FACS antibodies used in determining innate immune responses

Antibody	Fluorochrome	Source	Concentration (0.5×10^5 cells in 100µl volume)
CD11b	PE-Cy7	BD Pharmingen	0.05µg/ml (0.005µg)
Gr-1	APC-Cy7	BD Pharmingen	0.4µg/ml (0.04µg)
F4/80	PerCP-Cy5.5	eBioscience	1µg/ml (0.1µg)
CD124	PE	BD Pharmingen	0.4µg/ml (0.04µg)
MHCcII	efluor 450	eBioscience	0.4µg/ml (0.04µg)
SiglecF	PE	BD Pharmingen	0.2µg/ml (0.02µg)
CD16/CD32	N/A	BD Pharmingen	2.5µg/ml (0.25µg)
ckit	FITC	BD Pharmingen	0.5µg/ml (0.05µg)
CCR3	A647	BD Pharmingen	1µg/ml (0.1µg)
IgG2aκ	PE	BD Pharmingen	0.4µg/ml (0.04µg)

Table 2.4 – FACS antibodies used in determining adaptive immune responeses

Antibody	Fluorochrome	Source	Concentration (10×10^6 cells in 100µl volume)
CD3	V450	BD Horizon	0.01µg
CD4	APC eFlour 780	eBioscience	0.01µg
IFN-γ	PE	BD Pharmingen	0.06µg
IL-17	PerCP-Cy5.5	BD Pharmingen	0.06µg
B220	Alexa Flour 700	BD Pharmingen	0.01µg
CD44	FITC	BD Pharmingen	0.01µg
CD16/CD32	N/A	BD Pharmingen	0.01µg
CD11c	PE-Cy7	BD Pharmingen	0.01µg
F4/80	PerCP-Cy5.5	BD Pharmingen	0.01µg
MHCcII	APC	BD Pharmingen	0.01µg

Table 2.5 – FACS antibodies used in determining immune responses after *S. aureus* challenge

Antibody	Fluorochrome	Source
CD11b	BV510	Biolegend
F4/80	PECy7	eBioscience
Ly6G	efluor 450	BD Biosciences
CD18	PE	BD Pharingen
DHR	FITC	Sigma
MHCcII	APC eFlour 780	eBioscience
CXCR2	Alexa Flour 647	Biolegend
CD62L	PerCP-Cy5.5	eBioscience
NOS2	PE	eBioscience

2.1.4. Enzyme-linked immunosorbent assay (ELISA) materials

10X PBS

400g NaCl, 58g Na_2HPO_4, 10g KH_2PO_4, 10g KCl

Made up to a final volume of 5L with distilled (d) H_2O and brought to pH 7.2.

1% Bovine Serum Albumin (BSA)

10g BSA, 1L dH_2O.

3% BSA

30g BSA, 1L dH_2O.

10% Milk

100g Marvel dried milk (Fluka Analytical), 1L dH_2O.

Carbonate buffer

8.4g $NaHCO_3$, 3.56g Na_2CO_3.

Made up to a final volume of 5L with dH_2O and brought to pH 9.5.

Phosphate citrate buffer

10.19g $C_6H_8O_7$, 14.6g Na_2HPO_4.

Made up to a final volume of 1L with dH_2O and brought to pH 5.0.

0.05% PBS-Tween (Wash buffer)

8995ml dH_2O, 1000ml 10x PBS, 5ml Tween 20.

Stop solution

1M H_2SO_4.

ELISA antibodies

Cytokine (Table 2.6), chemokine (Table 2.7) and immunoglobulin (Table 2.10) antibodies were used at various concentrations depending on individual kits. Horseradish-peroxidase (HRP)-conjugated streptavidin concentrations are outlined in Table 2.9. Reagent diluents varied depending on individual ELISA kits (Table 2.8).

Table 2.6 – Antibodies used to measure cytokine concentrations by ELISA.

Antibody	Source	Concentration	Blocking Solution	Top Working Standard
IL-1β	R&D Systems	Capture – 4µg/ml Detection – 1µg/ml	1% BSA	1000pg/ml
IL-1α	Biolegend	Capture – 2µg/ml Detection – 0.1µg/ml	1% BSA	1000pg/ml
IL-17	Biolegend	Capture – 2µg/ml Detection – 0.4µg/ml	1% BSA	1000pg/ml
IL-6	BD Pharmingen	Capture – 1µg/ml Detection – 1µg/ml	3% BSA	5000pg/ml
IFN-γ	R&D Systems	Capture – 4µg/ml Detection – 0.1µg/ml	1% BSA	2000pg/ml
IL-13	R&D Systems	Capture – 4µg/ml Detection – 0.2µg/ml	1% BSA	4000pg/ml

IL-33	R&D Systems	Capture – 0.8µg/ml Detection – 0.4µg/ml	1% BSA	1000pg/ml
IL-10	Biolegend	Capture – 4µg/ml Detection – 0.3µg/ml	1% BSA	2000pg/ml
IL-4	BD Pharmingen	Capture – 2µg/ml Detection – 1µg/ml	10% Milk	2500pg/ml

Table 2.7 – Antibodies used to measure chemokine concentrations by ELISA.

Antibody	Source	Concentration	Blocking Solution	Top Working Standard
CXCL1	Peprotech	Capture – 100µg/ml Detection – 100µg/ml	1% BSA	1µg/ml
CXCL2	Peprotech	Capture – 100µg/ml Detection – 100µg/ml	1% BSA	1µg/ml
CCL2	R&D Systems	Capture – 0.2µg/ml Detection – 50ng/ml	1% BSA	250µg/ml
CCL3	R&D Systems	Capture – 0.4µg/ml Detection – 200ng/ml	1% BSA	500µg/ml
CCL13	Peprotech	Capture – 0.5µg/ml Detection – 1µg/ml	1% BSA	2ng/ml

Table 2.8 – Reagent diluents for various suppliers of ELISA antibodies

Supplier	Diluent
R&D	1% BSA
Biolegend	1% BSA
BD	PBS
Peprotech	0.05% Tween-20, 0.1% BSA

Table 2.9 – HRP-conjugated streptavidin concentrations

Antibody	Source	Concentration
IL-1β	R&D Systems	1/200 of stock
IL-1α	Biolegend	1/1000 of stock

IL-17	Biolegend	1/1000 of stock
IL-10	Biolegend	1/1000 of stock
IL-6	Sigma	700ng/ml
IFN-γ	R&D Systems	1/200 of stock
IL-13	R&D Systems	1/200 of stock
IL-33	R&D Systems	1/200 of stock
IL-4	Sigma	700ng/ml
CXCL1	Peprotech	1/2000 of stock
CXCL2	Peprotech	1/2000 of stock
CCL2	R&D Systems	1/200 of stock
CCL3	R&D Systems	1/200 of stock
CCL13	Peprotech	1/2000 of stock

Table 2.10 – Antibodies used to measure serum immunoglobulin titres by ELISA.

Antibody	Source	Concentration
IgG	Sigma-Aldrich	3μg/ml
IgG1	BD Pharmingen	0.1μg/ml
IgG2b	BD Pharmingen	0.1μg/ml
IgG2c	Abd Serotec	0.1μg/ml
IgE	BD OptEIA™	Lot specific

2.1.5. Measuring free dsDNA in the peritoneum

DNA released from cells in the peritoneum after injection was measured using the Quant-iT™ PicoGreen® dsDNA Assay Kit (Invitrogen).

2.1.6. Real time polymerase chain reaction (PCR) materials

RNA Isolation

High Pure RNA isolation kits were sourced from Roche (IN 46250-0414, USA) and used as per manufacturer's instructions.

Reverse transcription (RT) reagents (Table 2.11)

Table 2.11 – RT reagents for complementary DNA (cDNA) synthesis

Reagent	Supplier	Concentration
Deoxyribonucleotide triphosphates (dNTPs)	Promega	2.5mM/NTP
RT Buffer	Promega	-
Random hexamers	MWG Biotech	1μg/ml
RNaseOUT	Invitrogen	40U/μl
M-MLV Reverse Transcriptase	Promega	200U/μl

Quantitative PCR (qPCR) Reagents

Kapa SYBR® Fast qPCR Kit (Kapa Biosystems) containing ROX reference dye was used in combination with nuclease-free H_2O.

Primers

Primers (MWG Biotech) were directed against mouse genes and designed to be intron-spanning to avoid amplification of genomic DNA (Table 2.12). Dissociation curve analysis was performed after a completed real time qPCR to exclude non-specific products.

Table 2.12 – Primers

Primer	Forward	Reverse
β-actin	5'-TCCAGCCTTTCTTGGGT-3'	5'-GCACTGTGTTGGCATAGAGGTC-3'
IL-4	5'-GAGACTCTTTCGGGCTTTTC-3'	5'-TGATGCTCTTTAGGCTTTCCA-3'
IL-4Rα	5'-TCTGCATCCCGTTGTTTTGC-3'	5'-GCACCTGTGCATCCTGAATG-3'
IL-1α	5'-GACCATCTCTCTCTGAATCAG-3'	5'-GTGAAGTTGGACATCTTTGACG-3'
IL-1β	5'-GTGAAATGCCACCTTTTGACAGTGATGAG-3'	5'-CTGCTGCGAGATTTGAAGCTGGATG-3'
IL-13	5'- CCTGGCTCTTGCTTGCCTT-3'	5'- GGTCTTGTGTGATGTTGCTCA-3'
IL-10	5'-AGGCGCTGTCATCGATTTCTC-3'	5'-GACACCTTGGTCTTGGAGCTTAT-3'
IL-17	5'-TGTGAAGGTCAACCTCAAAGTC-3'	5'-AGGGATATCTATCAGGGTCTTCATT-3'
IL-12p40	5'-GTGTAACCAGAAAGGTGCGTT-3'	5'-TCGGACCCTGCAGGGAAC-3'

IL-9	5'- ATGTTGGTGACATACATCCTTGC-3'	5'-TGACGGTGGATCATCCTTCAG-3'

2.1.7. Endotoxin detection and removal materials

To remove endotoxin from antigen preparations, Detoxi-Gel endotoxin removing columns (Thermo Scientific) were used as per the manufacturer's instructions. To determine endotoxin contamination in ClfA preparations before and after being put through the endotoxin removal columns, a limulus amebocyte lysate (LAL) chromogenic endotoxin quantitation kit was used as per manufacturer's instructions (Thermo Scientific).

2.1.8. Materials for protein determination

To determine protein concentrations in ClfA preparations a bicinchoninic acid (BCA) assay was used as per manufacturer's instructions (Thermo Scientific)

2.2 Methods

2.2.1. Mice

Female C57BL/6 mice were obtained from Harlan Olac (Bicester, UK) and were used at 8–16 weeks of age. *Il1r1*$^{-/-}$ mice were obtained from Jackson Laboratories (Maine, United States of America) and bred in the TCD Bioresources Unit. Animals were maintained according to the regulations of the European Union and the Irish Department of Health. Animal studies were approved by the TCD Animal Research Ethics Committee (Ethical Approval Number 091210) and were performed under the appropriate licence (Licence Number B100/3321).

2.2.2. Cell culture

Cells were cultured at 37°C with an atmosphere maintained at 95% humidity and 5% CO_2.

2.2.2.1. Cell viability and counting

Cell viability was determined using a trypan blue exclusion method. 10µl of the cell suspension was added to 90µl of trypan blue and 10µl of this solution was loaded onto a KOVA Glasstic cell counter slide with grids (Hycor Biomedical Inc.). Cells were viewed under a light microscope and cell viability was assessed by dye exclusion. The number of cells/ml was ascertained using the following formula:

$$\text{number of cells/ml} = \text{cell number} \times 10^4 \text{ cells/ml} \times \text{dilution factor}$$

2.2.2.2. Culture of J558 granulocyte-macrophage colony-stimulating factor (GM-CSF)-expressing cell line

The murine gene for GM-CSF was cloned into a mammalian expression vector and transfected into the plasmacytoma line X63-AgS. These cells were grown for two passages in tissue culture flasks containing complete RPMI 1640 medium supplemented with the antibiotic geneticin (Gibco, final concentration of 1mg/ml geneticin) and were incubated at 37°C in a humidified environment (5% CO_2). Following the completion of the second passage, the cells were washed with complete RPMI 1640 medium and re-seeded at 1 x 10^6 cells/ml in the absence of geneticin. The cells were cultured to a medium density for the first passage without geneticin and were re-seeded at lower concentrations (2.5 x 10^5 cells/ml) for subsequent passages. The supernatant was collected from each passage up until passage 9. The supernatants were pooled and the concentration of GM-CSF was determined by ELISA (Section 2.2.4.1).

2.2.2.3. Isolation and culture of BMDCs

Murine BMDCs were prepared using protocols adapted from Lutz *et al.*[355]. Female mice were euthanized by cervical dislocation and their femurs and tibiae were dissected from the surrounding muscle tissue. BMDCs were isolated using a 27G needle by flushing the bone marrow from the femurs and tibiae of mice into a petri dish containing complete RPMI 1640 medium. The cells were broken up in the medium using a 19G needle to avoid aggregates. The cells were transferred to a 50ml tube (Greiner BioOne) and centrifuged at 1200 rotations per minute (rpm) for 5 mins. The supernatant was discarded and the pellet disrupted by adding 1ml 0.88% ammonium chloride and pipetting up and down for 1 min. 40ml complete RPMI 1640 medium was then added to wash the cells and the contents of the 50ml tube mixed well. The cells were centrifuged at 1200rpm for 5 mins then resuspended in 10ml complete RPMI 1640 medium for counting. Cell numbers were determined as described in Section 2.2.2.1.. Cells were seeded at 1 x 10^6 cells/ml in complete RPMI 1640 medium supplemented with supernatant obtained from a GM-CSF-expressing J558 cell line (final concentration of 20ng/ml GM-CSF unless otherwise stated) in T175 flasks (Greiner BioOne). The culture of this J558 cell line is described in Section 2.2.2.2.. The flasks were incubated at 37°C in a humidified atmosphere (5% CO_2).

After 3 days of incubation the cells were fed by adding 30ml complete RPMI 1640 medium supplemented with 40ng/ml GM-CSF. On day 6 the supernatant from each flask was discarded in order to remove any non-adherent cells (e.g. granulocytes) from the

culture. 30ml of sterile PBS, preheated to 37°C, was added to each flask. The cells were removed from the surface of the flask by repeated pipetting. The PBS was collected from each flask and added to a 50ml falcon tube containing 10ml of complete RPMI 1640 medium. 30ml of sterile 0.02% Ethylenediaminetetraacetic acid (EDTA) solution, preheated at 37°C, was added to each flask. The flasks were incubated for 10 mins at 37°C before cells were removed by repeated pipetting. The EDTA solution was removed from each flask and subsequently added to a 50ml falcon tube containing 10ml of complete RPMI 1640 medium. The cells in each of the 50ml falcon tubes were pelleted by centrifugation (1200rpm for 5 mins at 4°C). The cell pellets were resuspended and pooled in 10ml of complete RPMI 1640 medium, counted as described in Section 2.2.2.1 and seeded at 4.2 x 10^5 cells/ml (C57BL/6) in complete RPMI 1640 medium, supplemented with 40ng/ml GM-CSF.

On day 7 the cells were again fed by adding 30ml complete RPMI 1640 medium supplemented with 40ng/ml GM-CSF. On day 10, loosely adherent cells were harvested by gentle repeat pipetting. The cells were pelleted by centrifugation (1200rpm for 5 minutes at 4°C) and resuspended in 10ml of complete RPMI 1640 medium. Cell numbers were determined as described in Section 2.2.2.1 and the cells were plated at 6.25 x 10^5 cells/ml. On day 11, the cells were stimulated with particulates and TLR agonists and supernatants were collected 24 hours later for analysis of cytokine levels by ELISA.

2.2.2.4. Isolation and culture of splenocytes

Female C57BL/6 mice were euthanized by CO_2 and their spleens were isolated. The spleens were homogenised and passed through a 70μm cell strainer (BD) with complete RPMI 1640 medium to obtain a single cell suspension. The cell suspension was centrifuged at 1200rpm for 5 mins. The supernatant was decanted and the cells were resuspended in 1ml of 0.88% ammonium chloride for 2 mins before washing with complete RPMI 1640 medium. The cell suspension was centrifuged again at 1200rpm for 5 mins, and the supernatant was decanted. The splenocytes were resuspended in 5ml of complete RPMI 1640 T cell medium for counting. Cell numbers were determined as described in Section 2.2.2.1.. Splenocytes were used for FACS (Section 2.2.3), real time PCR (Section 2.2.6) or plated at 2 x 10^6 cells/ml in 200μl complete RPMI 1640 medium in 96-well round bottom tissue culture plates. Plated splenocytes were restimulated *ex vivo* with the appropriate treatments. The tissue culture plates were incubated at 37°C in a

humidified atmosphere (5% CO_2). Supernatants were collected either 24 or 72 hours later (indicated in figure legend) for analysis of cytokine levels by ELISA.

2.2.2.5. Isolation and culture of peritoneal exudates cells

Female mice (C57BL/6, *Il1r1*$^{-/-}$) were euthanized by CO_2. The peritoneal cavity was washed with 4ml of ice-cold PBS. The wash volume was collected and the peritoneal exudate cells (PECs) were centrifuged at 1200rpm for 5 mins. The supernatant was collected for further analysis and the PECs were resuspended in 1ml of complete RPMI 1640 medium. PEC numbers were determined as described in Section 2.2.2.1. PECs were used for FACS (Section 2.2.3), real time PCR (Section 2.2.6) or plated at 1 x 10^6 cells/ml in 200µl complete RPMI 1640 medium in 96-well round bottom tissue culture plates. Plated PECs were restimulated *ex vivo* with the appropriate treatments. The specific treatments and conditions for restimulation of PECs are outlined in each experimental figure legend. The tissue culture plates were incubated at 37°C in a humidified atmosphere (5% CO_2). Supernatants were collected either 24 or 72 hours later (indicated in figure legend) for analysis of cytokine levels by ELISA.

2.2.2.6. Isolation and culture of lymph node cells

Female C57BL/6 mice were euthanized by CO_2 and their mediastinal or inguinal lymph nodes were isolated. The lymph nodes were homogenised and passed through a 70µm cell strainer (BD) with complete RPMI 1640 medium to obtain a single cell suspension. The cell suspension was centrifuged at 1200rpm for 5 mins. The supernatant was decanted and the cells were resuspended in 1ml of 0.88% ammonium chloride for 1 min before washing with complete RPMI 1640 medium. The cell suspension was centrifuged again at 1200rpm for 5 mins, and the supernatant was decanted. The lymph node cells were resuspended in 1ml of complete RPMI 1640 T cell medium for counting. Cell numbers were determined as described in Section 2.2.2.1.. Lymph node cells were used for FACS (Section 2.2.3), real time PCR (Section 2.2.6) or plated at 1 x 10^6 cells/ml in 200µl complete RPMI 1640 medium in 96-well round bottom tissue culture plates.. Plated lymph node cells were restimulated *ex vivo* with the appropriate treatments. The specific treatments and conditions for restimulation of PECs are outlined in each experimental figure legend. The tissue culture plates were incubated at 37°C in a humidified atmosphere (5% CO_2). Supernatants were collected either 24 or 72 hours later (indicated in figure legend) for analysis of cytokine levels by ELISA.

2.2.3. Flow Cytometry/FACS

2.2.3.1. Innate immune responses in PECs

PECs were plated at 1 x 10^6 cells/ml in a 200µl volume of PBS in triplicate in a 96-well round bottom tissue culture plate and were centrifuged at 1200rpm for 5 mins. The supernatant was decanted and the cell pellet was resuspended in 50µl volume PBS and triplicates combined to yield a total of 6 x 10^5 cells per well. The cell suspension was centrifuged at 1200rpm for 5 mins, supernatant decanted and the cells were resuspended in 100µl of PBS supplemented with LIVE/DEAD fixable Aqua dead cell stain (dilution outlined in section 2.2.3.5). The cells were incubated at 4°C for 30 mins. The cell suspension was centrifuged at 1200rpm for 5 mins, the supernatant decanted and the cells washed in 200µl PBS. The cell suspension was centrifuged at 1200rpm for 5 mins, the supernatant decanted and the cells resuspended in 100µl FACS buffer supplemented with anti-mouse CD16/CD32 monoclonal antibody (dilution outlined in Table 2.3). The cells were incubated at 4°C for 10 mins. PECs were then incubated with the relevant fluorochrome-labelled antibodies for 30 mins on ice in the dark by adding a total volume of 10µl of antibodies to the cells (dilutions outlined in Table 2.3). After 30 mins, the cell suspension was centrifuged at 1200rpm for 5 mins, the supernatant decanted and the cell pellet washed in 200µl FACS buffer. PECs were centrifuged (1200rpm for 5 mins at 4°C) and the supernatant was decanted before the cells were resuspended in 200µl FACS buffer for analysis of immunofluorescence. Samples were acquired using summit software (Dako, Colorado) and the data was analysed using Flowjo™ software (Treestar, Oregon).

2.2.3.2. Intracellular cytokine staining

PECs were plated in triplicates at 2 x 10^6 cells/ml in a 200µl volume of complete RPMI 1640 medium in a 96-well round bottom tissue culture plate. Cells were stimulated with antigens and/or T cell stimulants (as described in individual figure legends) for 6 hours, along with Brefeldin A (10µg/ml) for 5 hours, disrupting the golgi apparatus in cells and restricting the secretion of intracellular cytokines. The cell suspension was centrifuged at 1200rpm for 5 mins, supernatant decanted and the cells were washed with 200µl PBS. The cell suspension was centrifuged again at 1200rpm for 5mins, then resuspended in 100µl of PBS supplemented with LIVE/DEAD fixable Aqua dead cell stain (dilution outlined in 2.2.3.5). The cells were incubated at 4°C for 30 mins. The cell suspension was centrifuged at 1200rpm for 5 mins, the supernatant decanted and the cells washed in 200µl PBS. The cell suspension was centrifuged at 1200rpm for 5 mins, the supernatant decanted and the cells resuspended in 100µl FACS buffer supplemented with anti-mouse CD16/CD32

monoclonal antibody (dilution outlined in Table 2.3). The cells were incubated at 4°C for 10 mins. PECs were then incubated with the relevant extra-cellular fluorochrome-labelled antibodies for 30 mins on ice in the dark by adding a total volume of 10µl of antibodies to the cells (dilutions outlined in Table 2.3). After 30 mins, the cell suspension was centrifuged at 1200rpm for 5 mins, the supernatant decanted and the cell pellet resuspended in 50µl 4% PFA to fix the cells. The cells were incubated at room temperature. After 15 mins 100µl of PBS was added and the cell suspension was centrifuged at 1200rpm for 5 mins and the supernatant decanted. The cells were resuspended in 50µl saponin that contained the intracellular fluorochrome-labelled antibodies (0.3µl/sample). The cells were incubated at room temperature. After 20 mins 100µl PBS was added and the cell suspension was centrifuged at 1200rpm for 5 mins. The cells were resuspended in 200µl FACS buffer for analysis of immunofluorescence. Samples were acquired using summit software (Dako, Colorado) and the data was analysed using Flowjo™ software (Treestar, Oregon).

2.2.3.3. OVA-specific $CD8^+$ tetramer staining

Splenocytes or lymph node cells were transferred to sterile FACS tube with lids (2 x 10^6 cells). The cells were washed twice with 2ml of sterile PBS and centrifuged at 1200rpm for 5 mins. Cell pellets were resuspended with 100µl of FACS buffer (that did not contain sodium azide) with 1ul of tetramer-PE per sample. The cells were incubated for 2h at 37°C 5% CO_2. Cells were washed twice with 2ml of sterile PBS and then cell pellets were then resuspended in 100µl of PBS supplemented with LIVE/DEAD fixable Aqua dead cell stain (dilution outlined in section 2.2.3.5). 50µl of extracellular antibodies (panel outlined in figure legend) in FACS buffer was added directly to cells and the cells were incubated at 4°C for 15 mins. The cells were again washed twice with 2ml of sterile PBS and then cell pellets were then resuspended in 150µl of FACS buffer for analysis of immunofluorescence. Samples were acquired immediately using summit software (Dako, Colorado) and the data was analysed using Flowjo™ software (Treestar, Oregon).

2.2.3.4. Influenza peptide-specific $CD4^+$ tetramer staining

Splenocytes or lymph node cells were transferred to a 96-well round bottom tissue culture plate (20 x 10^6 cells). The cells were centrifuged at 1200rpm for 5 mins and cell pellets resuspended in 25µl of diluted tetramer (1/100 in complete medium). Cells were incubated at 37°C for 2 hours, with gentle agitation every 20 mins to disrupt the cell pellet. The pellet was washed with PBS and then stained for cell death (Section 2.2.3.5). 50µl of

extracellular antibodies (panel outlined in figure legend) in FACS buffer was added directly to cells and the cells were incubated at 4°C for 15 mins. The cells were again washed twice with sterile PBS and then cell pellets were then resuspended in 150µl of FACS buffer for analysis of immunofluorescence. Samples were acquired immediately using summit software (Dako, Colorado) and the data was analysed using Flowjo™ software (Treestar, Oregon).

2.2.3.5. Cell death

LIVE/DEAD Fixable Aqua Dead Cell Stain was used at a 1/1000 dilution in PBS with a total volume of 100µl/sample in 96-well round bottom tissue culture plates. Cells were left to incubate for 30 mins and then washed with PBS.

2.2.4. ELISA

2.2.4.1. Measurement of cytokine and chemokine secretion

96-well high binding ELISA plates (Greiner Bio-one) were coated with 40µl per well of rat anti-mouse capture antibody diluted in PBS (dilutions outlined in Table 2.6 and 2.7) and were incubated overnight at 4°C. The ELISA plates were washed 4 times in wash buffer and incubated with 100µl per well of blocking solution (see Table 2.6 and 2.7) for 2 hours at room temperature. The blocking solution was washed from the ELISA plates as before and samples and standards were diluted in reagent diluents (Table 2.8) and added to the plates (top working standards outlined in Table 2.6 and 2.7). The ELISA plates were incubated overnight at 4°C and were subsequently washed in wash buffer as before. 40µl per well of biotinylated goat anti-mouse detection antibody, diluted in reagent diluents (see Table 2.6 and 2.7) was added to the plates which were incubated for either 1 hour (BD antibodies, Biolegend kits) or 2 hours (R&D kits, Peprotech kits) at room temperature in the dark.

The ELISA plates were then washed with wash buffer as before and incubated with 40µl per well of HRP-conjugated streptavidin (dilutions outlined in Table 2.9) diluted in appropriate reagent diluent for 20 mins at room temperature in the dark. Following this incubation step, the ELISA plates were once again washed with wash buffer. 0-phenylenediamine dihydrochloride (OPD) substrate was dissolved in phosphate citrate buffer (0.4mg/ml OPD) and hydrogen peroxide (0.7µl hydrogen peroxide per 1mg of OPD) was added to the solution. 40µl per well of this solution was added to the ELISA plates which were allowed to develop for the required time in the dark. The enzyme

reaction was halted by addition of 20µl per well of sulfuric acid (1M). The OD values were measured at 492nm using a Versa Max microplate reader. A standard curve was generated and this was then used to determine the cytokine concentration of the unknown replicates.

2.2.4.2. Measurement of serum antibodies

2.2.4.2.1. Antigen-specific IgG, IgG1 and IgG2b

Serum concentrations of antigen-specific IgG as well as the IgG subtypes IgG1 and IgG2b were determined using commercially available antibodies obtained from BD Pharmingen (Table 2.10). 96-well medium binding ELISA plates (Greiner Bio-one) were coated with 50µl per well of antigen (50µg/ml) diluted in carbonate buffer and incubated overnight at 4°C. The ELISA plates were washed with wash buffer and blocked with 100µl per well of 10% marvel dried milk. The blocking solution was washed from the ELISA plates before the serum samples were diluted in PBS and added to the plates. The samples were serially diluted across the plate and incubated overnight at 4°C. Plates were washed and 50µl per well of biotinylated anti-mouse detection antibody diluted in PBS (dilutions outlined in Table 2.9) was added to the plates which were incubated in the dark for 1 hour at 37°C. The ELISA plates were then washed and incubated with 50µl per well of HRP-conjugated streptavidin (700ng/ml) diluted in PBS for 20 mins at room temperature in the dark. Following this incubation step, the ELISA plates were once again washed. OPD substrate was dissolved in phosphate citrate buffer (0.4mg/ml OPD) and hydrogen peroxide (0.7µl hydrogen peroxide per 1mg of OPD) was added to the solution. 50µl per well of this solution was added to the ELISA plates which were allowed to develop for the required time in the dark. The enzyme reaction was halted following the addition of 25µl per well of sulfuric acid (1M). The OD values were obtained using a Versa Max microplate reader measuring absorbance at 492nm. Antibody concentrations were expressed as endpoint titres calculated by regression of a curve of OD values versus reciprocal serum levels to a cut off point of 2 standard deviations above a negative control.

2.2.4.2.2. Antigen-specific IgG2c

Serum concentrations of antigen-specific IgG2c were determined using a commercially available antibody obtained from Abd Serotec. 96-well medium binding ELISA plates (Greiner Bio-one) were coated with 50µl per well of antigen (50µg/ml) diluted in carbonate buffer and incubated overnight at 4°C. The ELISA plates were washed with wash buffer and blocked with 100µl per well of 10% marvel dried milk. The blocking solution was washed from the ELISA plates before the serum samples were diluted in PBS

and added to the plates. The samples were serially diluted across the plate and incubated overnight at 4°C. Plates were washed and biotinylated anti-mouse detection antibody conjugated to HRP, diluted in PBS (0.1µg/ml, 50µl final volume per well), was added to the plates which were incubated in the dark for 1 hour at 37°C. Following this incubation step, the ELISA plates were once again washed. OPD substrate was dissolved in phosphate citrate buffer (0.4mg/ml OPD) and hydrogen peroxide (0.7µl hydrogen peroxide per 1mg of OPD) was added to the solution. 50µl per well of this solution was added to the ELISA plates which were allowed to develop for the required time in the dark. The enzyme reaction was halted following the addition of 25µl per well of sulfuric acid (1M). The OD values were obtained using a Versa Max Microplate Reader measuring absorbance at 492nm. Antibody concentrations were expressed as endpoint titres calculated by regression of a curve of OD values versus reciprocal serum levels to a cut off point of 2 standard deviations above a negative control.

2.2.4.2.3. Total IgE and antigen-specific IgE

Serum concentrations of total IgE and antigen-specific IgE were determined using a commercially available antibody obtained from BD (OptEIA™). The protocol for total IgE was as per the manufacturer's instructions. The protocol for antigen-specific IgE replaced the capture antibody with 50µl per well of antigen (50µg/ml) diluted in carbonate buffer and incubated overnight at 4°C. The OD values were measured at 492nm using a Versa Max microplate reader. A standard curve was generated and this was then used to determine the cytokine concentration of the unknown replicates.

2.2.5. Measuring neutralising antibodies in serum

The presence of neutralising antibodies was determined by testing the ability of serum from immunised mice to inhibit the adherence of *S. aureus* to fibrinogen. Microtitre plates were coated with fibrinogen (2µg/ml) overnight at 4°C and blocked for 2 h at 37°C with 5% (w/v) BSA. *S. aureus* PS80 were grown to stationary phase, washed and incubated with mouse serum (1:60 dilution) for 30 min at room temperature before being added to the wells of a fibrinogen-coated plate and incubated for 1.5 h at 37°C. After washing with PBS, adherent cells were fixed with formaldehyde (25% v/v), stained with crystal violet and the A_{570} measured. Adherence was expressed as a percentage of bacterial adherence in the absence of serum and percentage inhibition was determined by subtracting the percentage adherence values from 100.

2.2.6. Real time PCR

RNA was extracted from cells as previously described (Section 2.1.6). Before qPCR could be carried out, cDNA was synthesised from the extracted RNA using a master mix outlined in Table 2.11. 5µl of the master mix was combined with 5µl of RNA and the components run in a thermocycler using the following program (Table 2.13).

Table 2.13 – cDNA synthesis thermocycler program

Temperature (°C)	Time (mins)
25	10
42	60
95	3
4	∞

qPCR was carried out with freshly synthesised cDNA and forward and reverse primers (5pmol/µl) using the Kapa SYBR® Fast qPCR Kit (Section 2.1.6). Samples were run on a Applied Biosystems 7500 Fast system for 40 cycles of 2 mins at 95°C followed by 3 seconds at 95°C, followed by one cycle of 30 seconds at 60°C. Dissociation curve analysis was performed after a completed real time qPCR to exclude non-specific products.

2.2.7. Animal studies

2.2.7.1. Peritonitis Model

Female mice (C57BL/6, *Il1r1*$^{-/-}$) were injected i.p. with 200µl volumes of specific treatments outlined in each experimental figure legend. The mice were euthanized by CO_2 at the time points indicated in each experimental figure legend. The peritoneal cavity was washed with 4ml of ice-cold sterile PBS. The wash volume was collected and the PECs were harvested for FACS analysis and/or *ex vivo* restimulation (See Sections 2.2.2.5 and 2.2.3.1). Where indicated, PEC supernatants, spleens, mediastinal lymph nodes and serum were also collected. Blood was taken by puncturing the heart and collected in eppendorf tubes (Starstedt). Tubes were centrifuged at 10,000rpm for 5 mins and the serum was removed and placed in fresh eppendorf tubes for analysis.

2.2.7.2. Adjuvant model

Female mice (C57BL/6) were injected i.p. or subcutaneously with 200µl volumes of specific treatments outlined in each experimental figure legend. Serum was taken on day

13 and mice were boosted i.p. or subcutaneously with identical treatments on day 14. On day 21 the mice were euthanized by CO_2. The PECs (i.p. model only), spleen and draining lymph nodes were collected and harvested for *ex vivo* restimulation and/or FACS (See Sections 2.2.2 and 2.2.3). The blood was collected and serum harvested for analysis of antigen-specific serum antibodies by ELISA. Blood was centrifuged at 10,000rpm for 5 mins, the serum removed and placed in fresh eppendorf tubes for analysis.

2.2.7.3. Challenge model

Female mice (C57BL/6) were injected subcutaneously with 200µl volumes of PBS, ClfA alone (1µg), or together with 50nm PS particles (4mg) or 100µm PS particles (4mg). Mice were boosted subcutaneously with identical treatments on day 14. On day 21 immunised mice were challenged with PS80 *S. aueus* via i.p. injection (5×10^8 colony forming units (CFU)). *S. aureus* PS80 is a clinically derived strain that expresses the capsular polysaccharide serotype 8, and has been previously described[356]. Challenge experiments were performed by Dr. Stephen Lalor, TCD.

2.2.7.3.1. Preparation of bacterial inoculum for *in vivo* challenge studies

Following overnight growth on CSA agar, a turbid solution of bacteria (1 ml) was prepared by scraping bacterial colonies using a sterile loop and agitating in sterile PBS. It was mixed thoroughly to ensure the bacteria were in solution. Appropriate dilutions were prepared and the OD of the bacterial solution was determined at 600nm using a spectrophotometer. The OD_{600nm} of the solution was adjusted to 0.45, which had previously been established to represent ~4×10^8 CFU/ml[357,358]. The amount of bacteria in the turbid solution was then adjusted to 5×10^9 CFU/ml which was used as the inoculum for all *in vivo* experiments. To confirm the inoculum concentration, serial dilutions of the bacterial suspension were spread onto Tryptic Soy Agar (TSA) plates and left to grow for 24 hr at 37°C. The following day the number of colonies visible on the plates was counted which represented the CFU/100 µl. Stocks of *S. aureus* (5×10^9 CFU/ml) in PBS were stored at -80°C for use during the course of a single *in vivo* experiment. Bacterial viability was confirmed after freezing and prior to injection by plating inoculum onto TSA.

2.2.7.3.2. Isolation of tissues

At 24 or 72 hours post challenge mice were sacrificed and systemic infection levels and immune responses were assessed. The PECs, spleen, liver and kidneys were isolated to assess bacterial burden. The peritoneal cavity was lavaged with sterile PBS (2 ml) in order

to collect the PECs. Total cell counts of PECs were determined using trypan blue staining to differentiate between live and dead cells on a haemocytometer under a light microscope. PECS were examined by flow cytometry using markers outlined in Table 2.5. Organs (spleen, liver and kidneys) were homogenized in 3 ml of sterile PBS using a homogenizer (Kinematica Polytron PT 2500E) with a 7mm blade. The homogenizer was cleaned between samples using 1M NaOH, sterile H_2O, 70% (v/v) EtOH and sterile PBS. Peritoneal lavage fluid and spleen, liver and kidney homogenate was prepared in PBS.

2.2.7.3.3. Quantification of bacterial burden

Serial dilutions of the peritoneal lavage fluid and disrupted spleen, liver and kidney solution were prepared in sterile PBS and 100µl spread onto TSA plates. Plates were incubated for 24 h at 37°C. The following day the number of colonies visible on the plates was counted which represented the CFU/100µl. All plates were kept at RT for a further 48 h to confirm a lack of contaminating bacterial species.

2.2.8. Statistical analysis

Statistical analysis was performed using Graphpad Prism 5 software. The means for 3 or more groups were compared by one-way analysis of variance (ANOVA). Where significant differences were found, the Tukey-Kramer multiple comparisons test was used to identify differences between individual groups. The means for 2 groups were compared using an unpaired Student's t-test.

Chapter 3

Innate immune responses to particles are dictated by particle size

3.1 Introduction

Micro- and nano-particles generated from a range of materials have been extensively studied as potential vaccine adjuvants. Differences in size, shape and chemical coating and their effects on the immune response have been compared across a range of particulate adjuvants, often using antibody titres as the main readout[269,351,352,354]. However, a detailed characterisation of the innate immune response to particles across a broad size range has not been conducted.

Cellular infiltration and local cytokine signalling are classical signs of inflammation. A number of studies have indicated that particle size influences cytokine production *in vitro*. For example, using the DC cell line BC-1, Chen *et al.* demonstrate that BC-1 cells stimulated with PS particles alone do not induce the secretion of cytokines. However, when CpG ODN are bound to the surface of PS particles, BC-1 cells secrete different cytokines depending on size, 100nm and 500nm particles inducing the secretion of IFN-α and IL-6 while 3μm particles induce IL-6 but no IFN-α secretion[359]. This is interesting since the pro-inflammatory cytokine IL-6 is involved in the acute phase response and $CD4^+$ T cell differentiation whereas IFN-α promotes activation of $CD8^+$ T cells which induce apoptosis in virally infected cells[360,361]. In addition, Sharp *et al.* reported that 430nm, 1μm, 10μm and 32μm PS particles are all capable of driving IL-1β secretion from LPS-primed BMDCs[52]. Stimulating human macrophages with Ti-alloy (mean size 0.7μm) and PMMA (1-10μm) particles induces the secretion of the monocyte chemotactic protein CCL2 and macrophage inflammatory protein CCL3, and the supernatant containing these chemokines enables monocyte migration[362]. Hence, particle size dramatically influences the cytokines produced by cells *in vitro,* and the simultaneous migration of inflammatory cells.

While *in vitro* assays can be informative, it is the soluble factors released by cells *in vivo* that influence the subsequent inflammatory response to particles. Tian *et al.* found that double-walled carbon nanotubes, 1-10μm in length, induce secretion of IL-6, IL-1β and CCL3 into the bronchoalveolar lavage fluid following intra-tracheal administration[363]. This correlated with an infiltration of neutrophils and pro-inflammatory macrophages into the alveolar region. In a separate model, particulate debris less than 5μm in size but of various shapes, resulting from *in vivo* degradation of total joint replacement (surgery involving removing parts of an arthritic or damaged joint and replacing them with a metal, plastic or

ceramic prosthesis) has also been shown to induce chemokine and cytokine production[364–367]. Hence it appears that chemokines that are secreted locally have crucial roles in determining the composition of the cellular infiltrate *in vivo*.

As mentioned, sterile inflammation is characterised by rapid recruitment of granulocytes to the site of damage following local chemokine and cytokine signalling. Resident macrophages and mast cells act as sentinels in tissue, secreting cytokines and chemokines such as IL-1β and CXCL1 to attract granulocytes such as neutrophils[5]. Importantly, neutrophil recruitment is soon followed by an infiltration of inflammatory macrophages and eosinophils, thus serving to propagate the inflammatory cascade[368]. Neutrophil recruitment following injection of several types and sizes of particles has been demonstrated. When comparing 30nm, 70nm and 300nm silica nano-particles, Lu *et al.* demonstrated that 70nm particles induce the highest level of neutrophil infiltration into the liver 6 hours after intravenous injection[369]. Using much larger particles of 1.2μm, 5.2μm and 12.5μm in diameter, PS particles were capable of initiating an inflammatory response in the peritoneum characterised by an influx of monocytes, macrophages, and neutrophils 24 hours after i.p. injection[370]. The intensity of the inflammatory response was greatest with the 1.2μm and 5.2μm PS particles[370]. Hence it is clear that across the literature, particles of various sizes and compositions are capable of inducing the infiltration of inflammatory cells to the local site. However, the upper size limit and the potential mechanisms underlying particle induced inflammation have not been addressed.

Preliminary histology data in our laboratory indicates that s.c. injection of nano-particles (50nm) promoted cellular infiltration, granuloma formation and necrosis at the injection site, whereas micro-particles (30μm) drove lower levels of cellular infiltration and cell death (Sharp, PhD thesis).

PS particles were chosen as model particles for analysis of specific innate immune responses since these particles were available in many different and well-defined sizes. PS particles of 50nm, 1μm, 10μm, 30μm and 100μm in diameter were chosen based on the hypothesis that the body comes into contact with many different sized pathogens, ranging from viruses at the nano-scale to bacteria 1-10μm in size and larger parasites 10-100μm in length. Therefore, there is a need to fully understand and characterise how size can influence innate immunity and the subsequent adaptive immune responses that follow.

3.2 Aims

Previous studies have compared the ability of 'small' particles against 'large' particles in generating inflammatory responses. However, there is inconsistency between studies in determining what is 'large' and what is 'small', with nano-particles and micro-particles rarely compared directly within a single study. The specific aims of this chapter were to characterise the inflammatory infiltrate into the peritoneum after i.p. injection with PS particles in the size range 50nm-100μm and subsequently to determine if the local responses influenced immune responses in secondary lymphatic organs such as the spleen and draining lymph nodes. Moreover, it has been proposed that IL-4 is a key cytokine in anti-inflammatory signalling in response to acute inflammation[371,372]. Thus the role of IL-4 in PS particle-mediated innate immune responses was investigated.

3.3 Results

3.3.1 50nm and 10μm PS particles promote cell recruitment into the injection site

The first question addressed was how particle size influences innate immunity *in vivo*. The peritoneum is a particularly convenient site to study modulation of the innate immune system as cell recruitment into this site in response to treatments can be easily assessed. C57BL/6 mice were injected i.p. with PBS or 4mg of PS particles (50nm, 1μm, 10μm, 30μm, 100μm) and were sacrificed after 24 or 72 hours. The concentration of particles injected was 4mg so that resuts could be correlated with preliminary data previously generated in the laboratory. Peritoneal exudate cells (PECs) were isolated and counted.

Interestingly, 50nm and 10μm PS particles were the only sizes that drove a significant increase in total PEC number 24 hours after injection (Figure 3.1A). As expected, the numbers of cells in the peritoneum had significantly decreased 72 hours after injection. However the increase in cell number in the peritoneum 72 hours after injection with 50nm PS particles was still significant when compared with PBS (Figure 3.1B).

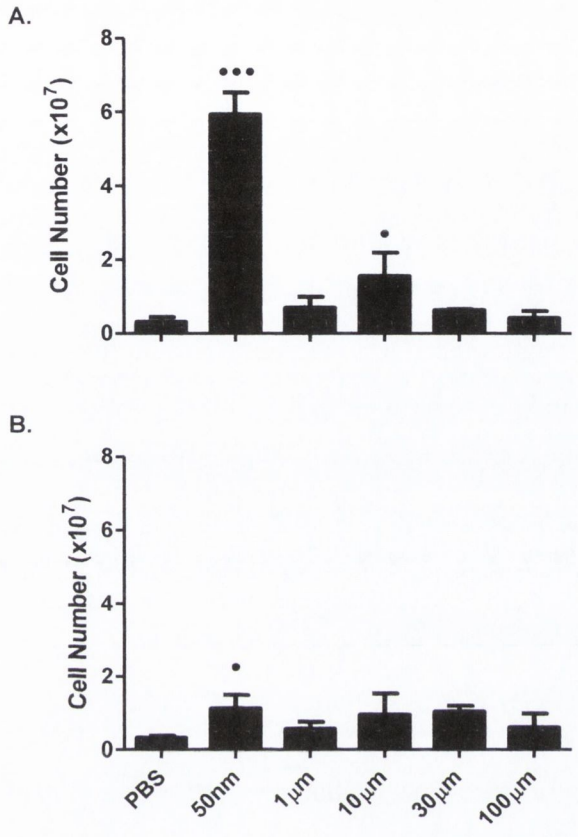

Figure 3.1 – 50nm and 10μm PS particles promote cell recruitment into the peritoneum. C57BL/6 mice were injected i.p. with PBS or 4mg of PS particles (50nm, 1μm, 10μm, 30μm or 100μm) in 200μl volumes. The mice were sacrificed after 24 hours (A) or 72 hours (B) and PECs were collected. Total PEC numbers were determined using a Glastic cell counter following trypan blue staining. Bar charts represent mean (+ standard deviation (SD)) for 3 (A) or 4 (B) mice per experimental group. These data are representative of two or three independent experiments. Versus PBS, • $p<0.05$, ••• $p<0.0001$.

3.3.2 Different sized particles elicit distinct inflammatory profiles *in vivo*

To determine whether different sized particles promote the recruitment of a distinct repertoire of innate immune cells into the peritoneum, C57BL/6 mice were injected i.p. with PBS or 4mg of PS particles (50nm, 1μm, 10μm, 30μm or 100μm) and were sacrificed after 24 or 72 hours. PECs were isolated and analysed by flow cytometry.

Interestingly, 24 hours after injection, 50nm particles drove a significant increase in both the percentage and total number of neutrophils ($CD11b^+$ $Gr1^{high}$ $F4/80^-$) in the peritoneum compared to PBS (Figure 3.2A, C). This increase was significantly higher than all of the other size particles tested with regard to total neutrophil number, and was also significantly higher than 1μm, 30μm and 100μm PS particles with regard to percentage of neutrophils in the peritoneum. 10μm PS particles also induced an infiltration of neutrophils, although to a lesser extent than 50nm PS particles at this time point (Figure 3.2A, C). However, 72 hours after injection 10μm PS particles were the only size capable of sustaining the recruitment of neutrophils to the peritoneum (Figure 3.2B, C).

In contrast to the profile seen with neutrophil recruitment, 10μm and 30μm PS particles optimally drove the recruitment of monocytes ($CD11b^+$ $F4/80^+$ $SiglecF^-$ side scatter $(SSC)^{low}$ $MHCcII^-$) into the site of injection after 24 hours (Figure 3.3A, C). To exclude the possibility that this population may contain myeloid DCs, DCs were gated as $MHCcII^+$ $CD11c^{+}$[139]. No difference in myeloid DC percentage was observed between mice injected with PBS and mice injected with PS particles (data not shown) indicating that the infiltration of $CD11b^+$ $F4/80^+$ $SiglecF^-$ SSC^{low} $MHCcII^-$ cells did not contain myeloid DCs. 72 hours after injection, 10μm PS particles exhibited a sustained increase in monocytes at the local site which was significantly greater than any of the other PS particle sizes (Figure 3.3B, D). Both 10μm and 30μm PS particles also recruited the greatest number of pro-inflammatory macrophages to the local site (Figure 3.4). Although 24 hours after injection the number of pro-inflammatory macrophages appears to be higher with 10μm and 30μm PS particles (Figure 3.4A,C), these differences were only significant 72 hours after injection (Figure 3.4B,D).

With the striking exception of 100μm particles, injection of all PS particles led to a reduction in resident macrophages ($CD11b^{high}$ $F4/80^{high}$) present in the peritoneum (Figure 3.5). This reduction in resident macrophages was statistically significant for all other sized

PS particles when compared with 100μm PS particles 24 hours after injection (Figure 3.5A, C). However, 72 hours after injection with 50nm, 1μm, 10μm and 30μm PS particles, although the percentage of resident macrophages remanded significantly lower than PBS, the number of resident macrophages was more similar to PBS for all sized PS particles (Figure 3.5B, D).

Interestingly, 50nm PS particles also drove recruitment of eosinophils ($CD11b^+$ $Gr1^-$ $SiglecF^+$) 24 hours after injection (Figure 3.6A, C). This result was not reflected in terms of percentage of cells in the peritoneum, but when presented as total number of eosinophils, this difference was highlighted. While larger sized PS particles of 10μm and 30μm also drove an increase in the percentage of eosinophils at this time point, when presented as total number of eosinophils in the peritoneum, the numbers were not significantly higher than those in PBS-injected mice (Figure 3.6C). However, 72 hours after injection, 50nm, 10μm and 30μm PS particles all drove an increase in eosinophil percentage and number when compared with PBS (Figure 3.6B, D).

In conclusion, 50nm and 10μm PS particles drove the most potent inflammatory responses at the site of injection which was characterised by recruitment of neutrophils, monocytes and eosinophils and concomitant depletion of resident macrophages. Interestingly, injection of 1μm particles did not drive significant inflammation. At the larger end of the size range, injection of 30μm PS particles induced the recruitment of monocytes, pro-inflammatory macrophages and eosinophils, but to a lesser extent than 50nm and 10μm PS particles. Injection of 100μm PS particles did not cause much inflammation and induced a similar profile to PBS-injected mice.

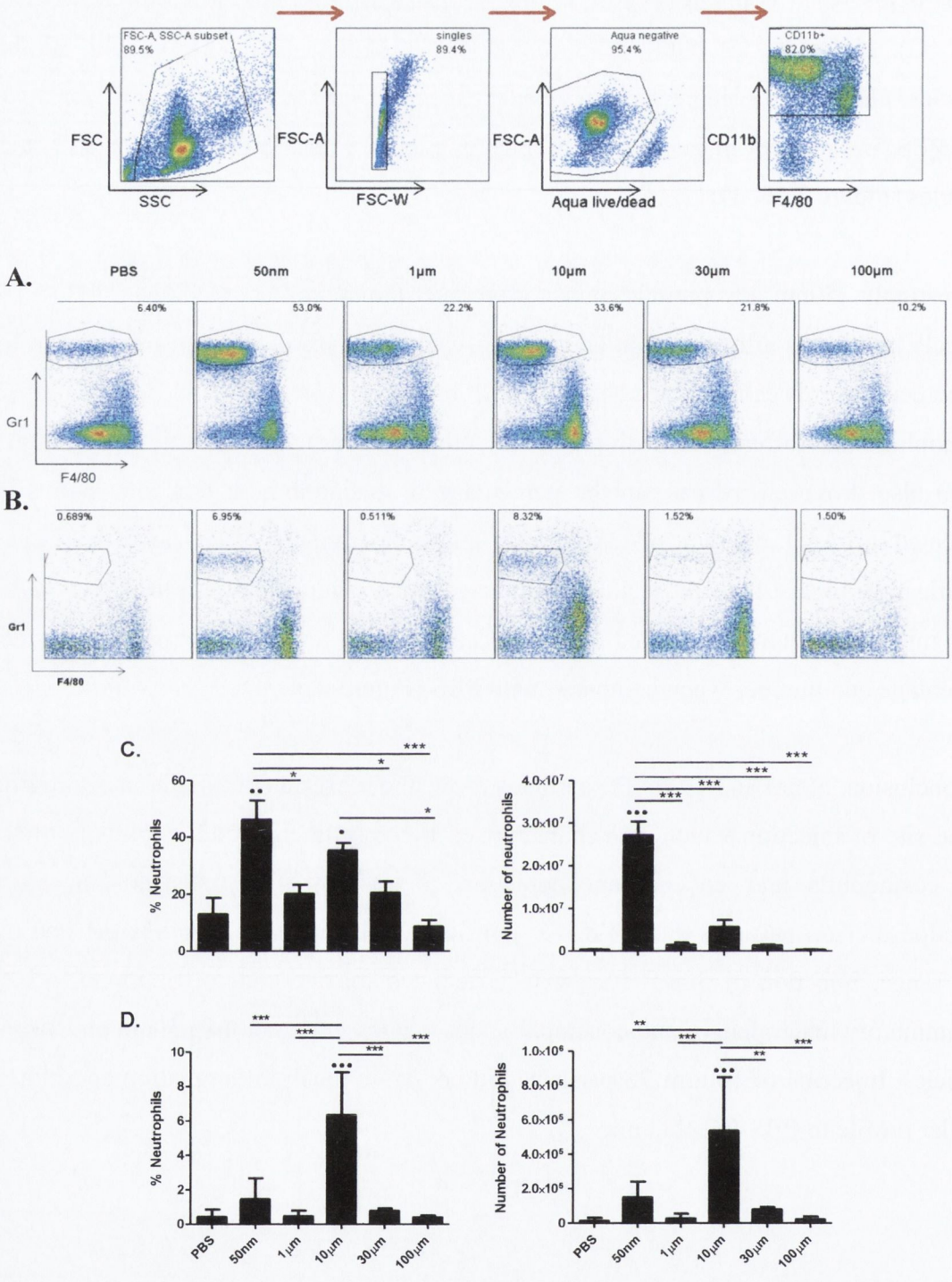

Figure 3.2 – 50nm and 10µm PS particles drive infiltration of neutrophils into the site of injection. C57BL/6 mice were injected i.p. with PBS or 4mg of PS particles (50nm, 1µm, 10µm, 30µm or 100µm) in 200µl volumes. The mice were sacrificed after 24 hours (A, C) or 72 hours (B, D) and PECs were collected. Neutrophils were gated as $CD11b^{+}$ $Gr1^{high}$ $F4/80^{-}$ and the data are graphed as percentage of live cells and number of live cells respectively. Bar charts represent mean (+ SD) for 3 or 4 mice per experimental group. Results are representative of two or three independent experiments. Versus PBS, • $p<0.05$, •• $p<0.01$, ••• $p<0.001$. Versus different sized PS particles, * $p<0.05$, ** $p<0.01$, *** $p<0.0001$.

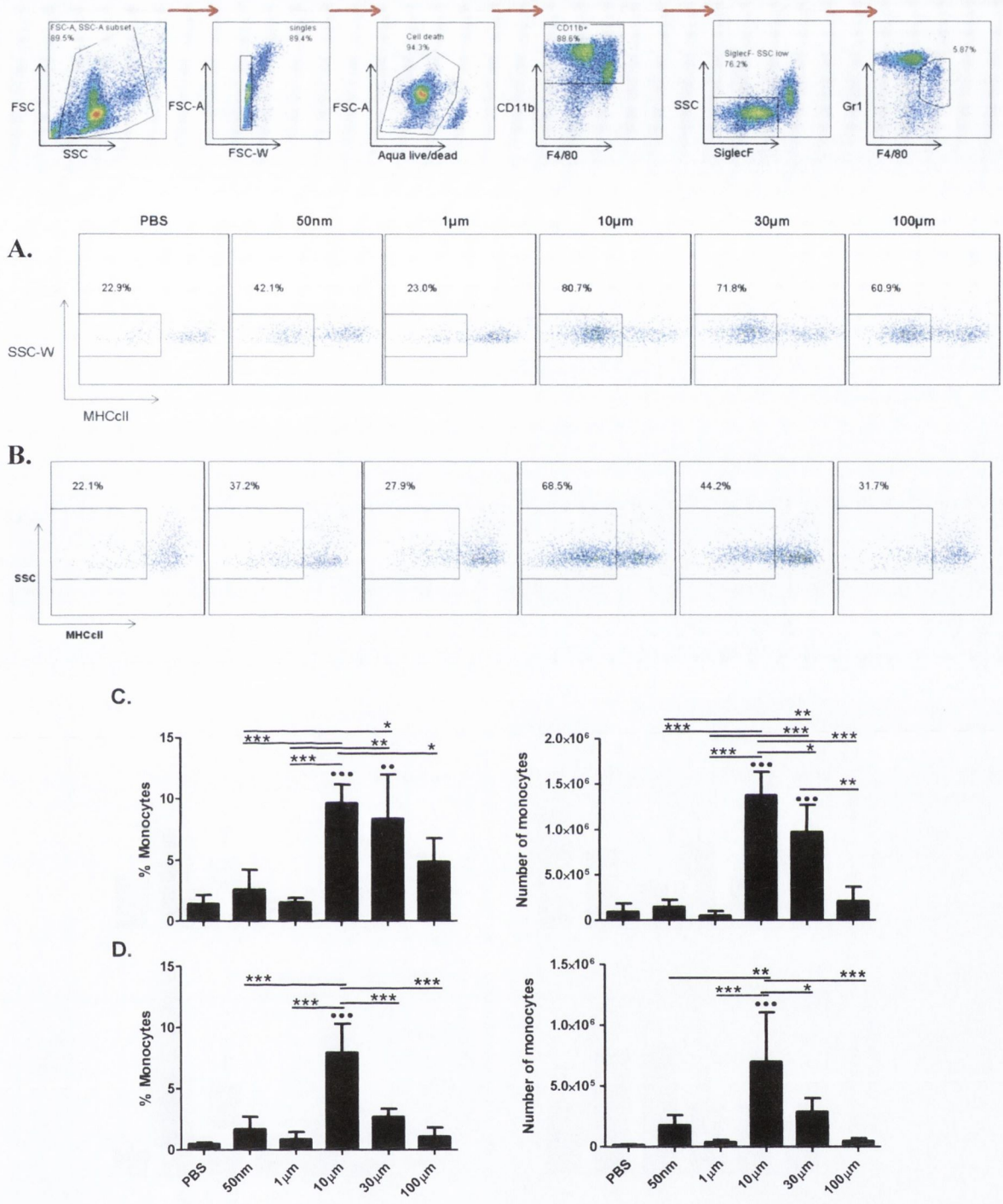

Figure 3.3 – 10µm PS particles are a potent stimulus for recruitment of monocytes into the site of injection. C57BL/6 mice were injected i.p. with PBS or 4mg of PS particles (50nm, 1µm, 10µm, 30µm or 100µm) in 200µl volumes. The mice were sacrificed after 24 or 72 hours and PECs were collected. Monocytes were gated as $CD11b^{+}$ $F4/80^{+}$ $SiglecF^{-}$ SSC^{low} $MHCcII^{-}$ and the data are graphed as percentage of live cells and number of live cells respectively. Bar charts represent mean (+ SD) for 3 or 4 mice per experimental group. Results are representative of two or three independent experiments. Versus PBS, •• $p<0.01$, ••• $p<0.0001$. Versus different sized PS particles, * $p<0.05$, ** $p<0.01$, *** $p<0.0001$.

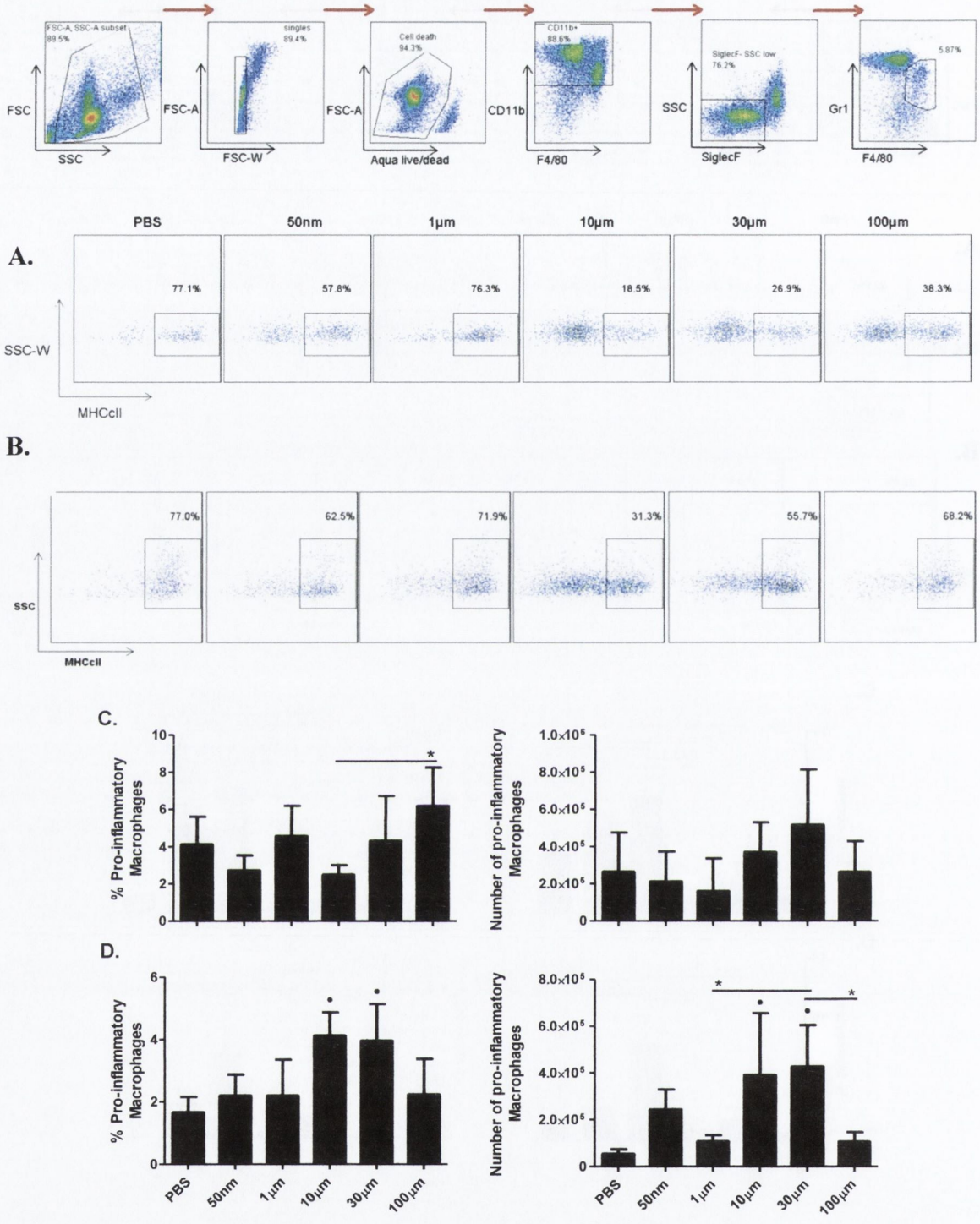

Figure 3.4 – 10µm and 30µm PS particles drive the recruitment of pro-inflammatory macrophages 72 hours after injection. C57BL/6 mice were injected i.p. with PBS or 4mg of PS particles (50nm, 1µm, 10µm, 30µm or 100µm) in 200µl volumes. The mice were sacrificed after 24 or 72 hours and PECs were collected. Pro-inflammatory macrophages were gated as $CD11b^{+}$ $F4/80^{+}$ $SiglecF^{-}$ SSC^{low} $MHCcII^{+}$ and the data are graphed as percentage of live cells and number of live cells respectively. Bar charts represent mean (+ SD) for 3 or 4 mice per experimental group. Results are representative of two or three independent experiments. Versus PBS, • $p<0.05$. Versus different sized PS particles, * $p<0.05$.

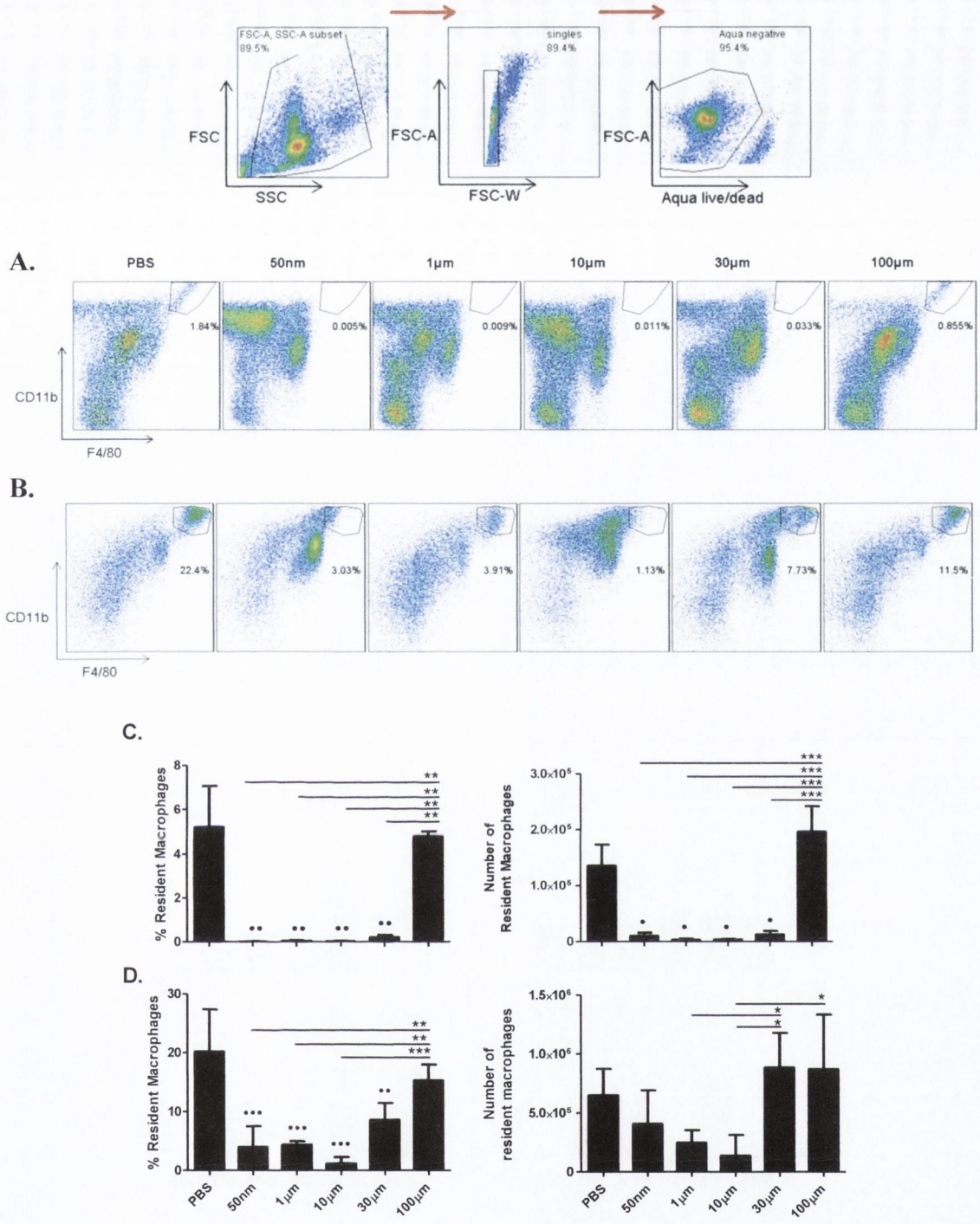

Figure 3.5 – With the exception of 100µm, injection of PS particles of all sizes effectively depletes resident peritoneal macrophages. C57BL/6 mice were injected i.p. with PBS or 4mg of PS particles (50nm, 1µm, 10µm, 30µm or 100µm) in 200µl volumes. The mice were sacrificed after 24 or 72 hours and PECs were collected. Resident macrophages were gated as $CD11b^{high}$ $F4/80^{high}$ and the data are graphed as percentage of live cells and number of live cells respectively. Bar charts represent mean (+ SD) for 3 or 4 mice per experimental group. Results are representative of two or three independent experiments. Versus PBS, • $p<0.05$, •• $p<0.01$, ••• $p<0.0001$. Versus different sized PS particles, * $p<0.05$, ** $p<0.01$, *** $p<0.0001$.

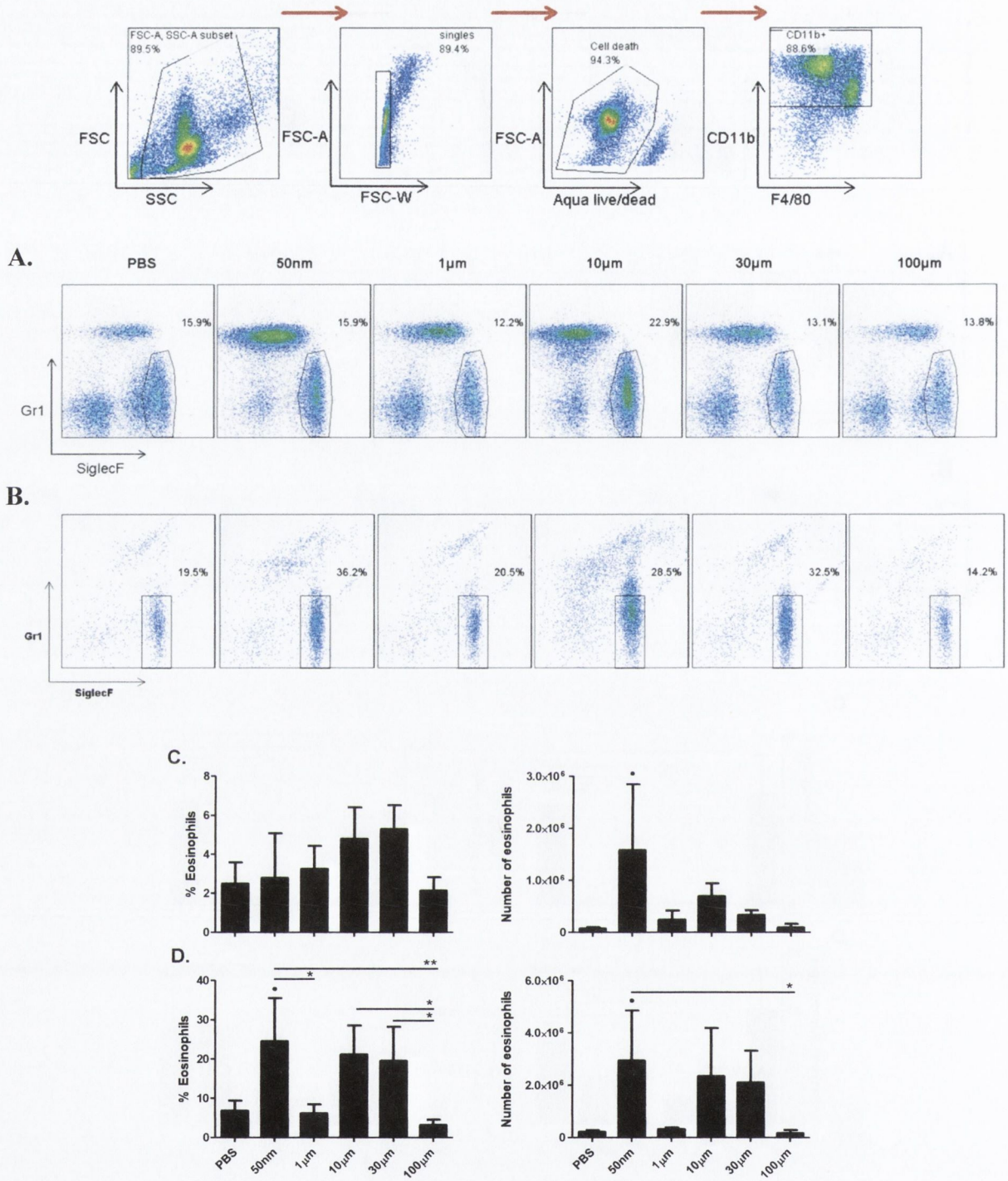

Figure 3.6 – 50nm, 10µm and 30µm PS particles drive recruitment of the greatest number of eosinophils to the site of injection. C57BL/6 mice were injected i.p. with PBS or 4mg of PS particles (50nm, 1µm, 10µm, 30µm or 100µm) in 200µl volumes. The mice were sacrificed after 24 or 72 hours and PECs were collected. Eosinophils were gated as $CD11b^+$ $Gr1^-$ $SiglecF^+$ and the data are graphed as percentage of live cells and number of live cells respectively. Bar charts represent mean (+ SD) for 3 or 4 mice per experimental group. Results are representative of two or three independent experiments. Versus PBS, • $p<0.05$. Versus different sized PS particles, * $p<0.05$, ** $p<0.01$.

3.3.3. 0.4mg and 4mg PS particles drive a comparable inflammatory response at the injection site

Given that the PS particles were injected by weight, it was necessary to confirm that the different inflammatory profiles observed were due exclusively to size differences and not due to varying numbers of particles. Therefore a dose response study using a peritonitis model was conducted with 50nm, 10μm and 100μm PS particles. C57BL/6 mice were injected i.p. with PBS or either 4mg or 0.4mg PS particles (50nm, 10μm or 100μm) and were sacrificed after 24 hours. PECs were isolated, counted and analysed by flow cytometry.

Comparable results in terms of neutrophil recruitment were obtained following injection of 4mg or 0.4mg of both 50nm and 10μm PS particles. Importantly, both 4mg and 0.4mg of 50nm PS particles induced neutrophil infiltration into the peritoneum to an equal degree (Figure 3.7). However, 50nm PS particles did not promote neutrophil recruitment to the same extent as shown previously (Figure 3.2). Importantly, both 4mg and 0.4mg concentrations of 10μm PS particles were also comparable in their ability to promote neutrophil recruitment into the peritoneum (Figure 3.7).

Since pro-inflammatory macrophage populations were low in number 24 hours after injection, we analysed this population together with monocytes in the peritoneum of mice injected with different numbers of particles and termed them 'macrophages' ($CD11b^+$ $SiglecF^-$ $F4/80^+$). Both 50nm and 10μm PS particles promoted a small increase in macrophages in the peritoneum and this was independent of particle number (Figure 3.8).

Eosinophils exhibited a similar trend to other granulocyte populations in so far as that the percentage and number of recruited cells was independent of the number of particles injected into the peritoneum (Figure 3.9). Again, 50nm PS particles drove significant eosinophil recruitment into the peritoneum after 24 hours through a process that was independent of PS particle number (Figure 3.9).

Given that the patterns of cell infiltration were comparable following injection of 0.4mg or 4mg PS particles, this suggests that it is the different sizes of the PS particles that promote different inflammatory profiles in the peritoneum rather than the administration of different numbers of particles.

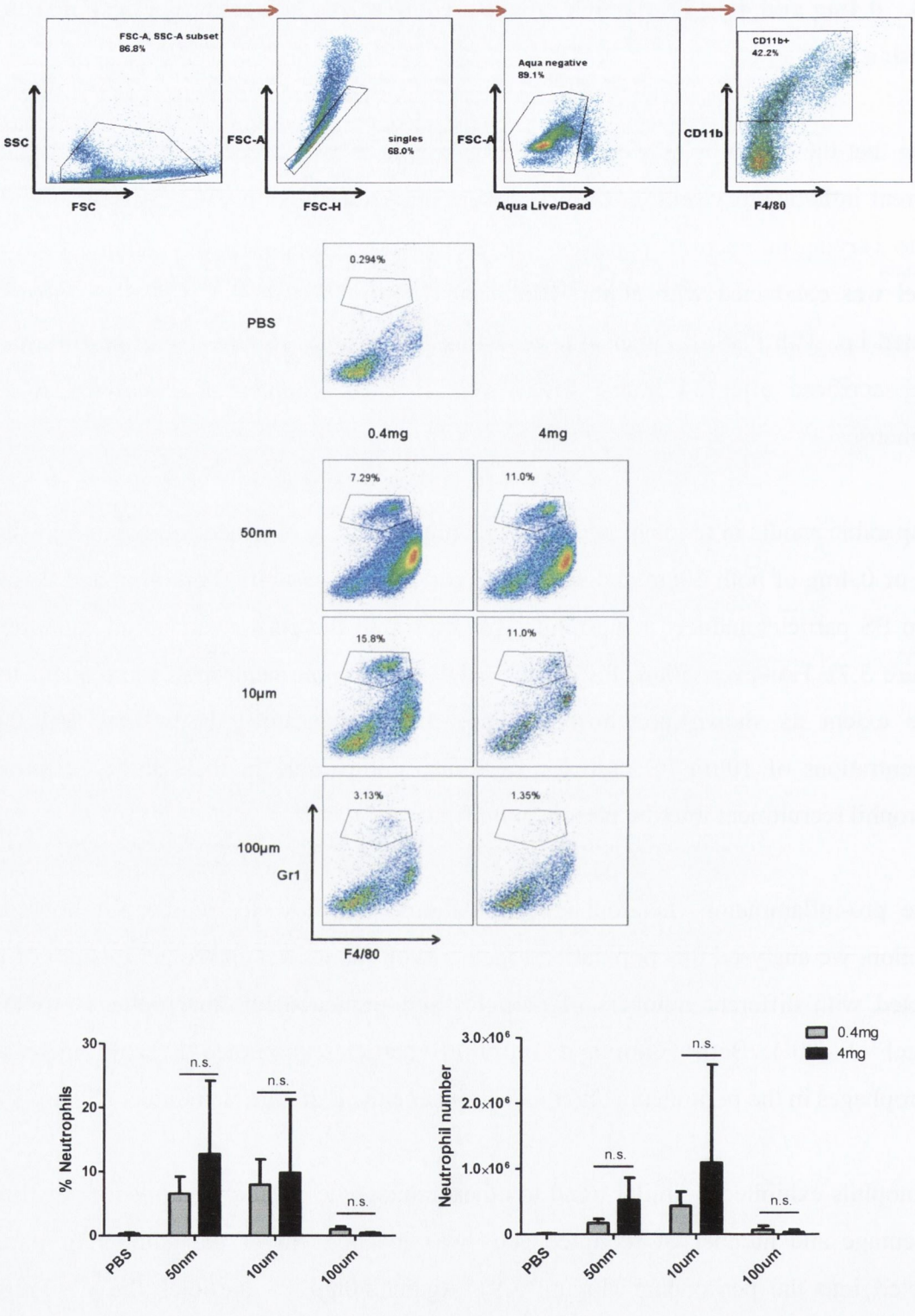

Figure 3.7 – Recruitment of neutrophils following PS particle injection was comparable when 4mg or 0.4mg of particles was administered. C57BL/6 mice were injected i.p. with PBS or 4mg/0.4mg PS particles (50nm, 10µm or 100µm) in 200µl volumes. The mice were sacrificed after 24 hours and PECs were collected. Neutrophils were gated as $CD11b^{+}$ $Gr1^{high}$ $F4/80^{-}$ and the data are graphed as percentage of live cells and number of live cells respectively. Bar charts represent mean (+ SD) for 3 mice per experimental group.

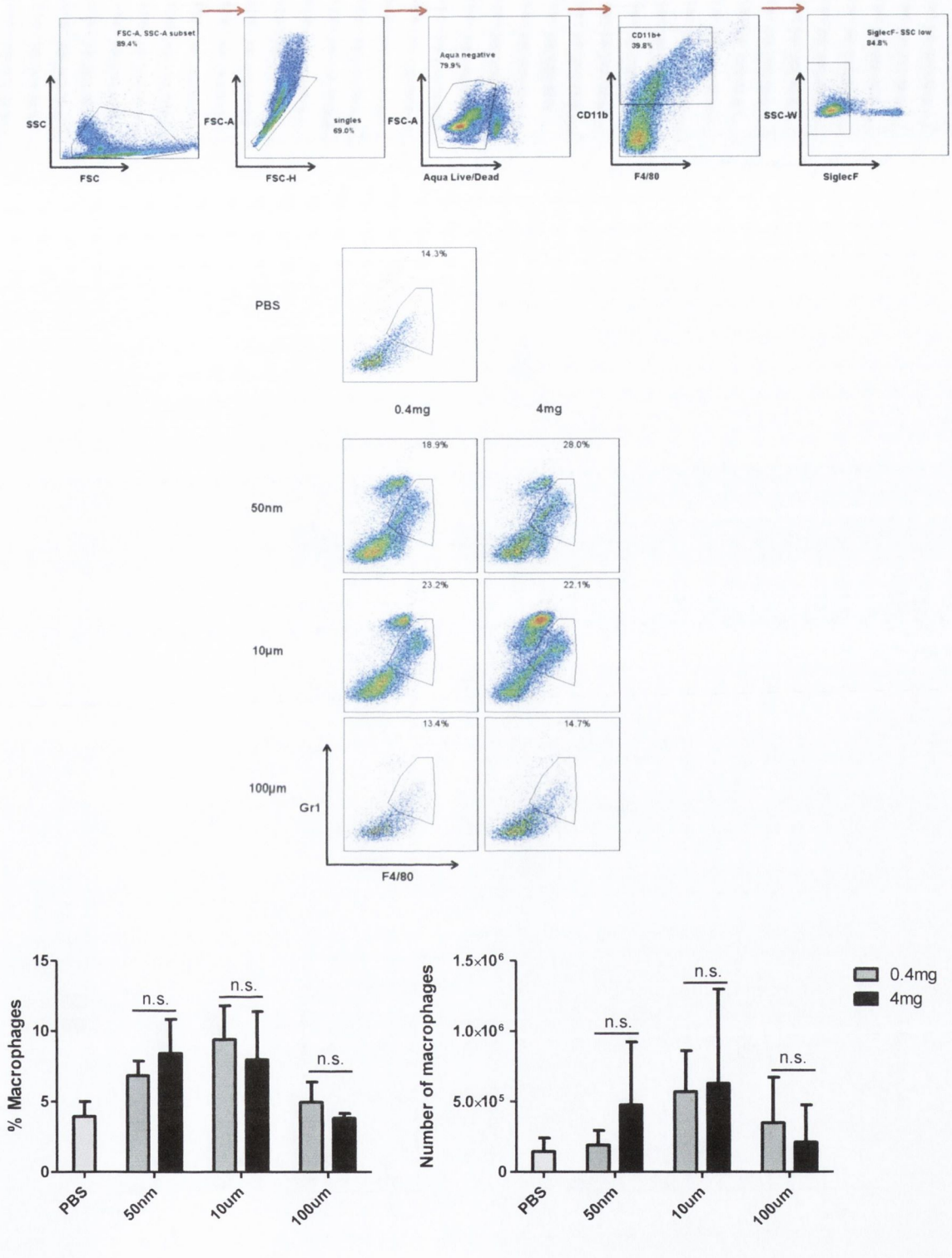

Figure 3.8 – Recruitment of macrophages following PS particle injection was comparable when 4mg or 0.4mg of particles was administered. C57BL/6 mice were injected i.p. with PBS or 4mg/0.4mg PS particles (50nm, 10µm or 100µm) in 200µl volumes. The mice were sacrificed after 24 hours and PECs were collected. Macrophages were gated as $CD11b^+$ $SiglecF^-$ $F4/80^+$ and the data are graphed as percentage of live cells and number of live cells respectively. Bar charts represent mean (+ SD) for 3 mice per experimental group.

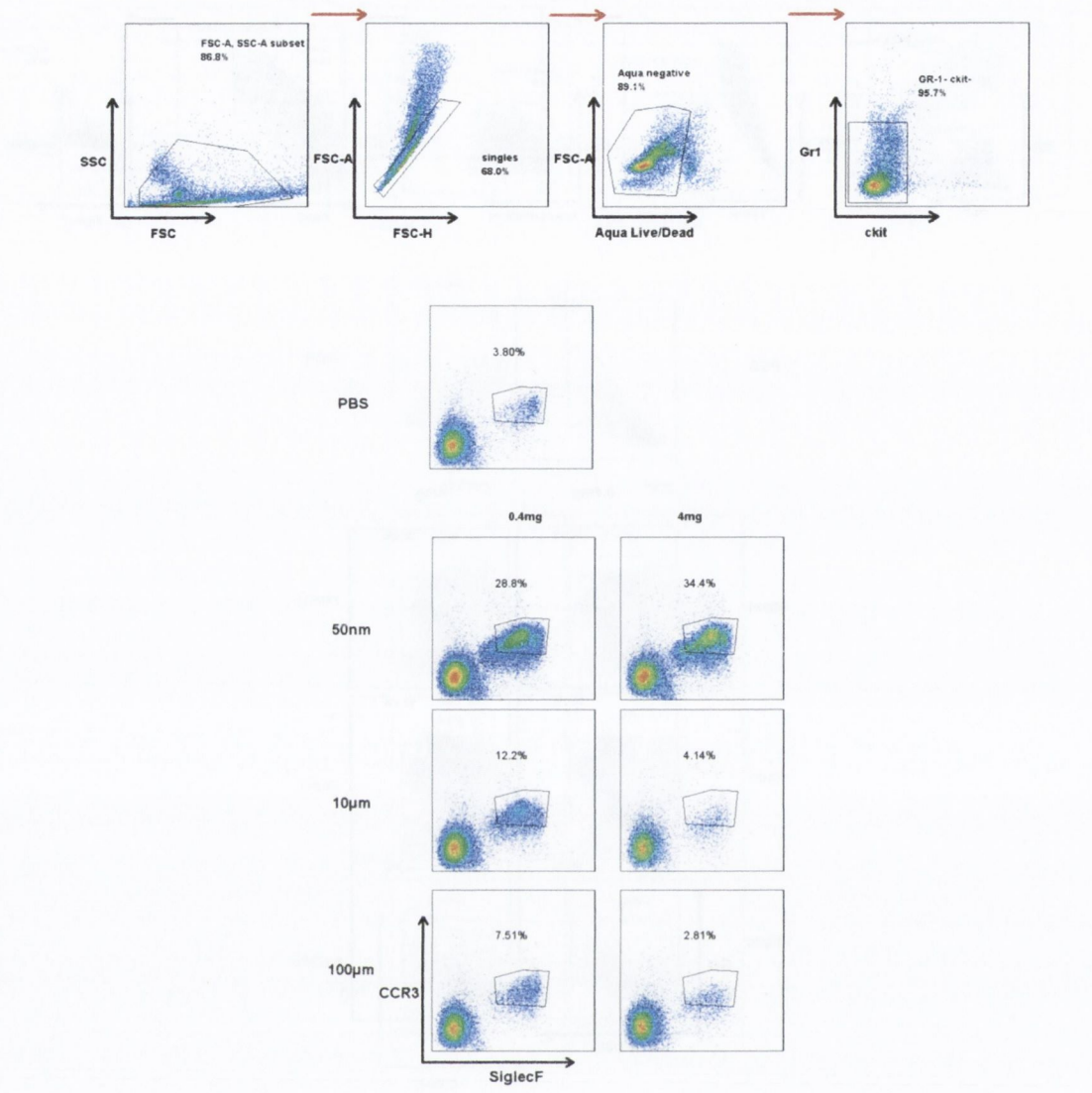

Figure 3.9 – Recruitment of eosinophils following PS particle injection was comparable when 4mg or 0.4mg of particles was administered. C57BL/6 mice were injected i.p. with PBS or 4mg/0.4mg PS particles (50nm, 10µm or 100µm) in 200µl volumes. The mice were sacrificed after 24 hours and PECs were collected. Eosinophils were gated as $Gr1^-$ $ckit^-$ $SiglecF^+$ $CCR3^+$ and the data are graphed as percentage of live cells and number of live cells respectively. Bar charts represent mean (+ SD) for 3 mice per experimental group. Versus PBS, ••• $p<0.0001$.

3.3.4. Injection of 50nm PS particles causes an infiltration of neutrophils which precedes that of macrophages

Since the inflammatory process has many stages, it was important to confirm that in selecting a 24 or 72 hour time point, earlier stages of inflammation for certain size PS particles were not being neglected. C57BL/6 mice were injected i.p. with PBS or PS particles (50nm, 10μm or 100μm) and were sacrificed after 1 or 3 hours. PECs were isolated, counted and analysed by flow cytometry.

Interestingly, neutrophils first appeared in the peritoneum of mice injected with 10μm PS particles but the increase over control was not significant (Figure 3.10). It was not until 3 hours after injection of PS particles that there was a significant increase in neutrophils in the peritoneum, and this was evident in both mice injected with 50nm and 10μm PS particles. Although 10μm PS particles appeared to have a 'head start' in terms of neutrophil infiltration 1 hour post injection, 50nm PS particles drove higher levels of neutrophil recruitment into the peritoneum after 3 hours (Figure 3.10), an effect which was still evident after 24 hours (Figure 3.2A,C).

Since early time points could precede differentiation of macrophages, both pro-inflammatory macrophages and monocytes were again combined within a $CD11b^+$ $F4/80^+$ gate. The appearance of macrophages in the peritoneum was not evident until 3 hours after injection with PS particles. Interestingly, 10μm PS particles drove the most significant infiltration of macrophages at this particular time point, however the number of macrophages was small (Figure 3.11). Of note, this difference in macrophage recruitment into the peritoneum of mice injected with 50nm and 10μm PS particles became more pronounced after 24 hours (Figure 3.3, 3.4). Importantly, eosinophils were not detectable after 1 hour or 3 hours after injection with PS particles (data not shown).

Interestingly, 100μm PS particles appeared to have no effect on cell recruitment into the injection site at early time points, thus reaffirming what was found after 24 and 72 hours (Figures 3.1). Remarkably, neutrophil infiltration 3 hours after injection with 50nm PS particles is still observed 24 hours later, and conversely macrophage infiltration after injection with 10μm PS particles was also still observed 72 hours later.

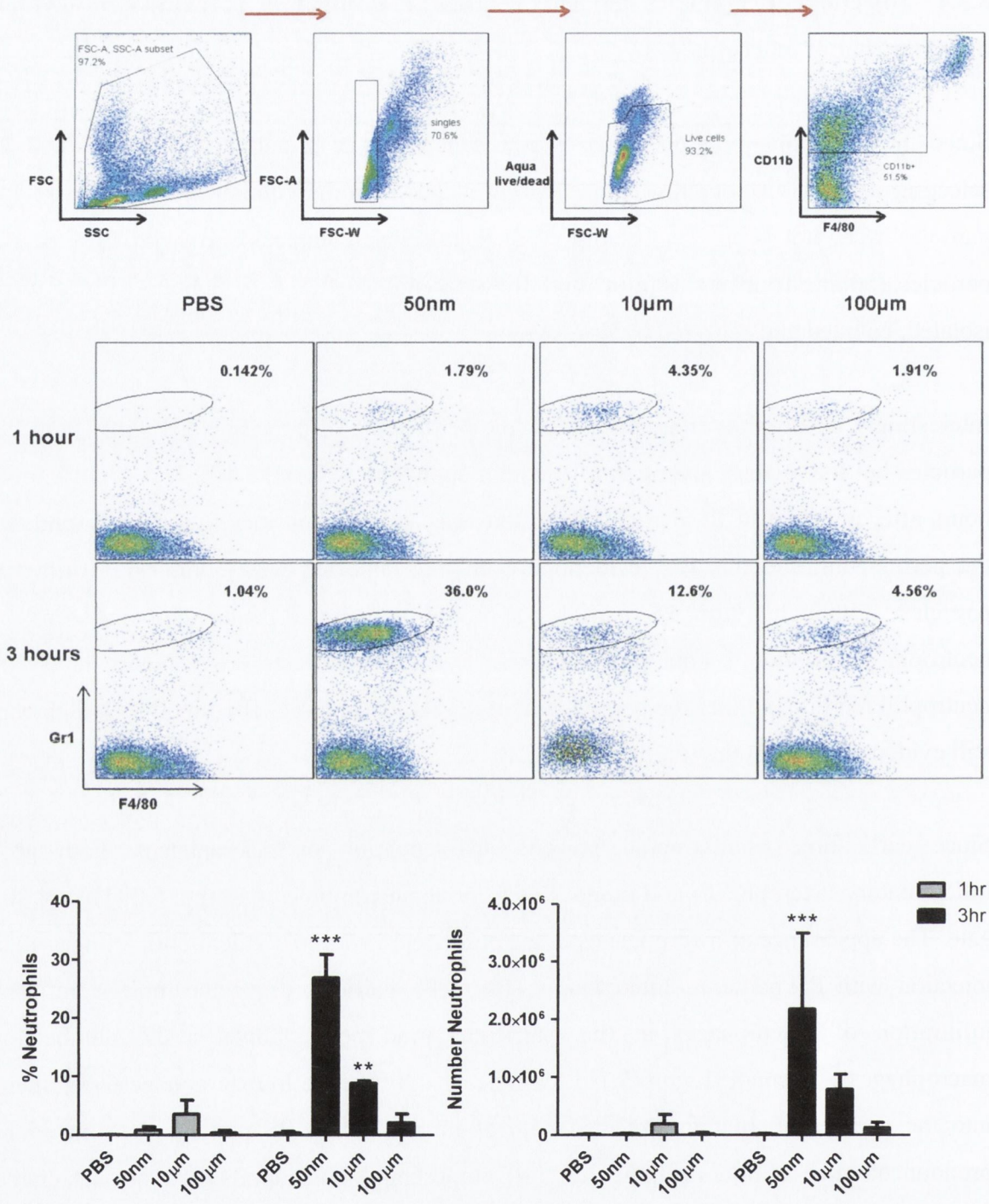

Figure 3.10 – 50nm PS particles drove neutrophil recruitment into the peritoneum 3 hours after injection. C57BL/6 mice were injected i.p. with PBS or 4mg of PS particles (50nm, 10µm or 100µm) in 200µl volumes. The mice were sacrificed after 1 hour or 3 hours and PECs were collected. Neutrophils were gated as $CD11b^{+}$ $Gr1^{high}$ $F4/80^{-}$ and the data are graphed as percentage of live cells and number of live cells respectively. Bar charts represent mean (+ SD) for 3 mice per experimental group. Versus group injected with corresponding treatments after 1 hr, ** $p<0.01$, *** $p<0.0001$.

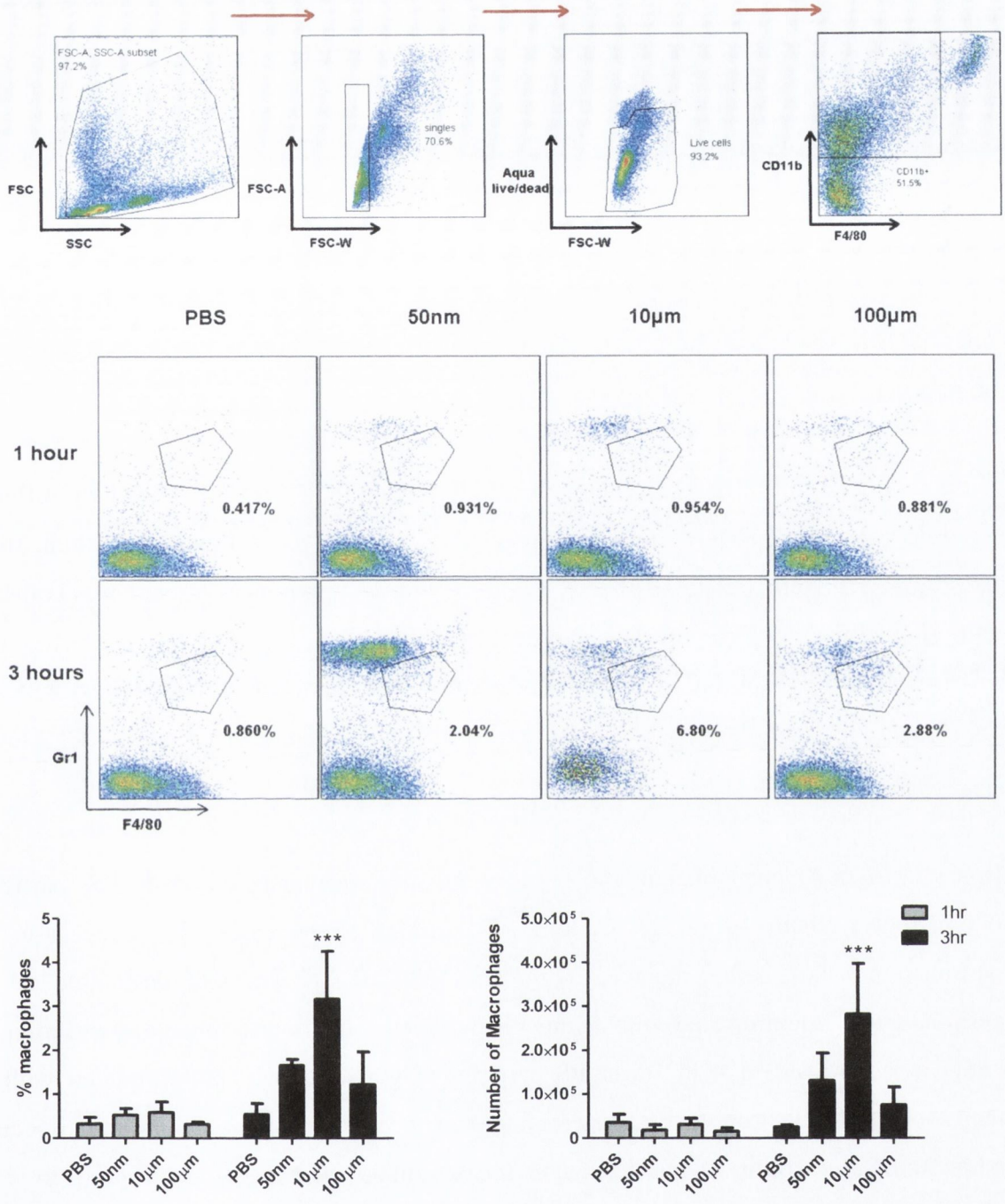

Figure 3.11 – Injection with 10µm PS particles drives recruitment of macrophages after 3 hours. C57BL/6 mice were injected i.p. with PBS or 4mg of PS particles (50nm, 10µm or 100µm) in 200µl volumes. The mice were sacrificed after 1 hour or 3 hours and PECs were collected. Macrophages were gated as $CD11b^{+}$ $F4/80^{+}$ and the data are graphed as percentage of live cells and number of live cells respectively. Bar charts represent mean (+ SD) for 3 mice per experimental group. Versus group injected with corresponding treatments after 1 hr, *** $p<0.0001$.

3.3.5 IL-1β, IL-33, CXCL1 and CXCL2 levels in the peritoneum correlate with subsequent cell infiltration after injection with PS particles

Significant amounts of inflammatory cells were recruited 3, 24 and 72 hours after injection with 50nm PS particles. Although cell recruitment into the peritoneum was most evident after 24 hours, it is conceivable that the cytokines/chemokines mediating this process might be elevated at a much earlier time point and may in fact be in decline after 24 hours. Therefore, it was crucial to assess several time points to determine cytokine levels in the peritoneum.

Hence, to determine the local chemoattractant signals that were influenced by different sized PS particles, C57BL/6 mice were injected i.p. with PBS or PS particles (50nm, 10μm or 100μm) and were sacrificed after 1, 3 or 24 hours. The peritoneal exudate was collected and chemokine/cytokine levels analysed by ELISA. Since IL-1 is a known pro-inflammatory mediator and neutrophil chemoattractant, there was a focus on cytokines of the IL-1 family, including IL-1β, IL-1α and IL-33. In addition, CXCL1 and CXCL2 levels were also determined.

IL-1α was not detectable in the peritoneum of mice injected with PS particles. Interestingly, 50nm, 10μm and 100μm PS particles all increased IL-1β levels in the peritoneum 1 hour after injection (Figure 3.12A). IL-1β was still detectable in the peritoneum of mice injected with 50nm PS particles 3 hours after injection and after 24 hours in mice injected with 10μm PS particles (Figure 3.12A). This correlated with an increase in both neutrophils and macrophages in the peritoneum 24 hours after injection with 50nm and 10μm PS particles and the sustained increase of neutrophils in mice injected with 10μm PS particles 72 hours after injection (Figures 3.2, 3.3). At all time points tested mice injected with 100μm PS particles had similar levels of IL-1β in the peritoneum compared to those injected with PBS (Figure 3.12A).

IL-33 was exclusively found in the peritoneum of mice injected with 50nm PS particles (Figure 3.12B), correlating with the ability of this particular size to drive the most significant recruitment of eosinophils into the site of injection (Figure 3.6). Both 50nm and 10μm PS particles drove CXCL1 production in the peritoneum 1 hour and 3 hours after injection, with significant levels of this chemokine still present 24 hours after injection with 50nm PS particles (Figure 3.12C). These particles were also capable of inducing the

secretion of CXCL2 in the peritoneum 3 hours after injection (Figure 3.12D). Interestingly, where 50nm PS particles primarily induced the secretion of CXCL1 24 hours after injection, 10μm PS particles induced the secretion of CXCL2 (Figure 3.12D).

In parallel with limited cell recruitment, 100μm PS particles did not drive any significant pro-inflammatory cytokine or chemokine production in the peritoneum at any of the time points tested (Figure 3.12). Therefore, only those PS particles that drove cell infiltration simultaneously induced the secretion of pro-inflammatory cytokines and chemokines at the injection site.

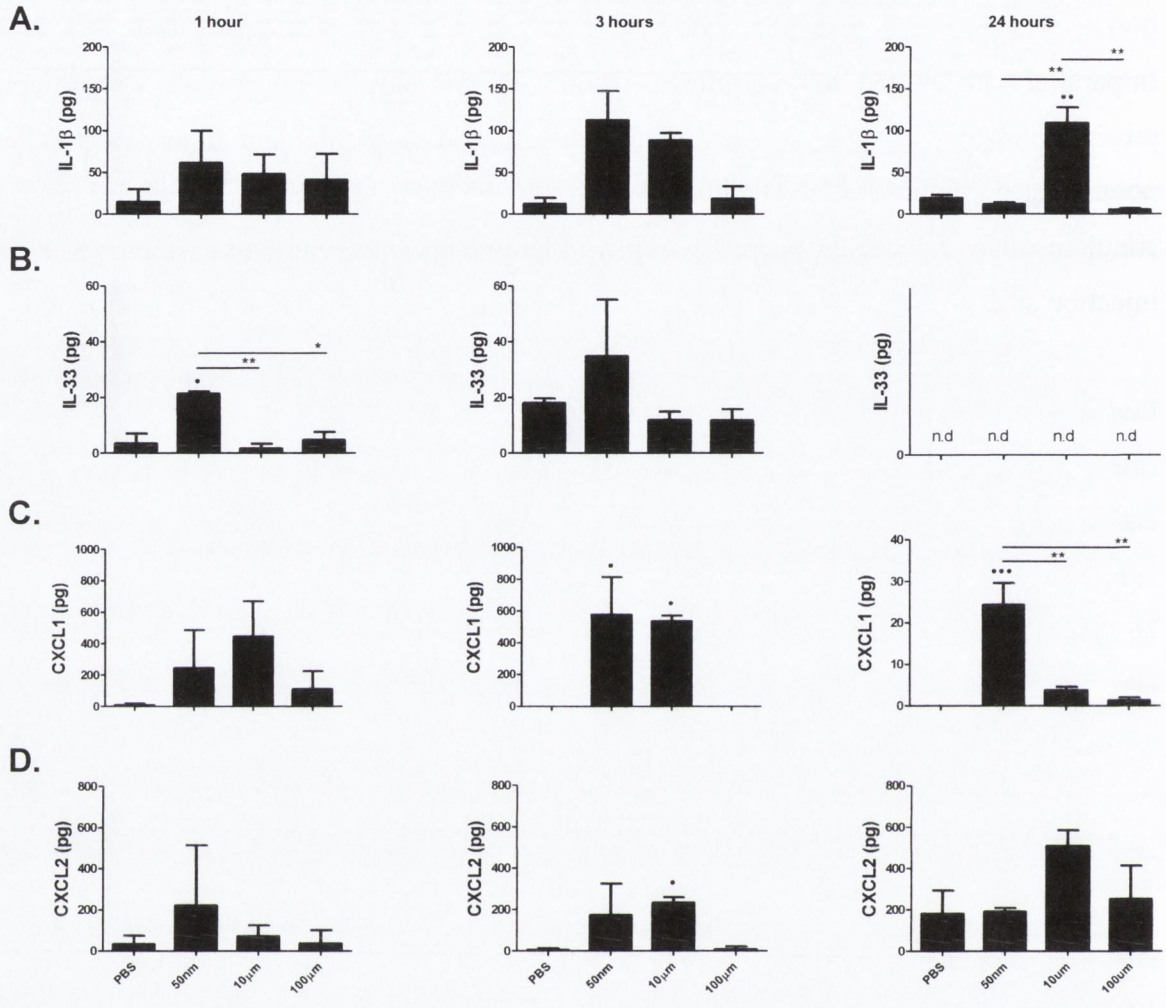

Figure 3.12 – 3 hours after injection is the optimal time to detect chemoattractant secretion. C57BL/6 mice were injected i.p. with PBS or 4mg PS particles (50nm, 10µm, or 100µm) in 200µl volumes. The mice were sacrificed after 1 hour and 3 hours and the peritoneal exudates collected. Cell supernatants were collected and concentrated using centrifugal filters. IL-1β, IL-33, CXCL1 and CXCL2 levels were determined by ELISA. Bar charts represent mean (+ SD) for 3 mice per experimental group. Results are representative of two or three independent experiments. Versus PBS, • $p<0.05$, •• $p<0.01$, ••• $p<0.0001$. Versus group injected with corresponding concentration of different sized particles, * $p<0.05$, ** $p<0.01$.

3.3.6 PS particles modulate cytokine and chemokine secretion 3 hours after injection

Since a selected panel of cytokines and chemokines were detected 3 hours after injection of PS particles (Figure 3.12), the presence of other chemoattractants known to be associated with the cell types recruited (Figures 3.2-3.6) were also assessed at this time point. C57BL/6 mice were injected i.p. with PBS or PS particles (50nm, 1μm, 10μm, 30μm or 100μm) and were sacrificed after 3 hours. The peritoneal exudate was collected and chemoattractant levels analysed by ELISA.

In comparison with Figure 3.12, 10μm PS particles drove the most significant amounts of IL-1β in this experiment, as well as significant amounts of CXCL1, CCL2, CCL3 and CCL13 (Figure 3.13). The induction of the secretion of these chemoattractants corresponds with the cellular infiltration of neutrophils (CXCL1, Figure 3.2) and monocytes (CCL2 and CCL3, Figure 3.3), as well as eosinophils after injection with 10μm and 30μm PS particles (CCL13, Figure 3.6). 50nm PS particles were also capable of driving CXCL1, CCL2 and CCL3, as well as CXCL2, the latter corresponding to the high numbers of neutrophils recruited after injection with 50nm PS particles (Figure 3.13). Similarly, 30μm PS particles induced the secretion of IL-1β, CCL2 and CCL13 again corresponding with the infiltration of monocytes, pro-inflammatory macrophages and eosinophils.

Interestingly, 1μm PS particles led to the secretion of significant levels of CXCL1, CCL2 and CCL3, however this did not appear to induce cell infiltration to the local site at the times analysed (Figure 3.13). 100μm PS particles did not induce the secretion of any chemoattractants 3 hours after injection.

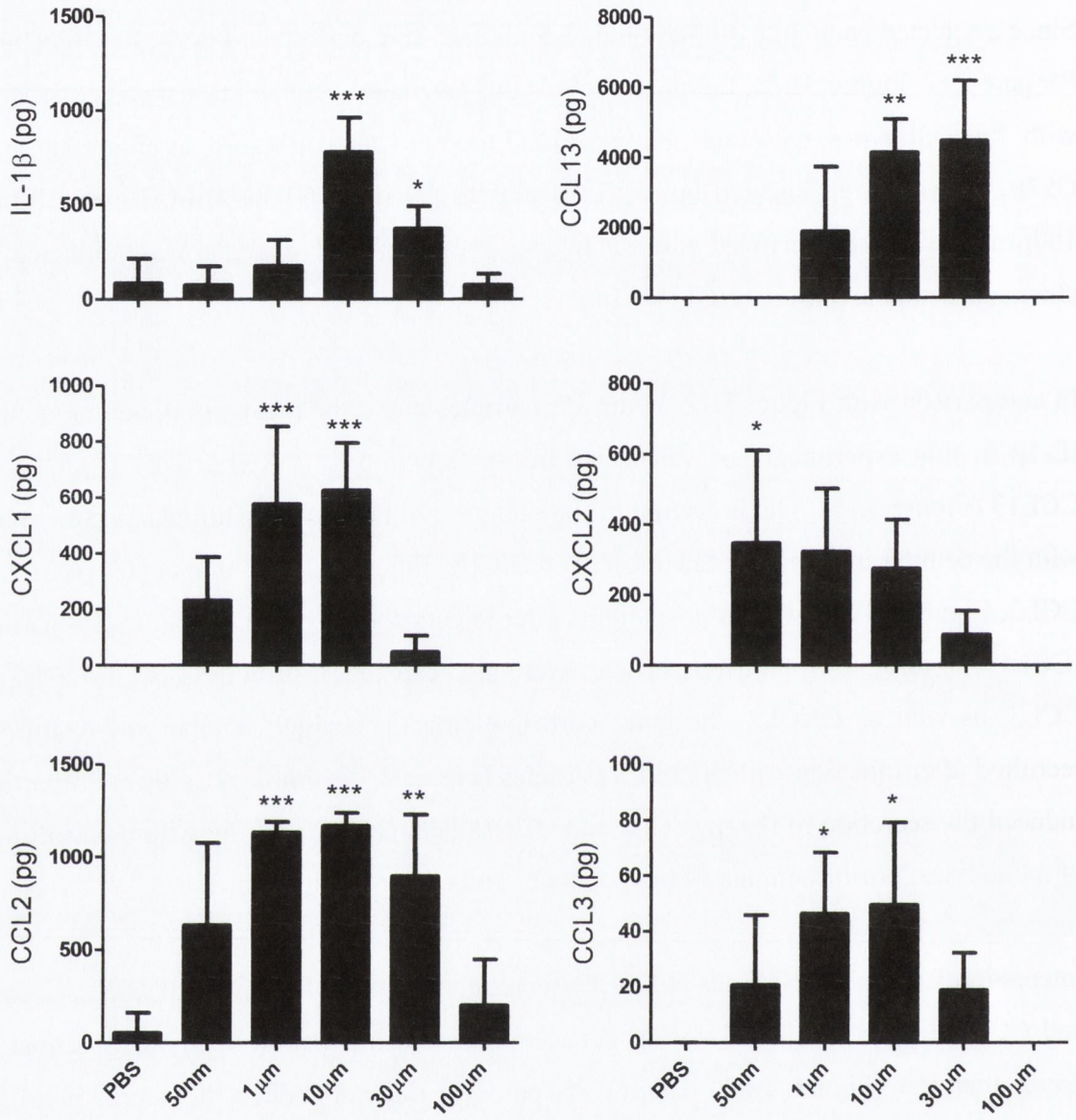

Figure 3.13 – Injection with all but 100μm PS particles drives chemoattractant secretion after 3 hours. C57BL/6 mice were injected i.p. with PBS or 4mg PS particles (50nm, 1μm, 10μm, 30μm or 100μm) in 200μl volumes. The mice were sacrificed after 3 hours and the peritoneal exudates collected. Cell supernatants were collected and concentrated using centrifugal filters. IL-1β, CXCL1, CXCL2, CCL2, CCL3 and CCL13 levels were determined by ELISA. Bar charts represent mean (+ SD) for 4 mice per experimental group. Results are representative of two independent experiments. Versus PBS, * $p<0.05$, ** $p<0.01$, *** $p<0.0001$.

3.3.7 Injection of PS particles does not induce detectable cell death

The immuno-stimulatory activity of a number of adjuvants has been reported to be at least partially dependent on their ability to induce necrotic cell death at the injection site. Since the release of IL-33, a DAMP known to be passively released from necrotic cells, was increased in mice injected with 50nm PS particles at early time points, it was important to establish whether cell recruitment into the peritoneum of mice injected with PS particles was due to PS particle-mediated toxicity. C57BL/6 mice were injected i.p. with PBS or PS particles (50nm, 10μm or 100μm) and were sacrificed after 1, 3, 24 or 72 hours. PECs were isolated, counted and stained with Aqua live/dead to assess cell death in the peritoneum.

Remarkably, PS particles of all sizes examined did not induce any significant cell death in the peritoneum 1, 3, or 24 hours after injection when compared to PBS (Figure 3.14A, B, C). 50nm and 100μm PS particles induced a small but significant amount of local necrosis 72 hours after injection (Figure 3.14D).

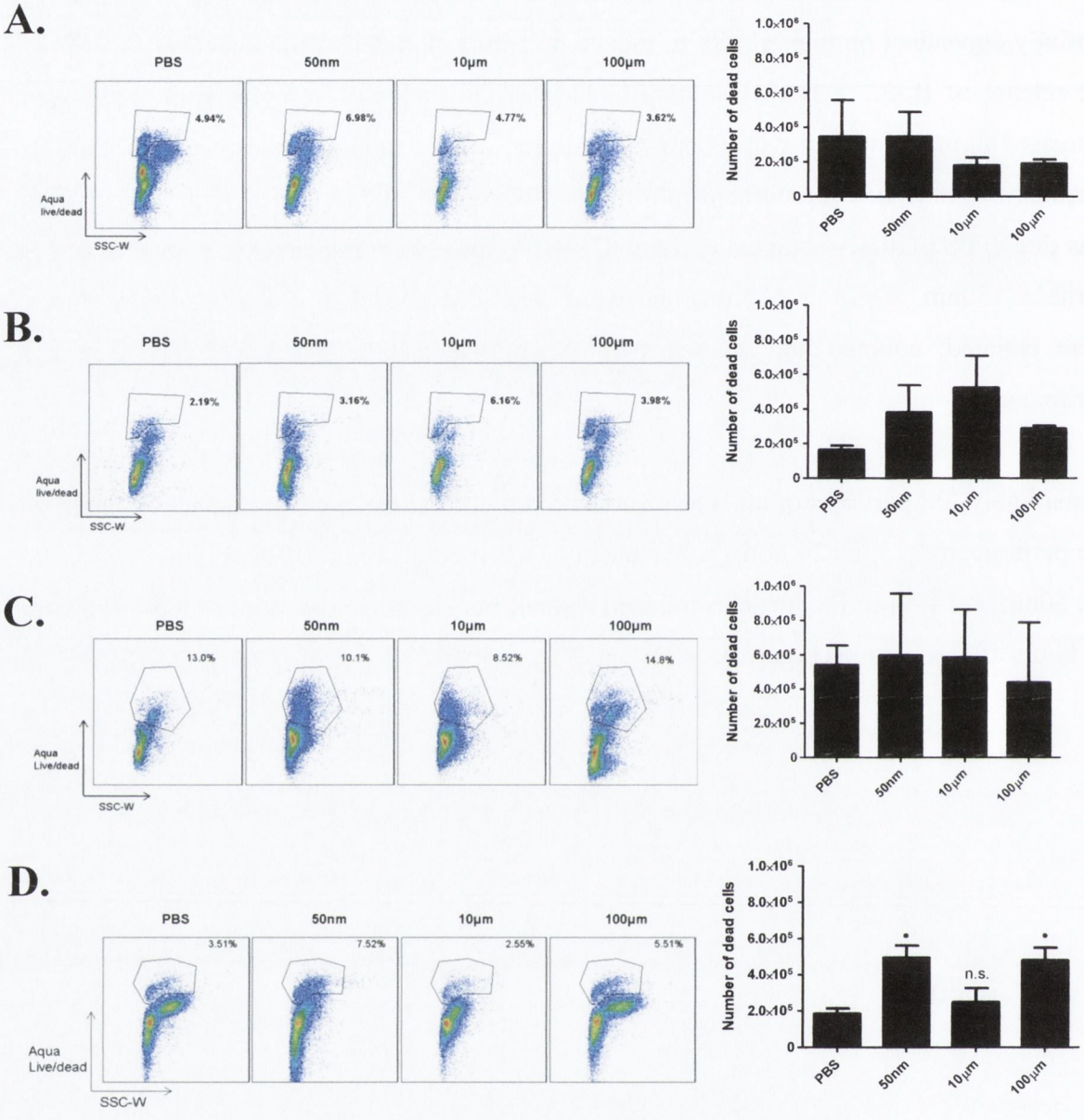

Figure 3.14 – Injection of PS particles did not induce detectable cell death up to 72 hours after injection. C57BL/6 mice were injected i.p. with PBS or 4mg of PS particles (50nm, 10µm or 100µm) in 200µl volumes. 1 hour (A), 3 hours (B), 24 hours (C) or 72 hours (D) later PECs were collected and stained with Aqua live/dead. Dead cells were gated as Aqua positive and the data are graphed as percentage of single cells. Bar charts represent mean (+ SD) for 3 or 4 mice per experimental group. Versus PBS, • $p<0.05$.

3.3.8 DNA is present in the peritoneum of mice injected with 50nm PS particles after 3 hours, but 10μm particles induce the release of local free DNA in the peritoneum at later time points.

The lack of PS particle-mediated toxicity at early time points when measured by flow cytometry was surprising. Necrotic cells are known to release their contents into the extracellular space and some viable granulocytes can release DNA as part of extracellular traps (ET). Hence free dsDNA in the peritoneal exudates was measured. C57BL/6 mice were injected i.p. with PBS or PS particles (50nm, 10μm or 100μm), were sacrificed after 1, 3, 24 or 72 hours and the peritoneal exudate was collected.

Interestingly 3 hours after injection with 50nm PS particles, free dsDNA was detected in the peritoneum (Figure 3.15). However, 24 and 72 hours after injection with 50nm PS particles, this free dsDNA was no longer present at significant levels when compared with mice injected with PBS. Intriguingly, at these later time points, injection with 10μm PS particles induced the release of free dsDNA in to the peritoneum (Figure 3.15). In contrast, injection with 100μm PS particles did not induce the release of free dsDNA into the peritoneum at any time point analysed.

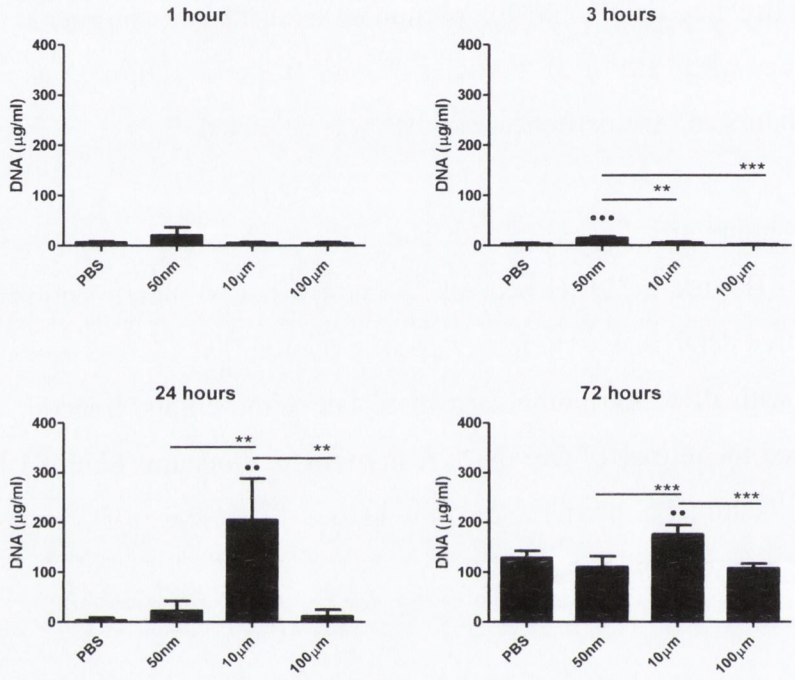

Figure 3.15 – Free DNA is present in the peritoneum 24 and 72 hours after injection with 10µm PS particles. C57BL/6 mice were injected i.p. with PBS or 4mg of PS particles (50nm, 10µm or 100µm) in 200µl volumes. 1, 3, 24 or 72 hours later the peritoneal exudates were collected. Cell supernatants were collected and free dsDNA measured. Bar charts represent mean (+ SD) for 3 or 4 mice per experimental group. Versus PBS, •• $p<0.01$, ••• $p<0.0001$. Versus group immunized with corresponding concentration of different sized particles, ** $p<0.01$, *** $p<0.0001$.

3.3.9 IL-1β is not present in significant levels in the serum of mice injected with PS particles.

Since the magnitude and type of local inflammation triggered by injection of PS particles was dependent on particle size, the systemic effects of injecting PS particles were also investigated. C57BL/6 mice were injected i.p. with PBS or PS particles (50nm, 10μm or 100μm) and were sacrificed after 1, 3 or 24 hours. Blood was isolated and IL-1β levels were determined in the serum by ELISA.

Although IL-1β levels were marginally increased in the serum of mice injected with both 50nm and 10μm PS particles after 3 hours, it was not significant compared with mice injected with PBS (Figure 3.16). Similarly, injection of 100μm particles did not result in systemic IL-1β secretion, correlating with a lack of IL-1β at the injection site (Figure 3.12A).

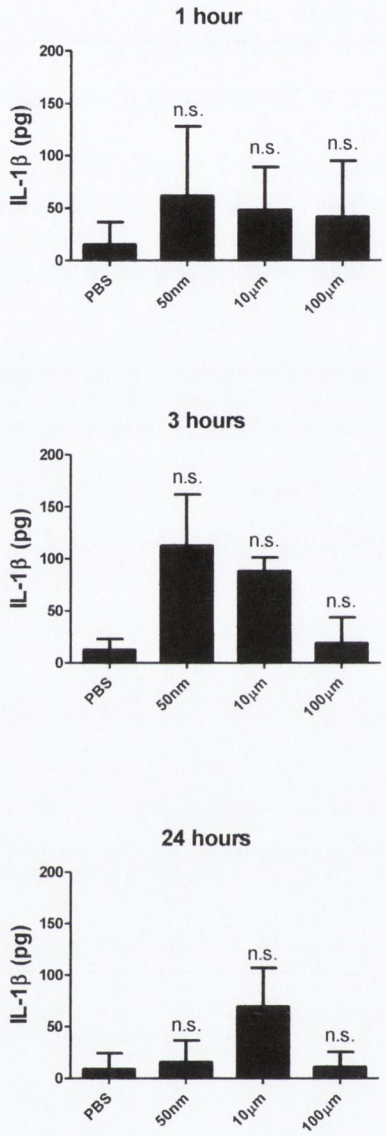

Figure 3.16 – Injection of 50nm and 10μm PS particles results in the presence of IL-1β in the blood at 3 hours and 24 hours. C57BL/6 mice were injected i.p. with PBS or 4mg PS particles (50nm, 10μm, or 100μm) in 200μl volumes. The mice were sacrificed after 1 hour, 3 hours or 24 hours and blood collected. IL-1β levels were measured in the serum by ELISA. Bar charts represent mean (+ SD) for 3 mice per experimental group.

3.3.10. Neutrophil recruitment in response to 50nm, but not 10μm, PS particles is dependent on IL-1R1

Having shown that IL-1β was present locally after i.p. injection of both 50nm and 10μm PS particles, the role of IL-1 in PS particle-induced inflammation was investigated. C57BL/6 and *Il1r1*$^{-/-}$ mice were injected i.p. with PBS or PS particles (50nm, 10μm, 100μm) and were sacrificed after 24 hours. PECs were isolated and analysed by flow cytometry.

Neutrophil recruitment into the peritoneum of mice injected with 50nm PS particles was completely IL-1R1-dependent (Figure 3.17). However, neutrophil recruitment following injection with 10μm PS particles was found to be IL-1R1-independent (Figure 3.17).

There were no significant differences between WT and *Il1r1*$^{-/-}$ mice in their ability to promote macrophage recruitment following injection with PS particles of all sizes tested (Figure 3.18). Interestingly, *Il1r1*$^{-/-}$ mice injected with 10μm PS particles had significantly more peritoneal macrophages than WT mice (Figure 3.18).

Increased numbers of eosinophils were recruited into the peritoneum of *Il1r1*$^{-/-}$ mice compared to WT mice following injection with PS particles (Figure 3.19). This trend was evident across all groups, but was found to be statistically significant when mice were injected with 10μm PS particles (Figure 3.19). Clearly the IL-1R1 was not required for eosinophil recruitment into the peritoneum after injection with PS particles (Figure 3.19).

These results indicate that the only population of cells analysed that requires the IL-1R1 for recruitment into the peritoneum in response to injection of PS particles are neutrophils. Interestingly, IL-1R1-dependent neutrophil recruitment was only evident in mice injected with 50nm PS particles. This infers that 10μm PS particles use a different mechanism to 50nm PS particles to mediate neutrophil infiltration into the site of injection.

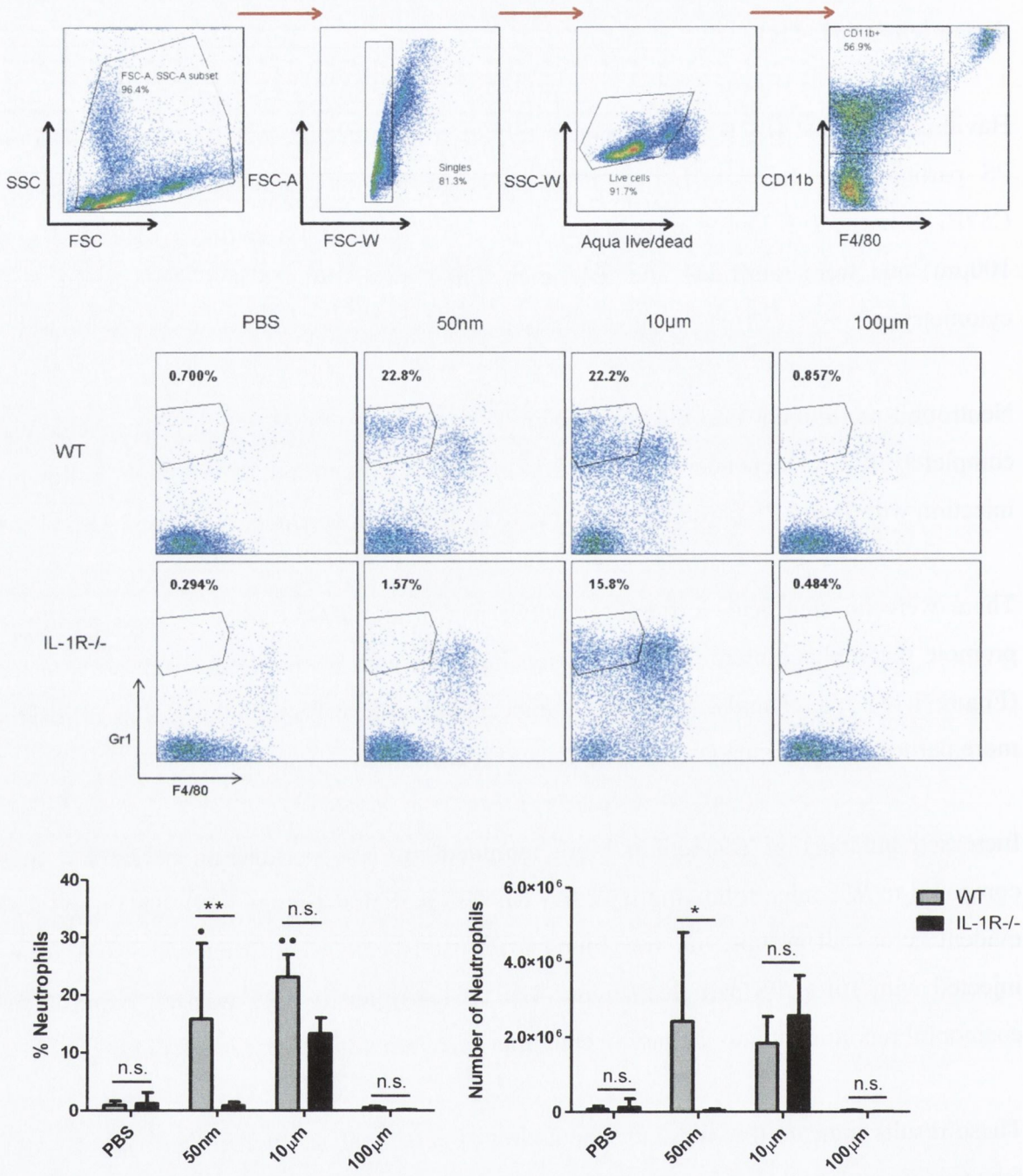

Figure 3.17 – IL-1R1 is required for neutrophil infiltration after injection of 50nm but not 10µm PS particles. C57BL/6 and *Il1r1*$^{-/-}$ mice were injected i.p. with PBS or 4mg of PS particles (50nm, 10µm or 100µm) in 200µl volumes. The mice were sacrificed after 24 hours and PECs were collected. Neutrophils were gated as CD11b^{+} Gr1^{high} F4/80^{-} and the data are graphed as percentage of live cells and number of live cells respectively. Bar charts represent mean (+ SD) for 3 mice per experimental group. Results representative of two independent experiments. Versus PBS of corresponding strain, • $p<0.05$, •• $p<0.01$. Versus corresponding particle size *Il1r1*$^{-/-}$ group, * $p<0.05$, ** $p<0.01$.

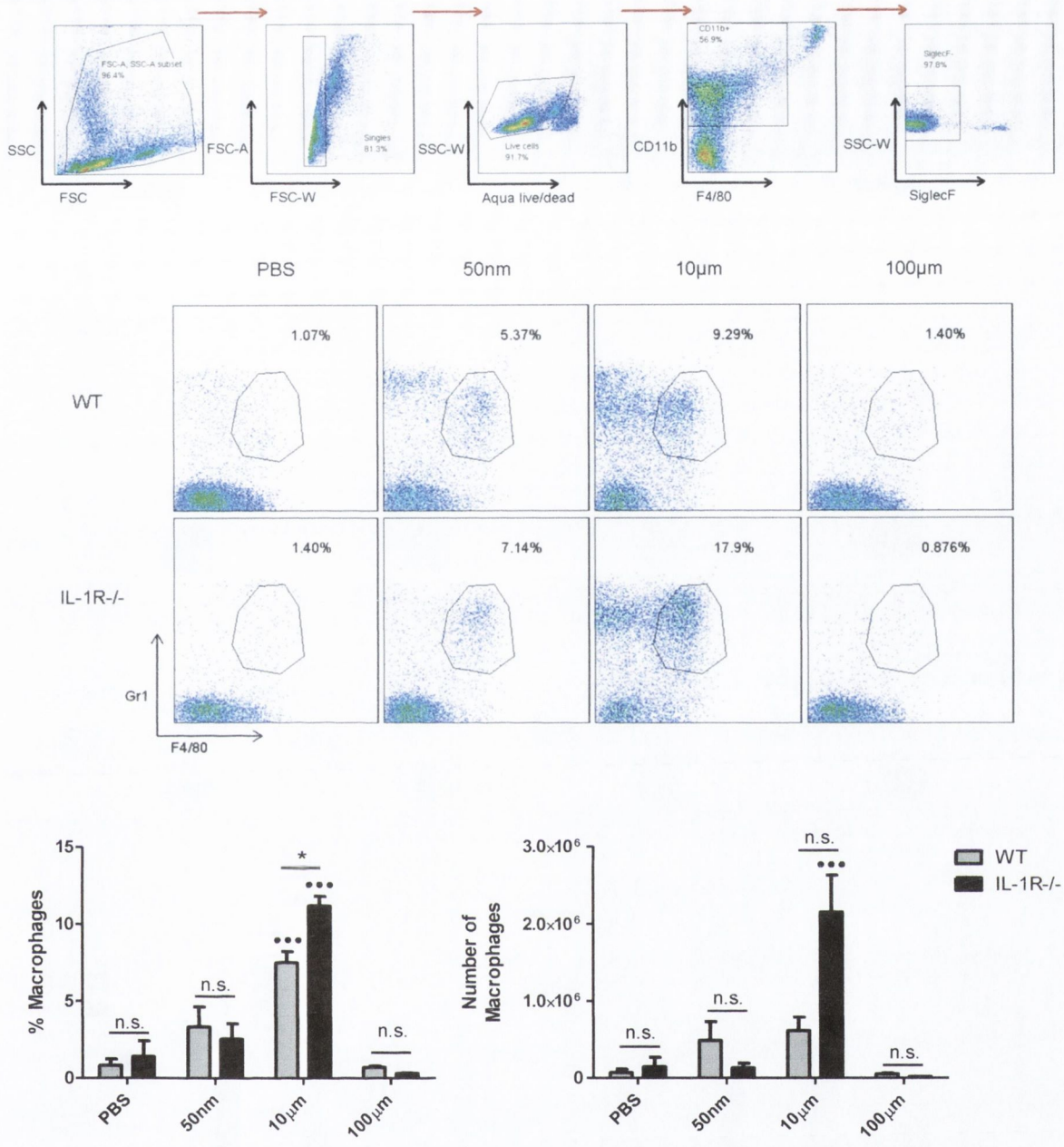

Figure 3.18 – Macrophage recruitment into the peritoneum is IL-1R1 independent for all sized PS particles. C57BL/6 and *Il1r1*$^{-/-}$ mice were injected i.p. with PBS or 4mg of PS particles (50nm, 10µm or 100µm) in 200µl volumes. The mice were sacrificed after 24 hours and PECs were collected. Macrophages were gated as CD11b^{+} F4/80^{+} SiglecF^{-} SSC^{low} and the data are graphed as percentage of live cells and number of live cells respectively. Results representative of two independent experiments. Bar charts represent mean (+ SD) for 3 mice per experimental group. Versus PBS of corresponding strain, ••• $p<0.0001$. Versus corresponding particle size *Il1r1*$^{-/-}$ group, * $p<0.05$.

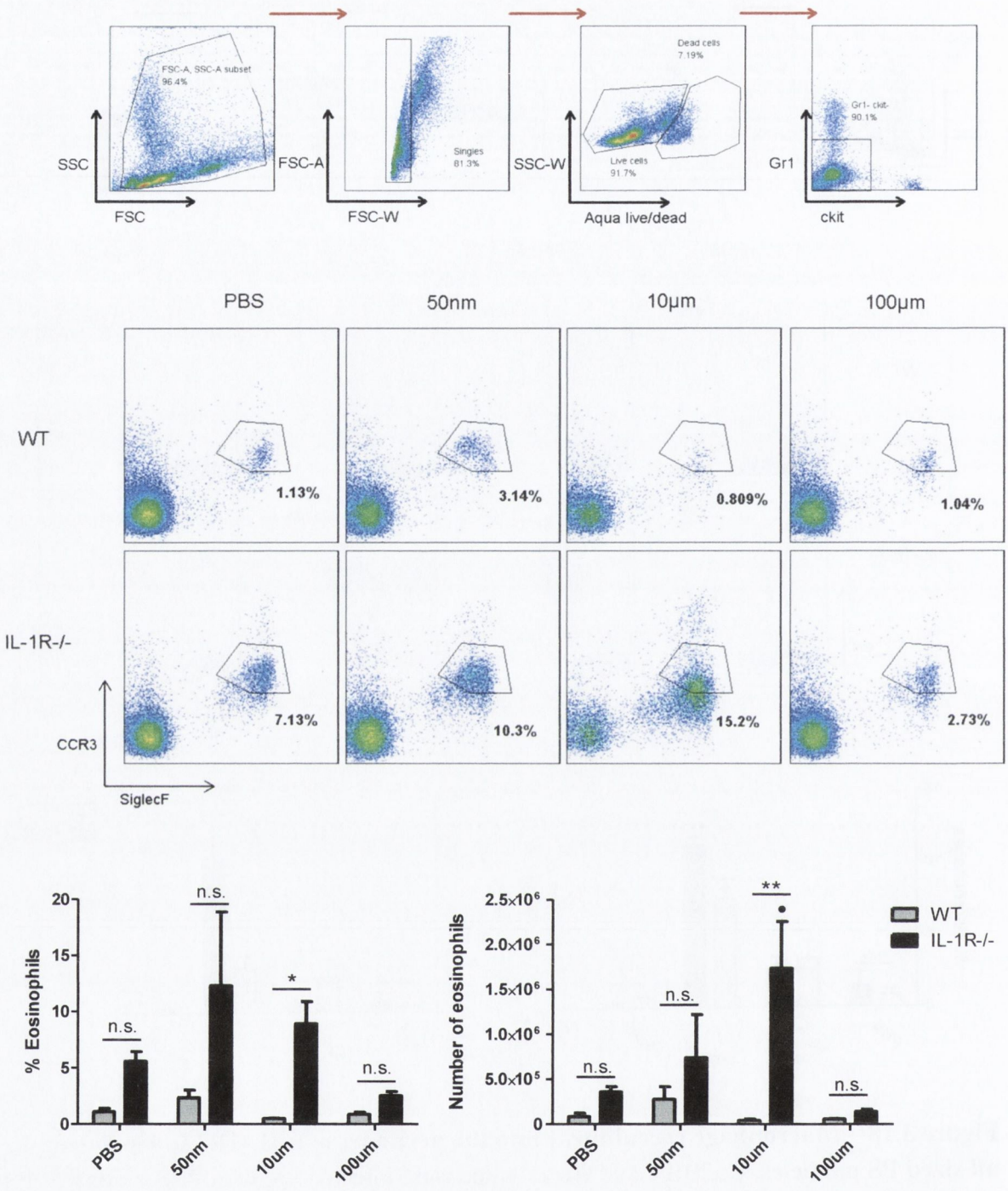

Figure 3.19 – Eosinophil recruitment into the peritoneum is IL-1R1 independent for all sized PS particles. C57BL/6 and *Il1r1*$^{-/-}$ mice were injected i.p. with PBS or 4mg of PS particles (50nm, 10µm or 100µm) in 200µl volumes. The mice were sacrificed after 24 hours and PECs were collected. Eosinophils were gated as Gr1^{-} ckit^{-} SiglecF^{+} CCR3^{+} and the data are graphed as percentage of live cells and number of live cells respectively. Bar charts represent mean (+ SD) for 3 mice per experimental group. Results representative of two independent experiments. Versus PBS of corresponding strain, • $p<0.05$. Versus corresponding particle size *Il1r1*$^{-/-}$ group, * $p<0.05$, ** $p<0.01$.

3.3.11. The neutrophil chemoattractants CXCL1, CXCL2 and IL-1β are induced in *Il1r1*$^{-/-}$ mice injected with 10μm PS particles

In order to determine whether the different mechanisms of neutrophil recruitment utilised by 50nm and 10μm PS particles were due to differential local neutrophil chemoattractant signalling, we analysed levels of chemokines and cytokines in the peritoneum known to be involved in neutrophil recruitment. C57BL/6 and *Il1r1*$^{-/-}$ mice were injected i.p. with PBS or PS particles (50nm, 10μm, 100μm) and were sacrificed after 24 hours. The peritoneal exudate was collected and CXCL1, CXCL2 and IL-1β levels were measured by ELISA.

The neutrophil chemoattractants CXCL1, CXCL2 and IL-1β were only detectable in the peritoneum of mice injected with 10μm PS particles after 24 hours. Interestingly, *Il1r1*$^{-/-}$ mice had significantly higher levels of both CXCL1 and CXCL2 than WT mice, whereas IL-1β levels were similar to those seen in WT mice (Figure 3.20). Although these chemoattractants were not found in mice injected with 50nm PS particles at this time point, it does not indicate that these signals are not involved in 50nm PS particle neutrophil recruitment in these mice, since CXCL1 and CXCL2 were present in the peritoneum of mice injected with 50nm PS particles at earlier time points (Figure 3.12C, D). These results indicate that in mice injected with 10μm PS particles, neutrophil recruitment is independent of the IL-1R1, as is the secretion of IL-1β, CXCL1 and CXCL2 in the peritoneum.

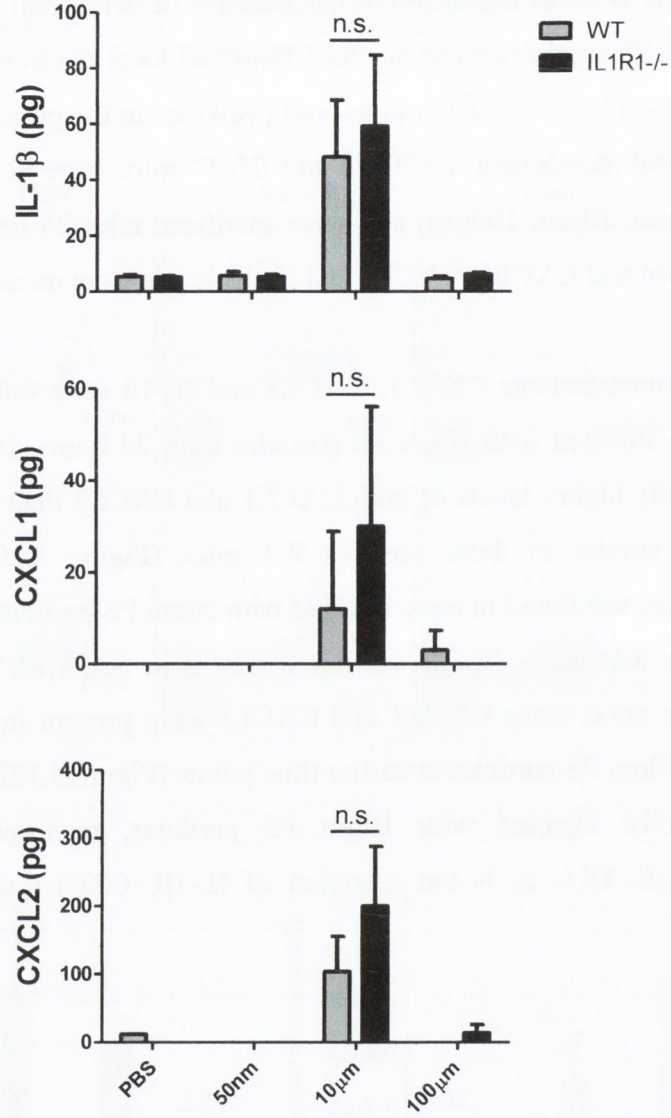

Figure 3.20 – Local chemokine and cytokine signals associated with neutrophil recruitment in response to 10μm PS particles are similar 24 hours after injection. C57BL/6 and *Il1r1*$^{-/-}$ mice were injected i.p. with PBS or 4mg of PS particles (50nm, 10μm or 100μm) in 200μl volumes. The mice were sacrificed after 24 hours and peritoneal exudates collected. Cell supernatants were collected and concentrated using centrifugal filters. IL-1β, CXCL1 and CXCL2 levels were determined by ELISA. Bar charts represent mean (+ SD) for 3 mice per experimental group. Results representative of two independent experiments.

3.3.12. PS particle size modulates cytokine production from restimulated PECs

Since we found that the peritoneal environment changed after injection with different sized PS particles, we next wanted to investigate if the cells present in the peritoneum after injection were functionally different and hence capable of inducing different immune responses. To assess if PS particle size could influence the ability of cells to secrete different cytokines in response to various stimuli, C57BL/6 mice were injected i.p. with PBS or PS particles (50nm, 1μm, 10μm, 30μm or 100μm) and were sacrificed after 24 or 72 hours. PECs were recovered and restimulated *ex vivo* with complete RPMI 1640 medium, LPS, heat-killed *Escherichia coli (*HK *E. coli*), anti-CD3 or anti-CD3 in combination with phorbol 12-myristate 13-acetate (PMA). Innate immune cells such as macrophages and/or DCs were activated *ex vivo* using LPS and HK *E. coli*. The cytokines TNF-α, IL-12p40 and IL-10 were measured to assess their activation *ex vivo*. The stimulant anti-CD3 engages CD3ε and was used to activate T cells, as was PMA which stimulates cells by activating protein kinase C[373]. To assess T cell activation, the secretion of cytokines indicative of T cell subsets was measured. Specifically, IFN-γ, IL-4, IL-17 and IL-10 were assayed in an attempt to characterise the ability of PS particles of different sizes to drive Th1, Th2, Th17 and Treg cell responses respectively.

Following restimulation with both HK *E. coli* and LPS, PECs recovered from mice injected with 10μm and 30μm PS particles secreted the most significant amounts of TNF-α and IL-12p40 and the most limited production of IL-10 when compared with PECs isolated from control mice injected with PBS (Figure 3.21).

Following restimulation with anti-CD3, PECs recovered 24 hours after mice were injected with PS particles did not elicit a significantly altered cytokine profile in comparison with PECs isolated from control mice injected with PBS (Figure 3.22). However, following restimulation with anti-CD3 in combination with PMA, PECs recovered from mice injected with 1μm and 10μm PS particles secreted increased levels of IL-4 and decreased levels of IL-10 when compared with PECs isolated from control mice injected with PBS (Figure 3.22). Furthermore, PECs from mice injected with 1μm PS particles also secreted higher concentrations of IL-17 than mice injected with PBS (Figure 3.22).

Interestingly, 72 hours after injection, PS particle size influenced the cytokine profiles from restimulated PECs. Following restimulation with anti-CD3, PECs recovered 72 hours

after mice were injected with 30μm and 100μm PS particles secreted increased levels of IL-4, IFN-γ, IL-17 but less IL-10 secretion than controls (Figure 3.23). Injection of 10μm PS particles induced a similar profile from restimulated PECs 72 hours after injection, including a significant increase in IL-4 secretion as well as an increase in IFN-γ and decrease in IL-10 secretion (Figure 3.23). Restimulation with anti-CD3 in combination with PMA elicited a similar size-dependent cytokine profile. Remarkably, all sized PS particles significantly reduced the ability of restimulated PECs to secrete IL-10 (Figure 3.23).

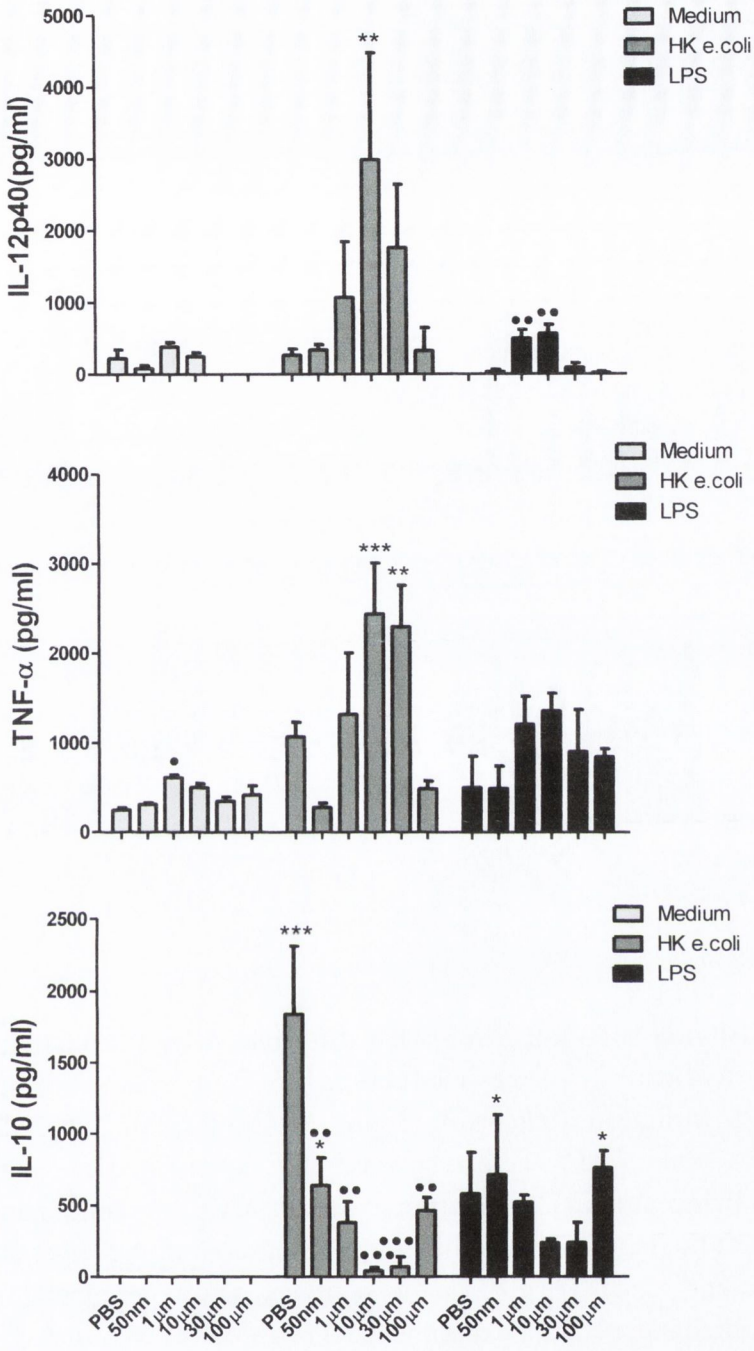

Figure 3.21 – 24 hours after injection with different sized PS particles restimulated PECs exhibit differential cytokine production. C57BL/6 mice were injected i.p. with PBS or 4mg of PS particles (50nm, 1μm, 10μm, 30μm or 100μm) in 200μl volumes and sacrificed after 24 hours. PECs were recovered and restimulated *ex vivo* with complete RPMI 1640 medium, HK *E. coli* (10 bacteria/cell) or LPS (1μg/ml). After 24 hours, cytokine profiles were measured in the supernatant by ELISA. Bar charts represent mean (+ standard error of the mean (SEM)) for 3 mice per experimental group. Results representative of two independent experiments. Versus cells restimulated with medium, * $p<0.05$, ** $p<0.01$, *** $p<0.0001$. Versus cells from mice injected with PBS and restimulated with the same stimulus, • $p<0.05$, •• $p<0.01$, ••• $p<0.0001$.

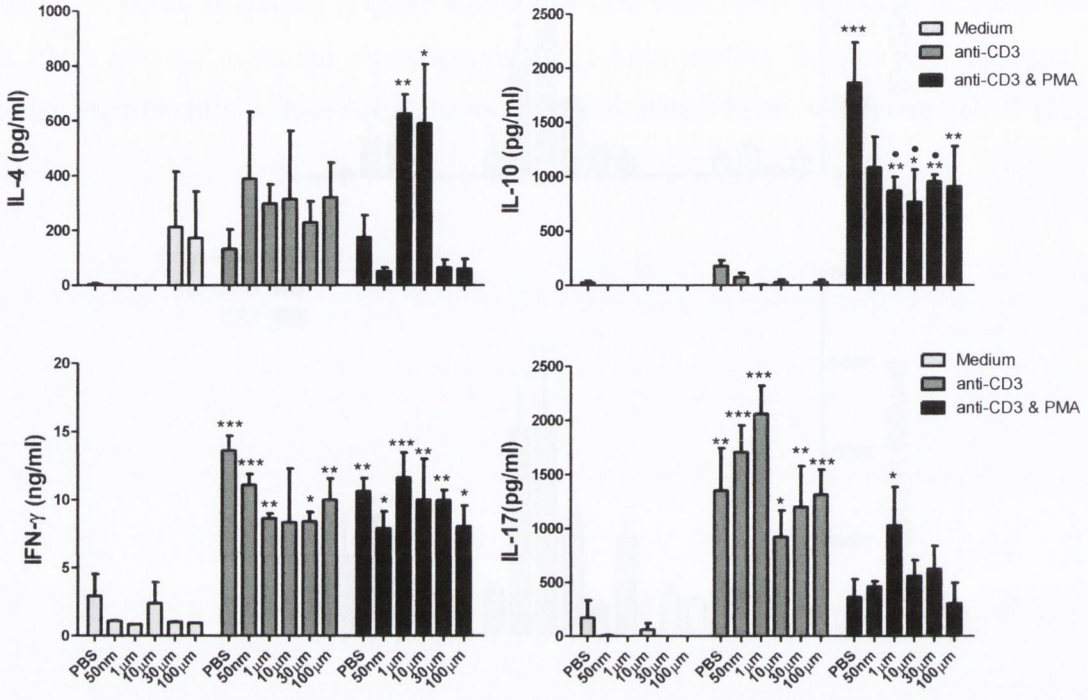

Figure 3.22 – 24 hours after injection with different sized PS particles restimulated PECs exhibit differential cytokine production. C57BL/6 mice were injected i.p. with PBS or 4mg of PS particles (50nm, 1µm, 10µm, 30µm or 100µm) in 200µl volumes and sacrificed after 24 hours. PECs were recovered and restimulated *ex vivo* with complete RPMI 1640 medium, anti-CD3 (0.2µg/ml) or anti-CD3 in combination with PMA (25ng/ml). After 72 hours, cytokine profiles were measured in the supernatant by ELISA. Bar charts represent mean (+ SEM) for 3 mice per experimental group. Results representative of three independent experiments. Versus cells restimulated with medium, * $p<0.05$, ** $p<0.01$, *** $p<0.0001$. Versus cells from mice injected with PBS and restimulated with the same stimulus, • $p<0.05$.

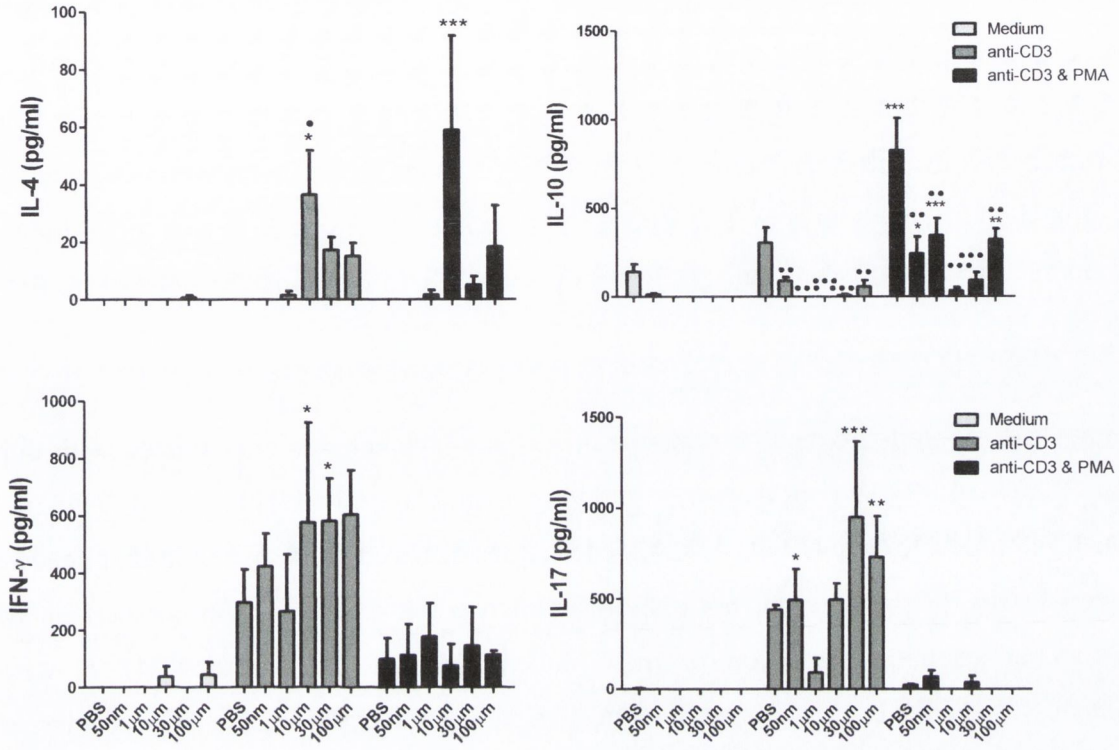

Figure 3.23 – 72 hours after injection with different sized PS particles restimulated PECs exhibit differential cytokine production. C57BL/6 mice were injected i.p. with PBS or 4mg of PS particles (50nm, 1μm, 10μm, 30μm or 100μm) in 200μl volumes and sacrificed after 72 hours. PECs were recovered and restimulated *ex vivo* with complete RPMI 1640 medium, anti-CD3 (0.2μg/ml) or anti-CD3 in combination with PMA (25ng/ml). After 72 hours, cytokine profiles were measured in the supernatant by ELISA. Bar charts represent mean (+ SEM) for 3 mice per experimental group. Results representative of two independent experiments. Versus cells restimulated with medium, * $p<0.05$, ** $p<0.01$, *** $p<0.0001$. Versus cells from mice injected with PBS and restimulated with the same stimulus, • $p<0.05$, •• $p<0.01$, ••• $p<0.0001$.

3.3.13. PS particle size modulates cytokine production from restimulated splenocytes

Having shown that cells at the site of injection are capable of being modulated to differentially induce the secretion of cytokines after restimulation, the ability of i.p. injection of PS particles to modulate cytokine profiles in splenocytes was investigated. To assess if PS particle size could influence the ability of splenocytes to secrete different cytokines, C57BL/6 mice were injected i.p. with PBS or PS particles (50nm, 1μm, 10μm, 30μm or 100μm) and were sacrificed after 24 or 72 hours. Splenocytes were recovered and restimulated *ex vivo* with complete RPMI 1640 medium, LPS or HK *E. coli* for 24 hours or complete RPMI 1640 medium, anti-CD3 or anti-CD3 in combination with PMA for 72 hours.

There was no modulation of cytokine profiles from splenocytes restimulated with either HK *E. coli* or LPS (data not known). Following restimulation with either anti-CD3 alone or anti-CD3 in combination with PMA, splenocytes recovered 24 hours after mice were injected with PS particles did not exhibit an altered cytokine profile in comparison with splenocytes isolated from control mice injected with PBS (Figure 3.24). However, splenocytes recovered 72 hours after mice were injected with 100μm PS particles, and upon restimulation with anti-CD3 in combination with PMA, secreted significantly more IL-4 than mice injected with PBS (Figure 3.25). Secretion of the other cytokines assayed for were not modulated based on PS particle size, apart from a reduction in IL-10, IFN-γ and IL-17 in splenocytes from mice injected with 1μm PS particles (Figure 3.25).

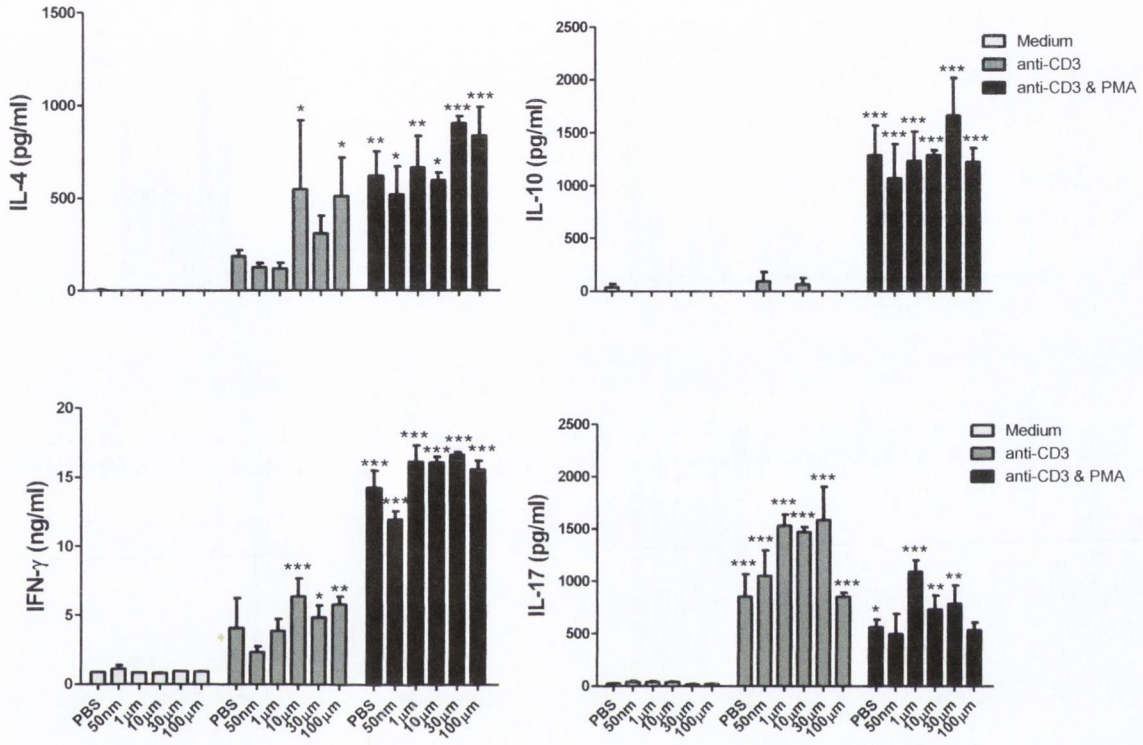

Figure 3.24 – Characterisation of the splenocyte response 24 hours after restimulation. C57BL/6 mice were injected i.p. with PBS or 4mg of PS particles (50nm, 1µm, 10µm, 30µm or 100µm) in 200µl volumes. The mice were sacrificed after 24 hours. Splenocytes were recovered and restimulated *ex vivo* with complete RPMI 1640 medium, anti-CD3 (0.2µg/ml) or anti-CD3 in combination with PMA (25ng/ml). After 24 hours, cytokine profiles were measured in the supernatant by ELISA. Bar charts represent mean (+ SEM) for 4 mice per experimental group. Results representative of two independent experiments. Versus cells restimulated with medium, * $p<0.05$, ** $p<0.01$, *** $p<0.0001$.

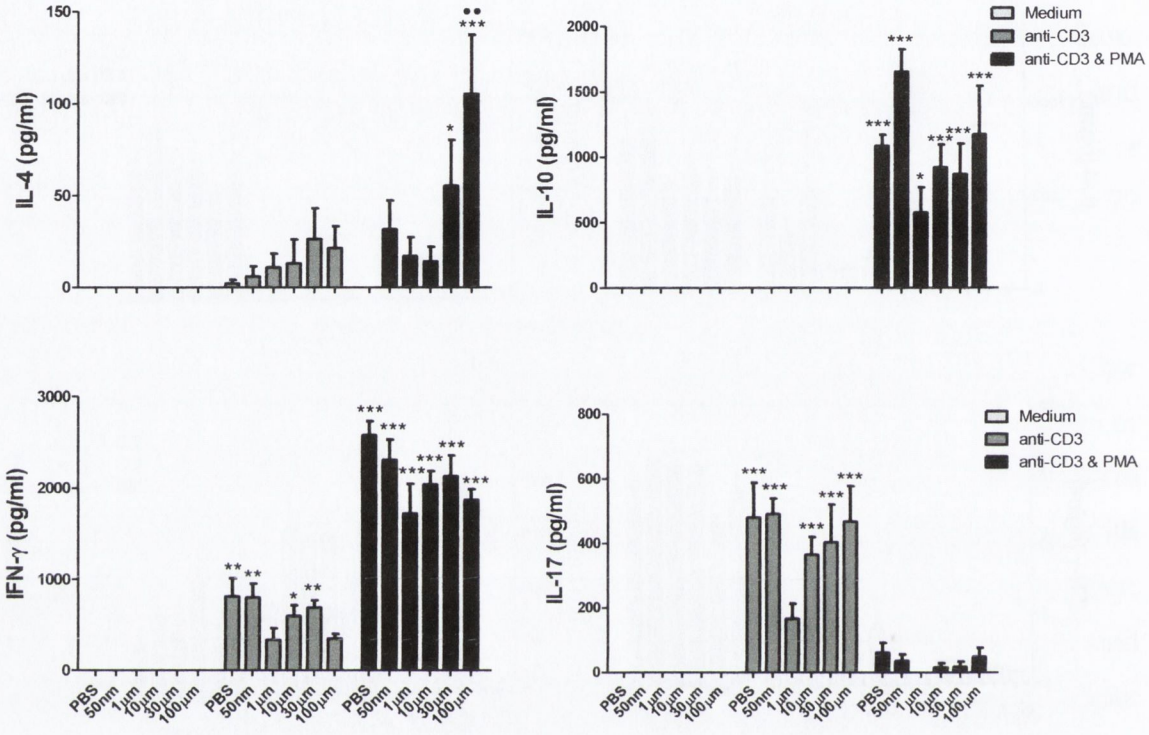

Figure 3.25 – Characterisation of the splenocyte response 72 hours after restimulation. C57BL/6 mice were injected i.p. with PBS or 4mg of PS particles (50nm, 1µm, 10µm, 30µm or 100µm) in 200µl volumes. The mice were sacrificed after 72 hours. Splenocytes were recovered and restimulated *ex vivo* with complete RPMI 1640 medium, anti-CD3 (0.2µg/ml) or anti-CD3 in combination with PMA (25ng/ml). After 24 hours, cytokine profiles were measured in the supernatant by ELISA. Bar charts represent mean (+ SEM) for 4 mice per experimental group. Results representative of two independent experiments. Versus cells restimulated with medium, * $p<0.05$, ** $p<0.01$, *** $p<0.0001$. Versus cells from mice injected with PBS and restimulated with the same stimulus, •• $p<0.01$.

3.3.14. PS particle size modulates cytokine production from restimulated lymph node cells

To determine if restimulated cells from the draining lymph nodes, the mediastinal lymph nodes, were also capable of secreting differential cytokine profiles, C57BL/6 mice were injected i.p. with PBS or PS particles (50nm, 1μm, 10μm, 30μm or 100μm) and sacrificed after 24 hours. Mediastinal lymph node cells were recovered and restimulated *ex vivo* with complete RPMI 1640 medium, LPS or HK *E. coli* for 24 hours or complete RPMI 1640 medium, anti-CD3 or anti-CD3 in combination with PMA for 72 hours.

There was no modulation of cytokine profiles from mediastinal lymph node cells restimulated with either HK *E. coli* or LPS (data not known). Following restimulation with either anti-CD3 or anti-CD3 in combination with PMA, mediastinal lymph node cells recovered 24 hours after mice were injected with PS particles elicited an altered cytokine profile in comparison with mediastinal lymph node cells isolated from control mice injected with PBS (Figure 3.26). Mediastinal lymph node cells recovered from mice injected with 30μm and 100μm PS particles produced less IL-4, IL-10, IFN-γ and IL-17 secretion than controls when restimulated with anti-CD3 and anti-CD3 in combination with PMA (Figure 3.26). Interestingly it was injection of smaller sized PS particles, specifically 50nm and 1μm, that enhanced the ability of restimulated mediastinal lymph node cells to secrete IL-10.

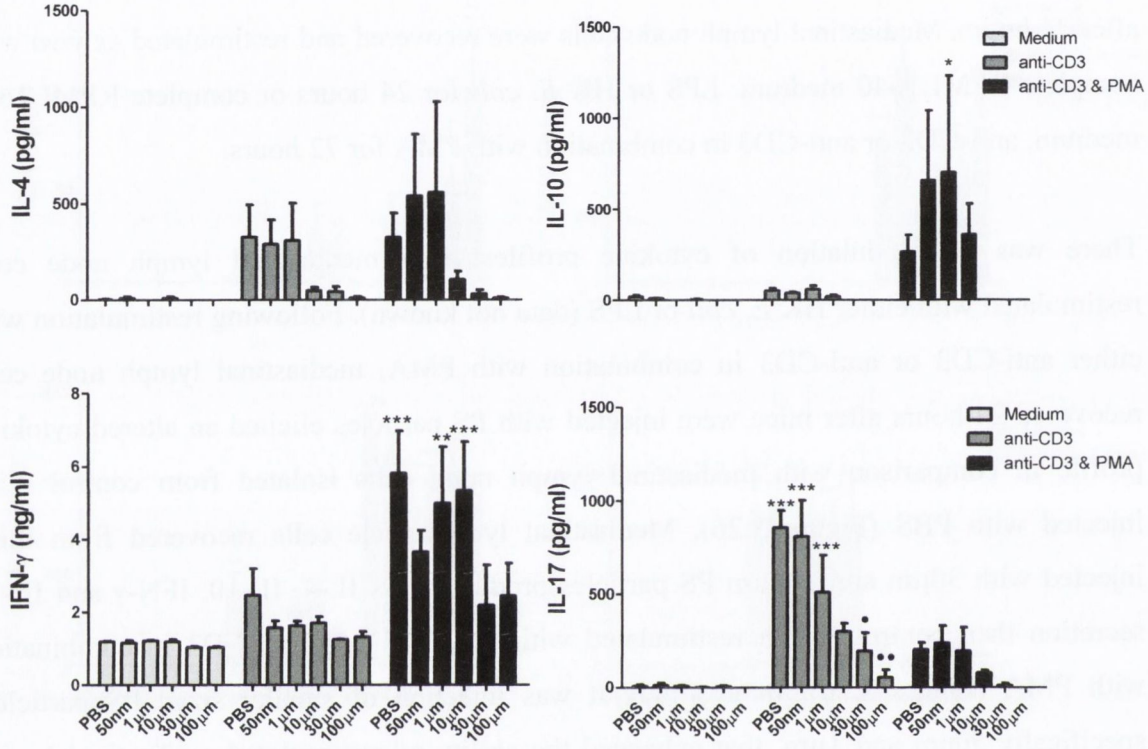

Figure 3.26 – Characterisation of the draining lymph node response 24 hours after restimulation. C57BL/6 mice were injected i.p. with PBS or 4mg of PS particles (50nm, 1μm, 10μm, 30μm or 100μm) in 200μl volumes. The mice were sacrificed after 24 hours. Mediastinal lymph node cells were recovered and restimulated *ex vivo* with complete RPMI 1640 medium, anti-CD3 (0.2μg/ml) or anti-CD3 in combination with PMA (25ng/ml). After 24 hours, cytokine profiles were measured in the supernatant by ELISA. Bar charts represent mean (+ SEM) for 3 mice per experimental group. Results representative of three independent experiments. Versus cells restimulated with medium, * $p<0.05$, ** $p<0.01$, *** $p<0.0001$. Versus cells from mice injected with PBS and restimulated with the same stimulus, • $p<0.05$, •• $p<0.01$.

3.3.15. IL-4 mRNA expression is up-regulated in PECs 3 hours after injection with PS particles

IL-4 secretion was significantly modulated from restimulated PECs, splenocytes and mediastinal lymph node cells recovered after injection with different sized PS particles, hence it was ascertained if IL-4 and IL-4Rα expression were differentially regulated in response to PS particle size. Real time PCR was used to analyse IL-4Rα and IL-4 mRNA expression. C57BL/6 mice were injected i.p. with PBS or PS particles (50nm, 1μm, 10μm, 30μm or 100μm) and were sacrificed after 3, 24 or 72 hours. PECs, splenocytes and mediastinal lymph node cells were isolated and Real time PCR was used to analyse mRNA expression in each of the tissues. β-actin, a housekeeping gene, was used to calculate mRNA fold induction. Since distal responses in the spleen and draining lymph nodes occur after the onset of a local response, mRNA expression was analysed at later time points only in these tissues.

Interestingly, 3 hours after injection with 1μm, 10μm and 30μm PS particles there was an increase in IL-4 mRNA expression in PECs (Figure 3.27). Neither the smallest (50nm) nor the largest (100μm) PS particles induced this increase in IL-4 mRNA expression. Injection with 10μm PS particles also induced an increase in IL-4Rα mRNA expression in PECs. At later time points, IL-4 and IL-4Rα mRNA expression in PECs taken from mice injected with all sized PS particles was similar to mice injected with PBS (Figure 3.27).

Correlating with the lack of IL-4Rα expression on splenocytes when analysed by FACS (data not shown), 24 and 72 hours after injection with PS particles there was no modulation of IL-4Rα mRNA expression in splenocytes (Figure 3.28). Similarly, there was no increase in IL-4 mRNA expression in splenocytes 24 and 72 hours after injection with PS particles.

In mediastinal lymph node cells there was also no modulation of IL-4Rα mRNA expression after injection with PS particles (Figure 3.29). However, IL-4 mRNA expression was induced in mediastinal lymph node cells 72 hours after injection with 50nm PS particles (Figure 3.29).

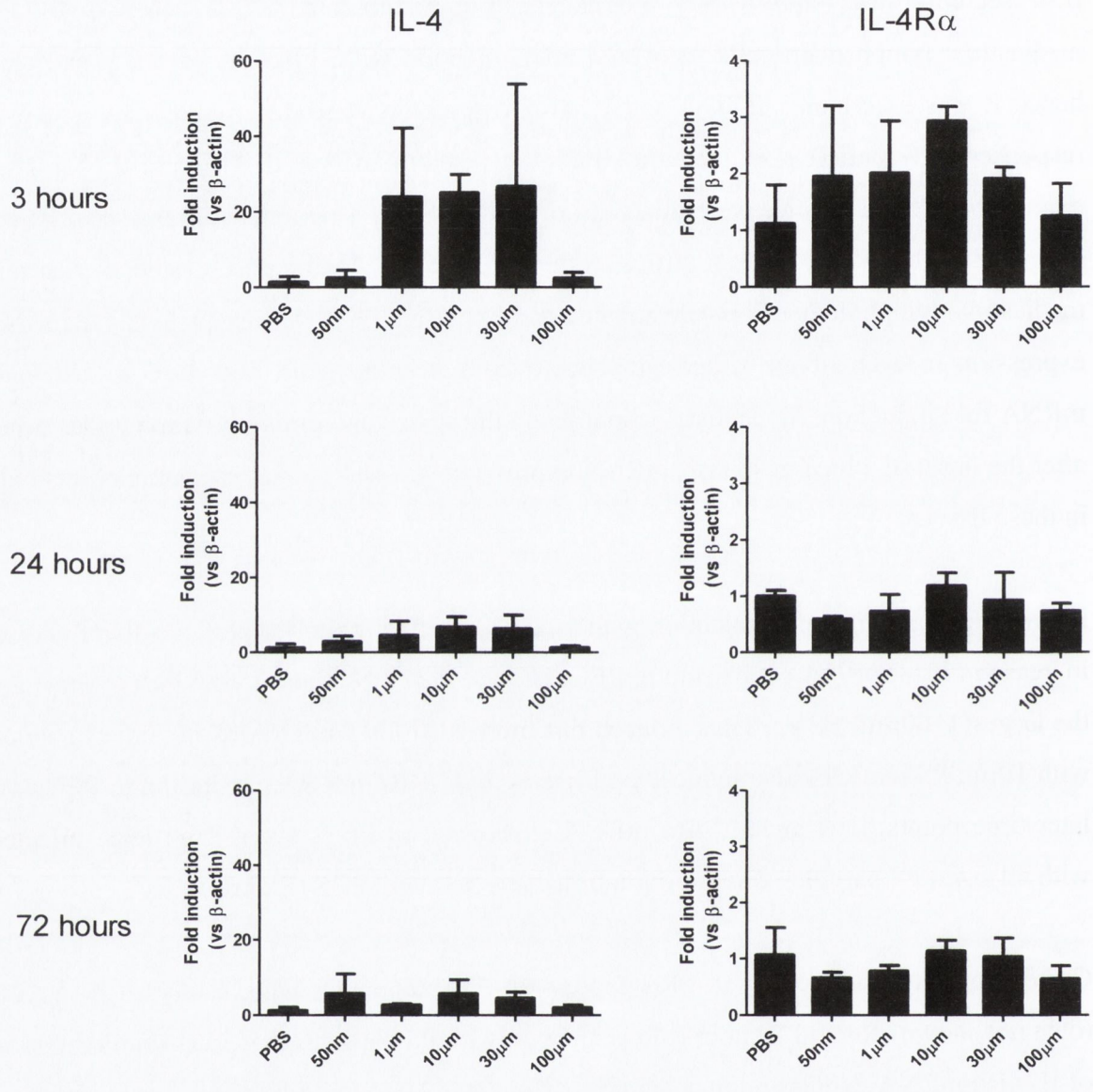

Figure 3.27 – PS particles modulate IL-4 and IL-4Rα mRNA expression in PECs 3 hours after injection. C57BL/6 mice were injected i.p. with PBS or 4mg of PS particles (50nm, 1μm, 10μm, 30μm or 100μm) in 200μl volumes. The mice were sacrificed after 3, 24 or 72 hours and PECs were isolated. RNA was extracted from cells and IL-4 and IL-4Rα mRNA expression was determined by real time PCR. Fold induction was determined against β-actin mRNA. Bar charts represent mean (+ SD) for 3 or 4 mice per experimental group. Results representative of two or three independent experiments.

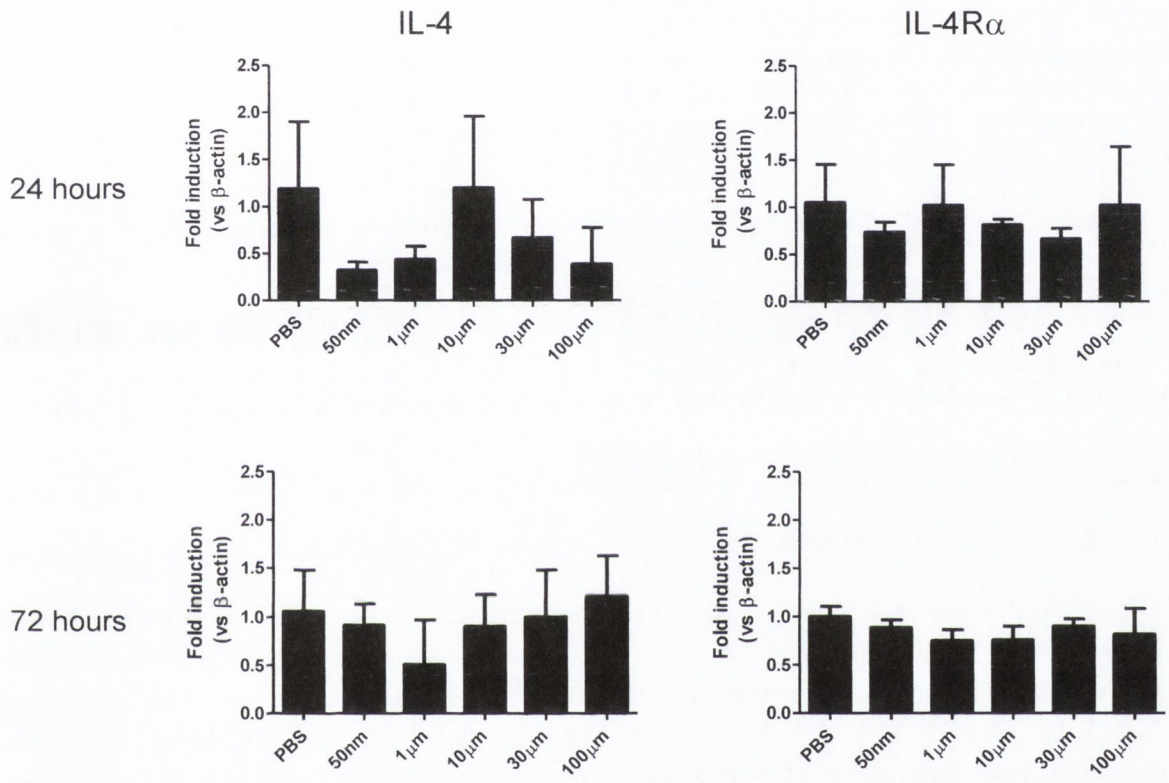

Figure 3.28 – Injection of PS particles has no effect on IL-4 or IL-4Rα mRNA expression in splenocytes. C57BL/6 mice were injected i.p. with PBS or 4mg of PS particles (50nm, 1μm, 10μm, 30μm or 100μm) in 200μl volumes. The mice were sacrificed after 24 or 72 hours and splenocytes were isolated. RNA was extracted from cells and IL-4 and IL-4Rα mRNA expression was determined by real time PCR. Fold induction was determined against β-actin mRNA. Bar charts represent mean (+ SD) for 3 or 4 mice per experimental group. Results representative of two or three independent experiments.

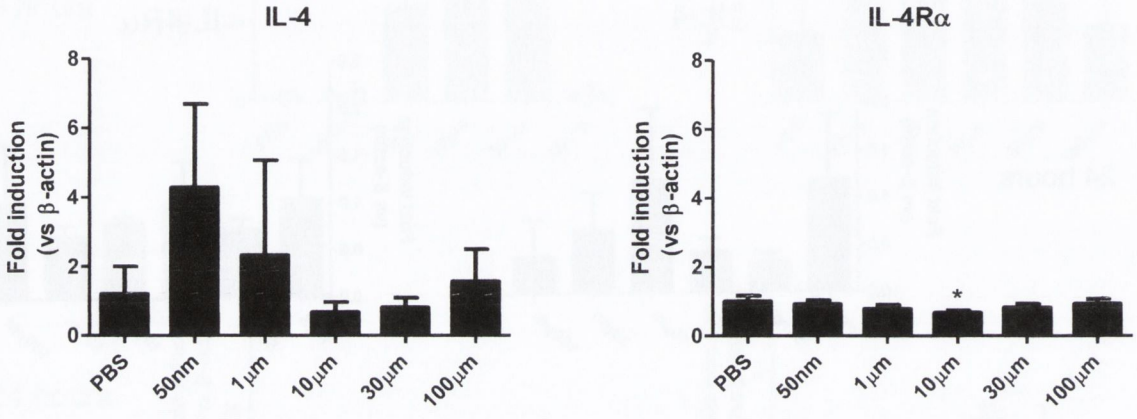

Figure 3.29 – 50nm PS particles drive IL-4 mRNA expression in mediastinal lymph node cells 72 hours after injection. C57BL/6 mice were injected i.p. with PBS or 4mg of PS particles (50nm, 1μm, 10μm, 30μm or 100μm) in 200μl volumes. The mice were sacrificed after 72 hours and mediastinal lymph node cells were isolated. RNA was extracted from cells and IL-4 and IL-4Rα mRNA expression was determined by real time PCR. Fold induction was determined against β-actin mRNA. Bar charts represent mean (+ SD) for 4 mice per experimental group. Results representative of two independent experiments. Versus PBS, * $p<0.05$.

3.3.16. IL-4Rα expression is not up-regulated in PECs 24 or 72 hours after injection with PS particles

Particle size influenced IL-4 mRNA expression in PECs (Figure 3.27) as well as influencing the ability to secrete IL-4 after restimulation (Figure 3.22, 3.23). To ascertain if IL-4 was involved in local regulation and/or signalling, the up-regulation of IL-4Rα on cells after injection with different sized PS particles was determined. First, a titration of the PE conjugated anti-CD124 (IL-4Rα) antibody was required. Alum was used to titrate the antibody as it is a potent driver of inflammation at the local site. C57BL/6 mice were injected i.p. with alum (1mg/mouse) and were sacrificed after 24 hours. PECs were isolated and PE conjugated anti-CD124 was used at several concentrations based on published data (0.2μg/ml, 0.4μg/ml, 1μg/ml, 2μg/ml or 4μg/ml)[372]. IL-4Rα expression was analysed using histograms.

Populations of cells were gated as before (Figure 3.2-3.7). All concentrations of antibody were capable of distinguishing an IL-4Rα positive population on all cell types (Figure 3.30). When focusing on eosinophils, 0.2μg/ml of PE conjugated anti-CD124 antibody did not separate an IL-4Rα positive and negative population as clearly as higher concentrations of the antibody (Figure 3.30). Hence in all further experiments 0.4μg/ml PE conjugated anti-CD124 was used.

To confirm that the commercial antibody was specific to the IL-4Rα, an isotype antibody on the same κ chain was included. C57BL/6 mice were injected i.p. with PBS or PS particles (50nm, 1μm, 10μm, 30μm or 100μm) and were sacrificed after 24 or 72 hours. PECs were isolated and analysed by flow cytometry as before using either the PE conjugated anti-CD124 or the PE conjugated isotype control. When compared with the isotype control, the commercial antibody stained a unique population as IL-4Rα positive when gated on live cells (Figure 3.31). This unique population was distinct in PECs isolated from mice injected with all sized PS particles. Using isotype controls and the most appropriate concentration of antibody as indicated by the titration study, the expression of IL-4Rα on individual cell populations was determined.

Using 0.4μg/ml PE conjugated anti-CD124 and comparing with isotype controls, C57BL/6 mice were injected i.p. with PBS or PS particles (50nm, 1μm, 10μm, 30μm or 100μm). PECs and splenocytes were isolated and analysed by flow cytometry for IL-4Rα

expression on infiltrating cell populations. IL-4Rα expression was unchanged on all splenocyte granulocyte and lymphocyte populations examined (data not shown).

IL-4Rα expression was also unchanged on neutrophils isolated from mice 24 and 72 hours after injection with different sized PS particles (Figure 3.32). A similar trend was seen with monocytes and pro-inflammatory macrophages (Figure 3.33, 3.34). Although eosinophils isolated from the peritoneum of mice 72 hours after injection with 1μm PS particles had a significantly higher IL-4Rα MFI value (Figure 3.35), this is not validated visually by histogram analysis and likely correlates with the number of eosinophils found in the peritoneum 72 hours after injection with 1μm PS particles (Figure 3.6D). Similarly, resident macrophage numbers were so low in the peritoneum 24 and 72 hours after injection with most sized PS particles that IL-4Rα MFI values were not calculable.

The expression of IL-4Rα on T cells and B cells was also examined. T cells were gated as $CD3^+$ $CD4^+$ or $CD3^+$ $CD8^+$ (Figure 3.36) and B cells were gated as $CD19^+$ (Figure 3.37). There was no increase in IL-4Rα expression on T cells or B cells after injection with PS particles (Figure 3.36, 3.37).

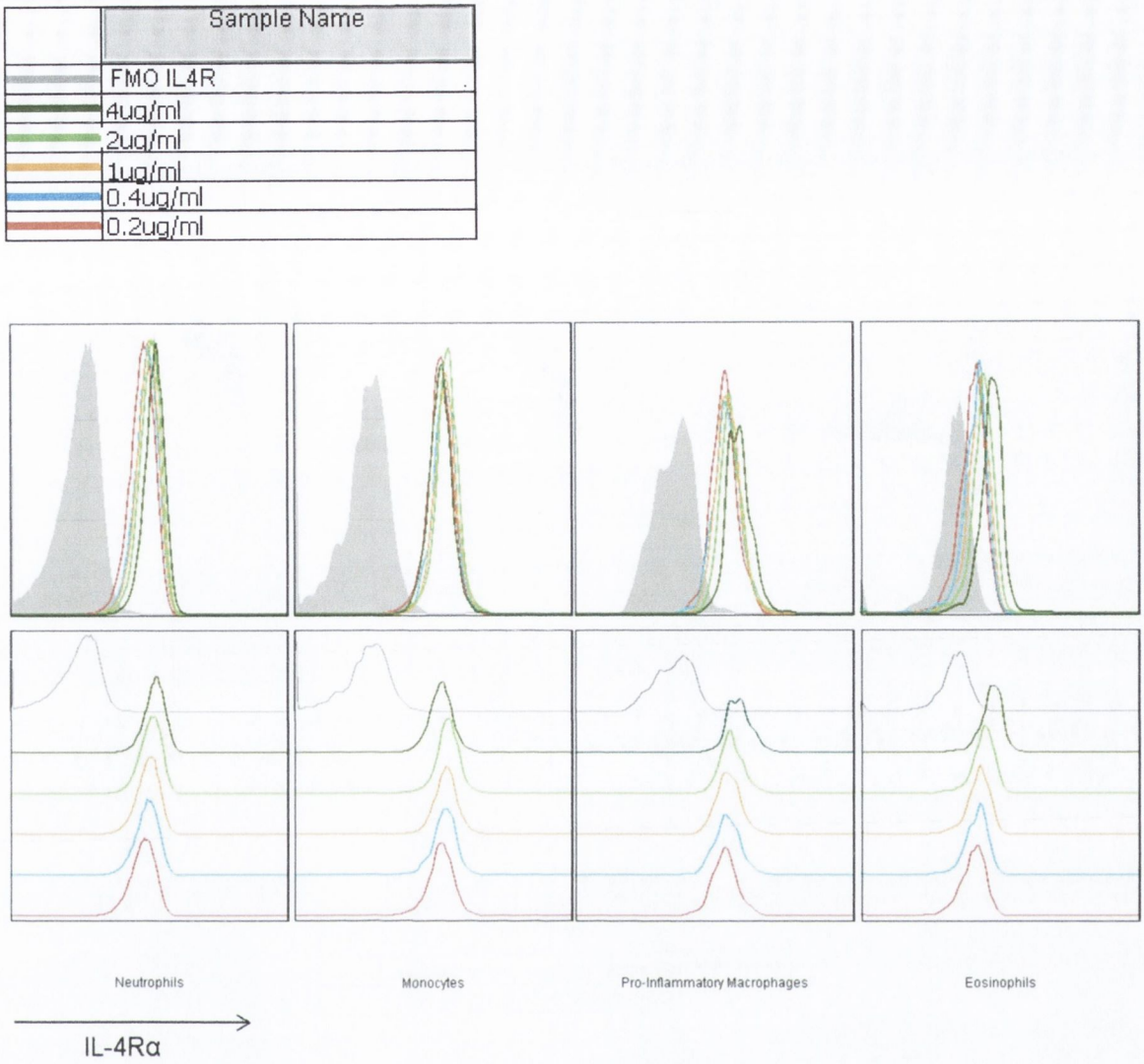

Figure 3.30 – Most concentrations of PE conjugated anti-CD124 distinguish IL-4Rα positive populations. C57BL/6 mice were injected i.p. with alum (1mg/mouse) in 200µl volumes and the mice were sacrificed after 24 hours. PECs were collected and cells incubated with extracellular cell markers along with either 0.2µg/ml, 0.4µg/ml, 1µg/ml, 2µg/ml or 4µg/ml of PE conjugated anti-CD124 antibody. MFI values are graphed both overlaid (top panel) and offset for neutrophils ($CD11b^+$ $Gr1^{high}$ $F4/80^-$), monocytes ($CD11b^+$ $F4/80^+$ $SiglecF^-$ SSC^{low} $MHCcII^-$), pro-inflammatory macrophages ($CD11b^+$ $F4/80^+$ $SiglecF^-$ SSC^{low} $MHCcII^+$) and eosinophils ($CD11b^+$ $Gr1^-$ $SiglecF^+$).

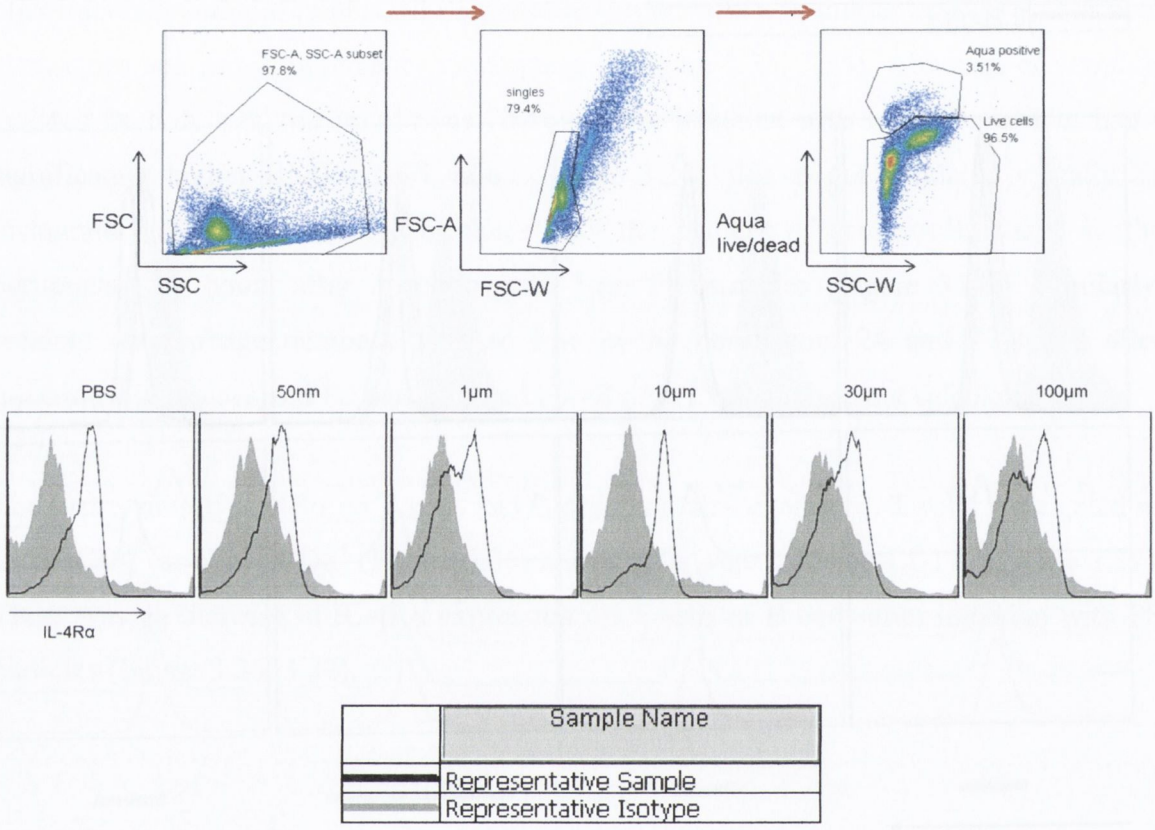

Figure 3.31 – PE conjugated anti-CD124 distinguishes IL-4Rα specific populations. C57BL/6 mice were injected i.p. with PBS or 4mg of PS particles (50nm, 1µm, 10µm, 30µm or 100µm) in 200µl volumes. The mice were sacrificed after 24 hours and PECs were collected. Live cells were gated as Aqua live/dead$^-$ and IL-4Rα expression represented on histograms.

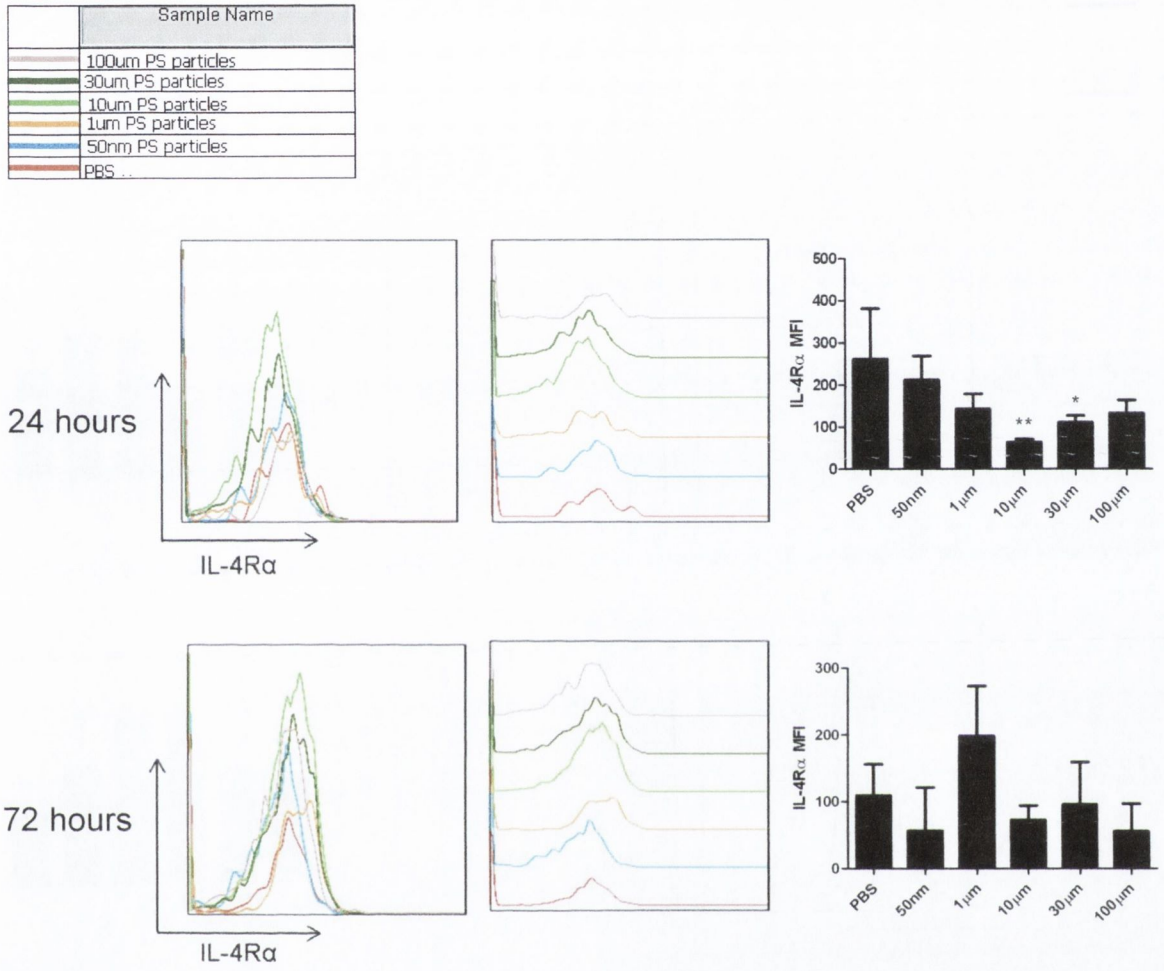

Figure 3.32 – Injection with PS particles does not enhance local neutrophil IL-4Rα expression. C57BL/6 mice were injected i.p. with PBS or 4mg of PS particles (50nm, 1μm, 10μm, 30μm or 100μm) in 200μl volumes. The mice were sacrificed after 24 or 72 hours and PECs were collected. Neutrophils were gated as $CD11b^{+}$ $Gr1^{high}$ $F4/80^{-}$ and IL-4Rα expression represented on histograms. IL-4Rα MFI values are graphed as bar charts and represent mean (+ SD) for 4 mice per experimental group. Results are representative of two independent experiments. Versus PBS, * $p<0.05$, ** $p<0.01$.

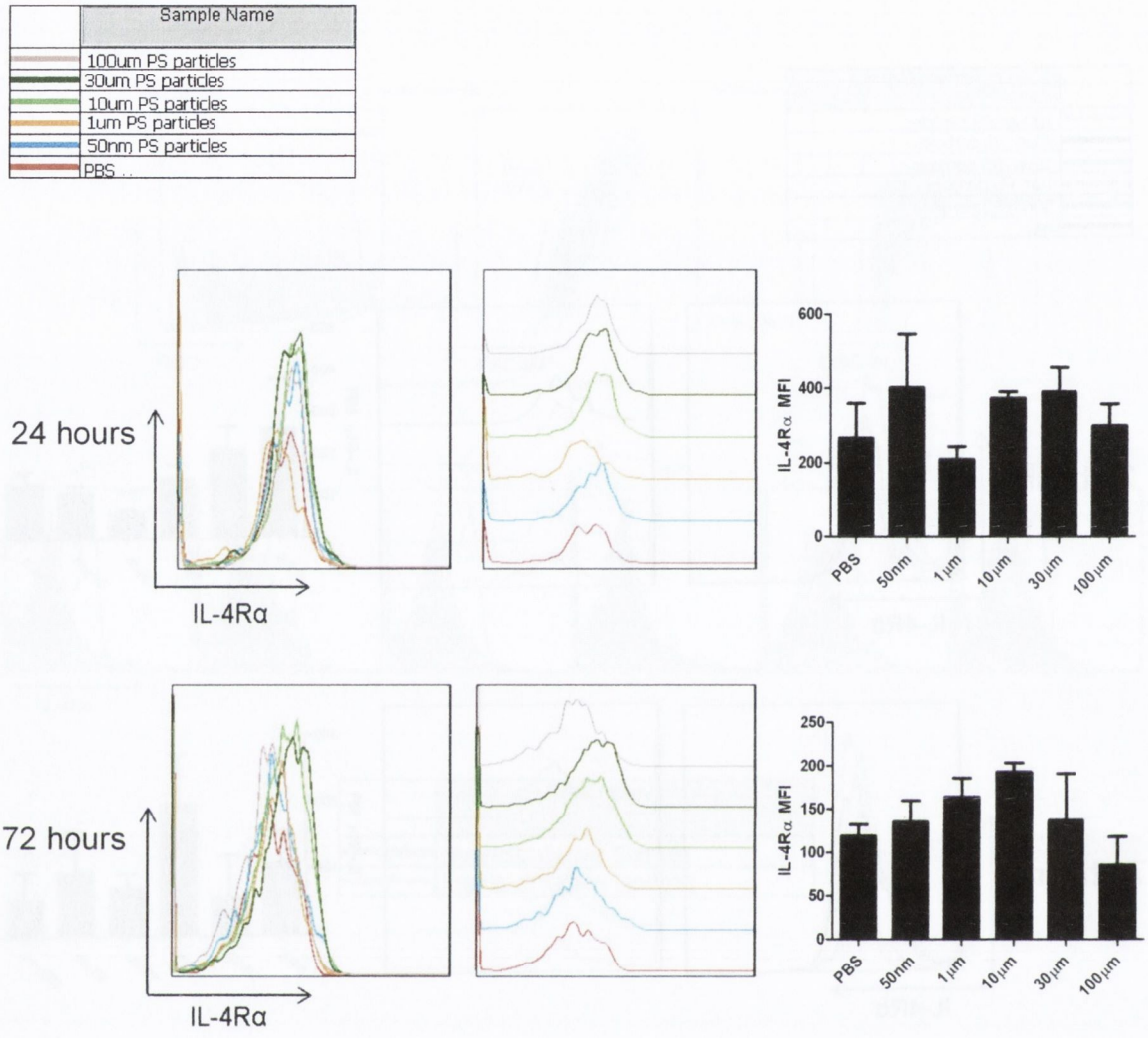

Figure 3.33 – Injection with PS particles does not enhance local monocyte IL-4Rα expression. C57BL/6 mice were injected i.p. with PBS or 4mg of PS particles (50nm, 1μm, 10μm, 30μm or 100μm) in 200μl volumes. The mice were sacrificed after 24 or 72 hours and PECs were collected. Monocytes were gated as $CD11b^{+}$ $F4/80^{+}$ $SiglecF^{-}$ SSC^{low} $MHCcII^{-}$ and IL-4Rα expression represented on histograms. IL-4Rα MFI values are graphed as bar charts and represent mean (+ SD) for 4 mice per experimental group. Results are representative of two independent experiments.

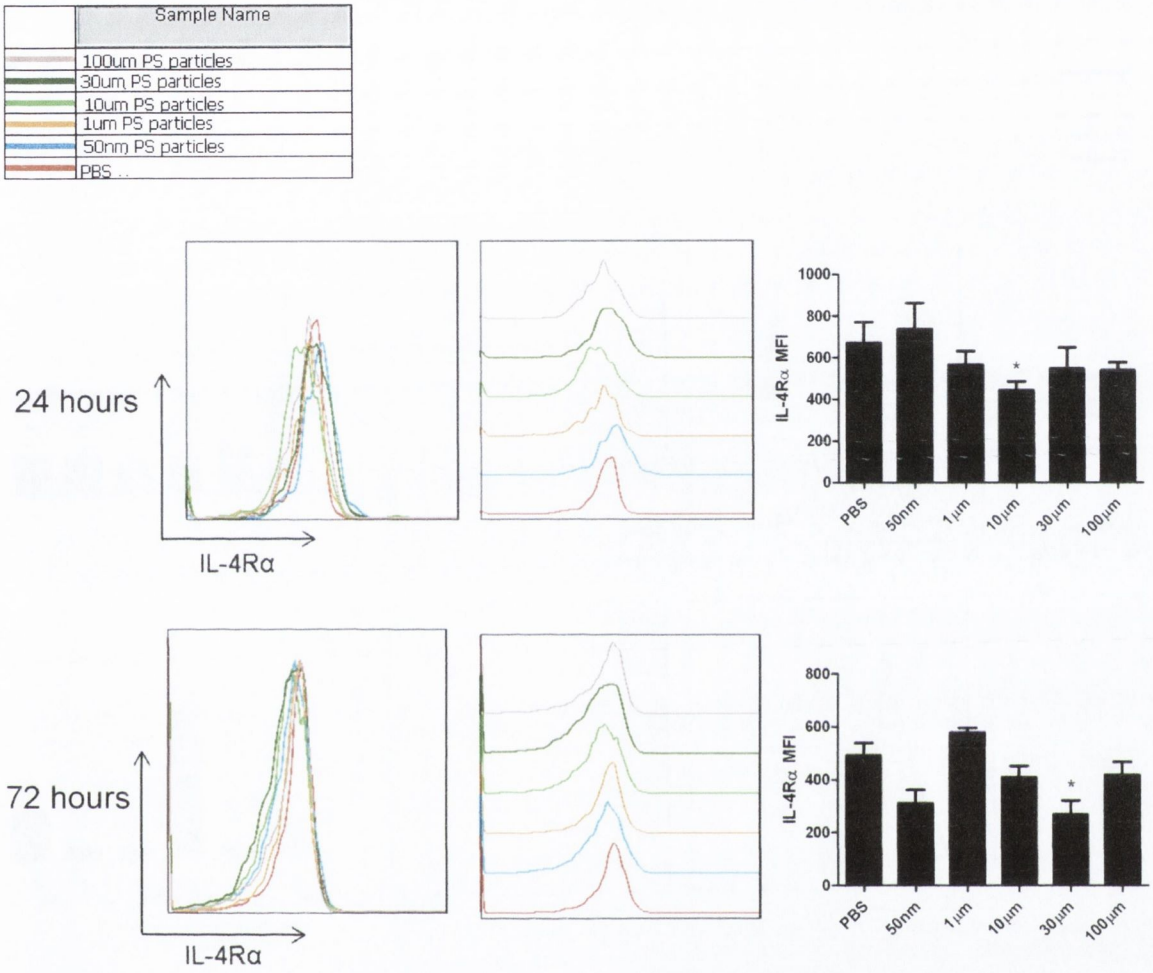

Figure 3.34 – Injection with PS particles does not enhance IL-4Rα expression in local pro-inflammatory macrophages. C57BL/6 mice were injected i.p. with PBS or 4mg of PS particles (50nm, 1μm, 10μm, 30μm or 100μm) in 200μl volumes. The mice were sacrificed after 24 or 72 hours and PECs were collected. Pro-inflammatory macrophages were gated as $CD11b^{+}$ $F4/80^{+}$ $SiglecF^{-}$ SSC^{low} $MHCcII^{+}$ and IL-4Rα expression represented on histograms. IL-4Rα MFI values are graphed as bar charts and represent mean (+ SD) for 4 mice per experimental group. Results are representative of two independent experiments. Versus PBS, * $p<0.05$.

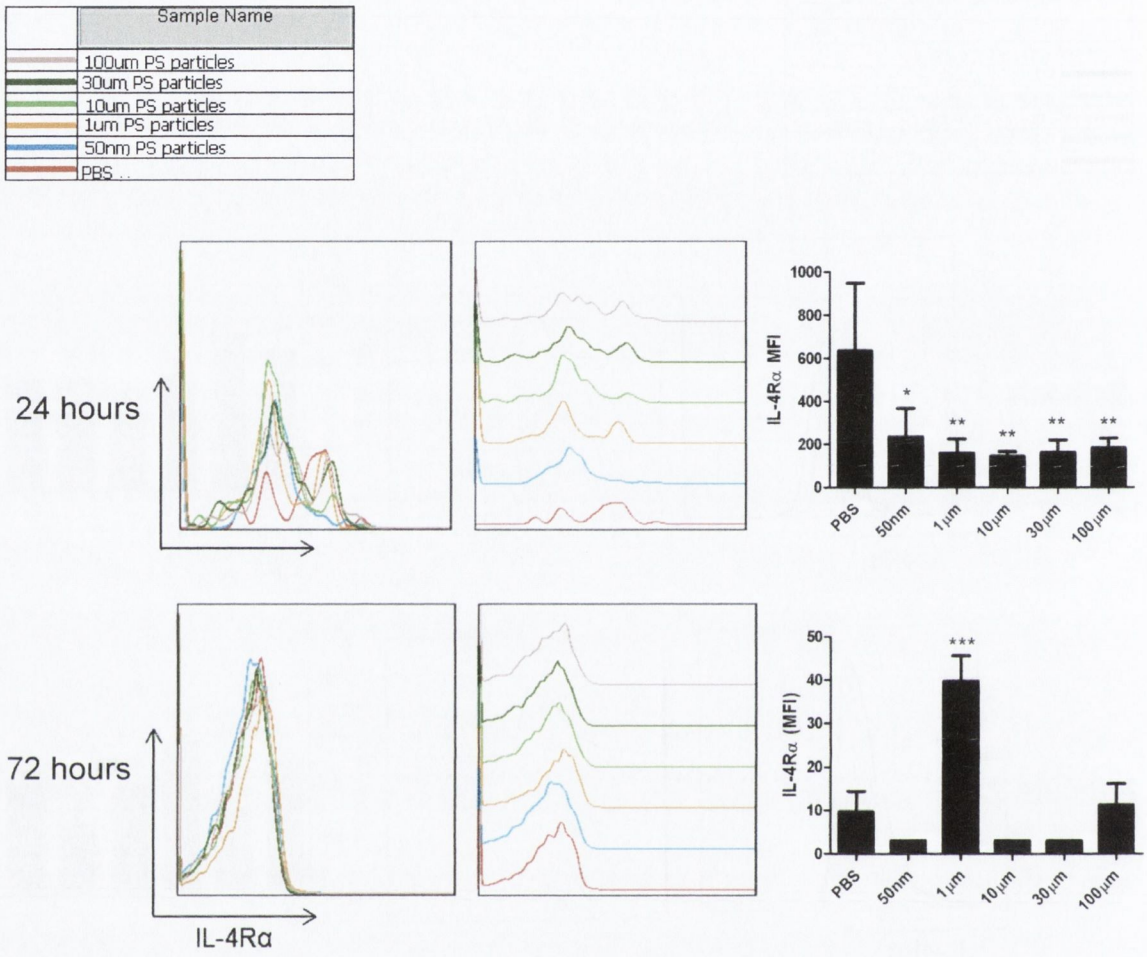

Figure 3.35 – Injection with PS particles does not enhance local eosinophil IL-4Rα expression 24 hours after injection. C57BL/6 mice were injected i.p. with PBS or 4mg of PS particles (50nm, 1μm, 10μm, 30μm or 100μm) in 200μl volumes. The mice were sacrificed after 24 or 72 hours and PECs were collected. Eosinophils were gated as $CD11b^{+}$ $Gr1^{-}$ $SiglecF^{+}$ and IL-4Rα expression represented on histograms. IL-4Rα MFI values are graphed as bar charts and represent mean (+ SD) for 4 mice per experimental group. Results are representative of two independent experiments. Versus PBS, * $p<0.05$, ** $p<0.01$, *** $p<0.0001$.

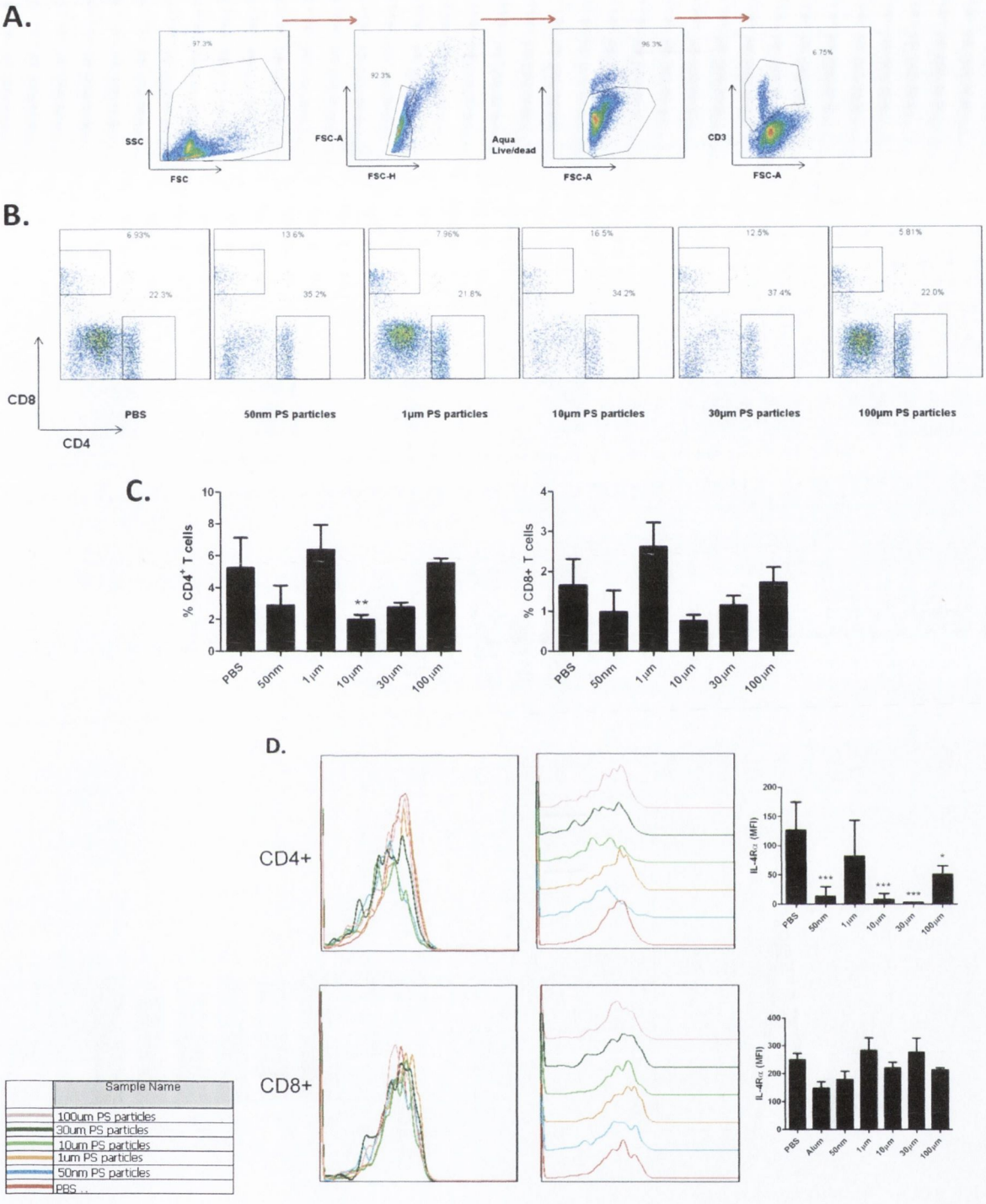

Figure 3.36 – Injection with PS particles does not enhance local T cell IL-4Rα expression. C57BL/6 mice were injected i.p. with PBS or 4mg of PS particles (50nm, 1µm, 10µm, 30µm or 100µm) in 200µl volumes. The mice were sacrificed after 72 hours and PECs were collected. T cells were gated as $CD3^+CD4^+$ or $CD3^+CD8^+$ (B, C) and IL-4Rα expression represented on histograms (D). IL-4Rα MFI values are graphed as bar charts and represent mean (+ SD) for 4 mice per experimental group. Versus PBS, * $p<0.05$, ** $p<0.01$, *** $p<0.0001$.

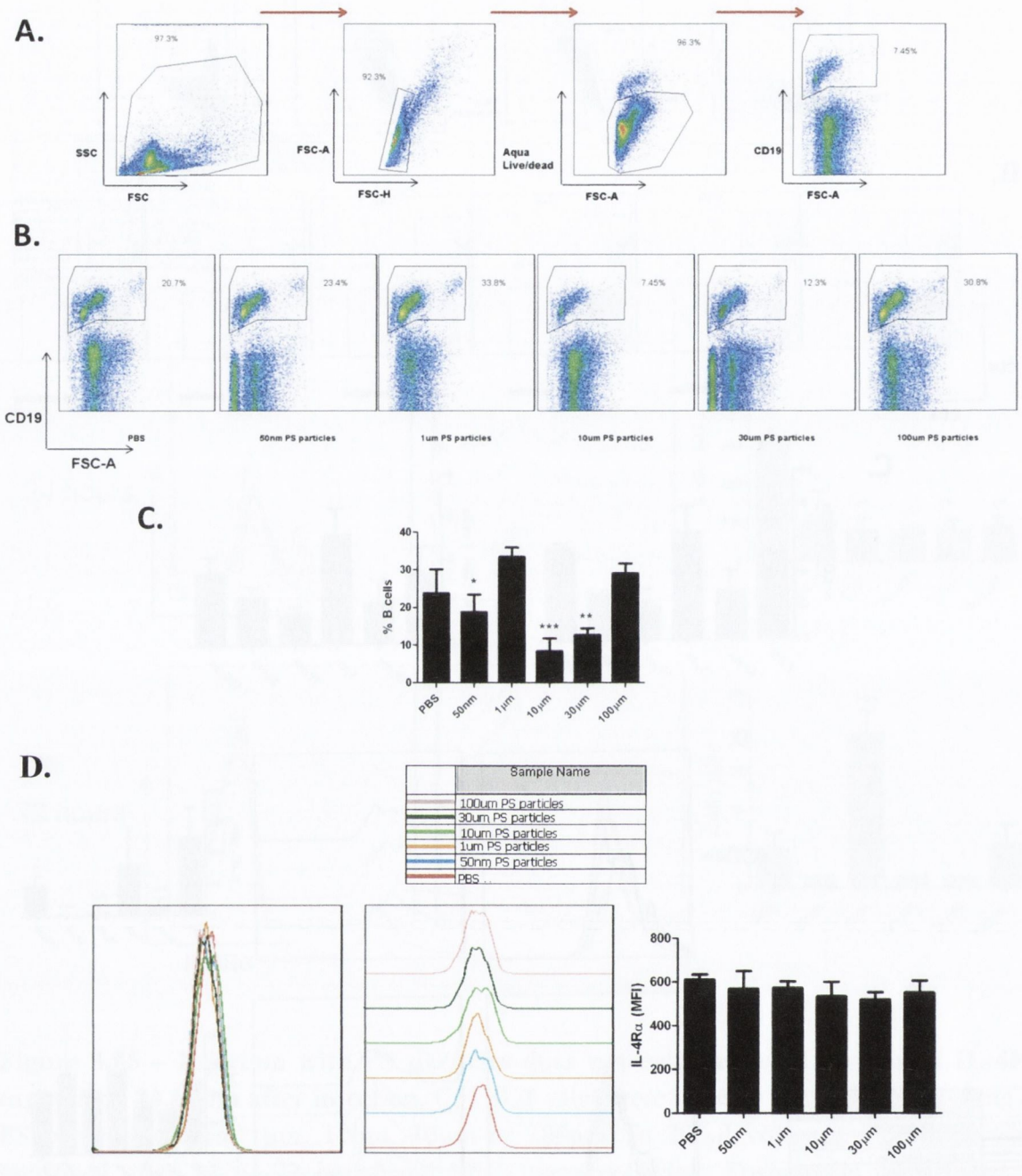

Figure 3.37 – Injection with PS particles does not enhance B cell IL-4Rα expression. C57BL/6 mice were injected i.p. with PBS or 4mg of PS particles (50nm, 1µm, 10µm, 30µm or 100µm) in 200µl volumes. The mice were sacrificed after 72 hours and PECs were collected. B cells were gated as $CD19^+$ (B, C) and IL-4Rα expression represented on histograms (D). IL-4Rα MFI values are graphed as bar charts and represent mean (+ SD) for 4 mice per experimental group. Versus PBS, * $p<0.05$, ** $p<0.01$, *** $p<0.0001$.

3.3.17. All sizes with the exception of 100μm PS particles can modulate mRNA cytokine expression 3 hours after injection

Based on the finding that expression of IL-4 and IL-4Rα mRNA was modulated to the greatest degree in PECs 3 hours after injection with PS particles (Figure 3.27), the mRNA expression of key pro-inflammatory mediators was also determined at this time point. C57BL/6 mice were injected i.p. with PBS or PS particles (50nm, 1μm, 10μm, 30μm or 100μm) and were sacrificed after 3 hours. PECs were isolated and real time PCR was used to analyse expression of inflammatory cytokines (IL-1α and IL-1β), as well as those associated with T cell differentiation (IL-10, IL-13, IL-17 and IL-12p40). β-actin, a housekeeping gene, was used to calculate mRNA fold induction.

50nm PS particles were the only size capable of inducing an increase in IL-1α mRNA expression 3 hours after injection. However, this size had no effect on IL-1β mRNA expression, whereas injection with 1μm, 10μm and 30μm PS particles all induced a significant increase in IL-1β mRNA expression when compared with PBS (Figure 3.38). Injection with both 1μm and 10μm PS particles simultaneously significantly up-regulated IL-10 mRNA expression at this time point (Figure 3.38).

Interestingly, the profile of IL-13 mRNA expression in PECs 3 hours after injection with PS particles (Figure 3.38) is similar to that of IL-4Rα (Figure 3.27), a component of the IL-13 receptor signalling pathway. All PS particle sizes except 100μm were capable of inducing small increases in both IL-13 and IL-4Rα mRNA expression in PECs (Figure 3.27, 3.38).

In parallel with the local cytokine and chemokine secretion and the cell restimulation data, mRNA expression of many cytokines was not modulated in a linear way that correlated with PS particle size. For example, IL-17 mRNA expression was significantly increased 3 hours after injection with 50nm and 10μm but not 1μm PS particles (Figure 3.38). The expression of IL-17 mRNA correlated with neutrophil infiltration after injection of 50nm and 10μm particles, indicating that IL-17 may be recruiting neutrophils to the injection site (Figure 3.2). In contrast, IL-12p40 mRNA expression was not changed in PECs 3 hours after injection with different sized PS particles (Figure 3.38). This does not negate that IL-12p19 and IL-12p35 mRNA could be modulated at this time point however these subunits were not investigated.

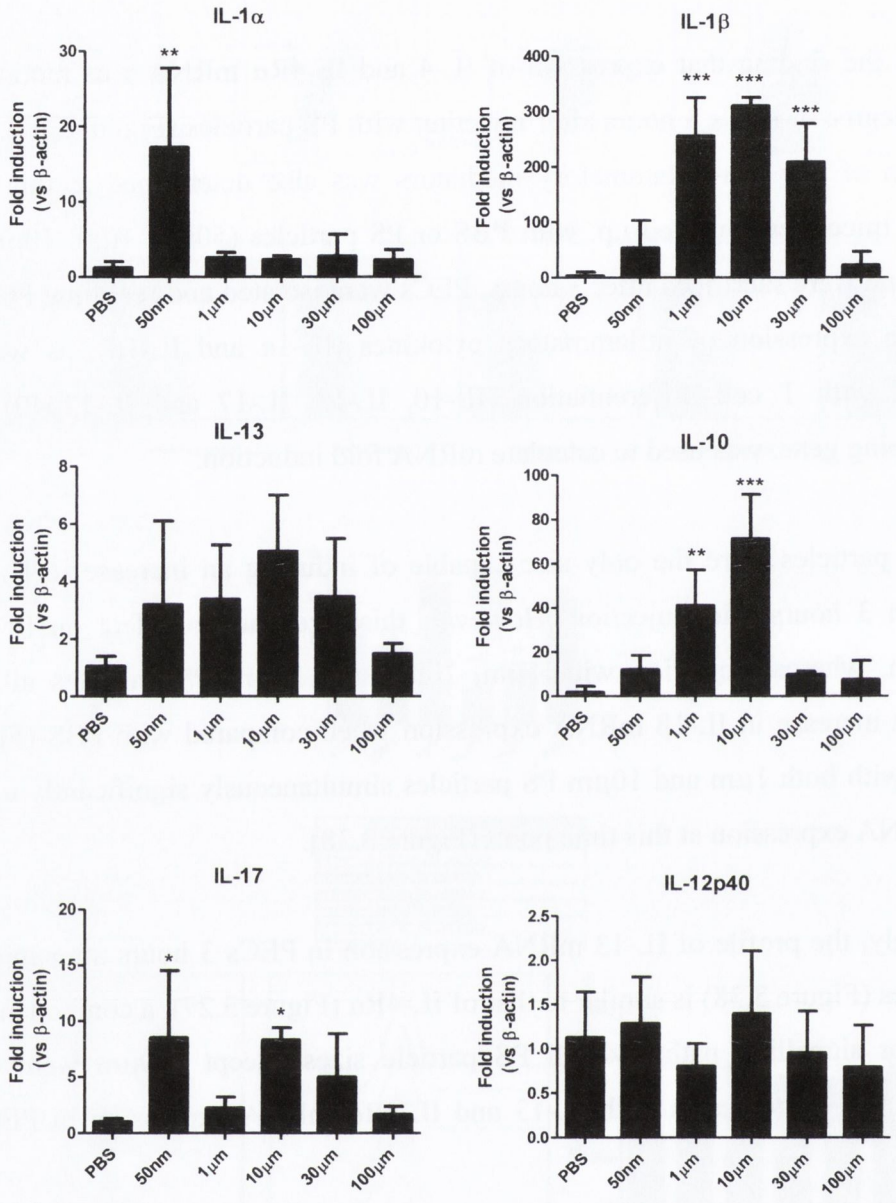

Figure 3.38 – PS particles modulate cytokine mRNA expression in PECs 3 hours after injection. C57BL/6 mice were injected i.p. with PBS or 4mg of PS particles (50nm, 1μm, 10μm, 30μm or 100μm) in 200μl volumes. The mice were sacrificed after 3 hours and PECs were isolated. RNA was extracted from cells and IL-1α, IL-1β, IL-10, IL-13, IL-17 and IL-12p40 mRNA expression was determined by real time PCR. Fold induction was determined against β-actin mRNA. Bar charts represent mean (+ SD) for 4 mice per experimental group. Results are representative of two independent experiments. Versus PBS, * $p<0.05$, ** $p<0.01$, *** $p<0.0001$.

3.3.18. Injection of 100μm PS particles induces the up-regulation of IL-9 mRNA in splenocytes

IL-4 mRNA expression in mediastinal lymph node cells was increased 72 hours after injection with 50nm PS particles (Figure 3.29). Since IL-13 is also involved in Th2-type responses, IL-13 mRNA expression was investigated. IL-4 has been proposed to have an anti-inflammatory role during acute inflammation as well as being involved in the differentiation of Th9 cells[174,371]. Hence the expression of IL-10 and IL-9 were investigated to determine if IL-10 was involved in regulating inflammation or IL-4 was inducing a Th9-type response.

C57BL/6 mice were injected i.p. with PBS or PS particles (50nm, 1μm, 10μm, 30μm or 100μm) and were sacrificed after 72 hours. Splenocytes and mediastinal lymph node cells were isolated and real time PCR was used to analyse IL-10, IL-13 and IL-9 mRNA expression from cells. β-actin, a housekeeping gene, was used to calculate mRNA fold induction.

Surprisingly, all sized PS particles except 50nm induced an increase in IL-10 mRNA expression in splenocytes 72 hours after injection. However this was not significant when compared with mice injected with PBS (Figure 3.39). These differences were not apparent in mediastinal lymph node cells at this time point (Figure 3.40). There was no change in IL-13 mRNA expression in splenocytes or mediastinal lymph node cells 72 hours after injection with PS particles (Figure 3.39, 3.40).

Finally, the ability of PS particles to induce modulation of IL-9 mRNA expression 72 hours after injection in splenocytes and mediastinal lymph nodes was investigated. Although the expression of IL-9 mRNA in mediastinal lymph node cells was unchanged 72 hours after injection with PS particles (Figure 3.40), 100μm PS particles induced a significant increase in IL-9 mRNA expression in splenocytes (Figure 3.39).

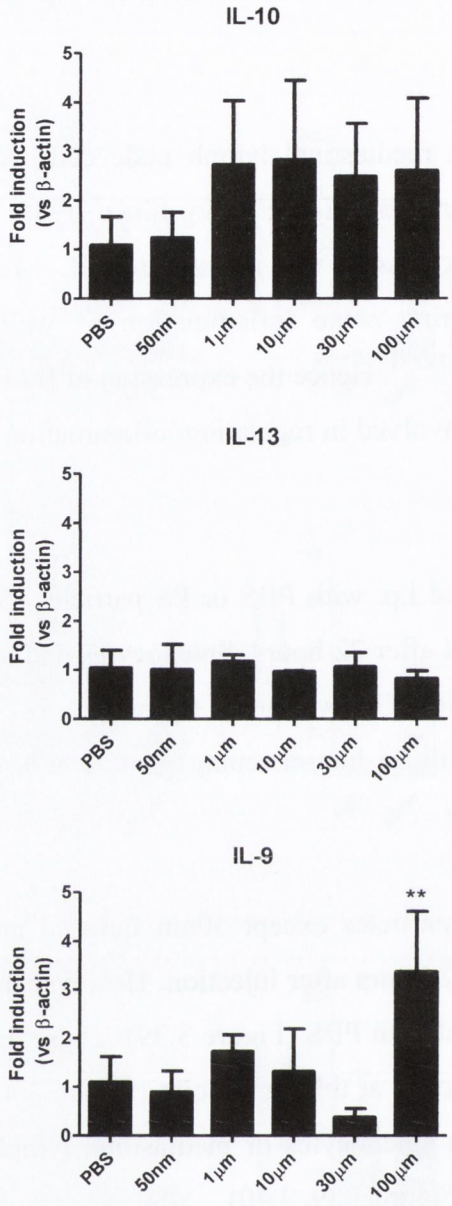

Figure 3.39 – 100μm PS particles up-regulate IL-9 mRNA expression in splenocytes 72 hours after injection. C57BL/6 mice were injected i.p. with PBS or 4mg of PS particles (50nm, 1μm, 10μm, 30μm or 100μm) in 200μl volumes. The mice were sacrificed after 72 hours and splenocytes were isolated. RNA was extracted from cells and IL-10, IL-13, and IL-9 mRNA expression was determined by real time PCR. Fold induction was determined against β-actin mRNA. Bar charts represent mean (+ SD) for 4 mice per experimental group. Results are representative of two independent experiments. Versus PBS, ** $p<0.01$.

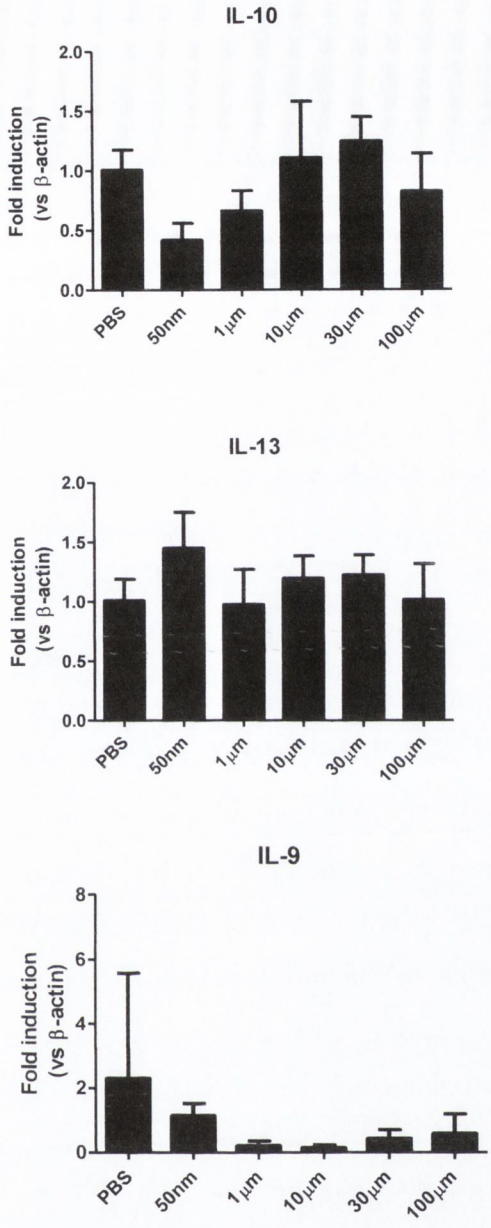

Figure 3.40 – PS particles do not modulate IL-10, IL-13 or IL-9 mRNA expression in mediastinal lymph node cells 72 hours after injection. C57BL/6 mice were injected i.p. with PBS or 4mg of PS particles (50nm, 1μm, 10μm, 30μm or 100μm) in 200μl volumes. The mice were sacrificed after 72 hours and mediastinal lymph node cells were isolated. RNA was extracted from cells and IL-10, IL-13, and IL-9 mRNA expression was determined by real time PCR. Fold induction was determined against β-actin mRNA. Bar charts represent mean (+ SD) for 4 mice per experimental group. Results are representative of two independent experiments.

3.4 Discussion

Previous studies have stressed the importance of particle size in dictating particle induced immunity. However, there are significant discrepancies in this field with some studies reporting that nano-particles and micro-particles induce Th1- and Th2-type responses respectively, whilst conversely other studies have reported the opposite[345,352,374]. These discrepancies may relate to the different particle compositions, the nature of the antigen or the route of vaccination. In contrast, relatively little work has been done on the relationship between particle size and the induction of innate immunity. Since the nature of an adaptive immune response is regulated by the innate immune system, the aim of this chapter was to characterise the innate immune response to a range of different sized particles of the same material[375].

The peritoneum is a convenient site to study cell recruitment. The resting peritoneum in mice is composed of approximately 50-60% B cells, 30% resident macrophages, 5-10% T cells and 1% DCs, as well as small populations of mast cells and eosinophils[376,377]. Macrophages are important inflammatory cells that influence the subsequent adaptive immune response through cytokine and chemokine signalling, as well as antigen presentation. Macrophages, as well as inflammatory DCs, differentiate from monocytes in the blood that migrate into tissues in response to various chemoattractants[378]. Based on work by Ghosn *et al.*, macrophage subsets were subdivided based on size and expression of the markers CD11b and F4/80[376]. Macrophages are described as pro-inflammatory ($CD11b^{+}$ $F4/80^{+}$ $SiglecF^{-}$ SSC^{low} $MHCcII^{+}$) or resident ($CD11b^{high}$ $F4/80^{high}$) peritoneal equivalents of M1 and M2 macrophages[10,13,376].

Injection of 50nm and 10μm PS particles induced recruitment of eosinophils, neutrophils and monocytes into the peritoneum whilst simultaneously depleting mast cells (preliminary results, data not shown) and resident macrophages. Due to inter-experiment variablility the number of cells recruited to the injection site varied between experiments. However trends with particle size and the number of cells recruited were consistant across all experiments. Injection of 30μm PS particles also led to the depletion of both resident macrophages and mast cells, but only induced significant infiltration of monocytes, pro-inflammatory macrophages and eosinophils 72 hours after injection. However, 1μm PS particles induced the depletion of resident macrophages without any significant cellular infiltration. This indicates that these sentinel cells detected an insult but that the inflammatory response was

either limited or regulated by inhibitory factors. The largest size PS particle (100μm) had a cellular profile similar to PBS, indicating that the immune system did not recognise the 100μm size particle.

The reason for the depletion of resident macrophages, the "macrophage disappearance reaction" (MDR), is currently unclear[379]. An obvious suggestion is cell death however cell viability in this study, along with other similar models involving MDR, remained high[380]. Two other hypotheses are tissue emigration of macrophages through draining lymphatics or disappearance due to increased tissue adherence[381]. Resident alveolar macrophages have been shown to migrate to draining lymph nodes during *Streptococcus pneumonia* exposure however conversely, alveolar macrophages have been shown to be refractory to migration to the draining lymph nodes after nasal administration of latex particles, hence the role of migration of resident macrophages is still unclear[382,383]. Bellingen *et al.* described how macrophage–mesothelial interactions were involved in adherence and subsequent migration of macrophages during peritoneal inflammation, however, studies requiring specific cell trafficking would be required to fully substantiate these findings[381,384]. At later time points of inflammation during zymosan peritonitis, substantial numbers of resident macrophages can be recovered, indicating local proliferation of cells that remain at the site of inflammation[385]. IL-4 has been shown to drive tissue-resident macrophage populations to expand by proliferation in the absence of peripheral monocyte recruitment[381,386,387]. Jenkins *et al.* have shown that both resident and recruited macrophages can alternatively activate and be driven to proliferate in a Th2 environment *in vivo*[386].

There appears to be no linear relationship regarding how size affects cell infiltration in this model. Small particles have larger surface areas relative to their size and it has been shown with PMMA particles that there exists a positive correlation between surface area and inflammatory potential[388,389]. Increased surface area positively influencing inflammation would explain the large infiltration of inflammatory cells evident after injection of 50nm and 10μm PS particles compared with 30μm and 100μm PS particles, but cannot account for the failure of 1μm PS particles to generate a similar inflammatory response.

Uptake of particles by phagocytes has been shown to influence inflammatory responses, and this is size-dependent. The process of internalisation by cells is both cell and particle dependent. Particles ranging between 20nm and 200nm in size are more likely endocytosed whereas larger particles such as those of 500nm or 5μm in size are primarily phagocytosed

or micropinocytosed[390–392]. However, uptake does not appear to be the only factor as 1μm PS particles were unable to induce a significant inflammatory response yet are more effectively phagocytosed than 10μm PS particles *in vitro*[52,393].

Injection of either 4mg or 0.4mg of particles led to comparable results which corresponds with other published work showing that particle number does not determine immune reactivity[354,394]. Using 500nm carboxylated PS particles to regulate inflammatory monocyte-derived macrophage migration in a model of West Nile virus encephalitis, Getts *et al.* found that doses higher than 0.355mg of particles had no added advantage in modulating macrophage infiltration and they suggested that saturation of particles may occur at this dose[395]. This suggests that in this study 0.4mg PS particles would have been sufficient in all experiments, as at this dose a threshold had already been reached in terms of the ability of PS particles to modulate the innate immune response. In an interesting systems biology study by Lu *et al.,* injecting silica nano-particles of various sizes intravenously, they found that although genes involved in inflammation, such as the chemoattractant CXCL1, were differentially expressed in a dose dependent manner, the cellular response pathways activated are conserved, independently of dose[369]. Remarkably, they found that cell infiltration, composed predominantly of neutrophils, was also generated differentially in terms of distinct gene expression profiles by different size nano-particles. This would indicate that although different particle sizes can generate similar inflammatory responses, this can be mediated through different pathways.

It has been suggested that cells are not able to detect properties such as volume or size until phagocytosis is complete[396]. However, the size of the particle may prevent the cell from successfully completing phagocytosis and hence initiating an immune response[397]. Despite the fact that 100μm PS particles appear to have no detectable effect on cell infiltration at the injection site, cells restimulated from mice injected with 100μm PS particles appeared to be modulated and capable of enhanced IL-4 secretion upon restimulation with anti-CD3 and anti-CD3 in combination with PMA. Similarly, restimulated PECs from mice injected with 30μm PS particles also exhibited elevated IL-4 secretion from T cells but unlike 100μm PS particles, were also capable of promoting significant increases in eosinophil and pro-inflammatory macrophages. If PS particles larger than 10μm are not being phagocytosed then they must be generating an innate immune response by an alternative mechanism[52].

One possible mechanism is through particle and cell membrane interactions. Since PS is a synthetic material it is highly unlikely that mammalian cells have evolved to specifically recognise this material using a PRR. However, scavenger receptors such as macrophage receptor with collagenous structure (MARCO) have been reported to recognise PS particles[395,398,399]. MARCO can bind both gram-negative and gram-positive bacteria and is expressed on macrophages and DCs, primarily in macrophages of the marginal zone of the spleen and lymph nodes[399,400]. PS particles of sizes 20nm, 200nm and 1μm were shown to associate with MARCO on the macrophage cell line J774.1 or with MARCO-transfected COS-7 cells by fluorescence microscopy[401]. MARCO-mediated PS particle uptake was also demonstrated using MARCO-transfected COS-7 which normally do not express the receptor[401]. Similarly MARCO-transfected Chinese hamster ovary (CHO-K1) cells internalised PS beads irrespective of particle size (20nm-1μm), whereas mock-transfected CHO-K1 cells did not[399]. *In vivo*, PS particles were shown to preferentially co-localize with splenic cell populations that expressed MARCO and PS particle uptake was shown to be significantly reduced in MARCO deficient mice[395]. These papers indicate that MARCO is a receptor that has some role in PS particle recognition, however the degree to which this interaction is specific is unclear and certainly electrostatic interactions between negative PS particles and the positively charged collagen-like domain of MARCO are important[402].

Receptor-independent, direct membrane binding leading to DC activation has also been reported[403–405]. Using atomic force microscopy to analyse real time single cell activation, uric acid crystals were found to directly engage the cellular membrane, particularly cholesterol components. This process was syk-dependent, leading to PI3K activation in DCs[403]. More recently, it has been shown that alum also binds plasma membrane lipids on DCs and that subsequent cholesterol-dependent lipid sorting activates an abortive phagocytic response that leads to antigen uptake[305]. It has also been demonstrated that direct particle-cell surface interactions are sufficient to activate osteoclastogenic signalling pathways in models of osteolysis[389,406]. Hence particles less than 10μm may be endocytosed or phagocytosed and drive an immune response whereas larger particles, unable to be internalised by cells may drive inflammation through cell surface contact.

Strikingly, 50nm and 10μm PS particles were the most potent drivers of local cell infiltration but induced recruitment of different innate immune cells into the peritoneum 3 hours after injection. 50nm PS particles principally drove infiltration of neutrophils whereas 10μm PS particles primarily mediated recruitment of macrophages. Although at

this time point the macrophages were not distinguished between monocytes or inflammatory macrophage classes (M1/M2), it is interesting to note that the inflammatory effect of wear particles (PMMA) from revised joint replacements (1-10μm) have been found to skew to an M1-like pro-inflammatory phenotype[407]. In addition, this data supports a study by Tomazic-Jezic *et al.* showing that that 10-12μm PS particles recruit pro-inflammatory macrophages that cannot phagocytose the particles but remain at the injection site to form multi-nucleate giant cells (MGCs) that are capable of ingesting these large particles[370]. MGCs are capable of releasing ROI and degradative enzymes into the privileged zone between the cell membrane and biomaterial surface, leading to degradation of the biomaterial and subsequent inflammation[408–410]. The process of giant cell formation is dependent on IL-4 and IL-13 signalling from degranulating mast cells at the site of injection and can lead to chronic inflammation[408,411,412]. It is possible that the apparent depletion of mast cells in the peritoneum after injection with (all but 100μm) PS particles is degranulation of these cells in response to injection with PS particles, thereby contributing to the formation of MGCs. Alternatively, the depletion of mast cells may be the result of down-regulation of ckit on the cell surface during, or subsequent to degranulation.

Supporting the hypothesis of MGC formation is the significant amounts of IL-4 released from restimulated PECs 72 hours after injection with 30μm and 100μm PS particles. The source of IL-4 from restimulated PECs is unclear and although PMA is known to activate T cells, it has also been shown to stimulate mast cells to secrete TNF-α *ex vivo* as well as to release histamine[413]. Particularly interesting is the observation that PECs from mice injected with 100μm PS particles, in the absence of macrophage recruitment, secrete IL-4 when restimulated with anti-CD3. As previously mentioned, this ability to secrete IL-4 may be important for macrophage proliferation[387]. Conversely, *in vivo* IL-4 secretion after injection with 30μm and 100μm PS particles could induce mast cell degranulation and the formation of MGCs to which some of the immune responses in secondary lymphoid organs, such as increased IL-9 mRNA expression, could be attributed.

Indeed, IL-4 is centrally involved in the differentiation of Th9 cells[174]. 72 hours after injection with 100μm PS particles, splenocytes significantly up-regulated the expression of IL-9 mRNA. However, injection with PS particles did not induce the up-regulation of IL-4 nor IL-4R mRNA in splenocytes at this time point. IL-9 has been compared closely with Th2-type cytokines, being associated with parasite infections and allergic responses[414–417].

The parallels between the immune response to large pathogens such as macro-parasites and 100μm PS particles is an intriguing one. The larger PS particles, 30μm and 100μm in diameter are comparable in size to schistosome, hookworm and threadworm eggs and drive innate responses involving IL-4 and IL-9, the same cytokines involved in the defence against these pathogens[418,419]. Irrespective of PAMPs and DAMPs, this implies that size can dictate innate immune responses.

Interestingly, different cells from the same ontogenic lineage have been shown to respond to various sizes of the same particulate in unique ways[420]. Thus pro-inflammatory macrophages may be capable of phagocytosing 50nm PS particles but form MGCs in response to injection with 10μm PS particles. Determining if this occurs would require histology staining at several time points at the site of injection, something that is not possible in the peritonitis model. However, using PS particles mixed with OVA, Fiona Sharp (PhD thesis, data unpublished) injected particles subcutaneously and found interesting differences in histological samples from mice immunised with different sized PS particles. Both 7 days and 21 days after injection, PBS or OVA did not result in significant local inflammatory changes. However, injection of 200nm PS particles led to large well-demarcated non-encapsulated inflammatory foci forming at the local site, with a core of particulate material surrounded by foamy macrophages and lymphocytes. Injection with 430nm PS particles resulted in similar features to 200nm PS particles at the local site except there were more particles left at the site of injection and neutrophils were also present. Interestingly, injection of 1μm PS particles induced the recruitment of small numbers of neutrophils, lymphocytes, foamy macrophages and the formation of local granulomas. Remarkably, and to a greater extent than 1μm, the local site of mice injected with 10μm PS particles contained large numbers of neutrophils at both 7 and 21 days post injection. Conversely, the largest size PS particles used, 30μm, only induced small discrete lesions with very little local inflammation evident and many particles remained at the injection site. These histological results correlate well with the cellular infiltration characterised by flow cytometry in this chapter, specifically regarding the ability of nano-particles to induce the recruitment of several inflammatory cells to the site of injection and large micro-particles exhibiting reduced cellular infiltration to the local site.

The dynamic changes in PEC composition and numbers were accompanied by the release of a number of pro-inflammatory cytokines and chemokines. IL-33 and CCL13 signalling correlated with the infiltration of eosinophils in mice injected with 50nm, 10μm and 30μm

PS particles. Specifically IL-33 correlated with eosinophil recruitment after injection with 50nm PS particles whereas CCL13 secretion appeared to relate to the recruitment of eosinophils after injection with 10μm and 30μm PS particles. CXCL1, CXCL2 and IL-1β secretion correlated with neutrophil recruitment and CCL2 and CCL3 secretion was concurrent with monocyte infiltration. Although injection with both 50nm and 10μm PS particles led to IL-1β secretion locally, recruitment of neutrophils in mice injected with 10μm PS particles was independent of the IL-1R1. IL-1 is a potent chemoattractant that is known to be involved in the recruitment of neutrophils and macrophages[421]. Specifically, IL-1α has been proposed to induce neutrophil recruitment whereas IL-1β promotes the recruitment and retention of macrophages[421]. Whether IL-1α and IL-1β are actively secreted or released during cell death is a current matter of debate[422–424]. Although in our model IL-1α protein could not be detected, the prolonged presence of IL-1β locally and in the serum correlated with a continued monocyte and pro-inflammatory macrophage presence after injection with 10μm PS particles. Yet intriguingly, IL-1 was not required for cell recruitment after injection with 10μm PS particles.

Several groups have shown that particulates such as alum, silica crystals, monosodium urate crystals and 1μm titanium particles all induce IL-1R-dependent recruitment of neutrophils[425–427]. However, there may be overlapping pathways involved in 10μm PS particle-induced neutrophil recruitment, thereby allowing for redundancy of the IL-1 signalling pathway. Interestingly, *Il1r1*$^{-/-}$ mice were comparable to WT mice in their ability to produce IL-1β, CXCL1 and CXCL2 in the peritoneum following injection with 10μm PS particles In fact, the chemokines CXCL1 and CXCL2 were significantly increased in *Il1r1*$^{-/-}$ mice. CXCL1 and CXCL2 have both been shown to be key factors in neutrophil recruitment and subsequent defence against pathogens[428–432]. Hence, in mice injected with 10μm PS particles, it is conceivable that neutrophils may be recruited into the peritoneum through classical chemokine signalling, thus rendering the IL-1R1 redundant.

Other neutrophil chemoattractants include processed complement components and lipid metabolites, as well as cytokines such as IL-17 and TNF-α which have been shown to be primarily involved in sustaining and enhancing neutrophil recruitment into sites of inflammation[433,434]. Indeed, injection with 10μm PS particles induced an up-regulation of IL-17 mRNA in PECs. Furthermore, it has been shown that in the presence of multiple chemoattractants, neutrophils must prioritize the signals they respond to, favouring 'end target' chemoattractants such as complement component 5a emanating from the site of

infection over intermediary endogenous chemoattractants such as IL-1 and leukotriene B4 encountered en route to sites of infection[435,436]. Nucleic acids are also known to drive sterile inflammation. Self DNA has also been reported to trigger antibody production, type I IFN secretion and cell proliferation, including the infiltration of neutrophils[437]. Interestingly injection of 10μm PS particles did induce an increase in exogenous dsDNA in the peritoneum which may be one mechanism by which 10μm PS particles induce neutrophil infiltration. The novel IL-1R1-independent pathway of neutrophil recruitment into the peritoneum following injection with 10μm PS particles will require further investigation in order to establish a more conclusive mechanism.

The release of dsDNA into the peritoneum after injection with 50nm and 10μm PS particles also indicates PS particle-mediated cell death and sequential DNA release. However, another possibility is that of ETosis, a form of programmed cell death where nuclear chromatin is thrown out of the cell in extracellular traps (ET)[438]. Neutrophils[7], eosinophils[439], mast cells[440] and macrophages[441] are all capable of ETosis. Flow cytometry analysis did not support the notion of PS particle mediated toxicity *in vivo*. Nevertheless mitochondrial chromatin can also form ET in the absence of cell death, although this appears to be a process limited to eosinophils and neutrophils[439,442]. DNA released from host cells is a known DAMP, along with the cytokines IL-1α and IL-33[437,443]. Injection of 50nm PS particles induced an increase in IL-33 levels in the peritoneum at 1 hour and 3 hours post injection, however as previously mentioned IL-1α levels were undetectable *in vivo*.

Remarkably, although injection with 100μm PS particles did not appear to induce the secretion of chemokines, cytokines or DAMPs locally, nor recruit cells to the local site, PECs recovered 72 hours after injection with 100μm were primed to secrete IL-4. From flow cytometry analysis it appeared that the peritoneum of mice injected with 100μm PS particles was of a similar composition to that of mice injected with PBS. Yet in the presence of the same stimulus the cytokine secretion profile is different. PECs from mice injected with 100μm PS particles exhibited an up-regulation of IL-4 and IL-17 and downregulation of IL-10 after restimulation with anti-CD3 when compared with mice injected with PBS. Interestingly the ability of PECs from mice injected with 100μm PS particles to secrete IL-4 after restimulation occurred in tandem with the reduced secretion of IL-4 from restimulated draining lymph node cells when compared to PBS. It is clear

from this data that injection of 100μm PS particles modulates responses in the secondary lymphoid organs, however the mechanisms by which this occurs are still unclear.

IL-4 is involved in many signalling pathways. It is primarily thought of as a Th2 type cytokine, involved in promoting the differentiation of naïve T cells towards a Th2 fate and stimulating positive feedback loops through STAT6 signalling. IL-4 is also known to drive the differentiation of Th9 cells alongside TGF-β and in the presence of IL-1β[174,175,177]. Recently, nitric oxide has been identified as a potent enhancer of polarisation of Th9 cells whilst simultaneously increasing the expression of IL-4R[444]. As previously mentioned in Section 1.1.1, in innate immune settings MPP^{type2} ILCs can differentiate into macrophages, basophils and mast cells, all of which are capable of secreting IL-4[141]. Interestingly, acute inflammation has recently been shown to promote IL-4 secretion which can act on myeloid cells to promote anti-inflammatory STAT6 signalling[372]. In this study, the increased IL-4 mRNA expression and secreted IL-4 after restimulation with anti-CD3 in combination with PMA, were both seen in mixed populations from the peritoneum of mice injected with large (10μm, 30μm and 100μm) PS particles. IL-4 signalling after injection with larger PS particles could be involved in regulating inflammation and restoring homeostasis, hence the limited cell infiltration seen after injection with 100μm PS particles. Wermeling *et al.* found that the anti-inflammatory ability of IL-4 depended directly on the expression of IL-4Rα on myeloid effector cells[372]. However, when IL-4Rα expression was determined on individual cell types there was no increase in expression after injection with PS particles on any individual cell populations examined. This may be due to the time points at which IL-4Rα expression was analysed, or that PS particles are not a strong enough stimulus to drive acute inflammation and up-regulate the IL-4Rα on myeloid cells in our peritoneal model. However, this chapter refutes the hypothesis that IL-4Rα is up-regulated on myeloid effector cells as a general response to inflammation to restore homeostasis[372]. In contrast, particles such as those of 1μm and 30μm in size were not the most inflammatory yet drove greater increases in IL-4 mRNA expression in PECs than 50nm PS particles. Supporting this, there was no increase in IL-4Rα expression on myeloid cells after injection with PS particles.

In conclusion, PS particles are capable of driving inflammation. However, the type and magnitude is dependent on particle size (Table 3.1, Figure 3.41).

Table 3.1 – Summary of the responses analysed in the peritoneum 24 hours after injection with PS particles

	50nm	1μm	10μm	30μm	100μm
Cells					
Neutrophils	x		IL1R1 independent		
Eosinophils	x		x	x	
Monocytes			x	x	
Pro-Inflammatory Macrophages			x	x	x
Resident Macrophages					x
Mast cells					x
Protein					
IL-1β	x		x	x	
IL-33	x				
CXCL1	x	x	x		
CXCL2	x		x		
CCL2		x	x	x	
CCL3			x	x	
CCL13			x	x	
mRNA					
IL-4		x	x	x	
IL-1α	x				
IL-1β		x	x	x	
IL-10		x	x		
IL-17	x		x		

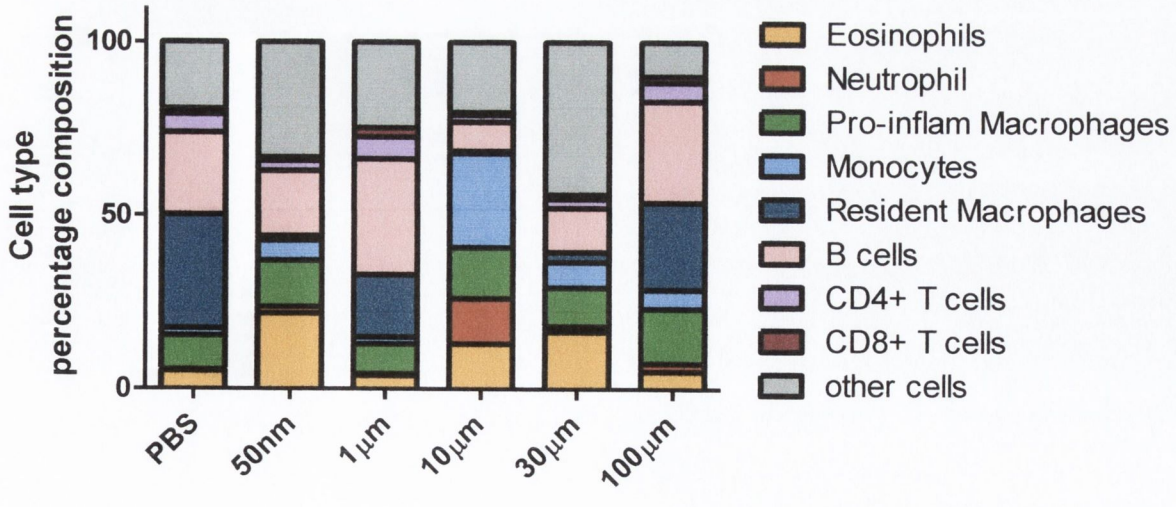

Figure 3.41 – Summary of the cell population percentages analysed in the peritoneum 72 hours after injection with PS particles.

Chapter 4

Adaptive immune responses to particles are dictated by particle size

4.1 Introduction

Alum is a particulate vaccine adjuvant that can induce effective, long-term humoral immunity. However, alum is not an effective promoter of Th1 or Th17 responses, thus rendering it unsuitable for use in vaccines against intracellular pathogens such as HIV and *M. tuberbulosis*[445,446]. Therefore, novel strategies are necessary to enhance cell-mediated immunity in response to particulate adjuvant formulations. Several studies have previously reported that the size of particles can dictate the magnitude of the ensuing adaptive immune response[269]. However, independent of particle composition, few studies have used a range of particle sizes from the nanometre to the micrometre scale[269]. In chapter 3, different sized particles were shown to modulate the innate immune system in distinct ways. Since the innate immune system determines the nature of the ensuing adaptive immune response, the affect of particle size on the adaptive immune response was also investigated.

As mentioned in Chapter 3, antibody titres are often used as a readout for adjuvanticity when comparing the ability of different sized particles to induce an adaptive immune response[269,351,352,354]. However, with very little consistency across studies with regards size range, route of administration and model antigen, results and trends can be difficult to interpret. For example, using s.c. injection and oral administration routes, PLG acid (A) particles containing BSA as a model antigen are more potent inducers of IgG when using 1μm particles rather than 5μm particles[447]. However, using PLA micro-particles encompassing OVA in a broader size range of 3-50μm, Nakaoka *et al.* demonstrated that 7-15μm particles drive the greatest antigen specific IgG response when administered i.p.[353]. In the nanometre range, Gutierro *et al.* found that when comparing 200nm, 500nm and 1μm PLGA particles loaded with BSA, 1μm particles drive the highest antigen-specific serum IgG response, independent of route of administration (s.c., intranasal or oral)[448]. Similarly, intramuscular vaccination with PLA particles loaded with HBsAg generate size-dependent antigen-specific IgG responses, with micro-particles (2-8μm) more effective than nano-particles (200-600nm)[352]. Although all of these studies compared particles of size 'small' against 'large', when this data is collated it is particles within the 1-10μm range that appear to generate the greatest antibody responses. However, it should be noted that Wendorf *et al.* reported that 110nm and 998nm PLG particles with absorbed antigens from *Neisseria meningitidis* type B or HIV-1 env glycoprotein gp140 generate identical antibody titres and also elicit similar serum bactericidal activity[449].

Although antibody-mediated humoral immunity is important for immunity to several pathogens, effective immune defence against HIV, TB and malaria requires strong cell mediated immunity. T cell responses after immunisation with particles have also been shown to be size dependent. For example, a study by Mottram *et al.* administering PS particles conjugated to OVA intra-dermally found that 40nm PS particles induce antigen-specific IFN-γ secretion from splenocytes whereas 93-123nm PS particles induce IL-4 secretion[345]. Interestingly when PLA particles containing HBsAg are injected intra-muscularly, nano-particles (200-600nm) were shown to elicit an IFN-γ response from proliferating T cells isolated from the lymph nodes whereas micro-particles (2-8μm) induced the secretion of IL-4[352]. However there are several discrepancies within and between these studies. Firstly, when size within groups spans a large spectrum, it is unclear which sized particle within the group is promoting the induction of the respective cytokines. Secondly, and intriguingly, particles of the smaller range promoted IFN-γ whereas larger particles promoted IL-4 secretion in both studies. However 'small' in one study is 'large' in another, again highlighting the difficulty in interpreting trends across studies. Discrepancies across the literature may in part be due to different materials, degree of polydispersity, particle concentrations, antigen, antigen dose, methods of antigen loading, route of administration and sterilisation[269].

A significant issue is the difficulty in producing mono-disperse preparations of polymeric particles with many materials. PS is an attractive model for use in particle size studies since as a material it can be used to make particularly uniform and mono-disperse particles. This study aimed to elucidate the relationship between PS particle size and the induction of an adaptive immune response across a broader particle size range than had previously been done, with the aim of consequently linking particle driven innate and adaptive immune responses.

The primary antigen chosen for the adjuvant studies was ClfA. ClfA is a *S. aureus* microbial surface component recognizing adhesive matrix molecules (MSCRAMM) that binds to fibrinogen and fibrin. Through this process ClfA promotes bacterial adhesion to immobilized fibrinogen in blood clots and also *ex vivo* to biomaterials conditioned with plasma proteins[450,451]. ClfA has also been shown to be anti-phagocytic and protects bacteria from opsono-phagocytosis[452]. ClfA has advantages as an antigen to assess particle-induced immune responses as it is a candidate *S. aureus* vaccine antigen[453–455]. A further advantage of using ClfA as an antigen is that functional antibody titres can be determined

and a challenge model is in place. Functional antibody titres can be determined by assessing the ability of antibodies in the serum of immunised mice to inhibit *S. aureus* adhesion to immobilised fibrinogen. If serum from a mouse has a high percentage of binding inhibition activity, it is then assumed that the serum contains neutralizing antibodies against ClfA.

4.2 Aims

This chapter aimed to explore the relationship between PS particle size and the adaptive immune response. The specific aims of this chapter were to titrate ClfA to a working concentration for our studies and to subsequently characterise the antibody and T cell responses after immunisation with ClfA mixed with PS particles in the range 50nm-100μm. Using this data, a *S. aureus* challenge experiment could then be conducted. To determine more specific roles for $CD8^+$ and $CD4^+$ T cells in PS particle size-dependent cellular responses, tetramers specific for OVA and the Influenza nucleoprotein $NP_{311-325}$ were used respectively.

4.3 Results

4.3.1. ClfA in combination with 10μm PS particles promotes enhanced antigen-specific serum antibody responses

The first aim of this chapter was to titrate ClfA to an appropriate dose for an adjuvant study. Based on preliminary experiments, 10μm PS particles were chosen for use in combination with ClfA at three different doses; 10μg, 1μg and 0.1μg per mouse. Female C57BL/6 mice were immunised s.c. on day 0 with PBS or ClfA either alone or in combination with 10μm PS particles. On day 14 the mice were boosted with these same treatments. Serum was collected on day 21 and antigen-specific antibody titres in the serum were measured as a positive correlate of adaptive immunity.

Injection of 10μg ClfA alone induced antigen-specific antibody titres in the serum (Figure 4.1). Importantly, ClfA-specific total IgG as well as the IgG subtypes IgG1 (Th2-type), IgG2b and IgG2c (Th1-type) were not significantly elevated in mice immunised with 10μg ClfA and PS particles compared with mice immunised with 10μg ClfA alone. Similarly, injection of 1μg ClfA alone induced antigen-specific antibody titres in the serum, although to a lesser extent than 10μg ClfA. However, injection of PS particles mixed with 1μg ClfA promoted increased antigen-specific IgG and IgG1 titres compared to those induced by 1μg ClfA alone (Figure 4.1). Mice immunised with the lowest dose of ClfA, 0.1μg, exhibited little or no antigen-specific antibody responses in the serum. Interestingly, however, injection of PS particles mixed with 0.1μg ClfA promoted increased total IgG and IgG1 compared with 0.1μg ClfA alone (Figure 4.1).

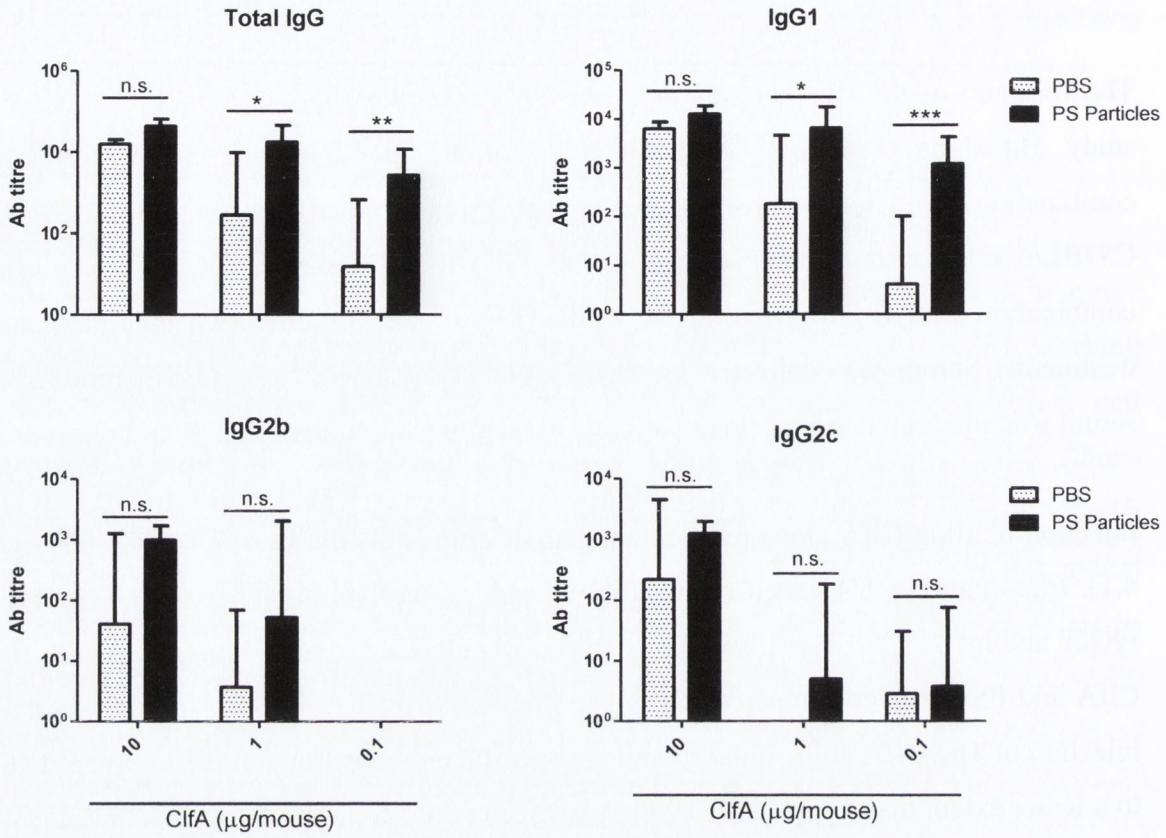

Figure 4.1 – Immunisation with ClfA mixed with 10μm PS particles promotes greater antigen-specific antibody responses compared with ClfA alone. Female C57BL/6 mice were immunised s.c. on day 0 with PBS or ClfA (10μg, 1μg or 0.1μg/mouse) either alone or mixed with 10μm PS particles (4mg/mouse) in 200μl volumes. The mice were boosted with these same treatments on day 14 and were sacrificed on day 21. Serum was collected and ClfA-specific antibody titres were determined in the serum by ELISA. Bar charts represent mean (+ SD) for 5 mice per experimental group. Versus ClfA alone (PBS) at corresponding concentration, * $p<0.05$, ** $p<0.01$, *** $p<0.0001$.

4.3.2. Vaccination with 1μg ClfA in combination with 10μm PS particles induces the production of serum neutralising antibodies against *S. aureus*

Although ClfA-specific antibodies were present in the serum of mice immunised with 10μm PS particles mixed with ClfA, this next study sought to address whether these antibodies were functional. Therefore, the ability of serum from vaccinated mice to inhibit *S. aureus* adhesion to immobilised fibrinogen was assessed.

Female C57BL/6 mice were immunised s.c. on day 0 with PBS or ClfA (10μg, 1μg or 0.1μg) either alone or in combination with 10μm PS particles. On day 14 the mice were boosted with these same treatments. Serum was collected on day 21 and the ability of serum to inhibit *S. aureus* adhesion to immobilised fibrinogen was assessed.

Interestingly, injection of 10μg ClfA with or without PS particles induced functional ClfA-specific antibodies in the serum (Figure 4.2). Doses of 1μg and 0.1μg ClfA alone did not drive functional antibodies against ClfA. However, when PS particles were combined with 1μg ClfA, functional ClfA-specific antibodies were detectable in the serum (Figure 4.2). The combination of 0.1μg ClfA and PS particles had no effect on functional antibodies.

From this titration study, it is clear that the *S. aureus* antigen ClfA is very immunogenic and the antigen alone is capable of driving functional antibodies in the serum. However, when the dose of ClfA was reduced to 1μg, adding PS particles had a clear enhancing effect on the induction of total ClfA-specific antibodies and particularly on ClfA neutralising antibodies. Based on these results, 1μg ClfA was chosen as the most appropriate dose to proceed with in further adjuvant studies.

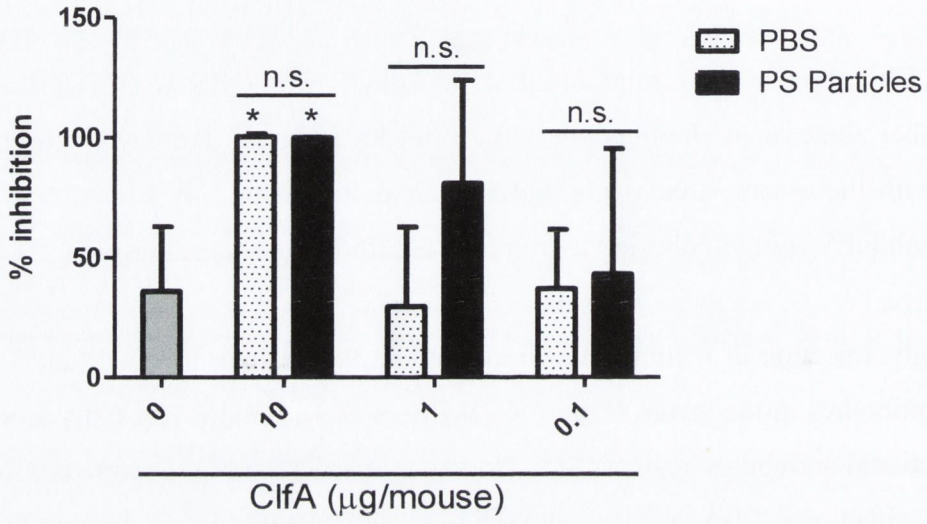

Figure 4.2 – Vaccination with 1μg ClfA mixed with 10μm PS particles induces the production of serum neutralising antibodies against *S. aureus*. Female C57BL/6 mice were immunised s.c. on day 0 with PBS or ClfA (10μg, 1μg or 0.1μg/mouse) either alone or mixed with 10μm PS particles (4mg/mouse) in 200μl volumes. The mice were boosted with these same treatments on day 14 and were sacrificed on day 21. Serum was collected. *S. aureus* PS80 bacteria incubated with PBS (no serum) were included as a control. Bar charts represent mean (+ SD) for 5 mice per experimental group. Versus PBS, * $p<0.05$.

4.3.3. The candidate antigen ClfA is highly immunogenic *in vivo* and is capable of driving antigen-specific antibody responses alone

After determining the most appropriate concentration of ClfA to use in an adjuvant study, it was important to next ascertain whether PS particle size can influence the adaptive immune response *in vivo*. In order to answer this question, an adjuvant model was employed. Female C57BL/6 mice were immunised s.c. on day 0 with PBS or ClfA (1μg) either alone or in combination with PS particles (50nm, 1μm, 10μm, 30μm or 100μm). On day 14 the mice were boosted with these same treatments and serum was collected on day 21.

As demonstrated previously, ClfA alone was capable of inducing robust antigen-specific antibody responses in the serum (Figure 4.3). However, ClfA alone induced an antigen specific antibody titre two logs higher than that observed in the previous titration study (Figure 4.1, 4.3). Hence, total IgG serum titres were not significantly different for any PS particle size tested when compared with ClfA alone. ClfA-specific IgG1 was significantly increased when ClfA was mixed with 1μm PS particles. Interestingly 50nm and 30μm PS particles exhibited an increase in ClfA-specific IgG2b, although this was not significant. Only 1μm PS particles led to the production of significantly higher ClfA-specific antibody titres in the serum compared to ClfA alone. This was in contrast to the previous study where ClfA at 1μg combined with 10μm PS particles was capable of inducing robust ClfA-specific antibody titres compared with ClfA alone (Figure 4.1). These results indicated that this particular preparation of ClfA may have been contaminated with endotoxin.

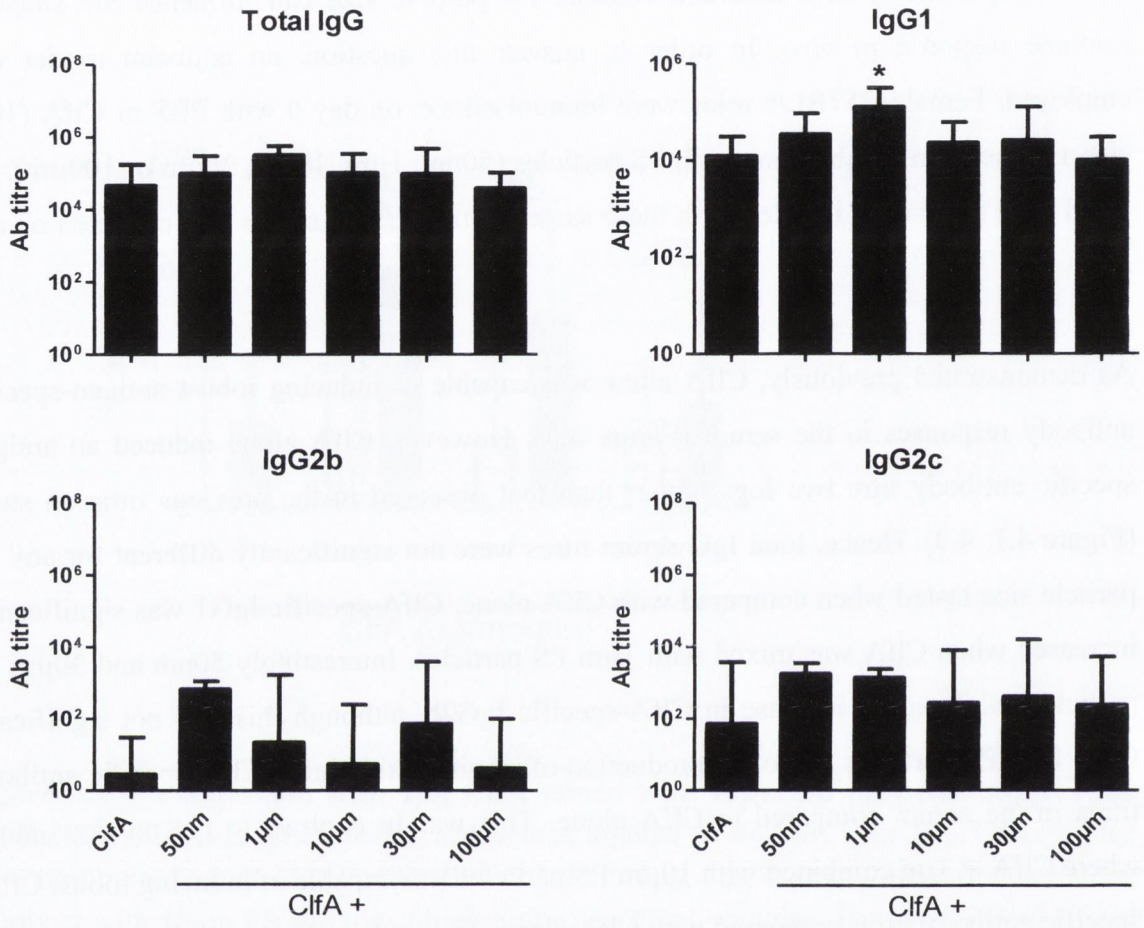

Figure 4.3 – 1μg ClfA alone is capable of driving antigen-specific antibody responses. Female C57BL/6 mice were immunised s.c. on day 0 with PBS or ClfA (1μg) either alone or in combination with PS particles (50nm, 1μm, 10μm, 30μm or 100μm)(4mg/mouse) in 200μl volumes. On day 14 the mice were immunised with these same treatments and on day 21 serum was collected. ClfA-specific antibody titres were determined in the serum by ELISA. Bar charts represent mean (+ SD) for 5 mice per experimental group. Versus ClfA alone, * $p<0.05$.

4.3.4. Removing endotoxin from ClfA preparation significantly reduces the ability of ClfA to stimulate BMDC secretion of IL-6

Figures 4.1 and 4.3 support the possibility that the preparation of ClfA was contaminated with endotoxin, hence LPS contamination was evaluated using an IL-6 ELISA. Concentrations as low as 10pg/ml LPS can induce the secretion of IL-6 from BMDCs, hence BMDCs were stimulated with ClfA and LPS to determine the ability of the ClfA preparation to drive IL-6[456]. 24 hours later, IL-6 secretion was measured in the supernatant in response to these stimuli.

BMDC stimulated with LPS alone induced the secretion of IL-6 (Figure 4.4A). BMDCs stimulated with ClfA alone were capable of secreting IL-6 in a concentration dependent manor (Figure 4.4A). Endotoxin removal resin was used to remove contaminants from the ClfA preparation. This assay works using porous cellulose beads that have been surface-modified with covalently attached polylysine chains which have a high affinity for LPS. The beads bind and remove pyrogens and allow non-endotoxin proteins to move through the resin. After the ClfA preparation was run through the endotoxin removal resin 9 times, murine BMDCs were stimulated as before and 24 hours later IL-6 secretion was measured in the supernatant.

Strikingly, no concentration of 'cleaned' ClfA tested was capable of stimulating BMDCs to secrete IL-6 (Figure 4.4B). To confirm whether the 'cleaned' preparation of ClfA contained any endotoxin, an LAL assay was employed. This assay measures the amount of endotoxin in a protein using a chromogenic signal generated in the presence of endotoxins. As expected, the amount of endotoxin in the preparation was significantly lower than before it was 'cleaned' as measured in endotoxin units (EU)/ml (Figure 4.4C). Importantly, the amount of residual endotoxin that remained in the ClfA preparation after being 'cleaned' was similar to endotoxin-free water (Figure 4.4C).

To determine if any non-specific binding had occurred in the endotoxin removal resin, a BCA assay was employed. Using a biuret reaction, this assay enables total protein concentration in a preparation to be determined. A small but insignificant amount of protein was lost using the endotoxin removal resin. The concentration of the ClfA preparation before being added to the resin was 365μg/ml and after running through the

resin was 321μg/ml (Figure 4.4D). All future studies were performed using ClfA that had been run through endotoxin removal columns and endotoxin concentrations confirmed.

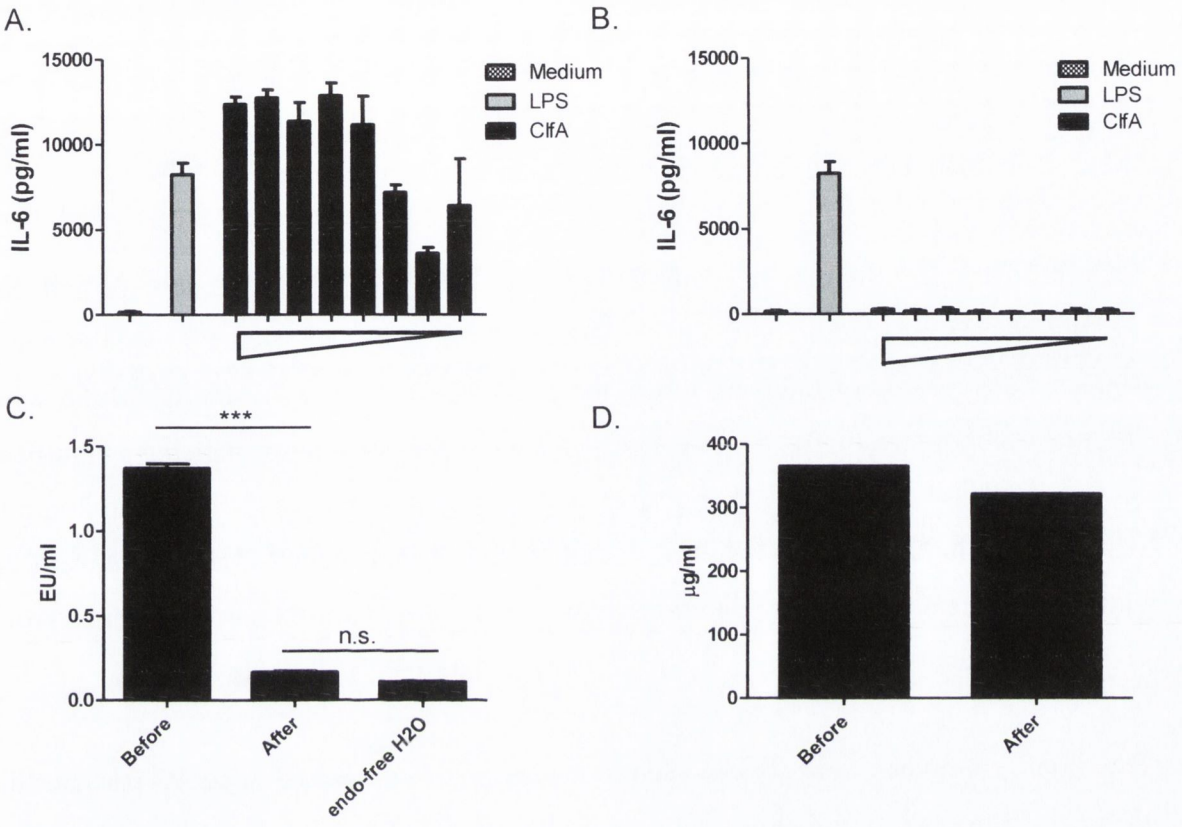

Figure 4.4 – ClfA preparation was contaminated with endotoxin and the ability of the antigen to stimulate BMDC to secrete IL-6 was reduced after endotoxin removal. (A, B) BMDCs from WT mice were plated at a concentration of 6.25 x 10^5 cells/ml. BMDCs were stimulated with LPS (10ng/ml) or ClfA before (A) or after (B) cleaning in endotoxin removal resin. ClfA was used at a top concentration of 100µg/ml and diluted 1:2 thereafter. 24 hours later the cells were centrifuged, supernatants collected and IL-6 secretion measured by ELISA. Bar charts represent mean (+ SEM). (C) LAL assay determining endotoxin concentration in ClfA preparations before and after cleaning in endotoxin removal resin, and in endotoxin-free water. Bar charts represent mean (+ SEM). Versus ClfA preparation before cleaning in endotoxin removal resin, *** $p<0.0001$. (D) Protein concentrations of ClfA preparations before and after cleaning in endotoxin removal resin using a BCA assay.

4.3.5 Subcutaneous immunisation with ClfA and PS particles promotes antigen-specific antibody responses with all but 100μm PS particles

In order to determine the relationship between PS particle size and the induction of antigen-specific antibodies using endotoxin-free ClfA, female C57BL/6 mice were immunised s.c. on day 0 with PBS or ClfA (1μg) either alone or in combination with PS particles (50nm, 1μm, 10μm, 30μm or 100μm). On day 14 the mice were boosted with these same treatments and serum was collected on day 21.

Importantly, mice immunised with ClfA alone were no longer capable of inducing significant antigen-specific antibody responses (Figure 4.5). All sized PS particles except 100μm were capable of inducing robust antigen-specific antibody responses in the serum (Figure 4.5A). Interestingly, 50nm PS particles were also capable of inducing a significant amount of class switched IgG2b and IgG2c antigen-specific antibodies. 1μm and 30μm PS particles also induced IgG2b responses in the serum (Figure 4.5A). Concentrations of IgE antibodies were also determined in the serum. Remarkably, 1μm PS particles were the only size particle capable of inducing an IgE response (Figure 4.5B).

Functional antibodies were also assayed in the serum of immunised mice. PS particles that drove the most robust antigen-specific total IgG and IgG2b also induced functional ClfA-specific antibodies in the serum (Figure 4.5C). Neither 10μm nor 100μm PS particle induced significant functional ClfA-specific antibodies in the serum (Figure 4.5C).

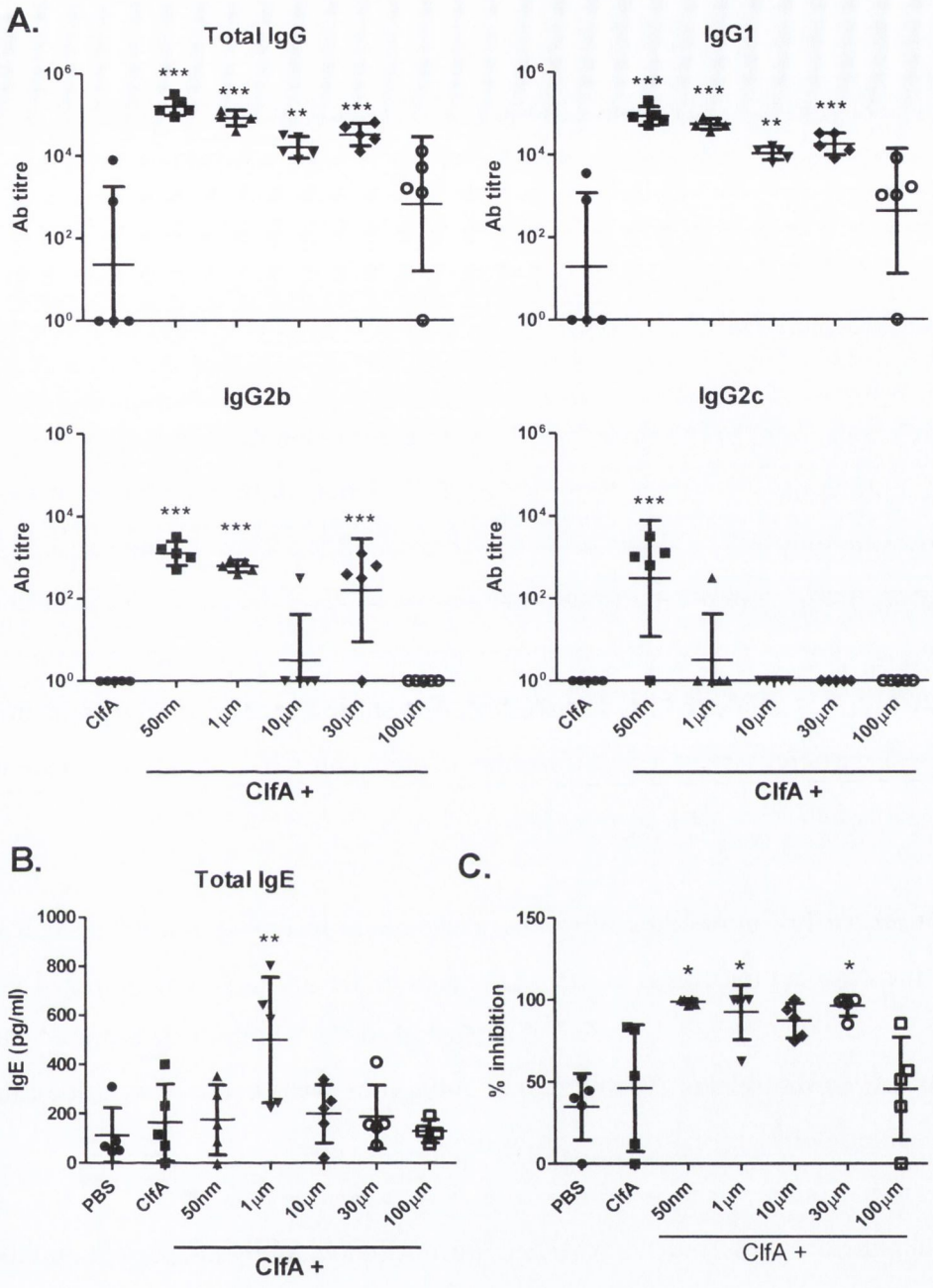

Figure 4.5 – Subcutaneous immunisation with ClfA mixed with PS particles promotes antigen-specific antibody responses with all but 100μm PS particles compared with ClfA alone. Female C57BL/6 mice were immunised s.c. on day 0 with PBS or ClfA (1μg) either alone or mixed with PS particles (4mg/mouse) in 200μl volumes. The mice were boosted with these same treatments on day 14 and were sacrificed on day 21. Serum was collected and ClfA-specific antibody titres (A), IgE antibody titres (B) and functional antibodies (C) were determined in the serum by ELISA (A,B) or inhibition assay (C). Dot plots represent mean (+ SD) for 5 mice per experimental group. Results are representative of two independent experiments. Versus ClfA alone, * $p<0.05$, ** $p<0.01$, *** $p<0.0001$.

4.3.6. Vaccination with 1mg PS particles and ClfA does not induce the production of significant antigen-specific antibodies

In order to determine if the concentration of PS particles was important in inducing antigen-specific antibody responses, female C57BL/6 mice were immunised s.c. on day 0 with PBS or ClfA (1μg) either alone or in combination with 1mg/mouse PS particles (50nm, 1μm, 10μm, 30μm or 100μm). On day 14 the mice were boosted with these same treatments and serum was collected on day 21.

Mice immunised with ClfA alone were capable of inducing antigen-specific antibody responses (Figure 4.6). However 50nm PS particles induced the production of the greatest antigen-specific total IgG antibody response (Figure 4.6A). This IgG response induced by immunisation with 50nm PS particles was primarily IgG1 (Figure 4.6A). In contrast to immunisation with 4mg, 1mg PS particles were not sufficient to induce antigen-specific IgG2b and IgG2c. Although the antigen-specific antibody response in mice immunised with 1mg PS particles was not significantly greater than ClfA alone, the trend with size was similar to when mice were immunised with 4mg PS particles (Figure 4.5).

Concentrations of IgE antibodies were also determined in the serum. PS particles did not induce an increase in production of IgE antibodies in the serum when compared with ClfA alone (Figure 4.6B). Antigen-specific IgE concentrations were not determined due to the absence of IgE in the serum. No functional antibodies were detected in mice immunised with ClfA mixed with 1mg PS particles (Figure 4.6C).

Since immunisation with 1mg PS particles did not induce antigen-specific antibody class switching or functional antibodies, the original 4mg/mouse dose of PS particles was used for all future experiments.

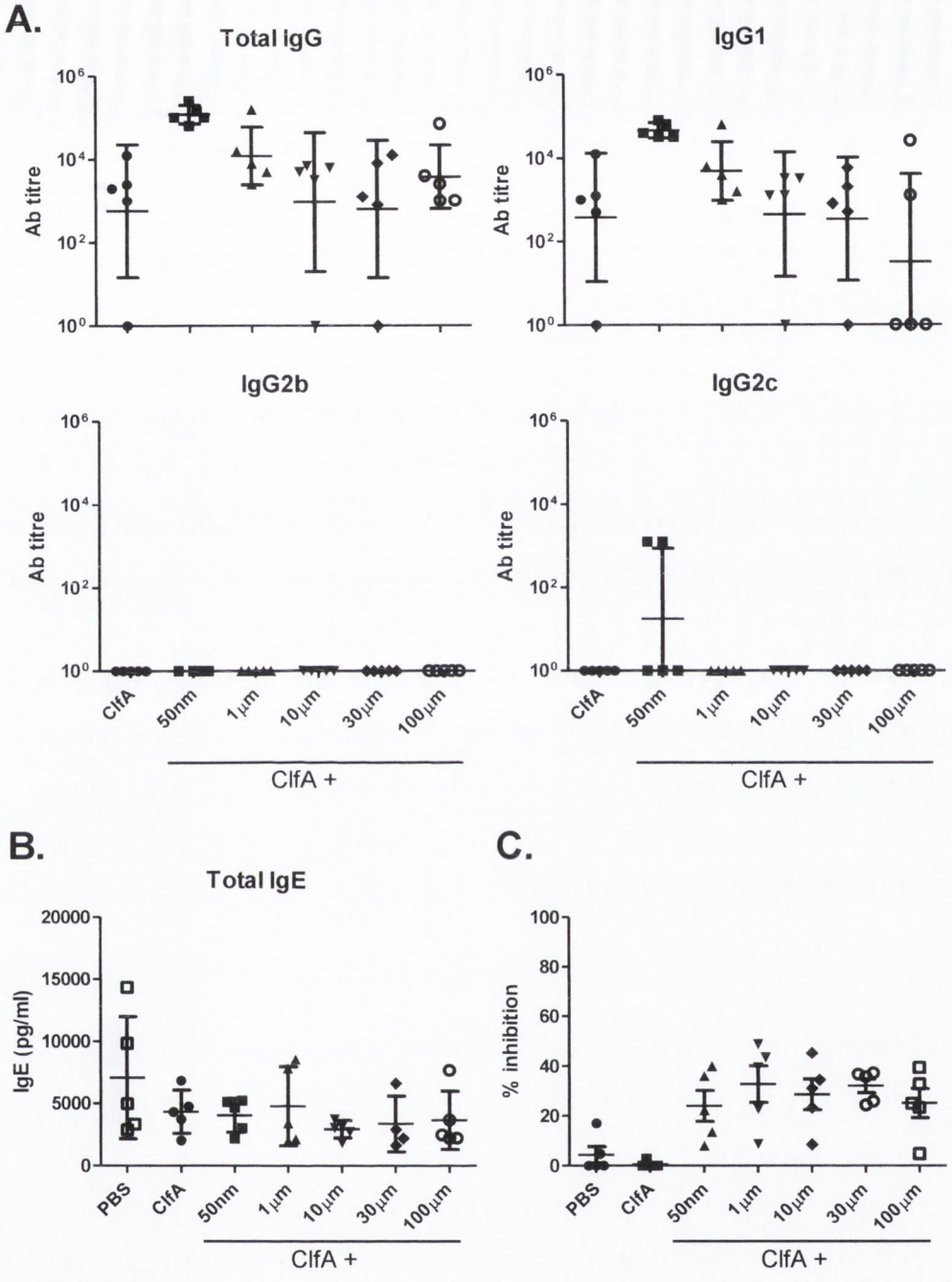

Figure 4.6 – 1mg of 50nm PS particles drives a greater increase in antigen-specific antibodies than larger PS particles. Female C57BL/6 mice were immunised s.c. on day 0 with PBS or ClfA (1μg) either alone or mixed with PS particles (1mg/mouse) in 200μl volumes. The mice were boosted with these same treatments on day 14 and were sacrificed on day 21. Serum was collected and ClfA-specific antibody titres (A), IgE antibody titres (B) and functional antibodies (C) were determined in the serum by ELISA (A,B) or inhibition assay (C). Dot plots represent mean (+ SD) for 5 mice per experimental group.

4.3.7. Route of administration influences the antigen-specific antibody response following immunisation with ClfA and 1μm PS particles

In order to determine if the route of immunisation was important in inducing antigen-specific antibody responses, female C57BL/6 mice were immunised i.p. on day 0 with PBS or ClfA (1μg) either alone or in combination with PS particles (50nm, 1μm, 10μm, 30μm or 100μm). On day 14 the mice were boosted with these same treatments and serum was collected on day 21.

50nm PS particles were again the most effective at driving antigen-specific antibody responses. Mice immunised with 50nm PS particles i.p. primarily generated IgG1, with a small production of IgG2b and IgG2c subclasses (Figure 4.7A). 50nm PS particles also induced the greatest induction of total IgE in the serum as well as antigen-specific IgE (Figure 4.7B). Interestingly, 10μm and 30μm PS particles were also capable of inducing the production of IgG1 antigen-specific antibodies but did not induce the production of IgE. Unlike s.c. immunisations there was no linear effect of size on antigen-specific antibodies, as 1μm and 100μm PS particles did not induce any significant antigen-specific IgG antibody response (Figure 4.7). However, 1μm PS particles did induce a small induction of IgE in the serum (Figure 4.7B).

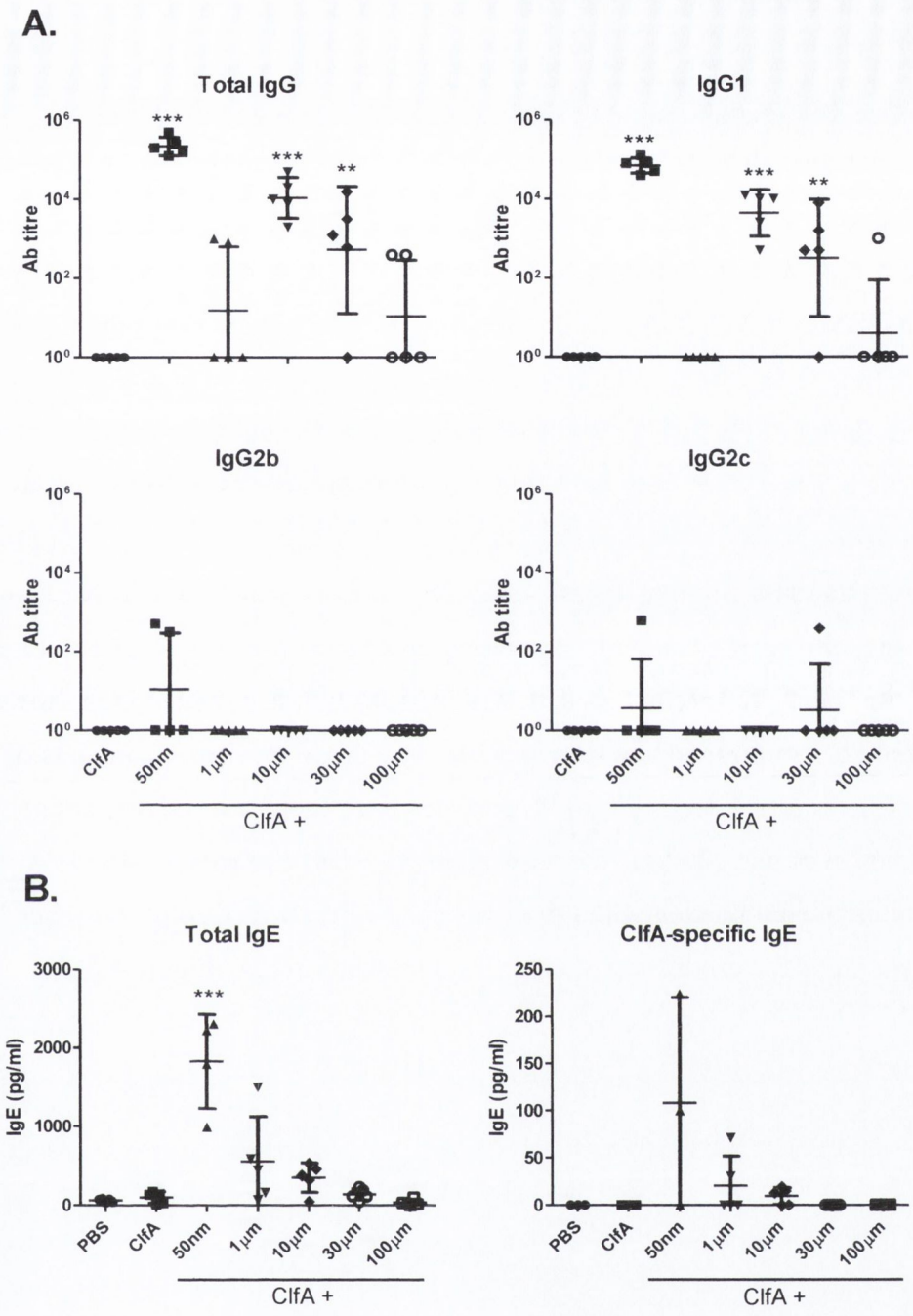

Figure 4.7 – Intra-peritoneal immunisation with ClfA mixed with PS particles promotes antigen-specific antibody responses. Female C57BL/6 mice were immunised i.p. on day 0 with PBS or ClfA (1μg) either alone or mixed with PS particles (4mg/mouse) in 200μl volumes. The mice were boosted with these same treatments on day 14 and were sacrificed on day 21. Serum was collected and ClfA-specific antibody titres (A) and IgE antibody titres (B) were determined in the serum by ELISA. Dot plots represent mean (+ SD) for 5 mice per experimental group. Results are representative of two independent experiments. Versus ClfA alone, ** $p<0.01$, *** $p<0.0001$.

4.3.8. The type and magnitude of OVA-specific antibody responses induced by PS particles can be dictated by particle size

PS particles were capable of inducing antigen-specific antibody responses in a size-dependent manner when co-injected with the *S. aureus* antigen ClfA. To determine whether this size-dependent response was antigen-dependent, an adjuvant model was established using the model antigen OVA. Female C57BL/6 mice were immunised i.p. on day 0 with PBS or OVA (1μg) either alone or in combination with alum (1mg) or PS particles (50nm, 1μm, 10μm, 30μm or 100μm). Alum was used as a positive control to compare the ability of PS particles to drive antigen-specific antibody responses. On day 14 the mice were boosted with these same treatments and serum was collected on day 21.

Interestingly, co-administration of all sized PS particles with OVA drove significantly enhanced antigen-specific antibody responses compared with OVA alone (Figure 4.8). IgG1 was the most prominent IgG subclass induced by all particle sizes. However, the smaller sized PS particles, 50nm, 1μm and 10μm all drove significant amounts of antigen-specific IgG2b (Figure 4.8A). 100μm PS particles were capable of driving antigen-specific antibodies however this size was the least effective when compared with OVA alone. As expected, alum in combination with OVA was the greatest driver of IgE however 10μm PS particles also drove the production of significant amounts of IgE (Figure 4.8B).

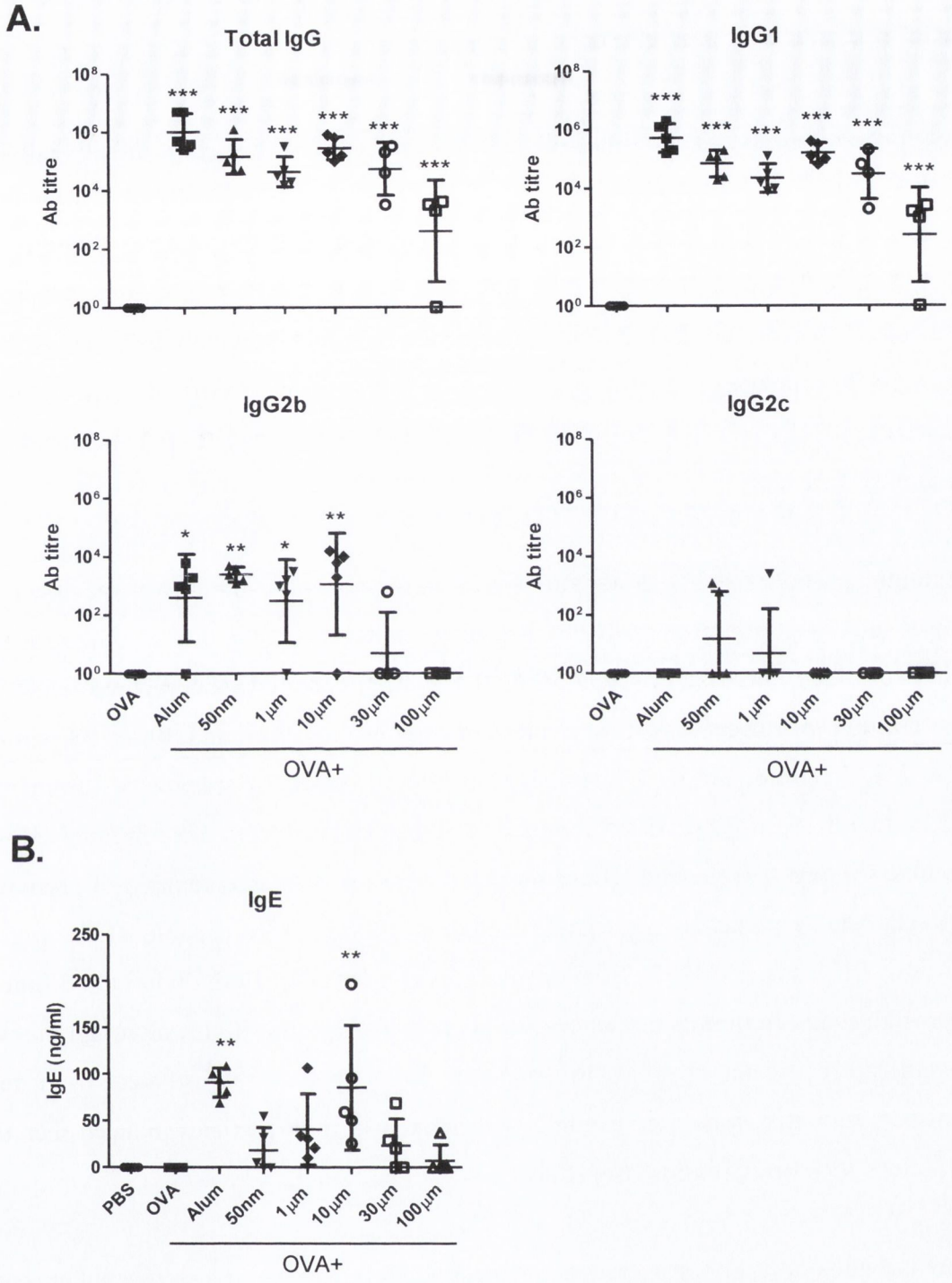

Figure 4.8 – Immunisation with PS particles and OVA promotes antigen-specific antibody responses. Female C57BL/6 mice were immunised i.p. on day 0 with PBS or OVA (1μg) either alone, or mixed with alum (1mg) or PS particles (4mg/mouse) in 200μl volumes. The mice were boosted with these same treatments on day 14 and were sacrificed on day 21. Serum was collected and OVA-specific antibody titres (A) and IgE antibody titres (B) were determined in the serum by ELISA. Dot plots represent mean (+ SD) for 5 mice per experimental group. Versus OVA alone, * $p<0.05$, ** $p<0.01$, *** $p<0.0001$.

4.3.9. The type and magnitude of ClfA-specific cellular immunity induced by PS particles is dictated by particle size

In order to determine the relationship between PS particle size and the induction of antigen-specific T cell responses, female C57BL/6 mice were immunised s.c. on day 0 with PBS or ClfA (1μg) either alone or in combination with PS particles (50nm, 1μm, 10μm, 30μm or 100μm). On day 14 the mice were immunised with the same treatments and on day 21 spleens and the draining lymph nodes (inguinal lymph nodes), were isolated. Cells were restimulated *ex vivo* and secretion of antigen-specific T cell cytokines characteristic of Th1 (IFN-γ), Th2 (IL-13), Th17 (IL-17) and Treg (IL-10) responses were subsequently measured.

Interestingly, particle size had a dramatic effect on the type of splenic ClfA-specific T cell responses induced. Immunisation with ClfA mixed with each of the different size particles led to a significant increase in secretion of IFN-γ from splenocytes compared with ClfA alone, although this effect was most evident in response to 10μm and 30μm PS particles (Figure 4.9). Secretion of IL-17 was significantly increased in splenocytes from mice immunised with 10μm PS particles compared to those isolated from mice immunised with ClfA alone (Figure 4.9). Indeed, 10μm particles were the only size capable of promoting this effect. All PS particle sizes tested, excluding 100μm, were capable of driving the secretion of ClfA-specific IL-13 from splenocytes (Figure 4.9). Both 50nm and 30μm PS particles induced secretion of the highest levels of ClfA-specific IL-13, although this was not significantly greater than IL-13 secretion from splenocytes isolated from mice immunised with ClfA alone. Interestingly, 50nm and 10μm PS particles induced secretion of the highest levels of ClfA-specific IL-10.

Inguinal lymph node cells were less responsive to ClfA restimulation *ex vivo*, but appeared to show a similar trend to splenocytes in mice immunised with 10μm PS particles and ClfA-specific IL-17 secretion (Figure 4.10).

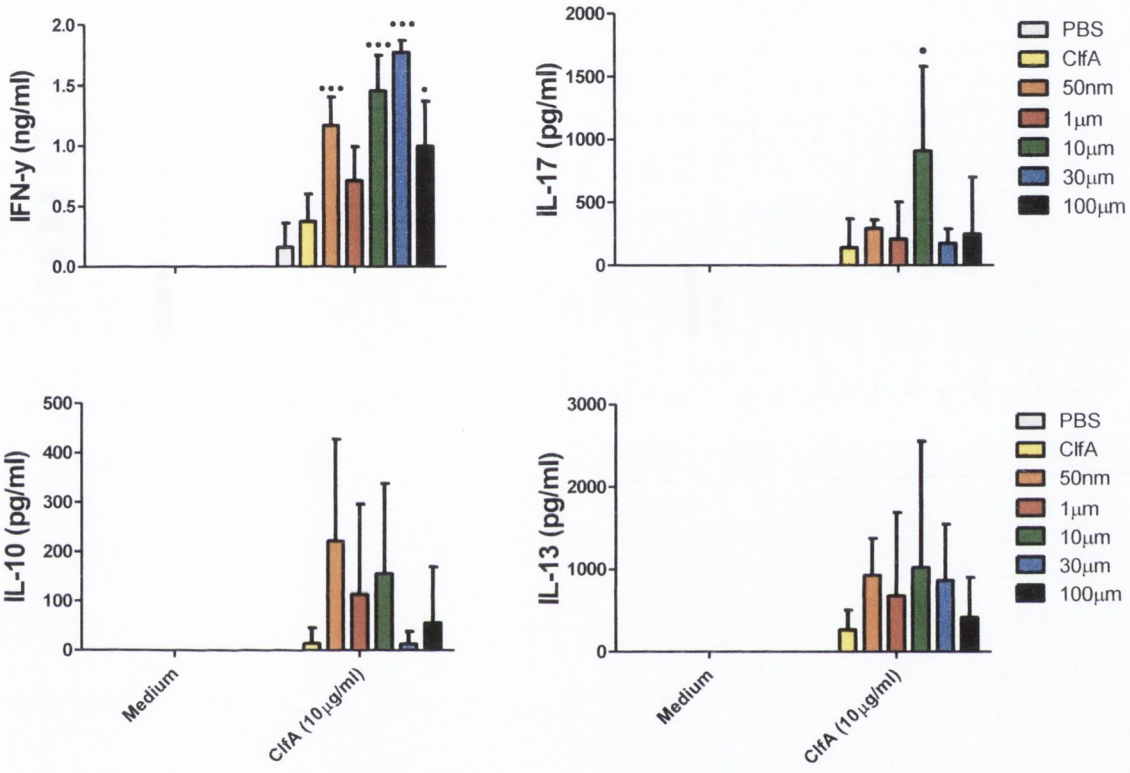

Figure 4.9 – Different sized particles drive distinct ClfA-specific T cell responses in splenocytes. Female C57BL/6 mice were immunised s.c. on day 0 with PBS or ClfA (1μg) either alone or in combination with PS particles (50nm, 1μm, 10μm, 30μm or 100μm) (4mg/mouse) in 200μl volumes. On day 14 the mice were immunised with these same treatments and on day 21 the spleens were collected. Splenocytes (2 x 10^6 cells/ml) were restimulated *ex vivo* with either medium alone or ClfA (10μg/ml). Levels of cytokines were measured in supernatants by ELISA after 72 hours. Bar charts represent mean (+ SD) for 5 mice per experimental group. Versus mice immunised with ClfA alone, • $p<0.05$, ••• $p<0.0001$.

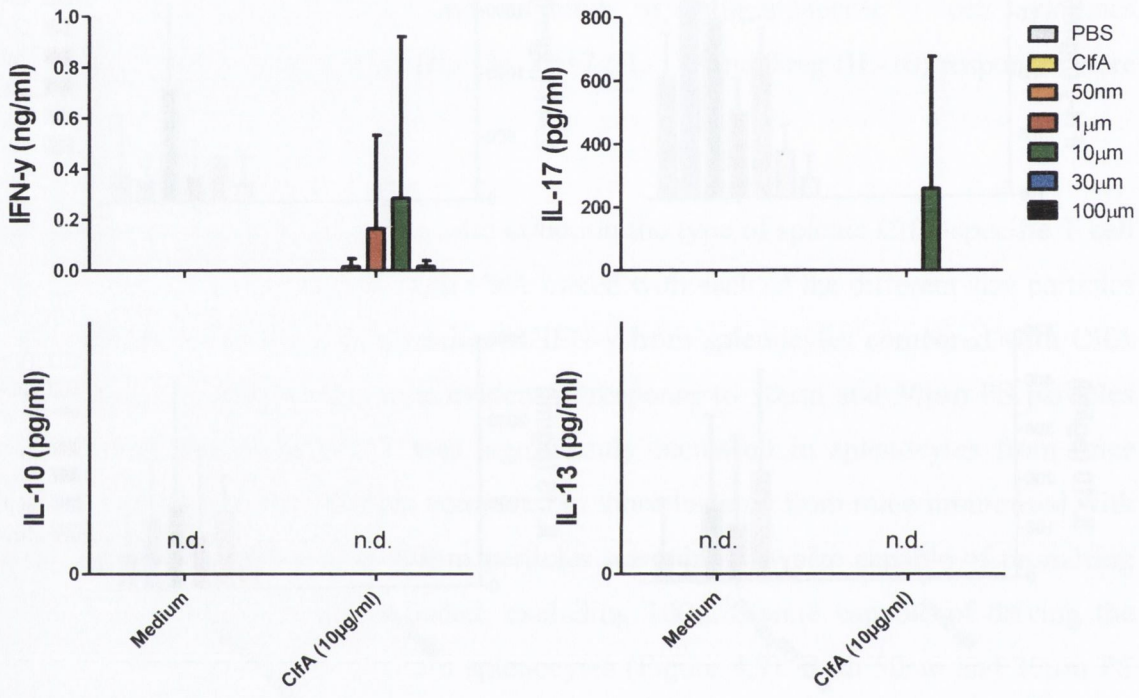

Figure 4.10 – Different sized particles drive distinct ClfA-specific T cell responses in inguinal lymph node cells. Female C57BL/6 mice were immunised s.c. on day 0 with PBS or ClfA (1μg) either alone or in combination with PS particles (50nm, 1μm, 10μm, 30μm or 100μm) (4mg/mouse) in 200μl volumes. On day 14 the mice were immunised with these same treatments and on day 21 the inguinal lymph nodes were collected. Inguinal lymph node cells (1 x 10^6 cells/ml) were restimulated *ex vivo* with either medium alone or ClfA (10μg/ml). Levels of cytokines were measured in supernatants by ELISA after 72 hours. Bar charts represent mean (+ SD) for 5 mice per experimental group.

4.3.10. The type and magnitude of ClfA-specific cellular immunity induced by PS particles depends on route of administration

Since route of administration was shown to affect antigen-specific antibody responses in the case of 1μm particles (Figure 4.7), the relationship between route of administration and the induction of antigen-specific T cell responses was determined. Female C57BL/6 mice were immunised i.p. on day 0 with PBS or ClfA (1μg) either alone or in combination with PS particles (50nm, 1μm, 10μm, 30μm or 100μm). On day 14 the mice were immunised with the same treatments and on day 21 PECs, spleens and the draining lymph nodes (mediastinal lymph nodes) were isolated. Cells were restimulated *ex vivo* and antigen-specific secretion of IFN-γ, IL-13, IL-17 and IL-10 was measured.

PECs, splenocytes and mediastinal lymph node cells were restimulated with anti-CD3 to assess cell viability and responsiveness. All cells responded to anti-CD3 stimulation as assessed by cytokine secretion measured by ELISA (data not shown). However splenocytes and mediastinal lymph node cells were unresponsive to ClfA restimulation *ex vivo* (data not shown). At the injection site, immunisation with ClfA mixed with 50nm PS particles led to an increase in secretion of antigen-specific IFN-γ from PECs compared with ClfA alone (Figure 4.11). However, immunisation with other PS particle sizes did not induce enhanced antigen-specific T cell responses from restimulated PECs (Figure 4.11).

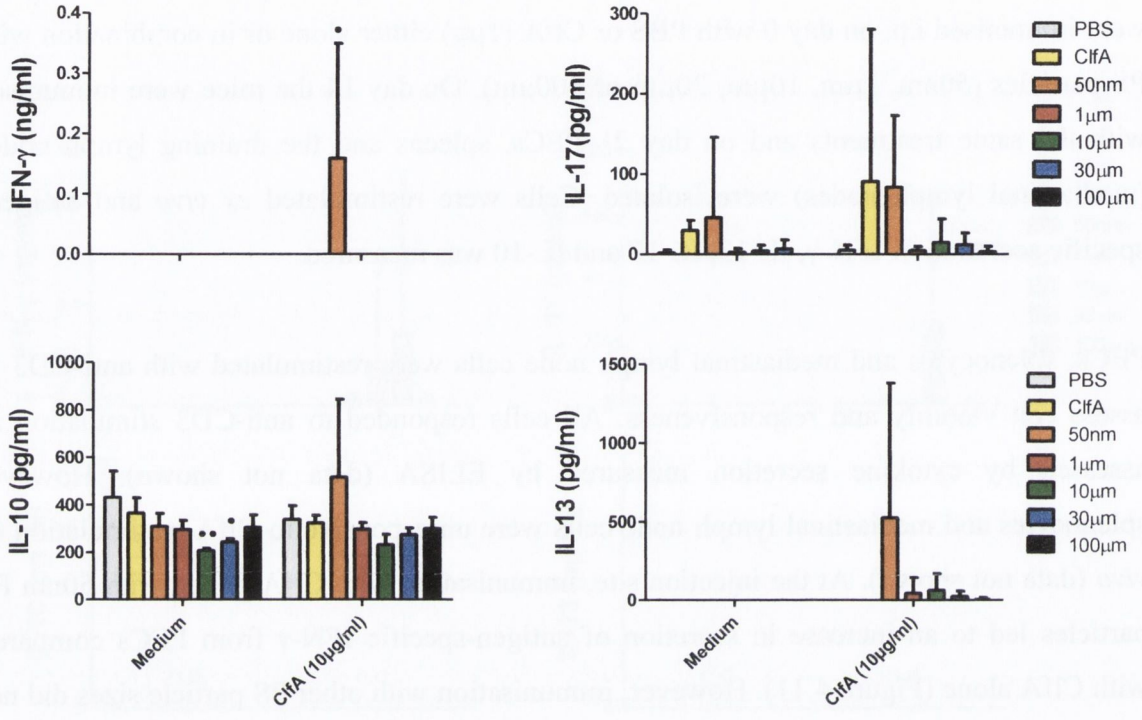

Figure 4.11 – Immunisation with 50nm PS particles and ClfA drives a ClfA-specific T cell response in PECs. Female C57BL/6 mice were immunised i.p. on day 0 with PBS or ClfA (1μg) either alone or in combination with PS particles (50nm, 1μm, 10μm, 30μm or 100μm) (4mg/mouse) in 200μl volumes. On day 14 the mice were immunised with these same treatments and on day 21 the PECs were collected. PECs (1 x 10^6 cells/ml) were restimulated *ex vivo* with either medium alone or ClfA (10μg/ml). Levels of cytokines were measured in supernatants by ELISA after 72 hours. Bar charts represent mean (+ SD) for 5 mice per experimental group. Versus mice immunised with ClfA alone, • $p<0.05$, •• $p<0.01$.

4.3.11. Vaccination with ClfA and 50nm PS particles induces the production of intracellular IFN-γ, but not IL-17, in PECs

To further investigate the source of the antigen-specific IFN-γ and possible IL-17 responses induced after i.p. immunisation with PS particles (Figure 4.11), female C57BL/6 mice were immunised i.p. on day 0 with PBS or ClfA (1μg) either alone or in combination with PS particles (50nm, 1μm, 10μm, 30μm or 100μm). On day 14 the mice were immunised with the same treatments and on day 21 PECs were isolated, restimulated and analysed by flow cytometry. PECs were restimulated *ex vivo* with either anti-CD28 alone (1μg/ml), ClfA alone (10μg/ml), PMA (0.1μg/ml) combined with ION (0.5μg/ml) or a combination of ClfA and anti-CD28 for 6 hours, the last 5 hours also including Brefeldin A (10μg/ml). Brefeldin A disrupts the function of the golgi apparatus in the cell and therefore inhibits newly translated proteins from leaving the cell. Intracellular IFN-γ and IL-17 levels were then assessed in $CD8^+$ T cells and $CD4^+$ T cell populations.

The positive control of PMA and ION enhanced intracellular IL-17 and IFN-γ in restimulated PECs (Figures 4.12-4.15). Restimulation with anti-CD28 or ClfA alone did not induce significant intracellular IL-17 or IFN-γ in $CD4^+$ or $CD8^+$ T cells (Figures 4.12-4.15).

PECs restimulated with anti-CD28 in combination with ClfA did not produce antigen-specific intracellular IL-17 in $CD4^+$ or $CD8^+$ T cells (Figure 4.12, 4.14), nor any antigen-specific IFN-γ from $CD8^+$ T cells (Figure 4.13). However, $CD4^+$ T cells produced antigen-specific intracellular IFN-γ following restimulation with anti-CD28 in combination with ClfA (Figure 4.15).

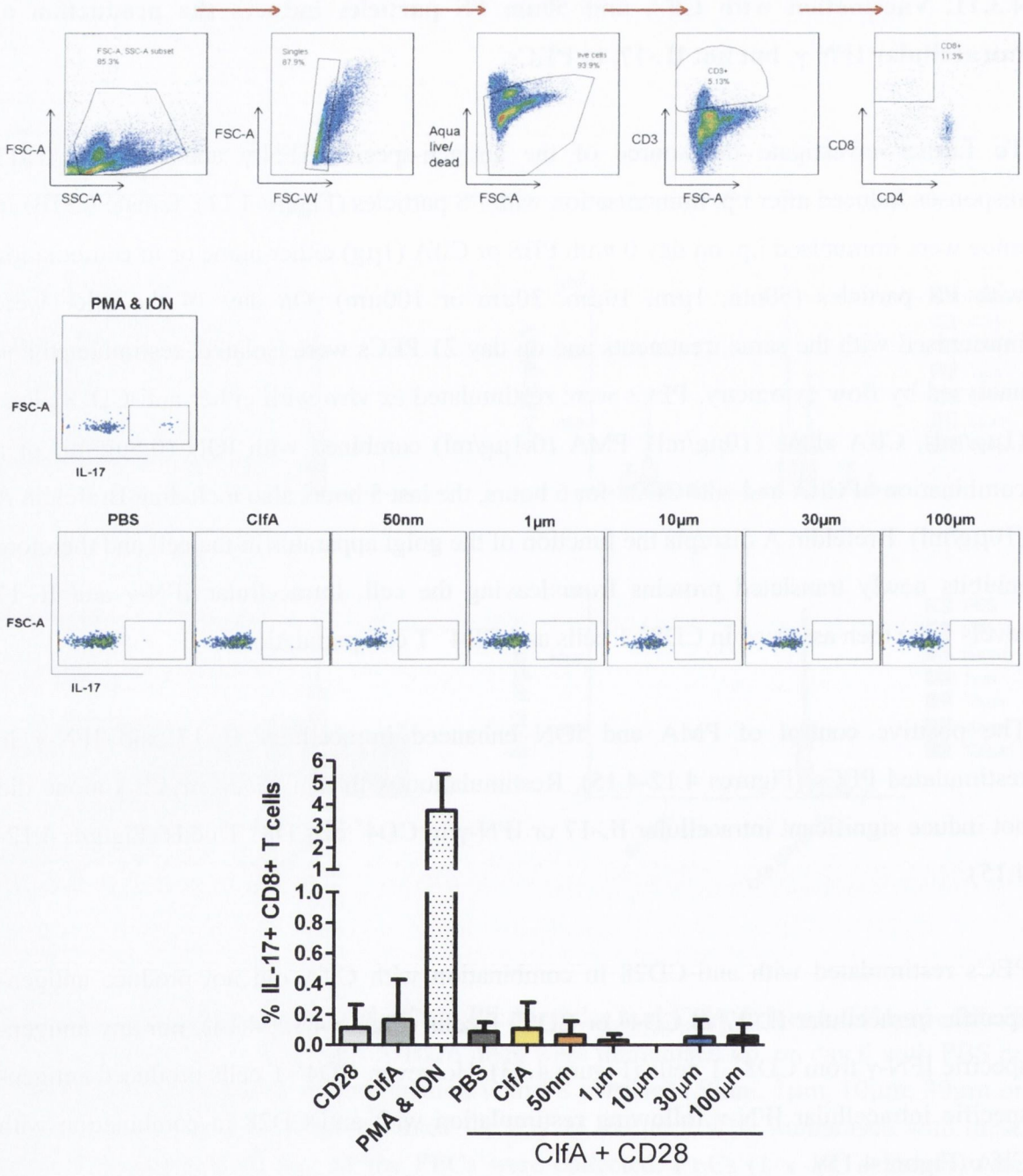

Figure 4.12 – Intra-peritoneal vaccination with ClfA and PS particles does not lead to detectable intracellular IL-17 in $CD8^+$ T cells after stimulation with ClfA and CD28. Female C57BL/6 mice were immunised i.p. on day 0 with PBS or ClfA (1μg) either alone or in combination with PS particles (50nm, 1μm, 10μm, 30μm or 100μm) (4mg/mouse) in 200μl volumes. On day 14 the mice were immunised with these same treatments and on day 21 the PECs were collected. PECs were restimulated *ex vivo* with either anti-CD28 alone (1μg/ml), ClfA alone (10μg/ml), PMA (0.1μg/ml) combined with ION (0.5μg/ml) or a combination of ClfA and anti-CD28 for 6 hours, the last 5 hours also including Brefeldin A (10μg/ml). $CD8^+$ $IL\text{-}17^+$ T cells were gated as $CD3^+$ $CD4^-$ $CD8^+$ and the data are graphed as a percentage of $CD8^+$ T cells. Bar charts represent mean (+ SD) for 5 mice per experimental group.

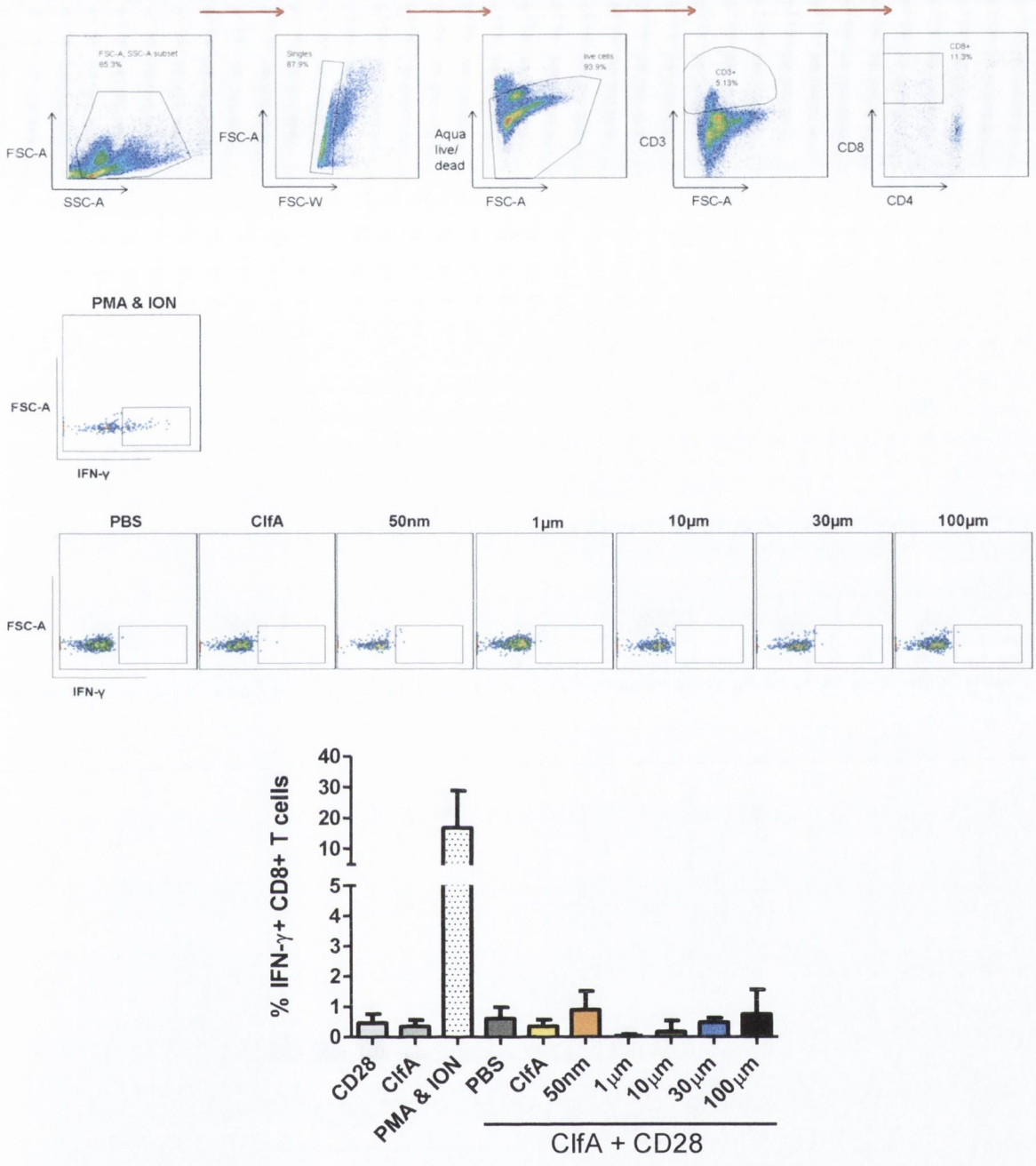

Figure 4.13 – Intra-peritoneal vaccination with ClfA and PS particles does not lead to detectable intracellular IFN-γ in $CD8^+$ T cells after stimulation with ClfA and CD28. Female C57BL/6 mice were immunised i.p. on day 0 with PBS or ClfA (1μg) either alone or in combination with PS particles (50nm, 1μm, 10μm, 30μm or 100μm) (4mg/mouse) in 200μl volumes. On day 14 the mice were immunised with these same treatments and on day 21 the PECs were collected. PECs were restimulated *ex vivo* with either anti-CD28 alone (1μg/ml), ClfA alone (10μg/ml), PMA (0.1μg/ml) combined with ION (0.5μg/ml) or a combination of ClfA and anti-CD28 for 6 hours, the last 5 hours also including Brefeldin A (10μg/ml). $CD8^+$ IFN-γ^+ T cells were gated as $CD3^+$ $CD4^-$ $CD8^+$ and the data are graphed as a percentage of $CD8^+$ T cells. Bar charts represent mean (+ SD) for 5 mice per experimental group.

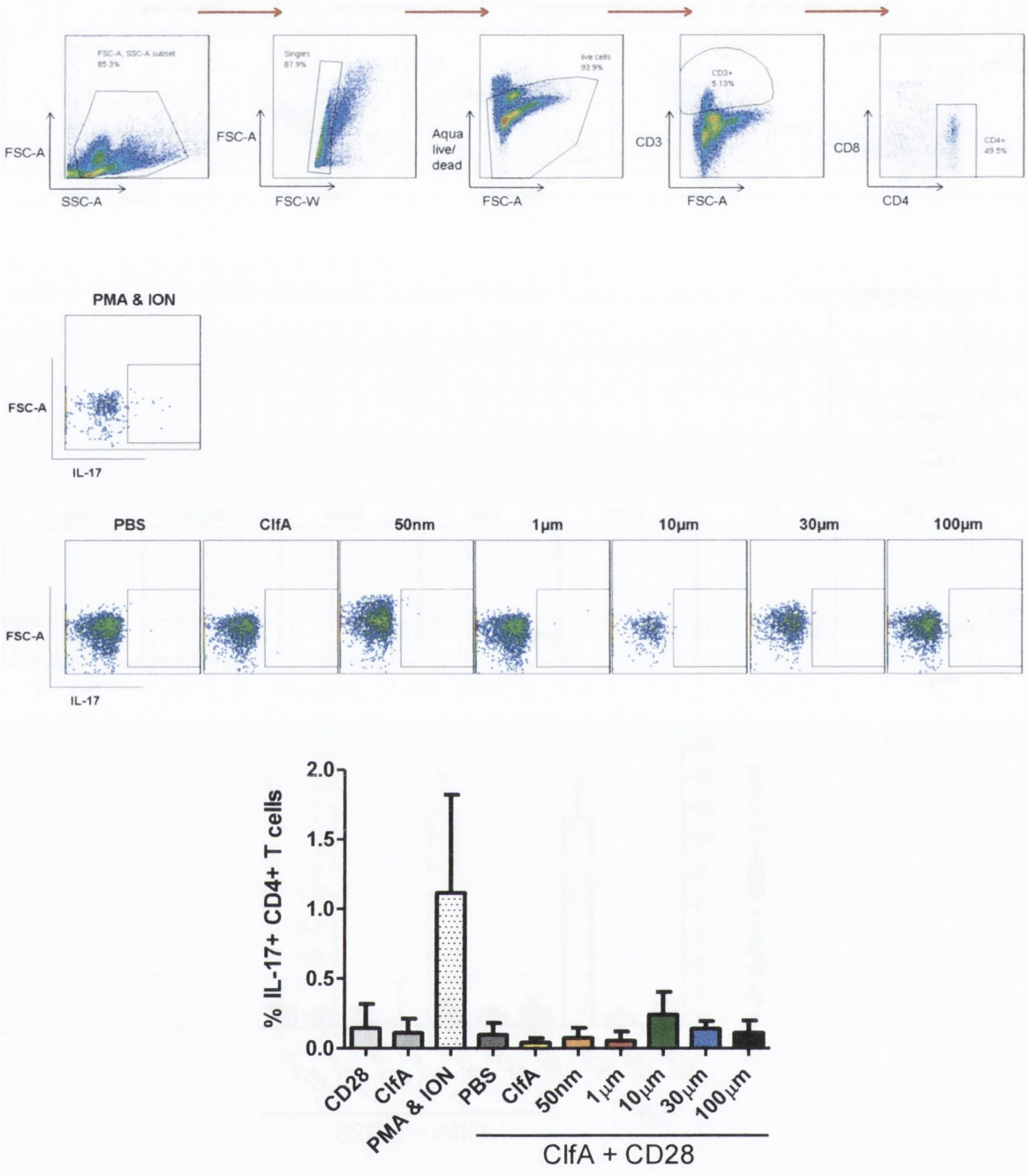

Figure 4.14 – Intra-peritoneal vaccination with ClfA and PS particles does not lead to detectable intracellular IL-17 in $CD4^+$ T cells after stimulation with ClfA and CD28. Female C57BL/6 mice were immunised i.p. on day 0 with PBS or ClfA (1µg) either alone or in combination with PS particles (50nm, 1µm, 10µm, 30µm or 100µm) (4mg/mouse) in 200µl volumes. On day 14 the mice were immunised with these same treatments and on day 21 the PECs were collected. PECs were restimulated *ex vivo* with either anti-CD28 alone (1µg/ml), ClfA alone (10µg/ml), PMA (0.1µg/ml) combined with ION (0.5µg/ml) or a combination of ClfA and anti-CD28 for 6 hours, the last 5 hours also including Brefeldin A (10µg/ml). $CD4^+$ $IL\text{-}17^+$ T cells were gated as $CD3^+$ $CD8^-$ $CD4^+$and the data are graphed as a percentage of $CD8^+$ T cells. Bar charts represent mean (+ SD) for 5 mice per experimental group.

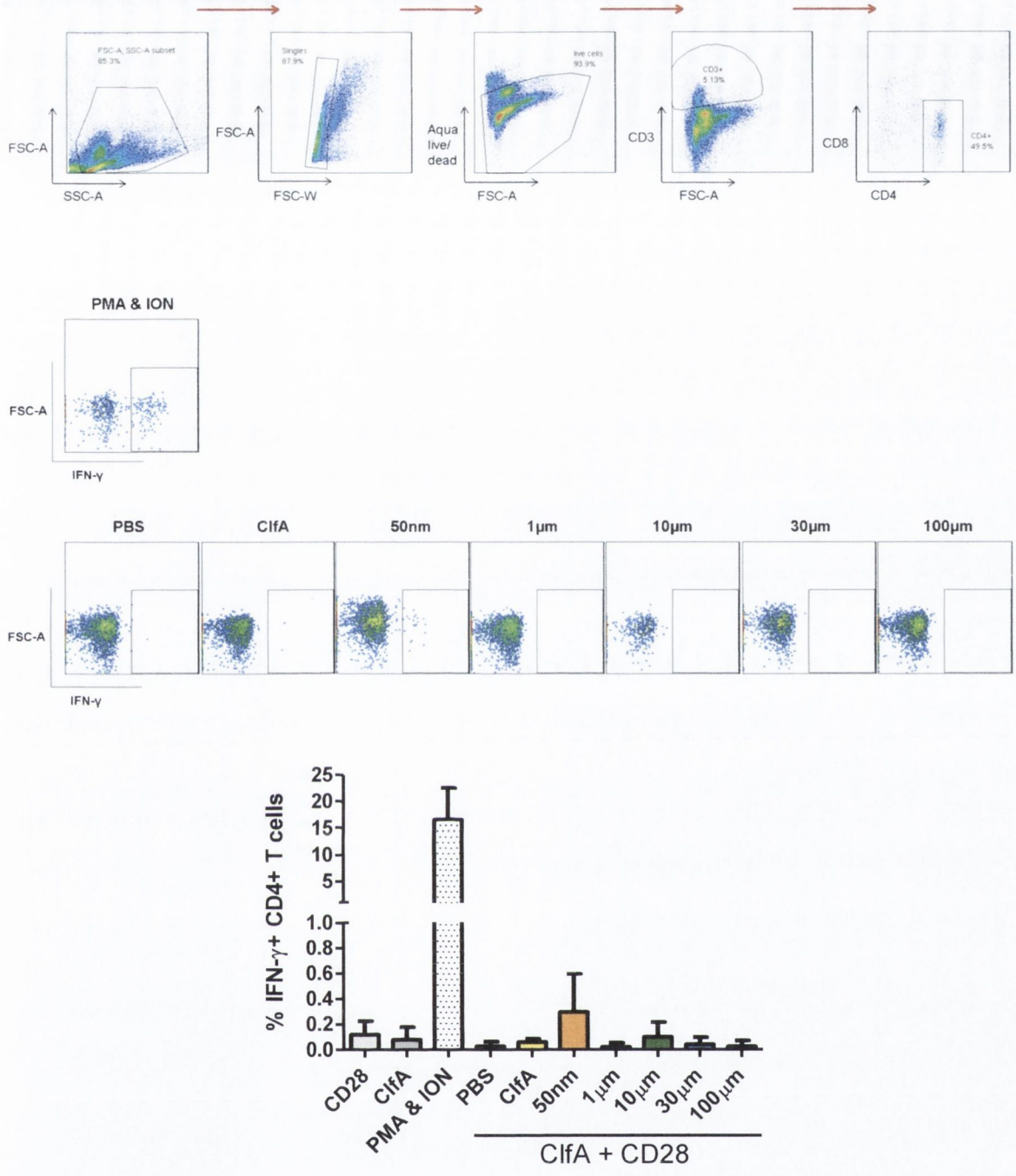

Figure 4.15 – Intra-peritoneal vaccination with ClfA and 50nm PS particles leads to intracellular IFN-γ in CD4$^+$ T cells after stimulation with ClfA and CD28.. Female C57BL/6 mice were immunised i.p. on day 0 with PBS or ClfA (1μg) either alone or in combination with PS particles (50nm, 1μm, 10μm, 30μm or 100μm) (4mg/mouse) in 200μl volumes. On day 14 the mice were immunised with these same treatments and on day 21 the PECs were collected. PECs were restimulated *ex vivo* with either anti-CD28 alone (1μg/ml), ClfA alone (10μg/ml), PMA (0.1μg/ml) combined with ION (0.5μg/ml) or a combination of ClfA and anti-CD28 for 6 hours, the last 5 hours also including Brefeldin A (10μg/ml). CD4$^+$ IFN-γ$^+$ T cells were gated as CD3$^+$ CD8$^-$ CD4$^+$ and the data are graphed as a percentage of CD8$^+$ T cells. Bar charts represent mean (+ SD) for 5 mice per experimental group.

4.3.12 Immunisation with OVA and 50nm PS particles induces OVA-specific IL-13 secretion from PECs

To verify if the T cell response generated after immunisation with ClfA and 50nm PS particles was dependent on the antigen used, an adjuvant model was established using OVA. Female C57BL/6 mice were immunised i.p. on day 0 with PBS or OVA (1μg) either alone or in combination with alum (1mg) or PS particles (50nm, 1μm, 10μm, 30μm or 100μm). Alum was used as a positive control to compare the ability of PS particles to drive antigen-specific antibody responses. On day 14 the mice were boosted with these same treatments and PECs, mediastinal lymph nodes and spleens were collected on day 21. Cells were restimulated *ex vivo* and antigen-specific cytokine secretion measured.

PECs, splenocytes and mediastinal lymph node cells were also restimulated with anti-CD3 to assess responsiveness. All cells responded to anti-CD3 stimulation as assessed by cytokine secretion measured by ELISA (data not shown). Antigen-specific cytokine production from splenocytes and mediastinal lymph node cells could not be detected (data not shown). Immunisation with 50nm PS particles and OVA induced enhanced antigen-specific IL-13 production by PECs when restimulated with OVA when compared with mice immunised with OVA alone (Figure 4.16).

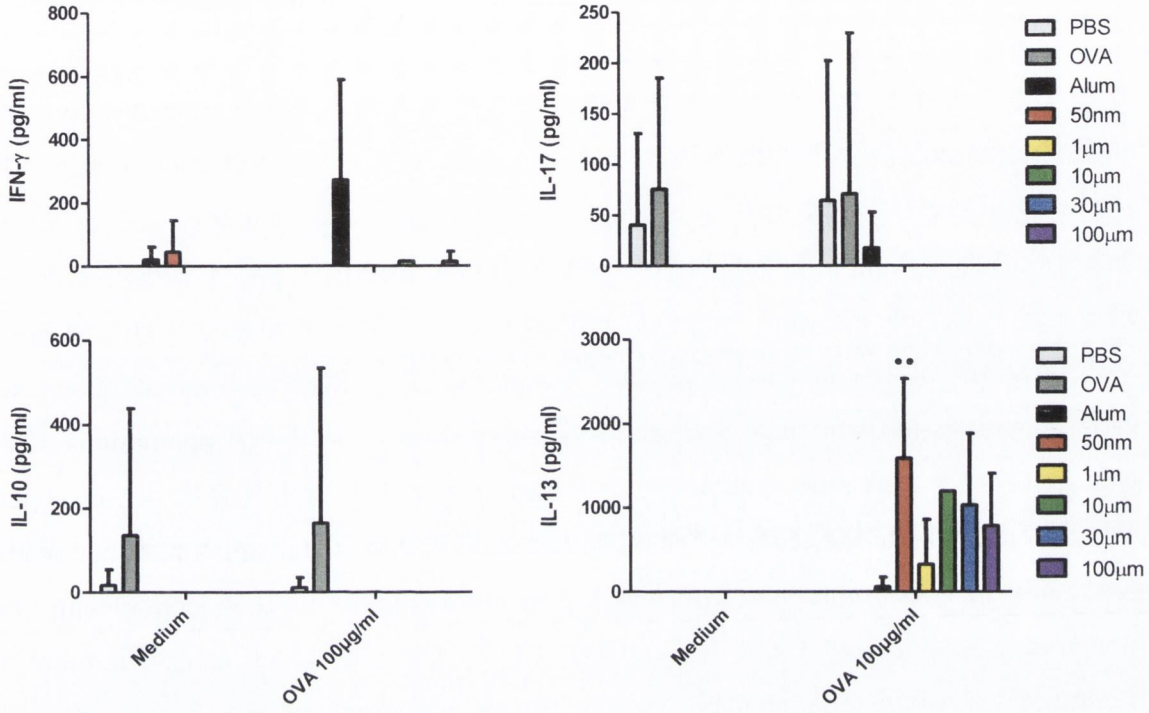

Figure 4.16 - Immunisation with PS particles and OVA drives OVA-specific IL-13 secretion from restimulated PECs. Female C57BL/6 mice were immunised i.p. on day 0 with PBS or OVA (1μg) either alone or in combination with alum (1mg) or PS particles (50nm, 1μm, 10μm, 30μm or 100μm) (4mg/mouse) in 200μl volumes. On day 14 the mice were immunised with these same treatments and on day 21 the PECs were collected. PECs (1×10^6 cells/ml) were restimulated *ex vivo* with either medium alone or OVA (100μg/ml). Levels of cytokines were measured in supernatants by ELISA after 72 hours. Bar charts represent mean (+ SD) for 5 mice per experimental group. Versus mice immunised with OVA alone, •• $p<0.01$.

4.3.13 50nm is the optimal particle size for promotion of antigen-specific $CD8^+$ T cell responses

To quantitatively determine if 50nm particles were capable of inducing antigen-specific $CD8^+$ T cell responses, an OVA-specific iTAg MHCcI tetramer was used.

Firstly, the tetramer needed to be titrated to an appropriate working concentration. Mice were immunised i.p. with either OVA alone (1μg) or OVA mixed with alum (1mg). Alum was used as a positive control as previous experiments in the laboratory had shown that immunisation with alum is capable of inducing OVA-specific $CD8^+$ T cells. Seven days after injection, spleens were isolated and splenocytes were incubated with a range of concentrations of the PE-conjugated OVA-specific iTAg MHCcI tetramer along with various markers to distinguish activated antigen-specific $CD8^+$ T cell populations. OVA-specific $CD8^+$ T cells were gated as $B220^-$ $F4/80^-$ $CD3^+$ $CD4^-$ $CD8^+$ $CD44^+$ tetramer $(tet)^+$. All concentrations of the tetramer tested were capable of distinguishing a tetramer positive population in mice immunised with OVA plus alum (Figure 4.17). Injection with OVA alone did not induce any $B220^-$ $F4/80^-$ $CD3^+$ $CD4^-$ $CD8^+$ $CD44^+$ tet^+ cells. Therefore, the minimum dose of the tetramer (1μl) was used for all future experiments.

Female C57BL/6 mice were immunised i.p. on day 0 with PBS or OVA (1μg) either alone or in combination with alum (1mg) or PS particles (50nm, 1μm, 10μm, 30μm or 100μm). On day 14 the mice were boosted with these same treatments and spleens and mediastinal lymph nodes were collected on day 21. Splenocytes and mediastinal lymph node cells were isolated, counted and incubated with the PE-conjugated OVA-specific iTAg MHCcI tetramer for 2 hours.

Immunisation with 50nm PS particles drove a significant increase in Tet^+ $CD8^+$ T cells in terms of percentage and number when compared with immunisation with OVA alone (Figures 4.18, 4.19). This was detectable in both the spleen and mediastinal lymph nodes. Interestingly, this response was significantly greater than that induced by OVA and alum in both tissues (Figure 4.18, 4.19). No other sized PS particle drove the induction of Tet^+ $CD8^+$ T cells.

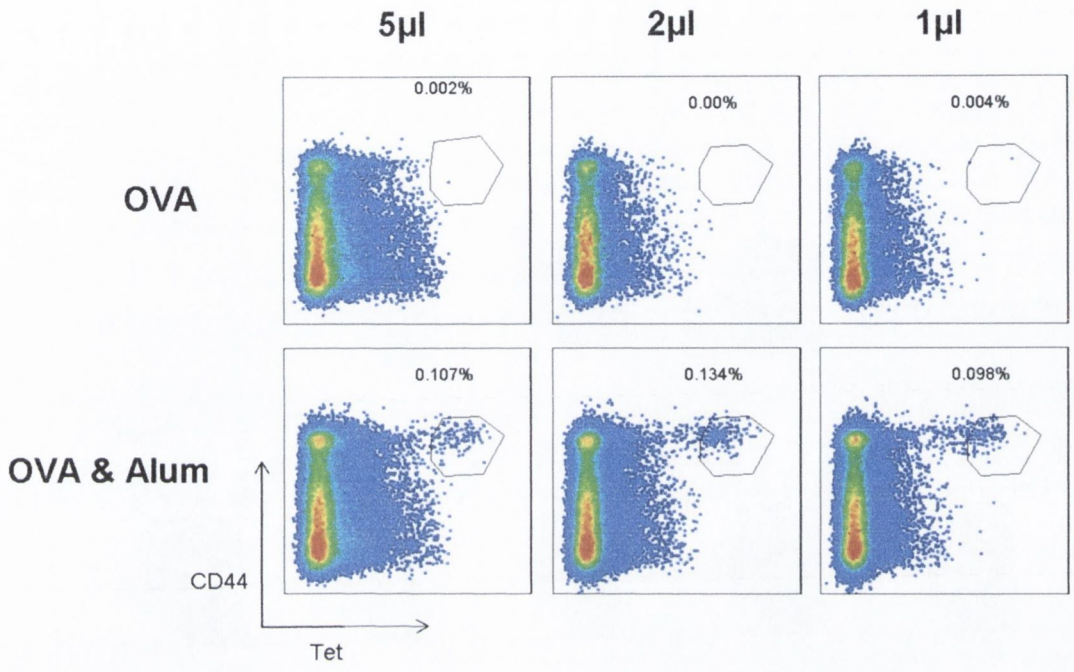

Figure 4.17 – All concentrations of PE-conjugated tetramer distinguish an antigen-specific CD8$^+$ T cell population. Female C57BL/6 mice were injected i.p. on day 0 with PBS or OVA (1µg) either alone or in combination with alum (1mg) in 200µl volumes. On day 7 spleens were collected. Splenocytes (2 x 10^6 cells) were incubated for 2 hours with either 5µl, 2µl or 1µl of PE-conjugated OVA-specific iTAg MHCcI tetramer and OVA-specific CD8+ T cells were gated as B220$^-$ F4/80$^-$ CD3$^+$ CD4$^-$ CD8$^+$ CD44$^+$ tet$^+$.

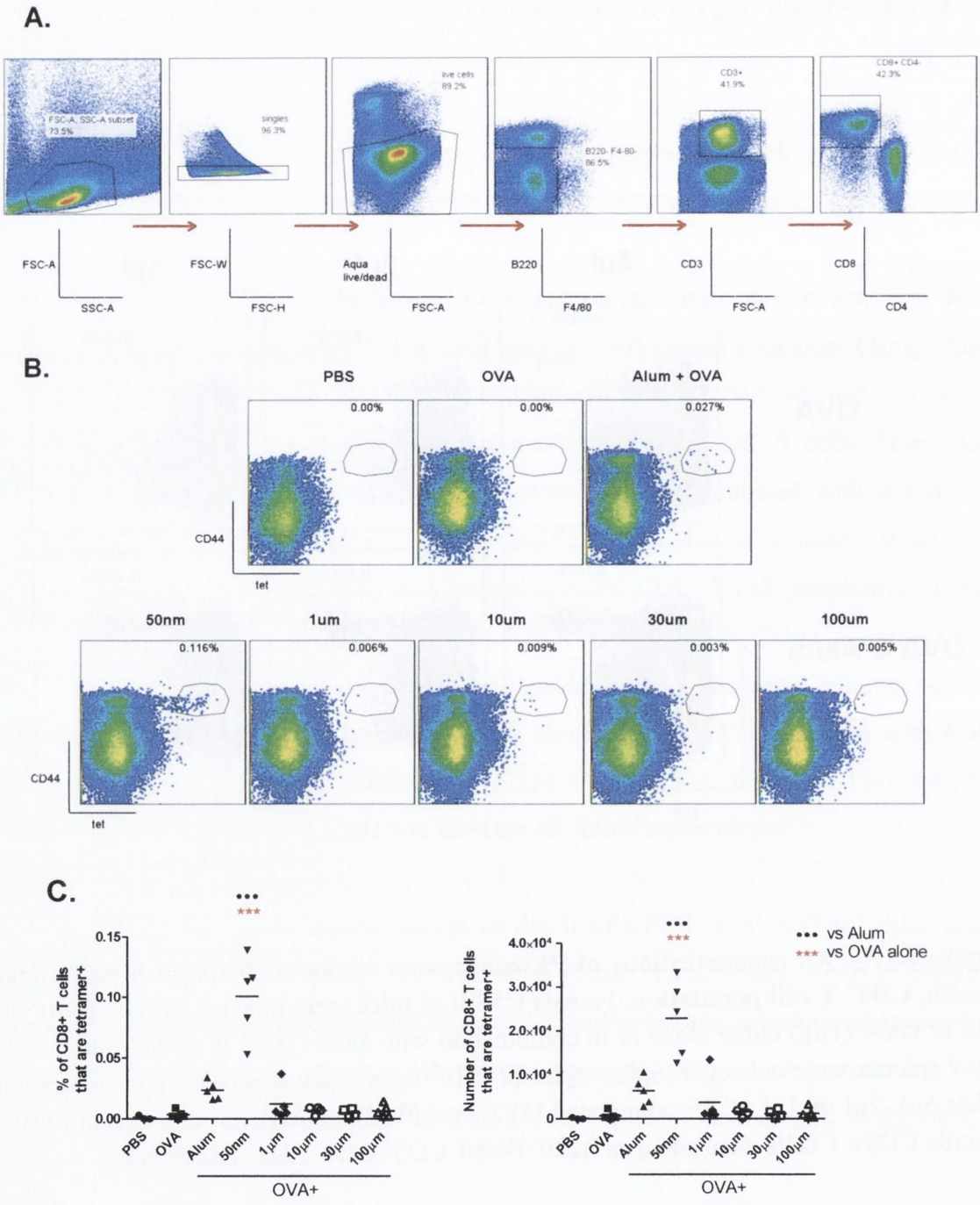

Figure 4.18 – Intra-peritoneal vaccination with OVA and 50nm PS particles drives antigen specific CD8$^+$ T cell expansion in the spleen. Female C57BL/6 mice were immunised i.p. on day 0 with PBS or OVA (1µg) either alone or in combination with alum (1mg) or PS particles (50nm, 1µm, 10µm, 30µm or 100µm) (4mg/mouse) in 200µl volumes. On day 14 the mice were immunised with these same treatments and on day 21 spleens were collected. Splenocytes were incubated with a PE-conjugated OVA-specific iTAg MHCcI tetramer for 2 hours and OVA-specific CD8+ T cells were gated as B220$^-$ F4/80$^-$ CD3$^+$ CD4$^-$ CD8$^+$ CD44$^+$ tet$^+$ (A, B). The data are graphed as a percentage or number of CD8$^+$ T cells that are tetramer$^+$ (C). Bar charts represent mean (+ SD) for 5 mice per experimental group. Versus alum, ••• $p<0.0001$. Versus OVA alone, *** $p<0.0001$.

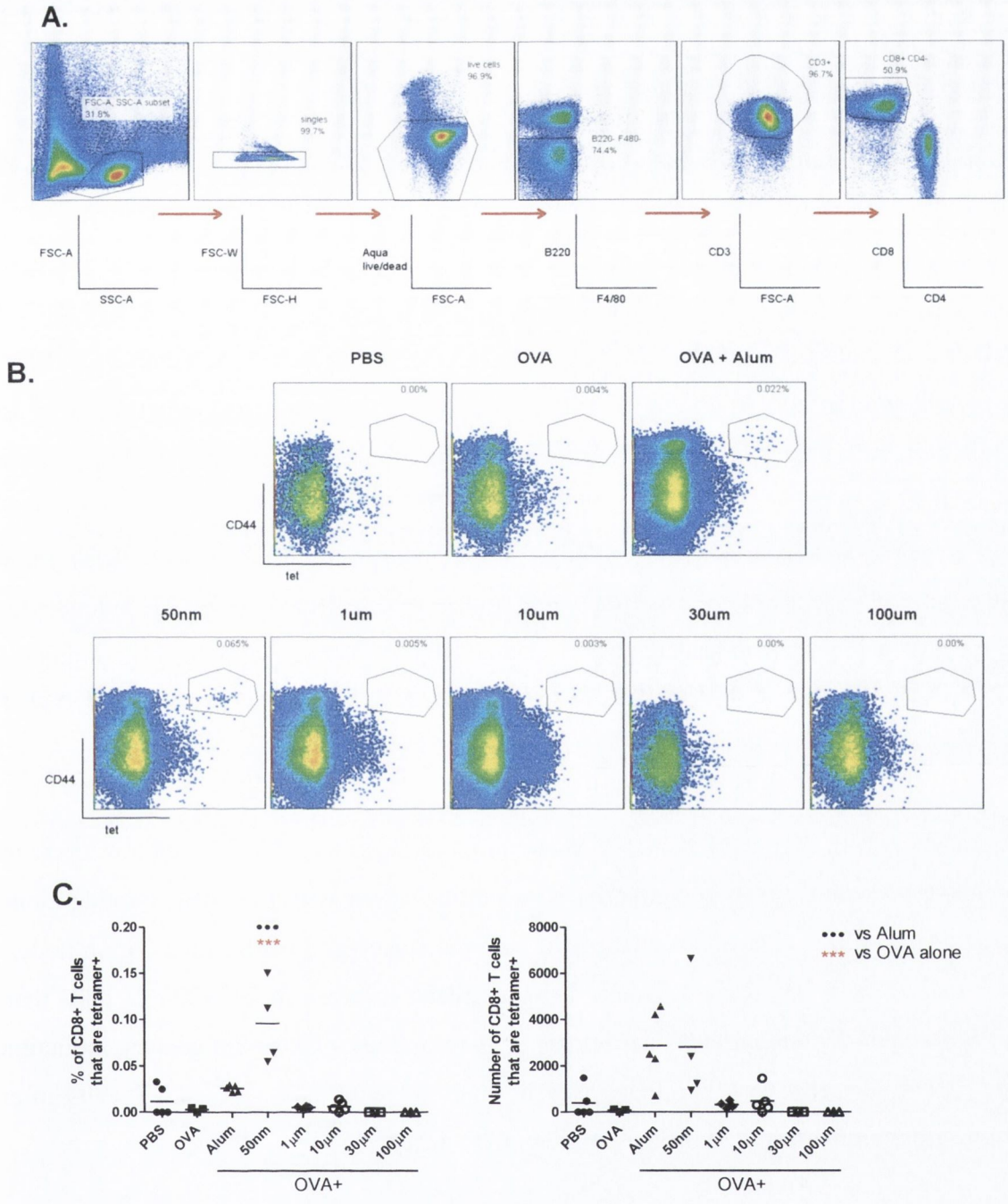

Figure 4.19 – Intra-peritoneal vaccination with OVA and 50nm PS particles drives antigen specific CD8$^+$ T cell expansion in the draining lymph nodes. Female C57BL/6 mice were immunised i.p. on day 0 with PBS or OVA (1µg) either alone or in combination with alum (1mg) or PS particles (50nm, 1µm, 10µm, 30µm or 100µm) (4mg/mouse) in 200µl volumes. On day 14 the mice were immunised with these same treatments and on day 21 mediastinal lymph nodes were collected. Mediastinal lymph node cells were incubated with a PE-conjugated OVA-specific iTAg MHCcI tetramer for 2 hours and OVA-specific CD8+ T cells were gated as B220$^-$ F4/80$^-$ CD3$^+$ CD4$^-$ CD8$^+$ CD44$^+$ tet$^+$ (A, B). The data are graphed as a percentage or number of CD8$^+$ T cells that are tetramer$^+$ (C). Bar charts represent mean (+ SD) for 5 mice per experimental group. Versus alum, ••• $p<0.0001$. Versus OVA alone, *** $p<0.0001$.

4.3.14 50nm is the optimal particle size for promotion of antigen-specific $CD4^+$ T cell responses

The ability of 50nm PS particles to drive a significant $CD8^+$ antigen-specific response as shown by tetramer positive cells by flow cytometry prompted the use of this method to detect $CD4^+$ antigen-specific cells after immunisation with PS particles. To detect antigen-specific $CD4^+$ T cells, a PE-conjugated influenza NP_{311}-specific I-A(b) restricted MHCcII tetramer was kindly donated by Dr. Tom Barr, University of Glasgow. Female C57BL/6 mice were immunised i.p. on day 0 with PBS or NP_{311} peptide (1μg) either alone or in combination with alum (1mg) or PS particles (50nm, 1μm, 10μm, 30μm or 100μm). Alum was used as a positive control to compare the ability of PS particles to drive antigen-specific $CD4^+$ T cell responses. On day 14 the mice were boosted with these same treatments and spleens and mediastinal lymph nodes were collected on day 21. Splenocytes and mediastinal lymph node cells were isolated and incubated with the PE-conjugated NP_{311}-specific I-A(b) restricted MHCcII tetramer for 2 hours and NP_{311}-specific CD4+ T cells were gated as $CD11c^-$ $F4/80^-$ $B220^-$ $CD3^+$ $CD4^+$ $CD44^+$ tet^+ (Figure 4.20A, B).

Immunisation with 50nm PS particles drove an increase in tet^+ $CD4^+$ T cells in terms of percentage and number when compared with immunisation with the NP_{311} peptide alone (Figures 4.20, 4.21). This was detectable in both the spleen and mediastinal lymph nodes. In contrast to the $CD8^+$ tetramer, alum drove a greater increase in tet^+ $CD4^+$ T cells than any PS particle. With regards PS particles, 50nm PS particles drove the greatest induction of tet^+ $CD4^+$ T cells however there was a small increase in tet^+ $CD4^+$ T cells after immunisation with 10μm PS particles (Figure 4.20, 4.21).

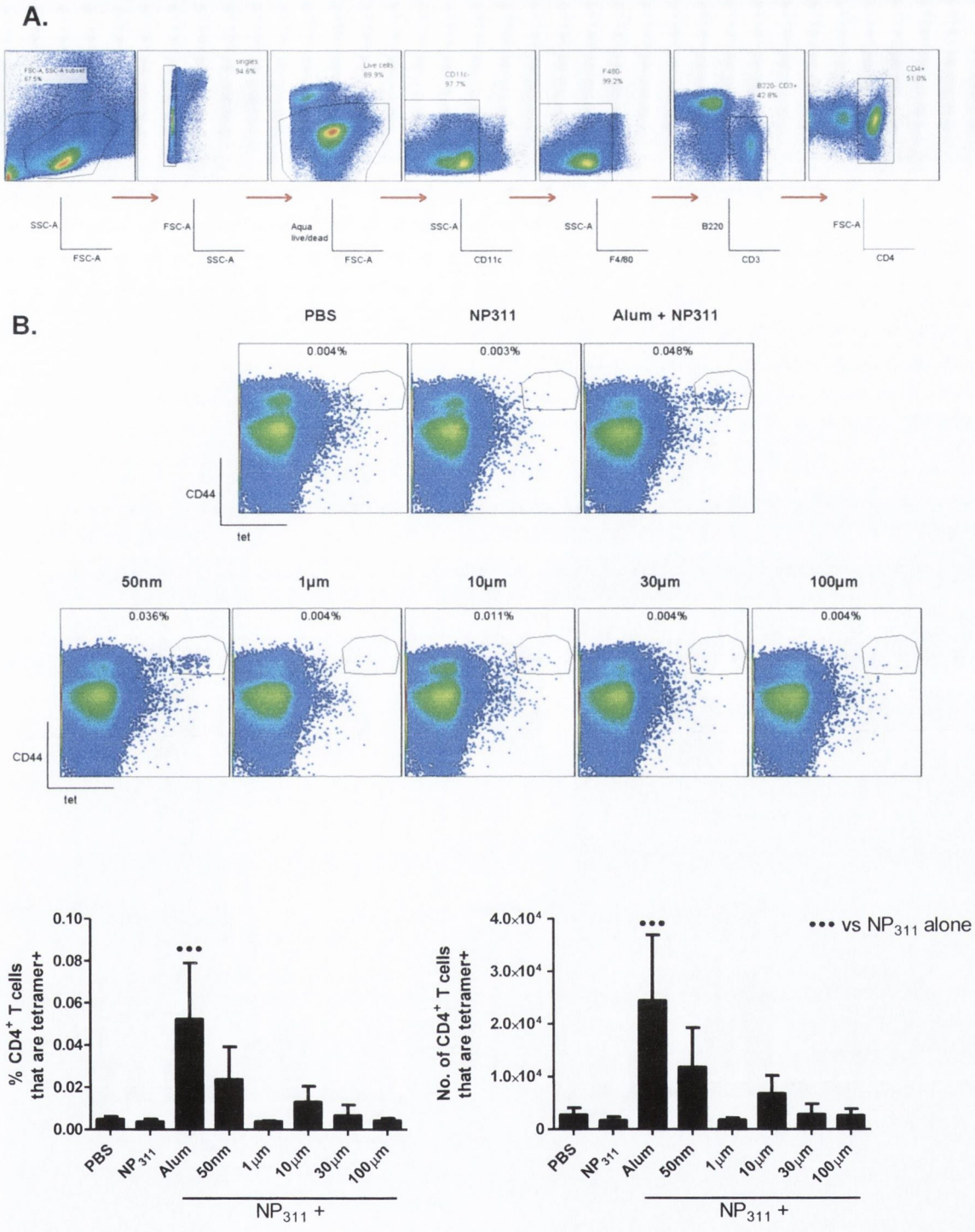

Figure 4.20 – Vaccination with NP_{311} and 50nm PS particles drives antigen specific $CD4^+$ T cell expansion in spenocytes. Female C57BL/6 mice were immunised i.p. on day 0 with PBS or NP_{311} (10µg) either alone or in combination with alum (1mg) or PS particles (50nm, 1µm, 10µm, 30µm or 100µm) (4mg/mouse) in 200µl volumes. On day 14, the mice were immunised with these same treatments and on day 21 splenocytes were collected. Cells were incubated with a PE-conjugated NP_{311}-specific I-A(b) restricted MHCcII tetramer and NP_{311}-specific CD4+ T cells were gated as $CD11c^-$ $F4/80^-$ $B220^-$ $CD3^+$ $CD4^+$ $CD44^+$ tet^+ (A, B). The data are graphed as a percentage or number of $CD4^+$ T cells that are $tetramer^+$ (C). Bar charts represent mean (+ SD) for 5 mice per experimental group. Versus NP_{311} alone, ••• $p<0.0001$.

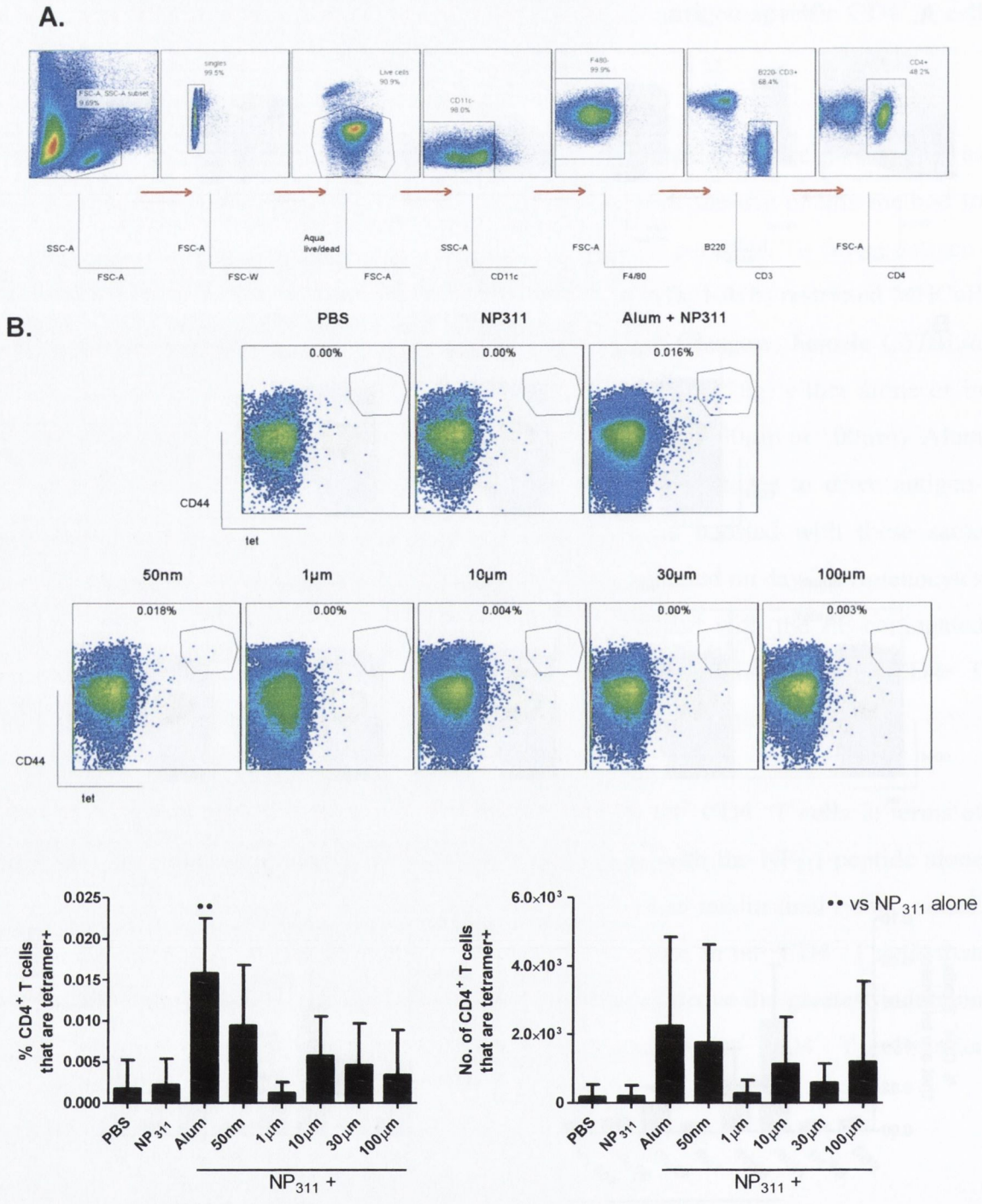

Figure 4.21 – Vaccination with NP_{311} and 50nm PS particles drives antigen specific $CD4^+$ T cell expansion in the draining lymph nodes. Female C57BL/6 mice were immunised i.p. on day 0 with PBS or NP_{311} (10μg) either alone or in combination with alum (1mg) or PS particles (50nm, 1μm, 10μm, 30μm or 100μm) (4mg/mouse) in 200μl volumes. On day 14, the mice were immunised with these same treatments and on day 21 mediastinal lymph node cells were collected. Cells were incubated with a PE-conjugated NP_{311}-specific I-A(b) restricted MHCcII tetramer and NP_{311}-specific CD4+ T cells were gated as $CD11c^-$ $F4/80^-$ $B220^-$ $CD3^+$ $CD4^+$ $CD44^+$ tet^+ (A, B). The data are graphed as a percentage or number of $CD4^+$ T cells that are $tetramer^+$ (C). Bar charts represent mean (+ SD) for 5 mice per experimental group. Versus NP_{311} alone, •• $p<0.0001$.

4.3.15 Vaccination with ClfA and 50nm PS particles induces the recruitment of activated neutrophils to the site of challenge which does not correlate with protection against *S. aureus* infection

Having shown that 50nm PS particles were capable of driving antigen-specific antibodies and the induction of both $CD8^+$ and $CD4^+$ T cell responses to a greater extent than any other particle size, the ability of these responses to protect in a challenge model was investigated. Work in our laboratory has recently demonstrated that nasal vaccine-induced protection against acute systemic *S. aureus* infection in mice is antibody-independent[457]. To determine if s.c. administration of PS particles could also induce protection via an antibody-independent mechanism, 100μm PS particles were used. Using ClfA as the antigen and challenging with a PS80 strain of *S. aureus*, female C57BL/6 mice were immunised subcutaneously with PBS or ClfA (1μg) alone or in combination with 50nm or 100μm PS particles (4mg). On day 14 the mice were boosted with the same treatments. Mice were challenged i.p. with 5×10^8 CFU PS80 on day 21 and PECs, livers, kidneys and spleens were isolated 24 or 72 hours after challenge to assess for protection.

The number of cells recruited to the site of challenge was significantly increased 24 hours after challenge in mice immunised with ClfA and 50nm PS particles compared with ClfA alone (Figure 4.22A). This infiltration was characterised by a significant increase in the number of neutrophils ($CD11b^+$ $F4/80^-$ $Ly6G^+$), as well as an enhanced number of macrophages ($CD11b^+$ $F4/80^+$ $Ly6G^-$) compared with ClfA alone (Figure 4.22B, C). Immunisation with either ClfA alone or ClfA combined with 100μm PS particles did not lead to an increased recruitment of cells into the peritoneum 24 hours after injection compared with the PBS control (Figure 4.22A). As expected, the number of inflammatory monocytes decreased over time as macrophage numbers increased, indicating differentiation of macrophages in the tissue (Figure 4.22B). The differentiation of macrophages appeared to occur earlier in mice immunised with 50nm PS particles as evidenced by the increased number of macrophages and decreased number of inflammatory monocytes at 24 hours (Figure 4.22B). Conversely, 72 hours after challenge, mice immunised with 50nm PS particles had the lowest number of cells at the site of challenge (Figure 4.22A).

To determine if cells recruited to the site of challenge were activated and therefore functional, the presence of the activation markers CD62L, CXCR2, nitric oxide synthase

(NOS)2, CD18 and MHCcII on neutrophils, inflammatory monocytes and macrophages was determined. CD62L is involved in the recruitment of neutrophils to inflamed tissue and is often down-regulated once at the site of inflammation[4]. Indeed, by 72 hours post challenge all neutrophils from all groups had down-regulated CD62L (Figure 4.23). The ligand for the neutrophil chemoattractants CXCL1 and CXCL2 is CXCR2[458]. As expected, all neutrophils were CXCR2 positive at both 24 hours and 72 hours post challenge. CD18 when paired with CD11b is known as the complement receptor 3 and is involved in various mechanisms of pathogen detection and phagocytosis[459,460]. Most neutrophils from all groups were CD18 positive and the percentage of $CD18^+$ neutrophils increased from 24 to 72 hours in all groups (Figure 4.23).

The expression of DHR (dihydrorhodamine) is an indirect measure of certain leukocytes function and oxidative burst. This is based on the fact that non-fluorescent DHR, when phagocytosed by activated neutrophils, can be oxidized by hydrogen peroxide (produced during the activated neutrophil respiratory oxidative burst) to rhodamine, a green fluorescent compound, which can be detected by flow cytometry. There was no difference between the different immunisation groups' neutrophil, inflammatory monocyte or macrophage oxidative burst functions, with 80-100% of all cells capable of oxidising DHR both 24 and 72 hours post challenge (Figure 4.23).

The activation markers of inflammatory monocytes and macrophages that were examined were MHCcII and NOS2. NOS2 is an effector molecule of activated macrophages and MHCcII is capable of presenting extracellular antigen on macrophage cell surfaces as described in Chapter 1[461]. As expected, inflammatory monocytes had low MHCcII and NOS2 expression 24 hours post challenge in all immunisation groups (Figure 4.23). 72 hours post challenge there was an increase in MHCcII expression in all groups, however mice immunised with 50nm PS particles had significantly fewer inflammatory monocytes that were $MHCcII^+$ than mice immunised with ClfA alone (Figure 4.23). Similarly, NOS2 expression on inflammatory monocytes from mice immunised with 50nm PS particles was significantly lower than that on inflammatory monocytes from mice immunised with ClfA alone (Figure 4.23).

Macrophages had the greatest MHCcII expression 72 hours post challenge. In a similar trend to inflammatory monocytes, macrophages from mice immunised with 50nm PS particles had significantly lower MHCcII expression than macrophages from mice

immunised with ClfA alone (Figure 4.23). NOS2 expression from macrophages was similar between all immunisation groups at both 24 and 72 hours post challenge (Figure 4.23).

Finally, to assess if the cell infiltration observed after challenge correlated with protection against *S. aureus* challenge, systemic infection levels were assessed. Bacterial burdens were quantified and 24 hours post challenge there were no significant differences in CFUs in the peritoneum, liver, spleen or kidney between mice immunised with ClfA alone and those immunised with ClfA and either 50nm or 100μm PS particles (Figure 4.24A). Remarkably, 72 hours after challenge there was still no difference in CFUs in the peritoneal cavity and the spleen in mice immunised with ClfA and PS particles compared with those immunised with PBS or ClfA alone (Figure 4.24B). 72 hours post challenge, immunisation with both 50nm and 100μm PS particles induced significantly reduced CFUs in the liver compared with mice immunised with PBS. However, immunisation with ClfA alone induced an even greater reduction in CFUs in the liver 72 hours post challenge (Figure 4.24B). Surprisingly, mice immunised with ClfA and 50nm PS particles had significantly higher CFUs in kidneys than mice immunised with either PBS or ClfA alone (Figure 4.24B).

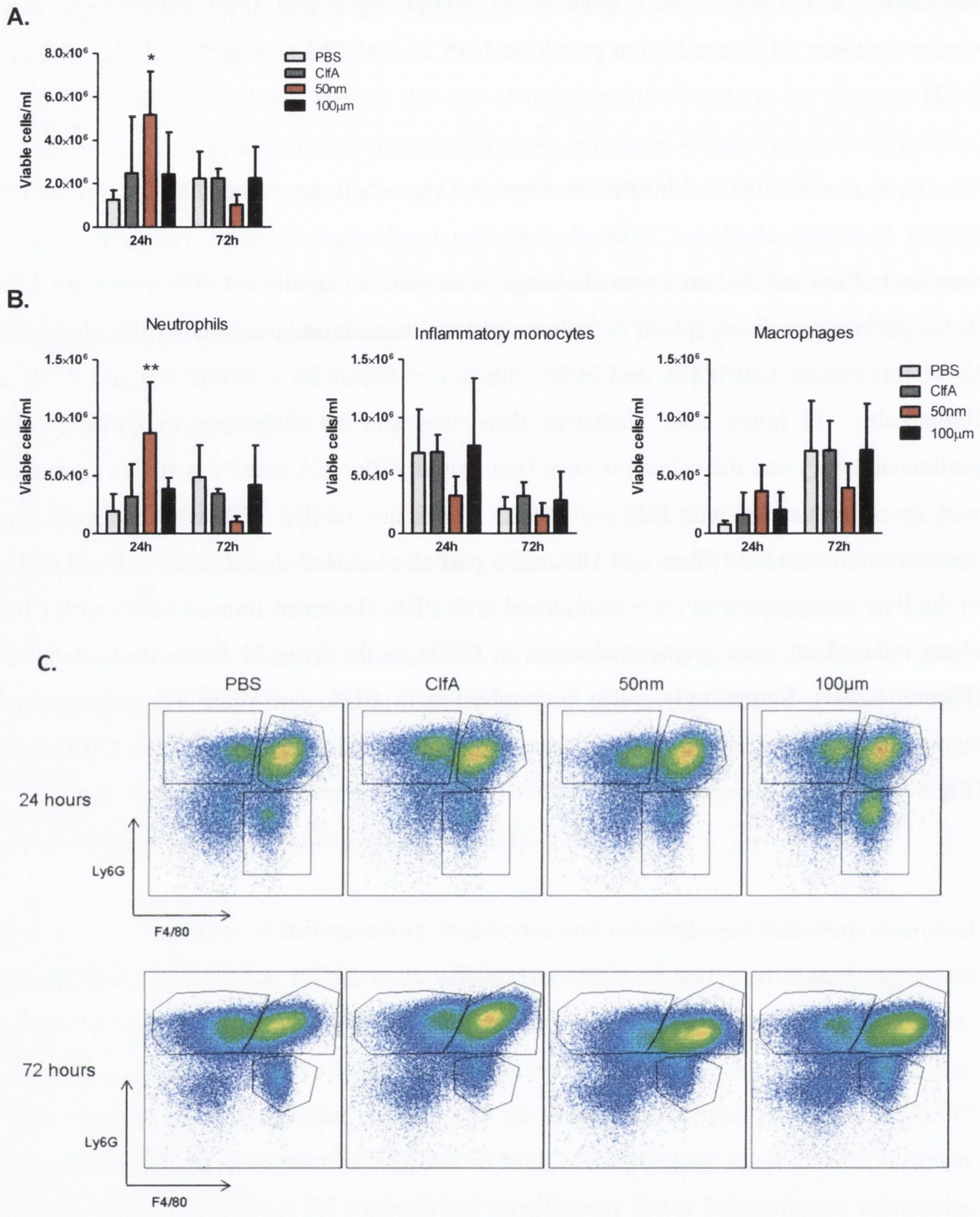

Figure 4.22 – Vaccination with ClfA and 50nm PS particles induces the greatest cell recruitment to the site of challenge. Female C57BL/6 mice were immunised s.c. on day 0 with PBS or ClfA (1µg) either alone or in combination with PS particles (50nm or 100µm) (4mg/mouse) in 200µl volumes. On day 14 the mice were immunised with these same treatments and on day 21 were challenged i.p. with $5x10^8$ CFU PS80 *S. aureus.* PECs were collected and counted (A) and Neutrophils ($CD11b^+$ $F480^-$ $Ly6G^+$), Inflammatory Monocytes ($CD11b^+$ $F480^+$ $Ly6G^+$) and Macrophages ($CD11b^+$ $F480^+$ $Ly6G^-$) were gated by flow cytometry (B, C). Bar charts represent mean (+ SD) for 5 mice per experimental group. Versus ClfA alone, * $p<0.05$, ** $p<0.01$.

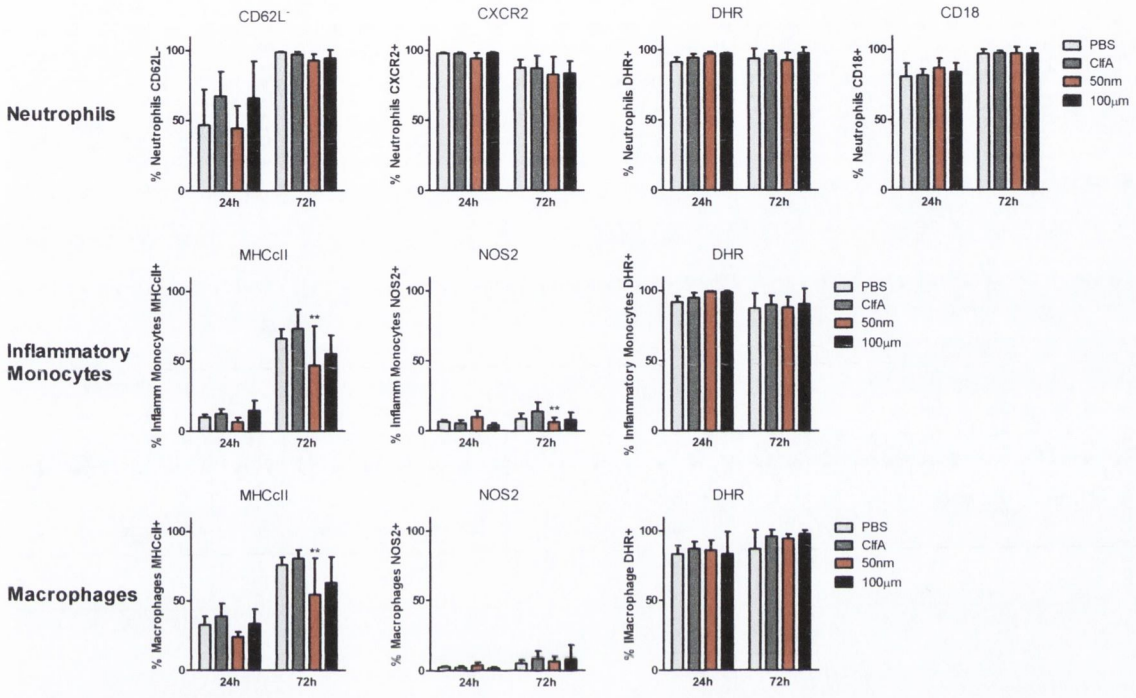

Figure 4.23 – Neutrophils, inflammatory monocytes and macrophages infiltrating to the site of challenge are all activated. Female C57BL/6 mice were immunised s.c. on day 0 with PBS or ClfA (1µg) either alone or in combination with PS particles (50nm or 100µm) (4mg/mouse) in 200µl volumes. On day 14 the mice were immunised with these same treatments and on day 21 were challenged i.p. with $5x10^8$ CFU PS80 *S. aureus.* PECs were collected and Neutrophils ($CD11b^+$ $F480^-$ $Ly6G^+$), Inflammatory Monocytes ($CD11b^+$ $F480^+$ $Ly6G^+$) and Macrophages ($CD11b^+$ $F480^+$ $Ly6G^-$) were gated by flow cytometry and activation markers assessed by flow cytomtery. Bar charts represent mean (+ SD) for 5 mice per experimental group. Versus ClfA alone, ** $p<0.01$.

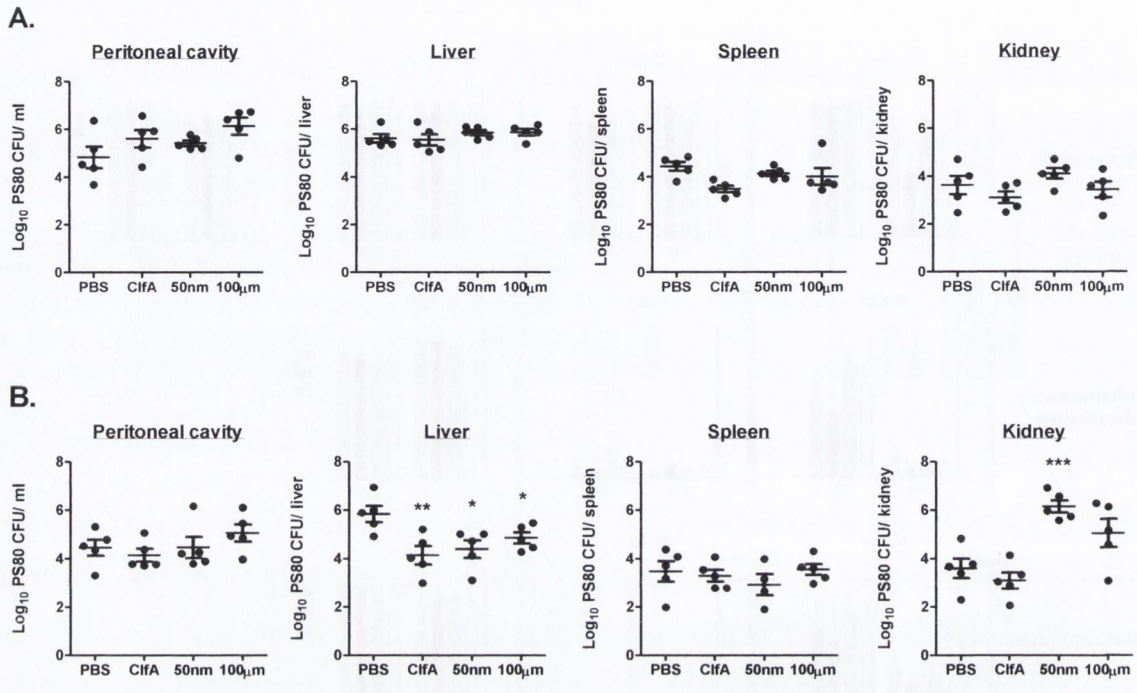

Figure 4.24 – Subcutaneous vaccination with ClfA and PS particles does not protect from *S. aureus* challenge. Female C57BL/6 mice were immunised s.c. on day 0 with PBS or ClfA (1µg) either alone or in combination with PS particles (50nm or 100µm) (4mg/mouse) in 200µl volumes. On day 14 the mice were immunised with these same treatments and on day 21 were challenged i.p. with $5x10^8$ CFU PS80 *S. aureus.* After 24 hours (A) or 72 hours (B) peritoneal exudates, livers, spleens and kidneys were isolated, homogenized and plated on agar plates and left at 37°C. Colonies were counted 24 hours later and graphed as CFU/tissue. Dot plots with SEM for 5 mice per experimental group. Versus PBS, * $p<0.05$, ** $p<0.01$, *** $p<0.0001$.

4.4 Discussion

Optimising adjuvant characteristics is crucial in vaccine design, specifically in the current age when efficient vaccines against intracellular pathogens causing diseases such as HIV, malaria and TB remain elusive. In this context adjuvants that facilitate the induction of potent cellular immunity with subunit antigens are required. Particle size is regarded as one of the key parameters in the efficacy of adjuvants but this field is notable for a lack of consensus regarding what size is optimal for adjuvanticity. Although nano-particles are favoured for drug delivery this is primarily due to the ability of nano-particles to permeate biological barriers[462,463]. However, the optimum size of particles for generating long lasting adaptive immune responses is still unclear[269,392]. Therefore, this study sought to elucidate the effects of a broad size range of particles on the adaptive immune response.

The literature on the importance of size in particulate adjuvant induced T cell responses is limited, antibody responses being more often used as a correlate of adjuvanticity. In general, the dogma is that smaller particles drive IFN-γ- and larger particles IL-4-producing antigen specific T cells, however as previously alluded to, 'small' and 'large' are relative terms. Intra-dermal administration of 40nm carboxylated PS particles conjugated to OVA have been found to induce the greatest IFN-γ $CD8^+$ responses when comparing T cell responses from particles in the range 20nm-2μm in diameter[345,354]. Similarly, Kanchan et al found that intra-muscular injection with HBsAg and 200-600nm PLA particles induced IFN-γ responses whereas 2-8μm PLA particles induced IL-4 responses, again indicating a Th1/Th2 bias between nano- and micro-particles[352]. In terms of $CD8^+$ T cell responses, mice immunised with PLG particles encapsulating peptides from either *Plasmodium berghei* circumsporozoite protein or influenza A virus NP had stronger CTL responses after parenteral administration of nano-particles (~500nm) than micro-particles (ranging between 2-30μm)[314].

Following on from the characterisation of the role of size in the induction of innate immune responses to PS particles following intra-peritoneal injection (chapter 3), in this chapter intra-peritoneal vaccination with antigen and PS particles was found to induce size-dependent adaptive immunity. Intra-peritoneal vaccination with 50nm PS particles and OVA induced significant proliferation of antigen-specific $CD8^+$ T cells. Similarly, 50nm particles were also the most effective at driving the proliferation of antigen-specific $CD4^+$ T cells when immunised with the influenza peptide NP_{311}. Particularly interesting was the

ability of 50nm PS particles to drive $CD8^+$ T cell proliferation to a significantly greater extent than alum. Alum is a known Th2-type adjuvant and is regarded as suboptimal at promoting Th1 and CTL responses. This observation sheds important light on adjuvant development and the clear need for the size of adjuvants to be critically assessed.

In the current study, of a range of particle sizes, only 50nm PS particles promoted antigen specific Th1 responses (intra-cellular IFN-γ from $CD4^+$ T cells) following i.p. injection with the *S. aureus* antigen, ClfA. Similarly, 50nm PS particles were the most effective at driving ClfA-specific IFN-γ as well as small amounts of IL-10 and IL-13 from restimulated PECs. In the case of the other particle sizes co-administered with ClfA there was no enhancement in antigen-specific T cell responses after intra-peritoneal injection. In contrast to the findings with ClfA, when OVA was used as the antigen, i.p. co-administration with 50nm PS particles selectively enhanced antigen-specific IL-13 producing cells in restimulated PECs. This highlights the importance of the antigen in assessing adjuvanticity and may caution against assuming that findings from 'model antigens' apply universally.

In terms of enhancing antigen-specific antibody induction, there are reports of nano-particles and micro-particles being equally effective at promoting IgG[464], micro-particles being more potent[352,353] and nano-particles being superior[354]. Therefore, based on the current literature, to reach an unambiguous conclusion it is vital to compare like with like. A problem is that while many papers indicate that 'smaller' particles enhanced antibody responses, a limited size range was used, often only in the micron range and with large polydispersity[353,447]. Hence the current study tackled confounding variables in the literature such as polydispersity, narrow size ranges and limited immunogenicity readouts by only using monodisperse particle preparations, examining a wide particle size range and measuring both antibody and T cell responses to determine adjuvanticity.

The current data supports studies suggesting that nano-particles induce more robust antigen-specific antibodies than micro-particles[354,465,466]. This is in contrast to numerous studies indicating that micron-sized particles are more potent than nano-sized particles at driving antigen-specific antibody responses[351,352,448,467]. Intra-peritoneal vaccination with 50nm PS particles and ClfA or OVA induced the highest titre of serum IgG antibodies, primarily IgG1. Crucially, intra-peritoneal immunisation with 50nm PS particles and ClfA induced neutralising antibodies in the serum that were capable of inhibiting the adherence

of *S. aureus* to fibrinogen. Interestingly, intra-peritoneal immunisation with all PS particles and OVA induced the production of antigen-specific IgG1 but titres reduced as particle size increased. Similarly, intra-peritoneal immunisation with 50nm, 10μm or 30μm particles and ClfA induced the production of antigen-specific IgG1. However, when 1μm or 100μm particles were administered with ClfA they did not induce the production of antigen-specific antibodies. Why 1μm and 100μm particles were incapable of inducing ClfA-specific antibody responses is unclear but such antigen-dependent effects emphasises the need to use several antigens when optimising particulate adjuvants characteristics.

While the data on i.p. vaccination are novel and very clear in pointing towards a greater potency of small nano-particles as adjuvants, subcutaneous vaccination is more clinically relevant. Therefore parallel studies were conducted into the importance of size in particle mediated enhancement in antigen-specific antibody responses after subcutaneous immunisation. In terms of the optimal particle size for antigen-specific antibody induction the current study is in agreement with much of the literature in that a 1μm particle size is efficient at driving antibody responses if administered subcutaneously. Interestingly, many studies using biodegradable particles have used an approximate 1μm size to optimize their vaccine components, neglecting optimising the particle size itself[311,468,469]. However, the current data indicate that 50nm particles are in fact more effective at inducing antigen-specific IgG1 and IgG2b than 1μm, and that larger particles, sized 10μm and 30μm, are also capable of inducing antigen-specific antibodies after subcutaneous vaccination.

Route-dependent adaptive immune responses have been reported in several models. Supporting the work of Nakaoka *et al.*, the current study found that serum antibody titres were influenced to a greater degree by particle size after intra-peritoneal injection than after subcutaneous injection[353]. Subcutaneous immunisation with all sized PS particles with the exception of 100μm induced ClfA-specific antibodies. However as previously mentioned, intra-peritoneal injection of 1μm and 100μm PS particles with ClfA failed to induce antigen-specific antibody responses. These observations argue against the possibility that particle interactions with the antigen compromise conformational integrity and indicates that the differences are route-dependent. The route of vaccination also influenced size-dependent T cell responses since micro-particles (1-100μm) were capable of driving an antigen-dependent T cell response after subcutaneous immunisation but not after intra-peritoneal administration.

One possible explanation for these route-dependent differences is particle distribution, with smaller particles more likely to migrate and interact with several cell types in an intra-peritoneal environment as opposed to subcutaneous tissue[353]. Interestingly the ability of particles to move through tissue is limited by size due to hindrance in the extracellular matrix[470]. It has been shown that PS particles of 20-200nm in size injected into the hind footpad can freely drain to the lymph nodes for antigen presentation, whereas larger particles of 0.5-2μm in size made of the same material are mostly dependent on DCs for transport to the lymph nodes[471]. However this will depend on the route of administration, with subcutaneous and intra-muscular injection leading to depot formation and prolonged particle-cell interactions.

Prolonged macrophage-micro-particle attachment and interaction has been proposed to function as a depot system facilitating continuous release of the entrapped antigen from the cell surface for subsequent processing and presentation[351,472]. In the present study, ClfA was not covalently attached to the PS particles surface, however, micro-particle injection could still lead to macrophage migration and hence ClfA sampling at the injection site. Johansen *et al.* suggested that reports on efficient primary immune responses induced by large micro-particles may be due to the fact that most formulations are poly-disperse and a small population of small-sized particles can be sufficient to induce a primary response[473]. However, they also suggested that for boosting antibody responses, larger micro-particles that are not readily phagocytosed and that liberate antigen extra-cellularly upon polymer degradation might be best suited[473]. Longer term studies have also indicated that after several months, antibody responses in the serum are similar between 1-10μm particles and 10-100μm particles, indicating that larger micro-particle induced antibody responses rise over time[474]. In fact, micro-particles have been chosen as adjuvants specifically for their ability to generate controlled release of antigens over prolonged periods[475].

However controlled release of antigen may be an over-simplistic explanation. In the present study antigen was not contained within the particles yet particles ranging 10-100μm in diameter were still capable of driving antigen-specific antibody and T cell responses. Depot removal after alum immunisation does not affect adjuvanticity and specific particle-cell interactions, as in the case of alum engaging cholesterol components to activate syk kinase-dependent signalling in DCs or MARCO engagement by PS particles (Chapter 3) may be more important in the induction of adaptive immune responses[298,304,403]. Clearly the exact mechanisms of action need to be elucidated further. In

particular, tetramer staining after subcutaneous immunisation would allow for quantification of the T cell response with different sized PS particles by this route, however, this was not feasible here due to time constraints.

The affect of particle size on the induction of antigen-specific T cell responses is dependent on route of administration, and this may be influenced by tissue-specific factors such as the predominant APCs. Newman *et al.* found that PLGA particles (ranging 700nm-5μm in diameter) delivered by intra-peritoneal injection were more likely to be taken up by macrophages ($CD18^+$ $DEC\text{-}205^-$ $CD86^{low}$) whereas intra-dermal administration of the same particles led to increased uptake and migration by DCs ($DEC\text{-}205^+$ $CD86^+$) to the draining lymph nodes[476]. In the lung, particle size has been shown to influence the type of APC that is targeted. For example, Blank *et al.* demonstrated size-dependent uptake and trafficking patterns of nano-particles by respiratory-tract DCs and alveolar macrophages to lung-draining lymph nodes, with high uptake leading to enhanced antigen-specific $CD4^+$ T cell proliferation[477]. Therefore the type, quantity and quality of T cell responses may be influenced by the specific APC populations present in the local tissue after vaccination[269,478].

In the current study, a critical step in verifying the type and magnitude of T cell responses promoted by PS particles was in preparing endotoxin-free ClfA for use in adjuvant studies. Despite performing a titration study, endotoxin contamination of the antigen appeared to influence our results. Tynan *et al.* have shown that LPS concentrations as low as 10pg/ml and 20pg/ml are sufficient to induce BMDC secretion of the pro-inflammatory cytokines IL-6 and TNF-α respectively[456]. Importantly, LPS at concentrations as low as 5pg/ml are capable of synergising with microbial and endogenous immuno-modulators to enhance BMDC secretion of specific pro-inflammatory cytokines. Our group has previously shown that combining MPL with porous silicon micro-particles can significantly augment the inflammatory response to particles *in vivo*[479]. Hence, eliminating all traces of endotoxin was crucial in determining the immunogenicity of ClfA in this model, as well as confirming the ability of PS particles of all sizes to generate antigen-specific adaptive immune responses.

ClfA is a surface protein of *S. aureus* and contributes to staphylococcal virulence during invasive infection[453,480,481]. The need for neutralising and opsonising antibodies[482–484], as well as the importance of a Th1/Th17 balance for protection against *S. aureus* infections in

mice has been demonstrated[457,485]. A recent study from the laboratory demonstrated that lectin targeted nasal vaccination using ClfA attached to 400nm PS particles can provide antibody-independent protection against *S. aureus* in mice[457]. However a clinically established correlate of protection is lacking which is a significant impediment to rational vaccine design[454,486]. Although most humans have pre-existing binding antibodies against ClfA, these antigen-specific antibodies have no neutralising activity as tested by their ability to inhibit *S. aureus* binding to human fibrinogen[455,486]. It has been suggested that the production of functional antibodies alongside competent effector cells such as neutrophils should protect against *S. aureus* infection[486]. Immunisation with 50nm PS particles and ClfA induced neutralising antibodies, as well as significant recruitment of activated neutrophils to the site of challenge as measured by DHR and CD18 expression. It is therefore surprising that 50nm PS particles when combined with ClfA did not protect against *S. aureus* challenge. Increased numbers of neutrophils in mice immunised with 50nm PS particles and ClfA did not reduce the bacterial burden in the peritoneum and in fact these neutrophils may have acted as trojan horses, enabling the bacteria to disseminate to the kidney[487]. *S. aureus* has been shown to possess numerous virulence mechanisms, including the ability to evade neutrophil phagocytosis and phagosomal degradation[488–491]. Hence the suggestion that neutrophils act as 'privileged sites' for *S. aureus* could explain the increased dissemination to the kidneys in mice immunised with 50nm PS particles and ClfA.

The increased infiltration of neutrophils after immunisation with 50nm particles and ClfA also implicates a role for trained immunity in this model. As previously described in chapter 1, innate cells can develop memory that is non-specific and in some cases provide protection from infection. Similar to the metabolic shift observed in proliferating cells, elevated glycolysis is required to provide the energy and metabolic substrates for the increased activation of trained immune cells[492]. In the current model, injection of 50nm PS particles appeared to induce neutrophil 'training' exemplified by the significant increase in neutrophils to the site of challenge. Monocytes, macrophages and NK cells are currently the only cells that have been implicated in trained immunity so further studies should be conducted to elucidate the basis of this enhanced neutrophil recruitment. Due to time constraints, the challenge experiment could not be repeated however future experiments should focus on finding the optimal size for innate training as well as incorporating a longer time between vaccination and challenge to focus on the benefit of the antigen-specific response.

Although many studies suggest that particles of 1μm in diameter are the most effective at driving antibody production, the current study counters this and indicates that 1μm is not a suitable size for promotion of robust, antigen-specific antibody responses, independent of route[351,352,448,467]. A crucial point is that the poly-dispersity of particle preparations within the literature precludes any definitive conclusions on which specific sizes are optimal for inducing antigen-specific immune responses[351,352,467]. In published studies where the mean particle size was in the order of 1μm, it is possible that it was actually a small population of smaller nano-particles that mediated the adjuvant effect. Secondly, making firm conclusions on the adjuvant potential of a specific particle size when a broad range of sizes have not been compared is unwise. Finally, comparing systemic and mucosal routes in the same study is unhelpful since the environments into which particles are injected are drastically different. In particular following mucosal delivery, particles firstly have to cross epithelial barriers which are highly size-dependent so the optimal sizes for trans-epithelial uptake and for activating innate and adaptive immunity may be different.

In summary the data from chapter 4 indicate that independent of the route of administration and independent of antigen, 50nm PS particles are the optimal PS particles to drive both antigen-specific antibody and T cell responses (Table 4.1, 4.2, 4.3).

Table 4.1 – Summary of the affect of particle size on the adaptive immune response after intra-peritoneal immunisation with ClfA

	50nm	1μm	10μm	30μm	100μm
Antigen-specific antibodies					
Total IgG	xxx		xxx	xx	
IgG1	xxx		xxx	xx	
IgG2b					
IgG2c					
IgE	xxx				
Cytokine after antigenic restimulation					
IFN-γ	x				
IL-13					
IL-17					
IL-10					

Table 4.2 – Summary of the affect of particle size on the adaptive immune response after intra-peritoneal immunisation with OVA

	50nm	1μm	10μm	30μm	100μm
Antigen-specific antibodies					
Total IgG	xxx	xxx	xxx	xxx	xxx
IgG1	xxx	xxx	xxx	xx	xxx
IgG2b	xx	x	xx		
IgG2c					
IgE			xx		
Cytokine after antigenic restimulation					
IFN-γ					
IL-13	xx				
IL-17					
IL-10					
Antigen-specific T cell proliferation					
CD8+	xxx				

x - Corresponds to statistical significance (p-value) based on One-way ANOVA compared with relevant control.

Table 4.3 – Summary of the affect of particle size on the adaptive immune response after subcutaneous immunisation

	50nm	1μm	10μm	30μm	100μm
Antigen-specific antibodies					
Total IgG	xxx	xxx	xx	xxx	
IgG1	xxx	xxx	xx	xxx	
IgG2b	xxx	xxx		xxx	
IgG2c	xxx				
IgE		xx			
Neutralising	x	x		x	
Cytokine after antigenic restimulation					
IFN-γ	xxx		xxx	xxx	x
IL-13					
IL-17			x		
IL-10					

x - Corresponds to statistical significance (p-value) based on One-way ANOVA compared with relevant control.

Chapter 5

General Discussion

The value of vaccination cannot be overstated. The implementation of recommended childhood vaccination programmes are estimated to avert up to 3 million deaths per year globally[493]. Although there is significant research ongoing into using attenuated viral vectors for vaccination[494,495], much of current vaccine development is focused on subunit vaccines that incorporate refined, often recombinant antigens that require effective adjuvants to enhance immunogenicity. As outlined in Chapter 1, there are many types of particulate adjuvants in development. However the size of these adjuvants, irrespective of composition, is rarely reported or optimised. The objective of this thesis was to determine how the size of particulate adjuvants can influence their capacity to induce and direct both the innate and the adaptive immune response.

Although PS particles are not approved for use in humans, as a material PS is widely used to elucidate the influence of particle size on the induction of immune responses[477,496–500]. As a polymer it can be used to generate particles of specific sizes, with minimal deviations making it highly mono-disperse. Fifis *et al.* have demonstrated that OVA conjugated to PS particles (40nm) elicits enhanced antigen-specific antibody titres when compared with a range of other adjuvants, including QuilA, MPL, alum and DC-OVA when injected intra-dermally[354]. PS particles have also been shown to enhance the expression of co-stimulatory markers on APCs in draining lymph nodes following intra-nasal instillation with OVA[477]. Regardless of specific composition, there is increasing evidence that the association of antigens with particles can significantly enhance immunogenicity and thus it is important to elucidate the influence of particle characteristics such as size in developing and optimising new adjuvants.

Particulate adjuvants induce a local pro-inflammatory environment to recruit immune cells to the injection site[501]. The accumulation of inflammatory factors at the site of injection correlates with the immunogenicity and efficacy of adjuvants, but the requirement for specific inflammatory mediators in inducing effective adaptive immune responses is still largely unclear. The recent development of effective nano-particle and mucosally-delivered nano-emulsion adjuvants indicates that strong adjuvanticity can be dissociated from significant or deleterious inflammation[502,503]. However, in the current study, 50nm PS particles induced the most significant inflammation as measured by cell infiltration and local chemokine signalling, and subsequently initiated significant adaptive responses as

measured by antigen-specific antibody production and antigen-specific T cell responses, independent of antigen or route of administration. However, 100μm PS particles were capable of inducing antigen-specific antibodies and some antigen-specific T cell responses when co-injected with ClfA subcutaneously, in the absence of significant inflammation. This indicates that inflammation, as measured by increased numbers of infiltrating cells and pro-inflammatory chemokines at the site of injection, is not always required to drive adaptive immunity[231]. Supporting this theory, cell depletion studies have shown that alum-mediated humoral and cellular responses are independent of mast cells, macrophages and eosinophils, and depletion of neutrophils had no impact on the antigen-specific immune responses induced by MF59[278,300].

One aspect of the initial hypothesis underlying this work was that nano-particles induce inflammation that may be detrimental to the host and induce a regulatory response that negatively influences the ensuing adaptive immune response. In support of our hypothesis, it has been suggested that using inflammation as a direct readout of adjuvanticity is unwise as there is often 'wasted inflammation' or excessive inflammation that causes local damage. Furthermore, only specific innate immune responses contribute to the onset of adaptive immunity, for example in the case of alum, as mentioned above[231]. Mosca *et al.* using genome wide microarray analysis have indicated that there may be 'adjuvant core response genes' that are common to many adjuvants (cytokines, chemokines and adhesion molecules) and hence may be necessary for adjuvanticity[504]. 50nm particles induced the most potent inflammatory response and also the most effective adaptive immune response, independent of the antigen used or route of administration (Figure 5.1). Hence, 50nm PS particles must drive the induction of some of the 'adjuvant core response genes' as well as other inflammatory mediators that may not be required for adjuvanticity.

The precise mechanisms by which 50nm PS particles induce increased inflammatory responses compared with larger PS particles are still unclear. Nano-particles have a higher contact surface area allowing for multi-valent interactions of antigens with cells[466]. Multi-valent interactions with cells are particularly beneficial for macro-molecules that predominantly promote antibody responses by cross-linking with BCRs[505]. Seydoux *et al.* demonstrated that PS particles in the range of 20nm-1μm in diameter did not alter cell viability or modify expression of the surface markers CD11b, CD11c, MHCcII, CD40, and CD86 *in vitro*[496]. Results from the current study indicate that PS particles in the range 50nm-100μm did not induce cell death *in vivo*, however the DAMPs IL-33 and dsDNA

were released into the peritoneum after injection with 50nm PS particles. As referred to in Chapter 3, dsDNA may be present in the peritoneum of these mice due to NET activation. IL-33 has been shown to be secreted by unconventional mechanisms, independent of cell death, that are discussed in depth elsewhere[506]. The release of these DAMPs may be responsible for driving the heightened inflammation seen after injection with 50nm PS particles compared with larger PS particles.

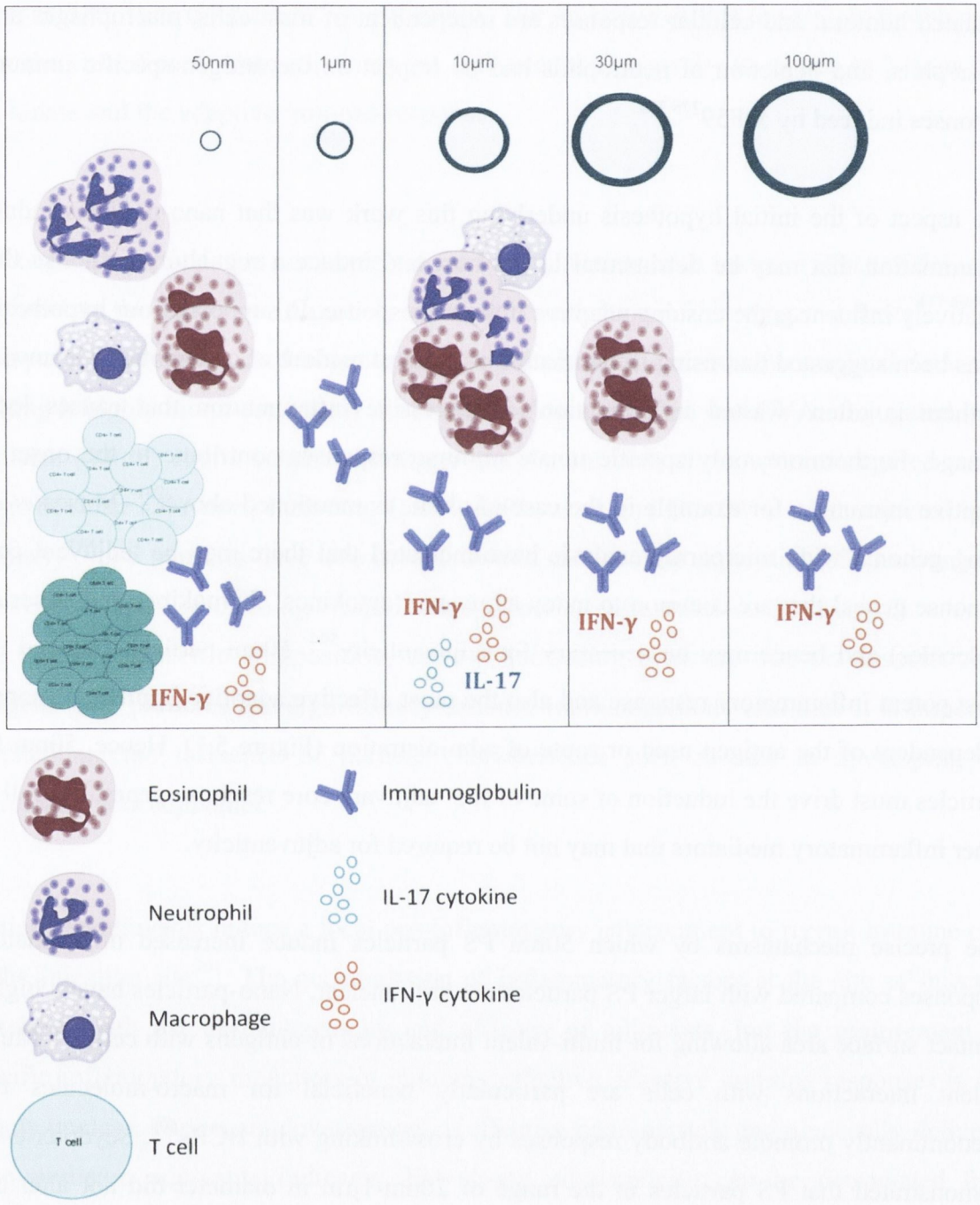

Figure 5.1 – Summary of the types of innate and adaptive responses generated after injection with different sized PS particles.

DNA could also contribute to the innate responses induced by 10μm particles, as mentioned in Chapter 3, possibly recruiting neutrophils through an IL-1R1-independent mechanism[507]. Interestingly, the size of microbes has been shown to influence the type of ensuing neutrophil response[397]. Branzk *et al.* demonstrated how *C. albicans* hyphae (~50μm long) selectively induced the release of NETs whereas smaller *C. albicans* yeast (~5μm diameter) induced phagocytosis and prevented NET release by down-regulating the translocation of neutrophil elastase to the nucleus[397,508,509]. These responses were shown to be independent of the expression of molecules on the surface of pathogens and NETs were suggested to function as an anti-microbial defence strategy for cells when pathogens were too large to be cleared by phagocytosis[397].

The key cell type with regard to bridging the innate and the adaptive responses in adjuvant induced immunity is the DC, with alum adjuvanticity shown to be DC-dependent[139]. Local resident APC populations, as well as the composition of the cellular infiltrate following adjuvant injection, will depend on the route of administration. For example, within different cutaneous layers there exist different APC populations; epidermal Langerhans cells in the epidermis, dermal DCs in the dermis and dermal macrophages in the hypodermis[510]. These distinct DC populations influence antigen uptake and hence the adaptive immune response generated. Route-dependent responses have been demonstrated using PLA nano-particles (200nm) coated with HIV-1 p24; intra-dermal administration induced both antigen-specific $CD8^+$ T cells and IgG responses, whereas injection by the subcutaneous route generated antigen-specific IgG responses only[511]. Looking in more detail, Mohanan *et al.* compared subcutaneous, intra-dermal, intra-muscular, and intra-lymphatic routes using OVA-loaded PLG particles (880nm) and found that all routes of administration induced similar titres of IgG1 but intra-lymphatic and subcutaneous administration were associated with higher IFN-γ production from splenocytes than intra-dermal and intra-muscular administration[512].

The differences between subcutaneous and intra-peritoneal routes in the current study may relate to the confined subcutaneous environment compared with the more dissipated space in the peritoneum, leading to a concentration of factors that allows promotion of greater T cell responses with 10-100μm particles after subcutaneous administration. Alternatively, particles may encounter macrophages more readily than DCs after intra-peritoneal injection, hence the processing of antigen may be less efficient. The differences in efficiency may be due to the distinct roles of the APCs, macrophages being involved

primarily in efficient scavenging of foreign material to promote clearance whilst DCs primarily involved in taking up antigens for antigen presentation and initiating an effective immune response[513,514].

Once inside a cell, the processing of particulates is known to be important for antigen-specific responses[345,515,516]. As mentioned in Chapter 3, particles as large as 10μm can be taken up by APCs[52]. It has been proposed that PS particles of 20-200nm in size are endocytosed leading to Th1-type T cell responses[269,345,516]. Nano-particles ability to leak out of endo-lysosomal compartments and escape into the cytosol also makes them more efficient at driving $CD8^+$ T cell immune responses than micro-particles[517,518]. Micro-particles have been shown to be internalised by phagocytosis or micro-pinocytosis, leading primarily to a humoral response[269,345,516]. However, Brewer *et al.* have shown that lipid vesicles of 560nm in size can end up in early endosome/phagosomes, increasing antigen presentation on MHCcII and driving T cell responses[519].

In the current study, although the mechanisms of uptake of particles by APCs was not elucidated, 50nm particles did induce the most potent $CD8^+$ and Th1-type responses. However these particles also induced the strongest humoral responses. Intriguingly, particles in the micro-particle range (10-100μm) were still capable of inducing antigen-specific antibody and T cell responses after subcutaneous vaccination (Figure 5.1). Nevertheless, particle size may influence the mechanism of uptake by APCs and hence the ability to promote a Th1 or Th2-type immune response.

Although the route of administration can affect the DC population targeted by vaccines, particle size can also influence the APC that is most likely to process and present the vaccine antigens. For example, PS particles less than 200nm in diameter injected into the hind footpad have been shown to drain to the lymph nodes through lymphatics where they are taken up by lymphoid resident DCs, whereas larger PS particles require cellular transport to the lymph nodes by skin resident DCs[471,520]. Highlighting the difference between nano- and micro-particles, 20nm PS particles were preferentially taken up by DC subpopulations in the conducting airways and lung parenchyma after intra-nasal administration compared with 1μm PS particles that were transported to the lung draining lymph nodes by migratory $CD11b^{low}$ DCs[477]. This correlated with enhanced antigen presentation to $CD4^+$ T cells in lung draining lymph nodes after administration with 20nm PS particles and OVA compared with 1μm PS particles[477].

Interestingly, uptake of PS particles (1μm in diameter) can be enhanced when particles display a positive surface charge[499]. However, administration of cationic particles may result in non-specific interactions with all cell types *in vivo*, due to electrostatic interaction with the negatively charged cell surfaces[499]. PS usually has a negative charge. Interestingly the receptor MARCO contains a collagen-like domain characterized by a lysine positively charged at the ε amino acid, enabling electrostatic interactions and particle uptake as exhibited by Getts *et al.*[402,500]. Although surface charge is important, equally, if not more important is the zeta potential of preparations. The zeta potential is a key indicator of the stability of colloidal dispersions and influences particle aggregation. The zeta potential of the PS particle preparations in the current study ranged from -27.5mV to -4.47mv (this excludes the zeta potential of 100μm PS particles as they were out of the measurement range of the equipment) with zeta potential reducing linearly with increasing particle size. Hence 50nm PS particles were the most stable particle preparation. Interestingly, it has been demonstrated that when particles are compared at a zeta potential of the same absolute value, differences between the phagocytosis of cationic particles compared with anionic particles were negated[393]. Hence zeta potential should be maintained as closely as possible across sizes to eliminate this as a variable in size-dependent uptake by APCs.

Additionally, whether particles are hydrophilic or hydrophobic may also influence the size-dependent affects previously published. Hydrophilic polyacrylamide hydrogel micro-particles cross-linked with acid-labile moieties of 35nm and 3.5μm in size were both readily taken up by macrophages *in vitro* and equally capable of inducing T cell proliferation[374]. The authors suggested that size may not be a critical factor in the stimulatory capacity of hydrophilic carrier systems compared with hydrophobic, surface-conjugated systems[374]. However, the functionality of the T cells as measured by OVA-specific cyto-toxicity *in vivo* was similar between 35nm and 3.5μm particles only if co-administered with immuno-stimulatory DNA[374].

Interestingly, in the current study the induction of both antibody and T cell responses was influenced by antigen after intra-peritoneal vaccination with PS particles. Co-injection of all sized PS particles with both ClfA and OVA induced antigen-specific antibodies, except with the 1μm size. Similarly, T cell responses induced after intra-peritoneal immunisation with PS particles were antigen-dependent. Immunisation with 50nm PS particles and OVA induced IL-13 production from restimulated PECs whereas immunisation with 50nm PS particles and ClfA induced IFN-γ production from restimulated PECs. Therefore the

antigen influenced the ability of 50nm PS particles to generate a Th1- or Th2-type response.

ClfA is known to interact with the C-terminal region of the fibrinogen gamma-chain through the 'dock, lock and latch' mechanism allowing *S. aureus* to clump in blood plasma[451,521,522]. However, it is also involved in immune evasion, binding complement factor 1 which subsequently decreases complement-mediated phagocytosis[523]. ClfA is therefore highly immunogenic and may have its own Th1/Th17-promoting modulatory activity. ClfA could synergise with specific particles to alter the activation of cells and drive a Th1-type response whilst OVA may lack this activity. Irrespective of antigen, 50nm PS particles were the most effective at driving both Th1- and Th2-type responses. Nevertheless, the data in the current study clearly indicates that studies investigating the potential of particulate adjuvants should be performed using the target candidate vaccine antigens rather than model antigens as the outcome may be dependent on the nature of the antigen.

In the general context of immunisation, the dogma is that by initiating an appropriate innate immune response, a specific and long lasting adaptive immune response will be generated. However the recently described concept of 'trained immunity' requires that the longevity of innate responses be analysed in detail after immunisation[102]. For example, the alum-adjuvanted pneumococcal conjugate vaccine has been shown to induce Th2-type polarisation of TLR agonist-induced mononuclear cell cytokine responses *in vitro,* indicating possible epigenetic remodelling and polarisation of APCs[102,524]. Numerous reports have shown that the BCG vaccine can alter responses to subsequently administered vaccines, with BCG vaccinated infants having higher concentrations of anti-pneumococcal polysaccharide IgGs, anti-*Haemophilus influenza* type b IgG and anti-tetanus toxoid IgG which could be interpreted as non-specific trained immunity[525].

In the current model, by selecting a specific particle size it is possible that the innate immune system could be trained to respond in specific ways. Arguably, immunisation with 50nm PS particles and ClfA induced innate 'training' as evidenced by the significant increase of neutrophils at the site of *S. aureus* challenge. Similarly, injection with 10μm particles could potentially induce a monocyte fuelled response to subsequent immunisations. More importantly, vaccine-mediated non-specific effects challenges the model in which vaccine and adjuvants are currently developed, focusing on individuals

being protected from specific pathogens[526]. Focusing on overall mortality and morbidity as a readout for vaccine efficacy has been suggested to enable the development of the most beneficial and all encompassing vaccines[526].

Building on the groundwork of this thesis, future work could explore many avenues. For example, determining the different processes in the lymph nodes that lead to the generation of an adaptive immune response after injection with PS particles and how this differs using different sizes. Specifically this would involve determining how the inflammation seen at the injection site translates to an adaptive response. Determining the cellular profile in the draining lymph nodes using flow cytometry and fluorescent particles at several times post injection would help elucidate how the PS particles are orchestrating the inflammatory response and subsequent adaptive response.

Other future work could build on quantifying T cell numbers after subcutaneous injection using tetramer staining. This would allow a comparison with the intra-peritoneal model, as well as elucidating if there are markers of inflammation that correlate with T cell differentiation. Generating a tetramer that was specific for both $CD4^+$ T cells and $CD8^+$ T cells would allow the quantification to be compared directly in the same model.

With regards the *S. aureus* challenge model, it would be interesting to see if other particle sizes were more or less capable of providing protection when injected with ClfA. 10μm PS particles were capable of inducing antigen-specific IFN-γ and IL-17 secretion after injection with ClfA, and these two cytokines are thought to be important in controlling *S. aureus* infections. In particular it would be interesting to determine if 10μm PS particles, when injected with ClfA, protect against *S.aureus* challenge.

To further translate this work it would be very interesting to perform similar adjuvant models using biodegradable particles such as PLGA, which are already used in the clinic for drug delivery. Determing antigen-specific T and B cell responses using PLGA would demonstrate if the particle size-dependent immune response is the same across different materials.

The affect that particles can have on the body is not just important in the context of vaccines, but has important implications for drug delivery, bioengineering and environmental particle exposure. This thesis has shown that size is a critical parameter in

determining innate and adaptive immune responses to particulates and therefore has important implications for adjuvant design as well as particle-based medicine in general. By understanding the distinct affects that the size of particles can have, adjuvants can be tailored to direct more specific responses with fewer undesired and unnecessary side effects. Our data indicates that although inflammation coincides with the most potent adaptive immune responses, antigen-specific antibodies and some T cell responses can still develop in the absence of significant inflammation.

Chapter 6

References

1 Turvey SE, Broide DH. Innate immunity. *J Allergy Clin Immunol* 2010; **125**: S24–32.

2 Luster AD. The role of chemokines in linking innate and adaptive immunity. *Curr Opin Immunol* 2002; **14**: 129–35.

3 Mestas J, Hughes CCW. Of Mice and Not Men: Differences between Mouse and Human Immunology. *J Immunol* 2004; **172**: 2731–8.

4 Nauseef WM, Borregaard N. Neutrophils at work. *Nat Immunol* 2014; **15**: 602–11.

5 Kolaczkowska E, Kubes P. Neutrophil recruitment and function in health and inflammation. *Nat Rev Immunol* 2013; **13**: 159–75.

6 Weiss SJ. Tissue destruction by neutrophils. *N Engl J Med* 1989; **320**: 365–76.

7 Brinkmann V, Reichard U, Goosmann C, *et al.* Neutrophil extracellular traps kill bacteria. *Science* 2004; **303**: 1532–5.

8 Chertov O, Ueda H, Xu LL, *et al.* Identification of human neutrophil-derived cathepsin G and azurocidin/CAP37 as chemoattractants for mononuclear cells and neutrophils. *J Exp Med* 1997; **186**: 739–47.

9 Bennouna S, Bliss SK, Curiel TJ, Denkers EY. Cross-talk in the innate immune system: neutrophils instruct recruitment and activation of dendritic cells during microbial infection. *J Immunol* 2003; **171**: 6052–8.

10 Gordon S, Martinez FO. Alternative activation of macrophages: mechanism and functions. *Immunity* 2010; **32**: 593–604.

11 Shi C, Pamer EG. Monocyte recruitment during infection and inflammation. *Nat Rev Immunol* 2011; **11**: 762–74.

12 Lolmede K, Campana L, Vezzoli M, *et al.* Inflammatory and alternatively activated human macrophages attract vessel-associated stem cells, relying on separate HMGB1- and MMP-9-dependent pathways. *J Leukoc Biol* 2009; **85**: 779–87.

13 Mills CD, Kincaid K, Alt JM, Heilman MJ, Hill AM. M-1/M-2 macrophages and the Th1/Th2 paradigm. *J Immunol* 2000; **164**: 6166–73.

14 Biswas SK, Mantovani A. Macrophage plasticity and interaction with lymphocyte subsets: cancer as a paradigm. *Nat Immunol* 2010; **11**: 889–96.

15 Stein M, Keshav S, Harris N, Gordon S. Interleukin 4 potently enhances murine macrophage mannose receptor activity: A marker of alternative immunologic macrophage activation. *Receptor* 1992; **176**: 287–92.

16 Cheong C, Matos I, Choi J-H, *et al.* Microbial stimulation fully differentiates monocytes to DC-SIGN/CD209(+) dendritic cells for immune T cell areas. *Cell* 2010; **143**: 416–29.

17 Abraham SN, St John AL. Mast cell-orchestrated immunity to pathogens. *Nat Rev Immunol* 2010; **10**: 440–52.

18 Enoksson M, Lyberg K, Möller-Westerberg C, Fallon PG, Nilsson G, Lunderius-Andersson C. Mast cells as sensors of cell injury through IL-33 recognition. *J Immunol* 2011; **186**: 2523–8.

19 Enoksson M, Möller-Westerberg C, Wicher G, *et al.* Intraperitoneal influx of neutrophils in response to IL-33 is mast cell-dependent. *Blood* 2013; **121**: 530–6.

20 Spencer LA, Melo RCN, Perez SAC, Bafford SP, Dvorak AM, Weller PF. Cytokine receptor-mediated trafficking of preformed IL-4 in eosinophils identifies an innate immune mechanism of cytokine secretion. *Proc Natl Acad Sci U S A* 2006; **103**: 3333–8.

21 Bandeira-Melo C, Sugiyama K, Woods LJ, Weller PF. Cutting edge: eotaxin elicits rapid vesicular transport-mediated release of preformed IL-4 from human eosinophils. *J Immunol* 2001; **166**: 4813–7.

22 Voehringer D, Van Rooijen N, Locksley RM. Eosinophils develop in distinct stages and are recruited to peripheral sites by alternatively activated macrophages. *J Leukoc Biol* 2007; **81**: 1434–44.

23 Heredia JE, Mukundan L, Chen FM, *et al.* Type 2 innate signals stimulate fibro/adipogenic progenitors to facilitate muscle regeneration. *Cell* 2013; **153**: 376–88.

24 Walker J a, Barlow JL, McKenzie ANJ. Innate lymphoid cells--how did we miss them? *Nat Rev Immunol* 2013; **13**: 75–87.

25 Lambrecht BN, Hammad H. Innate immune cells to the help. *Immunity* 2014; **40**: 313–4.

26 Kiessling R, Klein E, Pross H, Wigzell H. "Natural" killer cells in the mouse. II. Cytotoxic cells with specificity for mouse Moloney leukemia cells. Characteristics of the killer cell. *Eur J Immunol* 1975; **5**: 117–21.

27 Herberman RB, Nunn ME, Holden HT, Lavrin DH. Natural cytotoxic reactivity of mouse lymphoid cells against syngeneic and allogeneic tumors. II. Characterization of effector cells. *Int J Cancer* 1975; **16**: 230–9.

28 Bernink J, Mjösberg J, Spits H. Th1- and Th2-like subsets of innate lymphoid cells. *Immunol Rev* 2013; **252**: 133–8.

29 Gordon SM, Chaix J, Rupp LJ, *et al.* The transcription factors T-bet and Eomes control key checkpoints of natural killer cell maturation. *Immunity* 2012; **36**: 55–67.

30 Fallon PG, Ballantyne SJ, Mangan NE, *et al.* Identification of an interleukin (IL)-25-dependent cell population that provides IL-4, IL-5, and IL-13 at the onset of helminth expulsion. *J Exp Med* 2006; **203**: 1105–16.

31 Neill DR, Wong SH, Bellosi A, *et al.* Nuocytes represent a new innate effector leukocyte that mediates type-2 immunity. *Nature* 2010; **464**: 1367–70.

32 Price AE, Liang H-E, Sullivan BM, *et al.* Systemically dispersed innate IL-13-expressing cells in type 2 immunity. *Proc Natl Acad Sci U S A* 2010; **107**: 11489–94.

33 Spits H, Artis D, Colonna M, *et al.* Innate lymphoid cells--a proposal for uniform nomenclature. *Nat Rev Immunol* 2013; **13**: 145–9.

34 Eberl G, Marmon S, Sunshine M-J, Rennert PD, Choi Y, Littman DR. An essential function for the nuclear receptor RORgamma(t) in the generation of fetal lymphoid tissue inducer cells. *Nat Immunol* 2004; **5**: 64–73.

35 Sun Z, Unutmaz D, Zou YR, *et al.* Requirement for RORgamma in thymocyte survival and lymphoid organ development. *Science* 2000; **288**: 2369–73.

36 Sutton CE, Mielke L a, Mills KHG. IL-17-producing γδ T cells and innate lymphoid cells. *Eur J Immunol* 2012; **42**: 2221–31.

37 Doisne J-M, Soulard V, Bécourt C, *et al.* Cutting edge: crucial role of IL-1 and IL-23 in the innate IL-17 response of peripheral lymph node NK1.1- invariant NKT cells to bacteria. *J Immunol* 2011; **186**: 662–6.

38 Kono H, Onda A, Yanagida T. Molecular determinants of sterile inflammation. *Curr Opin Immunol* 2014; **26**: 147–56.

39 Ishii KJ, Koyama S, Nakagawa A, Coban C, Akira S. Host innate immune receptors and beyond: making sense of microbial infections. *Cell Host Microbe* 2008; **3**: 352–63.

40 Ozinsky A, Underhill DM, Fontenot JD, *et al.* The repertoire for pattern recognition of pathogens by the innate immune system is defined by cooperation between toll-like receptors. *Proc Natl Acad Sci U S A* 2000; **97**: 13766–71.

41 Hayashi F, Smith KD, Ozinsky A, *et al.* The innate immune response to bacterial flagellin is mediated by Toll-like receptor 5. *Nature* 2001; **410**: 1099–103.

42 Takeuchi O, Akira S. Pattern recognition receptors and inflammation. *Cell* 2010; **140**: 805–20.

43 Alexopoulou L, Holt AC, Medzhitov R, Flavell RA. Recognition of double-stranded RNA and activation of NF-kappaB by Toll-like receptor 3. *Nature* 2001; **413**: 732–8.

44 Heil F, Hemmi H, Hochrein H, *et al.* Species-specific recognition of single-stranded RNA via toll-like receptor 7 and 8. *Science* 2004; **303**: 1526–9.

45 Hemmi H, Takeuchi O, Kawai T, *et al.* A Toll-like receptor recognizes bacterial DNA. *Nature* 2000; **408**: 740–5.

46 Carty M, Goodbody R, Schröder M, Stack J, Moynagh PN, Bowie AG. The human adaptor SARM negatively regulates adaptor protein TRIF-dependent Toll-like receptor signaling. *Nat Immunol* 2006; **7**: 1074–81.

47 Reed SG, Orr MT, Fox CB. Key roles of adjuvants in modern vaccines. *Nat Med* 2013; **19**: 1597–608.

48 Robinson MJ, Sancho D, Slack EC, LeibundGut-Landmann S, Reis E Sousa C. Myeloid C-type lectins in innate immunity. *Nat Immunol* 2006; **7**: 1258–65.

49 Zhu L-L, Zhao X-Q, Jiang C, *et al.* C-type lectin receptors Dectin-3 and Dectin-2 form a heterodimeric pattern-recognition receptor for host defense against fungal infection. *Immunity* 2013; **39**: 324–34.

50 Kato H, Takeuchi O, Sato S, *et al.* Differential roles of MDA5 and RIG-I helicases in the recognition of RNA viruses. *Nature* 2006; **441**: 101–5.

51 Satoh T, Kato H, Kumagai Y, *et al.* LGP2 is a positive regulator of RIG-I- and MDA5-mediated antiviral responses. *Proc Natl Acad Sci U S A* 2010; **107**: 1512–7.

52 Sharp FA, Ruane D, Claass B, *et al.* Uptake of particulate vaccine adjuvants by dendritic cells activates the NALP3 inflammasome. *Proc Natl Acad Sci U S A* 2009; **106**: 870–5.

53 Mariathasan S, Weiss DS, Newton K, *et al.* Cryopyrin activates the inflammasome in response to toxins and ATP. *Nature* 2006; **440**: 228–32.

54 Gross O, Poeck H, Bscheider M, *et al.* Syk kinase signalling couples to the Nlrp3 inflammasome for anti-fungal host defence. *Nature* 2009; **459**: 433–6.

55 Boyden ED, Dietrich WF. Nalp1b controls mouse macrophage susceptibility to anthrax lethal toxin. *Nat Genet* 2006; **38**: 240–4.

56 Chamaillard M, Hashimoto M, Horie Y, *et al.* An essential role for NOD1 in host recognition of bacterial peptidoglycan containing diaminopimelic acid. *Nat Immunol* 2003; **4**: 702–7.

57 Girardin SE, Boneca IG, Viala J, *et al.* Nod2 is a general sensor of peptidoglycan through muramyl dipeptide (MDP) detection. *J Biol Chem* 2003; **278**: 8869–72.

58 Leemans JC, Cassel SL, Sutterwala FS. Sensing damage by the NLRP3 inflammasome. *Immunol Rev* 2011; **243**: 152–62.

59 Gürtler C, Bowie AG. Innate immune detection of microbial nucleic acids. *Trends Microbiol* 2013; **21**: 413–20.

60 Miyashita M, Oshiumi H, Matsumoto M, Seya T. DDX60, a DEXD/H box helicase, is a novel antiviral factor promoting RIG-I-like receptor-mediated signaling. *Mol Cell Biol* 2011; **31**: 3802–19.

61 Reikine S, Nguyen JB, Modis Y. Pattern recognition and signaling mechanisms of RIG-I and MDA5. *Front Immunol* 2014; **5**: 342.

62 Nussenzweig MC, Steinman RM, Gutchinov B, Cohn ZA. Dendritic cells are accessory cells for the development of anti- trinitrophenyl cytotoxic T lymphocytes. *J Exp Med* 1980; **152**: 1070–84.

63 Steinman RM, Cohn ZA. Identification of a novel cell type in peripheral lymphoid organs of mice. I. Morphology, quantitation, tissue distribution. *J Exp Med* 1973; **137**: 1142–62.

64 Steinman RM, Gutchinov B, Witmer MD, Nussenzweig MC. Lymphoid dendritic cells are potent stimulators of the primary mixed leukocyte reaction in mice. *J Exp Med* 1983; **157**: 5132–6.

65 Steinman RM. Decisions about dendritic cells: Past, present, and future. *Annu Rev Immunol* 2012; **30**: 1–22.

66 Koopmann JO, Hämmerling GJ, Momburg F. Generation, intracellular transport and loading of peptides associated with MHC class I molecules. *Curr Opin Immunol* 1997; **9**: 80–8.

67 Lennon-Duménil A-M, Bakker AH, Wolf-Bryant P, Ploegh HL, Lagaudrière-Gesbert C. A closer look at proteolysis and MHC-class-II-restricted antigen presentation. *Curr Opin Immunol* 2002; **14**: 15–21.

68 Bevan MJ. Cross-priming for a secondary cytotoxic response to minor H antigens with H-2 congenic cells which do not cross-react in the cytotoxic assay. *J Exp Med* 1976; **143**: 1283–8.

69 Bevan MJ. Minor H antigens introduced on H-2 different stimulating cells cross-react at the cytotoxic T cell level during in vivo priming. *J Immunol* 1976; **117**: 2233–8.

70 Liu YJ. Dendritic cell subsets and lineages, and their functions in innate and adaptive immunity. *Cell* 2001; **106**: 259–62.

71 Steinman RM. Dendritic cells: understanding immunogenicity. *Eur J Immunol* 2007; **37 Suppl 1**: S53–60.

72 Inaba K, Witmer MD, Steinman RM. Clustering of dendritic cells, helper T lymphocytes, and histocompatible B cells during primary antibody responses in vitro. *J Exp Med* 1984; **160**: 858–76.

73 Liu K, Victora GD, Schwickert TA, *et al.* In vivo analysis of dendritic cell development and homeostasis. *Science* 2009; **324**: 392–7.

74 Reizis B. Classical dendritic cells as a unique immune cell lineage. *J Exp Med* 2012; **209**: 1053–6.

75 Mellman I, Steinman RM. Dendritic cells: specialized and regulated antigen processing machines. *Cell* 2001; **106**: 255–8.

76 Merad M, Sathe P, Helft J, Miller J, Mortha A. The dendritic cell lineage: ontogeny and function of dendritic cells and their subsets in the steady state and the inflamed setting. *Annu Rev Immunol* 2013; **31**: 563–604.

77 Ardavin C, Wu L, Li CL, Shortman K. Thymic dendritic cells and T cells develop simultaneously in the thymus from a common precursor population. *Nature* 1993; **362**: 761–3.

78 Vremec D, Pooley J, Hochrein H, Wu L, Shortman K. CD4 and CD8 expression by dendritic cell subtypes in mouse thymus and spleen. *J Immunol* 2000; **164**: 2978–86.

79 Hochrein H, Shortman K, Vremec D, Scott B, Hertzog P, O'Keeffe M. Differential production of IL-12, IFN-alpha, and IFN-gamma by mouse dendritic cell subsets. *J Immunol* 2001; **166**: 5448–55.

80 Meredith MM, Liu K, Darrasse-Jeze G, *et al.* Expression of the zinc finger transcription factor zDC (Zbtb46, Btbd4) defines the classical dendritic cell lineage. *J Exp Med* 2012; **209**: 1153–65.

81 Satpathy AT, KC W, Albring JC, *et al.* Zbtb46 expression distinguishes classical dendritic cells and their committed progenitors from other immune lineages. *J Exp Med* 2012; **209**: 1135–52.

82 Grouard G, Rissoan M-C, Filgueira L, Durand I, Banchereau J, Liu Y-J. The enigmatic plasmacytoid T cells develop into dendritic cells with interleukin (IL)-3 and CD40-ligand. *J Exp Med* 1997; **185**: 1101–12.

83 Colonna M, Trinchieri G, Liu Y-J. Plasmacytoid dendritic cells in immunity. *Nat Immunol* 2004; **5**: 1219–26.

84 Ersland K, Wüthrich M, Klein BS. Dynamic interplay among monocyte-derived, dermal, and resident lymph node dendritic cells during the generation of vaccine immunity to fungi. *Cell Host Microbe* 2010; **7**: 474–87.

85 Bogunovic M, Ginhoux F, Helft J, *et al.* Origin of the lamina propria dendritic cell network. *Immunity* 2009; **31**: 513–25.

86 Varol C, Vallon-Eberhard A, Elinav E, *et al.* Intestinal lamina propria dendritic cell subsets have different origin and functions. *Immunity* 2009; **31**: 502–12.

87 Lewis KL, Caton ML, Bogunovic M, *et al.* Notch2 receptor signaling controls functional differentiation of dendritic cells in the spleen and intestine. *Immunity* 2011; **35**: 780–91.

88 Langlet C, Tamoutounour S, Henri S, *et al.* CD64 expression distinguishes monocyte-derived and conventional dendritic cells and reveals their distinct role during intramuscular immunization. *J Immunol* 2012; **188**: 1751–60.

89 Serbina N V, Salazar-mather TP, Biron CA, Kuziel WA, Pamer EG. TNF / iNOS-producing dendritic cells mediate innate immune defense against bacterial infection. *Immunity* 2003; **19**: 59–70.

90 Netea MG, Quintin J, van der Meer JWM. Trained immunity: a memory for innate host defense. *Cell Host Microbe* 2011; **9**: 355–61.

91 Slaughter A, Daniel X, Flors V, Luna E, Hohn B, Mauch-Mani B. Descendants of primed Arabidopsis plants exhibit resistance to biotic stress. *Plant Physiol* 2012; **158**: 835–43.

92 Fu ZQ, Dong X. Systemic acquired resistance: turning local infection into global defense. *Annu Rev Plant Biol* 2013; **64**: 839–63.

93 Faulhaber LM, Karp RD. A diphasic immune response against bacteria in the American cockroach. *Immunology* 1992; **75**: 378–81.

94 Arala-Chaves M, Sequeira T. Is there any kind of adaptive immunity in invertebrates? *Aquaculture* 2000; **191**: 247–58.

95 Moret Y, Siva-Jothy MT. Adaptive innate immunity? Responsive-mode prophylaxis in the mealworm beetle, Tenebrio molitor. *Proc Biol Sci* 2003; **270**: 2475–80.

96 Moret Y, Schmid-Hempel P. Immune defence in bumble-bee offspring. *Nature* 2001; **414**: 506.

97 Blanden R V. The host response to Calmette-Guerin Bacillus infection in mice. *J Exp Med* 1969; **129**: 1079–107.

98 Sher NA, Chaparas SD, Greenberg LE, Bernard S. Effects of BCG, Corynebacterium parvum, and methanol-extration residue in the reduction of mortality from Staphylococcus aureus and Candida albicans infections in immunosuppressed mice. *Infect Immun* 1975; **12**: 1325–30.

99 Van 't Wout JW, Poell R, van Furth R. The role of BCG/PPD-activated macrophages in resistance against systemic candidiasis in mice. *Scand J Immunol* 1992; **36**: 713–9.

100 Tribouley J, Tribouley-Duret J, Appriou M. Effect of Bacillus Callmette Guerin (BCG) on the receptivity of nude mice to Schistosoma mansoni. *C R Seances Soc Biol Fil* 1978; **172**: 902–4.

101 Bistoni F, Verducci G, Perito S, *et al.* Immunomodulation by a low-virulence, agerminative variant of Candida albicans. Further evidence for macrophage activation as one of the effector mechanisms of nonspecific anti-infectious protection. *J Med Vet Mycol* 1988; **26**: 285–99.

102 Levy O, Netea MG. Innate immune memory: implications for development of pediatric immunomodulatory agents and adjuvanted vaccines. *Pediatr Res* 2014; **75**: 184–8.

103 Bistoni F, Vecchiarelli A, Cenci E, Puccetti P, Marconi P, Cassone A. Evidence for macrophage-mediated protection against lethal Candida albicans infection. *Infect Immun* 1986; **51**: 668–74.

104 Rosenthal SR, Loewinsohn E, Graham ML, Liveright D, Thorne MG, Johnson V. BCG vaccination in tuberculous households. *Am Rev Respir Dis* 1961; **84**: 690–704.

105 Garly M-L, Martins CL, Balé C, *et al.* BCG scar and positive tuberculin reaction associated with reduced child mortality in West Africa. A non-specific beneficial effect of BCG? *Vaccine* 2003; **21**: 2782–90.

106 Kleinnijenhuis J, Quintin J, Preijers F, *et al.* Bacille Calmette-Guerin induces NOD2-dependent nonspecific protection from reinfection via epigenetic reprogramming of monocytes. *Proc Natl Acad Sci U S A* 2012; **109**: 17537–42.

107 Quintin J, Saeed S, Martens JHA, *et al.* Candida albicans infection affords protection against reinfection via functional reprogramming of monocytes. *Cell Host Microbe* 2012; **12**: 223–32.

108 Sun JC, Beilke JN, Lanier LL. Adaptive immune features of natural killer cells. *Nature* 2009; **457**: 557–61.

109 Paust S, Gill HS, Wang B-Z, *et al.* Critical role for the chemokine receptor CXCR6 in NK cell-mediated antigen-specific memory of haptens and viruses. *Nat Immunol* 2010; **11**: 1127–35.

110 Burgdorf S, Kautz A, Böhnert V, Knolle PA, Kurts C. Distinct pathways of antigen uptake and intracellular routing in CD4 and CD8 T cell activation. *Science (80-)* 2007; **316**: 612–6.

111 Zhang N, Bevan MJ. CD8(+) T cells: foot soldiers of the immune system. *Immunity* 2011; **35**: 161–8.

112 Comber JD, Philip R. MHC class I antigen presentation and implications for developing a new generation of therapeutic vaccines. *Ther Adv vaccines* 2014; **2**: 77–89.

113 Blum JS, Wearsch PA, Cresswell P. Pathways of antigen processing. *Annu Rev Immunol* 2013; **31**: 443–73.

114 Stemberger C, Huster KM, Koffler M, *et al.* A single naive CD8 + T Cell precursor can develop into diverse effector and memory subsets. *Immunity* 2007; **27**: 985–97.

115 Podack E, Konigsberg P. Cytolytic T cell granules. Isolation, structural, biochemical, and functional characterization. *J Exp Med* 1984; **160**: 695–710.

116 Lowin B, Peitsch MC, Tschopp J. Perforin and granzymes: crucial effector molecules in cytolytic T lymphocyte and natural killer cell-mediated cytotoxicity. *Curr Top Microbiol Immunol* 1995; **198**: 1–24.

117 Badovinac VP, Haring JS, Harty JT. Initial T cell receptor transgenic cell precursor frequency dictates critical aspects of the CD8(+) T cell response to infection. *Immunity* 2007; **26**: 827–41.

118 Watts TH. TNF/TNFR family members in costimulation of T cell responses. *Annu Rev Immunol* 2005; **23**: 23–68.

119 Curtsinger JM, Lins DC, Mescher MF. Signal 3 determines tolerance versus full activation of naive CD8 T cells: dissociating proliferation and development of effector function. *J Exp Med* 2003; **197**: 1141–51.

120 Seder RA, Boulay JL, Finkelman F, *et al.* CD8+ T cells can be primed in vitro to produce IL-4. *J Immunol* 1992; **148**: 1652–6.

121 Salgame P, Abrams JS, Clayberger C, *et al.* Differing lymphokine profiles of functional subsets of human CD4 and CD8 T cell clones. *Science* 1991; **254**: 279–82.

122 Croft M, Carter L, Swain SL, Dutton RW. Generation of polarized antigen-specific CD8 effector populations: reciprocal action of interleukin (IL)-4 and IL-12 in promoting type 2 versus type 1 cytokine profiles. *J Exp Med* 1994; **180**: 1715–28.

123 Vukmanovic-Stejic M, Vyas B, Gorak-Stolinska P, Noble A, Kemeny DM. Human Tc1 and Tc2/Tc0 CD8 T-cell clones display distinct cell surface and functional phenotypes. *Blood* 2000; **95**: 231–40.

124 Shrikant PA, Rao R, Li Q, *et al.* Regulating functional cell fates in CD8 T cells. *Immunol Res* 2010; **46**: 12–22.

125 Huber M, Lohoff M. IRF4 at the crossroads of effector T-cell fate decision. *Eur J Immunol* 2014; **44**: 1886–95.

126 O'Garra A, Arai N. The molecular basis of T helper 1 and T helper 2 cell differentiation. *Trends Cell Biol* 2000; **10**: 542–50.

127 Constant SL, Bottomly K. Induction of Th1 and Th2 CD4+ T cell responses: the alternative approaches. *Annu Rev Immunol* 1997; **15**: 297–322.

128 Gazzinelli RT, Hieny S, Wynn TA, Wolf S, Sher A. Interleukin 12 is required for the T-lymphocyte-independent induction of interferon gamma by an intracellular parasite and induces resistance in T-cell-deficient hosts. *Proc Natl Acad Sci U S A* 1993; **90**: 6115–9.

129 Hsieh CS, Macatonia SE, Tripp CS, Wolf SF, O'Garra A, Murphy KM. Development of TH1 CD4+ T cells through IL-12 produced by Listeria-induced macrophages. *Science* 1993; **260**: 547–9.

130 Seder RA, Gazzinelli R, Sher A, Paul WE. Interleukin 12 acts directly on CD4+ T cells to enhance priming for interferon gamma production and diminishes interleukin 4 inhibition of such priming. *Proc Natl Acad Sci U S A* 1993; **90**: 10188–92.

131 O'Garra A. Cytokines induce the development of functionally heterogeneous T helper cell subsets. *Immunity* 1998; **8**: 275–83.

132 Sims JE, Smith DE. The IL-1 family: regulators of immunity. *Nat Rev Immunol* 2010; **10**: 89–102.

133 Wan YY, Flavell RA. How diverse--CD4 effector T cells and their functions. *J Mol Cell Biol* 2009; **1**: 20–36.

134 Szabo SJ, Sullivan BM, Peng SL, Glimcher LH. Molecular mechanisms regulating Th1 immune responses. *Annu Rev Immunol* 2003; **21**: 713–58.

135 Mosmann TR, Coffman RL. TH1 and TH2 cells: different patterns of lymphokine secretion lead to different functional properties. *Annu Rev Immunol* 1989; **7**: 145–73.

136 Zheng W, Flavell RA. The transcription factor GATA-3 is necessary and sufficient for Th2 cytokine gene expression in CD4 T cells. *Cell* 1997; **89**: 587–96.

137 Zhu J, Guo L, Watson CJ, Hu-Li J, Paul WE. Stat6 is necessary and sufficient for IL-4's role in Th2 differentiation and cell expansion. *J Immunol* 2001; **166**: 7276–81.

138 Sokol CL, Chu N-Q, Yu S, Nish SA, Laufer TM, Medzhitov R. Basophils function as antigen-presenting cells for an allergen-induced T helper type 2 response. *Nat Immunol* 2009; **10**: 713–20.

139 Kool M, Soullié T, Van Nimwegen M, *et al.* Alum adjuvant boosts adaptive immunity by inducing uric acid and activating inflammatory dendritic cells. *J Exp Med* 2008; **205**: 869–82.

140 Perrigoue JG, Saenz SA, Siracusa MC, *et al.* MHC class II-dependent basophil-CD4+ T cell interactions promote T(H)2 cytokine-dependent immunity. *Nat Immunol* 2009; **10**: 697–705.

141 Saenz SA, Noti M, Artis D. Innate immune cell populations function as initiators and effectors in Th2 cytokine responses. *Trends Immunol* 2010; **31**: 407–13.

142 Williams JW, Tjota MY, Clay BS, *et al.* Transcription factor IRF4 drives dendritic cells to promote Th2 differentiation. *Nat Commun* 2013; **4**: 2990.

143 Gao Y, Nish SA, Jiang R, *et al.* Control of T helper 2 responses by transcription factor IRF4-dependent dendritic cells. *Immunity* 2013; **39**: 722–32.

144 Paul WE, Zhu J. How are T(H)2-type immune responses initiated and amplified? *Nat Rev Immunol* 2010; **10**: 225–35.

145 Nakae S, Nambu A, Sudo K, Iwakura Y. Suppression of immune induction of collagen-induced arthritis in IL-17-deficient mice. *J Immunol* 2003; **171**: 6173–7.

146 Jin D, Zhang L, Zheng J, Zhao Y. The inflammatory Th 17 subset in immunity against self and non-self antigens. *Autoimmunity* 2008; **41**: 154–62.

147 Veldhoen M, Hocking RJ, Atkins CJ, Locksley RM, Stockinger B. TGFbeta in the context of an inflammatory cytokine milieu supports de novo differentiation of IL-17-producing T cells. *Immunity* 2006; **24**: 179–89.

148 Ivanov II, McKenzie BS, Zhou L, *et al.* The orphan nuclear receptor RORgammat directs the differentiation program of proinflammatory IL-17+ T helper cells. *Cell* 2006; **126**: 1121–33.

149 Torchinsky MB, Garaude J, Martin AP, Blander JM. Innate immune recognition of infected apoptotic cells directs T(H)17 cell differentiation. *Nature* 2009; **458**: 78–82.

150 Aggarwal S, Ghilardi N, Xie M-H, de Sauvage FJ, Gurney AL. Interleukin-23 promotes a distinct CD4 T cell activation state characterized by the production of interleukin-17. *J Biol Chem* 2003; **278**: 1910–4.

151 Wolk K, Kunz S, Witte E, Friedrich M, Asadullah K, Sabat R. IL-22 increases the innate immunity of tissues. *Immunity* 2004; **21**: 241–54.

152 Liang SC, Tan X-Y, Luxenberg DP, *et al.* Interleukin (IL)-22 and IL-17 are coexpressed by Th17 cells and cooperatively enhance expression of antimicrobial peptides. *J Exp Med* 2006; **203**: 2271–9.

153 Tato CM, O'Shea JJ. Immunology: what does it mean to be just 17? *Nature* 2006; **441**: 166–8.

154 Witowski J, Ksiazek K, Jörres A. Interleukin-17: a mediator of inflammatory responses. *Cell Mol life Sci* 2004; **61**: 567–79.

155 Gratz IK, Campbell DJ. Organ-specific and memory treg cells: specificity, development, function, and maintenance. *Front Immunol* 2014; **5**: 333.

156 Thornton AM, Shevach EM. CD4+CD25+ Immunoregulatory T Cells Suppress Polyclonal T Cell Activation In Vitro by Inhibiting Interleukin 2 Production. *J Exp Med* 1998; **188**: 287–96.

157 Thornton AM, Shevach EM. Suppressor effector function of CD4+CD25+ immunoregulatory T cells is antigen nonspecific. *J Immunol* 2000; **164**: 183–90.

158 Shevach EM. CD4+ CD25+ suppressor T cells: more questions than answers. *Nat Rev Immunol* 2002; **2**: 389–400.

159 Chen W, Jin W, Hardegen N, *et al.* Conversion of peripheral CD4+CD25- naive T cells to CD4+CD25+ regulatory T cells by TGF-beta induction of transcription factor Foxp3. *J Exp Med* 2003; **198**: 1875–86.

160 Sakaguchi S, Yamaguchi T, Nomura T, Ono M. Regulatory T cells and immune tolerance. *Cell* 2008; **133**: 775–87.

161 Papiernik M, De Moraes ML, Pontoux C, Vasseur F, Pénit C. Regulatory CD4 T cells: expression of IL-2R alpha chain, resistance to clonal deletion and IL-2 dependency. *Int Immunol* 1998; **10**: 371–8.

162 Jordan MS, Boesteanu A, Reed AJ, *et al.* Thymic selection of CD4+CD25+ regulatory T cells induced by an agonist self-peptide. *Nat Immunol* 2001; **2**: 301–6.

163 Liu X, Nurieva RI, Dong C. Transcriptional regulation of follicular T-helper (Tfh) cells. *Immunol Rev* 2013; **252**: 139–45.

164 Breitfeld BD, Ohl L, Kremmer E, *et al.* Follicular B helper T Cells express CXC chemokine receptor 5 , localize to B Cell follicles , and support immunoglobulin production. *J Exp Med* 2000; **192**: 1545–15551.

165 Schaerli BP, Willimann K, Lang AB, Lipp M, Loetscher P, Moser B. CXC chemokine receptor 5 expression defines follicular homing T cells with B Cell helper function. *J Exp Med* 2000; **192**: 1553–62.

166 Ballesteros-Tato A, Randall TD. Priming of T follicular helper cells by dendritic cells. *Immunol Cell Biol* 2014; **92**: 22–7.

167 Nurieva RI, Chung Y, Hwang D, *et al.* Generation of T follicular helper cells is mediated by interleukin-21 but independent of T helper 1, 2, or 17 cell lineages. *Immunity* 2008; **29**: 138–49.

168 Nurieva RI, Chung Y, Martinez GJ, *et al.* Bcl6 mediates the development of T follicular helper cells. *Science* 2009; **325**: 1001–5.

169 Ansel KM, Ngo VN, Hyman PL, *et al.* A chemokine-driven positive feedback loop organizes lymphoid follicles. *Nature* 2000; **406**: 309–14.

170 Chtanova T, Tangye SG, Newton R, *et al.* T follicular helper cells express a distinctive transcriptional profile, reflecting their role as non-Th1/Th2 effector cells that provide help for B cells. *J Immunol* 2004; **173**: 68–78.

171 Vinuesa CG, Tangye SG, Moser B, Mackay CR. Follicular B helper T cells in antibody responses and autoimmunity. *Nat Rev Immunol* 2005; **5**: 853–65.

172 Fazilleau N, Mark L, McHeyzer-Williams LJ, McHeyzer-Williams MG. Follicular helper T cells: lineage and location. *Immunity* 2009; **30**: 324–35.

173 Quezada S a, Peggs KS. An antitumor boost to TH9 cells. *Nat Immunol* 2014; **15**: 703–5.

174 Dardalhon V, Awasthi A, Kwon H, *et al.* IL-4 inhibits TGF-beta-induced Foxp3+ T cells and, together with TGF-beta, generates IL-9+ IL-10+ Foxp3(-) effector T cells. *Nat Immunol* 2008; **9**: 1347–55.

175 Veldhoen M, Uyttenhove C, Van Snick J, *et al.* Transforming growth factor-beta "reprograms" the differentiation of T helper 2 cells and promotes an interleukin 9-producing subset. *Nat Immunol* 2008; **9**: 1341–6.

176 Schmitt E, Germann T, Goedert S, *et al.* IL-9 production of naive CD4+ T cells depends on IL-2, is synergistically enhanced by a combination of TGF-beta and IL-4, and is inhibited by IFN-gamma. *J Immunol* 1994; **153**: 3989–96.

177 Végran F, Berger H, Boidot R, *et al.* The transcription factor IRF1 dictates the IL-21-dependent anticancer functions of TH9 cells. *Nat Immunol* 2014; **15**. doi:10.1038/ni.2925.

178 Staudt V, Bothur E, Klein M, *et al.* Interferon-regulatory factor 4 is essential for the developmental program of T helper 9 cells. *Immunity* 2010; **33**: 192–202.

179 Kaech SM, Wherry EJ, Ahmed R. Effector and memory T-cell differentiation: implications for vaccine development. *Nat Rev Immunol* 2002; **2**: 251–62.

180 Sprent J, Surh CD. Normal T cell homeostasis: the conversion of naive cells into memory-phenotype cells. *Nat Immunol* 2011; **131**: 478–84.

181 Bachmann MF, Barner M, Viola A, Kopf M. Distinct kinetics of cytokine production and cytolysis in effector and memory T cells after viral infection. *Eur J Immunol* 1999; **29**: 291–9.

182 Veiga-Fernandes H, Walter U, Bourgeois C, McLean A, Rocha B. Response of naïve and memory CD8+ T cells to antigen stimulation in vivo. *Nat Immunol* 2000; **1**: 47–53.

183 Teague TK, Hildeman D, Kedl RM, *et al.* Activation changes the spectrum but not the diversity of genes expressed by T cells. *Proc Natl Acad Sci U S A* 1999; **96**: 12691–6.

184 Schenkel JM, Fraser KA, Vezys V, Masopust D. Sensing and alarm function of resident memory $CD8^+$ T cells. *Nat Immunol* 2013; **14**: 509–13.

185 Mueller SN, Zaid A, Carbone FR. Tissue-resident T cells: Dynamic players in skin immunity. *Front Immunol* 2014; **5**: 332.

186 Shin H, Iwasaki A. Tissue-resident memory T cells. *Immunol Rev* 2013; **255**: 165–81.

187 Surh CD, Sprent J. Homeostasis of naive and memory T cells. *Immunity* 2010; **29**: 848–62.

188 Zhang X, Sun S, Hwang I, Tough DF, Sprent J. Potent and selective stimulation of memory-phenotype CD8+ T cells in vivo by IL-15. *Immunity* 1998; **8**: 591–9.

189 Ku CC, Murakami M, Sakamato A, Kappler J, Marrack P. Control of homeostasis of CD8(+) memory T cells by opposing cytokines. *Science* 2000; **288**: 675–8.

190 Schluns KS, Kieper WC, Jameson SC, Lefrançois L. Interleukin-7 mediates the homeostasis of naïve and memory CD8 T cells in vivo. *Nat Immunol* 2000; **1**: 426–32.

191 Masopust D, Choo D, Vezys V, *et al.* Dynamic T cell migration program provides resident memory within intestinal epithelium. *J Exp Med* 2010; **207**: 553–64.

192 Klonowski KD, Williams KJ, Marzo AL, Blair DA, Lingenheld EG, Lefrançois L. Dynamics of blood-borne CD8 memory T cell migration in vivo. *Immunity* 2004; **20**: 551–62.

193 Wakim LM, Woodward-Davis A, Bevan MJ. Memory T cells persisting within the brain after local infection show functional adaptations to their tissue of residence. *Proc Natl Acad Sci U S A* 2010; **107**: 17872–9.

194 Gebhardt T, Wakim LM, Eidsmo L, Reading PC, Heath WR, Carbone FR. Memory T cells in nonlymphoid tissue that provide enhanced local immunity during infection with herpes simplex virus. *Nat Immunol* 2009; **10**: 524–30.

195 Boyman O, Létourneau S, Krieg C, Sprent J. Homeostatic proliferation and survival of naïve and memory T cells. *Eur J Immunol* 2009; **39**: 2088–94.

196 Bernasconi NL, Traggiai E, Lanzavecchia A. Maintenance of serological memory by polyclonal activation of human memory B cells. *Science* 2002; **298**: 2199–202.

197 Gray D. A role for antigen in the maintenance of immunological memory. *Nat Rev Immunol* 2002; **2**: 60–5.

198 León B, Ballesteros-tato A, Misra RS, Wojciechowski W, Lund FE. Unraveling effector functions of B cells during infection□: The hidden world beyond antibody production. *Infect Disord - Drug Tagets* 2012; **12**: 213–21.

199 Wu LC, Zarrin AA. The production and regulation of IgE by the immune system. *Nat Rev Immunol* 2014; **14**: 247–59.

200 Amanna IJ, Slifka MK. Mechanisms that determine plasma cell lifespan and the duration of humoral immunity. *Immunol Rev* 2010; **236**: 125–38.

201 Ward ES, Ghetie V. The effector functions of immunoglobulins: implications for therapy. *Ther Immunol* 1995; **2**: 77–94.

202 Chen K, Cerutti A. New insights into the enigma of immunoglobulin D. *Immunol Rev* 2010; **237**: 160–79.

203 Schroeder HW, Cavacini L. Structure and function of immunoglobulins. *J Allergy Clin Immunol* 2010; **125**: S41–52.

204 Radbruch A, Muehlinghaus G, Luger EO, *et al.* Competence and competition: the challenge of becoming a long-lived plasma cell. *Nat Rev Immunol* 2006; **6**: 741–50.

205 Snapper CM, Paul WE. Interferon-gamma and B cell stimulatory factor-1 reciprocally regulate Ig isotype production. *Science* 1987; **236**: 944–7.

206 Kühn R, Rajewsky K, Müller W. Generation and analysis of interleukin-4 deficient mice. *Science* 1991; **254**: 707–10.

207 Defrance T, Vanbervliet B, Brière F, Durand I, Rousset F, Banchereau J. Interleukin 10 and transforming growth factor beta cooperate to induce anti-CD40-activated naive human B cells to secrete immunoglobulin A. *J Exp Med* 1992; **175**: 671–82.

208 McHeyzer-Williams LJ, McHeyzer-Williams MG. Antigen-specific memory B cell development. *Annu Rev Immunol* 2005; **23**: 487–513.

209 Kruetzmann S, Rosado MM, Weber H, *et al.* Human immunoglobulin M memory B cells controlling Streptococcus pneumoniae infections are generated in the spleen. *J Exp Med* 2003; **197**: 939–45.

210 Stavnezer J. Immunoglobulin class switching. *Curr Opin Immunol* 1996; **8**: 199–205.

211 Hayakawa K, Hardy RR. Development and function of B-1 cells. *Curr Opin Immunol* 2000; **12**: 346–53.

212 Fairfax K a, Kallies A, Nutt SL, Tarlinton DM. Plasma cell development: from B-cell subsets to long-term survival niches. *Semin Immunol* 2008; **20**: 49–58.

213 Ochsenbein A, Fehr T, Lutz C, Suter M, Brombacher F, Hengartner H. Control of early viral and bacterial distribution and disease by natural antibodies. *Science* 1999; **286**: 2156–9.

214 Martin F, Oliver A, Kearney JF. Marginal zone and B1 B cells unite in the early response against T-independent blood borne particulate antigens. *Immunity* 2001; **14**: 617–29.

215 Martin F, Kearney JF. B1 cells: similarities and differences with other B cell subsets. *Curr Opin Immunol* 2001; **13**: 195–201.

216 Schwartz-Albiez R, Monteiro RC, Rodriguez M, Binder CJ, Shoenfeld Y. Natural antibodies, intravenous immunoglobulin and their role in autoimmunity, cancer and inflammation. *Clin Exp Immunol* 2009; **158 Suppl** : 43–50.

217 Hardy RR, K H. B cell development pathways. *Annu Rev Immunol* 2001; **19**: 595–621.

218 Zhang X. Regulatory functions of innate-like B cells. *Cell Mol Immunol* 2013; **10**: 113–21.

219 Pieper K, Grimbacher B, Eibel H. B-cell biology and development. *J Allergy Clin Immunol* 2013; **131**: 959–71.

220 Vitale G, Mion F, Pucillo C. Regulatory B cells: Evidence, developmental origin and population diversity. *Mol Immunol* 2010; **48**: 1–8.

221 Mauri C. Regulation of immunity and autoimmunity by B cells. *Curr Opin Immunol* 2010; **22**: 1–7.

222 Mizoguchi A, Mizoguchi E, Takedatsu H, Blumberg RS, Bhan AK. Chronic intestinal inflammatory condition generates IL-10-producing regulatory B cell subset characterized by CD1d upregulation. *Immunity* 2002; **16**: 219–30.

223 Gray D, Gray M. What are regulatory B cells? *Eur J Immunol* 2010; **40**: 2677–9.

224 Fillatreau S, Sweenie C, McGeachy M, Gray D, Anderton S. B cells regulate autoimmunity by provision of IL-10. *Nat Immunol* 2002; **3**: 944–50.

225 Wolf S, Dittel B, Hardardottir F, Janeway CJ. Experimental autoimmune encephalomyelitis induction in genetically B cell-deficient mice. *J Exp Med* 1996; **184**: 2271–8.

226 Amu S, Saunders S, Kronenberg M, Mangan N, Atzberger A, Fallon P. Regulatory B cells prevent and reverse allergic airway inflammation via FoxP3-positive T regulatory cells in a murine model. *J Allergy Clin Immunol* 2010; **125**: 1114–24.

227 Yanaba K, Bouaziz J-D, Haas K, Poe J, Fujjimoto M, Tedder T. A regulatory B cell subset with a unique CD1dhigh CD5+ phenotype controls T cell-dependent inflammatory responses. *Immunity* 2008; **28**: 639–50.

228 Peek LJ, Middaugh CR, Berkland C. Nanotechnology in vaccine delivery. *Adv Drug Deliv Rev* 2008; **60**: 915–28.

229 Orenstein W a, Seib K, Graham-Rowe D, Berkley S. Contemporary vaccine challenges: Improving global health one shot at a time. *Sci Transl Med* 2014; **6**: 253ps11.

230 Shepard CW, Simard EP, Finelli L, Fiore AE, Bell BP. Hepatitis B virus infection: epidemiology and vaccination. *Epidemiol Rev* 2006; **28**: 112–25.

231 Bergmann-Leitner E, Leitner W. Adjuvants in the driver's seat: How magnitude, type, fine specificity and longevity of immune responses are driven by distinct classes of immune potentiators. *Vaccines* 2014; **2**: 252–96.

232 Pulendran B, Ahmed R. Translating innate immunity into immunological memory: implications for vaccine development. *Cell* 2006; **124**: 849–63.

233 Vanneman M, Dranoff G. Combining immunotherapy and targeted therapies in cancer treatment. *Nat Rev Cancer* 2012; **12**: 237–51.

234 Plotkin S, Orenstein W, Offit P. Vaccines, 5th Editio. , Elsevier Health Sciences, 2008http://books.google.com/books?id=BFQq2-fIAJ8C&pgis=1 (accessed 15 Sep2014).

235 Ramon G. Sur la toxine et sur l'anatoxine diphtheriques. *Ann Inst Pasteur (Paris)* 1924; **38**: 1–10.

236 Guy B. The perfect mix: recent progress in adjuvant research. *Nat Rev Microbiol* 2007; **5**: 505–17.

237 Dubensky TW, Reed SG. Adjuvants for cancer vaccines. *Semin Immunol* 2010; **22**: 155–61.

238 Cluff CW. Monophosphoryl lipid A (MPL) as an adjuvant for anti-cancer vaccines: clinical results. *Adv Exp Med Biol* 2009; **667**: 111–23.

239 O'Hagan DT, De Gregorio E. The path to a successful vaccine adjuvant--'the long and winding road'. *Drug Discov Today* 2009; **14**: 541–51.

240 O'Hagan DT, Singh M. Microparticles as vaccine adjuvants and delivery systems. *Expert Rev Vaccines* 2003; **2**: 269–83.

241 Aranda F, Llopiz D, Díaz-Valdés N, *et al.* Adjuvant combination and antigen targeting as a strategy to induce polyfunctional and high-avidity T-cell responses against poorly immunogenic tumors. *Cancer Res* 2011; **71**: 3214–24.

242 Palucka K, Ueno H, Banchereau J. Recent developments in cancer vaccines. *J Immunol* 2011; **186**: 1325–31.

243 Kaisho T, Akira S. Toll-like receptors as adjuvant receptors. *Biochim Biophys Acta* 2002; **1589**: 1–13.

244 Haining WN, Davies J, Kanzler H, *et al.* CpG oligodeoxynucleotides alter lymphocyte and dendritic cell trafficking in humans. *Clin Cancer Res* 2008; **14**: 5626–34.

245 Jahrsdorfer B, Hartmann G, Racila E, *et al.* CpG DNA increases primary malignant B cell expression of costimulatory molecules and target antigens. *J Leukoc Biol* 2001; **69**: 81–8.

246 Gowen BB, Wong M-H, Jung K-H, *et al.* TLR3 is essential for the induction of protective immunity against Punta Toro Virus infection by the double-stranded RNA (dsRNA), poly(I:C12U), but not Poly(I:C): differential recognition of synthetic dsRNA molecules. *J Immunol* 2007; **178**: 5200–8.

247 Stahl-Hennig C, Eisenblätter M, Jasny E, *et al.* Synthetic double-stranded RNAs are adjuvants for the induction of T helper 1 and humoral immune responses to human papillomavirus in rhesus macaques. *PLoS Pathog* 2009; **5**: e1000373.

248 Trumpfheller C, Caskey M, Nchinda G, *et al.* The microbial mimic poly IC induces durable and protective CD4+ T cell immunity together with a dendritic cell targeted vaccine. *Proc Natl Acad Sci U S A* 2008; **105**: 2574–9.

249 Zhao Y, Yang J, Shi J, *et al.* The NLRC4 inflammasome receptors for bacterial flagellin and type III secretion apparatus. *Nature* 2011; **477**: 596–600.

250 Garaude J, Kent A, van Rooijen N, Blander JM. Simultaneous targeting of toll- and nod-like receptors induces effective tumor-specific immune responses. *Sci Transl Med* 2012; **4**: 120ra16.

251 Ulrich J, Myers K. Monophosphoryl lipid A as an adjuvant. Past experiences and new directions. *Pharm Biotechnol* 1995; **6**: 495–524.

252 Persing D, Coler R, Lacy M, *et al.* Taking toll: lipid A mimetics as adjuvants and immunomodulators. *Trends Microbiol* 2002; **10**: S32–7.

253 Didierlaurent AM, Morel S, Lockman L, *et al.* AS04, an aluminum salt- and TLR4 agonist-based adjuvant system, induces a transient localized innate immune response leading to enhanced adaptive immunity. *J Immunol* 2009; **183**: 6186–97.

254 Johnson DA. Synthetic TLR4-active glycolipids as vaccine adjuvants and stand-alone immunotherapeutics. *Curr Top Med Chem* 2008; **8**: 64–79.

255 Schoenen H, Bodendorfer B, Hitchens K, *et al.* Cutting edge: Mincle is essential for recognition and adjuvanticity of the mycobacterial cord factor and its synthetic analog trehalose-dibehenate. *J Immunol* 2010; **184**: 2756–60.

256 Ishikawa E, Ishikawa T, Morita YS, *et al.* Direct recognition of the mycobacterial glycolipid, trehalose dimycolate, by C-type lectin Mincle. *J Exp Med* 2009; **206**: 2879–88.

257 Tewari K, Flynn BJ, Boscardin SB, *et al.* Poly(I:C) is an effective adjuvant for antibody and multi-functional CD4+ T cell responses to Plasmodium falciparum circumsporozoite protein (CSP) and αDEC-CSP in non human primates. *Vaccine* 2010; **28**: 7256–66.

258 Kobiyama K, Takeshita F, Ishii KJ, *et al.* A signaling polypeptide derived from an innate immune adaptor molecule can be harnessed as a new class of vaccine adjuvant. *J Immunol* 2009; **182**: 1593–601.

259 Luke JM, Simon GG, Söderholm J, *et al.* Coexpressed RIG-I agonist enhances humoral immune response to influenza virus DNA vaccine. *J Virol* 2011; **85**: 1370–83.

260 Kastenmüller W, Kastenmüller K, Kurts C, Seder R a. Dendritic cell-targeted vaccines - hope or hype? *Nat Rev Immunol* 2014. doi:10.1038/nri3727.

261 Blander JM, Medzhitov R. Toll-dependent selection of microbial antigens for presentation by dendritic cells. *Nature* 2006; **440**: 808–12.

262 Wille-Reece U, Wu C -y., Flynn BJ, Kedl RM, Seder R a. Immunization with HIV-1 Gag Protein Conjugated to a TLR7/8 Agonist Results in the Generation of HIV-1 Gag-Specific Th1 and CD8+ T Cell Responses. *J Immunol* 2005; **174**: 7676–83.

263 Kensil C, Patel U, Lennick M, Marciani D. Separation and characterization of saponins with adjuvant activity from Quillaja saponaria Molina cortex. *J Immunol* 1991; **146**: 431–7.

264 Sun H-X, Xie Y, Ye Y-P. Advances in saponin-based adjuvants. *Vaccine* 2009; **27**: 1787–96.

265 Ragupathi G, Gardner JR, Livingston PO, Gin DY. Natural and synthetic saponin adjuvant QS-21 for vaccines against cancer. *Expert Rev Vaccines* 2011; **10**: 463–70.

266 Kim SK, Ragupathi G, Cappello S, Kagan E, Livingston PO. Effect of immunological adjuvant combinations on the antibody and T-cell response to vaccination with MUC1–KLH and GD3–KLH conjugates. *Vaccine* 2000; **19**: 530–7.

267 Vandepapelière P, Horsmans Y, Moris P, *et al.* Vaccine adjuvant systems containing monophosphoryl lipid A and QS21 induce strong and persistent humoral and T cell

responses against hepatitis B surface antigen in healthy adult volunteers. *Vaccine* 2008; **26**: 1375–86.

268 Schijns VEJC, Lavelle EC. Trends in vaccine adjuvants. *Expert Rev Vaccines* 2011; **10**: 539–50.

269 Oyewumi MO, Kumar A, Cui Z. Nano-microparticles as immune adjuvants: correlating particle sizes and the resultant immune responses. *Expert Rev Vaccines* 2010; **9**: 1095–107.

270 Le Moignic P. Les vaccines en emulsion dans les corps gras ou "lipo-vaccins". *Comptes Rendus la Soc Biol* 1916; : 201–3.

271 Morse MA, Clay TM, Lyerly HK. Handbook of cancer vaccines, Volume 1. , Humana Press, 2004.

272 Su SB, Silver PB, Grajewski RS, *et al.* Essential role of the MyD88 pathway, but nonessential roles of TLRs 2, 4, and 9, in the adjuvant effect promoting Th1-mediated autoimmunity. *J Immunol* 2005; **175**: 6303–10.

273 Eisenbarth SC, Colegio OR, O'Connor W, Sutterwala FS, Flavell RA. Crucial role for the Nalp3 inflammasome in the immunostimulatory properties of aluminium adjuvants. *Nature* 2008; **453**: 1122–6.

274 Gavin AL, Hoebe K, Duong B, *et al.* Adjuvant-enhanced antibody responses in the absence of toll-like receptor signaling. *Science* 2006; **314**: 1936–8.

275 Aucouturier J, Dupuis L, Ganne V. Adjuvants designed for veterinary and human vaccines. *Vaccine* 2001; **19**: 2666–72.

276 Aucouturier J, Ascarateil S, Dupuis L. The use of oil adjuvants in therapeutic vaccines. *Vaccine* 2006; **24**: S44–5.

277 Seubert A, Monaci E, Pizza M, O'Hagan DT, Wack A. The adjuvants aluminum hydroxide and MF59 induce monocyte and granulocyte chemoattractants and enhance monocyte differentiation toward dendritic cells. *J Immunol* 2008; **180**: 5402–12.

278 Calabro S, Tortoli M, Baudner BC, *et al.* Vaccine adjuvants alum and MF59 induce rapid recruitment of neutrophils and monocytes that participate in antigen transport to draining lymph nodes. *Vaccine* 2011; **29**: 1812–23.

279 Ellebedy AH, Lupfer C, Ghoneim HE, DeBeauchamp J, Kanneganti T-D, Webby RJ. Inflammasome-independent role of the apoptosis-associated speck-like protein containing CARD (ASC) in the adjuvant effect of MF59. *Proc Natl Acad Sci U S A* 2011; **108**: 2927–32.

280 Vono M, Taccone M, Caccin P, *et al.* The adjuvant MF59 induces ATP release from muscle that potentiates response to vaccination. *Proc Natl Acad Sci U S A* 2013; **110**: 21095–100.

281 Podda A, Del Giudice G. MF59-adjuvanted vaccines: increased immunogenicity with an optimal safety profile. *Expert Rev Vaccines* 2003; **2**: 197–203.

282 Anderson RC, Fox CB, Dutill TS, *et al.* Physicochemical characterization and biological activity of synthetic TLR4 agonist formulations. *Colloids Surf B Biointerfaces* 2010; **75**: 123–32.

283 Coler RN, Bertholet S, Moutaftsi M, *et al.* Development and characterization of synthetic glucopyranosyl lipid adjuvant system as a vaccine adjuvant. *PLoS One* 2011; **6**: e16333.

284 Orr MT, Fox CB, Baldwin SL, *et al.* Adjuvant formulation structure and composition are critical for the development of an effective vaccine against tuberculosis. *J Control Release* 2013; **172**: 190–200.

285 Morein B, Sundquist B, Höglund S, Dalsgaard K, Osterhaus A. Iscom, a novel structure for antigenic presentation of membrane proteins from enveloped viruses. *Nature* 1984; **308**: 457–60.

286 Barr IG, Mitchell GF. ISCOMs (immunostimulating complexes): the first decade. *Immunol Cell Biol* 1996; **74**: 8–25.

287 Claassen I, Osterhaus A. The iscom structure as an immune-enhancing moiety: experience with viral systems. *Res Immunol* 1992; **143**: 531–41.

288 Villacres-Eriksson M, Bergström-Mollaoglu M, Kåberg H, Lövgren K, Morein B. The induction of cell-associated and secreted IL-1 by iscoms, matrix or micelles in murine splenic cells. *Clin Exp Immunol* 1993; **93**: 120–5.

289 Behboudi S, Morein B, Villacres-Eriksson M. In vivo and in vitro induction of IL-6 by Quillaja saponaria molina triterpenoid formulations. *Cytokine* 1997; **9**: 682–7.

290 Behboudi S, Morein B, Villacres-Eriksson M. In vitro activation of antigen-presenting cells (APC) by defined composition of Quillaja saponaria Molina triterpenoids. *Clin Exp Immunol* 1996; **105**: 26–30.

291 Schnurr M, Orban M, Robson NC, *et al.* ISCOMATRIX Adjuvant induces efficient cross-presentation of tumor antigen by dendritic cells via rapid cytosolic antigen delivery and processing via tripeptidyl peptidase II. *J Immunol* 2009; **182**: 1253–9.

292 Brito L a, O'Hagan DT. Designing and building the next generation of improved vaccine adjuvants. *J Control Release* 2014; **190**: 563–79.

293 Clements CJ, Griffiths E. The global impact of vaccines containing aluminium adjuvants. *Vaccine* 2002; **20**: S24–33.

294 Li H, Willingham SB, Ting JP-Y, Re F. Cutting edge: inflammasome activation by alum and alum's adjuvant effect are mediated by NLRP3. *J Immunol* 2008; **181**: 17–21.

295 Franchi L, Núñez G. The Nlrp3 inflammasome is critical for aluminium hydroxide-mediated IL-1beta secretion but dispensable for adjuvant activity. *Eur J Immunol* 2008; **38**: 2085–9.

296 Glenny A, Pope C. The antigenic effect of intravenous injection of diphtheria toxin. *J Pathol Bacteriol* 1925; **28**: 273–8.

297 Glenny A, Buttle G, Stevens M. Rate of disappearance of diptheria toxoid injected into rabbits and guinea pigs: toxoid precipitated with alum. *J Pathol Bacteriol* 1931; **34**: 267–75.

298 Hutchison S, Benson RA, Gibson VB, Pollock AH, Garside P, Brewer JM. Antigen depot is not required for alum adjuvanticity. *Fed Am Soc Exp Biol* 2012; **26**: 1272–9.

299 Marichal T, Ohata K, Bedoret D, *et al.* DNA released from dying host cells mediates aluminum adjuvant activity. *Nat Med* 2011; **17**: 996–1002.

300 McKee AS, Munks MW, MacLeod MKL, *et al.* Alum induces innate immune responses through macrophage and mast cell sensors, but these sensors are not required for alum to act as an adjuvant for specific immunity. *J Immunol* 2009; **183**: 4403–14.

301 Jordan MB, Mills DM, Kappler J, Marrack P, Cambier JC. Promotion of B cell immune responses via an alum-induced myeloid cell population. *Science* 2004; **304**: 1808–10.

302 McKee AS, MacLeod M, White J, Crawford F, Kappler JW, Marrack P. Gr1+IL-4-producing innate cells are induced in response to Th2 stimuli and suppress Th1-dependent antibody responses. *Int Immunol* 2008; **20**: 659–69.

303 Wang H-B, Weller PF. Pivotal advance: eosinophils mediate early alum adjuvant-elicited B cell priming and IgM production. *J Leukoc Biol* 2008; **83**: 817–21.

304 Holt LB. Developments in Diptheria Prophylaxi. , Heinemann-Medical books Ltd, 1950http://books.google.ie/books/about/Developments_in_Diptheria_Prophylaxis.html?id=MJUwAAAAIAAJ&pgis=1 (accessed 28 May2013).

305 Flach TL, Ng G, Hari A, *et al.* Alum interaction with dendritic cell membrane lipids is essential for its adjuvanticity. *Nat Med* 2011; **17**: 479–87.

306 Men Y, Tamber H, Audran R, Gander B, Corradin G. Induction of a cytotoxic T lymphocyte response by immunization with a malaria specific CTL peptide entrapped in biodegradable polymer microspheres. *Vaccine* 1997; **15**: 1405–12.

307 Hamdy S, Haddadi A, Hung RW, Lavasanifar A. Targeting dendritic cells with nano-particulate PLGA cancer vaccine formulations. *Adv Drug Deliv Rev* 2011; **63**: 943–55.

308 Jain S, O'Hagan DT, Singh M. The long-term potential of biodegradable poly(lactide-co-glycolide) microparticles as the next-generation vaccine adjuvant. *Expert Rev Vaccines* 2011; **10**: 1731–42.

309 Malyala P, Chesko J, Ugozzoli M, *et al.* The potency of the adjuvant, CpG oligos, is enhanced by encapsulation in PLG microparticles. *J Pharm Sci* 2008; **97**: 1155–64.

310 Kazzaz J, Singh M, Ugozzoli M, Chesko J, Soenawan E, O'Hagan DT. Encapsulation of the immune potentiators MPL and RC529 in PLG microparticles enhances their potency. *J Control Release* 2006; **110**: 566–73.

311 Waeckerle-Men Y, Allmen EU, Gander B, *et al.* Encapsulation of proteins and peptides into biodegradable poly(D,L-lactide-co-glycolide) microspheres prolongs and enhances antigen presentation by human dendritic cells. *Vaccine* 2006; **24**: 1847–57.

312 Bachmann MF, Zinkernagel RM. Neutralizing antiviral B cell responses. *Annu Rev Immunol* 1997; **15**: 235–70.

313 Maloy KJ, Donachie AM, O'Hagan DT, Mowat AM. Induction of mucosal and systemic immune responses by immunization with ovalbumin entrapped in poly(lactide-co-glycolide) microparticles. *Immunology* 1994; **81**: 661–7.

314 Nixon DF, Hioe C, Chen PD, *et al.* Synthetic peptides entrapped in microparticles can elicit cytotoxic T cell activity. *Vaccine* 1996; **14**: 1523–30.

315 Men Y, Gander B, Merkle HP, Corradin G. Induction of sustained and elevated immune responses to weakly immunogenic synthetic malarial peptides by encapsulation in biodegradable polymer microspheres. *Vaccine* 1996; **14**: 1442–50.

316 Men Y, Thomasin C, Merkle HP, Gander B, Corradin G. A single administration of tetanus toxoid in biodegradable microspheres elicits T cell and antibody responses similar or superior to those obtained with aluminum hydroxide. *Vaccine* 1995; **13**: 683–9.

317 Zhao L, Seth A, Wibowo N, *et al.* Nanoparticle vaccines. *Vaccine* 2014; **32**: 327–37.

318 Maruyama K, Okuizumi S, Ishida O, Yamauchi H, Kikuchi H, Iwatsuru M. Phosphatidyl polyglycerols prolong liposome circulation in vivo. *Int J Pharm* 1994; **111**: 103–7.

319 Foged C, Arigita C, Sundblad A, Jiskoot W, Storm G, Frokjaer S. Interaction of dendritic cells with antigen-containing liposomes: effect of bilayer composition. *Vaccine* 2004; **22**: 1903–13.

320 Allison A, Gregoriadis G. Liposomes as immunological adjuvants. *Nature* 1974; **252**: 252–252.

321 Korsholm KS, Petersen R V, Agger EM, Andersen P. T-helper 1 and T-helper 2 adjuvants induce distinct differences in the magnitude, quality and kinetics of the early inflammatory response at the site of injection. *Immunology* 2010; **129**: 75–86.

322 Henriksen-Lacey M, Bramwell VW, Christensen D, Agger E-M, Andersen P, Perrie Y. Liposomes based on dimethyldioctadecylammonium promote a depot effect and enhance immunogenicity of soluble antigen. *J Control Release* 2010; **142**: 180–6.

323 Davidsen J, Rosenkrands I, Christensen D, *et al.* Characterization of cationic liposomes based on dimethyldioctadecylammonium and synthetic cord factor from M. tuberculosis (trehalose 6,6'-dibehenate)-a novel adjuvant inducing both strong CMI and antibody responses. *Biochim Biophys Acta* 2005; **1718**: 22–31.

324 Christensen D, Henriksen-Lacey M, Kamath AT, *et al.* A cationic vaccine adjuvant based on a saturated quaternary ammonium lipid have different in vivo distribution kinetics and display a distinct CD4 T cell-inducing capacity compared to its unsaturated analog. *J Control Release* 2012; **160**: 468–76.

325 Pinto V V, Salanti A, Joergensen LM, *et al.* The effect of adjuvants on the immune response induced by a DBL4ε-ID4 VAR2CSA based Plasmodium falciparum vaccine against placental malaria. *Vaccine* 2012; **30**: 572–9.

326 Fomsgaard A, Karlsson I, Gram G, *et al.* Development and preclinical safety evaluation of a new therapeutic HIV-1 vaccine based on 18 T-cell minimal epitope peptides applying a novel cationic adjuvant CAF01. *Vaccine* 2011; **29**: 7067–74.

327 Olsen AW, Andersen P, Follmann F. Characterization of protective immune responses promoted by human antigen targets in a urogenital Chlamydia trachomatis mouse model. *Vaccine* 2014; **32**: 685–92.

328 Rosenkrands I, Vingsbo-Lundberg C, Bundgaard TJ, *et al.* Enhanced humoral and cell-mediated immune responses after immunization with trivalent influenza vaccine adjuvanted with cationic liposomes. *Vaccine* 2011; **29**: 6283–91.

329 Christensen D, Lindenstrøm T, van de Wijdeven G, Andersen P, Agger EM. Syringe free vaccination with CAF01 Adjuvated Ag85B-ESAT-6 in Bioneedles provides strong and prolonged protection against tuberculosis. *PLoS One* 2010; **5**: e15043.

330 Scheerlinck J-PY, Greenwood DL V. Virus-sized vaccine delivery systems. *Drug Discov Today* 2008; **13**: 882–7.

331 Glück R, Moser C, Metcalfe IC. Influenza virosomes as an efficient system for adjuvanted vaccine delivery. *Expert Opin Biol Ther* 2004; **4**: 1139–45.

332 Grgacic EVL, Anderson DA. Virus-like particles: passport to immune recognition. *Methods* 2006; **40**: 60–5.

333 Huckriede A, Bungener L, Stegmann T, *et al.* The virosome concept for influenza vaccines. *Vaccine* 2005; **23 Suppl 1**: S26–38.

334 Bungener L, Serre K, Bijl L, *et al.* Virosome-mediated delivery of protein antigens to dendritic cells. *Vaccine* 2002; **20**: 2287–95.

335 Bungener L, Idema J, ter Veer W, Huckriede A, Daemen T, Wilschut J. Virosomes in vaccine development: induction of cytotoxic T lymphocyte activity with virosome-encapsulated protein antigens. *J Liposome Res*; **12**: 155–63.

336 Bachmann MF, Jennings GT. Vaccine delivery: a matter of size, geometry, kinetics and molecular patterns. *Nat Rev Immunol* 2010; **10**: 787–96.

337 Fritz JH, Brunner S, Birnstiel ML, *et al.* The artificial antimicrobial peptide KLKLLLLLKLK induces predominantly a TH2-type immune response to co-injected antigens. *Vaccine* 2004; **22**: 3274–84.

338 Schellack C, Prinz K, Egyed A, *et al.* IC31, a novel adjuvant signaling via TLR9, induces potent cellular and humoral immune responses. *Vaccine* 2006; **24**: 5461–72.

339 Aichinger MC, Ginzler M, Weghuber J, *et al.* Adjuvating the adjuvant: facilitated delivery of an immunomodulatory oligonucleotide to TLR9 by a cationic antimicrobial peptide in dendritic cells. *Vaccine* 2011; **29**: 426–36.

340 Garçon N, Chomez P, Van Mechelen M. GlaxoSmithKline Adjuvant Systems in vaccines: concepts, achievements and perspectives. *Expert Rev Vaccines* 2007; **6**: 723–39.

341 Morel S, Didierlaurent A, Bourguignon P, *et al.* Adjuvant System AS03 containing α-tocopherol modulates innate immune response and leads to improved adaptive immunity. *Vaccine* 2011; **29**: 2461–73.

342 Agnandji ST, Lell B, Fernandes JF, *et al.* A phase 3 trial of RTS,S/AS01 malaria vaccine in African infants. *N Engl J Med* 2012; **367**: 2284–95.

343 Kruit WHJ, Suciu S, Dreno B, *et al.* Selection of Immunostimulant AS15 for Active Immunization With MAGE-A3 Protein: Results of a Randomized Phase II Study of the European Organisation for Research and Treatment of Cancer Melanoma Group in Metastatic Melanoma. *J Clin Oncol* 2013; **May 28**: epub ahead of print.

344 Ott G, Barchfeld GL, Chernoff D, Radhakrishnan R, Van Hoogevest P, Van Nest G. MF59. Design and evaluation of a safe and potent adjuvant for human vaccines. *Pharm Biotechnol* 1995; **6**: 277–96.

345 Mottram PL, Leong D, Crimeen-irwin B, *et al.* Type 1 and 2 immunity following vaccination is influenced by nanoparticle size: Formulation of a model vaccine for respiratory syncytial virus. *Mol Pharm* 2006; **4**: 73–84.

346 Li X, Sloat BR, Yanasarn N, Cui Z. Relationship between the size of nanoparticles and their adjuvant activity: data from a study with an improved experimental design. *Eur J Pharm Biopharm* 2011; **78**: 107–16.

347 O'Hagan DT, Singh M, Ulmer JB. Microparticle-based technologies for vaccines. *Methods* 2006; **40**: 10–9.

348 O'Hagan DT, Jeffery H, Roberts MJ, McGee JP, Davis SS. Controlled release microparticles for vaccine development. *Vaccine* 1991; **9**: 768–71.

349 O'Hagan DT, Rahman D, McGee JP, *et al.* Biodegradable microparticles as controlled release antigen delivery systems. *Immunology* 1991; **73**: 239–42.

350 Johansen P, Raynaud C, Yang M, Colston MJ, Tascon RE, Lowrie DB. Anti-mycobacterial immunity induced by a single injection of M. leprae Hsp65-encoding plasmid DNA in biodegradable microparticles. *Immunol Lett* 2003; **90**: 81–5.

351 Katare YK, Muthukumaran T, Panda AK. Influence of particle size, antigen load , dose and additional adjuvant on the immune response from antigen loaded PLA microparticles. *Int J Pharm* 2005; **301**: 149–60.

352 Kanchan V, Panda AK. Interactions of antigen-loaded polylactide particles with macrophages and their correlation with the immune response. *Biomaterials* 2007; **28**: 5344–57.

353 Nakaoka R, Inoue Y, Tabata Y, Ikada Y. Size effect on the antibody production induced by biodegradable microspheres containing antigen. *Vaccine* 1996; **14**: 1251–6.

354 Fifis T, Gamvrellis A, Crimeen-irwin B, *et al.* Size-dependent immunogenicity: Therapeutic and protective properties of nano-vaccines against tumors. *J Immunol* 2004; **1**: 2–8.

355 Lutz MB, Kukutsch N, Ogilvie AL, *et al.* An advanced culture method for generating large quantities of highly pure dendritic cells from mouse bone marrow. *J Immunol Methods* 1999; **223**: 77–92.

356 Tzianabos AO, Wang JY, Lee JC. Structural rationale for the modulation of abscess formation by Staphylococcus aureus capsular polysaccharides. *Proc Natl Acad Sci U S A* 2001; **98**: 9365–70.

357 McLoughlin RM, Lee JC, Kasper DL, Tzianabos AO. IFN-gamma regulated chemokine production determines the outcome of Staphylococcus aureus infection. *J Immunol* 2008; **181**: 1323–32.

358 McLoughlin RM, Solinga RM, Rich J, *et al.* CD4+ T cells and CXC chemokines modulate the pathogenesis of Staphylococcus aureus wound infections. *Proc Natl Acad Sci U S A* 2006; **103**: 10408–13.

359 Chen HC, Sun B, Tran KK, Shen H. Effects of particle size on toll-like receptor 9-mediated cytokine profiles. *Biomaterials* 2011; **32**: 1731–7.

360 Van Snick J. Interleukin-6: an overview. *Annu Rev Immunol* 1990; **8**: 253–78.

361 Stetson DB, Medzhitov R. Type I interferons in host defense. *Immunity* 2006; **25**: 373–81.

362 Nakashima Y, Sun DH, Trindade MC, *et al.* Induction of macrophage C-C chemokine expression by titanium alloy and bone cement particles. *J bone Jt Surg Br Vol* 1999; **81**: 155–62.

363 Tian F, Habel NC, Yin R, *et al.* Pulmonary DWCNT exposure causes sustained local and low-level systemic inflammatory changes in mice. *Eur J Pharm Biopharm* 2013; **84**: 412–20.

364 Gu Q, Shi Q, Yang H. The role of TLR and chemokine in wear particle-induced aseptic loosening. *J Biomed Biotechnol* 2012; **2012**: 596870.

365 Jacobs JJ, Hallab NJ, Urban RM, Wimmer MA. Wear particles. *J Bone Joint Surg Am* 2006; **88 Suppl 2**: 99–102.

366 Abu-Amer Y, Darwech I, Clohisy JC. Aseptic loosening of total joint replacements: mechanisms underlying osteolysis and potential therapies. *Arthritis Res Ther* 2007; **9 Suppl 1**: S6.

367 Department of Research & Scientific Affairs, American Academy of Orthopaedic Surgeons. Rosemont, IL; AAOS; May 2014. http://orthoinfo.aaos.org/topic.cfm?topic=a00233.

368 Rankin JA. Biological Mediators of Acute Inflmmation. *AACN Clin Issues* 2004; **15**: 3–17.

369 Lu X, Jin T, Jin Y, *et al.* Toxicogenomic analysis of the particle dose- and size-response relationship of silica particles-induced toxicity in mice. *Nanotechnology* 2013; **24**: 015106.

370 Tomazic-Jezic VJ, Merritt K, Umbreit TH. Significance of the type and the size of biomaterial particles on phagocytosis and tissue distribution. *J Biomed Mater Res* 2001; **55**: 523–9.

371 Anthony RM, Kobayashi T, Wermeling F, Ravetch J V. Intravenous gammaglobulin suppresses inflammation through a novel T(H)2 pathway. *Nature* 2011; **475**: 110–3.

372 Wermeling F, Anthony RM, Brombacher F, Ravetch J V. Acute inflammation primes myeloid effector cells for anti-inflammatory STAT6 signaling. *Proc Natl Acad Sci U S A* 2013; **110**: 13487–91.

373 Kay JE. Mechanisms of T lymphocyte activation. *Immunol Lett* 1991; **29**: 51–4.

374 Cohen JA, Beaudette TT, Tseng WW, *et al.* T-cell activation by antigen-loaded pH-sensitive hydrogel particles in vivo: the effect of particle size. *Bioconjug Chem* 2009; **20**: 111–9.

375 Medzhitov R, Janeway CA. Innate immunity: impact on the adaptive immune response. *Curr Opin Immunol* 1997; **9**: 4–9.

376 Ghosn EEB, Cassado AA, Govoni GR, *et al.* Two physically, functionally, and developmentally distinct peritoneal macrophage subsets. *Proc Natl Acad Sci U S A* 2010; **107**: 2568–73.

377 Ray A, Dittel BN. Isolation of mouse peritoneal cavity cells. *J Vis Exp* 2010; : e1488.

378 Auffray C, Sieweke MH, Geissmann F. Blood monocytes: development, heterogeneity, and relationship with dendritic cells. *Annu Rev Immunol* 2009; **27**: 669–92.

379 Barth M, Hendrzak J, Melnicoff M, Morahans P. Review of the macrophage disappearance reaction. *J Leukoc Biol* 1995; **57**: 361–7.

380 Nelson DS, North RJ. The fate of peritoneal macrophages after the injection of antigen into guinea pigs with delayed-type hypersensitivity. *Lab Invest* 1965; **14**: 89–101.

381 Davies LC, Jenkins SJ, Allen JE, Taylor PR. Tissue-resident macrophages. *Nat Immunol* 2013; **14**: 986–95.

382 Jakubzick C, Tacke F, Llodra J, van Rooijen N, Randolph GJ. Modulation of Dendritic Cell Trafficking to and from the Airways. *J Immunol* 2006; **176**: 3578–84.

383 Kirby AC, Coles MC, Kaye PM. Alveolar macrophages transport pathogens to lung draining lymph nodes. *J Immunol* 2009; **183**: 1983–9.

384 Bellingan GJ, Xu P, Cooksley H, *et al.* Adhesion Molecule-dependent Mechanisms Regulate the Rate of Macrophage Clearance During the Resolution of Peritoneal Inflammation. *J Exp Med* 2002; **196**: 1515–21.

385 Davies LC, Rosas M, Smith PJ, Fraser DJ, Jones SA, Taylor PR. A quantifiable proliferative burst of tissue macrophages restores homeostatic macrophage populations after acute inflammation. *Eur J Immunol* 2011; **41**: 2155–64.

386 Jenkins SJ, Ruckerl D, Cook PC, *et al.* Local macrophage proliferation, rather than recruitment from the blood, is a signature of TH2 inflammation. *Science* 2011; **332**: 1284–8.

387 Jenkins SJ, Ruckerl D, Thomas GD, *et al.* IL-4 directly signals tissue-resident macrophages to proliferate beyond homeostatic levels controlled by CSF-1. *J Exp Med* 2013; **210**: 2477–91.

388 Gelb H, Schumacher HR, Cuckler J, Ducheyne P, Baker DG. In vivo inflammatory response to polymethylmethacrylate particulate debris: effect of size, morphology, and surface area. *J Orthop Res* 1994; **12**: 83–92.

389 González O, Smith RL, Goodman SB. Effect of size, concentration, surface area, and volume of polymethylmethacrylate particles on human macrophages in vitro. *J Biomed Mater Res* 1996; **30**: 463–73.

390 Reis e Sousa C, Stahl PD, Austyn JM. Phagocytosis of antigens by Langerhans cells in vitro. *J Exp Med* 1993; **178**: 509–19.

391 Sallusto F, Cella M, Danieli C, Lanzavecchia A. Dendritic cells use macropinocytosis and the mannose receptor to concentrate macromolecules in the major histocompatibility complex class II compartment: downregulation by cytokines and bacterial products. *J Exp Med* 1995; **182**: 389–400.

392 Xiang SD, Scholzen A, Minigo G, *et al.* Pathogen recognition and development of particulate vaccines: does size matter? *Methods* 2006; **40**: 1–9.

393 Tabata Y, Ikada Y. Effect of the size and surface charge of polymer microspheres on their phagocytosis by macrophage. *Biomaterials* 1988; **9**: 356–62.

394 Fifis T, Mottram P, Bogdanoska V, Hanley J, Plebanski M. Short peptide sequences containing MHC class I and/or class II epitopes linked to nano-beads induce strong immunity and inhibition of growth of antigen-specific tumour challenge in mice. *Vaccine* 2004; **23**: 258–66.

395 Getts DR, Terry RL, Getts MT, *et al.* Therapeutic inflammatory monocyte modulation using immune-modifying microparticles. *Sci Transl Med* 2014; **6**: 219ra7.

396 Champion JA, Walker A, Mitragotri S. Role of particle size in phagocytosis of polymeric microspheres. *Pharm Res* 2008; **25**: 1815–21.

397 Branzk N, Lubojemska A, Hardison SE, *et al.* Neutrophils sense microbe size and selectively release neutrophil extracellular traps in response to large pathogens. *Nat Immunol* 2014; : 1–11.

398 Palecanda A, Paulauskis J, Al-Mutairi E, *et al.* Role of the scavenger receptor MARCO in alveolar macrophage binding of unopsonized environmental particles. *J Exp Med* 1999; **189**: 1497–506.

399 Hirano S, Fujitani Y, Furuyama A, Kanno S. Macrophage receptor with collagenous structure (MARCO) is a dynamic adhesive molecule that enhances uptake of carbon nanotubes by CHO-K1 Cells. *Toxicol Appl Pharmacol* 2012; **259**: 96–103.

400 Elomaa O, Kangas M, Sahlberg C, *et al.* Cloning of a novel bacteria-binding receptor structurally related to scavenger receptors and expressed in a subset of macrophages. *Cell* 1995; **80**: 603–9.

401 Kanno S, Furuyama A, Hirano S. A murine scavenger receptor MARCO recognizes polystyrene nanoparticles. *Toxicol Sci* 2007; **97**: 398–406.

402 Chao Y, Makale M, Karmali PP, *et al.* Recognition of dextran-superparamagnetic iron oxide nanoparticle conjugates (Feridex) via macrophage scavenger receptor charged domains. *Bioconjug Chem* 2012; **23**: 1003–9.

403 Ng G, Sharma K, Ward SM, *et al.* Receptor-independent, direct membrane binding leads to cell-surface lipid sorting and Syk kinase activation in dendritic cells. *Immunity* 2008; **29**: 807–18.

404 Mandel N. Crystal-membrane interaction in kidney stone disease. *J Am Soc Nephrol* 1994; **5**: S37–45.

405 Mandel NS. The structural basis of crystal-induced membranolysis. *Arthritis Rheum* 1976; **19**: 439–45.

406 Gallo J, Kamínek P, Tichá V, Riháková P, Ditmar R. Particle disease. A comprehensive theory of periprosthetic osteolysis: a review. *Biomed Pap* 2002; **146**: 21–8.

407 Rao AJ, Gibon E, Ma T, Yao Z, Smith RL, Goodman SB. Revision joint replacement, wear particles, and macrophage polarization. *Acta Biomater* 2012; **8**: 2815–23.

408 Anderson JM, Rodriguez A, Chang DT. Foreign body reaction to biomaterials. *Semin Immunol* 2008; **20**: 86–100.

409 Henson PM. The immunologic release of constituents from neutrophil leukocytes. II. Mechanisms of release during phagocytosis, and adherence to nonphagocytosable surfaces. *J Immunol* 1971; **107**: 1547–57.

410 Henson PM. The immunologic release of constituents from neutrophil leukocytes. I. The role of antibody and complement on nonphagocytosable surfaces or phagocytosable particles. *J Immunol* 1971; **107**: 1535–46.

411 McNally AK, Anderson JM. Interleukin-4 induces foreign body giant cells from human monocytes/macrophages. Differential lymphokine regulation of macrophage fusion leads to morphological variants of multinucleated giant cells. *Am J Pathol* 1995; **147**: 1487–99.

412 DeFife KM, Jenney CR, McNally AK, Colton E, Anderson JM. Interleukin-13 induces human monocyte/macrophage fusion and macrophage mannose receptor expression. *J Immunol* 1997; **158**: 3385–90.

413 Puri N, Roche PA. Mast cells possess distinct secretory granule subsets whose exocytosis is regulated by different SNARE isoforms. *Proc Natl Acad Sci U S A* 2008; **105**: 2580–5.

414 Faulkner H, Humphreys N, Renauld JC, Van Snick J, Grencis R. Interleukin-9 is involved in host protective immunity to intestinal nematode infection. *Eur J Immunol* 1997; **27**: 2536–40.

415 Khan WI, Richard M, Akiho H, *et al.* Modulation of intestinal muscle contraction by interleukin-9 (IL-9) or IL-9 neutralization: correlation with worm expulsion in murine nematode infections. *Infect Immun* 2003; **71**: 2430–8.

416 Temann UA, Geba GP, Rankin JA, Flavell RA. Expression of interleukin 9 in the lungs of transgenic mice causes airway inflammation, mast cell hyperplasia, and bronchial hyperresponsiveness. *J Exp Med* 1998; **188**: 1307–20.

417 Shimbara A, Christodoulopoulos P, Soussi-Gounni A, *et al.* IL-9 and its receptor in allergic and nonallergic lung disease: increased expression in asthma. *J Allergy Clin Immunol* 2000; **105**: 108–15.

418 Pearce EJ, M Kane C, Sun J, J Taylor J, McKee AS, Cervi L. Th2 response polarization during infection with the helminth parasite Schistosoma mansoni. *Immunol Rev* 2004; **201**: 117–26.

419 Loukas A, Prociv P. Immune responses in hookworm infections. *Clin Microbiol Rev* 2001; **14**: 689–703.

420 Glant TT, Jacobs JJ. Response of three murine macrophage populations to particulate debris: bone resorption in organ cultures. *J Orthop Res* 1994; **12**: 720–31.

421 Rider P, Carmi Y, Guttman O, *et al.* IL-1α and IL-1β recruit different myeloid cells and promote different stages of sterile inflammation. *J Immunol* 2011; **187**: 4835–43.

422 Cohen I, Rider P, Carmi Y, *et al.* Differential release of chromatin-bound IL-1alpha discriminates between necrotic and apoptotic cell death by the ability to induce sterile inflammation. *Proc Natl Acad Sci U S A* 2010; **107**: 2574–9.

423 Fettelschoss A, Kistowska M, LeibundGut-Landmann S, *et al.* Inflammasome activation and IL-1β target IL-1α for secretion as opposed to surface expression. *Proc Natl Acad Sci U S A* 2011; **108**: 18055–60.

424 Miwa K, Asano M, Horai R, Iwakura Y, Nagata S, Suda T. Caspase 1-independent IL-1beta release and inflammation induced by the apoptosis inducer Fas ligand. *Nat Med* 1998; **4**: 1287–92.

425 Hornung V, Bauernfeind F, Halle A, *et al.* Silica crystals and aluminum salts mediate NALP-3 inflammasome activation via phagosomal destabilization. *Nat Immunol* 2010; **9**: 847–56.

426 Chen C-J, Shi Y, Hearn A, *et al.* MyD88-dependent IL-1 receptor signaling is essential for gouty inflammation stimulated by monosodium urate crystals. *J Clin Invest* 2006; **116**: 2262–71.

427 St Pierre C a, Chan M, Iwakura Y, Ayers DC, Kurt-Jones E a, Finberg RW. Periprosthetic osteolysis: characterizing the innate immune response to titanium wear-particles. *J Orthop Res* 2010; **28**: 1418–24.

428 De Filippo K, Henderson RB, Laschinger M, Hogg N. Neutrophil chemokines KC and macrophage-inflammatory protein-2 are newly synthesized by tissue macrophages using distinct TLR signaling pathways. *J Immunol* 2008; **180**: 4308–15.

429 McColl SR, Clark-Lewis I. Inhibition of murine neutrophil recruitment in vivo by CXC chemokine receptor antagonists. *J Immunol* 1999; **163**: 2829–35.

430 Zwijnenburg PJG, Polfliet MMJ, Florquin S, *et al.* CXC-chemokines KC and macrophage inflammatory protein-2 (MIP-2) synergistically induce leukocyte recruitment to the central nervous system in rats. *Immunol Lett* 2003; **85**: 1–4.

431 Mehrad B, Strieter RM, Moore TA, Tsai WC, Lira SA, Standiford TJ. CXC chemokine receptor-2 ligands are necessary components of neutrophil-mediated host defense in invasive pulmonary aspergillosis. *J Immunol* 1999; **163**: 6086–94.

432 Tsai WC, Strieter RM, Wilkowski JM, *et al.* Lung-specific transgenic expression of KC enhances resistance to Klebsiella pneumoniae in mice. *J Immunol* 1998; **161**: 2435–40.

433 Griffin GK, Newton G, Tarrio ML, *et al.* IL-17 and TNF-α sustain neutrophil recruitment during inflammation through synergistic effects on endothelial activation. *J Immunol* 2012; **188**: 6287–99.

434 Bokoch GM. Chemoattractant signaling and leukocyte activation. *Blood* 1995; **86**: 1649–60.

435 Campbell JJ, Foxman EF, Butcher EC. Chemoattractant receptor cross talk as a regulatory mechanism in leukocyte adhesion and migration. *Eur J Immunol* 1997; **27**: 2571–8.

436 Heit B, Tavener S, Raharjo E, Kubes P. An intracellular signaling hierarchy determines direction of migration in opposing chemotactic gradients. *J Cell Biol* 2002; **159**: 91–102.

437 Ablasser A, Hertrich C, Waßermann R, Hornung V. Nucleic acid driven sterile inflammation. *Clin Immunol* 2013; **147**: 207–15.

438 Goldmann O, Medina E. The expanding world of extracellular traps: not only neutrophils but much more. *Front Immunol* 2012; **3**: 420.

439 Yousefi S, Gold JA, Andina N, *et al.* Catapult-like release of mitochondrial DNA by eosinophils contributes to antibacterial defense. *Nat Med* 2008; **14**: 949–53.

440 Von Köckritz-Blickwede M, Goldmann O, Thulin P, *et al.* Phagocytosis-independent antimicrobial activity of mast cells by means of extracellular trap formation. *Blood* 2008; **111**: 3070–80.

441 Chow OA, von Köckritz-Blickwede M, Bright AT, *et al.* Statins enhance formation of phagocyte extracellular traps. *Cell Host Microbe* 2010; **8**: 445–54.

442 Yousefi S, Mihalache C, Kozlowski E, Schmid I, Simon HU. Viable neutrophils release mitochondrial DNA to form neutrophil extracellular traps. *Cell Death Differ* 2009; **16**: 1438–44.

443 Hirsiger S, Simmen H-P, Werner CML, Wanner GA, Rittirsch D. Danger signals activating the immune response after trauma. *Mediators Inflamm* 2012; **2012**: 315941.

444 Niedbala W, Besnard A-G, Nascimento DC, *et al.* Nitric oxide enhances Th9 cell differentiation and airway inflammation. *Nat Commun* 2014; **5**: 4575.

445 Lindblad EB, Elhay MJ, Silva R, Appelberg R, Andersen P. Adjuvant modulation of immune responses to tuberculosis subunit vaccines. *Infect Immun* 1997; **65**: 623–9.

446 Arthur LO, Bess JW, Waters DJ, *et al.* Challenge of chimpanzees (Pan troglodytes) immunized with human immunodeficiency virus envelope glycoprotein gp120. *J Virol* 1989; **63**: 5046–53.

447 Igartua M, Hernández RM, Esquisabel A, Gascón AR, Calvo MB, Pedraz JL. Enhanced immune response after subcutaneous and oral immunization with biodegradable PLGA microspheres. *J Control Release* 1998; **56**: 63–73.

448 Gutierro I, Hernández R., Igartua M, Gascón A., Pedraz J. Size dependent immune response after subcutaneous, oral and intranasal administration of BSA loaded nanospheres. *Vaccine* 2002; **21**: 67–77.

449 Wendorf J, Chesko J, Kazzaz J, *et al.* A comparison of anionic nanoparticles and microparticles as vaccine delivery systems. *Hum Vaccin* 2008; **4**: 44–9.

450 O'Brien L, Kerrigan SW, Kaw G, *et al.* Multiple mechanisms for the activation of human platelet aggregation by Staphylococcus aureus: roles for the clumping factors ClfA and ClfB, the serine-aspartate repeat protein SdrE and protein A. *Mol Microbiol* 2002; **44**: 1033–44.

451 McDevitt D, Nanavaty T, House-Pompeo K, *et al.* Characterization of the interaction between the Staphylococcus aureus clumping factor (ClfA) and fibrinogen. *Eur J Biochem* 1997; **247**: 416–24.

452 Higgins J, Loughman A, van Kessel KPM, van Strijp JAG, Foster TJ. Clumping factor A of Staphylococcus aureus inhibits phagocytosis by human polymorphonuclear leucocytes. *FEMS Microbiol Lett* 2006; **258**: 290–6.

453 Josefsson E, Hartford O, O'Brien L, Patti JM, Foster T. Protection against experimental Staphylococcus aureus arthritis by vaccination with clumping factor A, a novel virulence determinant. *J Infect Dis* 2001; **184**: 1572–80.

454 Bagnoli F, Bertholet S, Grandi G. Inferring reasons for the failure of Staphylococcus aureus vaccines in clinical trials. *Front Cell Infect Microbiol* 2012; **2**: 16.

455 Hawkins J, Kodali S, Matsuka Y V, *et al.* A recombinant clumping factor A-containing vaccine induces functional antibodies to Staphylococcus aureus that are not observed after natural exposure. *Clin Vaccine Immunol* 2012; **19**: 1641–50.

456 Tynan GA, McNaughton A, Jarnicki A, Tsuji T, Lavelle EC. Polymyxin B inadequately quenches the effects of contaminating lipopolysaccharide on murine dendritic cells. *PLoS One* 2012; **7**: e37261.

457 Misstear K, McNeela E a, Murphy AG, *et al.* Targeted nasal vaccination provides antibody-independent protection against Staphylococcus aureus. *J Infect Dis* 2014; **209**: 1479–84.

458 Bachelerie F, Ben-Baruch A, Burkhardt AM, *et al.* International Union of Basic and Clinical Pharmacology. LXXXIX. Update on the extended family of chemokine receptors and introducing a new nomenclature for atypical chemokine receptors. *Pharmacol Rev* 2014; **66**: 1–79.

459 Springer TA. Adhesion receptors of the immune system. *Nature* 1990; **346**: 425–34.

460 Arnaout MA. Leukocyte adhesion molecules deficiency: its structural basis, pathophysiology and implications for modulating the inflammatory response. *Immunol Rev* 1990; **114**: 145–80.

461 Lowenstein CJ, Padalko E. iNOS (NOS2) at a glance. *J Cell Sci* 2004; **117**: 2865–7.

462 Wu NZ, Da D, Rudoll TL, Needham D, Whorton AR, Dewhirst MW. Increased microvascular permeability contributes to preferential accumulation of Stealth liposomes in tumor tissue. *Cancer Res* 1993; **53**: 3765–70.

463 Kim GJ, Nie S. Targeted cancer nanotherapy. *Mater Today* 2005; **8**: 28–33.

464 Nagamoto T, Hattori Y, Takayama K, Maitani Y. Novel chitosan particles and chitosan-coated emulsions inducing immune response via intranasal vaccine delivery. *Pharm Res* 2004; **21**: 671–4.

465 Jung T, Kamm W, Breitenbach A, Hungerer KD, Hundt E, Kissel T. Tetanus toxoid loaded nanoparticles from sulfobutylated poly(vinyl alcohol)-graft-poly(lactide-co-glycolide): evaluation of antibody response after oral and nasal application in mice. *Pharm Res* 2001; **18**: 352–60.

466 Anish C, Khan N, Upadhyay AK, Sehgal D, Panda AK. Delivery of polysaccharides using polymer particles: Implications on size-dependent immunogenicity, opsonophagocytosis and protective immunity. *Mol Pharm* 2014; **11**: 922–37.

467 Mann JFS, Shakir E, Carter KC, Mullen AB, Alexander J, Ferro VA. Lipid vesicle size of an oral influenza vaccine delivery vehicle influences the Th1/Th2 bias in the immune response and protection against infection. *Vaccine* 2009; **27**: 3643–9.

468 Audran R, Peter K, Dannull J, *et al.* Encapsulation of peptides in biodegradable microspheres prolongs their MHC class-I presentation by dendritic cells and macrophages in vitro. *Vaccine* 2003; **21**: 1250–5.

469 De Temmerman M-L, Rejman J, Demeester J, Irvine DJ, Gander B, De Smedt SC. Particulate vaccines: on the quest for optimal delivery and immune response. *Drug Discov Today* 2011; **16**: 569–82.

470 Champion JA, Katare YK, Mitragotri S. Particle shape:A new design parameter for micro- and nanoscale drug delivery carriers. *J Control Release* 2007; **121**: 3–9.

471 Manolova V, Flace A, Bauer M, Schwarz K, Saudan P, Bachmann MF. Nanoparticles target distinct dendritic cell populations according to their size. *Eur J Immunol* 2008; **38**: 1404–13.

472 Horisawa E, Kubota K, Tuboi I, *et al.* Size-dependency of DL-lactide/glycolide copolymer particulates for intra-articular delivery system on phagocytosis in rat synovium. *Pharm Res* 2002; **19**: 132–9.

473 Johansen P, Gander B, Merkle HP, Sesardic D. Ambiguities in the preclinical quality assessment of microparticulate vaccines. *Trends Biotechnol* 2000; **18**: 203–11.

474 Men Y, Thomasin C, Merkle HP, Gander B, Corradin G. A single administration of tetanus toxoid in biodegradable microspheres elicits T cell and antibody responses similar or superior to those obtained with aluminum hydroxide. *Vaccine* 1995; **13**: 683–9.

475 Singh M, Li XM, Wang H, *et al.* Immunogenicity and protection in small-animal models with controlled-release tetanus toxoid microparticles as a single-dose vaccine. *Infect Immun* 1997; **65**: 1716–21.

476 Newman KD, Elamanchili P, Kwon GS, Samuel J. Uptake of poly (D , L -lactic-co-glycolic acid) microspheres by antigen-presenting cells in vivo. *J Biomed Mater Res* 2002; **60**: 480–6.

477 Blank F, Stumbles P a, Seydoux E, *et al.* Size-dependent uptake of particles by pulmonary antigen-presenting cell populations and trafficking to regional lymph nodes. *Am J Respir Cell Mol Biol* 2013; **49**: 67–77.

478 Balasse E, Odot J, Gatouillat G, Andry M-C, Madoulet C. Enhanced immune response induced by BSA loaded in hydroxyethylstarch microparticles. *Int J Pharm* 2008; **353**: 131–8.

479 Meraz IM, Hearnden CH, Liu X, *et al.* Multivalent presentation of MPL by porous silicon microparticles favors T helper 1 polarization enhancing the anti-tumor efficacy of doxorubicin nanoliposomes. *PLoS One* 2014; **9**: e94703.

480 McAdow M, Kim HK, Dedent AC, Hendrickx APA, Schneewind O, Missiakas DM. Preventing Staphylococcus aureus sepsis through the inhibition of its agglutination in blood. *PLoS Pathog* 2011; **7**: e1002307.

481 Moreillon P, Entenza JM, Francioli P, *et al.* Role of Staphylococcus aureus coagulase and clumping factor in pathogenesis of experimental endocarditis. *Infect Immun* 1995; **63**: 4738–43.

482 Bubeck Wardenburg J, Schneewind O. Vaccine protection against Staphylococcus aureus pneumonia. *J Exp Med* 2008; **205**: 287–94.

483 Kim HK, DeDent A, Cheng AG, *et al.* IsdA and IsdB antibodies protect mice against Staphylococcus aureus abscess formation and lethal challenge. *Vaccine* 2010; **28**: 6382–92.

484 Wertheim HFL, Vos MC, Ott A, *et al.* Risk and outcome of nosocomial Staphylococcus aureus bacteraemia in nasal carriers versus non-carriers. *Lancet*; **364**: 703–5.

485 Lin L, Ibrahim AS, Xu X, *et al.* Th1-Th17 cells mediate protective adaptive immunity against Staphylococcus aureus and Candida albicans infection in mice. *PLoS Pathog* 2009; **5**: e1000703.

486 Scully IL, Liberator P a, Jansen KU, Anderson AS. Covering all the bases: Preclinical development of an effective Staphylococcus aureus vaccine. *Front Immunol* 2014; **5**: 109.

487 Thwaites GE, Gant V. Are bloodstream leukocytes Trojan Horses for the metastasis of Staphylococcus aureus? *Nat Rev Microbiol* 2011; **9**: 215–22.

488 DeLeo FR, Diep BA, Otto M. Host defense and pathogenesis in Staphylococcus aureus infections. *Infect Dis Clin North Am* 2009; **23**: 17–34.

489 Anwar S, Prince LR, Foster SJ, Whyte MKB, Sabroe I. The rise and rise of Staphylococcus aureus: laughing in the face of granulocytes. *Clin Exp Immunol* 2009; **157**: 216–24.

490 Serruto D, Rappuoli R, Scarselli M, Gros P, van Strijp JAG. Molecular mechanisms of complement evasion: learning from staphylococci and meningococci. *Nat Rev Microbiol* 2010; **8**: 393–9.

491 Foster TJ. Colonization and infection of the human host by staphylococci: adhesion, survival and immune evasion. *Vet Dermatol* 2009; **20**: 456–70.

492 Cheng S-C, Quintin J, Cramer RA, *et al.* mTOR- and HIF-1 -mediated aerobic glycolysis as metabolic basis for trained immunity. *Science* 2014; **345**: 1250684–1250684.

493 Ehreth J. The value of vaccination: a global perspective. *Vaccine* 2003; **21**: 4105–17.

494 Ansari AA. Clinical features and pathobiology of Ebolavirus infection. *J Autoimmun* 2014. doi:10.1016/j.jaut.2014.09.001.

495 Andersen P, Woodworth JS. Tuberculosis vaccines - rethinking the current paradigm. *Trends Immunol* 2014; **35**: 387–95.

496 Seydoux E, Rothen-Rutishauser B, Nita IM, *et al.* Size-dependent accumulation of particles in lysosomes modulates dendritic cell function through impaired antigen degradation. *Int J Nanomedicine* 2014; **9**: 3885–902.

497 Makino K, Yamamoto N, Higuchi K, Harada N, Ohshima H, Terada H. Phagocytic uptake of polystyrene microspheres by alveolar macrophages: effects of the size and surface properties of the microspheres. *Colloids Surfaces B Biointerfaces* 2003; **27**: 33–9.

498 Nagao G, Ishii K, Hirota K, Makino K, Terada H. Role of lipid rafts in phagocytic uptake of polystyrene latex microspheres by macrophages. *Anticancer Res* 2010; **30**: 3167–76.

499 Foged C, Brodin B, Frokjaer S, Sundblad A. Particle size and surface charge affect particle uptake by human dendritic cells in an in vitro model. *Int J Pharm* 2005; **298**: 315–22.

500 Getts DR, Terry RL, Getts MT, *et al.* Therapeutic inflammatory monocyte modulation using immune-modifying microparticles. *Sci Transl Med* 2014; **6**: 219ra7.

501 Awate S, Babiuk LA, Mutwiri G. Mechanisms of action of adjuvants. *Front Immunol* 2013; **4**: 114.

502 Saade F, Honda-Okubo Y, Trec S, Petrovsky N. A novel hepatitis B vaccine containing Advax™, a polysaccharide adjuvant derived from delta inulin, induces robust humoral and cellular immunity with minimal reactogenicity in preclinical testing. *Vaccine* 2013; **31**: 1999–2007.

503 Wong PT, Wang SH, Ciotti S, *et al.* Formulation and characterization of nanoemulsion intranasal adjuvants: effects of surfactant composition on mucoadhesion and immunogenicity. *Mol Pharm* 2014; **11**: 531–44.

504 Mosca F, Tritto E, Muzzi A, *et al.* Molecular and cellular signatures of human vaccine adjuvants. *Proc Natl Acad Sci U S A* 2008; **105**: 10501–6.

505 Anish C, Goswami DG, Kanchan V, Mathew S, Panda AK. The immunogenic characteristics associated with multivalent display of Vi polysaccharide antigen using biodegradable polymer particles. *Biomaterials* 2012; **33**: 6843–57.

506 Lefrançais E, Cayrol C. Mechanisms of IL-33 processing and secretion: differences and similarities between IL-1 family members. *Eur Cytokine Netw* 2012; **23**: 120–7.

507 Sirois CM, Jin T, Miller AL, *et al.* RAGE is a nucleic acid receptor that promotes inflammatory responses to DNA. *J Exp Med* 2013; **210**: 2447–63.

508 Sudbery P, Gow N, Berman J. The distinct morphogenic states of Candida albicans. *Trends Microbiol* 2004; **12**: 317–24.

509 Sudbery PE. Growth of Candida albicans hyphae. *Nat Rev Microbiol* 2011; **9**: 737–48.

510 Romani N, Thurnher M, Idoyaga J, Steinman RM, Flacher V. Targeting of antigens to skin dendritic cells: possibilities to enhance vaccine efficacy. *Immunol Cell Biol* 2010; **88**: 424–30.

511 Liard C, Munier S, Arias M, *et al.* Targeting of HIV-p24 particle-based vaccine into differential skin layers induces distinct arms of the immune responses. *Vaccine* 2011; **29**: 6379–91.

512 Mohanan D, Slütter B, Henriksen-Lacey M, *et al.* Administration routes affect the quality of immune responses: A cross-sectional evaluation of particulate antigen-delivery systems. *J Control Release* 2010; **147**: 342–9.

513 Thiele L, Merkle HP, Walter E. Phagocytosis of synthetic particulate vaccine delivery systems to program dendritic cells. *Expert Rev Vaccines* 2002; **1**: 215–26.

514 Kiama SG, Cochand L, Karlsson L, Nicod LP, Gehr P. Evaluation of phagocytic activity in human monocyte-derived dendritic cells. *J Aerosol Med* 2001; **14**: 289–99.

515 Harding C V, Song R. Phagocytic processing of exogenous particulate antigens by macrophages for presentation by class I MHC molecules. *J Immunol* 1994; **153**: 4925–33.

516 Rice-Ficht AC, Arenas-Gamboa AM, Kahl-McDonagh MM, Ficht TA. Polymeric particles in vaccine delivery. *Curr Opin Microbiol* 2010; **13**: 106–12.

517 Panyam J, Zhou W-Z, Prabha S, Sahoo SK, Labhasetwar V. Rapid endo-lysosomal escape of poly(DL-lactide-co-glycolide) nanoparticles: implications for drug and gene delivery. *FASEB J* 2002; **16**: 1217–26.

518 Raychaudhuri S, Rock KL. Fully mobilizing host defense: building better vaccines. *Nat Biotechnol* 1998; **16**: 1025–31.

519 Brewer JM, Pollock KGJ, Tetley L, Russell DG. Vesicle size influences the trafficking, processing, and presentation of antigens in lipid vesicles. *J Immunol* 2004; **173**: 6143–50.

520 Reddy ST, Rehor A, Schmoekel HG, Hubbell JA, Swartz MA. In vivo targeting of dendritic cells in lymph nodes with poly(propylene sulfide) nanoparticles. *J Control Release* 2006; **112**: 26–34.

521 Ganesh VK, Rivera JJ, Smeds E, *et al.* A structural model of the Staphylococcus aureus ClfA-fibrinogen interaction opens new avenues for the design of anti-staphylococcal therapeutics. *PLoS Pathog* 2008; **4**: e1000226.

522 Foster TJ, Geoghegan J a, Ganesh VK, Höök M. Adhesion, invasion and evasion: the many functions of the surface proteins of Staphylococcus aureus. *Nat Rev Microbiol* 2014; **12**: 49–62.

523 Hair PS, Echague CG, Sholl AM, *et al.* Clumping factor A interaction with complement factor I increases C3b cleavage on the bacterial surface of Staphylococcus aureus and decreases complement-mediated phagocytosis. *Infect Immun* 2010; **78**: 1717–27.

524 Van den Biggelaar AHJ, Richmond PC, Pomat WS, *et al.* Neonatal pneumococcal conjugate vaccine immunization primes T cells for preferential Th2 cytokine expression: a randomized controlled trial in Papua New Guinea. *Vaccine* 2009; **27**: 1340–7.

525 Ritz N, Mui M, Balloch A, Curtis N. Non-specific effect of Bacille Calmette-Guérin vaccine on the immune response to routine immunisations. *Vaccine* 2013; **31**: 3098–103.

526 Aaby P, Kollmann TR, Benn CS. Nonspecific effects of neonatal and infant vaccination: public-health, immunological and conceptual challenges. *Nat Immunol* 2014; **15**: 895–9.

Appendix

Appendix I – Validation of particle size

		Size (d.nm):	% Intensity:	St Dev (d.nm):
Z-Average (d.nm): 45.66	Peak 1:	45.49	100.0	6.458
PdI: 0.097	Peak 2:	0.000	0.0	0.000
Intercept: 0.921	Peak 3:	0.000	0.0	0.000
Result quality : Good				

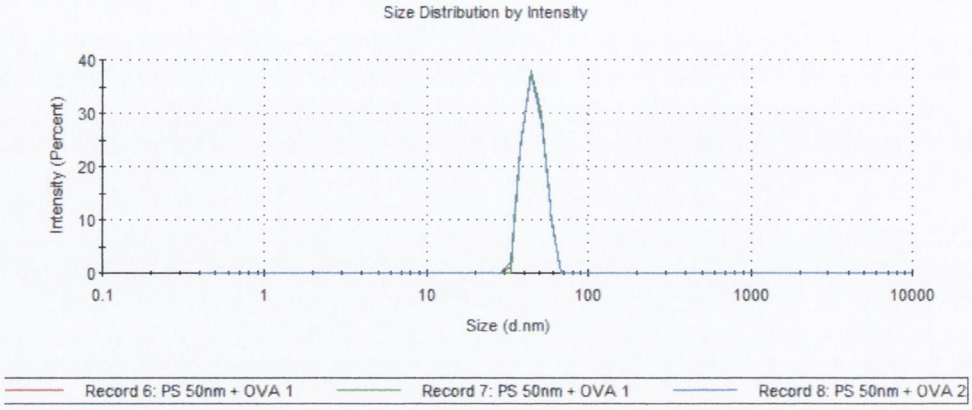

Figure I1 – Validation of 50nm particle size. The size of 50nm particles was analysed after mixing with 1µg OVA for 30 minutes at 4°C. Size was validated using the Malvern Zetasizer Nano ZS (Malvern Instruments Ltd, UK). One of three attempts (record 8) detected the particle size. Experiment performed by Dr. Dulce Bento.

		Size (d.nm):	% Intensity:	St Dev (d.nm):
Z-Average (d.nm): 1372	Peak 1:	1366	100.0	190.1
PdI: 0.093	Peak 2:	0.000	0.0	0.000
Intercept: 0.752	Peak 3:	0.000	0.0	0.000
Result quality : Good				

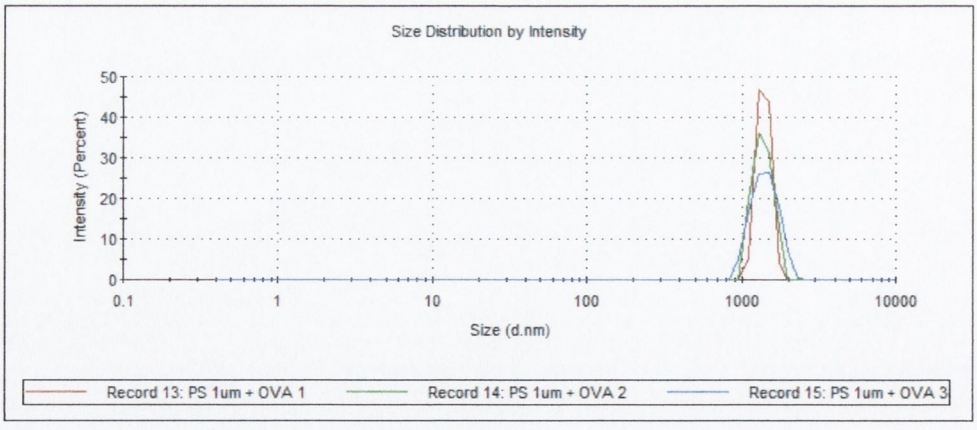

Figure I2 – Validation of 1µm particle size. The size of 1µm particles was analysed after mixing with 1µg OVA for 30 minutes at 4°C. Size was validated using the Malvern Zetasizer Nano ZS (Malvern Instruments Ltd, UK). An average of the three measurements recorded the particles at 1.372µm. Experiment performed by Dr. Dulce Bento.

OPEN ACCESS Freely available online

PLOS | ONE

Multivalent Presentation of MPL by Porous Silicon Microparticles Favors T Helper 1 Polarization Enhancing the Anti-Tumor Efficacy of Doxorubicin Nanoliposomes

Ismail M. Meraz[1☯], Claire H. Hearnden[2☯], Xuewu Liu[1], Marie Yang[2,3], Laura Williams[2,3], David J. Savage[4,5], Jianhua Gu[1], Jessica R. Rhudy[1], Kenji Yokoi[1], Ed C. Lavelle[2,3¶], Rita E. Serda[1,4*¶]

1 Nanomedicine, Houston Methodist Research Institute, Houston, Texas, United States of America, **2** Adjuvant Research Group, School of Biochemistry and Immunology, Trinity Biomedical Sciences Institute, Trinity College, Dublin, Ireland, **3** Advanced Materials and BioEngineering Research (AMBER), Centre for Research on Adaptive Nanostructures and Nanodevices (CRANN), Trinity College, Dublin, Ireland, **4** Michael E. DeBakey Department of Surgery, Baylor College of Medicine, Houston, Texas, United States of America, **5** The University of Texas School of Medicine, Houston, Texas, United States of America

Abstract

Porous silicon (pSi) microparticles, in diverse sizes and shapes, can be functionalized to present pathogen-associated molecular patterns that activate dendritic cells. Intraperitoneal injection of MPL-adsorbed pSi microparticles, in contrast to free MPL, resulted in the induction of local inflammation, reflected in the recruitment of neutrophils, eosinophils and proinflammatory monocytes, and the depletion of resident macrophages and mast cells at the injection site. Injection of microparticle-bound MPL resulted in enhanced secretion of the T helper 1 associated cytokines IFN-γ and TNF-α by peritoneal exudate and lymph node cells in response to secondary stimuli while decreasing the anti-inflammatory cytokine IL-10. MPL-pSi microparticles independently exhibited anti-tumor effects and enhanced tumor suppression by low dose doxorubicin nanoliposomes. Intravascular injection of the MPL-bound microparticles increased serum IL-1β levels, which was blocked by the IL-1 receptor antagonist Anakinra. The microparticles also potentiated tumor infiltration by dendritic cells, cytotoxic T lymphocytes, and F4/80$^+$ macrophages, however, a specific reduction was observed in CD204$^+$ macrophages.

Citation: Meraz IM, Hearnden CH, Liu X, Yang M, Williams L, et al. (2014) Multivalent Presentation of MPL by Porous Silicon Microparticles Favors T Helper 1 Polarization Enhancing the Anti-Tumor Efficacy of Doxorubicin Nanoliposomes. PLoS ONE 9(4): e94703. doi:10.1371/journal.pone.0094703

Editor: Muriel Moser, Université Libre de Bruxelles, Belgium

Received January 6, 2014; **Accepted** March 19, 2014; **Published** April 15, 2014

Copyright: © 2014 Meraz et al. This is an open-access article distributed under the terms of the Creative Commons Attribution License, which permits unrestricted use, distribution, and reproduction in any medium, provided the original author and source are credited.

Funding: This research was supported by Houston Methodist and Science Foundation Ireland (SFI Investigators Award 12/IA/1421) and the Irish Health Research Board (Scholars Programme in Immunology). The funders had no role in study design, data collection and analysis, decision to publish, or preparation of the manuscript.

Competing Interests: Xuewu Liu has a patent entitled "Porous particles and methods of making thereof," Patent Application Number 20080280140; and Rita Serda has a patent entitled "Mesoporous silicon particles for the presentation of tumor antigens and adjuvant for anti-cancer immunity," Patent Application Number: 2013019596. This does not alter the authors' adherence to PLOS ONE policies on sharing data and materials.

* E-mail: ritaserda@gmail.com

☯ These authors contributed equally to this work.

¶ These authors also contributed equally to this work.

Introduction

The physico-chemical properties of synthetic particles have a major impact on their cellular associations, biodistribution, degradation, and immuno-modulatory properties. Alum, an aluminum salt particulate used in vaccines, is thought to recruit immune cells to the site of injection, at least in part due to cytotoxic effects. [1] While macrophages internalize alum, dendritic cells (DC) are reported to exhibit no or limited uptake of alum. [2] Alum favors T helper (Th)2 immune responses and does not stimulate production of proinflammatory Th1 promoting cytokines by DCs or macrophages. [3–5] However, effective cancer immunotherapies require Th1 cytokines to arrest tumor growth, specifically interferon (IFN)-γ and tumor necrosis factor (TNF)-α. [6] To overcome this deficiency, a novel formulation containing alum and the Toll-like receptor (TLR)-4 ligand monophosphoryl lipid A (MPL) has been used to enhance adaptive immunity. [7] MPL, which is approved for clinical use in vaccines, induces secretion of IL-12 by antigen presenting cells (APC), leading to IFN-γ secretion by T and NK cells [8,9].

The NOD-like receptor family, pyrin domain containing 3 (NLRP3) inflammasome is a multiprotein complex that functions to activate caspase-1, leading to the proteolytic maturation and secretion of the proinflammatory cytokines interleukin (IL)-1β and IL-18. [10] Chemotherapeutics, such as doxorubicin, activate the NLRP3 inflammasome, and mice lacking components of the NLRP3 inflammasome fail to respond to chemotherapy unless exogenous IL-1β is provided [11].

As an alternative to alum, synthetic particles have the potential to support Th1 responses in the absence of cytotoxicity based on intrinsic particle properties, as well as through presentation of pathogen-associated molecular patterns or proinflammatory cytokines. In 2008, Eicke Latz *et al.* [12,13] reported that silica crystals activate the NALP3 inflammasome in PBMCs in a process dependent on phagocytosis. We previously demonstrated [14] that porous silicon (pSi) microparticles enhance lipopolysaccharide

(LPS) and MPL mediated DC secretion of proinflammatory cytokines that are associated with successful cancer immunosurveillance. [15] Direct attachment of the molecule to the particle surface generated a multivalent ligand for TLR-4, with superior activation of downstream pathways compared to free MPL or LPS leading to secretion of IL-1β and proinflammatory cytokines such as TNF-α. *In vitro*, pSi microparticle stimulated IL-1β secretion was caspase-dependent and slightly elevated in the presence of cytochalasin B, [14] which is known to induce frustrated phagocytosis, locking silicon microparticles on the cell surface in actin rings, thereby inducing sustained engagement of surface receptors. [16] pSi presentation of adsorbed MPL led to increased particle uptake by DC; elevated DC expression of costimulatory and major histocompatibility complex (MHC) class I and II molecules; stimulated migration of DC to the draining lymph node; and enhanced associations between DCs presenting the ovalbumin peptide SIINFEKL and T cells from C57BL/6-Tg(TcraTcrb) (OT-1) transgenic mice [14].

Intravenous injection of oxidized (anionic) or cationic pSi microparticles in mice has been shown to be inert with respect to endothelial cell cycle, mitosis [17] and *in vivo* tumor cell growth. [18,19] The biodistribution and biodegradability of pSi microparticles is well documented. [20–22] Functionally, pSi microparticles are proven carriers for nanoparticles, nucleic acids, peptides, and chemotherapeutic agents [23,24].

In this study, for the first time we examine in depth the *in vivo* immunomodulatory properties of pSi microparticles and the impact of multivalent presentation of MPL, as well as the combined potential of these agents to augment the immunomodulatory properties of chemotherapeutics. Using an immune competent mouse model of breast cancer, pSi microparticles in combination with doxorubicin-loaded nanoparticles (DOX-NPs) are administered by intravenous injection. In addition, the impact of intraperitoneal injection of microparticles of various sizes and aspect ratios are examined to explore the impact of geometry and size on intrinsic immunomodulatory properties. Cell recruitment to the site of injection and to the tumor microenvironment is explored, as is the impact of the microparticles on the cytokine milieu. MPL-adsorbed pSi microparticles are found to favor Th1 polarization in the tumor and have anti-tumor properties, independent of and additive to that induced by DOX-NPs.

Materials and Methods

Ethics Statement

All animal procedures were performed in accordance with protocols reviewed and approved by the Institutional Animal Care and Use Committee at Houston Methodist and Trinity College as appropriate.

Materials

LPS from *Escherichia coli* and MPL from *Salmonella enteric* serotype Minnesota RE 595 were purchased from Sigma-Aldrich (St. Louis, MO, USA). IL-1β, TNF-α and IFN-γ ELISA kits were purchased from R&D Systems, Inc. (Minneapolis, MN, USA; detection range 15.6–1000 pg/ml, 31.2–2000 pg/ml and 31.2–2000 pg/ml respectively). IL-10 ELISA kits were purchased from Biolegend, Inc. (San Diego, CA, USA; detection range of 31.3–2000 pg/ml). IL-12p40 capture (purified) and detection (biotin) antibodies were purchased from BD Pharmingen; detection range of 39.06–5000 pg/ml). If samples reached the top end of the standard curve for ELISA assays, samples were diluted 1:2 for more accurate readings. Alum was purchased from Brenntag Biosector (Alhydrogel). Liposomal Doxorubicin (DOX-N), 80–90 nm, was purchased from Avanti Polar Lipids, Inc. (Alabaster, AL, USA). 4T1-luc2-td Tomato Bioware Ultra Red mouse mammary cancer cells were purchased from Caliper Life Sciences (Hopkinton, MA, USA). Human THP-1 monocytes were purchased from American Type Culture Collection (ATCC; Manassas, VA, USA).

Animals Models

BALB/c (6–8 wk old) mice were obtained from Charles River Laboratories, Inc, Wilmington, MA, USA) and C57BL/6 mice from The Jackson Laboratory (Bar Harbor, ME, USA). NLRP3$^{-/-}$ mice were generously provided by Professor Jurg Tschopp and bred in the Trinity College Dublin Bioresources Unit.

Particle Fabrication

Starting with a p-type <100> wafer with resistivity of 0.005 ohm-cm as the substrate (Silicon Quest, Inc, Santa Clara, CA, USA), the wafer was exposed to 1:3 hydrofluoric acid (49%):ethanol solution, and electrochemically etched with a DC current density of 7 mA/cm^2 for 65 sec and 125 sec to form 200 and 400 nm thick porous silicon layers, respectively. The current density was then increased to 76 mA/cm^2, and kept for six sec to form a second porous layer, the high porosity release layer. The bilayer porous films were washed and spin-dried. An 80 nm thick low-temperature oxide (LTO) was deposited on the porous film in a LPCVD furnace at 400°C. The photolithography process was then carried out using an i-line contact aligner (KARL SUSS MA6 mask aligner). To make 1800×400 nm rod-shape microparticles, a dark-field photomask (chrome on quartz; HTA Photomask) consisting of a pattern array of 1800×400 nm rectangles with 2500 nm×1000 nm pitch was used. A thin NR9-250P photoresist (Futurrex Franklin, NJ, USA) layer was spun on the double-layer film at 3000 RPM and baked. The resist exposure time and development process were optimized to obtain clean 1800×400 nm patterns on 400 nm thick film. Discoidal microparticles with 2500, 1000 and 600 nm diameters were patterned on the 200 or 400 nm thick porous silicon films using NR9-500P photoresist (Futurrex Franklin, NJ, USA) and the dark-field photomasks consisting of arrays of circles with 2600, 1100 and 600 nm diameters, respectively. Both rod-shaped and discoidal patterns were transferred into the double-layer porous films by reactive ion etch in CF4 plasma (Plasmatherm BatchTop, 15 sccm CF4, 100 mTorr, 200 W RF). After striping the LTO in dilute HF, the as-made porous silicon particles were retained on the substrate allowing go through washing steps, followed by release using ultrasound in isopropyl alcohol. Particles were oxidized in a 35% H_2O_2 solution at 100°C for two hr.

Microparticles were treated with piranha solution (1 volume H_2O_2 and 2 volumes of H_2SO_4) to chemically oxidize the surface. The suspension was heated to 110–120°C for two hr, centrifuged and washed in deionized water repeatedly. Amine surface modification was achieved using a 2% (v/v) 3-aminopropyl triethoxy-silane (APTES) (Sigma-Aldrich) solution in 95% isopropanol and 5% water for two hr at 35°C with agitation at 1300 RPM.

MPL was adsorbed to pSi microparticles by immersion in a 1 mg/ml aqueous solution of MPL followed by two wash steps. The binding density of MPL was determined by imaging using a Bruker Multimode Atomic Force Microscope as described previously and the amount of bound MPL was determined by Western blot analysis or quantitating fluorescent ligand bound to the microparticles [14].

Cationic MPL liposomes were made by dissolving lipids and cholesterol at a molar ratio of 7:3:1 DPPC:Cholesterol:DOTAP in

a 3:1 solution of chloroform and methanol. MPL (250 μg per 40 mg lipid) was added from a Chloroform: Methanol (3:1) stock solution. Solvent was extracted at 55°C using a Hei-Vap Series Heidolph Rotary Evaporator (Heidolph Instruments GmbH & Co., Schwabach, Germany). PBS was added and the mixture was heated at 52°C for three min, vortexed for 2.5 min, and then sonicated for 30 sec with three repeats. A Malvern Zetasizer (Worcestershire, UK) was used to measure particle size and surface potential.

Preparation of Bone Marrow-derived Dendritic Cells (BMDC)

BMDCs were prepared as previously described. [14] Briefly, bone marrow cells were harvested from the femurs and tibias of mice and filtered through a cell strainer (BD Biosciences, San Jose, CA, USA). RBC was lysed with ACK lysis buffer (Quality Biologicals, Inc., Gaithersburg, MD, USA), and cells were washed and cultured in six-well plates at 10^6 cells/ml (3 ml/well) in RPMI 1640 (Sigma-Aldrich) supplemented with 10% fetal bovine serum (FBS) (Atlanta Biologicals, Lawrenceville, GA, USA), 100 U/ml penicillin/streptomycin (Fishers Scientific, Waltham, MA, USA), 50 μM 2-mercaptoethanol (Sigma-Aldrich), and mouse granulocyte-macrophage colony stimulating factor (GM-CSF) (20 ng/ml; Pierce, Rockford, IL, USA) plus or minus IL-4 (100 ng/ml) as indicated for 7–10 days. Half of the media was replaced every 2–3 days with fresh media and cytokines.

Imaging Microparticle Uptake by BMDC using Electron Microscopy

BMDC cells were plated in 24 well plates containing 5×7 mm silicon chip specimen supports (Ted Pella, Inc., Redding, CA, USA) at 1×10^5 cells per well. The next day, cells were incubated with pSi microparticles for one hr at 37°C at a 1:20 cell to microparticle ratio. Cells were processed for SEM imaging as previously described.[14a, 16] Specimens were mounted on SEM stubs (Ted Pella, Inc.) using conductive adhesive tape (12 mm OD PELCO Tabs, Ted Pella, Inc.), and sputter-coated with a four nm layer of platinum/palladium (80:20) using a Cressington Sputter Coater 208 HR (Ted Pella, Inc.). For microparticle imaging, pSi microparticles in IPA were dried on SEM stubs. SEM images were acquired under high vacuum, at 10–15 kV, spot size 3.0, using a Nova NanoSEM Scanning Electron Microscope (FEI Company, Hillsboro, OR, USA). Gamma levels of the micrographs were adjusted to enhance image contrast and brightness.

For transmission electron microscopy, GM-CSF-stimulated BMDC were cultured on poly-l-lysine glass slides, and then incubated with TLR ligand-bound pSi microparticles (1:20 ratio) for four hr followed by washing and fixation in 2% glutaraldehyde in 0.1 M cacodylate buffer, pH 7.4. After washing with cacodylate buffer, cells were incubated in a mixture of osmium tetroxide and 1% potassium ferrocyanate in 0.1 M cacodylate buffer for 30 min at 48°C. Cells were then dehydrated in increasing concentrations of ethanol and embedded with a mixture of epon and araldite. After polymerization at 60°C, glass slides were removed from the resin by freezing in liquid nitrogen. Ultrathin sections were counter-stained with uranyl acetate and imaged using a JEOL 1210 microscope equipped with an AMT Imaging System (JEOL, Peabody, MA, USA). Gamma adjustments were made to the micrographs to enhance image contrast and brightness.

Alum uptake by BMDC (GM-CSF and IL-4 culture; five days) was examined by transmission electron microscopy following treatment with 2 μg/ml Imject alum (Thermo Scientific) for four hr. Cells were washed in PBS twice followed by fixation in TRUMPS fixative and processing as described in the preceding paragraph.

Evaluation of Cell Viability

BMDCs were incubated with three doses of alum (25, 12.5, and 6.25 μg/ml), LPS (10 ng/ml), or pSi microparticles at a dose of 20 microparticles/cell for 24 hr. Cells were washed and stained with Aqua Live/Dead and evaluated using flow cytometry. Samples were acquired using Summit software (Dako, Colorado, USA) and the data were analysed using FlowJo software (Treestar, Oregon, USA).

pSi Microparticle-mediated Leukocyte Infiltration

Female mice (C57BL/6) were injected intraperitoneally with either PBS, Alum (0.3 mg/mouse), 0.3 mg pSi microparticles, MPL (50 μg/mouse) or pSi particles loaded with MPL. After 24 hr the mice were euthanized by CO_2, the peritoneal cavity was washed with PBS and the peritoneal extrudate cells (PEC) were harvested for flow cytometry analysis and/or *ex vivo* restimulation. For restimulation experiments, PECs were plated at 1×10^6 cells/ml and restimulated with either CpG (5 μg/ml) or Heat-killed E. coli (10 bacteria:1 cell) for 24 hr. Supernatants were collected and IFN-γ, TNF-α, IL-12p40 and IL-10 concentrations were determined by ELISA.

For flow cytometry analysis, PECs (1×10^6 cells/ml) were incubated for 30 min with AQUA fluorescent dye (0.5 μl) (Invitrogen) and for an additional 30 min with antibodies specific for CD11b (0.005 μg) (M1/70 : BD Pharmingen), Gr-1 (0.04 μg) (RB6-8C5 : BD Pharmingen), F4/80 (0.1 μg) (BM8 : eBioscience), ckit (0.5 μg) (2B8 : BD Pharmingen), CD11c (0.1 μg) (HL3 : BD Pharmingen), MHCcII (0.04 μg) (M5/114.15.2 : BD Pharmingen), CD19 (0.1 μg) (1D3 : BD Pharmingen), Ly6C (0.25 μg) (AL-21 : BD Pharmingen) and SiglecF (0.02 μg) (E50-2440 : BD Pharmingen). Samples were acquired using a Becton Dickinson FACSCanto flow cytometer equipped with Summit software (Dako, Colorado, USA) and the data was analysed using FlowJo^T software (Treestar, Oregon, USA).

Therapeutic Efficacy Studies

Breast cancer tumors were established in BALB/c mice by intramammary injection of 1×10^5 4T1 cells. On day 10–14, mice were inoculated weekly by intravenous tail vein injection as follows: PBS control, DOX-NP (2.5 or 5.0 mg/kg); MPL (10 μg); MPL-pSi microparticles (5×10^8); or the hybrid combination of DOX-NP/MPL-pSi particles. Alternatively, mice were injected intratumorally with PBS, MPL (10 μg), or MPL-liposomes (1000 μg lipid/6.25 μg MPL; 50 μl). Kineret (anakinra, 30 mg/dose; Amgen, Thousand Oaks, CA, USA) was administered 3 times per week by intraperitoneal injection. Tumor growth was monitored by caliper measurements 3× per week and based on luciferase expression weekly with the Xenogen IVIS-200 System (Perkin Elmer Inc., Waltham, MA, USA) following intraperitoneal injection of 150 mg/kg RediJect D-Luciferin (Perkin Elmer Inc.). Mice were sacrificed 24–26 days after initiation of tumor growth, blood was collected by cardiac puncture, and tumor and spleen were collected for weight, size and immunohistochemical staining.

Immunohistochemistry

Tissues were quick frozen in OCT (Tissue-Tek) and stored at −80°C. Tissue sections (10 μm) were fixed with ice-cold acetone for 15 min at −20°C and washed three times with PBS followed by blocking with 5% FBS. Fluorescence-labeled primary antibodies

[e-flour 615 CD8 (clone 53-6.7; 1:50), e-flour 570 ki67 (clone solA15; 1:100; eBioscience, San Diego, CA, USA); FITC F4/80 (MCA497A488; 1:100), Alexa Fluor 647 CD204 (MCA1322; 1:50, AbD Serotec, Raleigh NC), Alexa Fluor 647 Gr-1 (clone RB6-8C5; 1:100; Biolegend), FITC CD11b (clone M1/70, 1:100; Biolegend); and 33D1 (1:50, BD Biosciences, San Jose, CA, USA; secondary anti-rat IgG Alexa Fluor 647; Invitrogen)] were incubated with tissues overnight at 4°C in the presence of 5% FBS. Slides were then washed three times with PBS and mounted with ProLong Gold AntiFade with DAPI (Invitrogen). Images were taken using an A1 Nikon confocal microscope (Belmont, CA, USA) and percent positive cells were determined by manual counting or using Image J software (National Institute of Health) equipped with the ITCN (Image-based tool for counting nuclei) Plugin (Thomas Kuo and Jiyun Byun; Center for Bio-image Informatics at UC Santa Barbara, CA, USA) with analysis of 3–6 arbitrary regions representing randomly selected tissues from greater than one mouse per group.

ELISA

Cytokines were measured by ELISA using kits purchased from R&D Systems (IFN-γ, TNF-α, and IL-1β), Biolegend (IL-10), and BD Pharmingen (IL-12p40) according to the manufacturer's instructions. Briefly, 96-well high binding ELISA plates were coated with purified anti-IL-12p40 antibody (0.5 μg/ml) diluted with PBS at 4°C overnight. After three washes, non-specific binding was blocked using 1% BSA for two hr at room temperature. The standards and PEC samples were then added and the plate incubated for two hr at room temperature. After five washes, biotin anti-IL-12p40 antibody (1 μg/ml) was added for two hr, followed by HRP-conjugated streptavidin for 20 min. Absorbance was measured at 490 nm within 30 min of adding the stop solution. Mean absorbance was compared to a standard curve.

IL-1β secretion in plasma was measured by ELISA using the BD OptEIA kit (BD Biosciences, San Diego, CA, USA; detection limit 31.3–2000 pg/ml) according to the manufacturer's instructions. Briefly, 96-well ELISA plates were coated with IL-1β antibody diluted with coating buffer at 4°C overnight. After three washes, non-specific binding was blocked using blocking buffer provided by the manufacturer for one hr at room temperature. The standards and plasma samples were then added and the plate incubated for two hr at room temperature. After five washes, mouse HRP conjugated anti-IgG antibody was added for an additional hr, followed by substrate solution for 30 min. Absorbance was measured at 450 nm within 30 min of adding the stop solution. Mean absorbance was compared to a standard curve.

Wildtype or NLRP3$^{-/-}$ BMDCs were plated at 6.25×10^5 cells/ml and primed with LPS at 1 or 10 ng/ml for one hr before pSi particles were added based on a dose of 40 microparticles/cell or on silicon content (0.006 mg/ml high dose). After 24 hr, supernatants were collected and IL-1β concentrations were determined by ELISA.

In vivo cytokine release was measured in BALB/c mice 4T1 tumors following subcutaneous injection of free MPL or 5×10^8 control or MPL-pSi microparticles (10 μg MPL equivalents; n = 3/group). Blood samples were collected at various time points post injection via retinal orbital access and serum was prepared by centrifugation at 2500 g for 10 min. Serum samples were stored at −80°C and analyzed by ELISA.

Statistics

Statistical analysis was performed using Graphpad Prism 5 software. The means for three or more groups were compared by one-way ANOVA. Where significant differences were found, the Tukey-Kramer multiple comparisons test was used to identify differences between individual groups. For differences in restimulation data, a two-way ANOVA was used, followed by a bonferroni posttest. Alternatively, statistical comparisons were performed using a two-sample, equal variance, two-tailed T test. Error bars in graphical presentations represent standard deviations.

Results

Fabrication of pSi Microparticles

Discoidal (D) and rod-shaped (R) pSi microparticles were fabricated by a process that consists of electrochemical etching of silicon films to create pores, photolithographic patterning of microparticle dimensions on pSi films, and reactive ion etch (RIE). As the porous structure and microparticle size are controlled independently, pSi microparticles with a wide range of dimensions, shapes and pore morphologies can be fabricated. Scanning electron micrographs of rod-shape and a variety of discoidal microparticles, with a mean pore size of 30 nm and a porosity of approximately 65%, are shown in **Figure 1a**. Particle lengths, widths, and abbreviations used in this study are presented in **Table 1**, along with a comparison of silicon content per microparticle number equivalents.

The fabrication process began with a heavily doped silicon wafer. A bi-layer porous silicon film consisting of a device layer and a release layer was formed using step-current electrochemical etching in a hydrofluoric acid/ethanol solution. The release layer, with high porosity, was retained on the substrate, able to withstand extensive handling including flush and photoresist stripping, but collapsing rapidly upon sonication. The bi-layer porous film was then capped by an 80 nm low temperature oxide (LTO) deposited in a low pressure chemical vapor deposition furnace. A direct photolithographic process was followed to pattern the particle array on the LTO capped film. The particle patterns were transferred onto the bi-layer porous film by one-step RIE in CF4 plasma. After removing the residual photoresist and LTO layers, the resulting microparticles were retained on the wafer as an array. The monodispersed microparticles were obtained by ultrasonic treatment of the on-wafer microparticle array.

BMDC Uptake of pSi Particles

To assess the impact of microparticle geometry and size on cellular interactions, various imaging modalities were used to capture various phases of microparticle uptake. Early uptake of the various microparticle formulations by BMDC induced membrane spreading across the microparticle surface that included actin cup formation and wrapping of microparticles in pseudopodia. Scanning electron micrographs shown in Figure 1b display cells one hr after addition of microparticles to the cell culture media. Further support for microparticle internalization by BMDC is presented in confocal micrographs three hr after microparticle addition (Figure 1c). Microparticles are visualized based on photoluminescence properties, while nuclei are labeled with Hoechst. Complete microparticle internalization and localization within phagosomes is presented in transmission electron micrographs of BMDC four hr after microparticle introduction (Figure 1d). Similar engulfment of alum (Imject) by BMDC is shown in electron micrographs in Figure 1e. BMDC were treated with 2 μg/ml alum for four hr. Internalization is apparent in two intracellular locations, with one region (boxed) shown at higher magnification in the far right image.

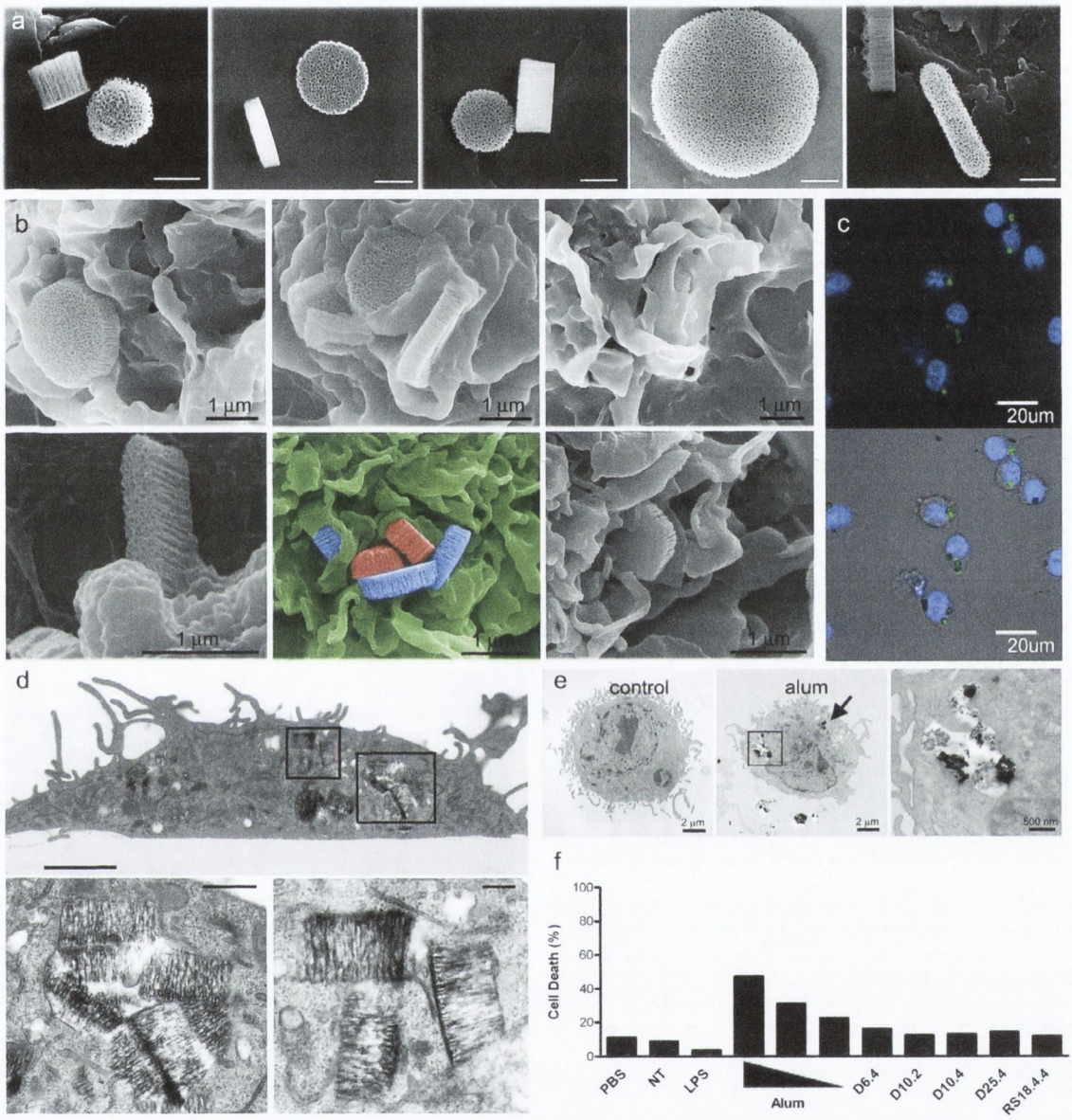

Figure 1. pSi microparticle association with BMDC and biocompatibility. a) Scanning electron micrographs show pSi microparticles of varying dimensions (bars 500 nm). b) SEM images show cellular association of 2500×400 nm pSi microparticles with BMDC at various stages of uptake (top row) and cellular association with rod-shaped (left, bottom row) and smaller discoidal particles [600 nm (middle) and 1000 nm (right)]. c) BMDCs, treated with five D25.4 microparticles/cell for three hr, were imaged using confocal microscopy. d) TEM images show BMDC with internalized TLR4-ligand (LPS) bound pSi microparticles four hr after microparticle introduction. Seven 1000×400 nm discoidal microparticles are seen in the cell in the upper image (boxed regions; bar 2 μm) and in the magnified regions below (bars 1 and 0.5 μm). e) TEM images show control (left) and alum-treated BMDC four hr after introduction of 2 μg/ml alum. The boxed region showing internalized alum is magnified in the image to the right. f) BMDCs were incubated with LPS (10 ng/ml), alum (25, 12.5 and 6.25 μg/ml), or pSi microparticles (20 particles/cell) for 24 hr. Cellular necrosis was evaluated using the LIVE/DEAD® Aqua dead cell stain.
doi:10.1371/journal.pone.0094703.g001

Cytotoxicity of Adjuvants

Microparticle compatibility with primary BMDC was assessed using flow cytometry to measure cell viability. While treatment of BMDC with alum (25, 12.5, and 6.25 μg/ml; Brenntag Biosector) induced 22–49% cell death after 24 hr of incubation at 37°C, parallel exposure of BMDC to pSi caused no cell death above control levels at a dose of 20 particles per cell (Figure 1f). When microparticle toxicity was compared using equivalent doses of

Table 1. Size and shape characteristics of pSi microparticles.

Abbreviation	Length (nm)	Width (nm)	Shape	mg Si/1e9 particles
D6.4	600	400	discoidal	0.11
D10.2	1000	200	discoidal	0.16
D10.4	1000	400	discoidal	0.3
D25.4	2500	400	discoidal	2.0
R18.4.4	1800	400×400	rod	0.3

doi:10.1371/journal.pone.0094703.t001

silicon across the spectrum, the largest microparticles (D25.4) displayed low levels of toxicity in a dose dependent manner (Figure S1).

Impact of Size and Shape on pSi Microparticle Uptake by APC

Microparticle uptake by antigen presenting macrophage-like (THP-1) cells varied by size and aspect ratio *in vitro* when microparticles were added to the culture media and time to settle on the cell surface was included in the kinetic analysis (**Figure 2a**). The largest microparticles (D25.4) had the greatest uptake across the four hr observation window, while the rod-shaped microparticles (RS18.4.4) displayed the lowest uptake. In contrast, uptake was similar for all microparticle sizes and shapes when contact with the cell surface was achieved prior to kinetic analysis by preincubation on ice.

Synergistic Recruitment of Inflammatory Cells and Production of Proinflammatory Cytokines

To assess the ability of pSi microparticles to drive the secretion of the proinflammatory cytokine IL-1β, the effect of a broad range of pSi microparticle geometries on IL-1β production by BMDCs was assessed. All geometries of pSi microparticles induced significant IL-1β secretion from LPS-primed BMDCs, whether primed with 1 ng/ml (Figure 2b) or 10 ng/ml (Figure 2c) LPS. pSi microparticle mediated IL-1β secretion by BMDCs was NLRP3-dependent and independent of particle geometry (Figure 2d). Similar results were obtained when microparticles were normalized for silicon content (Figure S2).

Since all geometries of pSi microparticles promoted comparable secretion of the pro-inflammatory cytokine IL-1β, we investigated if these microparticles exhibited differing immunomodulatory effects *in vivo*. Female C57BL/6 mice were injected intraperitoneally (i.p.) with PBS or pSi microparticles in a range of geometries. The various pSi microparticle formulations induced comparable neutrophil ($CD11b^{+}$ $Gr1^{high}$ $F4/80^{-}$; Figure 2e) and eosinophil ($Gr1^{-}$ $ckit^{-}$ $SiglecF^{+}$; Figure 2f) recruitment into the peritoneum as well as a comparable reduction in the number of resident macrophages ($CD11b^{high}$ $F4/80^{high}$; Figure 2g) 24 hr after injection, indicating the ability of pSi microparticles to induce local inflammatory responses independent of geometry over the range of parameters used. The number of DCs ($CD19^{-}$ $CD11c^{+}$ $MHCcII^{+}$), monocytes ($CD19^{-}$ $CD11c^{-}$ $CD11b^{+}$ $Ly6C^{+}$) and proinflammatory macrophages ($CD19^{-}$ $CD11c^{-}$ $Gr1^{low}$ $MHCcII^{+}$) were similar to PBS after injection with all geometries of microparticles (Figure S3).

Since D10.4 discoidal microparticles promoted secretion of the proinflammatory cytokine IL-1β, while exhibiting low levels of toxicity to BMDCs *in vitro*, we investigated the immunomodulatory effects of these particles in combination with MPL to evaluate potential synergistic induction of immune responses.

Female C57BL/6 mice were injected i.p. with PBS, pSi microparticles, MPL or MPL adsorbed onto pSi microparticles and the mice were sacrificed after 24 hr. Injection of microparticles with MPL resulted in a pronounced synergistic effect on neutrophil (**Figure 3a**) and proinflammatory monocyte ($CD11b^{inter}$ $F4/80^{inter}$ $Gr\text{-}1^{low/inter}$ SSC^{low}; Figure 3b) recruitment into the peritoneum. While MPL alone did not drive the recruitment of inflammatory cells to the site of injection, pSi microparticles independently promoted eosinophil recruitment into the peritoneum (Figure 3d). Furthermore, the combination of MPL and pSi microparticles, as well as pSi microparticles alone, resulted in depletion of both resident macrophage (Figure 3c) and mast cell numbers ($SiglecF^{-}$ $ckit^{+}$; Figure 3e).

In order to determine whether pSi microparticles could modulate the cytokine profile of peritoneal exudate cells (PECs) at the injection site or in the draining lymph nodes, female C57BL/6 mice were injected i.p. with PBS, pSi microparticles, MPL or MPL absorbed onto pSi microparticles and the mice were sacrificed after 24 hr. PECs and mediastinal lymph node cells were isolated and restimulated *ex vivo* with the TLR9 agonist CpG or heat killed (HK) *E.coli*. Subsequently, secretion of the cytokines IFN-γ, TNF-α, IL-12p40 and IL-10 were measured.

PECs and mediastinal lymph node cells isolated from mice injected with MPL-pSi microparticles exhibited a significant increase in secretion of the proinflammatory cytokines IFN-γ, TNF-α and IL-12p40 (**Figure 4**). Injection of microparticles alone resulted in enhanced IFN-γ in response to stimulation with HK *E. coli*, as well as IL-12p40 and TNF-α in response to CpG or HK *E. coli*. In contrast, IL-10 production in response to both pathogen recognition receptor agonists was significantly reduced in these mice compared to controls. Injection of MPL alone was capable of priming PECs for enhanced IL-12p40 and TNF-α secretion in response to CpG. Production of these cytokines by PECs was significantly enhanced in mice injected with particles and MPL. In parallel, injection of MPL-pSi microparticles resulted in significantly less production of the anti-inflammatory cytokine IL-10 in comparison to cells from mice injected with either pSi microparticles or MPL alone. Importantly and in contrast to the PEC data, only the injection of MPL-pSi resulted in significantly enhanced IFN-γ, TNF-α and IL-12p40 production by restimulated mediastinal lymph node cells. Specifically lymph node cells from mice injected with MPL-pSi microparticles secreted TNF-α in response to both CpG and HK *E. coli*, as well as IL-12p40 in response to CpG and IFN-γ in response to HK *E. coli*.

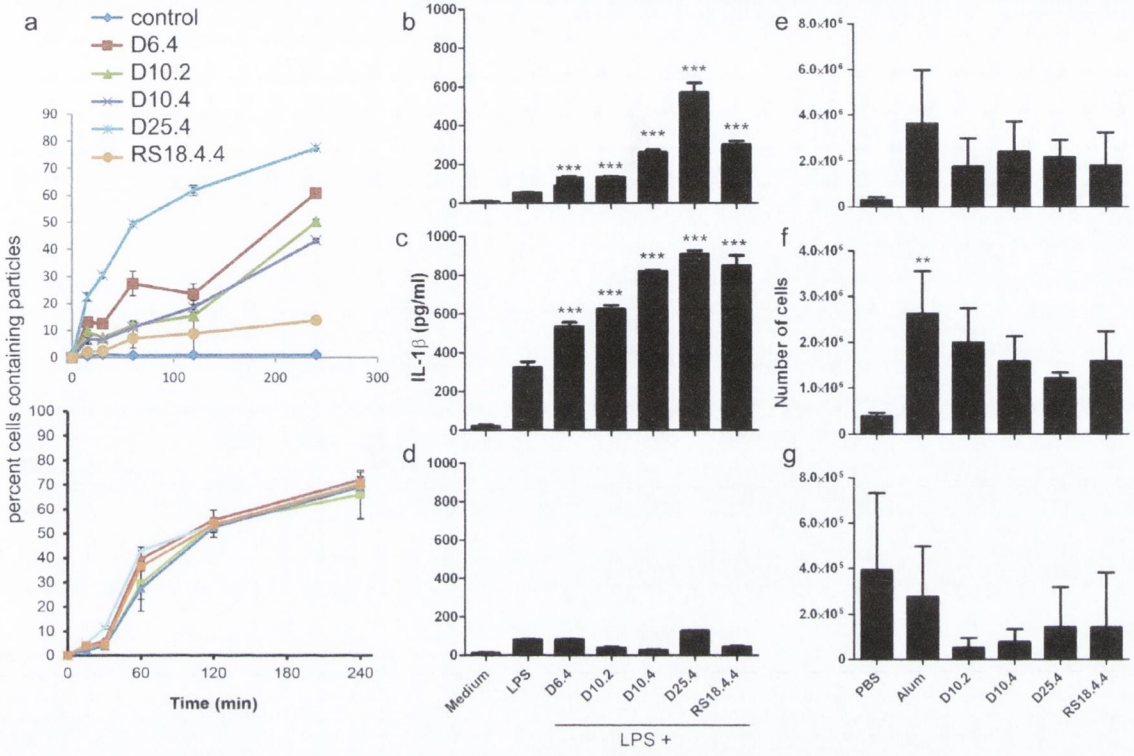

Figure 2. pSi microparticles are immunomodulatory both *in vitro* and *in vivo*. a) Fluorescent microparticle uptake by human monocytes (THP-1 cells) was measured by flow cytometry at select time points after adding microparticles to the cell culture media (top) or after settling of the microparticles on the cell surface by incubation of cells and microparticles on ice for 60 min (bottom) prior to adding warm media (37°C) and transferring to an incubator (n = 3/group). B-D) Wildtype (WT) (b, c) or NLRP3$^{-/-}$ (d) BMDCs were primed with 1 ng/ml (b) or 10 ng/ml (c, d) LPS, followed one hr later with 40 particles/cell using pSi microparticles of varying geometries. After 24 hours, supernatants were collected and IL-1β concentrations were determined by ELISA (***$p<0.001$). E-G) Female C57BL/6 mice were injected i.p. with PBS, Alum or D10.2, D10.4, D25.4 and RS18.4.4 pSi microparticles (0.3 mg/mouse) and the mice were sacrificed after 24 hr. PECs were isolated and stained with various markers to identify cell populations in the peritoneum, specifically the number of neutrophils (e; CD11b^{+} Gr1^{high} F4/80^{-}), eosinophils (f; Gr1^{-} ckit^{-} SiglecF^{+}) and resident macrophages (g; CD11b^{high} F4/80^{high}). **$p<0.01$ compared to PBS group, n = 3/group.
doi:10.1371/journal.pone.0094703.g002

Suppression of Tumor Growth by MPL-pSi Microparticles and DOX-NPs

To examine tumor growth inhibition by particle-presented chemotherapeutics and MPL, BALB/c mice bearing intramammary 4T1-luciferase breast tumors were injected with doxorubicin-loaded nanoliposomes (DOX-NPs; 5 mg/kg), MPL-pSi microparticles (5×10^{8}; 10 μg MPL equivalent), or combined DOX-NPs and MPL-pSi by tail vein injection 7–12 days after tumor initiation. Tumor growth was monitored by caliper measurements and luciferase expression using the IVIS Imaging System 200. MPL-pSi microparticle treated mice exhibited significantly reduced tumor growth based on caliper measurements, and mice receiving combined MPL-pSi microparticles and DOX-NPs exhibited arrest of tumor growth (**Figure 5a**). The mean final tumor size is presented in Figure 5b, and actual tumor images are shown in Figure 5c. The majority of mice treated with MPL-pSi showed a visible reduction in tumor mass with no growth of tumors in mice treated with DOX-NPs. Inoculation of mice with MPL-pSi or DOX-NPs also reduced tumor-associated splenomegaly (Figure 5c). Images of photon emission from luciferase positive tumor cells are shown in Figure 5d, further supporting reduced tumor growth in the presence of MPL-pSi and showing complete loss of detectable tumor cells in most animals treated with DOX-NPs.

Enhanced Tumor Ablation with Combined MPL-pSi and DOX-NPs Compared to Single Agent Therapy

While treatment with MPL-pSi reduced tumor growth when administered as a solo therapeutic agent, the synergistic or additive effect when co-administered with chemotherapy was masked due to strong anti-cancer effects at 5 mg/kg DOX-NPs. Therefore, mice were treated with half the effective DOX-NP dose, alone or in combination with MPL-pSi microparticles. Adjuvant MPL-pSi therapy significantly elevated suppression of tumor growth above that exhibited by treatment with DOX-NPs alone, as measured using calipers (Figure 5e) and based on the final tumor mass (Figure 5f). Visual inspection of the excised tumors and corresponding spleens (with reduced hypertrophy) are displayed in Figure 5g. Photon emission data from day 24 (Figure 5h) mirrored images of the excised tumors. Quantitation of the bioluminescence data is presented as total flux (photon/sec) in Figure 5i.

The relative increase in tumor blockade due to the addition of MPL microparticles to liposomal chemotherapy is displayed in

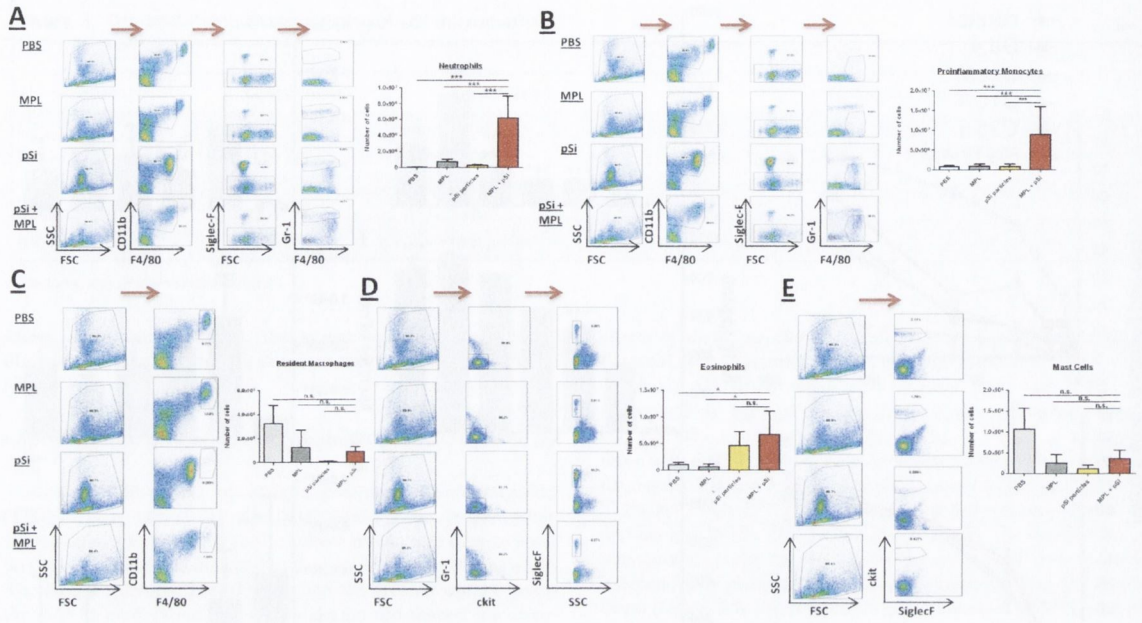

Figure 3. Injection of pSi microparticles with the TLR4 agonist MPL induces a synergistic recruitment of inflammatory cells. Female wild-type C57BL/6 mice were injected with PBS, MPL (50 μg/mouse), pSi microparticles (5×10^8) or MPL plus pSi microparticles. The mice were sacrificed 24 hr later and PECs were isolated. PECs were stained with various markers to identify cell populations in the peritoneum at this time point, specifically the number of neutrophils (a; $CD11b^+$ $SiglecF^-$ $Gr\text{-}1^+$), M1-like macrophages (b; $CD11b^+$ $SiglecF^-$ $F4/80^+$), M2-like macrophages (c; $CD11b^{high}$ $F4/80^{high}$), eosinophils (d; $Gr\text{-}1^-$ $ckit^-$ $SiglecF^-$) and mast cells (e; $ckit^+$ $SiglecF^-$). Indicated variable versus MPL+pSi, *p<0.05, ***p<0.001, n = 3/group.
doi:10.1371/journal.pone.0094703.g003

Figure 5j. Blockade due to liposomes alone is shown in blue and the increase due to adjuvant microparticles is shown in red, supporting an additive effect of the combined therapy. We anticipate that the enhancing effect of microparticles will be even greater with smaller doses of DOX-NPs.

Adjuvant Properties of MPL-nanoliposomes

To further determine if multivalent presentation of MPL is responsible for enhanced adjuvant properties compared to free MPL, we examined the impact of MPL-nanoliposomes and free MPL on 4T1 tumor growth. MPL-nanoliposomes had a mean size near 100 nm based on dynamic light scattering and the zeta potential was 40±2.5 mV. Similar to intravenous inoculation of mice with MPL-pSi microparticles, intratumoral inoculation with MPL-nanoliposomes reduced tumor growth significantly, while free MPL failed to alter tumor growth (Figure 5k).

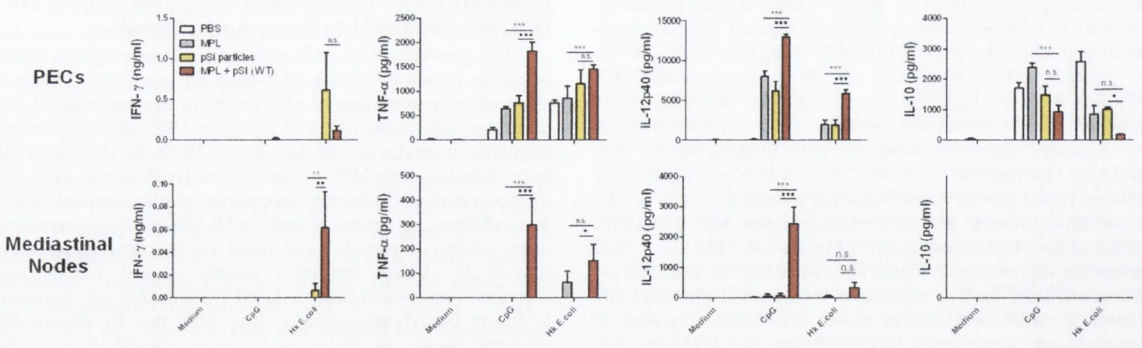

Figure 4. Injection of pSi microparticles with the TLR4 agonist MPL induces a synergistic production of proinflammatory cytokines. PECs were restimulated with CpG (5 μg/ml) or HK E. coli (10 E. coli : 1 PEC)(F). After 24 hr, supernatants were collected and analyzed for the cytokines IFN-γ, TNF-α, IL-12p40 and IL-10 by ELISA. MPL versus MPL-pSi, **p<0.01, ***p<0.001; pSi versus MPL-pSi, •p<0.05, •••p<0.001, n = 3/group.
doi:10.1371/journal.pone.0094703.g004

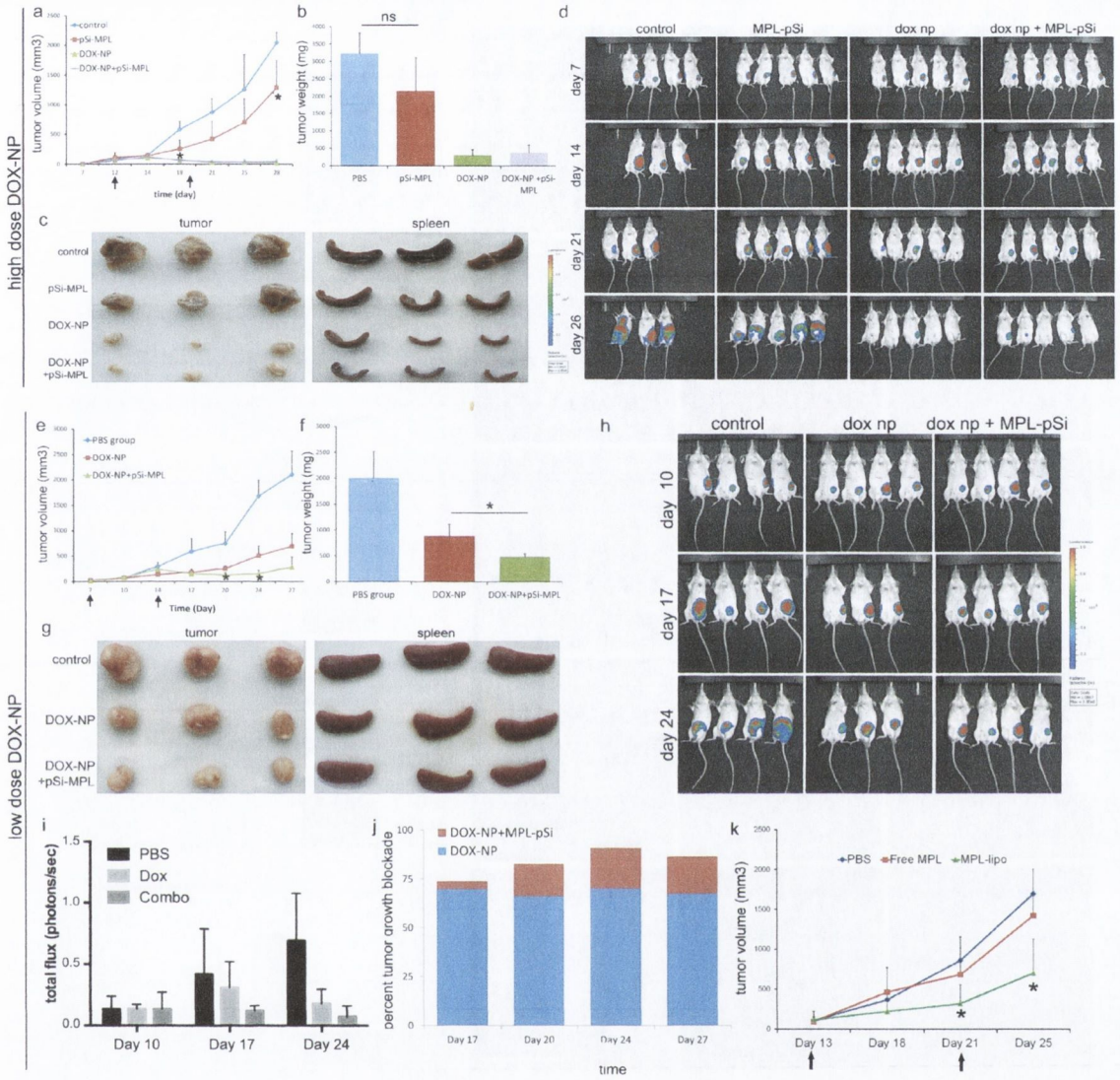

Figure 5. Combination therapy is superior to single agent therapy in a mouse model of breast cancer. a) 4T1 tumor growth in BALB/c mice was monitored using calipers. Mice were treated intravenously with MPL-pSi microparticles (5×10^8) with and without high dose DOX-NPs weekly as indicated by arrows. Control verses MPL-pSi, *$p<0.05$, n = 3–5/group. b) Final mass of excised tumor. c) Images showing the relative size of extracted tumors and spleens. d) Mice were imaged weekly using the IVIS imaging system five min following injection with luciferin. e) Caliper-derived tumor volume measurements over time for BALB/c mice treated intravenously with low dose DOX-NPs in the presence or absence of MPL-pSi microparticles (5×10^8) (time of microparticle injections indicated by arrows; DOX-NPs verses DOX-NPs plus MPL-pSi, *$p<0.05$, n = 3–4/group). f) Final weights of excised tumors, *$p<0.05$. g) Relative size of excised tumors and spleens. h) Weekly IVIS imaging of mice injected with luciferin. i) Quantitation of the bioluminescence data is presented as total flux in protons/sec. j) Increase in tumor growth blockade due to MPL-pSi microparticles (red) over that induced by DOX-NPs (blue) shown graphically across time. k) Similar to A & E, 4T1 tumor growth was monitored in BALB/c mice using calipers. Mice were injected with PBS (control), MPL-liposomes, or free MPL as indicated by the arrows (control vs MPL liposome, *$p<0.05$, n = 3/group).

doi:10.1371/journal.pone.0094703.g005

Alterations in Immune Cell Profiles of Tumor and Lymphatic Tissue Following Particle-based Therapy

DOX-NP therapy caused a significant, dramatic reduction in the number of $Ki67^+$ proliferating cells in the tumor (**Figure 6 a,b**). In order to examine the impact of DOX-NPs (low dose), alone and in combination with MPL-pSi, on the population of tumor-infiltrating immune cells, we examined $CD8^+$ cytotoxic T lymphocytes (CTL), $F4/80^+$ and $CD204^+$ myeloid cells, and $33D1^+$ DC in the tumors of control and particle-treated animals. Immunofluorescence staining of frozen tumor sections revealed increases in the proportion of both CTL and $F4/80^+$ myeloid cells following DOX-NP treatment, with significant further increases

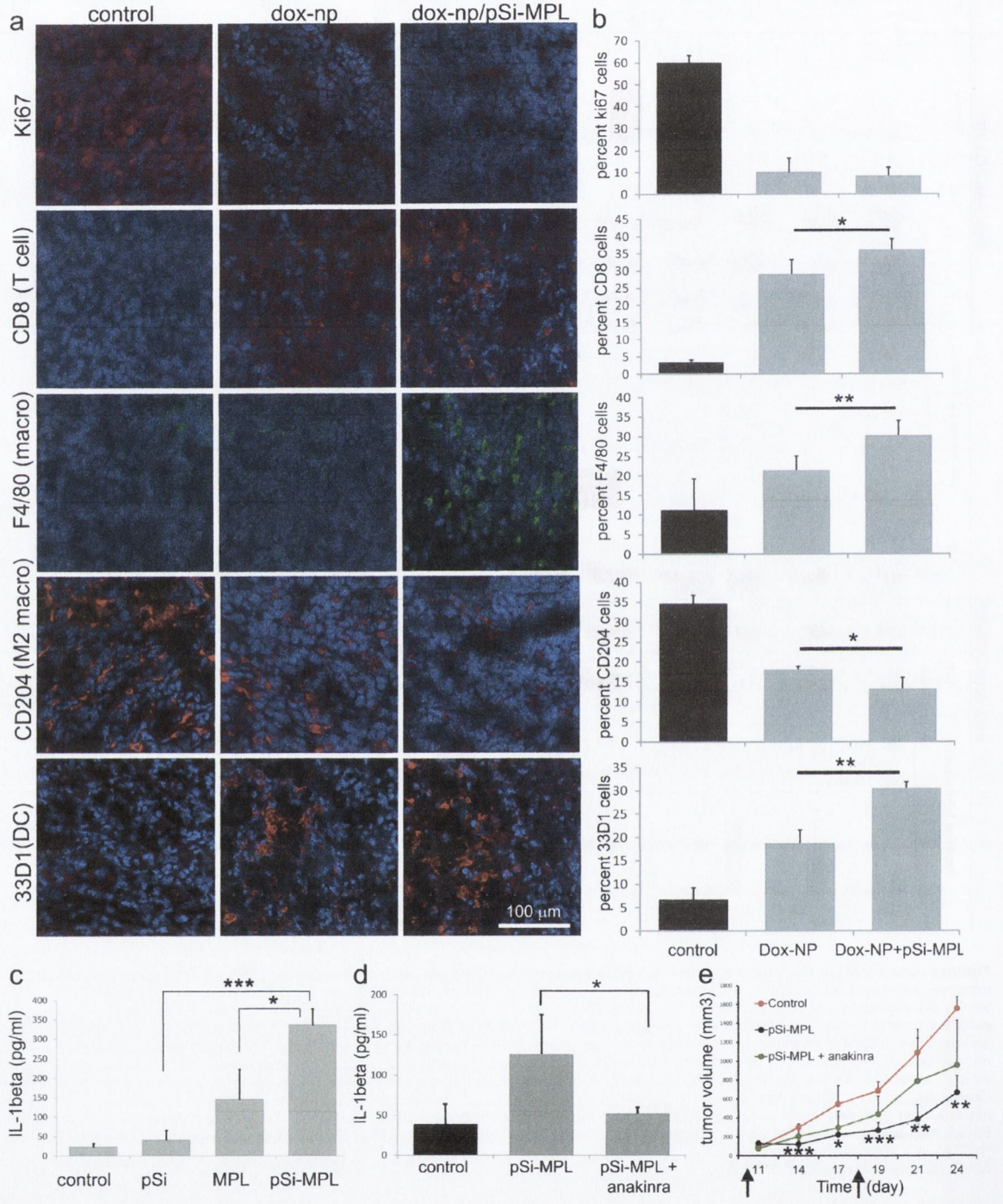

Figure 6. Combined chemo and MPL-pSi therapy inhibits cellular proliferation and stimulates tumor infiltration by immune cells which is partly IL-1 dependent. a) Excised tumors from mice treated with low dose DOX-NPs with or without pSi-MPL microparticles were stained with antibodies specific for Ki67 (red), CD8 (red), F4/80 (green), CD204 (red), or 33D1 (red). Nuclei were stained with Prolong Gold Antifade Reagent with DAPI (blue). b) The percentage of the population comprised of each cell type is shown graphically as the mean of 3–4 regions in randomly selected tissues representing at least two animals per group. *$p<0.05$; **$p<0.01$. c) Plasma IL-1β level six hr after intravenous injection of free MPL or 5×10^8 control or MPL-pSi microparticles (10 μg MPL equivalents; n = 3/group; ***$p<0.001$; *$p<0.05$). d) Effect of anakinra on MPL-pSi microparticle-induced

changes in plasma IL-1β six hr after injection (30 mg, 3×/week; *p<0.05; n = 3/group). e) Tumor growth of mice injected with MPL-pSi microparticles (weekly as indicated by arrows) with and without anakinra (30 mg, 3×/week; n = 3/group). Control verses MPL-pSi, *p<0.05; **p<0.01; ***p<0.001.
doi:10.1371/journal.pone.0094703.g006

induced by inoculation with MPL-pSi (Figure 6a,b). $33D1^+$ DC were similarly increased; however, the majority of DCs were localized to the tumor periphery. Conversely, $CD204^+$ alternatively activated M2 macrophages were reduced in the tumors of particle-treated mice.

Mice administered MPL-pSi intravenously displayed significantly elevated IL-1β in the serum six hr after treatment compared to mice treated with control pSi microparticles (*p<0.0002) or free MPL [(**p<0.02; Figure 6c]. Anakinra (Kineret), a recombinant soluble IL-1 receptor antagonist, blocked IL-1β secretion in MPL-pSi treated mice (Figure 6d) and reduced the anti-tumor efficacy of the microparticles, however, due the small number of mice used in the study, tumor size in these mice was not significantly different from that of control animals (n = 3/group; Figure 6e).

Myeloid populations were also examined by immunofluorescence staining of the draining lymph nodes and spleen of particle-treated mice. For mice treated with a therapeutic dose of DOX-NPs, $F4/80^+$ and $CD204^+$ myeloid cells in the draining lymph nodes were phenotypically similar to control and combination treated mice nine days following the final injection of DOX-NPs and pSi-MPL (Figure S4 a,b; middle row). Similar data was obtained for the spleen with respect to $F4/80^+$ and $CD204^+$ macrophages (Figure S4 a,b; top row). The population of $Gr\text{-}1^+/CD11b^+$ myeloid derived suppressor cells (MDSC) in the spleen were similar with respect to percentage of MDSC, however, since the size of the spleens was drastically reduced in treated mice, the absolute number of MDSC was correspondingly reduced with treatment. Interestingly, the percentage of $Gr\text{-}1^+/CD11b^-$ cells increased in mice treated with combination DOX-NP and MPL-pSi microparticles.

Discussion

Following internalization of tumor antigens, mature DCs are able to activate T lymphocytes having high tumor antigen avidity, leading to antigen-specific cytolytic responses [25]. Herein we show that pSi microparticles are internalized by DC, regardless of their geometric presentation within the study parameters, and in contrast to alum, are nontoxic. Furthermore, pSi microparticles stimulate NLRP3 inflammasome dependent IL-1β secretion by DCs.

IL-12 has potent anti-tumor effects, based in part on blockade of T regulatory cell secretion of IL-10 and TGF-β. [26] Since alum can suppress IL-12 secretion by DCs [4] and is not an effective promoter of Th1 responses, alternative adjuvant systems for cancer vaccines are required. In this study, in situ multivalent presentation of MPL by pSi microparticles elevated MPL-induced secretion of the Th1 cytokines IFN-γ, and TNF-α, and decreased levels of the immunosuppressive cytokine IL-10. Injection of MPL-pSi also favored the recruitment of neutrophils, eosinophils and proinflammatory monocytes, while reducing numbers of resident macrophages and mast cells.

As cancer progresses, tumor cells evade immune defenses and become increasingly refractory to chemotherapies. Tumors are rich in MDSC, a heterogeneous cell population that has characteristics of both M1 and M2 macrophages and inhibits both innate and adaptive immunity. [27] Since a variety of chemotherapeutics, including gemcitabine and doxorubicin, are reported to decrease MDSCs and thereby have favorable immunologic effects, leading to reduced splenomegaly in addition to blockade of tumor growth, [28] we evaluated the population of MDSC in the spleen of control and treated mice. While there was no significant difference between control and treated mice with respect to percentage of $Gr\text{-}1^+/CD11b^+$ cells on day 9 after the second injection with particles, the absolute number of MDSC was reduced to a degree corresponding to the large reduction in spleen mass. Similar results were reported by Alizadeh et al. [29], who observed lower percentages of MDSC on days 2 and 5 after doxorubicin treatment of mice with 4T1 tumors, but no difference of day 11. We did however observe an increase in the percentage of $Gr\text{-}1^+$ cells in the spleen of mice receiving combination therapy, which may represent $Gr\text{-}1^+/CD11b^-$ plasmacytoid DCs [30].

This study demonstrated that injection of mice bearing 4T1 tumors with MPL-pSi microparticles independently reduced tumor growth and stimulated a Th1 bias in the tumor microenvironment. Mice receiving DOX-NPs exhibited increases in the percentage of CTLs, $F4/80^+$ macrophages, and DC in the tumor, with further increases induced by inoculation with MPL-pSi. Conversely, injection of DOX-NPs decreased the proportion of $CD204^+$ macrophages, which are associated with tumor aggressiveness, [31] with augmentation of the effect stimulated by addition of MPL-pSi. Anakinra, a competitive inhibitor of IL-1, blocked MPL-pSi induced secretion of IL-1β, and reduced the anti-tumor properties of the microparticles. In summary, multivalent presentation of MPL by pSi enables a bias towards Th1 polarization, functioning as an attractive adjuvant for combination immunotherapy and for future applications in vaccine development.

Supporting Information

Figure S1 Influence of alum and pSi microparticles on cell viability. D10.4, D25.4 or R18.4.4 pSi microparticles were normalized for silicon content and added to LPS primed (10 ng/ml) BMDCs at a top concentration of 0.006 mg/ml silicon, parallel to alum (50 μg/ml) or LPS (10 ng/ml) for 24 hr. Percent cell death, based on propidium iodide uptake, is displayed.
(DOCX)

Figure S2 pSi microparticle-stimulated secretion of IL-1β. Microparticles were normalized for silicon content and added to LPS primed (10 ng/ml) WT (top) and $NLRP3^{-/-}$ (bottom) BMDCs in decending concentrations with a top concentration of 0.006 mg/ml Si. IL-1β secretion was determined by ELISA.
(DOCX)

Figure S3 Influence of alum and pSi microparticle geometry on number of DC, monocytes and pro-inflammatory macrophages recruited to site of injection. Female wild-type C57BL/6 mice were injected intraperitoneally with PBS, Alum (0.3 mg/mouse) or pSi microparticles with geometries D10.2, D10.4, D25.4 or RS18.4.4 (0.3 mg/mouse). The mice were sacrificed 24 hr later and PECs were isolated and stained for flow cytometry to determine numbers of DC (a), monocytes (b) and pro-inflammatory macrophages (c).
(DOCX)

Figure S4 Macrophage and MDSC populations in the draining lymph node and spleen of treated mice. a) Spleen and lymph node sections from BALB/c mice treated with DOX-NPs and MPL pSi microparticles were stained with fluorescent antibodies for F/80 (green) and CD204 (red)

macrophages; and Gr-1 (green) and CD11b (red) MDSCs. b) The proportion of positive cells in each population was determined in randomly selected tissues selecting 4–6 regions of interest based on DAPI staining and then counting cell populations using Image J software and the ITCN plugin. The percentage of positive cells in each population was determined by dividing the number of cells of interest by the total number of cells based on DAPI staining.
(DOCX)

Acknowledgments

We acknowledge use of The Houston Methodist Research Institute Scanning Electron Microscopy Core, directed by R.E. Serda, and the Baylor College of Medicine Microscopy Core. We thank James P. Barrish, Technical Specialist in the Department of Pathology Electron Microscopy Facility at Texas Children's Hospital, for TEM sample preparation and imaging.

Author Contributions

Conceived and designed the experiments: RES EL. Performed the experiments: IM CHH MY LW DJS JG JR KY. Analyzed the data: IM CHH MY DJS EL RES. Contributed reagents/materials/analysis tools: XL. Wrote the paper: RES CHH EL.

References

1. Kool M, Soullie T, van Nimwegen M, Willart MA, Muskens F, et al. (2008) Alum adjuvant boosts adaptive immunity by inducing uric acid and activating inflammatory dendritic cells. J Exp Med 205: 869–882.
2. Flach TL, Ng G, Hari A, Desrosiers MD, Zhang P, et al. (2011) Alum interaction with dendritic cell membrane lipids is essential for its adjuvanticity. Nat Med 17: 479–487.
3. Rimaniol AC, Gras G, Clayette P (2007) In vitro interactions between macrophages and aluminum-containing adjuvants. Vaccine 25: 6784–6792.
4. Mori A, Oleszycka E, Sharp FA, Coleman M, Ozasa Y, et al. (2012) The vaccine adjuvant alum inhibits IL-12 by promoting PI3 kinase signaling while chitosan does not inhibit IL-12 and enhances Th1 and Th17 responses. Eur J Immunol 42: 2709–2719.
5. Brewer JM (2006) (How) do aluminium adjuvants work? Immunology Letters 102: 10–15.
6. Braumuller H, Wieder T, Brenner E, Assmann S, Hahn M, et al. (2013) T-helper-1-cell cytokines drive cancer into senescence. Nature 494: 361–365.
7. Didierlaurent AM, Morel S, Lockman L, Giannini SL, Bisteau M, et al. (2009) AS04, an aluminum salt- and TLR4 agonist-based adjuvant system, induces a transient localized innate immune response leading to enhanced adaptive immunity. J Immunol 183: 6186–6197.
8. Trinchieri G (2003) Interleukin-12 and the regulation of innate resistance and adaptive immunity. Nat Rev Immunol 3: 133–146.
9. Martin M, Michalek SM, Katz J (2003) Role of innate immune factors in the adjuvant activity of monophosphoryl lipid A. Infect Immun 71: 2498–2507.
10. Schmidt RL, Lenz LL (2012) Distinct licensing of IL-18 and IL-1beta secretion in response to NLRP3 inflammasome activation. PLoS ONE 7: e45186.
11. Ghiringhelli F, Apetoh L, Tesniere A, Aymeric L, Ma Y, et al. (2009) Activation of the NLRP3 inflammasome in dendritic cells induces IL-1beta-dependent adaptive immunity against tumors. Nat Med 15: 1170–1178.
12. Latz E, Schoenemeyer A, Visintin A, Fitzgerald KA, Monks BG, et al. (2004) TLR9 signals after translocating from the ER to CpG DNA in the lysosome. Nat Immunol 5: 190–198.
13. Hornung V, Bauernfeind F, Halle A, Samstad EO, Kono H, et al. (2008) Silica crystals and aluminum salts activate the NALP3 inflammasome through phagosomal destabilization. Nat Immunol 9: 847–856.
14. Meraz IM, Melendez B, Gu J, Wong ST, Liu X, et al. (2012) Activation of the Inflammasome and Enhanced Migration of Microparticle-Stimulated Dendritic Cells to the Draining Lymph Node. Mol Pharm.
15. Haabeth OA, Lorvik KB, Hammarstrom C, Donaldson IM, Haraldsen G, et al. (2011) Inflammation driven by tumour-specific Th1 cells protects against B-cell cancer. Nat Commun 2: 240.
16. Serda RE, Gu J, Bhavane RC, Liu X, Chiappini C, et al. (2009) The association of silicon microparticles with endothelial cells in drug delivery to the vasculature. Biomaterials 30: 2440–2448.
17. Serda RE, Ferrati S, Godin B, Tasciotti E, Liu X, et al. (2009) Mitotic trafficking of silicon microparticles. Nanoscale 1: 250–259.
18. Blanco E, Sangai T, Hsiao A, Ferrati S, Bai L, et al. (2013) Multistage delivery of chemotherapeutic nanoparticles for breast cancer treatment. Cancer Lett 334: 245–252.
19. Shen H, Rodriguez-Aguayo C, Xu R, Gonzalez-Villasana V, Mai J, et al. (2013) Enhancing chemotherapy response with sustained EphA2 silencing using multistage vector delivery. Clin Cancer Res 19: 1806–1815.
20. Godin B, Chiappini C, Srinivasan S, Alexander JF, Yokoi K, et al. (2012) Discoidal Porous Silicon Particles: Fabrication and Biodistribution in Breast Cancer Bearing Mice. Adv Funct Mater 22: 4225–4235.
21. Decuzzi P, Godin B, Tanaka T, Lee SY, Chiappini C, et al. (2009) Size and shape effects in the biodistribution of intravascularly injected particles. J Control Release.
22. Savage DJ, Liu X, Curley SA, Ferrari M, Serda RE (2013) Porous silicon advances in drug delivery and immunotherapy. Curr Opin Pharmacol.
23. Tanaka T, Mangala LS, Vivas-Mejia PE, Nieves-Alicea R, Mann AP, et al. (2010) Sustained small interfering RNA delivery by mesoporous silicon particles. Cancer Res 70: 3687–3696.
24. Serda RE, Mack A, Pulikkathara M, Zaske AM, Chiappini C, et al. (2010) Cellular Association and Assembly of a Multistage Delivery System. Small.
25. Serda RE (2013) Particle platforms for cancer immunotherapy. International Journal of Cancer 8: 1683–1696.
26. Malvicini M, Ingolotti M, Piccioni F, Garcia M, Bayo J, et al. (2011) Reversal of gastrointestinal carcinoma-induced immunosuppression and induction of antitumoural immunity by a combination of cyclophosphamide and gene transfer of IL-12. Mol Oncol 5: 242–255.
27. Umemura N, Saio M, Suwa T, Kitoh Y, Bai J, et al. (2008) Tumor-infiltrating myeloid-derived suppressor cells are pleiotropic-inflamed monocytes/macrophages that bear M1- and M2-type characteristics. J Leukoc Biol 83: 1136–1144.
28. Le HK, Graham L, Cha E, Morales JK, Manjili MH, et al. (2009) Gemcitabine directly inhibits myeloid derived suppressor cells in BALB/c mice bearing 4T1 mammary carcinoma and augments expansion of T cells from tumor-bearing mice. Int Immunopharmacol 9: 900–909.
29. Alizadeh D, Trad M, Hanke NT, Larmonier CB, Janikashvili N, et al. (2014) Doxorubicin eliminates myeloid-derived suppressor cells and enhances the efficacy of adoptive T-cell transfer in breast cancer. Cancer Res 74: 104–118.
30. Nakano H, Yanagita M, Gunn MD (2001) CD11c(+)B220(+)Gr-1(+) cells in mouse lymph nodes and spleen display characteristics of plasmacytoid dendritic cells. J Exp Med 194: 1171–1178.
31. Shigeoka M, Urakawa N, Nakamura T, Nishio M, Watajima T, et al. (2013) Tumor associated macrophage expressing CD204 is associated with tumor aggressiveness of esophageal squamous cell carcinoma. Cancer Sci 104: 1112–1119.

Graham A. Tynan,[1,2] Claire H. Hearnden,[1] Ewa Oleszycka,[1] Claire L. Lyons,[3] Graham Coutts,[4] Jean O'Connell,[5] Michelle A. Corrigan,[5] Lydia Lynch,[5] Matthew Campbell,[6] John J. Callanan,[7] Kenneth H. Mok,[8] Justin Geoghegan,[9] Cliona O'Farrelly,[10] Stuart M. Allan,[4] Helen M. Roche,[3] Donal B. O'Shea,[5] and Ed C. Lavelle[1,2]

Endogenous Oils Derived From Human Adipocytes Are Potent Adjuvants That Promote IL-1α–Dependent Inflammation

Diabetes 2014;63:2037–2050 | DOI: 10.2337/db13-1476

Obesity is characterized by chronic inflammation associated with neutrophil and M1 macrophage infiltration into white adipose tissue. However, the mechanisms underlying this process remain largely unknown. Based on the ability of oil-based adjuvants to induce immune responses, we hypothesized that endogenous oils derived from necrotic adipocytes may function as an immunological "danger signal." Here we show that endogenous oils of human origin are potent adjuvants, enhancing antibody responses to a level comparable to Freund's incomplete adjuvant. The endogenous oils were capable of promoting interleukin (IL)-1α–dependent recruitment of neutrophils and M1-like macrophages, while simultaneously diminishing M2-like macrophages. We found that endogenous oils from subcutaneous and omental adipocytes, and from healthy and unhealthy obese individuals, promoted comparable inflammatory responses. Furthermore, we also confirmed that white adipocytes in visceral fat of metabolically unhealthy obese (MUO) individuals are significantly larger than those in metabolically healthy obese individuals. Since adipocyte size is positively correlated with adipocyte death, we propose that endogenous oils have a higher propensity to be released from hypertrophied visceral fat in MUO individuals and that this is the key factor in driving inflammation. In summary, this study shows that adipocytes contain a potent oil adjuvant which drives IL-1α–dependent proinflammatory responses in vivo.

Obesity is characterized by chronic, low-grade inflammation resulting in insulin resistance. Understanding the mechanisms underlying this inflammation would provide valuable insights into the disease and potentially offer new therapeutic targets. Early studies showing that sodium salicylate can reverse the symptoms of type 2 diabetes (1) highlighted roles for inhibitor of κB kinase β (IKKβ) and Jun N-terminal kinase (JNK) in this process. JNK can directly phosphorylate Serine307 on insulin receptor substrate 1, thus impairing insulin signaling and mediating obesity-induced insulin resistance (2). IKKβ can also phosphorylate insulin receptor substrate 1 (3), and myeloid-specific deletion of IKKβ in obese mice protects against insulin resistance (4). In addition, IKKβ-mediated translocation of nuclear factor-κB into the nucleus

[1]Adjuvant Research Group, School of Biochemistry and Immunology, Trinity Biomedical Sciences Institute, Trinity College Dublin, Dublin, Ireland
[2]Immunology Research Centre, Trinity Biomedical Sciences Institute, Trinity College Dublin, Dublin, Ireland
[3]Nutrigenomics Research Group, University College Dublin Conway Institute, University College Dublin, Dublin, Ireland
[4]Faculty of Life Sciences, University of Manchester, Manchester, U.K.
[5]Obesity Immunology Group, Education and Research Centre, St. Vincent's University Hospital, University College Dublin, Dublin, Ireland
[6]Smurfit Institute of Genetics, Trinity College Dublin, Dublin, Ireland
[7]Veterinary Pathobiology, University College Dublin School of Veterinary Medicine, University College Dublin, Dublin, Ireland
[8]Protein Folding and Biomolecular Nuclear Magnetic Resonance Spectroscopy Group, School of Biochemistry and Immunology, Trinity Biomedical Sciences Institute, Trinity College Dublin, Dublin, Ireland
[9]Department of Hepatobiliary Surgery, St. Vincent's University Hospital, Dublin, Ireland
[10]Comparative Immunology Group, School of Biochemistry and Immunology, Trinity Biomedical Sciences Institute, Trinity College Dublin, Dublin, Ireland
Corresponding author: Ed C. Lavelle, lavellee@tcd.ie.

Received 24 September 2013 and accepted 19 January 2014.
This article contains Supplementary Data online at http://diabetes.diabetesjournals.org/lookup/suppl/doi:10.2337/db13-1476/-/DC1.

© 2014 by the American Diabetes Association. See http://creativecommons.org/licenses/by-nc-nd/3.0/ for details.

See accompanying article, p. 1844.

results in transcription of a plethora of proinflammatory cytokines that further activate JNK and IKKβ in a positive feedback loop (5). Hotamisligil et al. (6) first demonstrated a role for proinflammatory cytokines in driving obesity-induced insulin resistance when reporting that neutralization of tumor necrosis factor (TNF)-α in genetically obese rats improved insulin sensitivity. Subsequently, it was shown that genetic or diet-induced obese mice deficient in TNF-α are protected from insulin resistance (7).

White adipose tissue (WAT) contains resident macrophages that, in nonobese individuals, have an anti-inflammatory profile with an "alternatively activated" phenotype and are referred to as M2 macrophages. The polarization of resident M2 macrophages is achieved under the influence of the cytokines interleukin (IL)-4 and IL-13, which are primarily secreted by T helper (Th) 2 cells and innate lymphoid cells (8,9). However, eosinophils and regulatory T cells are also important for alternative activation of M2 macrophages in WAT through production of IL-4 (10) and IL-10 (11), respectively. Crucially, obesity induces a phenotypic shift from M2 to M1 adipose tissue macrophages, which exhibit a proinflammatory profile and a "classically activated" phenotype (12). M1 macrophages originate from bone marrow precursors and subsequently infiltrate WAT (13). There is a significant increase in the number of proinflammatory M1 macrophages in obesity, particularly in visceral fat, which is more closely associated with pathology than subcutaneous fat (14,15). Th1 cells present in WAT promote the polarization of infiltrating macrophages toward an M1 phenotype by secreting the Th1 signature cytokine interferon (IFN)-γ (8). In addition, cytotoxic T cells (16), B cells (17), and mast cells (18) contribute to obesity-induced inflammation. Neutrophils also play a crucial role in the chronic inflammation associated with obesity and transiently infiltrate intra-abdominal tissue during the early stages of high-fat feeding (19,20).

Currently, the mechanisms responsible for neutrophil and M1 macrophage infiltration into WAT and the inflammatory response associated with obesity remain largely unknown. However, it has been reported that adipocytes in WAT of obese mice exhibit features of necrosis and subsequently release endogenous dietary oils into the extracellular milieu. Macrophages are recruited exclusively to sites of necrotic adipocyte death where they aggregate to form crown-like structures (21). Based on the established ability of oil-based vaccine adjuvants to induce potent immune responses (22–24), we hypothesized that endogenous oils derived from necrotic adipocytes may function as a potent immunological "danger signal," thus providing a crucial link between obesity and chronic immune stimulation.

RESEARCH DESIGN AND METHODS

Reagents

The reagents used were Freund's incomplete adjuvant (FIA; Sigma-Aldrich), alum (Alhydrogel, Brenntag Biosector), Pam3CSK4 (Pam3; InvivoGen), CpG (Oligos Etc. Inc.), and 10 μm polystyrene (PS) particles (Phosphorex Inc.).

Animals

C57BL/6, C3H/HeN, and C3H/HeJ mice were obtained from Harlan Olac (Bicester, U.K.), *Il1r1*$^{-/-}$ mice were obtained from The Jackson Laboratory (Bar Harbor, ME) and *Nlrp3*$^{-/-}$ breeding pairs were provided by the late Jurg Tschopp (University of Lausanne, Switzerland). These mice were housed in the Bioresources Unit in Trinity College Dublin. Animals were maintained according to the regulations of the European Union and the Irish Department of Health. Animal studies were approved by the Trinity College Dublin Animal Research Ethics Committee (ethical approval number 091210) and were performed under license number B100/3321. *Il1α/β*$^{-/-}$ and *Il1α*$^{-/-}$ mice were provided by Stuart Allan (University of Manchester, U.K.), and experiments involving these mice were performed at the University of Manchester under the Animals (Scientific Procedures) Act 1986 (license number PPL 40/3617).

Defining Profile of Individuals

Obese individuals had a BMI of >30. The metabolic profile of obese individuals was determined as described previously (25) and as outlined in Supplementary Table 1, according to the International Diabetes Federation worldwide consensus definition of the metabolic syndrome of 2006. Healthy lean individuals were nonmalignant and noninflammatory and had a BMI of <25.

Human Adipose Tissue

With informed consent, omental and subcutaneous adipose tissue biopsies were obtained from obese patients undergoing bariatric surgery and healthy lean patients undergoing a laparoscopic colonoscopy for exploratory reasons at St. Vincent's University Hospital (Elm Park, Dublin, Ireland). The St. Vincent's University Hospital Ethics and Medical Research Committee approved the use of these patient samples for this study.

Isolation of Human Omental and Subcutaneous Oils from WAT

Adipocytes were isolated as described previously (25) and were centrifuged at 2,500*g* for 1 min to release endogenous oils. Where indicated, a lipid-extraction procedure was performed using the Bligh and Dyer method described previously (26). When testing for immunostimulatory activity in vivo, the individual fractions were further separated with reversed-phase high-performance liquid chromatography. When preparing samples for fatty acid compositional profiling, the organic layer containing the lipid fraction was transesterified using 14% boron trifluoride-methanol as described previously (27) and was analyzed by gas chromatography as described previously (28).

Histological Analysis of Human Adipose Tissue

Omental adipose tissue was immediately fixed in formalin, paraffin-embedded, sectioned at 5 μm, and stained with hematoxylin and eosin. Adipocyte size was determined using Image Pro Plus 7 software.

Endotoxin-Free Ovalbumin

Ovalbumin (OVA; Sigma-Aldrich) was resuspended in sterile PBS (Biosera). This preparation was filter sterilized with a 0.22 μm syringe-driven filter (Millipore) and passed through three separate endotoxin removal columns (Pierce) three times each.

Heat-Killed *Escherichia coli*

BL21 strain *E. coli* were killed by heating at 70°C for 15 min.

Isolation and Culture of Peritoneal Exudate Cells

Mice were killed by cervical dislocation, and the peritoneal cavity was washed with 5 mL of ice-cold PBS. The wash fluid was collected, and peritoneal exudate cells (PECs) were pelleted by centrifugation. The supernatant was collected, and PECs were resuspended in RPMI 1640 medium (Biosera). PEC numbers were determined by light microscopy using a KOVA Glasstic cell counter slide with grids (Medical Supply Co. Ltd.) following trypan blue (Sigma-Aldrich) exclusion. PECs (1×10^6/mL) were incubated at 37°C in a humidified atmosphere (5% CO_2).

Flow Cytometry

PECs (1×10^6) were preincubated for 10 min with an anti-CD16/CD32 monoclonal antibody (0.25 μg; BD Pharmingen). PECs were then incubated for 30 min with AQUA fluorescent dye (0.5 μL; Invitrogen) and for an additional 30 min with antibodies specific for CD11b (0.005 μg; BD Pharmingen), Gr-1 (0.04 μg; BD Pharmingen), F4/80 (0.1 μg; eBioscience), and SiglecF (0.02 μg; BD Pharmingen). Samples were acquired with a FACSCanto II flow cytometer using FACSDiva software (BD Biosciences), and the data were analyzed using FlowJo software (Treestar, Oregon).

Dot plots are shown in the figures as a single representative population from each treatment group.

Measurement of Cytokines by ELISA

The concentration of the cytokine IL-12p40 was measured by ELISA using antibodies obtained from BD Pharmingen. Concentrations of the cytokines TNF-α, IL-10, and IL-12p70 were measured with DuoSet ELISA Development Kits (R&D Systems).

Measurement of Antigen-Specific Serum Antibodies by ELISA

Titres of antigen-specific total serum IgG as well as the IgG subtypes IgG1, IgG2b, and IgG2c were determined using commercially available antibodies from Sigma-Aldrich (total IgG), BD Pharmingen (IgG1 and IgG2b), and AbD Serotec (IgG2c).

Statistical Analysis

Statistical analysis was performed using GraphPad Prism 5 software. The means for three or more groups were compared by one-way ANOVA. Where significant differences were found, the Tukey–Kramer multiple comparisons test was used to identify differences between individual groups. The means for two groups were compared using an unpaired Student *t* test.

RESULTS

Endogenous Omental Oils Are Potent Adjuvants

Oil-based emulsions such as MF59 and FIA are potent vaccine adjuvants. Therefore, the first question addressed was whether endogenous oils derived from the human omentum of metabolically healthy obese (MHO) individuals (oils were derived from MHO individuals for each experiment, unless stated otherwise) could function as an endogenous adjuvant. Remarkably, mixing OVA with endogenous oils significantly enhanced antigen-specific IgG1, IgG2b, and IgG2c responses to a degree comparable to FIA (Fig. 1*A*).

In order to rule out the possibility that nonlipid components were responsible for the immunostimulatory activity of the preparation of endogenous oils, a lipid-extraction procedure was performed. The aqueous phase containing nonlipid components failed to enhance any of the OVA-specific IgG subtypes tested. However, the organic fraction containing nonpolar lipids potently enhanced OVA-specific antibody titres in the serum, including IgG1, IgG2b, and IgG2c (Fig. 1*B*). Thus it is likely that lipids, and not nonlipid components, are responsible for the immunostimulatory activity of the endogenous oils in vivo.

Endogenous Oils Promote Recruitment of Neutrophils and M1-Like Macrophages

Since oil-in-water adjuvants have been shown to act as powerful chemoattractants for macrophages and granulocytes (29), we investigated whether endogenous oils can promote inflammatory cell recruitment. The peritoneum was chosen as a relevant site to study oil-driven modulation of the innate immune system, as endogenous oils from necrotic adipocytes may leak into the abdomen of obese humans. Furthermore, the application of intraperitoneal injection to demonstrate the immunostimulatory activity of endogenous inducers of sterile inflammation, including monosodium urate crystals (30) and necrotic cells (31), is well established. Remarkably, the endogenous oils induced almost a threefold increase in PEC number after 24 h (Fig. 2*A*).

Neutrophil and M1 macrophage infiltration into WAT is a hallmark of obesity-induced inflammation (12,19). Given the significant increase in total PEC number following injection with endogenous oils, the capacity of the endogenous oils to promote neutrophil and M1 macrophage infiltration was determined. Importantly, "M1-like" and "M2-like" macrophages represent the peritoneal equivalent of M1 and M2 macrophages, respectively (32,33).

There was almost a complete absence of neutrophils ($CD11b^{inter}$ $F4/80^-$ $Gr\text{-}1^{high}$) in the peritoneum of control mice. However, injection of the endogenous oils induced neutrophil recruitment after only 15 min, and the magnitude of this response increased with time, being highest after 24 h (Fig. 2*B*). The endogenous oils also promoted significant infiltration of M1-like macrophages ($CD11b^{inter}$

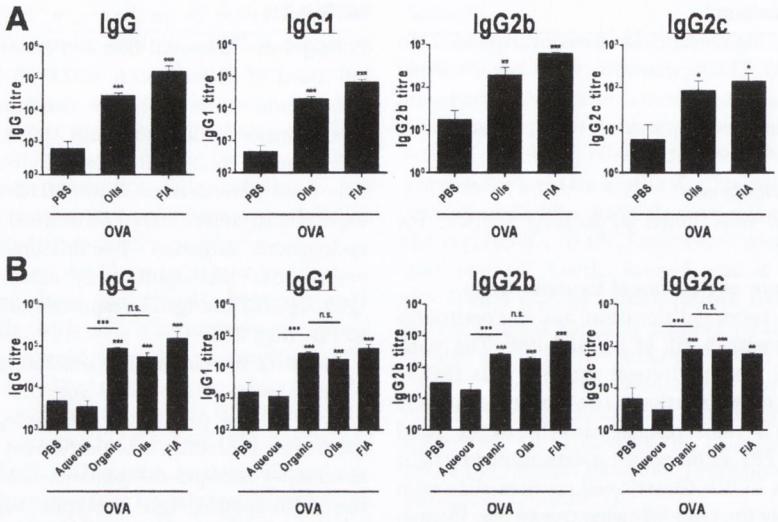

Figure 1—Endogenous oils have potent adjuvant properties. *A*: Female C57BL/6 mice were immunized intraperitoneally on day 0 with PBS or OVA (200 μg/mouse) either alone or mixed with an equal volume (100 μL) of endogenous oils derived from the human omentum. OVA was also mixed with an equal volume (100 μL) of FIA, and this solution was emulsified by sonication. The mice were boosted with these same treatments on day 14 and were killed on day 21. Blood samples were recovered and the serum was removed following centrifugation. OVA-specific antibody titres (IgG, IgG1, IgG2b, and IgG2c) in the serum were determined by ELISA. Results are mean titres (+SEM) for five mice per group. Versus PBS (OVA): *, $P < 0.05$; **, $P < 0.01$; ***, $P < 0.001$. *B*: Female C57BL/6 mice were immunized intraperitoneally with PBS or OVA (200 μg/mouse) either alone or mixed with an equal volume (100 μL) of endogenous oils or an aqueous or organic fraction derived from this preparation following a lipid-extraction procedure. OVA was also mixed with an equal volume (100 μL) of FIA, and this solution was emulsified by sonication. The mice were boosted with these same treatments on day 14 and were killed on day 21. Blood samples were recovered and the serum was removed following centrifugation. OVA-specific antibody titres (IgG, IgG1, IgG2b,, and IgG2c) in the serum were determined by ELISA. Results are mean titres (+SEM) for four mice per group. Versus PBS (OVA), **, $P < 0.01$; ***, $P < 0.001$. Organic fraction (OVA) versus aqueous fraction (OVA): •••, $P < 0.001$. n.s., not significant.

F4/80^{inter} SSC^{low}) into the injection site. Recruitment of these cells was only detectable after 3 h but was again most prominent after 24 h (Fig. 2*C*). The endogenous oils concomitantly mediated the rapid depletion of M2-like macrophages (CD11b^{high} F4/80^{high}) (Fig. 2*D*). Furthermore, these effects were still observed when as little as 1 μL of endogenous oils was injected (Supplementary Fig. 1*A* and *B*).

The immunostimulatory activity of a number of adjuvants has been reported to be at least partially dependent on their ability to induce necrotic cell death at the injection site (34,35). However, we found that the endogenous oils failed to exhibit significant toxicity in contrast to alum (Supplementary Fig. 2*A* and *B*). Therefore, the immunostimulatory activity of the endogenous oils is not likely to be mediated by toxicity. In support of this finding, the oil-in-water emulsion FIA also failed to induce necrotic cell death at the injection site (Supplementary Fig. 2*C*).

Endogenous Oils Enhance the Production of Proinflammatory Cytokines, Including TNF-α, and Decrease the Production of IL-10

Under steady-state conditions, resident macrophages serve to dampen immune responses in WAT through secretion of anti-inflammatory cytokines such as IL-10 (12). In obesity, however, WAT recruits M1 macrophages that secrete proinflammatory cytokines such as TNF-α (13) and IL-12 (36–38).

Importantly, PECs isolated from mice injected with endogenous oils exhibited a significant increase in secretion of TNF-α and IL-12p40 following restimulation with pattern recognition receptor (PRR) agonists, whereas IL-12p70 release was selectively augmented following restimulation with heat-killed (HK) *E. coli*. In contrast, PECs isolated from mice injected with endogenous oils secreted significantly less IL-10 in comparison with those isolated from mice injected with PBS (Fig. 2*E*). These effects were also apparent in PECs derived from mice injected with only 1 μL of endogenous oils (Supplementary Fig. 1*C*). Thus injection of endogenous oils recruits inflammatory cells into the peritoneum and primes PECs for secretion of proinflammatory cytokines, which parallels that seen in the inflamed WAT of obese individuals.

Endogenous Oils Derived From Subcutaneous Adipocytes Promote Innate Immune Responses Comparable to Those Derived From Omental Adipocytes

Accumulation of visceral fat is associated with adverse metabolic conditions such as type 2 diabetes and fatty liver and cardiovascular disease (39). Therefore, this study

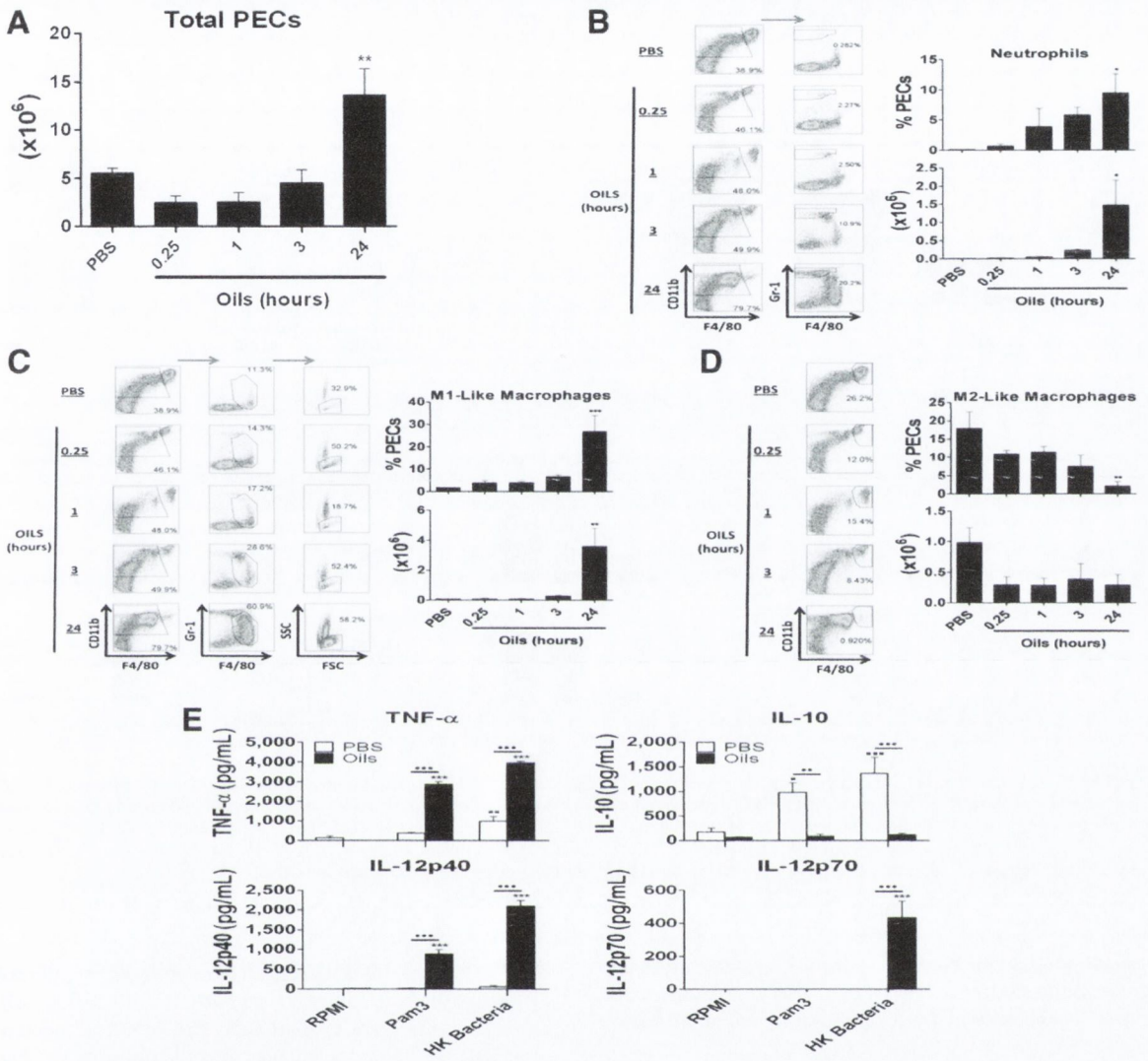

Figure 2—Endogenous oils promote the recruitment of inflammatory cells. *A*: Female C57BL/6 mice were immunized intraperitoneally with PBS or endogenous oils (10 μL/mouse). The mice were killed after the indicated number of hours (0.25 for PBS), and total PEC numbers were determined. *B*: Neutrophils ($CD11b^{inter}$ $F4/80^{-}$ $Gr\text{-}1^{high}$), (*C*) M1-like macrophages ($CD11b^{inter}$ $F4/80^{inter}$ SSC^{low}), and (*D*) M2-like macrophages ($CD11b^{high}$ $F4/80^{high}$) were identified by flow cytometry. Bar graphs represent mean (+SEM) cell numbers for three mice per group. Versus PBS: *, $P < 0.05$; **, $P < 0.01$; ***, $P < 0.001$. *E*: Female C57BL/6 mice were immunized as described (*A*). The mice were killed 24 h later. PECs were restimulated with RPMI, Pam3 (5 μg/mL), or HK *E. coli* (10 *E. coli*: 1 PEC). After 24 h, supernatants were analyzed for TNF-α, IL-10, IL-12p40, and IL-12p70 by ELISA. Results are mean cytokine concentrations (+SEM) for four mice per group tested individually in triplicate. Versus PECs from oil-injected mice restimulated with RPMI: **, $P < 0.01$; ***, $P < 0.001$. Versus PECs from PBS-injected mice restimulated with RPMI: ■, $P < 0.05$; ■■, $P < 0.01$; ■■■, $P < 0.001$. PECs from oil-injected mice versus PECs from PBS-injected mice for corresponding stimulus: ●●, $P < 0.01$; ●●●, $P < 0.001$.

next sought to address the question of whether cell recruitment into the injection site was an immunostimulatory property specific for endogenous oils derived from omental adipocytes or was also characteristic of endogenous oils derived from the less metabolically active subcutaneous fat.

Endogenous oils derived from subcutaneous and omental adipocytes were comparable in their capacity to recruit cells into the peritoneum (Fig. 3*A*). Both forms of endogenous oils also promoted similar recruitment of neutrophils and M1-like macrophages (Fig. 3*B* and *C*) while simultaneously depleting the M2-like macrophage population (Fig. 3*D*). Ultimately, there was no significant difference between endogenous oils derived from subcutaneous or omental adipocytes in their respective ability to promote inflammatory effects in the peritoneum.

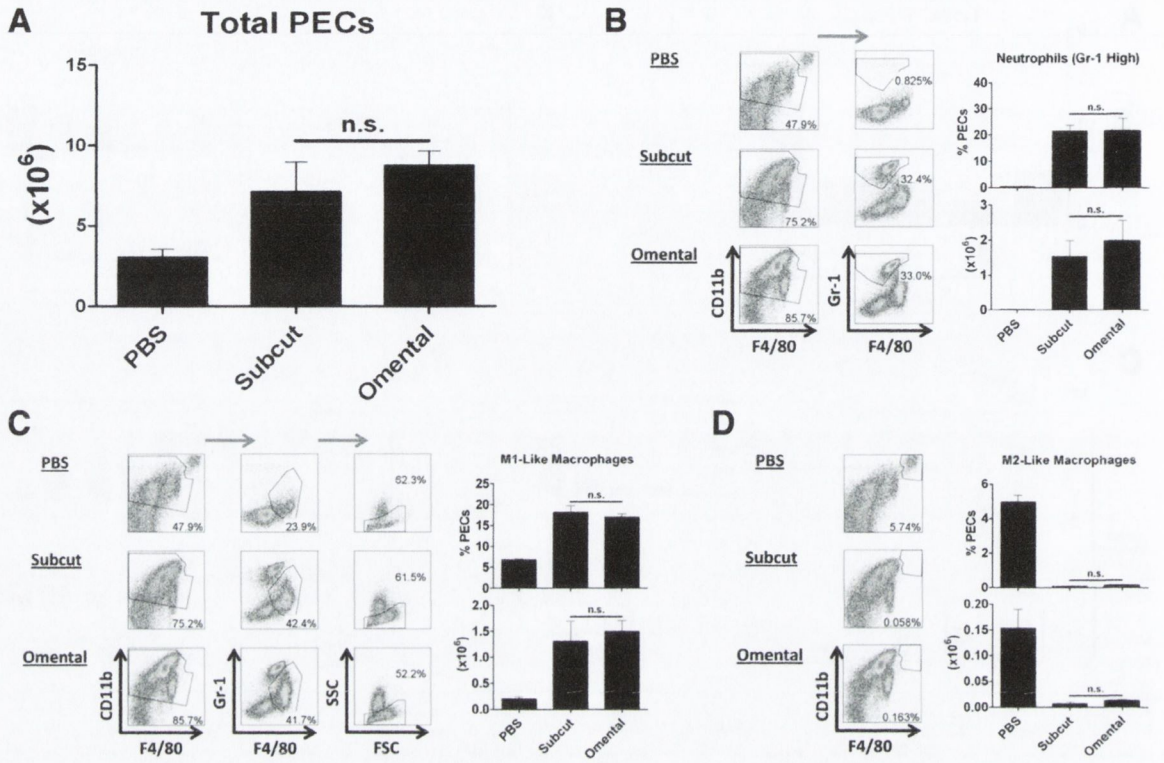

Figure 3—Endogenous oils derived from subcutaneous adipocytes and omental adipocytes are equally immunogenic. (*A*) Female C57BL/6 mice were immunized intraperitoneally with PBS or endogenous oils derived from either subcutaneous or omental adipocytes (10 μL/mouse) from the same obese individual. The mice were killed 24 h later and total PEC numbers were determined. (*B*) Neutrophils ($CD11b^{inter}$ $F4/80^{-}$ $Gr\text{-}1^{high}$), (*C*) M1-like macrophages ($CD11b^{inter}$ $F4/80^{inter}$ SSC^{low}), and (*D*) M2-like macrophages ($CD11b^{high}$ $F4/80^{high}$) were identified by flow cytometry. Bar graphs represent mean (+SEM) cell numbers for three mice per group. n.s., not significant.

Endogenous Oils Derived From Visceral Fat of MHO, Metabolically Unhealthy Obese, and Lean Individuals Are Comparable in Their Ability to Drive Inflammation

Since both the omental and subcutaneous oils elicited immunostimulatory effects in vivo, it was hypothesized that the ability of endogenous oils to promote obesity-induced inflammation was dependent on their release from ruptured adipocytes in WAT rather than their specific composition. Importantly, there is a positive correlation between adipocyte hypertrophy and adipocyte necrosis in visceral fat of obese mice and humans (21). In agreement with previous work (25), MHO individuals possessed an average adipocyte diameter of ~75 μm, but metabolically unhealthy obese (MUO) individuals had significantly larger adipocytes, which were ~85 μm in diameter, thus representing almost a 15% increase in adipocyte size (Fig. 4*A*).

Since adipocyte size is positively correlated with adipocyte death, we propose that endogenous oils have a higher propensity to be released from hypertrophied visceral fat in MUO individuals and that this is the key factor in driving inflammation. In support of this hypothesis, endogenous oils derived from MHO and MUO individuals both increased total PEC number, with no significant difference in their ability to promote this effect (Fig. 4*B*). Similar results were evident for recruitment of neutrophils and M1-like macrophages into the peritoneum (Fig. 4*C*), while both treatments effectively depleted the resident M2-like macrophage population (Fig. 4*D*). This comparable capacity of endogenous oils derived from MHO and MUO individuals to modulate the local PEC population was also reflected in terms of PEC cytokine secretion following ex vivo restimulation (Fig. 4*E*).

The immunostimulatory effects outlined above in response to endogenous oils derived from MHO and MUO individuals were also observed following injection with endogenous oils isolated from healthy lean individuals (Fig. 5*A–C*). These findings confirm that endogenous oils derived from adipocytes in WAT of MHO, MUO, and lean individuals are equally immunostimulatory. Analysis of the fatty acid profile of endogenous oil preparations derived from MHO, MUO, and lean individuals did not reveal significant differences in composition between the different groups. Furthermore, there was minimal variability between individuals, regardless of their BMI or metabolic state (Fig. 5*D*).

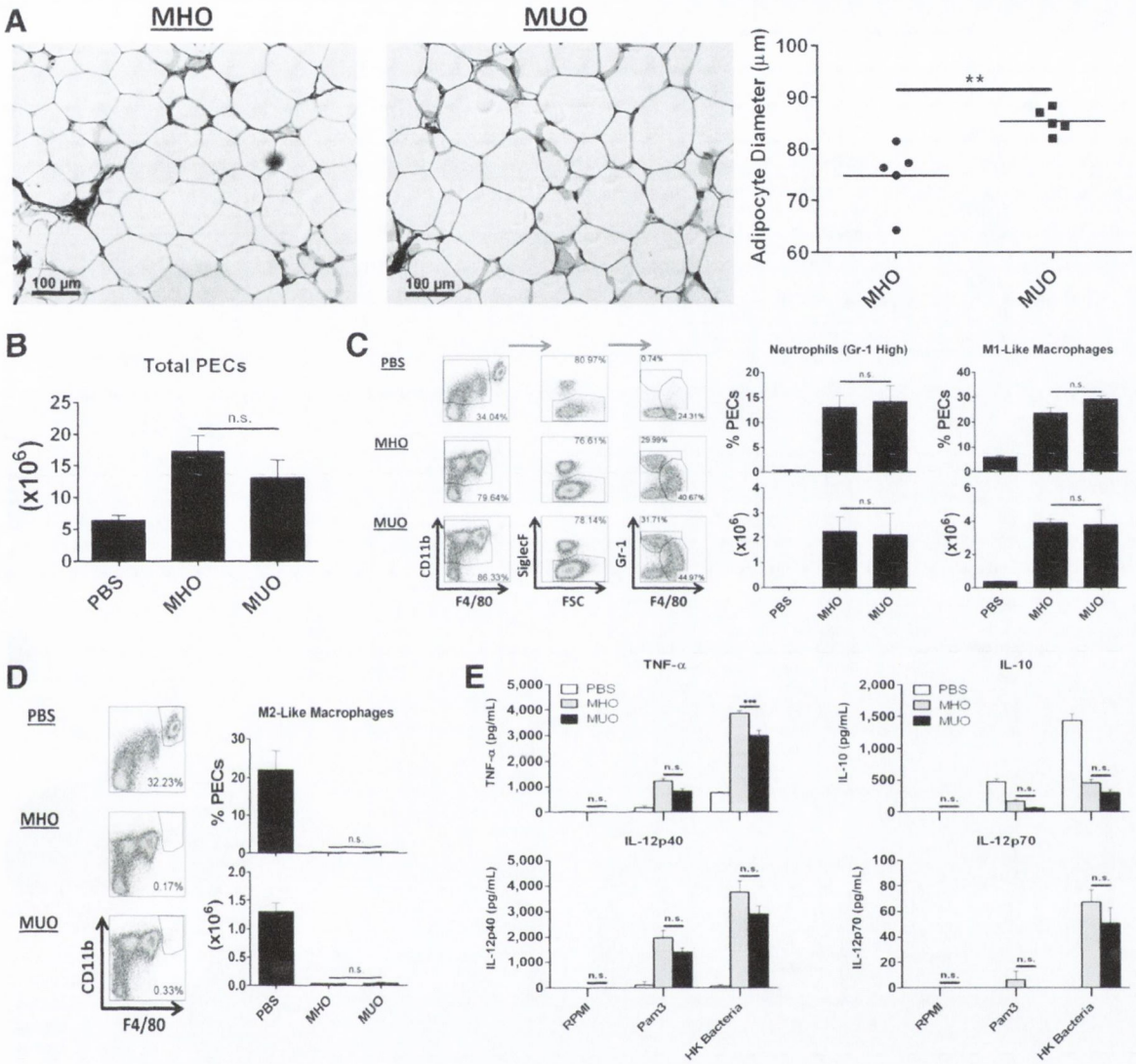

Figure 4—Endogenous oils are released from the hypertrophied visceral fat of MUO individuals and subsequently promote inflammation. *A*: Approximately 10–30 g of omental adipose tissue was obtained during bariatric surgery. A piece of this tissue was immediately fixed in formalin, prior to paraffin mounting and preparation of hematoxylin and eosin sections. Adipocyte size was determined using Image-Pro Plus 7 software. The mean diameter of a range of adipocytes from five MHO individuals and five MUO individuals was calculated from 10 separate photographs of randomized areas of the same section. Single representative image of a section containing WAT from an MHO individual and also a section containing WAT from an MUO individual. Scatter plot represents mean for five individuals per group. Versus MHO: **, $P < 0.01$. *B*: Female C57BL/6 mice were immunized intraperitoneally with PBS or endogenous oils derived from omental adipocytes of an MHO or MUO individual (10 μL/mouse). The mice were killed 24 h later, and total PEC numbers were determined. *C*: Neutrophils ($CD11b^{inter}$ $F4/80^{-}$ $Gr\text{-}1^{high}$), M1-like macrophages ($CD11b^{inter}$ $F4/80^{inter}$ $SiglecF^{-}$), and (*D*) M2-like macrophages ($CD11b^{high}$ $F4/80^{high}$) were identified by flow cytometry. Bar graphs represent mean (+SEM) cell numbers for four mice per group. *E*: Female C57BL/6 mice were immunized as described (*B*). The mice were killed 24 h later, and PECs were isolated. PECs were restimulated with RPMI, Pam3 (5 μg/mL), or HK *E. coli* (10 *E. coli*: 1 PEC). After 24 h, supernatants were analyzed for TNF-α, IL-10, IL-12p40, and IL-12p70 by ELISA. Results are mean cytokine concentrations (+SEM) for four mice per group tested individually in triplicate. MHO versus MUO for corresponding stimulus: ●●●, $P < 0.001$. n.s., not significant.

Toll-Like Receptor 4 Is Dispensable for Cell Recruitment Into the Peritoneum in Response to Endogenous Oils

Saturated fatty acids have previously been shown to promote cytokine production in macrophages in vitro in a Toll-like receptor 4 (TLR4)-dependent manner (40,41). Since the preparation of endogenous oils derived from the human omentum contains free fatty acids, this study next investigated whether TLR4 is required for inflammatory cell recruitment into the peritoneum in response to these oils.

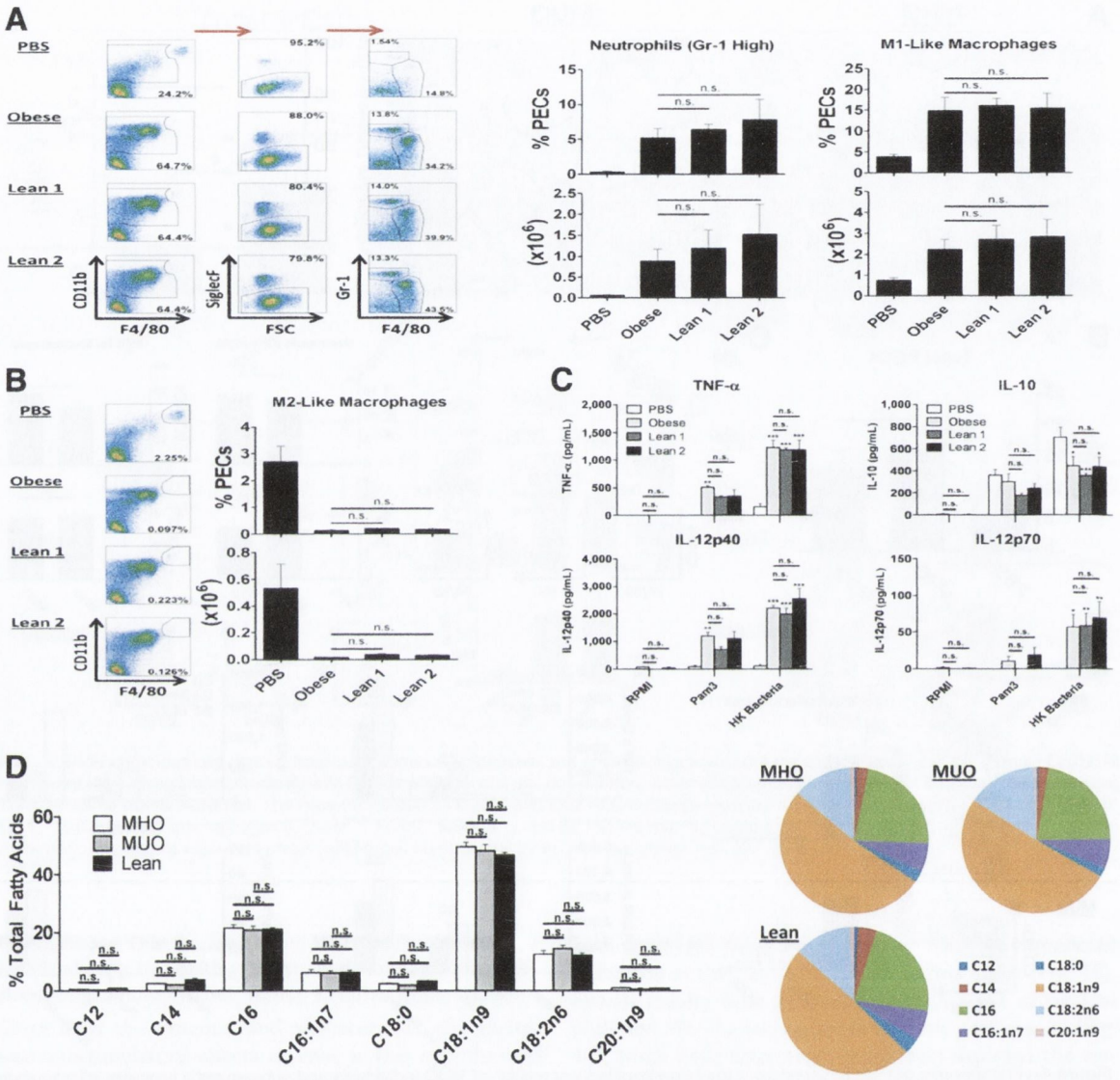

Figure 5—Endogenous oils derived from omental adipocytes of MHO, MUO, and lean individuals share an identical fatty acid profile. *A*: Female C57BL/6 mice were immunized intraperitoneally with PBS or endogenous oils derived from omental adipocytes of an MHO or one of two lean individuals (10 μL/mouse). The mice were killed 24 h later, and neutrophils ($CD11b^{inter}$ $F4/80^{-}$ $Gr\text{-}1^{high}$), M1-like macrophages ($CD11b^{inter}$ $F4/80^{inter}$ $SiglecF^{-}$), and (*B*) M2-like macrophages ($CD11b^{high}$ $F4/80^{high}$) were identified by flow cytometry. Bar graphs represent mean (+SEM) cell numbers for four mice per group. *C*: Female C57BL/6 mice were immunized as described (*A*). The mice were killed 24 h later, and PECs were isolated. PECs were restimulated with RPMI, Pam3 (5 μg/mL), or HK *E. coli* (10 *E. coli*: 1 PEC). After 24 h, supernatants were analyzed for TNF-α, IL-10, IL-12p40, and IL-12p70 by ELISA. Results are mean cytokine concentrations (+SEM) for four mice per group tested individually in triplicate. PECs from oil-injected mice versus PECs from PBS-injected mice for corresponding stimulus: *, $P < 0.05$; **, $P < 0.01$; ***, $P < 0.001$. *D*: Fatty acid profiles of endogenous oil preparations derived from omental adipocytes of five MHO, five MUO, and five lean individuals were analyzed by gas chromatography following a lipid-extraction and transesterification procedure. Bar graphs and pie charts represent mean (+SEM for bar charts) fatty acid composition as a relative percentage of the total of the quantified fatty acids present in the tissue. n.s., not significant.

Injection of endogenous oils increased total PEC number in both wild-type C3H/HeN mice and TLR4-defective C3H/HeJ mice, but there was no significant difference in total PEC number between the two mouse strains (Fig. 6*A*). The endogenous oils also induced comparable recruitment of neutrophils into the peritoneum of both C3H/HeN and C3H/HeJ mice. Similar results were evident for M1-like macrophages (Fig. 6*B*). Ultimately, TLR4 was dispensable for the immunostimulatory effects of the endogenous oils. Therefore, signaling through TLR4 by free fatty

acids does not appear to be responsible for mediating these effects.

Neutrophil and M1-Like Macrophage Recruitment Into the Peritoneum Following Injection With Endogenous Oils Is IL-1R–Dependent

IL-1α and IL-1β are powerful chemoattractants that may be involved in promoting cell recruitment into the peritoneum (31,42), and the IL-1R has been implicated in compromised insulin sensitivity (43). Both cytokines were elevated significantly at the injection site after 3 h in response to endogenous oils (Fig. 6*C*). Therefore, this study sought to determine their role in the subsequent recruitment of inflammatory cells.

The endogenous oils increased total PEC number in wild-type mice, whereas cell recruitment into the peritoneum in response to endogenous oils was completely abrogated in *Il1r1*$^{-/-}$ mice (Fig. 7*A*). Neutrophil and M1-like macrophage recruitment was entirely dependent on the IL-1R (Fig. 7*B*). In contrast, injection of 10 μm PS particles effectively recruited both of these inflammatory cell types into the peritoneum (Fig. 7*C*). Thus the requirement for the IL-1R in recruitment of neutrophils and M1-like macrophages was specific for injection with endogenous oils.

Interestingly, the saturated fatty acid palmitate has been reported to activate the NLRP3 inflammasome (44) and is present within the preparation of endogenous oils derived from necrotic adipocytes (Fig. 5*D*). However, the endogenous oils increased total PEC number in both C57BL/6 and *Nlrp3*$^{-/-}$ mice (Supplementary Fig. 3*A*). Neutrophil recruitment was marginally reduced in *Nlrp3*$^{-/-}$ mice, whereas M1-like macrophage recruitment was totally independent of this inflammasome (Supplementary Fig. 3*B*). This result eliminates the possibility that the observed effects are a result of palmitate-mediated NLRP3 activation.

Modulation of PEC Cytokine Secretion by Endogenous Oils Is IL-1R–Dependent

Since the endogenous oils were capable of modulating the local PEC population and the cytokine secretion profile of PECs following ex vivo restimulation with PRR agonists (Fig. 2*E*), this study next addressed the question of whether this effect was also dependent on the IL-1R.

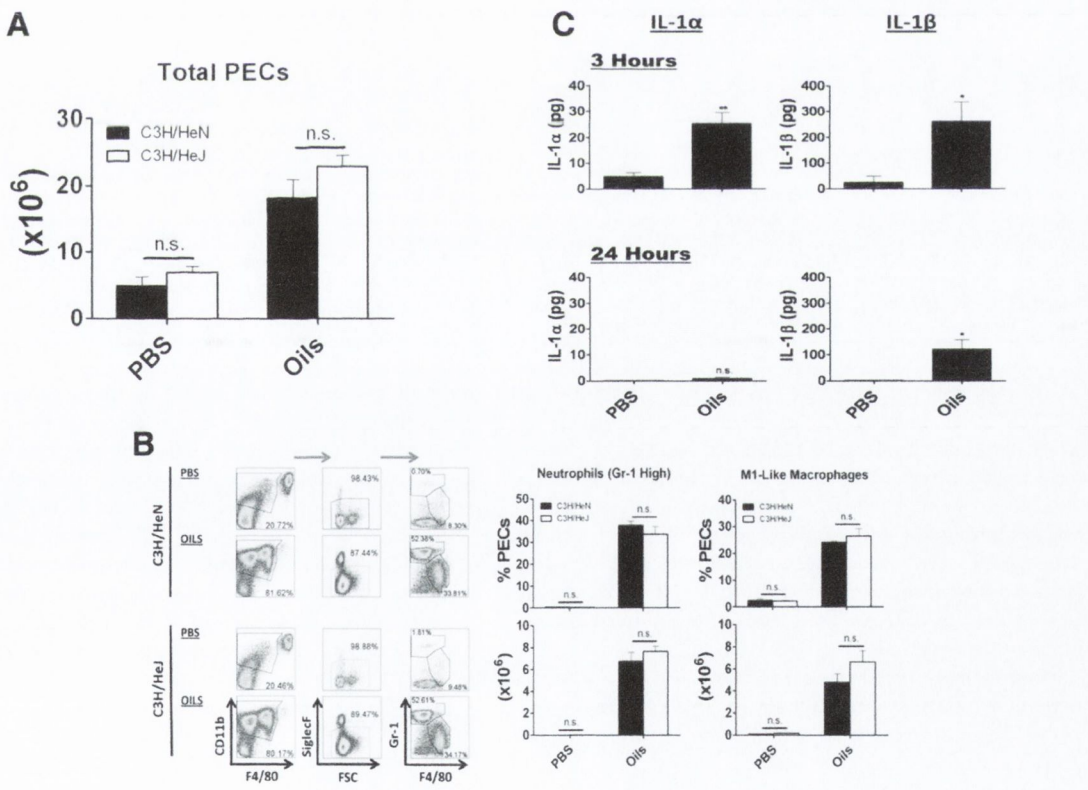

Figure 6—Neutrophil and M1-like macrophage recruitment in response to endogenous oils is independent of TLR4. *A*: Female C3H/HeN and C3H/HeJ mice were immunized intraperitoneally with PBS or endogenous oils (10 μL/mouse). The mice were killed 24 h later, and total PEC numbers were determined. *B*: Neutrophils (CD11b^{inter} F4/80^{-} Gr-1^{high}) and M1-like macrophages (CD11b^{inter} F4/80^{inter} SiglecF^{-}) were identified by flow cytometry. Bar graphs represent mean (+SEM) cell numbers for four mice per group. *C*: Female C57BL/6 mice were immunized as described in *A*. The mice were killed either 3 or 24 h later. PECs were isolated, and PEC supernatants were collected. PEC supernatants were tested for the cytokines IL-1α and IL-1β by ELISA. Results are mean cytokine concentrations (+SEM) for three mice per group. Versus PBS: *, $P < 0.05$; **, $P < 0.01$. n.s., not significant.

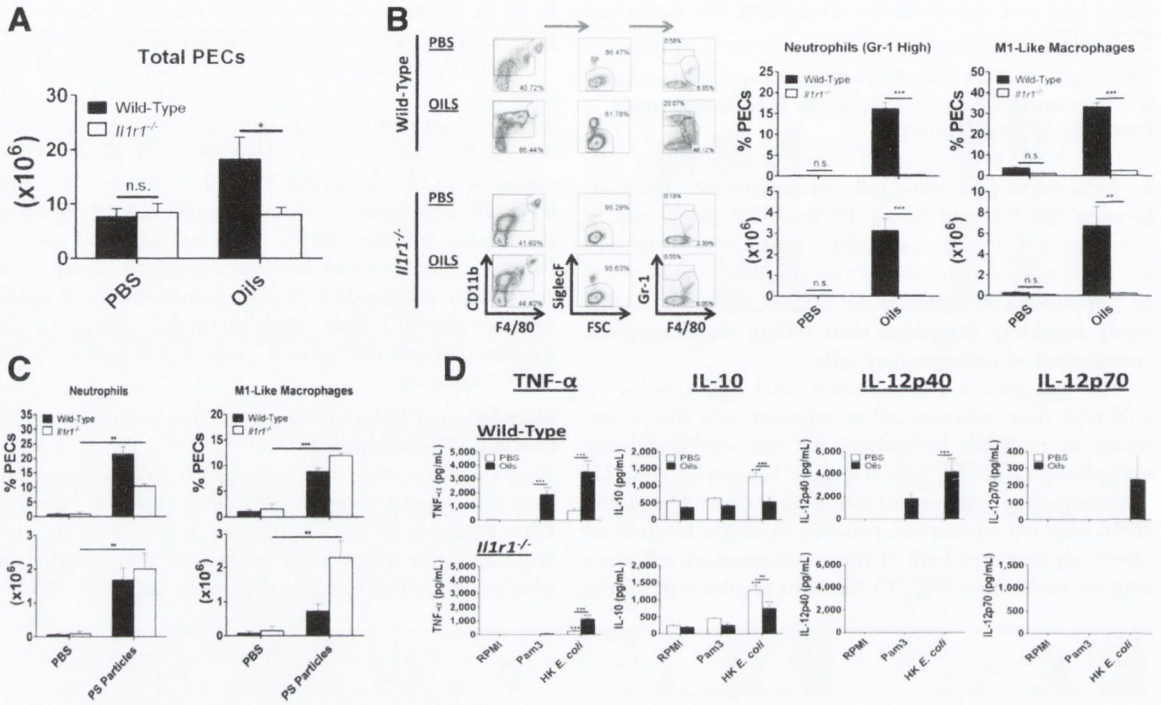

Figure 7—Endogenous oils mediate cell recruitment into the peritoneum through a process dependent on the IL-1R. *A*: Female wild-type C57BL/6 and *Il1r1*$^{-/-}$ mice were immunized intraperitoneally with PBS or endogenous oils (10 μL/mouse) and were killed 24 h later. PEC numbers were determined. *B*: Neutrophils (CD11b^{inter} F4/80^{-} Gr-1^{high}) and M1-like macrophages (CD11b^{inter} F4/80^{inter} SiglecF^{-}) were identified (four mice per group). *C*: Female C57BL/6 and *Il1r1*$^{-/-}$ mice were immunized intraperitoneally with PBS or 10 μm PS particles (4 mg/mouse). The mice were killed 24 h later. Neutrophils and M1-like macrophages were identified (three mice per group). Bar graphs represent mean (+SEM) cell numbers. Versus wild-type for corresponding treatment: *, $P < 0.05$; **, $P < 0.01$; ***, $P < 0.001$. *D*: Female wild-type C57BL/6 and *Il1r1*$^{-/-}$ mice were immunized as described (*A*) and were killed 24 h later. PECs were restimulated with RPMI, Pam3 (5 μg/mL), or HK *E. coli* (10 *E. coli*: 1 PEC). After 24 h, supernatants were analyzed for TNF-α, IL-10, IL-12p40, and IL-12p70 by ELISA. Results are mean cytokine concentrations (+SEM) for four mice/group tested individually in triplicate. Versus PECs from oil-injected mice restimulated with RPMI: ***, $P < 0.001$. Versus PECs from PBS-injected mice restimulated with RPMI: ■■■, $P < 0.001$. PECs from oil-injected mice versus PECs from PBS-injected mice for corresponding stimulus: ●●, $P < 0.01$; ●●●, $P < 0.001$. n.s., not significant.

In contrast to wild-type mice, PECs isolated from *Il1r1*$^{-/-}$ mice injected with endogenous oils failed to secrete detectable levels of IL-12p40 and IL-12p70 following restimulation with PRR agonists. Furthermore, secretion of TNF-α by these cells was completely abrogated following restimulation with Pam3 and significantly reduced when cells were restimulated with HK *E. coli*. However, as in wild-type mice, a reduction in IL-10 synthesis was still evident in PECs isolated from *Il1r1*$^{-/-}$ mice injected with endogenous oils (Fig. 7*D*).

Interestingly, PECs isolated from *Nlrp3*$^{-/-}$ or wild-type mice injected with endogenous oils exhibited an almost identical profile with regard to each of the cytokines tested (Supplementary Fig. 3*C*).

IL-1α Is the Key Cytokine Responsible for Driving Neutrophil and M1-Like Macrophage Recruitment in Response to Endogenous Oils

Both IL-1α and IL-1β are important IL-1 family members that signal through the IL-1R (45). Therefore, the next aim was to determine which of these cytokines was primarily responsible for mediating the observed effects. Neutrophil and M1-like macrophage recruitment was attenuated in *Il1αβ*$^{-/-}$ mice following injection with endogenous oils (Fig. 8*A*). Intriguingly, however, similar results were also found in *Il1α*$^{-/-}$ mice (Fig. 8*A*), thus confirming that IL-1α is the key IL-1 family member responsible for promoting inflammation in response to endogenous oils. In support of this observation, modulation of the cytokine profile associated with the PEC population following ex vivo restimulation was also IL-1α dependent (Fig. 8*B*).

DISCUSSION

This is the first study to directly test the inflammatory potential of a pure preparation of endogenous oils derived from adipocytes of both lean and obese individuals and demonstrates that these oils have remarkably potent inflammatory effects.

Using a peritonitis model, the endogenous oils increased total PEC number, specifically recruiting M1-like macrophages while simultaneously depleting the M2-like

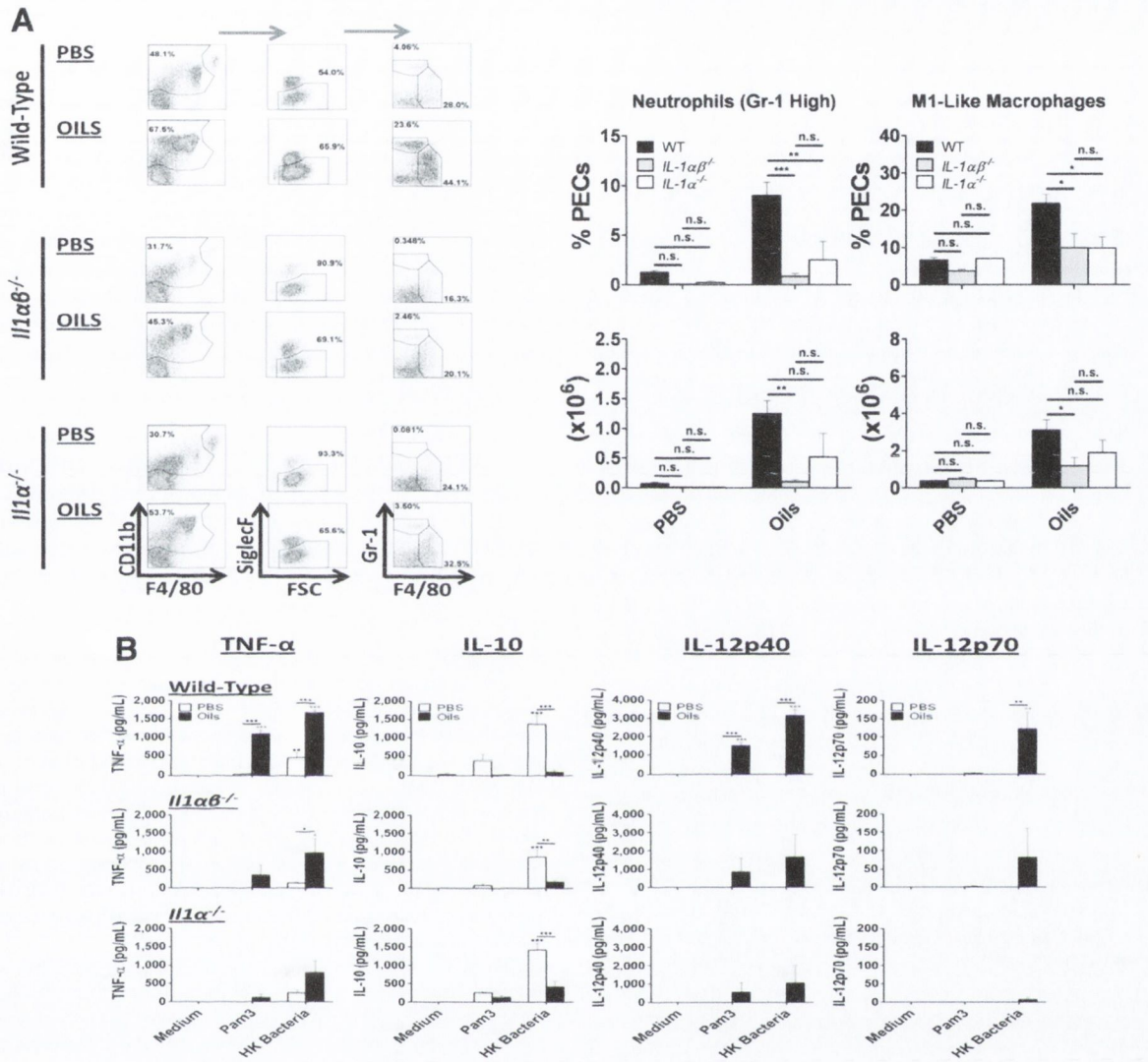

Figure 8—Neutrophil and M1-like macrophage recruitment into the peritoneum in response to endogenous oils is Il-1α–dependent. *A*: Female wild-type C57BL/6, *Il1αβ*$^{-/-}$, and *Il1α*$^{-/-}$ mice were immunized intraperitoneally with PBS or endogenous oils (10 μL/mouse). The mice were killed 24 h later, and neutrophils (CD11b^{inter} F4/80^{-} Gr-1^{high}) and M1-like macrophages (CD11b^{inter} F4/80^{inter} SiglecF^{-}) were identified by flow cytometry. Bar graphs represent mean (+SEM) cell numbers for four mice per group. Versus wild-type for corresponding treatment: *, $P < 0.05$; **, $P < 0.01$; ***, $P < 0.001$. *B*: Female wild-type C57BL/6, *Il1αβ*$^{-/-}$, and *Il1α*$^{-/-}$ mice were immunized as described in *A*. The mice were killed 24 h later, and PECs were restimulated with RPMI, Pam3 (5 μg/mL), or HK *E. coli* (10 *E. coli*: 1 PEC). After 24 h, supernatants were collected and analyzed for the cytokines TNF-α, IL-10, IL-12p40, and IL-12p70 by ELISA. Results are mean cytokine concentrations (+SEM) for four mice per group tested individually in triplicate. Versus PECs from oil-injected mice restimulated with RPMI: *, $P < 0.05$; **, $P < 0.01$; ***, $P < 0.001$. Versus PECs from PBS-injected mice restimulated with RPMI: ■■, $P < 0.01$; ■■■, $P < 0.001$. PECs from oil-injected mice versus PECs from PBS-injected mice for corresponding stimulus: ●, $P < 0.05$; ●●, $P < 0.01$; ●●●, $P < 0.001$. WT, wild-type; n.s., not significant.

resident macrophage population. Comprehensive studies by Ghosn et al. (33) and Spence et al. (32) have recently characterized M1-like and M2-like macrophages and clearly distinguished these coexisting populations using both phenotypic and functional criteria. M1-like macrophages are derived from blood monocytes and are only present at very low levels in the peritoneum of naïve mice. However, following injection with an inflammatory stimulus such as lipopolysaccharide or thioglycolate, M1-like macrophages become the dominant macrophage population in the peritoneum. M2-like macrophages are resident cells and are the dominant macrophage population in the peritoneum of naïve mice. In contrast to M1-like macrophages, however, the M2-like macrophage population is almost

undetectable in the peritoneum following injection with an inflammatory stimulus (32,33). Injection of endogenous oils strongly promoted the recruitment of M1-like macrophages and depletion of M2-like macrophages and furthermore also potently induced neutrophil recruitment into the peritoneum. Indeed, the fact that endogenous oils are capable of mediating infiltration of two of the most important cell populations in obesity-induced inflammation suggests that these oils may play a prominent role in this process.

The remarkable proinflammatory effects of omental oils were evident following injection of as little as 1 μL of the oil. Taking an average adipocyte diameter and volume as 100 μm and $4/3\pi r3$, respectively, we calculate that 1 μL endogenous oils is the equivalent volume released from only approximately 2×10^3 necrotic adipocytes.

Neutrophil recruitment was only marginally reduced in *Nlrp3*$^{-/-}$ mice, and M1-like macrophage recruitment was completely NLRP3-independent, thus ruling out a major role for palmitate-dependent NLRP3 activation in this process. In addition, TLR4 is not required for cell recruitment in response to the oils, thereby eliminating the possibility that signaling through TLR4 by free fatty acids is mediating these effects.

Our data suggest that the immunostimulatory activity of endogenous oils is, in fact, mediated by their physicochemical properties rather than by a specific danger signal. Our hypothesis is that most/all triglycerides are, in fact, immunostimulatory but only those that are released from necrotic adipocytes and are therefore exposed to the immune system will signal danger to the host and mediate inflammation. In support of this hypothesis, endogenous oils derived from subcutaneous adipocytes are as potent as those derived from omental adipocytes of the same obese individual, despite the fact that visceral fat is more closely associated with adverse metabolic outcomes than subcutaneous fat (46–48). Furthermore, there is no significant difference in the fatty acid profile or immunostimulatory activity of endogenous oils derived from MHO, MUO, and lean individuals.

We show that IL-1α is the key cytokine responsible for the inflammatory properties of the endogenous oils. Interestingly, Freigang et al. (49) recently demonstrated that oleic acid–mediated neutrophil recruitment into the peritoneum is IL-1α dependent. Furthermore, it was also reported that oleic acid can drive IL-1α production by primary macrophages in vitro and that this cytokine contributes to atherosclerosis in vivo (49). Given the crucial role of IL-1α in responding to endogenous oils demonstrated in the current study, it is conceivable that oleic acid is also playing a significant role in our model. In contrast to previous studies, the purified endogenous oils shown to be highly immunostimulatory here are derived directly from human WAT and thus differ from preparations from atherosclerotic plaques or from fatty acids that have been dissolved in an organic solvent, mixed with an emulsifying agent, and tested in isolation.

We also demonstrate a crucial role for IL-1α in mediating M1-like macrophage recruitment into the peritoneum, an effect that was not previously reported following injection of oleic acid. While Freigang et al. have demonstrated that a number of fatty acids can promote IL-1α release in vitro, none of these fatty acids was capable of driving IL-1β production from lipopolysaccharide-primed macrophages (49). In contrast, our data show that endogenous oils can induce rapid production of IL-1β in the peritoneum, although this does not appear to be decisive in terms of the local inflammatory response. In addition, we found that endogenous oils can prime PECs for secretion of proinflammatory cytokines, which parallels that seen in the inflamed WAT of obese individuals.

These findings open a new avenue of investigation into the mechanism underlying the pathology associated with obesity-induced inflammation. Moreover, the demonstration of the potent inflammatory properties of oils derived from human adipocytes provides a new concept that will inform further research in this field.

Acknowledgments. The authors thank Andrew Hogan (Obesity Immunology Group, Education and Research Centre, St. Vincent's University Hospital, University College Dublin, Dublin, Ireland) for helpful discussions, Barry Moran (Flow Cytometry Facility, School of Biochemistry and Immunology, Trinity Biomedical Sciences Institute, Trinity College Dublin, Dublin, Ireland) for advice on flow cytometry, and Eamonn FitzPatrick (University College Dublin School of Veterinary Medicine, University College Dublin, Dublin, Ireland) for assistance with Image-Pro Plus 7 software. The authors also thank Nicole Howe and Martin Caffrey (both of the Membrane Structural and Functional Biology Group, School of Biochemistry and Immunology, Trinity Biomedical Sciences Institute, Trinity College Dublin, Dublin, Ireland) for helpful advice and assistance with injecting small volumes of endogenous oils into mice.

Funding. This work was supported by Science Foundation Ireland (SFI) as part of the Immunology Research Centre SFI Strategic Research Cluster (07/SRC/B1144) and has emanated in part from research supported by a research grant from SFI under grant numbers 12/1A/1421. C.L.L. and H.M.R. are supported by a research grant from SFI under grant number 11/PI/1119.

The funders had no role in study design, data collection and analysis, decision to publish, or preparation of the manuscript.

Duality of Interest. No potential conflicts of interest relevant to this article were reported.

Author Contributions. G.A.T. conceived, designed, and performed the experiments; analyzed the data; and wrote the manuscript. C.H.H., E.O., and G.C. performed the experiments and analyzed the data. C.L.L. performed the experiments, analyzed the data, and performed the lipid-extraction procedure. J.O.C. and M.A.C. isolated adipocytes from WAT biopsies and provided WAT sections. L.L. isolated adipocytes from WAT biopsies, provided WAT sections, edited the manuscript, and contributed to discussion. M.C., C.O.F., H.M.R., and D.B.O.S. edited the manuscript and contributed to discussion. J.J.C. performed hematoxylin and eosin staining of WAT sections. K.H.M. performed the lipid-extraction procedure. J.G. performed bariatric surgery and obtained WAT biopsies. S.M.A. provided *Il1α/β*$^{-/-}$ and *Il1α*$^{-/-}$ mice. E.C.L. conceived and designed the experiments, made the initial observation, supervised the project, edited the manuscript, contributed to discussion, and secured funding. E.C.L. is the guarantor of this work and, as such, had full access to all the data in the study and takes responsibility for the integrity of the data and the accuracy of the data analysis.

References

1. Reid J. A new outlook on the action of salicylate. Scott Med J 1957;2:91–96
2. Aguirre V, Uchida T, Yenush L, Davis R, White MF. The c-Jun NH(2)-terminal kinase promotes insulin resistance during association with insulin receptor substrate-1 and phosphorylation of Ser(307). J Biol Chem 2000;275:9047–9054
3. Gao Z, Hwang D, Bataille F, et al. Serine phosphorylation of insulin receptor substrate 1 by inhibitor kappa B kinase complex. J Biol Chem 2002;277:48115–48121
4. Arkan MC, Hevener AL, Greten FR, et al. IKK-beta links inflammation to obesity-induced insulin resistance. Nat Med 2005;11:191–198
5. Shoelson SE, Lee J, Goldfine AB. Inflammation and insulin resistance. J Clin Invest 2006;116:1793–1801
6. Hotamisligil GS, Shargill NS, Spiegelman BM. Adipose expression of tumor necrosis factor-alpha: direct role in obesity-linked insulin resistance. Science 1993;259:87–91
7. Uysal KT, Wiesbrock SM, Marino MW, Hotamisligil GS. Protection from obesity-induced insulin resistance in mice lacking TNF-alpha function. Nature 1997;389:610–614
8. Winer S, Winer DA. The adaptive immune system as a fundamental regulator of adipose tissue inflammation and insulin resistance. Immunol Cell Biol 2012;90:755–762
9. Moro K, Yamada T, Tanabe M, et al. Innate production of T(H)2 cytokines by adipose tissue-associated c-Kit(+)Sca-1(+) lymphoid cells. Nature 2010;463:540–544
10. Wu D, Molofsky AB, Liang HE, et al. Eosinophils sustain adipose alternatively activated macrophages associated with glucose homeostasis. Science 2011;332:243–247
11. Feuerer M, Herrero L, Cipolletta D, et al. Lean, but not obese, fat is enriched for a unique population of regulatory T cells that affect metabolic parameters. Nat Med 2009;15:930–939
12. Lumeng CN, Bodzin JL, Saltiel AR. Obesity induces a phenotypic switch in adipose tissue macrophage polarization. J Clin Invest 2007;117:175–184
13. Weisberg SP, McCann D, Desai M, Rosenbaum M, Leibel RL, Ferrante AW Jr. Obesity is associated with macrophage accumulation in adipose tissue. J Clin Invest 2003;112:1796–1808
14. Weisberg SP, Hunter D, Huber R, et al. CCR2 modulates inflammatory and metabolic effects of high-fat feeding. J Clin Invest 2006;116:115–124
15. Matsuzawa Y, Shimomura I, Nakamura T, Keno Y, Kotani K, Tokunaga K. Pathophysiology and pathogenesis of visceral fat obesity. Obes Res 1995;3 (Suppl. 2):187S–194S
16. Nishimura S, Manabe I, Nagasaki M, et al. CD8+ effector T cells contribute to macrophage recruitment and adipose tissue inflammation in obesity. Nat Med 2009;15:914–920
17. Winer DA, Winer S, Shen L, et al. B cells promote insulin resistance through modulation of T cells and production of pathogenic IgG antibodies. Nat Med 2011;17:610–617
18. Liu J, Divoux A, Sun J, et al. Genetic deficiency and pharmacological stabilization of mast cells reduce diet-induced obesity and diabetes in mice. Nat Med 2009;15:940–945
19. Elgazar-Carmon V, Rudich A, Hadad N, Levy R. Neutrophils transiently infiltrate intra-abdominal fat early in the course of high-fat feeding. J Lipid Res 2008;49:1894–1903
20. Talukdar S, Oh Y, Bandyopadhyay G, et al. Neutrophils mediate insulin resistance in mice fed a high-fat diet through secreted elastase. Nat Med 2012;18:1407–1412
21. Cinti S, Mitchell G, Barbatelli G, et al. Adipocyte death defines macrophage localization and function in adipose tissue of obese mice and humans. J Lipid Res 2005;46:2347–2355
22. Higgins DA, Carlson JR, Van Nest G. MF59 adjuvant enhances the immunogenicity of influenza vaccine in both young and old mice. Vaccine 1996;14:478–484
23. Ramon G. Sur l'augmentation anormale de l'antitoxine chez les chevaux producteurs de serum antidiptherique. Bull Soc Centr Med Vet 1925;101:227–234
24. Freund J, Casals J, Hosmer EP. Sensitization and antibody formation after injection of tubercle bacilli and paraffin oil. Proc Soc Exp Biol 1937;37:509–513
25. O'Connell J, Lynch L, Cawood TJ, et al. The relationship of omental and subcutaneous adipocyte size to metabolic disease in severe obesity. PLoS ONE 2010;5:e9997
26. Bligh EG, Dyer WJ. A rapid method of total lipid extraction and purification. Can J Biochem Physiol 1959;37:911–917
27. Rule DC. Direct transesterification of total fatty acids of adipose tissue, and of freeze-dried muscle and liver with boron-trifluoride in methanol. Meat Sci 1997;46:23–32
28. Phillips CM, Goumidi L, Bertrais S, et al. Complement component 3 polymorphisms interact with polyunsaturated fatty acids to modulate risk of metabolic syndrome. Am J Clin Nutr 2009;90:1665–1673
29. Seubert A, Monaci E, Pizza M, O'Hagan DT, Wack A. The adjuvants aluminum hydroxide and MF59 induce monocyte and granulocyte chemoattractants and enhance monocyte differentiation toward dendritic cells. J Immunol 2008;180:5402–5412
30. Chen CJ, Shi Y, Hearn A, et al. MyD88-dependent IL-1 receptor signaling is essential for gouty inflammation stimulated by monosodium urate crystals. J Clin Invest 2006;116:2262–2271
31. Chen CJ, Kono H, Golenbock D, Reed G, Akira S, Rock KL. Identification of a key pathway required for the sterile inflammatory response triggered by dying cells. Nat Med 2007;13:851–856
32. Spence S, Fitzsimons A, Boyd CR, et al. Suppressors of cytokine signaling 2 and 3 diametrically control macrophage polarization. Immunity 2013;38:66–78
33. Ghosn EE, Cassado AA, Govoni GR, et al. Two physically, functionally, and developmentally distinct peritoneal macrophage subsets. Proc Natl Acad Sci U S A 2010;107:2568–2573
34. Marichal T, Ohata K, Bedoret D, et al. DNA released from dying host cells mediates aluminum adjuvant activity. Nat Med 2011;17:996–1002
35. Kool M, Soullié T, van Nimwegen M, et al. Alum adjuvant boosts adaptive immunity by inducing uric acid and activating inflammatory dendritic cells. J Exp Med 2008;205:869–882
36. Wegner M, Winiarska H, Bobkiewicz-Kozłowska T, Dworacka M. IL-12 serum levels in patients with type 2 diabetes treated with sulphonylureas. Cytokine 2008;42:312–316
37. Surendar J, Mohan V, Rao MM, Babu S, Aravindhan V. Increased levels of both Th1 and Th2 cytokines in subjects with metabolic syndrome (CURES-103). Diabetes Technol Ther 2011;13:477–482
38. Wen Y, Gu J, Li SL, Reddy MA, Natarajan R, Nadler JL. Elevated glucose and diabetes promote interleukin-12 cytokine gene expression in mouse macrophages. Endocrinology 2006;147:2518–2525
39. Matsuzawa Y, Shimomura I, Nakamura T, Keno Y, Tokunaga K. Pathophysiology and pathogenesis of visceral fat obesity. Diabetes Res Clin Pract 1994;24(Suppl.):S111–S116
40. Lee JY, Sohn KH, Rhee SH, Hwang D. Saturated fatty acids, but not unsaturated fatty acids, induce the expression of cyclooxygenase-2 mediated through Toll-like receptor 4. J Biol Chem 2001;276:16683–16689
41. Shi H, Kokoeva MV, Inouye K, Tzameli I, Yin H, Flier JS. TLR4 links innate immunity and fatty acid-induced insulin resistance. J Clin Invest 2006;116:3015–3025
42. Rider P, Carmi Y, Guttman O, et al. IL-1α and IL-1β recruit different myeloid cells and promote different stages of sterile inflammation. J Immunol 2011;187:4835–4843

43. McGillicuddy FC, Harford KA, Reynolds CM, et al. Lack of interleukin-1 receptor I (IL-1RI) protects mice from high-fat diet-induced adipose tissue inflammation coincident with improved glucose homeostasis. Diabetes 2011;60:1688–1698

44. Wen H, Gris D, Lei Y, et al. Fatty acid-induced NLRP3-ASC inflammasome activation interferes with insulin signaling. Nat Immunol 2011;12:408–415

45. Dinarello CA. Biologic basis for interleukin-1 in disease. Blood 1996;87:2095–2147

46. Barzilai N, She L, Liu BQ, et al. Surgical removal of visceral fat reverses hepatic insulin resistance. Diabetes 1999;48:94–98

47. Gabriely I, Ma XH, Yang XM, et al. Removal of visceral fat prevents insulin resistance and glucose intolerance of aging: an adipokine-mediated process? Diabetes 2002;51:2951–2958

48. Klein S, Fontana L, Young VL, et al. Absence of an effect of liposuction on insulin action and risk factors for coronary heart disease. N Engl J Med 2004;350:2549–2557

49. Freigang S, Ampenberger F, Weiss A, et al. Fatty acid-induced mitochondrial uncoupling elicits inflammasome-independent IL-1α and sterile vascular inflammation in atherosclerosis. Nat Immunol 2013;14:1045–1053

Chapter 5

NLRP3 Inflammasome Activation and Cytotoxicity Induced by Particulate Adjuvants

Marie Yang, Claire H.A. Hearnden, Ewa Oleszycka, and Ed C. Lavelle

Abstract

The ability of particulate materials to provoke inflammatory immune responses has been well documented. In the case of endogenous and environmental particulates, these effects can often lead to pathological disorders. In contrast, particulate adjuvants incorporated into vaccines promote immune responses, which in turn provide efficient protection against infectious diseases. In recent years, studies have revealed that the NLRP3 inflammasome plays a key role in particulate-driven inflammation and its associated cytotoxicity. Hence, this chapter covers protocols useful to (1) assess NLRP3 inflammasome activation triggered by particulate adjuvants or materials in mouse bone marrow-derived dendritic cell (BMDCs) differentiated cultures, and (2) measure particle-induced cytotoxicity. More specifically, protocols are described for the preparation and differentiation of BMDCs, their priming and stimulation using particulate NLRP3 agonists such as monosodium urate monohydrate (MSU) and the vaccine adjuvant alum. We then detail protocols to assess particulate-driven cytotoxicity via flow cytometry using annexin V-propidium iodide (PI) and novel dye LIVE/DEAD® aqua stain. General considerations are provided that warn against the use of endotoxin-contaminated particles and emphasize the use of experimental controls. Suggestions are also outlined for further assessment of the immunomodulatory effects of particulate materials in vivo using the mouse peritonitis model.

Key words Particulate adjuvants, NLRP3 inflammasome, Cytotoxicity, IL-1β, Caspase-1

1 Introduction

Exposure to particulate materials can provoke inflammatory responses and exert cytotoxic effects. Chronic environmental exposure to particles such as silica crystals and asbestos fibers, for example, can cause deposits in the lung leading to mesothelioma [1, 2]. Similarly, endogenous particulate stimuli, such as uric acid crystals, resulting from oxidative stress, injury or abnormal metabolism, may lead to the development of inflammatory and autoimmune disorders. On the other hand, particulate vaccine adjuvants, particularly alum salts, play a vital role in the promotion of protective immune responses in subunit vaccines. As part of the innate

Christine M. De Nardo and Eicke Latz (eds.), *The Inflammasome: Methods and Protocols*, Methods in Molecular Biology, vol. 1040, DOI 10.1007/978-1-62703-523-1_5, © Springer Science+Business Media New York 2013

immune system, inflammasomes govern the processing and secretion of caspase-1 and the pro-inflammatory cytokines IL-1β and IL-18. NLRP3 is currently one of the best-characterized inflammasomes. It consists of three main protein components, the Nod-like receptor (NLR)-family protein NLRP3, pro-caspase-1, and the apoptosis-associated speck-like protein containing a CARD (ASC) adapter, which bridges interactions between the former two. Upon inflammasome assembly, auto-activation of caspase-1 results in cleavage of IL-1β, and subsequent secretion of its biologically active form. The NLRP3 inflammasome is unique in its induction, as it is activated by a range of ligands that are highly structurally diverse [3, 4]. Here, we place the emphasis on particulate materials. The first evidence that particulate materials could activate the NLRP3 inflammasome came from investigations on the inflammatory properties of monosodium urate monohydrate (MSU) crystals [5], the etiologic agent of gout. Using primary cultures, silica crystals and asbestos fibers were also shown to activate the NLRP3 inflammasome, and in vivo, mice deficient for NLRP3 exhibited reduced pulmonary inflammation [4, 6]. Subsequently, particles with adjuvant activity such as alum and chitosan [7–9], and likewise poly(lactide-co-glycolide) (PLG) and polystyrene microparticles [10, 11], were also reported as strong activators of the NLRP3 inflammasome. Recent studies subsequently revealed that NLRP3 played a critical role in adjuvant driven cellular immunity [8] and as such, exploitation of this pathway by vaccines may enhance efficacy, thus reinforcing the importance of investigating NLRP3 activation and understanding the underlying mechanisms. Hence, this chapter details methods to assess particle-induced NLRP3 inflammasome activation in mouse bone marrow-derived dendritic cells (BMDCs).

Assessing the effects of particulate compounds on the viability of cells grown in culture is a common predictor of potential toxic effects in target tissues or whole organisms. In this chapter, we thus also describe protocols to measure the cytotoxic responses classically associated with particulate stimuli. There are a number of assays to choose from, which are primarily based on either measurement of metabolic activity or DNA fragmentation or plasma membrane integrity. In this chapter, we describe two easy-to-perform binding assays: (a) an improved methodology based on the classical AnnexinV-PI staining protocol and (b) the use of a novel generation of amine-reactive fluorescent dyes exemplified by LIVE/DEAD® (Invitrogen) aqua stain. Both represent sensitive, reliable, and convenient methods to distinguish viable cells from necrotic or apoptotic cells based on the principle on plasma membrane integrity (*see* **Notes 1–3**).

2 Materials

All solutions should be prepared using deionized water and brought to the appropriate pH using hydrochloric acid or sodium hydroxide. Store all solutions at room temperature (RT) unless otherwise specified.

2.1 Measurement of Inflammasome Activation

2.1.1 Harvesting and Differentiation of Mouse Bone Marrow Cells into BMDCs

1. Mice (*see* **Note 4**).
2. Ice.
3. A cell culture facility equipped with a 37 °C, 5 % CO_2 water-jacketed cell culture incubator, a laminar flow hood, and a centrifuge capable of holding cell culture plates and tubes.
4. Flushing medium: RPMI 1640, supplemented with 8–10 % Fetal Calf Serum (FCS), 2 mM l-glutamine, 100 IU/mL penicillin, and 100 μg/mL streptomycin.
5. Scissors and forceps.
6. Paper towels.
7. 5, 10, and 25 mL serological pipettes.
8. Pipette filler.
9. 70 % Ethanol.
10. Sterile 50 mL centrifuge tubes.
11. 100 μm cell strainers for use with 50 mL centrifuge tubes.
12. 2 and 20 mL syringes.
13. 19G and 27G needles.
14. Solution of 0.88 % Ammonium Chloride (*see* **Note 5**), filter-sterilized using a 0.22 μm syringe filter.
15. 0.4 % Trypan blue solution.
16. Hemocytometer.
17. BMDC differentiation medium (BMDC Medium): RPMI 1640 supplemented with 8–10 % FCS, 2 mM l-glutamine, 100 IU/mL penicillin, and 100 μg/mL streptomycin, and 20 ng/mL of recombinant murine GM-CSF (*see* **Note 6**).
18. 0.02 % EDTA solution.
19. Sterile, non-tissue culture grade 10 cm petri dishes.

2.1.2 Priming and Stimulation of BMDCs

1. 8- or 12-Tip multichannel pipette with a volume of 50–200 μL per tip.
2. Micropipettes.
3. Sterile pipette tips: 2–200 μL volume and 200–1,000 μL volume.
4. 96-well flat-bottom cell culture plates.

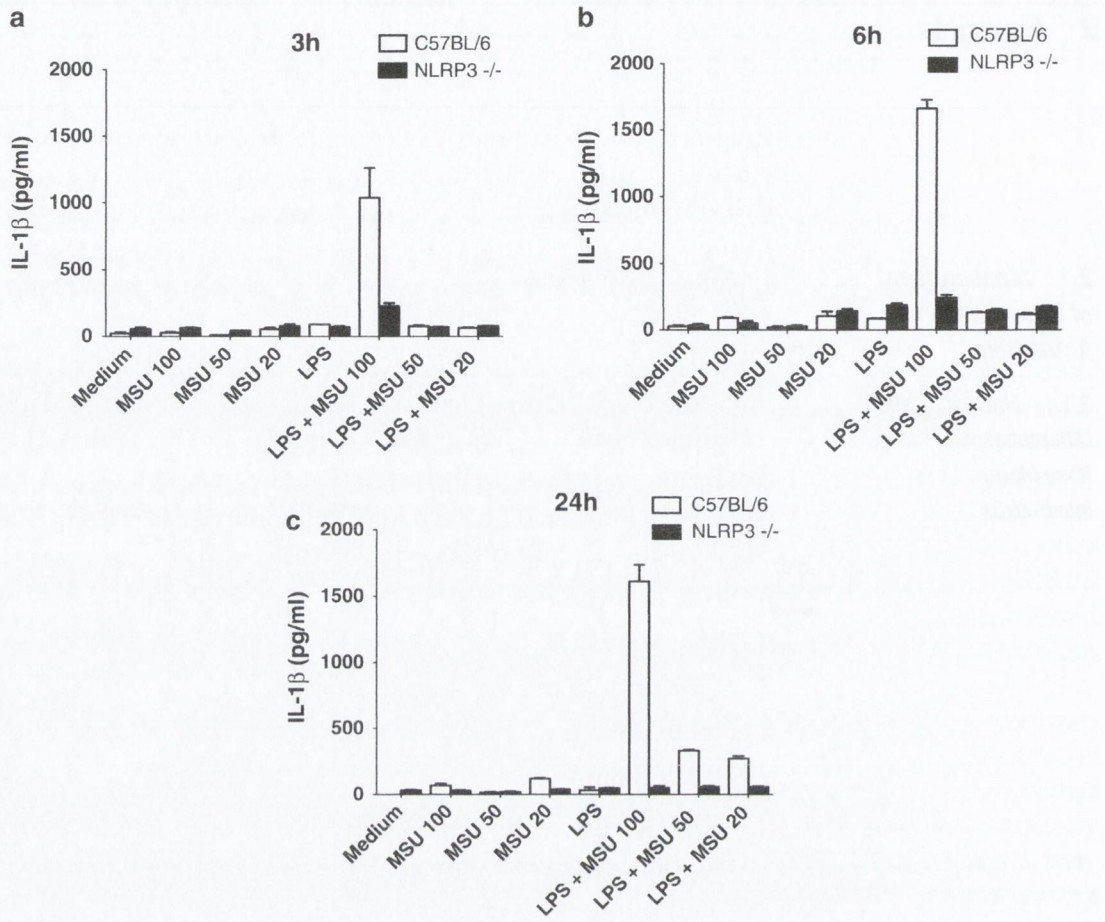

Fig. 1 Kinetics of IL-1β secretion. BMDCs from C57BL/6 and NLRP3–/– mice were left untreated or primed with LPS for 2 h prior to exposure with MSU at 20, 50, and 100 μg/mL for (**a**) 3, (**b**) 6, and (**c**) 24 h. Cell culture supernatants were collected, and IL-1β ELISA (R&D Systems) was performed. All values are represented as mean +/– SD

5. 100 μg/mL *Escherichia coli* K14 ultrapure Lipopolysaccharide (LPS).
6. Inflammasome activators: for example 1 M Adenosine-5′-triphosphate (ATP), 5 mM aluminum hydroxide (e.g., clinically approved Alhydrogel® formulation), or 40 mg/mL of silica.
7. Priming medium: same composition as BMDC differentiation medium (*see* Subheading 2.1.1).
8. 1× sterile PBS.

2.1.3 *ELISA Analysis*

This section emphasizes the use of ELISA kits for the detection of IL-1β (*see* Fig. 1) and IL-18 as these are processed by caspase-1. However, other cytokines such as IL-6, TNF-α, or IL-12 may also be quantified in the culture supernatants (*see* **Note 7**).

1. High binding flat-bottomed ELISA plates.
2. 1× PBS: 80.0 g NaCl, 14.4 g Na_2HPO_4, 2.4 g KH_2PO_4, 2.0 g KCl. Add deionized H_2O up to 10 L and pH to 7.2 with HCl.

3. ELISA wash buffer: 1× PBS with 0.05 % Tween-20.
4. ELISA dilution buffer: 1× PBS with 1 % BSA.
5. ELISA blocking buffer: 1× PBS with 3 % BSA.
6. Stop solution: 2N sulfuric acid.
7. 5, 10, and 25 mL serological pipettes.
8. Pipette filler.
9. Paper towel.
10. Washbasin or 96-well automatic microplate washer.
11. 8- or 12-tip multichannel pipette with a volume of 50–200 µL per tip.
12. 2–200 µL volume pipette tips.
13. Standard, capture antibody, detection biotin-labelled antibody and avidin-HRP conjugate for cytokine/chemokine of choice.
14. HRP substrate *o*-Phenylenediamine (dihydrochloride) (OPD) solution: 50 mL phosphate citrate buffer (10.19 g anhydrous citric acid, 14.6 g Na_2HPO_4, make up to 1 L with deionized water, pH 5), 20 mg *o*-Phenylenediamine tablet (Sigma), 14 µL Hydrogen peroxide added just before use.
15. 96-well microplate reader.

2.1.4 Western Blot Analysis

1. BMDC differentiated cultures, as described in Subheading 3.1.1.
2. Stimulation medium: RPMI 1640 medium containing less than 5 % FCS.
3. 6- and 12-well tissue culture plates.
4. Micropipettes.
5. Pipette tips: 2–200 µL volume and 200–1,000 µL volume.
6. Toll-like Receptor (TLR) ligands, e.g., LPS at 100 ng/mL (to be used at a final concentration of 1 ng/mL with BMDC cultures).
7. 1× PBS.
8. Particulates of choice: for example aluminum hydroxide (e.g., clinically approved Alhydrogel® formulation) or biodegradable microparticles (e.g., silicon, PLGA).
9. 15 mL centrifuge tubes.
10. Strataclean® beads (Agilent).
11. Vortex.
12. 1.5 mL tubes.
13. Heating block.
14. 15 % polyacrylamide gel (*see* **Note 8**).
15. 1× Laemmli sample buffer: 62.5 mM Tris–HCl, pH 6.8, 25 % glycerol, 2 % SDS, 0.01 % Bromophenol Blue, 5 % Beta-mercaptoethanol (or alternatively use the Biorad Laemmli Sample buffer (Biorad) with the addition of 5 % beta-mercaptoethanol).

16. Western blot transfer buffer: 25 mM Tris, 192 mM glycine, 20 % methanol v/v.
17. Polyvinylidene Difluoride (PVDF) membrane (*see* **Note 9**).
18. Prestained protein molecular weight markers (*see* **Note 10**).
19. Tris-buffered Saline with Tween-20 (TBST): TBS (25 mM Tris, 150 mM NaCl, 2 mM KCl, pH 7.4) and 0.1 % Tween-20.
20. Blocking solution: 5 % nonfat milk in TBST.
21. Rabbit anti-mouse caspase-1 primary antibody (Santa Cruz Labs).
22. HRP-conjugated anti-Rabbit IgG (Jackson ImmunoResearch Lab).
23. Western Blot Stripping buffer (*see* **Note 11**).
24. Goat anti-mouse IL-1β (R&D Systems).
25. HRP-conjugated anti-Goat (Jackson ImmunoResearch Lab).
26. Enhanced chemiluminescence (ECL) substrate (*see* **Note 12**): Millipore ECL detection reagent A + B solutions or home-made reagents A and B mixed at a ratio of 1:1. For reagent A: 0.5 mL luminal, 0.22 mL *p*-coumaric acid, 5 mL 1 M Tris–HCl, pH 8.5, make up to 50 mL with distilled water. For reagent B: 5 mL 1 M Tris–HCl, pH 8.5, 30.5 µL 30 % H_2O_2, make up to 50 mL with deionized water.
27. X-ray films.
28. Developer machine with developing and fixation solutions.
29. Dark room.

2.1.5 Determination of ASC Oligomerization Using Confocal Bioimaging of Live THP-1 Cells

1. THP-1-ASC-GFP cell line [12].
2. DMEM High Glucose Glutamax™ (Invitrogen) medium supplemented with 10 % FCS, 100 IU/mL penicillin and 100 µg/mL streptomycin.
3. DMEM medium containing phorbol 12-myristate-13-acetate (PMA) at 0.5 mM.
4. 35 mm cover glass bottom culture dishes.
5. Hoechst 33342 (for nuclear staining) and CellMask™ deep red (for plasma membrane staining).
6. Confocal microscope equipped with temperature and CO_2-controlled chamber.
7. Particulate stimuli of choice, e.g., aluminum hydroxide (e.g., clinically approved Alhydrogel® formulation), biodegradable particles (e.g., silicon or PLGA).
8. Imaging software for further image processing, e.g., Image *J* software (National Institute of Health, USA).

2.2 Measuring Cytotoxicity

2.2.1 Annexin-Binding Assay in BMDC Cultures

1. BMDC differentiation medium, as described in Subheading 2.1.1.
2. BMDC differentiated cultures (*see* **Note 13** and Subheading 3.1.1)
3. T-175 tissue culture flasks.
4. 96-well or 24-well tissue culture plates (*see* **Note 14**).
5. Hemocytometer or counting chamber.
6. Annexin V-FITC solution: e.g., Promega or homemade (*see* **Notes 15** and **16**) at a stock concentration of 2.5 mg/mL.
7. PI stock solution: we recommend preparing a 1 mg/mL stock solution in PBS and storing at 4 °C protected from light for up to 1 year. Use at a final concentration of 10 μg/mL (e.g., 1 μL in 100 μL of sample), just prior to analysis.
8. 10× concentrated annexin V-binding buffer: 10 mM of HEPES-NaOH, pH 7.4, 150 mM NaCl, 1.5 mM KCl, 1 mM $MgCl_2$, 1.8 mM $CaCl_2$. Store at 4 °C for up to 1 year. Prepare 1× annexin V-binding buffer by making up a 1:10 dilution with distilled water just prior to use (*see* **Note 17**).
9. Necrosis/apoptosis-inducing reagents, e.g., actinomycin-D, cycloheximide, staurosporine, or others, diluted at a concentration deemed optimal.
10. LIVE/DEAD® (Invitrogen) fixable aqua dead cell dye.
11. Cell fixative (*see* **Note 18**).
12. 1× PBS solution.
13. FACS buffer: PBS buffer supplemented with 2 % FCS and 0.05 % sodium azide.
14. FACS analysis tubes compatible with flow cytometer.
15. Flow cytometer and analytical software, e.g., FlowJo® (TreeStar).

3 Methods

3.1 Quantification of Inflammasome Activation

3.1.1 Murine Bone-Marrow Derived Dendritic Cell Differentiation

Perform all procedures in a laminar flow hood to maintain a sterile environment at all times. All animal procedures must be carried out by adequately trained staff and comply with rules set forth by your designated animal facility. Use BMDC medium, PBS and EDTA solutions, pre-warmed to 37 °C unless otherwise stated.

1. **Day 0:** Sacrifice mice by a method in accordance with your institute's animal regulations.
2. Using sterile scissors, cut away as much fat and muscle as possible from the femur and tibia and place the leg in a 50 mL tube containing flushing medium on ice.
3. Transfer the bones with medium into a petri dish and separate femurs from the tibiae.

4. Fill a 20 mL syringe with flushing medium, attach a 27G needle and flush the bone marrow through the bones into a fresh sterile petri dish (*see* **Note 19**).
5. Break up cell aggregates by passing the cells repeatedly through a 20 mL syringe equipped with a 19G needle.
6. Transfer cells to a 50 mL tube and centrifuge at 300 × *g* for 5 min.
7. Pour off the supernatant and resuspend the cell pellet in 1 mL of ammonium chloride solution to lyse red blood cells. Leave the ammonium chloride solution on the cells for 2 min at RT and then fill the tube with flushing medium (~ 40 mL) and mix by inversion.
8. Centrifuge the tubes at 300 × *g* for 5 min.
9. Pour off the supernatant and resuspend the cell pellet in 10 mL of BMDC medium.
10. Count the cells (*see* **Note 20**) and adjust to the required concentration with BMDC medium (*see* **Note 21**).
11. Differentiate the cells into DCs in T-175 tissue culture flasks: add between 30 and 38 mL of cell suspension at 1×10^6 cells/mL per flask and incubate at 37 °C, 5 % CO_2 for 3 days.
12. **Day 3**: Feed cells by adding 30 mL of pre-warmed BMDC medium, per flask and incubate at 37 °C, 5 % CO_2 for another 3 days.
13. **Day 6**: For each tissue culture flask, fill two 50 mL tubes with 10 mL of pre-warmed BMDC medium.
14. Carefully take the flasks out of the incubator & discard the supernatant by pipetting gently.
15. Add 30 mL of sterile pre-warmed PBS to each flask. Gently agitate the flask by moving contents from side-to-side. PBS should appear cloudy as loosely adherent cells become detached.
16. Gently pipette the PBS solution over the adherent/semi-adherent cells (flushing) approximately 10 times.
17. Transfer the PBS containing cells from the flask to one of the 50 mL tubes containing 10 mL BMDC medium.
18. Add 25 mL of pre-warmed EDTA to each flask and incubate at 37 °C for 10 min.
19. Gently agitate the flask, flush the cells 5×, as in **steps 15** and **16** above, and transfer the cell suspension into the second 50 mL tube containing 10 mL BMDC medium.
20. Centrifuge both 50 mL tubes at 300 × *g* for 5 min, pour off the supernatant, and then pool and resuspend the cell pellets in 10 mL of BMDC medium.

21. Count the cells using a 1:10 dilution (*see* **Note 20**) and adjust the cells to a concentration of 7×10^5 cells/mL (for mouse strains BALB/c, C3H/HeN, or C3H/HeJ) or 4.5×10^5 cells/mL (for mouse strain C57BL/6) using BMDC medium.
22. Continue to differentiate the cells into DCs in a T-175 tissue culture flask by adding between 30 and 38 mL of cell suspension per flask and incubating at 37 °C, 5 % CO_2 for a further 2 days.
23. **Day 8**: Feed cells by adding 30 mL of pre-warmed BMDC medium per flask and incubate at 37 °C, 5 % CO_2 for a further 2 days.
24. **Day 10**: Remove loosely adherent cells by gentle repeat pipetting off the medium and then transfer to a 50 mL tube and centrifuge at $300 \times g$ for 5 min.
25. Pour off the supernatant and pool pellets from each tube into 10 mL of BMDC medium.
26. Count cells using a 1:10 dilution (*see* **Note 20**) and adjust the cells to a concentration of 6.25×10^5 cells/mL if assessing cytokine responses, or $1–2 \times 10^6$ cells/mL if using cells for Western blot or FACS analysis, using BMDC medium.
27. Plate cells in round bottomed 96-well plates for cytokine analysis (200 µL/well) or 12-well/24-well plates (1–2 mL/well) for protein/FACS analysis and incubate at 37 °C, 5 % CO_2 overnight.
28. **Day 11**: Stimulate cells as required (*see* **Notes 22** and **23** and Subheading 3.1.2).

3.1.2 Priming and Stimulation of BMDCs

1. Prime cells using TLR agonists (e.g., LPS at 1 ng/mL final concentration) for at least 2 h prior to incubation with particulate materials.
2. Activate the inflammasome with particulates as outlined in **item 6** of Subheading 2.1.2 at the concentrations indicated.
3. Stimulate cells in triplicate and include triplicate blank wells and all relevant positive and negative controls.
4. After a 24 h incubation period, centrifuge the cells at $300 \times g$ for 5 min and collect the supernatant from the plates for ELISA analysis, according to manufacturer's instructions.

3.1.3 ELISA Analysis of BMDC Supernatants

ELISA should be carried out according to the manufacturer's instructions. Detection of specific cytokines or chemokines requires different concentrations of antibodies, blocking solutions and different incubation times. A general procedure is outlined below:

1. Coat the 96-well plate: dilute capture antibody in coating buffer as per manufacturer instructions and transfer 40–100 µL to each well of a high affinity, protein-binding ELISA plate.

2. Seal plate to prevent evaporation and incubate at 4 °C overnight.
3. Bring the plate to RT, flick off the capture antibody solution and wash plate 3× with ELISA wash buffer (*see* Subheading 2.1.3).
4. Block nonspecific binding sites by adding 200 µL/well of blocking solution to each well.
5. Seal plate and incubate at RT for 1 h.
6. Wash plate 3× with ELISA wash buffer and firmly blot plate against clean paper towels.
7. Dilute standards and samples to desired concentrations in ELISA dilution buffer and add 40–100 µL/well to the plate.
8. Seal the plate and incubate at RT for 2 h or at 4 °C overnight.
9. Wash plate 5× with ELISA wash buffer and firmly blot plate against clean paper towels.
10. Dilute biotin-labelled detection antibody in ELISA dilution buffer, as per manufacturer instructions. Add 40–100 µL/well of diluted antibody to plate.
11. Seal the plate and incubate at RT for 1 h.
12. Wash plate 3× with ELISA wash buffer and firmly blot plate against clean paper towels.
13. Dilute Avidin-HRP conjugate or other enzyme conjugate in ELISA dilution buffer, as per manufacturer instructions. Add 40–100 µL/well onto plate.
14. Seal the plate and incubate at RT for 30–60 min.
15. Wash plate 5× with ELISA wash buffer and firmly blot plate against clean paper towels.
16. Transfer 40–100 µL/well of HRP substrate solution into plate and incubate at RT for 5–30 min, while monitoring color development.
17. Stop color development reaction by adding 20–50 µL/well of stop solution.
18. Read the optical density (OD) for each well with a microplate reader set to 492 nm.

3.1.4 Western Blot Analysis

Western blot analysis should be carried out when BMDCs have been differentiated appropriately and plated on day 10 (*see* Subheading 3.1.1).

1. Plate differentiated BMDCs in a 12-well plate at a density of $0.5–1 \times 10^5$ cells/mL (1 mL/well) in BMDC stimulation medium containing less than 5 % FCS (*see* **Notes 24** and **25**) and incubate at 37 °C, 5 % CO_2 overnight.

2. On the following day, carefully remove and discard 0.5 mL of supernatant from each well. If using 6-well plates, remove 0.75–1.0 mL/well.
3. Prime with TLR ligands (e.g., LPS at final concentration of 1 ng/mL for BMDCs) in 10–20 μL of BMDC stimulation medium containing no more than 5 % of FCS and incubate for 3 h at 37 °C, 5 % CO_2.
4. Add particulates (20–40 μL/well of particulates for a maximum of 250 μL/well) to a microplate at optimized concentrations. Incubate for 3, 6, 18 and 24 h (*see* **Note 26**) for detection of cleaved caspase-1 and/or IL-1β.
5. Collect supernatant using a micropipette with sterile tips into 1.5 mL centrifuge tubes. Spin tubes at 500×*g* for 2 min to remove any cell debris.
6. Add 10 μL of Strataclean® beads/mL of supernatant collected. Make sure Strataclean® beads are fully dispersed in solution by gently vortexing. The solution color should be white.
7. Vortex tubes for 15 s and let tubes stand for 2–3 min. Repeat three times.
8. Centrifuge tubes in a microcentrifuge at 12,000×*g* for up to 10 min (or until the beads form a distinct depot at the bottom of the tube).
9. Carefully remove the supernatant. Resuspend the beads in a small volume of 1× Laemmli sample buffer (no more than 50–60 μL if you started with 1 mL of supernatant) and vigorously pipette up and down 6×.
10. Heat tubes at 95 °C for a maximum of 10 min.
11. Spin microcentrifuge tubes at 12,000×*g* for up to 10 min.
12. Load 20–30 μL/well of each sample and 5–10 μL/well of prestained markers to a 15 % polyacrylamide gel.
13. Run gel at 100–110 V for 1–2 h until the migration front reaches about ¾ of the way down the gel (*see* **Note 27**).
14. Prepare a 20 % MeOH Western blot transfer buffer and proceed to either wet or dry transfer—this is a personal preference (*see* **Note 28**).
15. Once transfer has completed, block the membrane(s) with 5 % nonfat milk in TBST, for 30 min at RT with agitation.
16. Wash membrane 3× for 5 min with TBST at RT with agitation.
17. Incubate PVDF membrane with rabbit anti-mouse caspase-1 primary antibody at 1:1,000 dilution in 5 % nonfat milk in TBST, overnight at 4 °C.
18. Wash membrane 5× for 3 min using TBST with agitation at RT.

19. Incubate membrane with HRP-conjugated anti-Rabbit antibody at 1:10,000 dilution in 5 % nonfat milk in TBST, for 2 h at RT.
20. Wash membrane 6× for 3 min with TBST at RT with agitation.
21. Proceed to ECL reaction using in-house solutions or Millipore ECL detection reagent A + B solution (*see* **item 26** of Subheading 2.1.4). Incubate membrane in solution for 2 min then blot dry.
22. Expose membrane to films in dark room and run through developer machine.
23. If probing for IL-1β: strip membrane for a maximum of 10 min using Western Blot Stripping buffer or as instructed by manufacturer.
24. Wash membrane 3× for 5 min with TBST at RT with agitation.
25. Incubate membrane with goat anti-mouse IL-1β at 1:1,000 dilution in 5 % nonfat milk in TBST, overnight at 4 °C.
26. Wash membrane 5× for 3 min with TBST at RT with agitation.
27. Incubate PVDF membrane with HRP-conjugated anti-Goat at 1:20,000 dilution in 5 % nonfat milk in TBST, for 2 h at RT.
28. Wash membrane 6× for 3 min with TBST at RT with agitation.
29. Proceed to ECL reaction using in-house solutions or Millipore ECL detection reagent A + B solution (*see* **item 26** of Subheading 2.1.4). Incubate membrane in solution for 2 min then blot dry.
30. Expose membrane to films in dark room and run through developer machine (*see* Fig. 2 [10]).

3.1.5 Determination of ASC-Activation Using Confocal Bio-imaging of Live THP-1 Cells

The THP1-ASC-GFP cells represent an ideal in vitro system to study and observe, in real time or by time-lapse imaging, the effect of a broad range of stimuli on the behavior of ASC in live cells and the consequences of ASC oligomerization on cell viability [13].

1. Pellet exponentially growing THP-1–ASC–GFP cells by centrifugation at 300 × *g* for 5 min.
2. Resuspend the cells in fresh DMEM medium containing phorbol 12-myristate-13-acetate (PMA) (0.5 mM) at a density of 5×10^5 cells/mL. Pipette 1 mL of the suspended cells into 35 mm cover glass bottom culture dishes and allow cells to adhere for 2 h.
3. Remove the PMA-containing medium and replace it with fresh DMEM medium without PMA (*see* **Note 29**).
4. If nuclear and/or plasma membrane staining is desired, stain cells with Hoechst 33342 and/or CellMask™ Red plasma membrane stains according to the manufacturer's instructions.

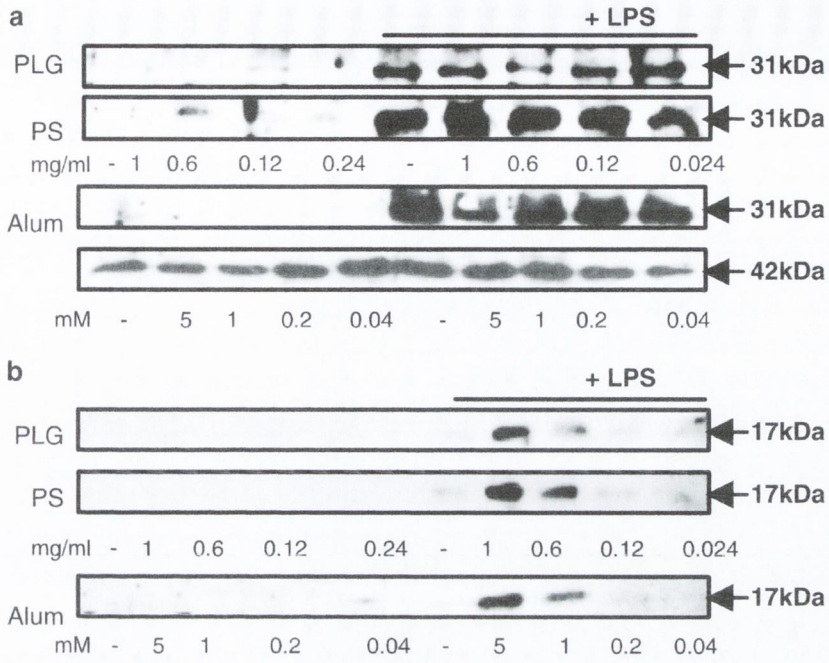

Fig. 2 Western blot analysis. BMDC cultures were incubated with particles alone (poly(lactide-co-glycolide) (PLG), polystyrene (PS) microparticles, or Alhydrogel®), LPS alone, or LPS + particles for period of 24 h. (**a**) Pro-IL-1β (31 kDa) and β-actin (42 kDa) in cell lysates. (**b**) Mature IL-1β (17 kDa) in supernatants

5. Place the culture dish in the microscope sample chamber maintained at 37–38 °C and 5 % CO_2 (*see* **Note 30**).
6. Stimulate the cells with LPS (1–5 μg/mL) or other pro-inflammatory stimuli. Ten minutes after LPS stimulation, start recording images from the GFP, Hoechst, and other fluorescence markers simultaneously every 10 s for 30–60 min (*see* **Note 31**).
7. Add particulate stimuli (e.g., MSU, alum salts) to petri dish at concentrations deemed optimal and continue recording (*see* **Note 32**).

3.2 Measuring Cytotoxicity

3.2.1 BMDC Cultures

1. Grow and differentiate BMDC cultures until day 10, as described in Subheading 3.1.1.
2. On day 10, take out T-175 tissue culture flask and verify cell viability and morphology under a light microscope (*see* **Note 33**).
3. Gently pipette the BMDCs cultures up and down to detach cells, as described in Subheading 3.1.1. BMDCs should detach from the bottom of the flask.
4. Transfer the cell suspension into 50 mL tubes and centrifuge at 300 × *g* for 5 min.
5. Discard supernatant and resuspend cell pellet in 5 mL of BMDC medium and count the cells (*see* **Note 20**).

6. Plate 5–10 × 10^3 cells per well in a 96-well plate (or 5–10 × 10^4 cells per well in a 24-well plate) and incubate overnight at 37 °C, 5 % CO_2 to allow cells to adhere.
7. Stimulate BMDCs cultures with particulates at various concentrations in order to assess dose–response effects. Use untreated BMDCs as a negative control and BMDCs stimulated with apoptosis- or necrosis-inducing agents as positive controls (*see* **Note 34**).
8. Incubate cells with particulates (*see* **Notes 35** and **36**) for a predefined period of time, e.g., 3, 6, and 24 h at 37 °C (*see* **Note 37**).

3.2.2 AnnexinV-PI Binding Assay

1. Centrifuge treated BMDC single cell suspension at 300 × *g* for 5 min, discard supernatants and resuspend in 200 µL binding buffer/sample (at no more than 2 × 10^6 cells/mL).
2. Incubate BMDC samples with 1 µg/mL Annexin V-FITC (or at the concentration deemed optimal for your setup) for 5 min.
3. Centrifuge at 500 × *g* for 5 min, discard supernatant and resuspend in 200 µL of binding buffer.
4. Transfer each sample into appropriately labelled FACS tubes.
5. Add PI directly into FACS tubes at a final concentration of 1 µg/mL, just prior to the acquisition of samples on the flow cytometer (*see* **Note 38**).
6. Analyze samples by flow cytometry within 1 h (*see* **Note 39**).

3.2.3 LIVE/DEAD® Aqua Staining

1. Bring one vial of LIVE/DEAD® aqua fluorescent reactive dye (*see* **Note 40**) and one vial of anhydrous DMSO (*see* **Note 41**) to RT.
2. Add 50 µL of anhydrous DMSO to one vial of reactive dye, as per manufacturer instructions (*see* **Note 42**). Mix well and visually confirm that the dye has completely dissolved.
3. At the end of the BMDC stimulation period with particulate compounds, centrifuge microplate at 300 × *g* for 5 min.
4. Discard the supernatant and resuspend in 200 µL/well of PBS for 96-well plate.
5. Count BMDCs and adjust density with PBS such that cell density is no more than 1 × 10^6 cells/mL, as per manufacturer instructions.
6. Add 1 µL of the reconstituted fluorescent reactive dye to 1 mL of the BMDC suspension and mix well.
7. Incubate on ice for 15–20 min, protected from light.
8. Centrifuge the cells at 300 × *g* for 5 min, discard supernatants and resuspend in 200 µL/well of PBS.
9. If fixation is required, carefully remove supernatant and add 100–200 µL/well of cell fixative (*see* **Notes 43** and **44**).
10. Incubate at RT for 10 min.

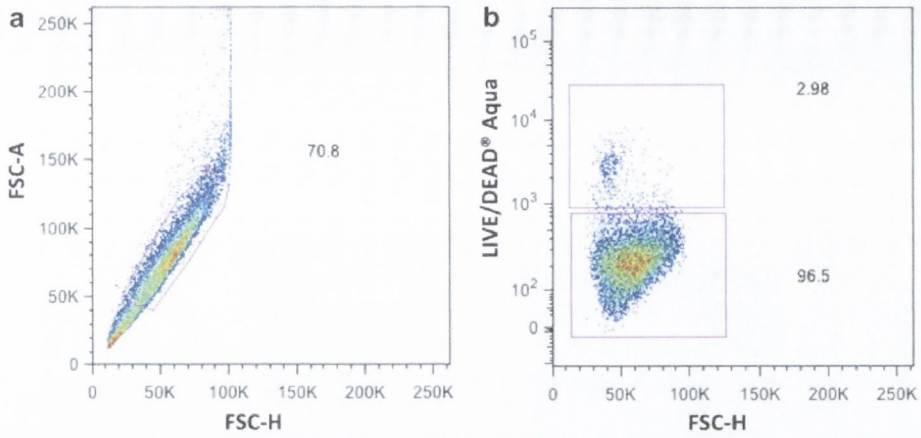

Fig. 3 Common gating strategy to remove doublets and dead cells in the cell analysis. (**a**) The first histogram uses the measurements of forward scatter area (FSC-A) and forward scatter height (FSC-H) to determine the single cells (*pink polygon*) from the doublets. (**b**) Following the staining reaction with LIVE/DEAD aqua, the cells were fixed in BD Cytofix/Cytoperm™ and analyzed by flow cytometry. The live cell population (*lower panel*, 96.5 %) is easily distinguished from the killed population (*upper panel*, 2.98 %)

11. Centrifuge the cells at 300 × *g* for 5 min, discard supernatant and wash cells once with 200 µL/well of FACS staining buffer.
12. Analyze samples by flow cytometry within 48 h using an analyzer equipped with a violet laser (*see* Figs. 3 and 4, and **Note 45**).

4 Notes

1. Annexin V-PI staining is a convenient way to discriminate early apoptosis from late apoptosis and necrosis. Early apoptotic cells express phosphatidylserine (PS) on the outer leaflet of the plasma membrane and PS can thus be stained with labelled annexin V. In contrast, late apoptotic cells and necrotic cells lose their cell membrane integrity and are permeable to vital dyes, such as PI.
2. The compound 7-amino-actinomycin (or 7-ADD) can be used as a DNA marker—it forms stable complexes with double strand DNA—in lieu of PI, at a concentration of 50 mg/mL, i.e., 20 µL/100 µL sample, e.g., use 1×10^6 cells in a 100 µL experimental sample. The maximum absorption of the 7-AAD/DNA complex is compatible with the blue excitation wavelength of 488 nm for cytometers fitted with an argon laser. The peak fluorescence emission in the deep red band (635–675 nm) of the 7-AAD/DNA complex permits optimal use of this probe when it is combined with Fluorescein Isothiocyanate conjugated antibodies (FITC) and R Phycoerythrin (PE). Indeed, in contrast to PI, the 7-AAD/DNA complex has a reduced overlapping emission spectrum with FITC and PE.
3. Regarding the performance of the LIVE/DEAD® aqua stain, the manufacturer states that the difference in intensity between live and dead cell population is greater than 50-fold.

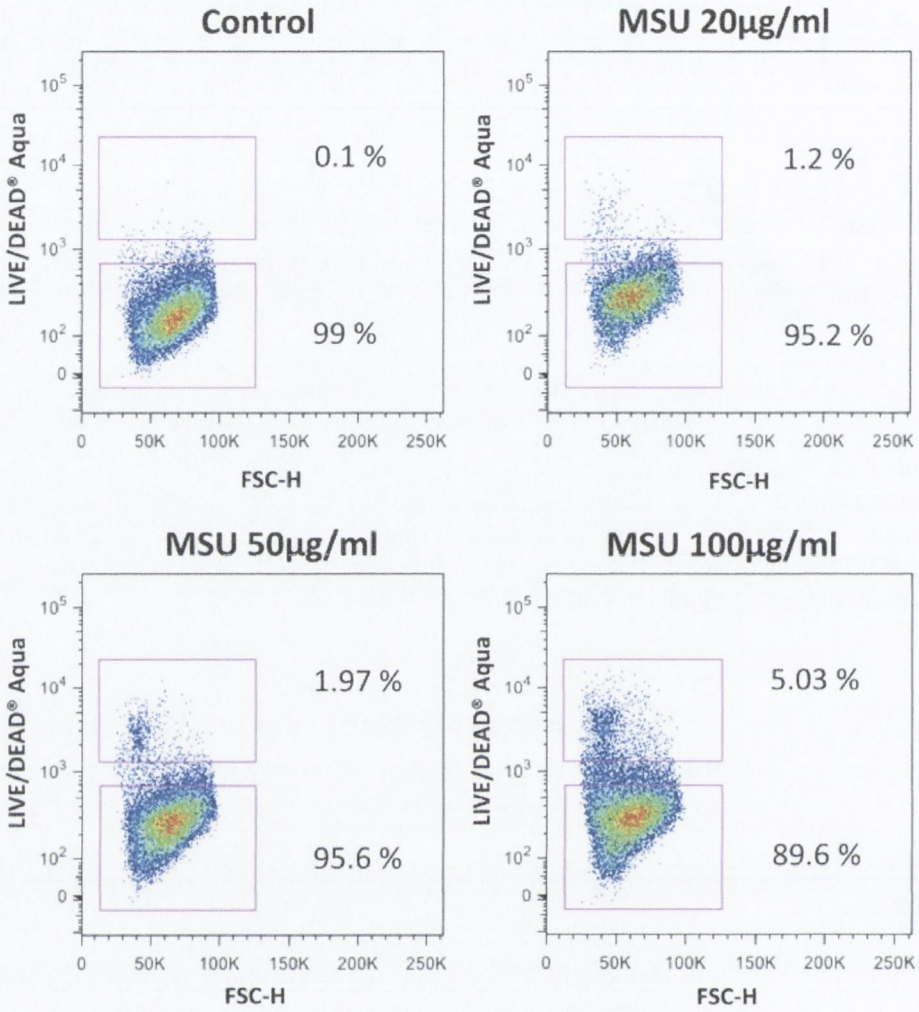

Fig. 4 Dose–response analysis of MSU-induced cell toxicity in BMDC cultures (C57BL/6) after 6 h incubation. MSU was used at concentrations ranging from 20 to 100 µg/mL

4. Depending on the age and strain of mice, and on the efficiency of the procedure, one mouse typically generates up to $20–40 \times 10^6$ BMDCs.
5. Alternatively, a commercially available solution of red blood cell (RBC) lysis buffer can also be used.
6. As a more economical alternative to the use of commercial recombinant mouse GM-CSF, prepare BMDC differentiation medium supplemented with 20 % conditioned medium from mouse GM-CSF producing J558 cells [14].
7. We recommend that other cytokines, e.g., IL-6, TNF-α, and IL-12 concentrations be measured to ensure that NLRP3 inflammasome activation is particle-driven and specific, and that chemical inhibitors are not modulating inflammasome-independent cytokines.

8. The apparent molecular masses of the pro- and cleaved forms of IL-1β are approximately 31 kDa and 17 kDa respectively, in SDS-PAGE under reducing conditions, while the caspase-1 precursor and cleaved forms have apparent molecular weights of approximately 45 kDa and 10 kDa, respectively. In order to obtain optimal separation between these two proteins and their cleaved form, we found that 15 % polyacrylamide gels were optimal.
9. The ability of membranes to bind proteins varies greatly depending on the amounts of protein present in the samples, the incubation times and the potential loss of proteins following incubation with different detergents or blocking agents. We compared the quality of the immunoblots using PVDF vs. nitrocellulose membrane using the protocol described herein and we consistently found that PVDF membrane performed better than nitrocellulose, particularly for the immunodetection of cleaved caspase-1. Note that PVDF membranes must be hydrated in 100 % methanol and then rinsed with deionized water before being placed in the transfer buffer to equilibrate.
10. We recommend the use of a low range prestained protein ladder, e.g., 3.4–100 kDa. It will serve the double purpose of confirming the apparent molecular weight of your protein bands and provide an indication on the efficiency of your protein transfer from the gel onto the membrane.
11. Our lab determined that the Restore™ (or Restore™ PLUS) Western blot stripping buffer from Thermo Scientific performed particularly well.
12. An alternative to ECL detection is the use of infrared detection (Odyssey®).
13. This chapter details materials and methods for determining the cytotoxic effects of particulate materials on BMDC cultures, but a similar approach is applicable to other antigen presenting cells, such as macrophages. Other cell types, doses and concentrations will require prior optimization. For titration procedures, detailed protocols have been described elsewhere [15].
14. Depending on the amount of particulate materials available for use, a plate format or 2 mL reaction tubes may be used.
15. A recent study described a detailed step-by-step procedure to express and purify milligram amounts of "home-made" annexin V within 3 days [16]. The method explains the expression of recombinant annexin V in competent DH5α *E. coli* bacteria, its purification using NI-NTA agarose, and its conjugation to the FITC fluorochrome. More specifically, human annexin V was cloned into the bacterial expression vector pProEx.Htb which encodes ampicillin resistance and incorporates an

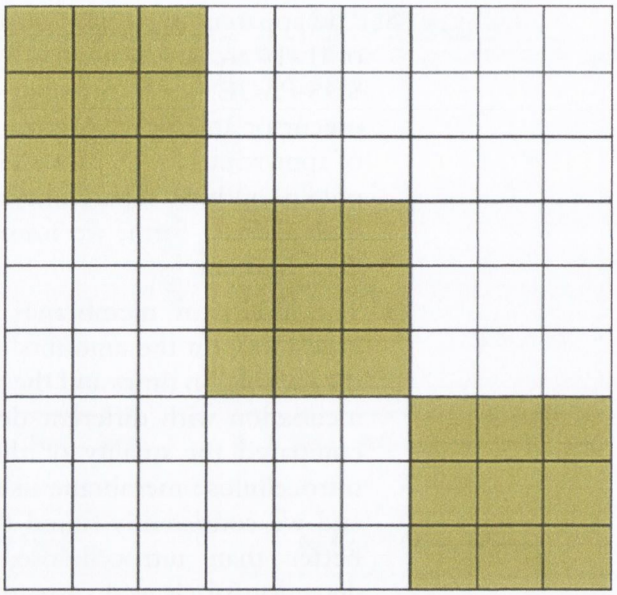

Fig. 5 Hemocytometer chamber and cell counting strategy

N-terminal poly-histidine tag. The resulting plasmid (i.e., pProEx.Htb.annexin V) is made freely available upon request to investigators working in nonprofit organizations.

16. General considerations for a successful Annexin-V binding assay: cells should *not* be fixed or permeabilized (e.g., paraformaldehyde or methanol) and similarly, trypsinization or scraping to detach cells should be carefully considered as this may damage the plasma membrane, resulting in false positives [16].
17. A recent study [16] determined that calcium was required at a concentration of 1–3 mM for optimal binding of annexin V to PS. For most cell types, a concentration of 1.8 mM calcium is ideal.
18. Cell fixative: either BD Cytofix/Cytoperm™ solution or a solution of 0.4 % paraformaldehyde may be used.
19. When flushing the femur and tibiae through with medium using a 27G needle, the flushing liquid coming out should be a red color and if flushed through correctly the bone should become clear/white when all the cells are flushed out. To ensure all cells are removed, flush each bone through from both ends.
20. A 1:10 dilution is usually adequate for cell counting, i.e., 90 µL of trypan blue solution and 10 µL of cells, mix well and transfer to a hemocytometer slide. Count the cells as follows: count three larger squares (of 9 smaller squares each, *see* Fig. 5), get the average of the three and calculate the number of cells per mL using the following formula:

$$\text{Cells/mL} = \text{average cell count} \times \text{dilution factor } (10) \times 10^4$$

21. Our lab has determined that different mouse strains required different seeding density on day 6 in order to reach optimal growth and differentiation on day 10.
22. Investigators may wish to use chemical inhibitors such as YVAD-fmk (caspase-1 inhibitor), bafilomycin A (inhibitor of the vacuolar H+ ATPase), or CA-074-Me (cathepsin B inhibitor) in order to gain further insight into the mechanisms of inflammasome activation [10]. The materials in Subheading 2.1.2 should also be used when planning to assess the effects of chemical inhibitors. They may be used in a similar manner to that described for priming and stimulating BMDCs (Subheading 3.1.2) and may be added before, at the same time, or after BMDCs have been primed. Advised concentrations of inhibitors are final concentrations and should be adjusted depending on the volume of cells in the well and the volume of the inhibitor to be added. Concentrations should be optimized in preliminary experiments or should be sourced from the literature. Note that chemical inhibitors could also affect priming (e.g., induction of NF-κB), thus, caution should be taken and controls included, ensuring that the inhibitor effect can be attributed to modulation of inflammasome activation rather than pro-IL-1β or IL-18 induction.
23. When priming and/or stimulating cells, note that the concentrations advised are for a final concentration in a well, i.e., 40 mg/mL silica final concentration. For example in a 96-well plate if there are 200 μL cells already in the well and the advised amount of 25 μL of the stimulant made up in priming medium is added, the concentration in the well will be diluted 1 in 9. Therefore stock solutions should be made up to a concentration nine times greater than the final concentration and 25 μL added per well in a 96-well plate.
24. We recommended using no more than 5 % FCS, to avoid the possibility of protein overloading which could negatively affect the quality of protein band signals. If difficulties are encountered (e.g., poor band resolution or slow migration during electrophoresis), decrease the concentration of FCS to 2 % and incubate for a maximum of 6 h. A further decrease in FCS concentration will affect the responsiveness of the BMDCs to TLR stimulation and/or particulate materials, and thus the quality of the signal.
25. We recommend running each experimental condition in triplicate wells so supernatants can be pooled, thus increasing signal intensity.
26. The optimal incubation period will be largely dependent on the characteristics of your particulate material. Longer incubation periods may be required depending on the particle–cell

ratio and the quality of the cell preparation, e.g., cell viability and maturation. Using the protocol described herein, our lab has determined that an incubation period of 3–6 h was optimal for the detection of caspase-1 and IL-1β in cell supernatants upon stimulation with particulates such as carbon nanotubes, silicon nanoparticles, alum, MSU, and polystyrene beads.

27. The use of prestained molecular weight markers helps to ensure that the caspase-1 p10 protein band remains within the gel; however, its apparent molecular mass may be lower, e.g., 7 kDa [12]. Thus, we recommend not allowing the migration front to go beyond ¾ way down the gel, as the caspase-1 (p10) band signal may be lost.
28. For wet transfer, proceed to transfer at 25 V (maximum 400 mA) and at 4 °C with stirring for at least 2 h. For dry transfer, a transfer at 15 V for 30–60 min should be sufficient.
29. At this stage, the cells are ready to be treated with particulate materials and/or pro-inflammatory agents. Cells are usually left in fresh medium without PMA overnight, but shorter times can be used.
30. We use an Olympus FV1000 confocal microscope system controlled by Olympus FLUOVIEW® viewer software and equipped with a temperature- and CO_2-regulated chamber, but comparable microscopes can be used. It is critical that the temperature of the sample be maintained between 37 and 38 °C and CO_2 be maintained at 5 %. Temperatures below 37 °C may reduce ASC-oligomers formation.
31. For example, use the following settings: GFP is excited with a 488 nm argon laser and its 505- to 545-nm emitted light is collected in a photomultiplier tube (PMT). Hoechst is excited with a 405 nm HeNe laser and its 420- to 480-nm emitted light is collected in a second PMT. Transmitted laser light is collected to produce a differential interference microscopic image. The eight-bit images are converted to a RGB format, the median is filtered to eliminate noise, montaged or overlayed, and can be converted into movie files at five frames per second using software such as Metamorph 7.3 (Molecular Devices Corp.).
32. In unstimulated cells, ASC–GFP should be distributed evenly in the cytoplasm and nucleus. However, ASC begins to oligomerize and may form single clusters as early as 10 min after stimulation with crude LPS or other stimuli [13]. ASC oligomers (observed as bright green specks) may not form simultaneously in all cells and some cells may not form any oligomers even after prolonged stimulation. Usually one ASC oligomer only will be formed in each cell, and this will precede morphological changes characteristic of pyroptosis. See supplementary movies

in reference [13]. ASC oligomer-induced pyroptosis can thus be seen within a period of 1–3 h and be simultaneously monitored by the release of intracellular LDH [13].

33. Cells should appear large and irregularly shaped.
34. Solutions of cycloheximide (protein synthesis inhibitor) and actinomycin D (RNA synthesis inhibitor) or a solution of staurosporine (a wide spectrum apoptosis inducer) can be used as positive controls. Concentrations and incubation times for necrosis/apoptosis induction may vary depending on the cell type used and the specific experimental set up, and thus, should be optimized in preliminary experiments.
35. It is critical to bring potential endotoxin contamination to low pg/mL values. We have observed that LPS concentrations as low as 10 and 20 pg/mL were able to induce secretion of IL-6 and TNF-α respectively, in BMDC differentiated cultures [17].
36. Further assessment of the innate immunomodulatory properties of particulate adjuvants or materials may be carried out in vivo using the mouse peritonitis model: mice can be challenged intraperitoneally with particulate solutions (50–200 μL/mouse at a range of concentrations, e.g., 100–1,000 μg of particles per mouse) for a period of 1–24 h in order to characterize inflammatory cell recruitment patterns. Peritoneal lavages are collected using 3–5 mL of sterile PBS solution. Mice challenged with PBS serve as negative controls. Peritoneal cells collected at different time points can then be stained for extracellular markers and analyzed by multicolor flow cytometry. A classic observation is the recruitment of inflammatory cells such as granulocyte and monocyte populations while resident macrophages are depleted. Further details can be found elsewhere [5, 10].
37. In preliminary experiments, we recommend incubation of the particulate material for a period of 24 h and determine if concentrations of IL-1β are significantly different from negative control wells. A dose–response may be evident between 3 and 24 h, i.e., the longer the incubation period, the higher the concentrations of IL-1β responses in the supernatant. However, this is not always the case, as potent stimuli cytokine secretion may be maximal after only a few hours.
38. Nonviable cells take up PI and its fluorescence can be detected on the FL2 channel (on most flow cytometers) while apoptotic cells display phosphatidylserine on their surface, which binds annexin V such that annexin V- FITC be detected on the FL1 channel (on most flow cytometers).
39. When carrying out annexin V-PI assay, samples should be analyzed within 1 h of completion of cell staining, due to toxicity issues and the risk of generating false positives. We suggest the

following gating strategy: exclude small cell particles or dead cell debris, which are recognized as a tail in the lower part of the dot plot. Then, set up the flow cytometer such that the distribution of the annexin V-FITC negative population is in the first two decades of the FL1 parameter and the distribution of the PI negative population is in the first two decades of the FL2 parameter. BMDCs treated with necrosis or apoptosis-inducing agents are used to set up single and double positive populations, thus gating at least 95 % of dead (early and late apoptotic or secondary necrotic) cells. Untreated BMDCs are used to set apart 95 % of viable cells. When using multicolor flow cytometry, e.g., FITC–annexin V and PI staining, it is important to compensate for spectral overlap between the different fluorochromes used. Refer to flow cytometer manual for specific instructions regarding compensation settings.

40. Other dyes besides LIVE/DEAD® Aqua are available. The single-color LIVE/DEAD® Fixable Dead cell stain kits from Invitrogen are identical except for the fluorescent color of the included dye, i.e., blue, violet, aqua, yellow, green, red, far red, or near-infra red (IR). Each of them has their specific excitation and emission wavelengths. For further details, see: http://www.invitrogen.com/
41. DMSO is hazardous; avoid contact with skin and eyes and do not swallow. Handle reagents containing DMSO using equipment and practices appropriate for the hazards posed by such materials.
42. This solution will be further diluted 1:1,000 in cell suspension.
43. Permeabilization and fixation reagents such as BD Cytofix/Cytoperm (BD Pharmingen) or 0.5 % PFA will not change the stability of the LIVE/DEAD® aqua dye nor will the dye leak out of the cells.
44. Staining for cell surface markers should be performed prior to fixation of the samples but after staining with LIVE/DEAD® aqua stain.
45. The Aqua fluorescent reactive dye (Invitrogen) is efficiently excited with ~405 nm light (or UV light) and has fluorescence emission monitored at ~525 nm.

References

1. Couillin I, Petrilli V, Martinon F (2011) The inflammasomes. Progress in inflammation research. Springer, Basel
2. Valavanidis A, Fiotakis K, Vlachogianni T (2008) Airborne particulate matter and human health: toxicological assessment and importance of size and composition of particles for oxidative damage and carcinogenic mechanisms. J Environ Sci Health C Environ Carcinog Ecotoxicol Rev 26(4):339–362

3. Strowig T, Henao-Mejia J, Elinav E, Flavell R (2012) Inflammasomes in health and disease. Nature 481(7381):278–286
4. Hornung V, Bauernfeind F, Halle A, Samstad EO, Kono H, Rock KL (2008) Silica crystals and aluminum salts activate the NALP3 inflammasome through phagosomal destabilization. Nat Immunol 9(8):847–856
5. Martinon F, Petrilli V, Mayor A, Tardivel A, Tschopp J (2006) Gout-associated uric acid crystals activate the NALP3 inflammasome. Nature 440:237–241
6. Dostert C, Pétrilli V, Van Bruggen R, Steele C, Mossman BT, Tschopp J (2008) Innate immune activation through Nalp3 inflammasome sensing of asbestos and silica. Science 320(5876):674–677
7. Li H, Willingham SB, Ting JP, Re F (2008) Cutting edge: inflammasome activation by alum and alum's adjuvant effect are mediated by NLRP3. J Immunol 181(1):17–21
8. Mori A, Oleszycka E, Sharp FA, Coleman M, Ozasa Y, Singh M, O'Hagan DT, Tajber L, Corrigan OI, McNeela EA, Lavelle EC (2012) The vaccine adjuvant alum inhibits IL-12 by promoting PI3 kinase signaling while chitosan does not inhibit IL-12 and enhances Th1 and Th17 responses. Eur J Immunol. doi: 10.1002/cji.201242372
9. Bueter CL, Lee CK, Rathinam VA, Healy GJ, Taron CH, Specht CA, Levitz SM (2011) Chitosan but not chitin activates the inflammasome by a mechanism dependent upon phagocytosis. J Biol Chem 286(41):35447–35455
10. Sharp FA, Ruane D, Claass B, Creagh E, Harris J, Malyala P, Singh M, O'Hagan DT, Pétrilli V, Tschopp J, O'Neill LAJ, Lavelle EC (2009) Uptake of particulate vaccine adjuvants by dendritic cells activates the NALP3 inflammasome. Proc Natl Acad Sci USA 106(3):870–875
11. Demento SL, Eisenbarth SC, Foellmer HG, Platt C, Caplan MJ, Mark Saltzman W, Mellman I, Ledizet M, Fikrig E, Flavell RA, Fahmy TM (2009) Inflammasome-activating nanoparticles as modular systems for optimizing vaccine efficacy. Vaccine 27(23):3013–3021
12. Doyle SL, Campbell M, Ozaki E, Salomon RG, Mori A, Kenna PF, Farrar GJ, Kiang AS, Humphries MM, Lavelle EC, O'Neill LA, Hollyfield JG, Humphries P (2012) NLRP3 has a protective role in age-related macular degeneration through the induction of IL-18 by drusen components. Nat Med 18(5):791–798
13. Fernandes-Alnemri T, Wu J, Yu JW, Datta P, Miller B, Jankowski W, Rosenberg S, Zhang J, Alnemri ES (2007) The pyroptosome: a supramolecular assembly of ASC dimers mediating inflammatory cell death via caspase-1 activation. Cell Death Differ 14(9):1590–1604
14. de Brito C, Tomkowiak M, Ghittoni R, Caux C, Leverrier Y, Marvel J (2011) CpG promotes cross-presentation of dead cell-associated antigens by pre-CD8α+ dendritic cells. J Immunol 186(3):1503–1511
15. Perfetto SP, Chattopadhyay PK, Lamoreaux L, Nguyen R, Ambrozak D, Koup RA, Roederer M (2010) Amine-reactive dyes for dead cell discrimination in fixed samples. Curr Protoc Cytom Chapter: Unit–9.34
16. Logue SE, Elgendy M, Martin S (2009) Expression, purification and use of recombinant annexin V for the detection of apoptotic cells. Nat Protoc 4(9):1383–1395
17. Tynan GA, McNaughton A, Jarnicki A, Tsuji T, Lavelle EC (2012) Polymyxin B inadequately quenches the effects of contaminating lipopolysaccharide on murine dendritic cells. PLoS One 7(5):e37261

Website Reference

Invitrogen web site of LIVE/DEAD® fixable dyes: http://www.invitrogen.com/site/us/en/home/Global/invitrogen-search-results.html?searchTerm=live+%2F+dead+fixable&searchRows=15&searchTypes=meta.collection%3Acmgtbuyproduct%3A&zeroCategories=meta.collection%3Amrdb%3A

small
Carbon Nanotubes

Functionalization of Carbon Nanoparticles Modulates Inflammatory Cell Recruitment and NLRP3 Inflammasome Activation

Marie Yang, Kevin Flavin, Ilona Kopf, Gabor Radics, Claire H. A. Hearnden, Gavin J. McManus, Barry Moran, Adrian Villalta-Cerdas, Luis A. Echegoyen, Silvia Giordani, and Ed C. Lavelle**

The inflammatory effects of carbon nanoparticles (NPs) are highly disputed. Here it is demonstrated that endotoxin-free preparations of raw carbon nanotubes (CNTs) are very limited in their capacity to promote inflammatory responses in vitro, as well as in vivo. Upon purification and selective oxidation of raw CNTs, a higher dispersibility is achieved in physiological solutions, but this process also enhances their inflammatory activity. In synergy with toll-like receptor (TLR) ligands, CNTs promote NLRP3 inflammasome activation and it is shown for the first time that this property extends to spherical carbon nano-onions (CNOs) of 6 nm in size. In contrast, the benzoic acid functionalization of purified CNTs and CNOs leads to significantly attenuated inflammatory properties. This is evidenced by a reduced secretion of the inflammatory cytokine IL-1β, and a pronounced decrease in the recruitment of neutrophils and monocytes following injection into mice. Collectively, these results reveal that the inflammatory properties of carbon NPs are highly dependent on their physicochemical characteristics and crucially, that chemical surface functionalization allows significant moderation of these properties.

1. Introduction

The discovery of carbon nanotubes (CNTs)[1] is regarded as a cornerstone in the advent of nanotechnology. CNTs are nano-sized rolls made of sheets of graphene and are classically coined as single-walled carbon nanotubes (SWCNTs) when they comprise one layer of atoms, while those made of multiple layers are known as multi-walled carbon nanotubes (MWCNTs). The present study focuses on SWCNTs as they were reported to show improved biocompatibility

Dr. M. Yang, Dr. K. Flavin, Dr. I. Kopf, Dr. G. Radics, Dr. S. Giordani,[+]
Dr. E. C Lavelle
Centre for Research on Adaptive Nanostructures and Nanodevices (CRANN)
Trinity College, Dublin 2, Ireland
E-mail: giordans@tcd.ie; lavellee@tcd.ie
Dr. M. Yang, C. H. A. Hearnden, Dr. E. C Lavelle
Adjuvant Research Group
School of Biochemistry and Immunology
Trinity Biomedical Sciences Institute, Trinity College, Dublin 2, Ireland
Dr. K. Flavin, Dr. I. Kopf, Dr. G. Radics, Dr. S. Giordani
School of Chemistry
Trinity Biomedical Sciences Institute
Trinity College Dublin, Dublin 2, Ireland
Dr. G. J. McManus, B. Moran
School of Biochemistry and Immunology
Trinity Biomedical Sciences Institute
Trinity College, Dublin 2, Ireland
Dr. A. Villalta-Cerdas, Prof. L. A. Echegoyen
Department of Chemistry
University of Texas at El Paso
El Paso, Texas, USA
[+]Present address: Italian Institute of Technology, Via Morego 30, 16163 Genova, Italy.

DOI: 10.1002/smll.201300481

© 2013 Wiley-VCH Verlag GmbH & Co. KGaA, Weinheim

and lower cytotoxicity compared to MWCNTs.[2] In addition, SWCNTs represent more homogeneous preparations.[3] While their unique properties have generated tremendous interest in material-based applications, CNTs have also been investigated for biomedical applications including the thermal ablation of tumor cells and drug delivery.[4] The antimicrobial activity and capacity of CNT composites to act as growth scaffolds for bone formation or repair, and neuronal growth have also been reported. Despite encouraging findings, concerns over the toxic and inflammatory properties of CNTs have been raised,[2] particularly in the context of occupational hazards and biomedical applications. Their high aspect ratio (length-to-width) led to concerns that CNTs may cause lung pathologies similar to those caused by asbestos fibres. Authors have attributed a variety of deleterious effects to CNTs: granulomatous inflammation, release of cytosolic enzymes, pulmonary fibrosis, reactive oxygen-induced damage, DNA fragmentation and mitotic spindle disruption (reviewed in [5]). In contrast, other biocompatibility studies have reported no or limited cytotoxicity to macrophages, fibroblasts and osteoblasts,[6–9] and the absence of any tissue damage or inflammation in vivo in mice.[10,11]

These conflicting observations prompted us to revisit the inflammatory potential of carbon nanoparticles, with a particular focus on CNTs and carbon nano-onions (CNOs), a group of carbon allotropes[12–13] that remains underexplored and whose immunomodulatory properties are unknown.

Most studies concerned with the inflammatory properties of CNTs were carried out using "as-prepared" or raw non-functionalized CNTs (*r*-CNTs). However, *r*-CNTs are generally impure as they contain ill-defined amounts of carbonaceous impurities,[14,15] metal catalyst residues[10,16] and microbial contaminants.[17] It is highly probable that such impurities may have contributed to the toxic and immunomodulatory properties previously attributed to CNTs.[18] In the present study, we ruled out the involvement of such impurities by subjecting *r*-CNTs to a rigorous process of purification[19] and ensured that all experiments were carried out in endotoxin-free conditions using medical grade water and ultra pure grade reagents during both synthetic, in vitro and in vivo work.[20] CNTs possess the inherent tendency to form aggregates in both aqueous and organic solvents and this can be addressed by means of surface functionalization. We recently reported the purification and selective oxidation of CNTs (*p*-CNT) while minimizing the effects of the chemical treatment on their integrity or shape,[19] however the consequence of this on their inflammatory properties was not investigated.

Insoluble aluminium salts—generically referred to as alum[21]—have served as particulate immunopotentiators in vaccines for over 80 years and millions of doses of alum-containing vaccines have been administered to healthy patients. A large body of evidence showed that alum exerts cytotoxic and inflammatory effects both in vitro and in vivo,[22] however, these effects are clearly acceptable given the excellent record of alum as a clinically applied vaccine adjuvant. Here, the immunomodulatory properties of CNTs and CNOs were compared to those of alum. In recent years, the NLRP3 inflammasome has been implicated in the inflammatory properties of particulate materials, including those of alum. Along with the adaptor protein ASC (apoptotic speck protein containing a caspase recruitment domain) and procaspase-1, NLRP3 forms a molecular platform responsible for the catalytic activation of caspase-1, and the cleavage and release of the inflammatory cytokines IL-1β and IL-18.[23] Previous studies have described NLRP3 inflammasome activation by raw non-functionalized multi-walled CNTs.[24,25] Here, in the context of their potential biomedical applications, we present a comprehensive analysis of the inflammatory and NLRP3 inflammasome activation properties of raw, purified and functionalized single-walled CNTs and small CNOs. We show that these properties are dependent on the physicochemical characteristics of the carbon allotrope and importantly that surface functionalization represents a convenient and controlled means to temper these inflammatory attributes.

2. Results

2.1. Preparation and Characterization of Carbon Nanotubes and Nano-Onions

r-CNTs were purified following a novel and recently described procedure,[19] (**Figure 1**A), which allows for the preparation of high purity *p*-CNT, where both carbonaceous impurities and iron catalyst are removed with high efficiency. This procedure takes advantage of a short nitric acid oxidation treatment to reduce structural/electronic degradation of the CNTs and sodium hydroxide treatments to remove carboxylated carbonaceous impurities. Essential to the purification, however, is the second oxidation step with hydrogen peroxide, which facilitates decomposition of the remaining carbonaceous impurities and full conversion of oxygenated groups to carboxylic acid functionalities (Figure 1A). AFM analysis of *r*-CNTs vs *p*-CNT was carried out to confirm the purity of the samples used in the study (Supporting Information Figure S1). Size distribution analysis of *p*-CNT revealed an average length ranging from 128 to 445 nm and an average diameter of 0.7 to 1 nm (Supporting Information Figure S2). The CNOs used in the study were synthesized according to a previously described procedure by annealing of nanodiamonds[26] which leads to highly pure materials with homogeneous diameters of 5-7 nm (Figure 1 and Supporting Information Figure S2).

Both *p*-CNT and *p*-CNO were subsequently functionalized to produce *f*-CNT (Figure 1A) and *f*-CNO (Figure 1B), using a previously described[27–29] one-pot Tour reaction comprising aminobenzoic acid and isoamylnitrite. This reaction was chosen because of its simplicity, versatility and the fact that its chemistry occurs at the sidewall of the carbon NPs. Evidence of the covalent modification is provided in Supporting Information Figure S3, with spectra showing a substantial enhancement of the D-band (activated by the presence of defects on the carbon NPs following the chemical treatment). FTIR analysis of the samples following the chemical treatment shows the appearance of aromatic C-H deformation vibrations (1290–990 cm^{-1}), aromatic C = C (1600 and 1475 cm^{-1}) and C-O (≈1625 and ≈1725 cm^{-1}) stretching vibrations, and O-H vibrations (1300 cm^{-1}). While the Zeta potential of −33.8mV for *p*-CNT indicates an increase in

© 2013 Wiley-VCH Verlag GmbH & Co. KGaA, Weinheim

DOI: 10.1002/smll.201300481

NANO MICRO small

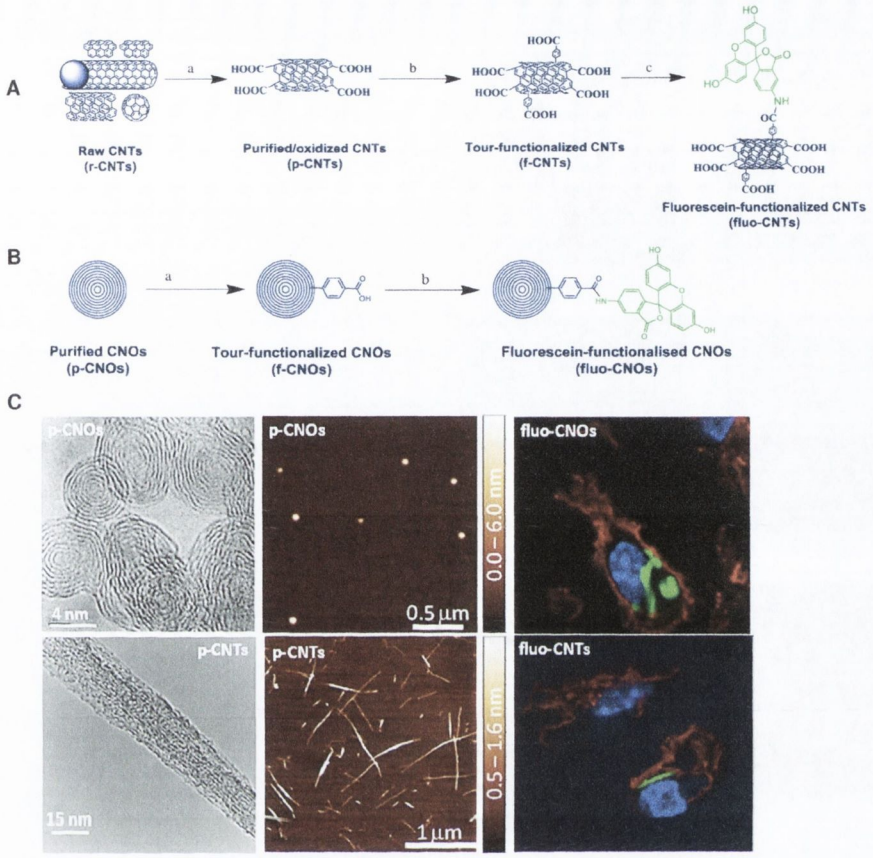

Figure 1. Schematic of carbon nanoparticle purification and functionalization. A) CNT purification and functionalization protocol. a) 7.9 M HNO_3, 100 °C, 4.5 h; 2 M NaOH, 100 °C, 12h (2×); 10% H_2O_2, 100 °C, 1 h; 2% H_2O_2, 20 °C, 12 h; 2 M NaOH, 100 °C, 12 h. b) 4-aminobenzoic acid, isoamyl nitrite, NMP, 70 °C, 14 h, N_2. c) DMAP, N-hydroxysuccinimide, DMF, 10 min; EDCI, 3 h, N_2; Fluoresceinamine, 60 °C, 6 days, N_2. B) CNO functionalization protocol. a) aminobenzoic acid, isoamyl nitrite, DMF, N2, 60 °C, 16 h; b) DMAP, N-hydroxysuccinimide, DMF, 10 min; EDCI, 3 h, N_2; Fluoresceinamine, 60 °C, 6 days, N_2. C) Visualization of carbon nanoparticles. High resolution TEM images of p-CNOs and p-CNTs nanoparticles (left panels). AFM topographs of p-CNO and p-CNT deposited on mica (middle panels). Confocal microscopy of C57BL/6 BMDCs incubated in the presence of fluorescein (green) labelled -CNT and -CNO for 18 h, then washed in PBS, fixed, and stained with wheat germ agglutinin-Alexa Fluor594 (red) and nuclei stain Hoescht (blue) (right panels).

polarity relative to *r*-CNT (–23.7 mV) (Supporting Information Figure S5, B), the further lowering in the Zeta potential to –38.7 mV for *f*-CNT and to –16.8 mV for *f*-CNO at pH 7.3 is in agreement with the successful surface functionalization.

To allow for in vitro visualization of the functionalized particles, a standard amide coupling reaction was used to covalently attach fluoresceinamine, thus producing *fluo*-CNTs and *fluo*-CNOs (Figure 1). The absorption and emission spectra of fluorescein-functionalized materials are represented in Supporting Information Figure S4. To minimize contamination of all purified and functionalized materials by microbial contaminants, such as endotoxins, samples were dispersed in NMP by water bath sonication (80 kHz), dialyzed against medical grade sterile water for 5 days and lyophilized until dry in sterile glass containers.

During functionalization, the size of individual CNPs does not change significantly as evidenced by AFM measurements. The agglomeration tendency changes are shown by DLS measurements performed in saline buffer, which was used as the particle suspension vehicle for the immunological studies. The initial particle sizes for *f*-CNOs and fluo-CNOs were 170 ± 11 nm and 136 ± 9 nm, respectively, after sonication and the agglomeration curve as a function of time is represented in Figure S5. Unlike the round CNO particles, CNTs are rod like structures with high aspect ratios and angle dependent light scattering, and are characterized by their effective hydrodynamic diameter in single angle light scattering.[30] Following the same sample preparation and measurement conditions as above, CNTs showed multimodal distribution of particle sizes in all cases (Supporting Information Figure S5C).

2.2. Dendritic Cells and Macrophages Take up Carbon NPs

We sought to evaluate the ability of macrophages (Macs) and dendritic cells (DCs) to internalize single-walled CNTs

© 2013 Wiley-VCH Verlag GmbH & Co. KGaA, Weinheim

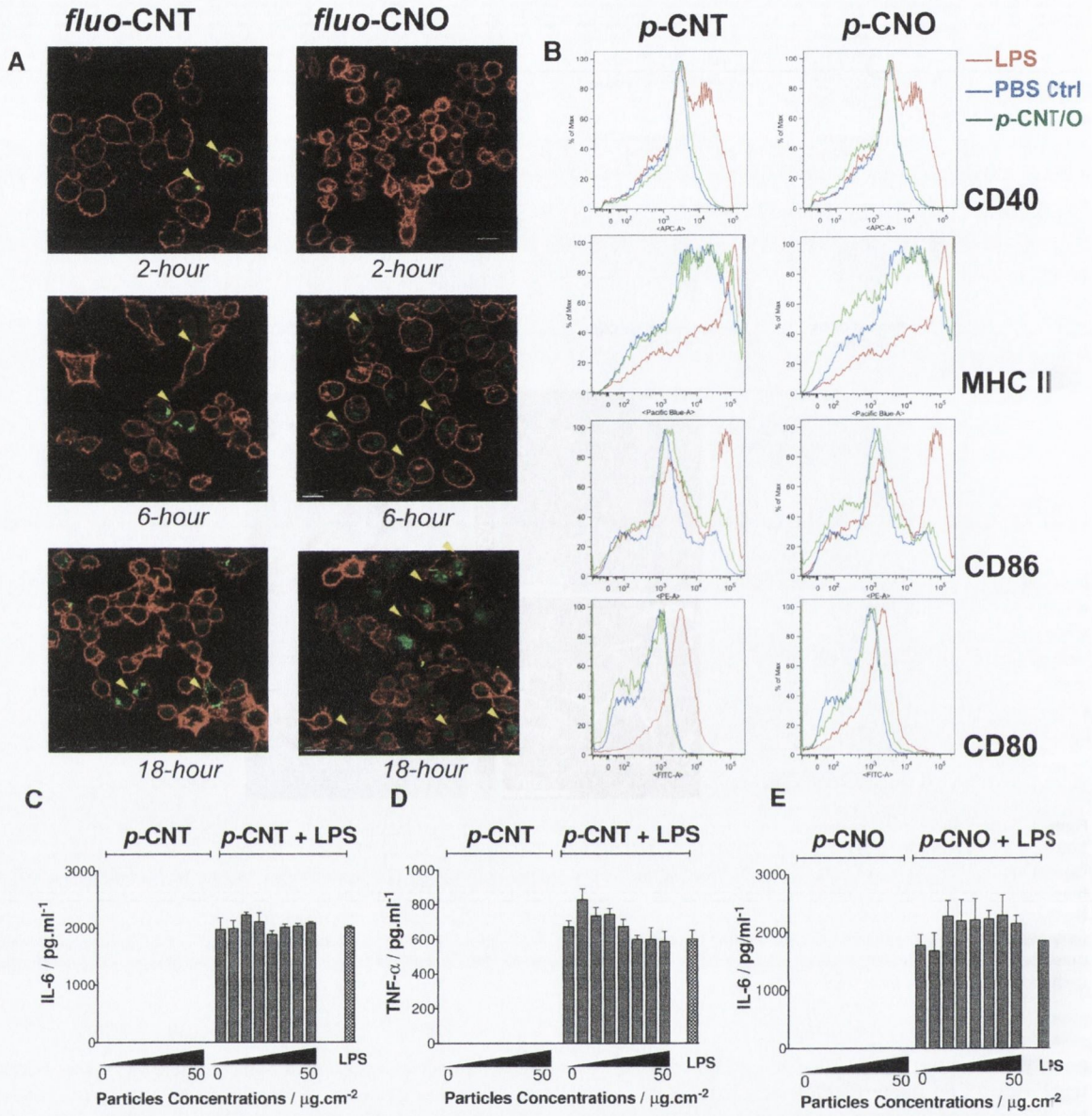

Figure 2. CNTs and CNOs are efficiently taken up by antigen-presenting cells, but do not induce maturation of dendritic cells nor production of inflammatory cytokines. A) Confocal microscopy of wild-type iBMM incubated in the presence of fluorescein (green) labelled-CNT and -CNO for 2, 6, and 18 h, then washed in PBS, fixed, and stained with wheat germ agglutinin-Alexa Fluor594 (red). Original magnification, ×60. B) The expression of the maturation markers CD40, CD80, CD86 and MHCII (I-A/I-E) was measured by flow cytometric analysis in BMDC cultures treated with either alum, p-CNT or p-CNO at 50 µg cm^{-2} for 24 h. C,E) Quantification of IL-6 (C,E) and TNF-α (D) in supernatants of BMDC cultures incubated for 24 h with p-CNT ± 1 ng mL^{-1} of LPS or p-CNO ± 1 ng mL^{-1} of LPS at concentrations ranging from 0.4–50 µg cm^{-2}.

and small CNOs, using confocal microscopy. Immortalized bone-marrow derived mouse macrophages (iBMM) were incubated in the presence of fluorescein-labeled CNTs (*fluo*-CNTs) and small CNOs (*fluo*-CNOs) over a time course of 18 h (**Figure 2**A). Results indicate that the internalization of *fluo*-CNOs by iBMM occurs to a higher degree compared to *fluo*-CNTs, as indicated by a greater number of green patches (yellow arrowheads), particularly at 6 and 18 h. Similarly, confocal imaging of mouse bone-marrow-derived dendritic cells (BMDCs) revealed the uptake of carbon NPs (Supporting Information Figure S6), although to a lesser extent than in Macs. This is not surprising as Macs are known to exhibit higher phagocytic activity than DCs.[31]

Live imaging of iBMMs incubated in the presence of *p*-CNT and *p*-CNO (50 µg cm^{-2}) shows that dendrites are being formed within 30 min of incubation indicating that

© 2013 Wiley-VCH Verlag GmbH & Co. KGaA, Weinheim

DOI: 10.1002/smll.201300481

carbon NPs are being actively sensed by professional antigen-presenting cells (Supporting Information Movies 1–3). Previous studies have documented the ability of CNTs to induce activation and maturation of DCs,[32,33] while others reported contradictory findings.[34–35] These conflicting results prompted us to assess the expression of surface markers CD40, CD80, CD86 and MHC class II (I-A/I-E) in BMDC cultures treated with either alum or highly purified *p*-CNT or *p*-CNO at a range of concentrations (Figure 2B). There was no distinguishable effect on expression of any of these cell surface markers when compared to their respective controls (Figure 2B). Studies have also described that commercial preparations of carbon nanotubes could induce the production of the cytokines IL-6, TNF-α and IL-1β by RAW 264.7 macrophages[36] as well as systemically (plasma) in vivo,[37] however, most of these studies fail to report endotoxin content. Our study indicates in contrast that neither *p*-CNTs nor *p*-CNOs induce secretion of the inflammatory cytokines IL-6 or TNF-α and did not significantly alter LPS-induced secretion of these two inflammatory cytokines (Figure 2 C–E). Using the LAL Chromogenic Endotoxin quantification kit (Pierce), we found that in correlation with the IL-6 readout from BMDCs cultures, the absorbance values for all the CNT and CNO preparations used in these studies were not greater than those of the negative control, endotoxin-free water (Supporting Information Figure S7). Likewise, we also demonstrated that CNTs and CNOs induced negligible death in BMDC cultures (Supporting Information Figure S8).

2.3. Purified Carbon NPs Promote Secretion of IL-1β in a NLRP3- and Dose-Dependent Manner

The particulate nature of CNTs and CNOs prompted us to investigate their ability to promote the secretion of IL-1β and the involvement of the NLRP3 inflammasome. BMDCs stimulated with LPS (1 ng mL^{-1}) alone or *p*-CNT alone secreted low or undetectable amounts of IL-1β, while stimulation of LPS-primed cells from C57BL/6 mice with *p*-CNT alone resulted in significantly enhanced secretion of IL-1β (**$p = 0.0014$, **Figure 3**A) in a dose-dependent manner. Most interestingly, we show for the first time that, similarly to *p*-CNT, small *p*-CNOs can induce the release of IL-1β by DC upon TLR-ligand priming (* $p = 0.022$, Figure 3B), albeit to a lesser extent than p-CNTs. Indeed, at concentrations ranging from 0.35–50 $\mu g.mL^{-1}$, small *p*-CNOs were 2-5 times less potent than *p*-CNTs at inducing the secretion of IL-1β (**$p = 0.0012$). Importantly, these effects were not restricted to priming with LPS (a TLR4 agonist), as a synergistic IL-1β production was also obtained upon priming with the TLR2 agonist Pam3CSK4 and the TLR9 agonist CpG (Supporting Information Figure S9).

Previously, Yazdi et al.[38] reported that CNTs failed to induce activation of the NLRP3 inflammasome in bone-marrow derived macrophages in contrast to two other studies which found that raw non-functionalized multi-walled CNTs could induce its activation. These latter investigations were carried out on human primary macrophages or monocytes using siRNA-based approaches.[24,25] Here, we show that the secretion of IL-1β in response to LPS plus alum, *p*-CNT or *p*-CNO was abolished in BMDCs generated from $NLRP3^{-/-}$ mice (Figure 3C,D). To confirm that this effect on IL-1β secretion was not reflective of a generalized hyporesponsiveness of $NLRP3^{-/-}$ cells, we assayed the same supernatants for IL-6, whose production occurs independently of caspase-1 activation.[39] IL-6 was secreted at comparable level in cells stimulated with LPS alone or LPS plus *p*-CNT/*p*-CNO in both wild type and $NLRP3^{-/-}$ cells (Supporting Information Figure S10). In order to provide more direct evidence that both CNTs and CNOs induce activation of the NLRP3 inflammasome, we tested their ability to induce oligomerization of ASC which is essential for full activation of the NLRP3 inflammasome.[40] We thus performed confocal imaging of THP-1 cells stably transfected with ASC-GFP (ASC-GFP-THP-1 cells) and visualized the cells by confocal microscopy (Figure 3E). No or very few ASC-GFP specks were observed when ASC-GFP-THP-1 cells were treated with PBS, LPS alone or *p*-CNT alone. On the other hand, when cells were pulsed with LPS and incubated in the presence of *p*-CNT, multiple and larger green specks were visible (Figure 3E, yellow arrows). Addition of the cathepsin B inhibitor Ca-074-Me to BMDC cultures primed with LPS resulted in an impaired production of IL-1β (Figure 3F), suggesting that lysosomal damage and release of cathepsin B is essential for carbon particle-induced NLRP3 inflammasome activation.[41,42] The involvement of caspase-1 was determined by the use of the caspase-1 inhibitory peptide YVAD-fmk, which led to a significant decrease of IL-1β secretion (Figure 3F). Finally, we also showed that lysosomal acidification and potassium efflux were required for inflammasome activation by carbon NPs (Supporting Information Figure S11).

2.4. Chemical Functionalization of Carbon NPs Attenuates Their Inflammatory Properties in Vitro and in Vivo

Having shown that *p*-CNT and *p*-CNO could activate the NLRP3 inflammasome in the presence of TLR ligands, we investigated whether chemical functionalization could modulate these inflammatory properties. Incubation of LPS-primed BMDCs in the presence of *p*-CNT resulted in significantly greater production of IL-1β compared to incubation with *raw*-CNT, while in contrast, IL-1β production by cells incubated with *f*-CNT was significantly lower than with *r*-CNT (**Figure 4**A, ***$p < 0.001$, r-CNT *vs.* *p*-CNT and *f*-CNT at concentrations of 6-50 $\mu g\ cm^{-2}$). Similarly, the benzoic acid-functionalization of *p*-CNOs led to a significant reduction in particle-induced secretion of IL-1β (Figure 4B, * $p < 0.05$, p-CNO vs *f*-CNO at concentrations of 3–50 $\mu g\ cm^{-2}$). For both CNTs and CNOs, benzoic acid-functionalization led to an enhanced dispersibility in both organic and aqueous diluents, a difference that remained visible up to 24 h after sonication (as shown for CNOs, Figure 4C). Another noteworthy observation was that CNOs were less inflammatory than CNTs, regardless of their functionalization status.

To further understand the modulatory properties of carbon NPs on innate immune responses, we carried out studies using a mouse peritonitis model. C57BL/6 mice

DOI: 10.1002/smll.201300481
© 2013 Wiley-VCH Verlag GmbH & Co. KGaA, Weinheim

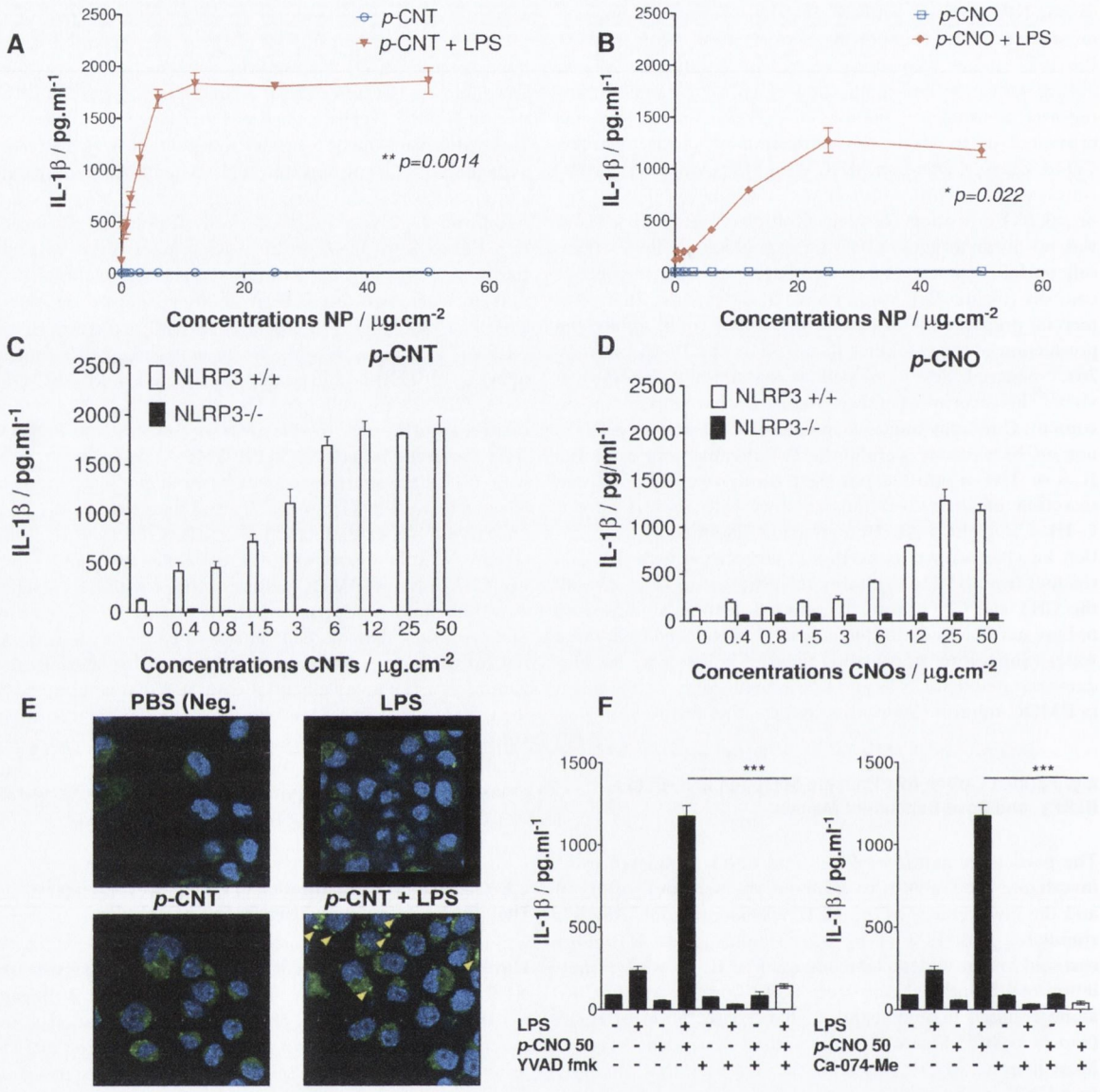

Figure 3. CNTs and CNOs induce the synergistic secretion of IL-1β in a NLRP3-dependent manner. A) Carbon nanotubes and B) nano-onions (dose range: 0.4–50 μg cm^{-2}) were added to C57BL/6 BMDC cultures either alone or in combination with LPS (1 ng mL^{-1}). Supernatants were collected after 24 h incubation and assayed by ELISA (*p* = CNO vs *f*-CNO t-test; *r*-CNT vs *p*-CNT or *f*-CNT (ANOVA and Dunnett's post hoc test, $*p < 0.05$, *** $p < 0.001$). C) Carbon nanotubes and D) nano-onions (dose range: 0.4–50 μg cm^{-2}) were added to either C57BL/6 or $NLRP3^{-/-}$ BMDC cultures either alone or in combination with LPS (1 ng mL^{-1}). Supernatants were collected after 24 h incubation and assayed by ELISA. E, ASC-GFP THP-1 cells were left untreated (PBS), treated with LPS (1 μg mL^{-1}) or treated with LPS +/− p-CNT (25 μg cm^{-2}) for 6 h and observed by confocal fluorescence microscopy (Original magnification: 40×). F, ELISA for IL-1β. Resting or LPS-primed BMDCs were stimulated with p-CNO (25 μg cm^{-2}) in the absence or presence of the cathepsin B inhibitor Ca-074-Me (10 μM) or the caspase-1 inhibitor YVAD-fmk (***$p < 0.001$, *p*-CNO+LPS *vs.* *p*-CNO+LPS+ chemical inhibitor).

were administered with PBS vehicle suspensions containing alum, *r*-CNT, *p*-CNT, *f*-CNT, *p*-CNO or *f*-CNO. The nature of the infiltrating cells recruited into the peritoneal cavity was determined using flow cytometry at 3 h post-injection (**Figure 5**). $CD11b^{+}F4/80^{+}$ macrophages are one of the most prominent resident cell populations in the mouse peritoneum. Here, in line with previous reports,[43,44] we observed a dramatic reduction (from 29.6% to 3.4%) in the number of $CD11b^{+}F4/80^{+}$ expressing cells when mice were injected with alum (Figure 5, top panel). We show for the first time that injection of CNT or CNO also results in a depletion of resident peritoneal macrophages. Specifically, depletion of resident macrophages occurred in mice administered with *p*-CNT (from 29.6% to 4.13%), *f*-CNT (from 29.6% to 12.6%),

© 2013 Wiley-VCH Verlag GmbH & Co. KGaA, Weinheim
small 2013,
DOI: 10.1002/smll.201300481

NANO MICRO small

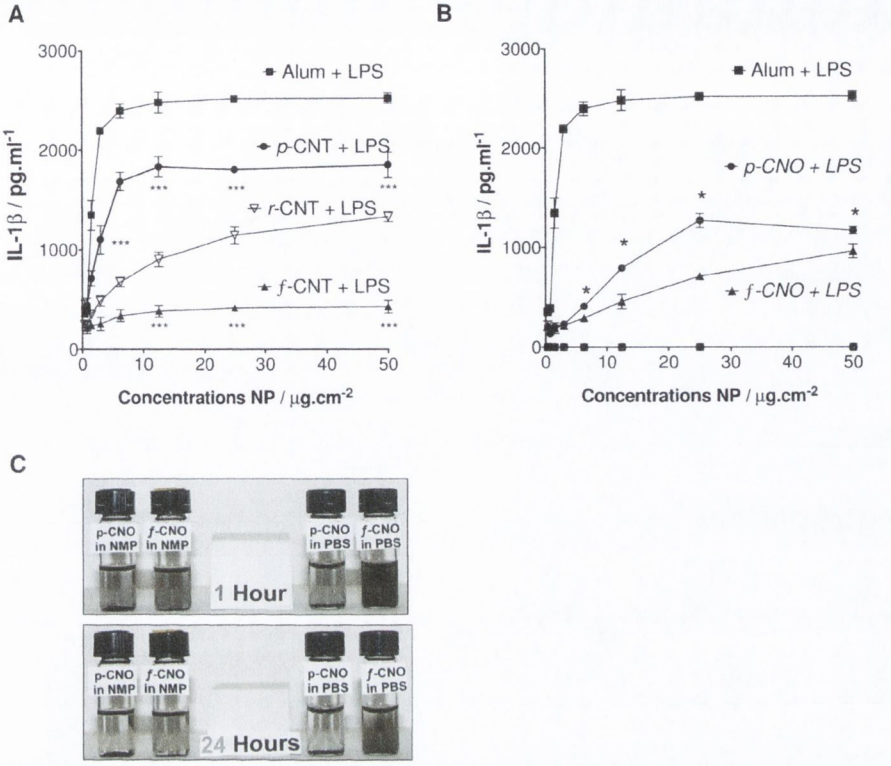

Figure 4. Tour-functionalization of *p*-CNOs and *p*-CNTs attenuates their inflammatory properties in vitro. A,B) Raw *r*-CNTs, *p*-CNT, *p*-CNO, *f*-CNT or *f*-CNO (dose range: 0.25–50 μg cm^{-2}) were added to C57BL/6 BMDC cultures in combination with LPS (1 ng mL^{-1}) or with LPS alone. Supernatants were collected after 24 h incubation and cytokines were assayed by ELISA (*p* = CNO vs *f*-CNO t-test; *r*-CNT vs. *p*-CNT or *f*-CNT ANOVA and Dunnett's *post hoc* test, * $p < 0.05$, *** $p < 0.001$). C) Photograph showing increased dispersibility of *p*-CNOs and *f*-CNOs in organic (NMP) and aqueous (PBS) solvents upon Tour-functionalization at 1 and 24 h after sonication.

p-CNO (from 29.6% to 16.8%) and *f*-CNO (from 29.6% to 20.5%) preparations (*** $p < 0.001$, Dunn's post hoc test) in comparison to PBS control group). Remarkably, no significant changes were observed in mice injected with *r*-CNT (from 29.5% to 25.7%) (Figure 5, top panel). In contrast to the depletion of resident macrophages, a marked recruitment of $Ly6G^{+}SiglecF^{-}$ neutrophils and $CD11c^{-}Ly6C^{High}$ inflammatory monocytes—described in the literature as potential DC precursors[44]—was detected in mice administered with *p*-CNT, *f*-CNT, *p*-CNO and *f*-CNO, as well as in the alum group (Figure 5B,C). Here again, there was no significant neutrophil or monocyte recruitment in the *r*-CNT group in comparison to the PBS group. Within each subset of carbon NPs, the benzoic acid-functionalized particles were consistently 2-5 times less effective than their purified counterparts at recruiting inflammatory cells (Histograms, * $p < 0.05$ and ** $p < 0.01$, Dunn's post hoc test, Figure 5B). Most interestingly, and in line with the in vitro results presented earlier, CNOs were consistently less potent than CNTs at inducing either resident macrophage depletion or neutrophil and monocyte recruitment (* $p < 0.05$, two-tailed t-test).

In view of these results on the regulation of innate immunity by carbon nanoparticles, we then assessed the potential of purified and functionalized carbon NPs to modulate adaptive immune responses. An adjuvant study was carried out to assess whether co-administration of carbon NPs with human serum albumin (HSA) in mice can enhance antigen specific cellular or humoral immunity. In contrast to the established vaccine adjuvant alum, none of the carbon NPs preparations tested induced a significant increase in specific antibody responses (HSA-specific IgG and IgG1) (Supporting Information Figure S12A). Instead, we found that carbon NPs, and CNOs in particular, promoted secretion of the immunosuppressive cytokine IL-10 in mediastinal lymph node cultures (Supporting Information Figure S12B, *** $p < 0.001$, Dunnett's test individual group vs HSA group).

3. Discussion

The current lack of consensus on the inflammatory properties of carbon NPs represents a significant issue regarding their application in the biomedical field. Here we explored the ability of carbon nanotubes and nano-onions to promote inflammation, how this relates to their physicochemical properties and the use of surface functionalization to modulate their inflammatory properties.

DOI: 10.1002/smll.201300481
© 2013 Wiley-VCH Verlag GmbH & Co. KGaA, Weinheim

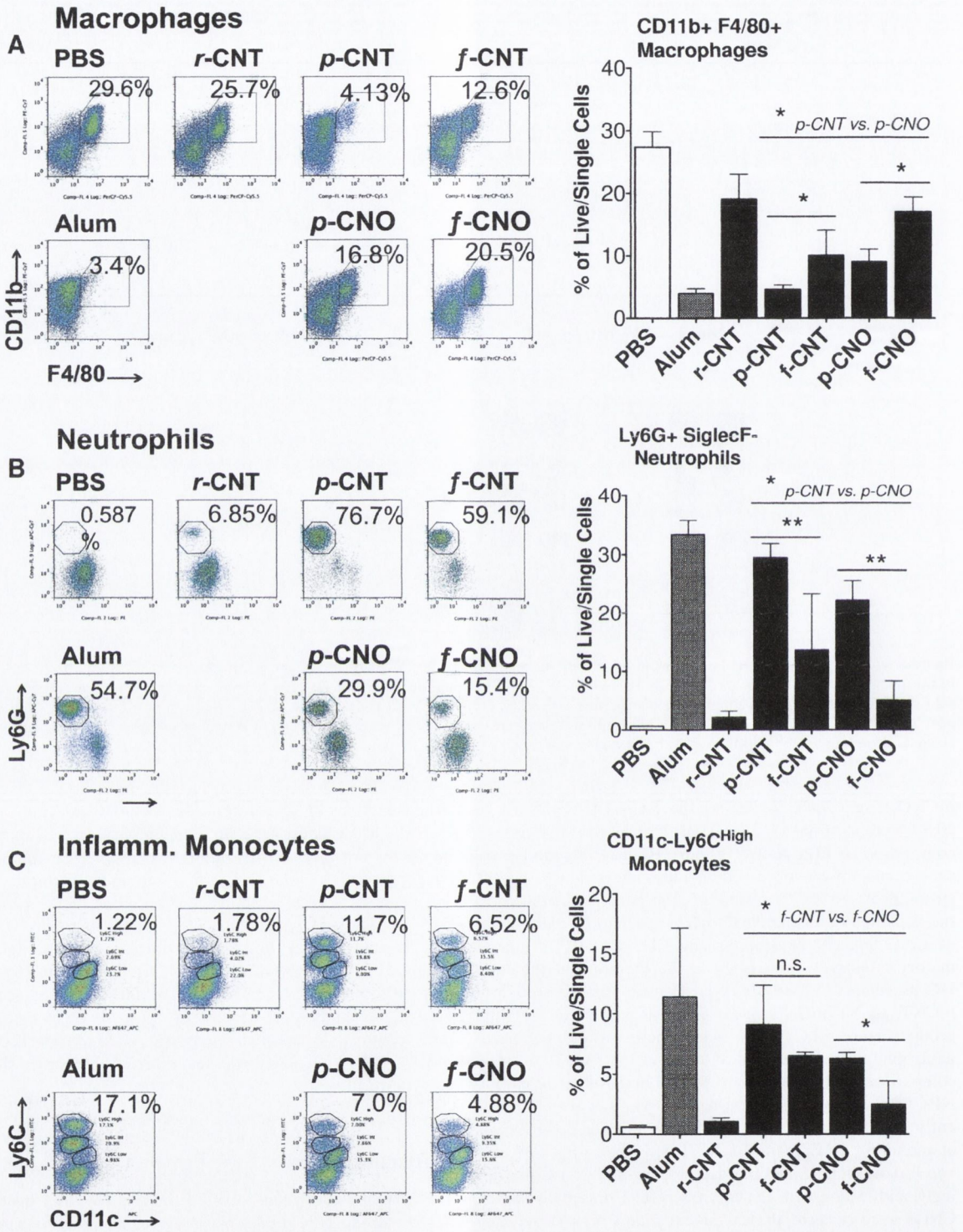

Figure 5. Tour-functionalization modulates the inflammatory properties of CNTs and CNOs in vivo. A–C) Female C57BL/6 mice (n = 3–5) aged 6–8 weeks were injected intraperitoneally with PBS vehicle, Alum (250 μg/mouse), r-CNTs (250 μg/mouse), *p*-CNT (250 μg/mouse), *f*-CNT (250 μg/mouse), *p*-CNO (250 μg/mouse) or *f*-CNO (250 μg/mouse). After 3 hr, peritoneal lavage cells were collected and cell recruitment was analysed by flow cytometry. The combinations of markers used to characterize the peritoneal cell recruitment were defined as follows: A) $CD11b^{High}$ F4/80+ macrophages, (B $Ly6G^{+}$ Siglec F^{-} neutrophils, and C) $CD11c^{-}Ly6C^{High}$ inflammatory monocytes. Results are expressed as a percentage of single/live cells (* $p < 0.05$, ** $p < 0.01$, Dunn's post hoc test).

© 2013 Wiley-VCH Verlag GmbH & Co. KGaA, Weinheim
small 2013,
DOI: 10.1002/smll.201300481

NANO MICRO small

Firstly, we established that highly purified preparations of CNTs and CNOs fail to induce dendritic cell maturation (Figure 2B) or to stimulate any detectable level of inflammatory cytokine secretion (Figure 2C–E) in vitro. These results are in line with Brewer et al.,[45] who demonstrated that particulate materials, including commercial vaccine adjuvants such as alum salts, are unable to act as TLR agonists and do not induce DC maturation.[46] The results are, however, in contrast to earlier reports which documented the inflammatory potential of commercial CNTs[33] and their ability to induce DC maturation and secretion of cytokines such as IL-6 and TNF-α.[47,48] It is possible that in these reports, the *raw* preparations tested may have contained immunostimulatory contaminants[17,49] although differences in assay systems and cell types may also contribute to the differences observed.

Secondly, we describe for the first time, as anticipated by their particulate nature,[50] that not only single-walled CNTs but also small CNOs promote secretion of the proinflammatory cytokine IL-1β by BMDC in a NLRP3- and dose-dependent manner, in the presence of TLR ligands (Figure 3). An earlier study reported that large CNOs (30 nm diameter) were 10 times less cytotoxic than multi-walled CNTs using a human skin fibroblast cell line.[51] Here, we found that small CNOs exhibit an inflammatory profile that is weaker than that of single-walled CNTs both in vitro with respect to the release of IL-1β by BMDCs (Figure 4, $^{**}p < 0.01$, not shown) and in vivo with respect to the recruitment of neutrophils and inflammatory monocytes (Figure 5, $^{*}p < 0.05$). It is highly probable that the long fiber-like morphology of CNTs *vs.* the spherical shape and minute size[26] of CNOs may contribute to these differences. We determined that CNOs were taken up by antigen-presenting cells (Figure 1A,B and Supporting Information S6) to a greater extent than CNTs. However, CNOs were less competent at inducing NLRP3 inflammasome activation and secretion of IL-1β, suggesting that the magnitude of the response is not strictly proportional to particle uptake. Similarly, we found that in vivo CNOs were more efficiently targeted to draining lymph nodes (Supporting Information Figure S13A) when compared to single walled-CNTs. This finding was supported by raman spectral analysis (Supporting Information Figure S7B). Overall, by virtue of their weak inflammatory potential and low cytotoxicity (Supporting Information Figure S9), yet efficient uptake by antigen-presenting cells and transport to lymph nodes, CNOs may represent a safer and more efficient alternative to CNTs for applications such as drug delivery[52] or in biocomposite materials.[53]

Thirdly, we assessed the impact of surface functionalization on the inflammatory response to carbon nanoparticles.[54] In striking contrast to the relative immunological inertia of *r*-CNTs, purified *p*-CNTs and *p*-CNOs were highly potent at recruiting innate cells including neutrophils and monocytes (Figure 5). Remarkably however, the benzoic acid-functionalization of both purified carbon NPs resulted in a significantly reduced inflammation in vitro with regard to the release of IL-1β (Figure 4) as well as in vivo with regard to the recruitment of innate inflammatory cells (Figure 5). To our knowledge, this study is the first to describe the potential for selective oxidation and surface chemical functionalization to exert fine control over the inflammatory properties of carbon nanoparticles.

We sought to comprehend the basis for the differential inflammatory abilities of *r*-CNTs vs. *p*-CNT vs. *f*-CNT as well as *p*-CNOs vs. f-CNOs, and therefore carried out detailed studies on particle agglomeration, size and polarity. The zeta potential of carbon particles was determined and can be categorized as follows: *r*-CNTs>*p*-CNTs>*f*-CNTs and *p*-CNOs>*f*-CNOs (Supporting Information Figure S5). A decreasing zeta potential denotes an increased polarity, which correlates well with the enhanced dispersibility in aqueous solvents[19] and is evidenced in Figure 4 (photograph). The contrasting inflammatory effects of CNTs and CNOs may reflect differences in size but these particles also differ in other physical characteristics including shape. A size-dependent effect has indeed been described in previous studies investigating the inflammatory profile of particulate materials,[55,56] which found that larger particles are generally less inflammatory than their smaller counterparts. While strong hydrophobic forces are known to induce spontaneous and rapid agglomeration in *r*-CNTs, it is reasonable to suggest that an increased polarity in *p*-CNTs may have hampered this agglomeration leading to the formation of smaller sized-aggregates over the same period of time and hence the enhanced inflammatory responses induced by *p*-CNTs than *r*-CNTs. However, further lowering of zeta potential in *f*-CNTs as a result of benzoic acid functionalization resulted in a decreased inflammatory potential compared with *p*-CNT (Figures 4 and 5). Therefore, despite the enhanced dispersibility of *f*-CNTs (and *f*-CNOs), their inherent polarity led to a reduced local inflammatory response.

4. Conclusion

Our study suggests that the inflammatory properties of carbon NPs, in particular CNTs, may have been overestimated in the current literature and importantly, that simple and carefully designed functionalization strategies may allow for tight control of carbon NP-induced inflammation. Specifically we found that raw CNT induced very limited inflammation in vitro or in vivo while purified CNT induced marked inflammasome activation in vitro and inflammatory responses in vivo which were significantly attenuated by benzoic acid functionalization. We further show that CNO promote less inflammation than carbon nanotubes and this can be further reduced by surface functionalization.

5. Experimental Section

Preparation of Carbon Nanotubes and Nano-Onions for in Vitro and in Vivo Studies: Raw single walled carbon nanotubes (*r*-CNTs) produced by the HiPco technique were purchased from Unidym, Inc. (Lot no R0513). Reagents and solvents used for the purification and chemical functionalization of carbon NPs were purchased as reagent-grade from Fisher Scientific Ireland Ltd, or Sigma-Aldrich Ireland and used without further purification.

Highly Purified Selectively Oxidized CNTs (p-CNTs): Synthesis was performed as previously described.[19] A 300 mg quantity of raw SWNTs was dispersed in 7.9 M HNO_3 (1000 mL) by sonication

DOI: 10.1002/smll.201300481
© 2013 Wiley-VCH Verlag GmbH & Co. KGaA, Weinheim

(sonic waterbath, at 80 kHz) at maximum power for 5 min and subsequently at minimum power for 10 min. The mixture was then stirred under reflux at 100 °C for 4.5 h and quenched with ice. The dispersion was then filtered through a Millipore system (0.2 μm Isopore filter) and washed with distilled water until the filtrate ran neutral. The wet solid was transferred to a Teflon tube, dispersed in 2 M NaOH by sonication for 5 min and subsequently stirred overnight at 100 °C under a nitrogen atmosphere. The mixture was cooled to room temperature, filtered through an Isopore filter and washed with a further 500 mL of 2 M NaOH. The solid was washed with distilled water until the filtrate pH became neutral and the sample was subjected to the NaOH treatment one additional time. Following filtration, the wet solid was dispersed in 10% H_2O_2 by sonication for 5 min and subsequently stirred for 1 h at 100 °C. The dispersion was quenched with ice (800 g, diluting to 2% H_2O_2) and allowed to stand for 12 h. The wet solid was subsequently subjected to two further NaOH treatments (as above), and filtered. The solid was then washed with 2 M NaOH (400mL), followed by distilled water until neutral pH, and a further 1 M HCl (400 mL), followed by distilled water until neutral pH. The wet solid was re-dispersed in distilled water and lyophilized to afford 51 mg of black solid (yield: 17%). A portion of this material was dialyzed (10–13 kDa CO) against medical grade (endotoxin free) sterile water (Baxter) for 5 days. The 5-day dialysis entailed two daily changes of water preceded by a 60- to 90-min sonication at 80 kHz. At the end of the dialysis period, all preparations were placed in sterile glass containers and lyophilized until dry.

Pristine CNOs (p-CNOs): Synthesis was performed by annealing of nanodiamonds as previously described.[26] Briefly, high purity ultradispersed nanodiamonds (Molto Ig, Inc.) were annealed in a graphite crucible at 1650 °C in an Astro carbonization furnace under a partial pressure of helium (approx. 150mm). The temperature was maintained for 1 hr and the sample was cooled to RT over a period of 1 h. This procedure was followed by annealing of the sample in air at 400 °C to remove amorphous carbon and the recovered material was composed mainly of pristine CNOs, 95% recovered mass.

Tour-functionalized CNTs (f-CNTs): Synthesis was performed according to a procedure previously described.[27] A 45 mg quantity of *p*-CNTs was dispersed in N-Methyl-2-pyrrolidone (NMP, 200 mL) by sonication for 20 min. Following addition of 4-aminobenzoic acid (1.1g), the reaction mixture was put under a nitrogen atmosphere. The reaction mixture was stirred overnight at 70 °C, following addition of isoamyl nitrite (1.6 mL) *via* syringe. After cooling to room temperature, the mixture was briefly sonicated to redisperse the sample and was then filtered through a 0.2 μm fluoropore FG filter, and washed with NMP until the filtrate ran clear. The sample was redispersed in NMP (50 mL), and the entire procedure was repeated an additional two times. Finally, the solid was washed with methanol and dried under vacuum to afford 49 mg of black solid. A portion of this material was dialyzed (10-13kDa CO) against medical grade sterile water (Baxter) for 5 days. The 5-day dialysis entailed two daily changes of water preceded by a 60- to 90-min sonication at 80kHz. At the end of the dialysis period, all preparations were placed in sterile glass containers and lyophilized until dry.

Tour-functionalized CNOs (f-CNOs): Synthesis was performed using similar reaction conditions as previously described.[28] A 40 mg quantity was dispersed in DMF (100 mL) by sonication. To this dispersion was added firstly the 4-aminobenzoic acid (3.3 g) and subsequently isoamyl nitrite (5.36 mL) under a nitrogen atmosphere. The reaction was stirred overnight at 60 °C and subsequently allowed to cool to room temperature. The CNOs were separated from the reaction solution by centrifugation. Fresh DMF was added following removal of the supernatant. This procedure was repeatedly conducted until the supernatant solution remained colorless. This was repeated with toluene and methanol and the black solid was finally dried under reduced pressure to afford 38 mg of black solid (yield: 95%). A portion of this material was dialyzed (10–13 kDa CO) against medical grade sterile water (Baxter) for 5 days. The 5-day dialysis entailed two daily changes of water preceded by a 60- to 90-min sonication at 80kHz. At the end of the dialysis period, all preparations were placed in sterile glass containers and lyophilized until dry.

Fluoroscein-Functionalized CNTs (Fluo-CNTs): A 13 mg quantity of *f*-CNTs was dispersed in dry dimethylformamide (DMF) by sonication for 1 h. Dimethylaminopyridine (DMAP) and N-hydroxysuccinimide were added to the mixture and sonicated at minimum power for 10 min. Subsequently, 1-ethyl-3-(3-dimethylaminopropyl)carbodiimide (EDCI) was added and the dispersion was sonicated for 3 hours at low power under a N_2 atmosphere. Finally, fluorosceinamine was added and the dispersion was allowed to stir at 60 °C for 6 days under a N_2 atmosphere. The dispersion was briefly sonicated to redisperse the sample and was then filtered through a 0.2 μm fluoropore FG filter, washing with DMF until the filtrate ran clear. The sample was redispersed in DMF, and the entire procedure was repeated an additional two times. Finally, this material was dialyzed (10–13 kDa CO) against medical grade sterile water (Baxter) for 5 days. The 5-day dialysis entailed two daily changes of water preceded by a 60- to 90-min water bath sonication at 80 kHz. At the end of the dialysis period, all preparations were placed in sterile glass containers and lyophilized until dry.

Fluoroscein-Functionalized CNOs (Fluo-CNOs): An 8 mg quantity of *f*-CNOs was dispersed in dry DMF by sonication for 1 h. Dimethylaminopyridine (DMAP) and N-hydroxysuccinimide were added to the mixture sonicated at minimum power for 10 min. Subsequently, 1-Ethyl-3-(3-dimethylaminopropyl)carbodiimide (EDCI) was added and the dispersion was sonicated for 3 h at low power under a N_2 atmosphere. Finally, fluorosceinamine was added and the dispersion was allowed to stir at 60 °C for 6 days under a N_2 atmosphere. The dispersion was centrifuged at a rcf of 6870g for 60 min and the supernatant removed. The wet solid was redispersed in DMF and again separated from the supernatant by centrifugation (this was repeated an additional two times). Finally, this material was dialyzed (10-13 kDa CO) against medical grade endotoxin-free sterile water (Baxter) for 5 days. The 5-day dialysis entailed two daily changes of water preceded by a 60- to 90-min sonication at 80 kHz. At the end of the dialysis period, all preparations were placed in sterile glass containers and lyophilized until dry.

Prior to in vitro or in vivo experiments, all formulations were prepared by weighing the freeze-dried preparations into sterile glass tubes and diluting them down to the desired concentrations in sterile, endotoxin-free, phosphate buffered saline (PBS) solution. The solutions were then sonicated for 15 min at 30 kHz, 100% intensity, followed by a sonication at 80 kHz for 90–120 min.

Characterization of Carbon Nanotubes and Nano-Onions: Dynamic light scattering (DLS) and zeta potential measurements were conducted on a Malvern Zetasizer Nano ZS system (Malvern Instruments Ltd.) using a HeNe laser (633 nm). For the measurement of zeta potential the carbon nanoparticles (35 μg) were

© 2013 Wiley-VCH Verlag GmbH & Co. KGaA, Weinheim

DOI: 10.1002/smll.201300481

NANO MICRO small

dispersed in low ionic strength 0.01 M phosphate buffer (1.4 mL, pH 7.3) by sonicating them for 15 min at 30 kHz and then for 90 min at 80 kHz prior to measurement. The measurement was conducted at 25 °C six times and the average was calculated. For the DLS measurements the samples were prepared the same way as for the zeta potential measurements but using the sterile phosphate buffered saline (PBS) solution as solvent to replicate the sample preparation used for the in vitro and in vivo experiments. The DLS measurement was carried out repeatedly for a duration of 200 min to observe the agglomeration tendency as a function of time.

AFM: Topographic images were collected in semi-contact mode with an NTEGRA Spectra inverted configuration system (NT-MDT). Silicon tips with reflectance gold coating on the back, tip apex radius 10 nm, force constant 2 N/m and frequency 170 kHz were used (NSG01 (NT-MDT)). The data were collected with NT-MDT Nova software and analysed with WSxM SPM freeware.[57] Samples were prepared by dispersing the nanotubes in high purity DMF by sonication, spray coating them onto freshly cleaved mica substrates and drying them overnight in the oven at 100 °C. For the SWNT size distribution analysis, samples were dispersed at lower concentration in order to adequately estimate single nanoparticle size. Statistical analysis was performed on samples of >100 SWNTs. The contour length of individual SWNTs was measured using the segmented line profiling tool from WSxM SPM freeware. Statistical analysis of CNO size was performed using ImageJ.

Micro-Raman Scattering: Measurements were performed at room temperature in backscattering geometry using a NTEGRA Spectra Upright configuration system (NT-MDT) coupled with an InVia spectrometer (Renishaw) equipped with a 1024 × 256 pixels CCD camera. As excitation sources a HeNe laser (λ_{ex} 633 nm) and an Ar^+ laser (λ_{ex} 514 nm) in combination with a 1800 or 2400 lines mm^{-1} grating, respectively, were used. Measurements were taken with 10 s of exposure time. The laser spot was focused on the sample surface using a 100× long working distance objective (NA 0.7). Raman spectra were collected on numerous spots of the sample. Data were collected and analysed with Renishaw WiRE software.

TEM: Measurements of CNTs and CNOs were performed with a Hitachi Model 9500 and FEI Titan operated at 300 kV, respectively. CNO samples were prepared from dispersion followed by deposition on the copper grids. CNT samples were prepared by drop coating SWNT dispersions in DMF onto a lacey carbon coated 400 mesh copper grid.

FTIR: Spectra were measured in the solid state on a PerkinElmer FTIR Spectrometer Spectrum 100 with a universal ATR sampling accessory (diamond/ZnSe crystal). The spectra for functionalized CNOs and SWNTs were recorded at 256 scans, with a 4 cm^{-1} resolution.

UV-Vis Absorption: Spectra were recorded on a Perkin Elmer UV/Vis Spectrometer Lambda 35 after 1 cycle, with an interval of 1 nm, slit width of 2 nm and scan speed of 240 nm min^{-1}. Absorption spectroscopy was carried out on a Perkin Elmer UV-vis/NIR Lambda 1050 Absorption Photospectrometer. All spectra were recorded on supernatants after 1 cycle, with an interval of 1 nm, slit width 2 nm and scan speed of 240 nm min^{-1}. Samples were either dispersed in NMP or DMF by sonication (3–4 h) and measurements were carried out in a 1 cm quartz cell on the dispersion supernatant following centrifugation at 8000 RPM (900 × g) for 90 min (to remove aggregates and large bundles). Emission spectra were taken in a HORIBA Jobin Yvon Fluorolog-3 Spectrofluorometer equipped with a 450 xenon CV lamp after 1 cycle, with slit width of 10 nm and integration time 0.1 s.

Raman Spectroscopic Analysis of Lymph Node Tissue: Micro-Raman scattering measurements were carried out at room temperature in backscattering geometry using a NTEGRA Spectra Upright configuration (NT-MDT) coupled with an InVia spectrometer (Renishaw) equipped with a 1024 × 256 pixels CCD camera. As excitation sources an Ar^+ laser (λ_{exc} 514 nm) in combination with a 2400 lines mm^{-1} grating was used. In all measurements the laser power did not exceed 5 mW. Measurements were taken with 10 s of exposure time and 1 accumulation. The laser spot was focused on the sample surface using a 100× long working distance objective (NA 0.7). Spectroscopic data were collected and analysed with Renishaw WiRE software. Lymph nodes for Raman analyses were put on a cleaned silicon substrate and covered with a thin layer of fixation solution (4% paraformaldehyde).

Mice Source and Husbandry: Female C57BL/6 wild-type mice aged 8–12 weeks were obtained from Harlan Laboratories (Oxon, UK). $NLRP3^{-/-}$ mice[58] were age- and gender-matched with C57BL/6 wild-type mice for each set of experiments. Animals were maintained on a light/dark cycle with at least 12 h of light and water was provided ad libitum. All animal experiments were conducted according to the regulations of the European Union and the Irish Department of Health, and all procedures were approved by the Animal Ethics Committee (reference number 091210) at Trinity College Dublin.

Measurement of Dendritic Cell Activation: Murine bone-marrow-derived dendritic cells (BMDC) generated as previously described[59] were plated out on day 10 and primed with TLR agonists (LPS, CpG, Pam3CSK4) on day 11 for 1–2 h prior to stimulation with either alum (Brenntag Biosector, Frederikssund, Denmark) or carbon nanoparticles (*r*-CNT, *p*-CNT, *f*-CNT, *p*-CNO or *f*-CNO) at the concentrations indicated. When specified, cells were pretreated with the following chemical inhibitors prior to the addition of particulate materials: 250 nM bafilomycin (an inhibitor of lysosomal acidification) or 10μM CA-074-Me (a cathepsin B inhibitor), 50 mM KCl (for inhibition of potassium efflux). Supernatants were collected and analysed for IL-1β by ELISA (R&D Systems). IL-6 (BD Biosciences), TNF-α and IL-10 (ELISA Max set, Biolegend) were also determined by ELISA according to the manufacturers' instructions. In addition to cytokine secretion the effect of particulates on expression of costimulatory molecule expression was assessed by flow cytometry as described previously.[60] All in vitro experiments were carried out independently a minimum of 3 times.

Innate Immune Responses to Carbon Nanoparticles (Peritonitis Model): Female C57BL/6 mice (n = 3–5) aged 6–8 weeks were injected intraperitoneally with PBS vehicle, Alum (250 μg/mouse), *r*-CNTs (250 μg/mouse), *p*-CNT (250 μg/mouse), *f*-CNT (250 μg/mouse), *p*-CNO (250 μg/mouse) or *f*-CNO (250 μg/mouse). After 3 h, peritoneal lavage cells were collected and cell recruitment was analysed by flow cytometry. In order to determine the nature of the infiltrating cells, peritoneal exudate cells were stained with the following fluorescently labeled antibodies (eBiosciences, Biolegend or BD Pharmingen): CD11b-PE Cy7, Gr1-APC Cy7, F4/80 PerCP Cy5.5, Siglec F-PE, CD3-APC Cy7, CD11c APC, MHC II-PE, CD19-perCP Cy5.5, Ly6C-FITC. A Canto II (BD Biosciences) or CyAN (Dako) flow cytometer was used, and data were analysed using FlowJo software (Tree Star Inc., Ashland, OR, USA). Results were expressed as a percentage of single/live cells (Mean ± SD, $*p < 0.05$, $**p < 0.01$).

DOI: 10.1002/smll.201300481
© 2013 Wiley-VCH Verlag GmbH & Co. KGaA, Weinheim

Cell Viability of Bone-Marrow Derived Dendritic Cell Cultures: Murine bone-marrow-derived dendritic cells (BMDC) generated as previously described[59] were plated out on day 10 and incubated for 24 h on day 11 in the presence of (A) carbon nanotubes (*p*-CNT), (B) nano-onions (*p*-CNO) and (C) Alum at a range of concentrations 1–100 μg cm^{-2}. Cell viability was assessed using the LIVE/DEAD Aqua stain according to the manufacturers' instructions.

Adjuvant Properties of Carbon Nanoparticles: Female C57BL/6 mice (n = 5) were immunized intraperitoneally on days 0 and 14 with endotoxin-free Dulbecco's PBS, human serum albumin (HSA, Novozyme BioPharma UK Ltd, 50 μg/mouse) alone or HSA (50 μg/mouse) mixed with Alum (200 μg/mouse), *r*-CNTs (200 μg/mouse), *p*-CNT (200 μg/mouse), *f*-CNT (200 μg/mouse), *p*-CNO (200 μg/mouse) or *f*-CNO (200 μg/mouse). On day 21, whole blood, spleens and peritoneal lavage cells were collected. Antigen-specific serum IgG and IgG1 titers were determined by ELISA (IgG: Sigma; IgG1: antibody pairs from BD PharMingen). Mediastinal lymph node single cell suspensions were prepared and further cultured with HSA (10 μg/mL) or medium only for 72 h. Supernatants were collected and IL-10, IL-4, IL-17A and IFN-γ concentrations were determined using Max ELISA kits (Biolegend).

Confocal Microscopy Analysis: Immortalized bone marrow-derived macrophages (iBMM) from wild type C57BL/6 mice were generated using J2 transforming retroviruses (expressing Raf and Myc), as described previously.[41] iBMM or bone-marrow derived dendritic cells (5×10^5 cells mL^{-1}) were cultured on glass coverslips at 37 °C for 0–18 h with carbon nanoparticles (25 μg cm^{-2}). Cells were fixed with 2% paraformaldehyde for 20 min and stained with Alexa-Fluor 594-conjugated wheat germ agglutinin (WGA; 10 μg mL^{-1}) for 30 min. Immediately before mounting, Hoechst nuclear stain was applied to the sections for 10 min and excess was washed away. Cells were mounted onto glass slides with Dakomation mounting medium (Dako) and analysed on a Zeiss LSM 510 microscope with LSM 5 software (version 4) and Adobe Photoshop. Stably transfected mouse THP-1 expressing ASC-GFP were prepared according to a protocol previously described.[61]

Statistics: Cytokine concentrations measured by ELISA assays were subjected to ANOVA analyses. Where significant differences were found, the Dunnett's multiple comparisons post hoc test was then performed. Statistical differences in the cell numbers determined by FACS analyses were assessed using the Kruskall–Wallis test, followed by Dunn's post hoc test. Wherever applicable, omparisons between two groups were carried out using two-tailed Student's t-test. Statistical calculations were performed using the GraphPad Prism 5 package (GraphPad Software Inc., San Diego, CA, USA) and Excel. In all cases, p-values ≤0.05 were considered statistically significant (*$p < 0.05$, **$p < 0.01$ and ***$p < 0.001$). Results are representative of three independent experiments, but similarly performed.

Supporting Information

Supporting Information is available from the Wiley Online Library or from the author.

Acknowledgements

This work was supported by Science Foundation Ireland (CSET pathfinder grant 48S55 and Giordani PIYRA 07/Y12/1052). This publication has emanated from research supported in part by a research grant from Science Foundation Ireland (SFI) under Grant Number 12/IA/1421. S.G. wishes to thank the L'Oreal UNESCO For Women in Science Fellowship. L.E. and A.V.C. wish to thank the U.S. National Science Foundation, grants CHE-1110967 and DMR-1205302, and the Robert A. Welch foundation #AH-0033 for generous support. We thank Dr. Jim Harris for taking mediastinal lymph node photographs and for advice on confocal microscopy analysis. Immortalized macrophages from wild-type mice were a kind gift from Douglas Golenbock, University of Massachusetts Medical School, Worcester, MA. We also thank Rebecca Coll, Dr. Sarah Doyle and Dr. Jennifer K. Dowling for technical assistance with ASC-GFP-THP-1 cells. We thank Eoghan Delany for support with the Tour-functionalization of carbon nano-onions and Nicola Pesenti for support with Raman spectroscopic measurements and statistical data analysis of carbon nanoparticle size distribution. We also would like to thank Ruza Leko for designing the ToC and cover figures.

[1] S. Iijima, *Nature* **1991**, *354*, 56.
[2] X. Zhao, R. Liu, *Environ. Int.* **2012**, *40*, 244.
[3] N. Sinha, J. T. Yeow, *IEEE Trans. Nanobiosci.* **2005**, *4*, 180.
[4] S. Y. Madani, N. Naderi, O. Dissanayake, A. Tan, A. M. Seifalian, *Int. J. Nanomed.* **2011**, *6*, 2963.
[5] Y. Liu, Y. Zhao, B. Sun, C. Chen, *Acc Chem Res* **2013**, *46*, 702.
[6] S. K. Smart, A. I. Cassady, G. Q. Lu, D. J. Martin, *Carbon* **2006**, *44*, 1034.
[7] L. A. Thomson, F. C. Law, N. Rushton, J. Franks, *Biomaterials* **1991**, *12*, 37.
[8] M. Allen, F. Law, N. Rushton, *Clin. Mater.* **1994**, *17*, 1.
[9] S. Linder, W. Pinkowski, M. Aepfelbacher, *Biomaterials* **2002**, *23*, 767.
[10] T. Thurnherr, C. Brandenberger, K. Fischer, L. Diener, P. Manser, X. Maeder-Althaus, J.-P. Kaiser, H. F. Krug, B. Rothen-Rutishauser, P. Wick, *Toxicol. Lett.* **2011**, *200*, 176.
[11] M. L. Schipper, N. Nakayama-Ratchford, C. R. Davis, N. W. S. Kam, P. Chu, Z. Liu, X. M. Sun, H. J. Dai, S. S. Gambhir, *Nat. Nanotechnol.* **2008**, *3*, 2.16.
[12] D. Urgate, *Nature* **1992**, *359*, 707.
[13] M. Ghosh, S. K. Sonkar, M. Saxena, S. Sarkar, *Small* **2011**, *7*, 3170.
[14] E. L. Chng, M. Pumera, *Chemistry* **2012**, *18*, 1401.
[15] E. Del Canto, K. Flavin, D. Movia, C. Navio, C. Bittencourt, S. Giordani, *Chem. Mater.* **2011**, *23*, 67.
[16] V. E. Kagan, Y. Y. Tyurina, V. A. Tyurin, N. V. Konduru, A. I. Potapovich, A. N. Osipov, E. R. Kisin, D. Schwegler-Berry, R. Mercer, V. Castranova, A. A. Shvedova, *Toxicol. Lett.* **2006**, *165*, 88.
[17] L. G. Delogu, S. M. Stanford, E. Santelli, A. Magrini, A. Bergamaschi, K. Motamedchaboki, N. Rosato, T. Mustelin, N. Bottini, M. Bottini, *J. Nanosci. Nanotechnol.* **2010**, *10*.
[18] K. Pulskamp, S. Diabaté, H. F. Krug, *Toxicol. Lett.* **2007**, *168*, 58.
[19] F. Flavin, I. Kopf, E. Del Canto, C. Navio, C. Bittencourt, S. Giordani, *J. Mater. Chem.* **2011**, *21*, 17881.
[20] G. A. Tynan, A. McNaughton, A. Jarnicki, T. Tsuji, E. C. Lavelle, *PloS One* **2012**, *7*, e37261.

© 2013 Wiley-VCH Verlag GmbH & Co. KGaA, Weinheim

DOI: 10.1002/smll.201300481

[21] S. L. Hem, H. Hogenesch, *Exp. Rev. Vaccines* **2007**, *6*, 685.
[22] M. W. Munks, A. S. McKee, M. K. MacLeod, R. L. Powell, J. L. Degen, N. A. Reisdorph, J. W. Kappler, P. Marrack, *Blood* **2010**, *116*, 5191.
[23] K. Schroder, J. Tschopp, *Cell* **2010**, *140*, 821.
[24] E. Meunier, A. Coste, D. Olagnier, H. Authier, L. Lefèvre, C. Dardenne, J. Bernad, M. Béraud, E. Flahaut, B. Pipy, *Nanomedicine* **2012**, *8*, 987.
[25] J. Palomäki, E. Välimäki, J. Sund, M. Vippola, P. A. Clausen, K. A. Jensen, K. Savolainen, S. Matikainen, H. Alenius, *ACS Nano* **2011**, *5*, 6861.
[26] A. S. Rettenbacher, B. Elliott, J. S. Hudson, A. Amirkhanian, L. Echegoyen, *Chemistry* **2005**, *12*, 376.
[27] K. Flavin, K. Lawrence, J. Bartelmess, M. Tasior, C. Navio, C. Bittencourt, D. F. O'Shea, D. M. Guldi, S. Giordani, *ACS Nano* **2011**, *5*, 1198.
[28] K. Flavin, N. Chaur, L. Echegoyen, S. Giordani, *Org. Lett.* **2010**, *12*, 840.
[29] M. S. Strano, C. A. Dyke, M. L. Usrey, P. W. Barone, M. J. Allen, H. Shan, C. Kittrell, R. H. Hauge, J. M. Tour, R. E. Smalley, *Science* **2003**, *301*, 1519.
[30] B. Smith, K. Wepasnick, K. E. Schrote, A. R. Bertele, W. P. Ball, C. O'Melia, D. H. Fairbrother, *Environ. Sci. Technol.* **2009**, *43*, 819.
[31] A. Savina, S. Amigorena, *Immunol Rev.* **2007**, *219*, 143.
[32] D. Yang, Y. Zhao, H. Guo, Y. Li, P. Tewary, G. Xing, W. Hou, J. J. Oppenheim, N. Zhang, *ACS Nano* **2010**, *4*, 1178.
[33] K. Inoue, R. Yanagisawa, E. Koike, M. Nishikawa, H. Takano, *Free Radical Biol. Med.* **2010**, *48*, 924.
[34] A. V. Tkach, G. V. Shurin, M. R. Shurin, E. R. Kisin, A. R. Murray, S. H. Young, A. Star, B. Fadeel, V. E. Kagan, A. A. Shvedova, *ACS Nano* **2011**, *5*, 5755.
[35] J. Palomäki, P. Karisola, L. Pylkkänen, K. Savolainen, H. Alenius, *Toxicology* **2010**, *267*, 125.
[36] T. Zhang, M. Tang, L. Kong, H. Li, T. Zhang, S. Zhang, Y. Xue, Y. Pu, *J. Hazard Mater.* **2012**, *219-220*, 203.
[37] D. Crouzier, S. Follot, E. Gentilhomme, E. Flahaut, R. Arnaud, V. Dabouis, C. Castel-larin, J. C. Debouzy, *Toxicology* **2010**, *272*, 39.
[38] A. S. Yazdi, G. Guarda, N. Riteau, S. K. Drexler, A. Tardivel, I. Couillin, J. Tschopp, *Proc. Natl. Acad. Sci. USA* **2010**, *107*, 19449.
[39] H. Li, S. B. Willingham, J. P. Ting, F. Re, *J. Immunol.* **2008**, *181*, 17.
[40] T. Fernandes-Alnemri, J. Wu, J. W. Yu, P. Datta, B. Miller, W. Jankowski, S. Rosenberg, J. Zhang, E. S. Alnemri, *Cell Death Differ.* **2007**, *14*, 1590.
[41] A. Halle, V. Hornung, G. C. Petzold, C. R. Stewart, B. G. Monks, T. Reinheckel, K. A. Fitzgerald, E. Latz, K. J. Moore, D. T. Golenbock, *Nat. Immunol.* **2008**, *9*, 857.
[42] V. Hornung, F. Bauernfeind, A. Halle, E. O. Samstad, H. Kono, K. L. Rock, *Nat. Immunol.* **2008**, *9*, 847.
[43] M. Kool, T. Thomas Soullié, M. van Nimwegen, M. A. M. Willart, F. Muskens, S. Jung, H. C. Hoogsteden, H. Hammad, B. N. Lambrecht, *J. Exp. Med.* **2008**, *205*, 869.
[44] S. Calabro, M. Tortoli, B. C. Baudner, A. Pacitto, M. Cortese, D. T. O'Hagan, E. De Gregorio, A. Seubert, A. Wack, *Vaccine* **2011**, *29*, 1812.
[45] H. Sun, K. G. Pollock, J. M. Brewer, *Vaccine* **2003**, *21*, 849.
[46] A. S. McKee, M. W. Munks, P. Marrack, *Immunity* **2007**, *27*, 687.
[47] L. Yan, F. Zhao, S. Li, Z. Hu, Y. Zhao, *Nanoscale* **2011**, *3*, 362.
[48] M. V. Ivanova, C. Lamprecht, M. J. Loureiro, J. T. Huzil, M. Foldvari, *Int. J. Nanomed.* **2012**, *7*, 403.
[49] R. K. Esch, L. Han, K. K. Foarde, D. S. Ensor, *Nanotoxicology* **2010**, *4*, 73.
[50] F. A. Sharp, D. Ruane, B. Claass, E. Creagh, J. Harris, P. Malyala, M. Singh, D. T. O'Hagan, V. Pétrilli, J. Tschopp, L. A. J. O'Neill, E. C. Lavelle, *Proc. Natl. Acad. Sci. USA* **2009**, *106*, 870.
[51] L. Ding, J. Stilwell, T. Zhang, O. Elboudwarej, H. Jiang, J. P. Selegue, P. A. Cooke, J. W. Gray, F. F. Chen, *Nano Lett.* **2005**, *5*, 2448.
[52] P. Urban, J. J. Valle-Delgado, E. Moles, J. Marques, C. Diez, X. Fernandez-Busquets, *Curr. Drug Targets* **2012**, *13*, 1158.
[53] B. Zhang, C. T. Kwok, *J. Mater. Sci. Mater. Med.* **2011**, *22*, 2249.
[54] Z. Liu, S. Tabakman, K. Welsher, H. Dai, *Nano Res.* **2009**, *2*, 85.
[55] H. L. Karlsson, J. Gustafsson, P. Cronholm, L. Möller, *Toxicol. Lett.* **2009**, *188*, 112.
[56] H. Yang, C. Liu, D. Yang, H. Zhang, Z. Xi, *J. Appl. Toxicol.* **2009**, *29*, 69.
[57] I. Horcas, R. Fernández, J. M. Gómez-Rodríguez, J. Colchero, J. Gómez-Herrero, A. M. Baro, *Rev. Sci. Instrum.* **2007**, *78*, 13705.
[58] F. Martinon, V. Petrilli, A. Mayor, A. Tardivel, J. Tschopp, *Nature* **2006**, *440*, 237.
[59] M. B. Lutz, N. Kukutsch, A. L. Ogilvie, S. Rössner, F. Koch, N. Romani, G. Schuler, *J. Immunol. Methods* **1999**, *223*, 77.
[60] E. A. McNeela, A. Burke, D. R. Neill, C. Baxter, V. E. Fernandes, D. Ferreira, S. Smeaton, R. El-Rachkidy, R. M. McLoughlin, A. Mori, B. Moran, K. A. Fitzgerald, J. Tschopp, V. Pétrilli, P. W. Andrew, A. Kadioglu, E. C. Lavelle, *PLoS Pathog.* **2010**, *6*, e 1001191.
[61] S. L. Doyle, M. Campbell, E. Ozaki, R. G. Salomon, A. Mori, P. F. Kenna, G. J. Farrar, A. S. Kiang, M. M. Humphries, E. C. Lavelle, L. A. O'Neill, J. G. Hollyfield, P. Humphries, *Nat. Med.* **2012**, *18*, 791.

Received: February 14, 2013
Revised: May 9, 2013
Published online:

© 2013 Wiley-VCH Verlag GmbH & Co. KGaA, Weinheim

Autophagy Regulates IL-23 Secretion and Innate T Cell Responses through Effects on IL-1 Secretion

Celia Peral de Castro,*,† Sarah A. Jones,*,† Clíona Ní Cheallaigh,‡ Claire A. Hearnden,‡ Laura Williams,* Jan Winter,‡ Ed C. Lavelle,†,‡ Kingston H. G. Mills,*,† and James Harris*,†

Autophagy controls IL-1β secretion by regulating inflammasome activation and by targeting pro–IL-1β for degradation. In this article, we show that inhibition of autophagy, either with the PI3K inhibitors 3-methyladenine, wortmannin, and LY294002 or with small interfering RNA against autophagy proteins augmented the secretion of IL-23 by human and mouse macrophages and dendritic cells in response to specific TLR agonists. This process occurred at the transcriptional level and was dependent on reactive oxygen species and IL-1R signaling; it was abrogated with an IL-1R antagonist or with IL-1–neutralizing Abs, whereas treatment with either rIL-1α or IL-1β induced IL-23 secretion. Dendritic cells treated with LPS and 3-methyladenine secreted enhanced levels of both IL-1β and IL-23, and supernatants from these cells stimulated the innate secretion of IL-17, IFN-γ, and IL-22 by γδ T cells. These data demonstrate that autophagy has a potentially pivotal role to play in the induction and regulation of inflammatory responses by innate immune cells, largely driven by IL-1 and its consequential effects on IL-23 secretion. ***The Journal of Immunology*****, 2012, 189: 4144–4153.**

Autophagy is a highly conserved homeostatic mechanism that orchestrates the sequestration and degradation of damaged or noxious cytosolic constituents, including organelles, and regulates the catabolism of macromolecules during nutrient deprivation. More recently, autophagy has been shown to regulate inflammation and immune responses to infection. In particular, autophagy can mediate the intracellular killing of some bacteria by macrophages (1) and is involved in the presentation of Ags via MHC class I and class II molecules (2). Autophagy is regulated by cytokines; in macrophages, it is induced by IFN-γ and TNF-α (3, 4) and inhibited by IL-4, IL-13, and IL-10 (5-8). Numerous studies have also demonstrated a role for autophagy in regulating the secretion of cytokines (reviewed in Ref. 9), including members of the IL-1 family.

Inhibition of autophagy allows the processing and secretion of the proinflammatory cytokine IL-1β in response to TLR3 and TLR4 agonists, and this process may be dependent on TIR domain-containing adaptor protein inducing IFN-β (TRIF), reactive oxygen species (ROS), and mitochondrial DNA (10–13). In addition, inhibition of autophagy enhances the secretion of IL-1α and IL-18 in response to LPS (10). Conversely, autophagosomes have been shown to target both pro–IL-1β and the inflammasome components ASC and NLRP3 within cells, thus directly regulating the production and availability of IL-1β (10, 14). Moreover, both IL-1β and IL-1α induce autophagy in macrophages (15), suggesting that these cytokines might regulate their own secretion. These data, together with studies showing that autophagy alters disease outcomes in animal models of sepsis (10, 11) and colitis (12), suggest that autophagy is a potent regulator of inflammatory responses. Supporting this, polymorphisms in human *ATG16L1*, a protein involved in autophagosome formation, have been associated with an increased risk of Crohn's disease (16, 17).

Both IL-1β and IL-1α, as well as IL-18, can drive IL-17 secretion by Th17 and γδ T cells, but only in the presence of IL-23 (18–20). This pathway can drive inflammatory pathologies in multiple autoimmune diseases, including multiple sclerosis and rheumatoid arthritis (21–24), and is important in immunity to infection (18, 25, 26). In this study, we demonstrate that inhibition of autophagy promotes the secretion of IL-1α, IL-1β, and IL-23 by macrophages and dendritic cells (DC), which in turn influences the innate secretion of IL-17, IFN-γ, and IL-22 by γδ T cells. Moreover, this is dependent on IL-1 and NF-κB signaling, and both IL-1α and IL-1β augment IL-23 production. These data demonstrate a potentially pivotal role for autophagy in regulating inflammatory cytokines and innate T cell-driven immune responses.

Materials and Methods

Materials and reagents

Wortmannin, LY294002, and rapamycin were from Sigma-Aldrich (Poole, U.K.), and 3-methyladenine (3-MA) was from Sigma-Aldrich or Merck Millipore (Billerica, MA). Hydrocinnamoyl-L-valyl pyrrolidine (IL-1R antagonist [IL-1Ra]) and BAY 11-7082 (NF-κB inhibitor) were from Merck Millipore. LPS from *Escherichia coli* serotype R515 was from Enzo Life Sciences (Exeter, U.K.), and polyinosinic:polycytidylic acid [poly(I:C)], R837, and CpG were from InvivoGen (San Diego, CA). PP242 was from Chemdea (Ridgewood, NJ). Recombinant human (rh)IL-1β was from

*Immune Regulation Research Group, School of Biochemistry and Immunology, Trinity Biomedical Sciences Institute, Trinity College, Dublin 2, Ireland; †Immunology Research Centre, Trinity College, Dublin 2, Ireland; and ‡Adjuvant Research Group, School of Biochemistry and Immunology, Trinity Biomedical Sciences Institute, Trinity College, Dublin 2, Ireland

Received for publication July 12, 2012. Accepted for publication August 10, 2012.

This work was supported by Science Foundation Ireland as part of the Immunology Research Centre, Science Foundation Ireland Strategic Research Cluster (Grant 07/SRC/B1144).

Address correspondence and reprint requests to Dr. James Harris, School of Biochemistry and Immunology, Trinity Biomedical Sciences Institute, Trinity College, Dublin 2, Ireland. E-mail address: jaharris@tcd.ie

The online version of this article contains supplemental material.

Abbreviations used in this article: BMDC, bone marrow-derived dendritic cell; DC, dendritic cell; iBMM, immortalized bone marrow-derived macrophage; IL-1Ra, IL-1R antagonist; 3-MA, 3-methyladenine; mTOR, mammalian target of rapamycin; poly(I:C), polyinosinic:polycytidylic acid; rh, recombinant human; ROS, reactive oxygen species; siRNA, small interfering RNA; TRIF, TIR domain-containing adaptor protein inducing IFN-β.

Copyright © 2012 by The American Association of Immunologists, Inc. 0022-1767/12/$16.00

www.jimmunol.org/cgi/doi/10.4049/jimmunol.1201946

Downloaded from http://www.jimmunol.org/ at IRIS - IReL Consortia on June 18, 2013

Immunotools (Friesoythe, Germany). Granzyme B-cleaved and full-length murine IL-1α were gifts from Prof. S. Martin (Trinity College Dublin, Ireland).

Cell culture

C57BL/6 mice were obtained from Harlan Olac (Bicester, U.K.) and were used at 8–16 wk of age. Animals were maintained according to the regulations of the European Union and the Irish Department of Health. Bone marrow-derived DC (BMDC) were generated as previously described (27) and grown in RPMI 1640 medium (Biosera, East Sussex, U.K.) with 10% FCS, L-glutamine (2 mM), and penicillin and streptomycin (50 U/ml and 50 μg/ml, respectively) (complete medium). The medium was supplemented with GM-CSF (40 ng/ml). Cells were plated out on day 10 and stimulated on day 11. BMDC from $TRIF^{+/+}$ and $TRIF^{-/-}$ mice were provided by Prof. K. Fitzgerald (University of Massachusetts Medical Center, Worcester, MA).

$CD3^+$ T cell isolation and culture

$CD3^+$ T cells were purified from spleens of C57BL/6 mice using magnetic beads for negative selection (*Pan* T Cell Isolation Kit II, mouse; Miltenyi Biotec), according to the manufacturer's instructions. In some experiments, cells were cultured with IL-1β (10 ng/ml), IL-23 (10 ng/ml), LPS (10 or 100 ng/ml), 3-MA (5–10 mM), IL-1Ra (5 μg/ml), or combinations thereof. Alternatively, $CD3^+$ T cells were cultured with supernatants (50 μl/200 μl $CD3^+$ cells) obtained from DCs cultured for 24 h with 3-MA (5–10 mM) in the presence or absence of LPS (10 ng/ml). Similarly, $CD3^+$ T cells were cultured with supernatants obtained from immortalized bone marrow-derived macrophages (iBMM) transfected with control (scrambled), beclin I, or Atg7 small interfering RNA (siRNA) stimulated for 18 h with LPS (10–100 ng/ml). After 72 h, IL-17A, IL-17F, and IFN-γ concentrations in supernatants were determined by ELISA.

For characterization of γδ T cells, lymph node T cells depleted of γδ T cells (2×10^5) or γδ T cells (2×10^4) enriched from lymph nodes using a $TCR\gamma/\delta^+$ T cell MACS Isolation kit, according to manufacturer's instructions (Miltenyi Biotec), were cultured for 72 h in 200 μl complete medium. Supernatants (50 μl) or recombinant cytokines were added to each well, as described above. Cytokine (IL-17A, IL-22, and IFN-γ) secretion was measured by ELISA.

iBMM cell lines

iBMM from wild-type C57BL/6, generated using J2 transforming retroviruses, were a gift from Prof. D. Golenbock (University of Massachusetts Medical Center). iBMM stably expressing EGFP-LC3 (GFP-LC3) were generated as previously described (10) and expanded under constant selection with 10 μg/ml puromycin. All iBMM were grown in complete medium.

Mycobacterium tuberculosis *culture*

M. tuberculosis strain H37Rv was grown in Middlebrook 7H9 broth with 0.2% glycerol and albumin–dextrose catalase supplement. Mycobacteria were grown to log phase before use, declumped by vortexing with glass beads for 60 s, and resuspended in RPMI 1640 medium with 10% FCS before use.

Macrophage and DC transfection

iBMM or BMDC were transfected by nucleoporation with an Amaxa Nucleofector Device (Lonza, Wokingham, U.K.) as described previously (5). iBMM were harvested after 2–3 d in culture and resuspended in 100 μl of the appropriate electroporation buffer (Lonza AG) with 10 nM siGENOME SMARTpool siRNA against beclin 1, Atg7, or siGENOME nontargeting control siRNA (Thermo Scientific, Lafayette, CO). Transfected cells were incubated overnight in complete medium before stimulation with LPS for 24 h. Targeting efficiency was analyzed by Western blot for beclin 1 and Atg7.

ELISA

Cytokine secretion in cell culture supernatants was measured by ELISA, according to the manufacturer's standard protocols (R&D Systems, Abingdon, U.K.; eBioscience, San Diego, CA; and BD Biosciences, San Diego, CA). Absorbance was read on a Multiscan FC plate reader and analyzed with SkanIt for Multiscan FC software (Thermo Scientific).

Propidium iodide incorporation assay

BMDC were grown and stimulated in 96 well U-bottom tissue culture plates. After treatment with LPS and 3-MA, cells were incubated with propidium iodide (1 μg/ml) for 5 min. A CyAN (DakoCytomation, Dublin, Ireland) flow cytometer was used to analyze fluorescence, and the data were analyzed using FlowJo software (Tree Star, Ashland, OR).

Quantitative PCR

Mouse BMDC were stimulated for 4 h with 3-MA (2.5–10 mM) in the presence or absence of LPS (10 ng/ml). RNA was purified with the TRIzol (Invitrogen)/chloroform method; this process was followed by transcription into cDNA with a High-Capacity cDNA Reverse Transcription Kit (Applied Biosystems). Real-time PCR for the detection of IL-23p19 (*il23a*) (Mm00518984_m1) and IL-1β (*il1b*) (Mm00434228_m1) mRNA was performed with predesigned TaqMan gene expression assays (Applied Biosystems) using a 7500 Fast Real-Time PCR machine (Applied Biosystems). Expression was normalized to 18s rRNA.

Confocal microscopy

Immortalized GFP-$LC3^+$ iBMM were grown and stimulated on nitric acid-treated glass coverslips (19 mm diameter) in 12-well plates. Cells were fixed with 2% paraformaldehyde for 30 min at room temperature and permeabilized for 10 min with Triton X-100 (0.1% in PBS). All subsequent steps were conducted at room temperature. The cells were blocked with 5% goat serum in PBS with 1% BSA (blocking buffer) for 1 h and stained with primary Ab (1/200 in blocking buffer) for 1 h. After washing with PBS (five times), the cells were stained with Alexa Fluor 568-conjugated goat anti-rabbit IgG (1/500 in blocking buffer; Life Technologies, Grand Island, NY) for 1 h. In some experiments, cells were stained with tetramethylrhodamine isothiocyanate–phalloidin (American Peptide, Sunnyvale, CA) at 1 μg/ml to stain polymerized actin. The coverslips were mounted onto glass slides with fluorescent Mounting medium (DakoCytomation) and analyzed on an Olympus FV1000 laser scanning confocal microscope.

Immunoblotting

BMDC and immortalized iBMM were washed twice with PBS and lysed, according to a previously described protocol (28). Samples were loaded and separated on 10, 12, or 15% SDS-polyacrylamide gels and transferred to a nitrocellulose membrane. The membrane was blocked for 1 h with 5% milk in PBS/Tween 20 (0.1%). After washing with PBS/Tween 20, the membrane was probed with primary Ab (1/500 in 3% BSA) overnight at 4°C, washed three times with PBS/Tween, and probed with HRP-conjugated secondary Ab (1/2000 in PBS) for 1 h at room temperature. The membrane was washed three times with PBS/Tween 20 and developed with freshly prepared luminol-based detection solution. Densitometric analysis of blots was conducted using ImageJ software (National Institutes of Health, Bethesda, MD).

LPS challenge in vivo

Female BALB/c mice were injected i.p. with 200 μl PBS, LPS (10 μg/mouse in 200 μl PBS), or LPS with rapamycin (1.5 mg/kg in 200 μl PBS). After 4 h, mice were bled, and ELISA analysis was performed on plasma samples.

Statistical analysis

Unless otherwise stated, data sets were analyzed for statistical significance ($p < 0.05$) using one-way ANOVA, followed by a Bonferroni post hoc test. Statistical analysis was conducted using GraphPad Prism software.

Results

The autophagy inhibitor 3-MA enhances LPS-induced secretion of IL-23

3-MA is a PI3K inhibitor that blocks autophagic degradation of proteins (29). Our previous work has demonstrated that treatment of murine macrophages and DC with 3-MA stimulates the secretion of IL-1β, IL-1α, and IL-18 in responses to specific TLR ligands (10). To determine whether IL-23 secretion was also regulated by autophagy, we treated human PMA-differentiated THP-1 monocyte/macrophages with 3-MA and LPS overnight and measured cytokines in the supernatants. At concentrations of 2.5 mM and above, 3-MA stimulated the secretion of both IL-23 and IL-1β in response to LPS (Fig. 1A, 1B). IL-1α secretion by THP-1 cells was also stimulated under these conditions (Supplemental

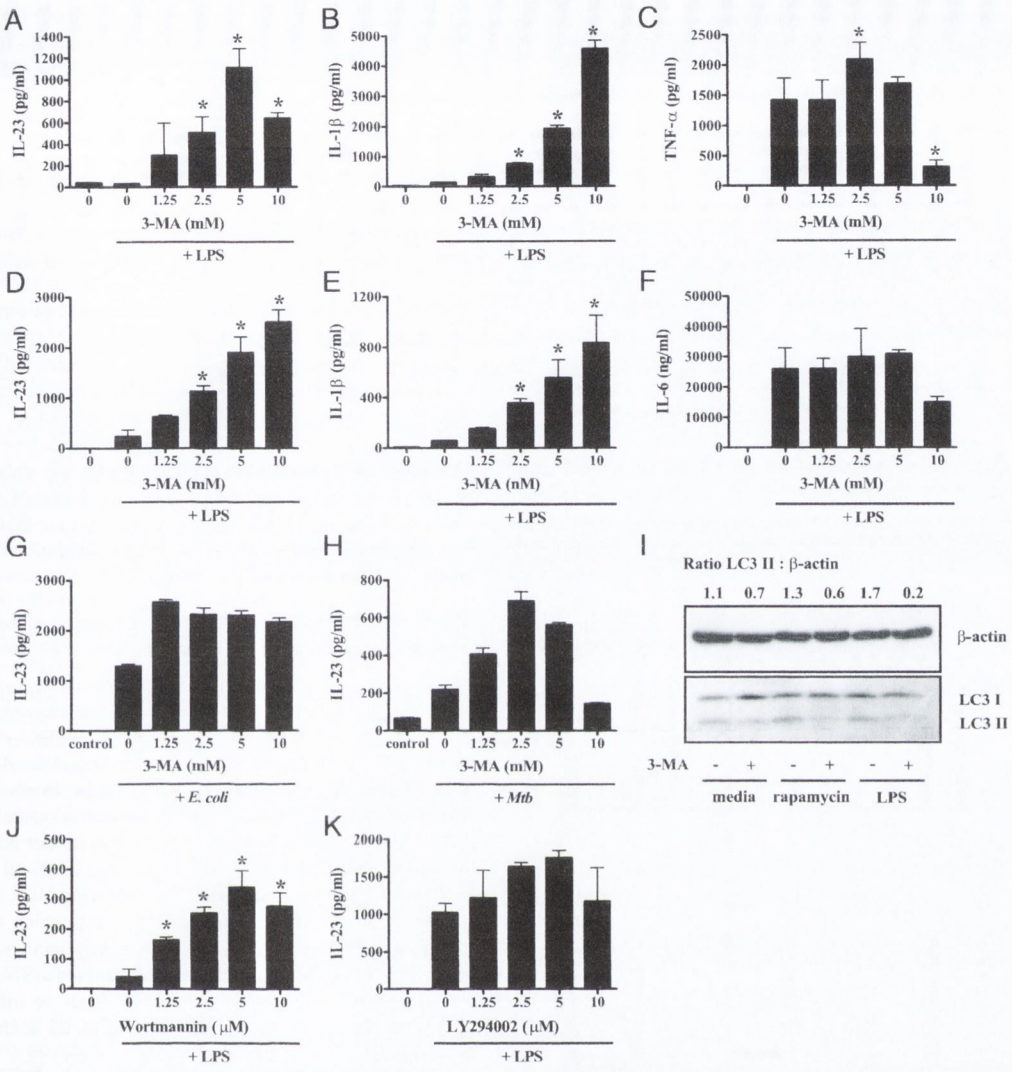

FIGURE 1. Inhibition of autophagy enhances LPS-induced secretion of IL-23 by macrophages and DC. PMA-differentiated human THP-1 cells (**A–C**) or murine bone marrow-derived dendritic cells (BMDC) (**D–F**) were treated with LPS (100 or 10 ng/ml) for 24 h in the presence of 3-MA at different concentrations and levels of IL-23 (A, D), IL-1β (B, E), TNF-α (C), and IL-6 (F) in the supernatants measured by ELISA. BMDC (**G**) or PMA-differentiated THP-1 cells (**H**) were treated with heat-killed *E. coli* (multiplicity of infection 10:1 bacteria:cells) (G) or live *Mycobacterium tuberculosis* strain H37Rv (multiplicity of infection 10:1) (H) in the presence of different concentrations of 3-MA for 24 h and IL-23 secretion measured by ELISA. (**I**) Lysates from BMDC treated with bafilomycin (100 nM) and rapamycin or LPS in the presence or absence of 3-MA (10 mM) were stained for LC3 I (cytosolic) and LC3 II (lipidated, membrane-bound) by Western blot analysis. The samples were stained for β-actin as a loading control. (**J** and **K**) BMDC were treated with LPS (10 ng/ml) in the presence of wortmannin (J) or LY294002 (K) at different concentrations and IL-23 secretion measured by ELISA of culture supernatants. Data represent mean values + SD ($n \geq 3$); *$p < 0.05$ compared with LPS only, one-way ANOVA with Bonferroni's multiple comparison test.

Fig. 1A). In contrast, LPS-induced TNF-α secretion was enhanced by 3-MA at 2.5 mM but inhibited by 10 mM (Fig. 1C). In primary murine BMDC, 3-MA increased LPS-induced secretion of IL-23 and IL-1β (Fig. 1D, 1E), as well as IL-1α (Supplemental Fig. 1B). Levels of IL-6 secreted by these cells were not significantly affected (Fig. 1F). This effect was also observed in primary human monocyte-derived DC in which 3-MA augmented LPS-induced IL-23 secretion but inhibited TNF-α secretion (Supplemental Fig. 1C, 1D). In addition, 3-MA enhanced the secretion of IL-23 by BMDC in response to heat-killed *E. coli* (Fig. 1G). Secretion of IL-1α and IL-1β was also increased in response to *E. coli* with 3-MA (Supplemental Fig. 1E, 1F), whereas IL-6 secretion was either unaffected or inhibited (Supplemental Fig. 1G). Similarly, stimulation of THP-1 cells with 3-MA enhanced IL-23 secretion in response to live virulent *M. tuberculosis* H37Rv (Fig. 1H), whereas TNF-α secretion was either unaffected or inhibited (Supplemental Fig. 1H). To confirm the autophagy-inhibiting activity of 3-MA, we treated BMDC with the autophagy inducer rapamycin or with LPS for 2 h in the presence or absence of 3-MA and bafilomycin (to inhibit autophagic flux (30)) and measured levels of LC3 I (cytosolic) and LC3 II (lipidated autophagosomal membrane-bound) by Western blotting. Both rapamycin and LPS increased the amount of LC3 II present, indicating an increase in autophagosome biogenesis, whereas 3-MA inhibited this effect (Fig. 1I).

Treatment with other broad-range PI3K inhibitors has also been shown to inhibit autophagy (30). In our model, LPS-induced IL-23 secretion by BMDC was increased in the presence of the PI3K

Downloaded from http://www.jimmunol.org/ at IRIS - IReL Consortia on June 18, 2013

inhibitors wortmannin and LY294002 (Fig. 1J, 1K), and both IL-1β and IL-23 secretion were enhanced by LY294002 in THP-1 cells (Supplemental Fig. 1I, 1J). These data demonstrate that autophagy-inhibiting drugs augment IL-23 secretion by macrophages and DC in response to microbial stimuli.

IL-1β secretion in the absence of autophagy is dependent on the TLR adaptor molecule TRIF and thus only occurs in response to TLR3 and TLR4 agonists, which signal through this pathway (10, 12). In this study, we also observed enhanced secretion of IL-23 by 3-MA–treated BMDC in response to TLR3 and TLR4 ligands but not ligands of other TLRs. Both IL-23 and IL-1β secretion were increased in cells treated with 3-MA in combination with the TLR3 ligand poly(I:C) or the TLR4 ligands LPS and monophosphoryl lipid A (which preferentially signals through TRIF) but not the TLR2 ligand PAM_3CysK_4, the TLR7 agonist R837 (imiquimod), the TLR7/8 agonist R848, or the TLR9 ligand CpG (Fig. 2A–D). Both IL-1β and IL-23 secretion were augmented by 3-MA in response to zymosan, a ligand for TLR2, but which also signals through binding to dectin-1 (Fig. 2C, 2D). To determine whether the effect of 3-MA on IL-23 secretion was dependent on signaling through TRIF, which has been previously demonstrated for IL-1β secretion (10, 12), we treated BMDC from wild-type and $TRIF^{-/-}$ mice with LPS and 3-MA. Both IL-1β and IL-23 secretion was inhibited in the $TRIF^{-/-}$ cells (Fig. 2E, 2F).

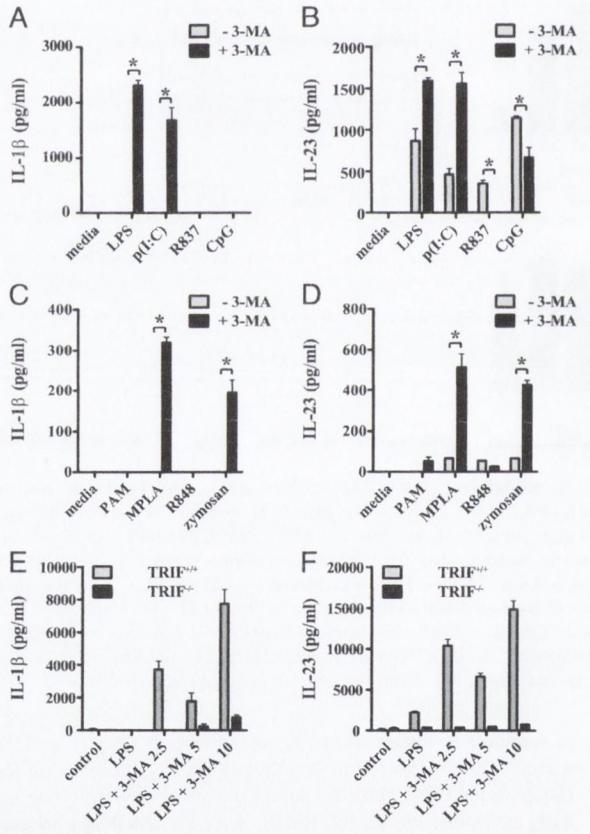

FIGURE 2. IL-23 secretion in autophagy-deficient cells is dependent on specific TLRs. Murine BMDC were treated with different TLR ligands (10 ng/ml LPS, 1 μg/ml poly(I:C), 1 μg/ml R837, 10 μg/ml CpG, 1 μg/ml PAM_3CysK_4, 500 ng/ml monophosphoryl lipid A (MPLA), 1 μg/ml R848, and 1 μg/ml zymosan) in the presence or absence of 3-MA (10 mM), and culture supernatants were tested by ELISA for IL-1β (**A**, **C**) or IL-23 (**B**, **D**). (**E** and **F**) Murine BMDC from $TRIF^{+/+}$ and $TRIF^{-/-}$ mice were treated with LPS in the presence or absence of 3-MA at different concentrations and culture supernatants tested by ELISA for IL-1β (E) or IL-23 (F). Data represent mean values + SD ($n \geq 3$); $^*p < 0.05$ difference between +3-MA and −3-MA, one-way ANOVA with Bonferroni's multiple comparison test.

Specific knockdown of autophagy proteins enhances LPS-induced secretion of IL-23

Knockdown of autophagy-specific genes, using siRNA targeting beclin 1 and Atg7, enhances LPS-induced secretion of IL-1β by macrophages (10, 12). In this study, we found that siRNA depletion of beclin 1 in murine iBMM enhanced secretion of IL-1α and IL-1β but did not affect secretion of IL-12/23 p40 (Fig. 3A-D). Moreover, knockdown of either beclin 1 or Atg7 enhanced secretion of IL-23, but not TNF-α, in response to LPS (Fig. 3E–H), replicating the effects produced by treatment with 3-MA. Inhibition of autophagy with 3-MA has been demonstrated to drive IL-1β secretion by human PBMC in response to *M. tuberculosis* (31). Similarly, we show in this study that knockdown of beclin 1 in BMDC, even though only partial, significantly enhanced IL-23 but not TNF-α secretion in response to irradiated *M. tuberculosis* strain H37Rv (Fig. 3I, 3J). These data demonstrate that in microbe-activated macrophages and DC, the specific inhibition of autophagy enhances IL-23 secretion.

Inhibition of autophagy alters IL-23 expression at the transcriptional level

The effects of autophagy inhibition on LPS-driven IL-1β secretion have previously been shown to occur at the transcriptional level (31, 32). In this study, we examined cytokine mRNA expression in murine BMDC in response to LPS and 3-MA. After 4-h treatment with LPS, expression of IL-1β mRNA was increased, but this was unaffected by 3-MA (Fig. 4A). However, expression of IL-23 mRNA was enhanced by LPS, and this was further augmented by the addition of 3-MA (Fig. 4B). Expression of IL-10 mRNA was increased by LPS but unaffected by 3-MA (Fig. 4C). Similarly, in iBMM transfected with beclin 1 siRNA, expression of IL-23p19 mRNA in response to LPS was significantly increased after 4 h compared with cells transfected with scrambled siRNA (Fig. 4D). Thus, inhibition of autophagy not only leads to inflammasome activation but also to the upregulation of IL-23 at the transcriptional level.

Secretion of IL-23 in response to 3-MA and LPS is dependent on IL-1 signaling

In human PBMC exposed to wheat gliadin, IL-23 secretion is driven by IL-1 signaling (33). To determine whether IL-23 secretion was dependent on IL-1 signaling in our model, we treated BMDC and PMA-differentiated THP-1 cells with LPS and 3-MA in the presence or absence of hydrocinnamoyl-L-valyl pyrrolidine, an IL-1Ra. In BMDC, IL-1Ra inhibited the secretion of both IL-23 and IL-1β in response to LPS and 3-MA but had no effect on IL-12p40 or IL-12/23p70 secretion (Fig. 5A–D), whereas in THP-1 cells, IL-1Ra inhibited the secretion of IL-23, but not IL-1β, in response to LPS and 3-MA (Fig. 5E, 5F). In THP-1 cells, a neutralizing Ab against IL-1β inhibited IL-23 secretion at all concentrations tested, whereas a neutralizing Ab against IL-1α had a small inhibitory effect only at the lowest concentration tested (Fig. 6A). Similarly, secretion of IL-23 by THP-1 cells stimulated with heat-killed *E. coli* and 3-MA was inhibited with neutralizing Abs against IL-1β but not IL-1α (Fig. 6B). To further assess the ability of IL-1 to induce IL-23 secretion, THP-1 cells were treated with rhIL-1α or rhIL-1β. At 10 ng/ml, rhIL-1α induced IL-23 secretion, both in the presence and absence of LPS (Fig. 6C). Similarly, rhIL-1β stimulated IL-23 secretion by THP-1 cells, regardless of exposure to LPS (Fig. 6D).

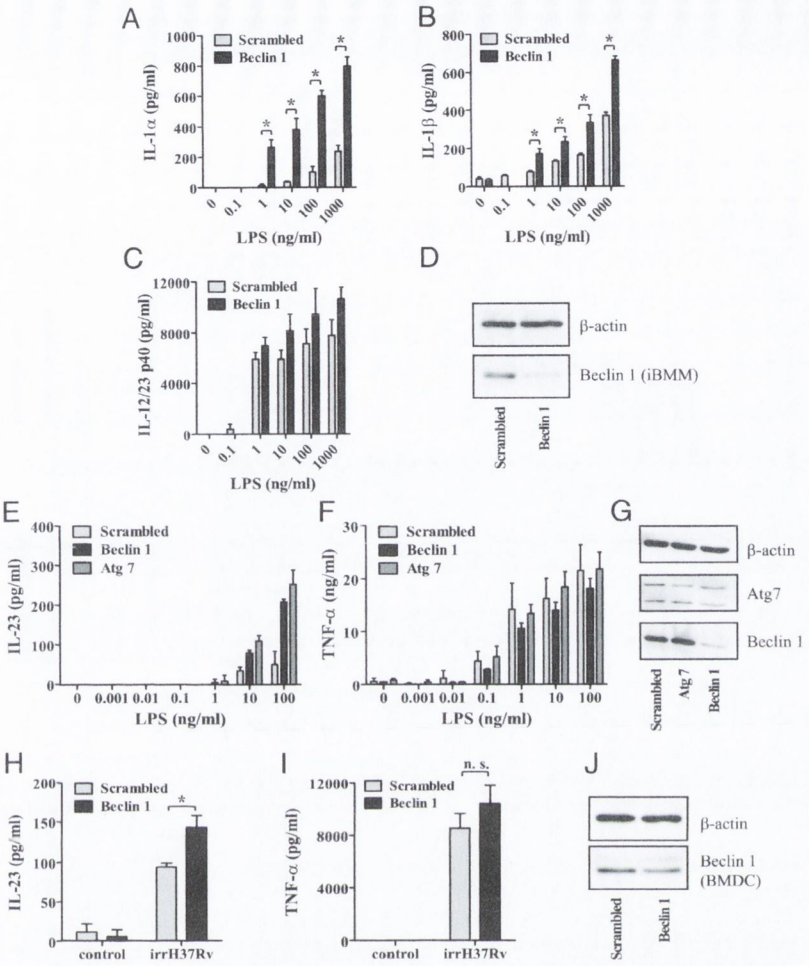

FIGURE 3. siRNA-targeted inhibition of autophagy enhances LPS-induced IL-23 secretion. (**A–C**) Murine iBMM were transfected with siRNA against beclin 1 or nontargeting ("scrambled") siRNA and treated with LPS at different concentrations for 24 h. Secretion of IL-1α (A), IL-1β (B), and IL-12/23 p40 (C) were measured from culture supernatants by ELISA. (**D**) Western blot analysis of beclin 1 levels in transfected iBMM from (A)–(C). (**E** and **F**) iBMM were transfected with siRNA against beclin 1, Atg7, or scrambled siRNA and treated with LPS at different concentrations for 24 h. Secretion of IL-23 (E) and TNF-α (F) were measured from culture supernatants by ELISA. (**G**) Western blot analysis of beclin 1 and Atg7 levels in transfected iBMM from (E) and (F). (**H** and **I**) Murine BMDC were transfected with siRNA against beclin 1 or scrambled siRNA and treated with irradiated *M. tuberculosis* strain H37Rv (multiplicity of infection 10:1 bacteria:cells) for 24 h. Culture supernatants were analyzed by ELISA for IL-23 (H) and TNF-α (I). (**J**) Western blot analysis of beclin 1 levels in BMDC transfected with scrambled or beclin 1 siRNA. Data represent mean values + SD ($n \geq 3$); $^*p < 0.05$ compared with corresponding scrambled control, one-way ANOVA with Bonferroni's multiple comparison test.

Because the IL-1R1 is known to signal through the NF-κB pathway, we assessed the effects of a NF-κB inhibitor, BAY 11-7082, on LPS/IL-1β–induced IL-23 secretion. In PMA-differentiated THP-1 cells, the inhibitor abrogated the effects of LPS and rhIL-1β, but not LPS alone, on IL-23 secretion (Fig. 6E). In addition, LPS and rhIL-1β enhanced the secretion of TNF-α by THP-1 cells, and this was again inhibited by the NF-κB inhibitor (Fig. 6F). These data suggest that activation of NF-κB via the IL-1R1 stimulates the production of IL-23 as well as TNF-α.

Previous reports have suggested that ROS promote activation of the inflammasome and secretion of IL-1β in autophagy-deficient cells (10, 12). Given the role of IL-1β in promoting IL-23 secretion, we assessed the potential role of ROS on IL-23 secretion by BMDC. The ROS scavenger *N*-acetyl-L-cysteine completely abrogated the secretion of IL-23 in response to LPS and 3-MA in BMDC at all concentrations tested (Supplemental Fig. 2A). In addition, at higher concentrations, *N*-acetyl-L-cysteine inhibited the secretion of IL-1β and IL-1α (Supplemental Fig. 2B, 2C). IL-6 secretion was affected only at the highest concentration (50 mM) (Supplemental Fig. 2D). Taken together, these data demonstrate that IL-23 secretion in autophagy-deficient cells is directly regulated by IL-1 signaling and is dependent on the generation of ROS.

IL-23 is not sequestered by autophagosomes

Our previous work demonstrated that in LPS-stimulated iBMM, autophagosomes sequester pro–IL-1β for degradation (10). To assess whether the same was true for IL-23, we stained LPS-treated GFP-LC3–expressing iBMM with Ab against IL-1β or IL-23 and examined the cells by confocal microscopy. As previously shown, after overnight treatment with LPS, IL-1β colocalized with GFP-LC3 (Fig. 7A). However, no IL-23 could be detected in GFP-LC3$^+$ autophagosomes (Fig. 7B). This would suggest that unlike IL-1β, intracellular IL-23 is not sequestered by autophagosomes.

To determine the effect of autophagy induction on IL-23 production, we treated BMDC with LPS and PP242, an autophagy-inducing mammalian target of rapamycin (mTOR) inhibitor. At all concentrations tested, PP242 inhibited LPS-induced IL-23 production (Fig. 7C) Moreover, when another mTOR inhibitor, rapamycin, was administered i.p. in a murine model of endotoxin-induced sepsis, it abrogated the stimulatory effects of LPS on serum IL-23 (Fig. 7D), as we have previously demonstrated for IL-1β (10). These data would suggest that although blocking autophagy allows IL-23 production through the enhancement of IL-1 secretion, the induction of autophagy has the opposite effect and downregulates IL-23 secretion.

Both IL-1β and IL-1α can induce autophagy (15), suggesting that these cytokines may limit their own secretion. In agreement with this, we found that both IL-1β and IL-1α increased autophagosome formation in GFP-LC3–expressing iBMM (Supplemental Fig. 3A, 3B). Interestingly, granzyme B-processed IL-1α, which has recently been shown to have greater proinflammatory

Downloaded from http://www.jimmunol.org/ at IRIS - IReL Consortia on June 18, 2013

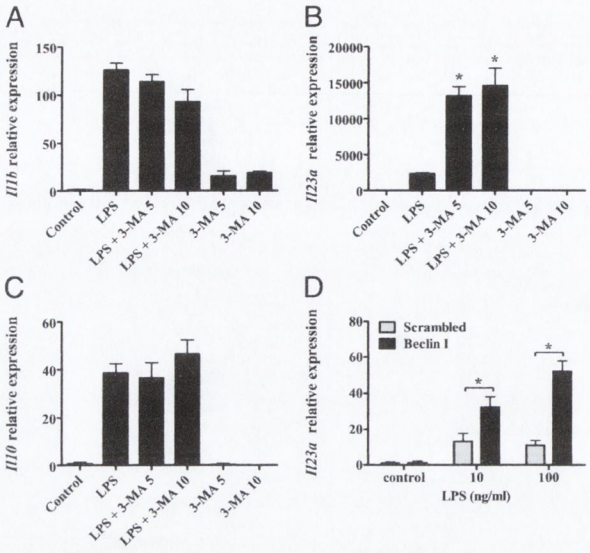

FIGURE 4. Inhibition of autophagy enhances IL-23 secretion at the transcriptional level. Levels of IL-1β (*Il1b*) (**A**), IL-23p19 (*Il23a*) (**B**), and IL-10 (*Il10*) (**C**) mRNA in murine BMDC treated with LPS (10 ng/ml) and 3-MA (5 or 10 mM) or 3-MA alone for 4 h were measured by quantitative PCR. Data represent mean values + SD. $*p < 0.05$ compared with LPS alone, one-way ANOVA with Bonferroni's multiple comparison test. (**D**) Murine iBMM were transfected with siRNA against beclin 1 or with nontargeting ("scrambled") siRNA and treated with LPS (10 and 100 ng/ml) for 4 h, and levels of *Il23a* were measured by quantitative PCR. Data represent mean values + SD ($n \geq 3$); $*p < 0.05$, one-way ANOVA with Bonferroni's multiple comparison test.

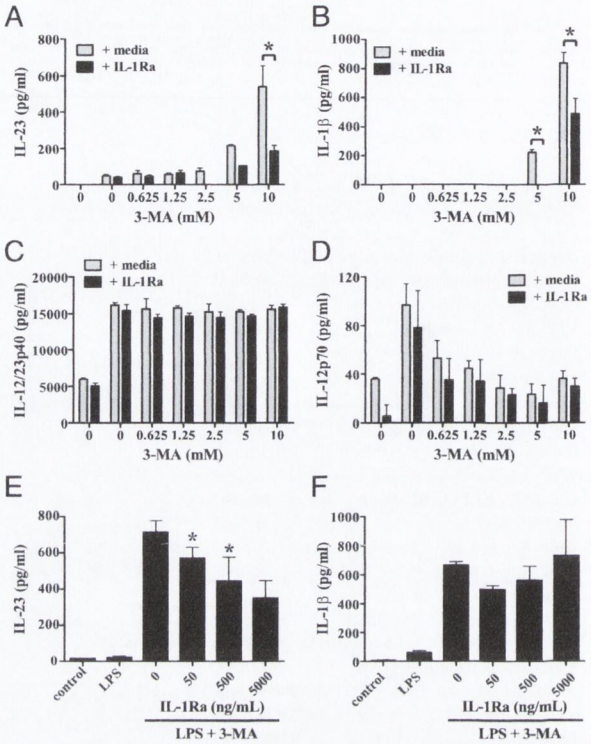

FIGURE 5. IL-23 secretion in autophagy-deficient cells is dependent on IL-1 signaling. (**A–D**) Murine BMDC were treated with LPS (10 ng/ml) and 3-MA at different concentrations in the presence or absence of the IL-1Ra hydrocinnamoyl-L-valyl pyrrolidine (5 μg/ml) for 24 h. Culture supernatants were analyzed by ELISA for IL-23 (A), IL-1β (B), IL-12/23p40 (C), and IL-12p70 (D). Human PMA-differentiated THP-1 cells were treated with LPS (100 ng/ml) and 3-MA (5 mM) with the IL-1Ra at different concentrations for 24 h, and supernatants were tested by ELISA for IL-23 (**E**) and IL-1β (**F**). Data represent mean values + SD ($n \geq 3$); $*p < 0.05$ difference between +IL-1Ra and −IL-1Ra, one-way ANOVA with Bonferroni's multiple comparison test.

effects than the full-length form (34), was a more potent autophagosome inducer (Supplemental Fig. 3B). In addition, IL-23 increased autophagosome formation in GFP-LC3–expressing iBMM (Supplemental Fig. 3C). These data would indicate that autophagy represents a negative feedback mechanism for the control of IL-1β secretion and the subsequent production of IL-23.

Impaired autophagy in activated macrophages and DC stimulates innate cytokine secretion by γδ T cells

Given that IL-1 and IL-23 synergistically stimulate TCR-independent IL-17 production by Th17 cells (20) and that the inhibition of autophagy in macrophages and DC enhances the secretion of IL-1β, IL-1α, and IL-23, we sought to determine whether this could, in turn, stimulate innate Th17-like cytokine responses in vitro. Supernatants from BMDC treated with LPS and 3-MA (to induce IL-1β and IL-23 secretion; Supplemental Fig. 4A, 4B) stimulated IL-17A and IL-17F secretion by MACS-purified splenic $CD3^+$ T cells (Fig. 8A, 8B). These supernatants also enhanced T cell secretion of IFN-γ (Fig. 8C). Moreover, LPS and 3-MA had no direct effect on T cells (Fig. 8D–F), suggesting that this effect was due to soluble factors secreted by the 3-MA–treated BMDC. Supernatants from iBMM transfected with siRNA against beclin 1 similarly enhanced secretion of IL-17A from splenic T cells (Supplemental Fig. 4C-H), demonstrating that this effect is due to impaired autophagy. Because γδ T cells are a key source of innate cytokines secreted in response to IL-1β and IL-23 in the absence of TCR stimulation (20), we isolated $\gamma\delta^+$ and $\gamma\delta^-$ T cells from lymph nodes and assessed their capacity to produce IL-17, IL-22, and IFN-γ when exposed to supernatants from autophagy-deficient DC. When cultured with supernatants from BMDC treated with LPS and 3-MA or with recombinant IL-1β and IL-23, γδ T cells were responsible for the majority of IL-17, IL-22, and IFN-γ secretion (Fig. 8G–L). Thus, our data demonstrate that, through the regulation of IL-1β and IL-23 secretion, autophagy can influence innate cytokine production through the indirect stimulation of γδ T cells.

Discussion

Numerous cytokines have been shown to regulate autophagy in macrophages and DC (9). In particular, IFN-γ, TNF-α, IL-1α, and IL-1β increase autophagosome formation in macrophages (3, 4, 15), whereas IL-4, IL-13, and IL-10 inhibit autophagy (5–8). More recent studies have also demonstrated that autophagy can directly influence the secretion of cytokines, including IL-1β. Inhibition of autophagy enhances IL-1β production and secretion, because of the intracellular accumulation of endogenous inflammasome-activating factors, such as mitochondrial DNA and ROS (10–13, 31, 32). Conversely, autophagosomes themselves can directly target pro–IL-1β and the inflammasome components ASC and NLRP3 (10, 14). In addition, autophagy can regulate the secretion of IL-18 and IL-1α, although the mechanisms behind the latter may be different to those characterized for IL-1β (10, 12). In the current study, we have demonstrated that the inhibition of autophagy can also enhance IL-23 secretion in response to LPS and whole bacteria. A previous study has reported that wortmannin, but not LY294002, enhances IL-23 secretion by human DC in response to

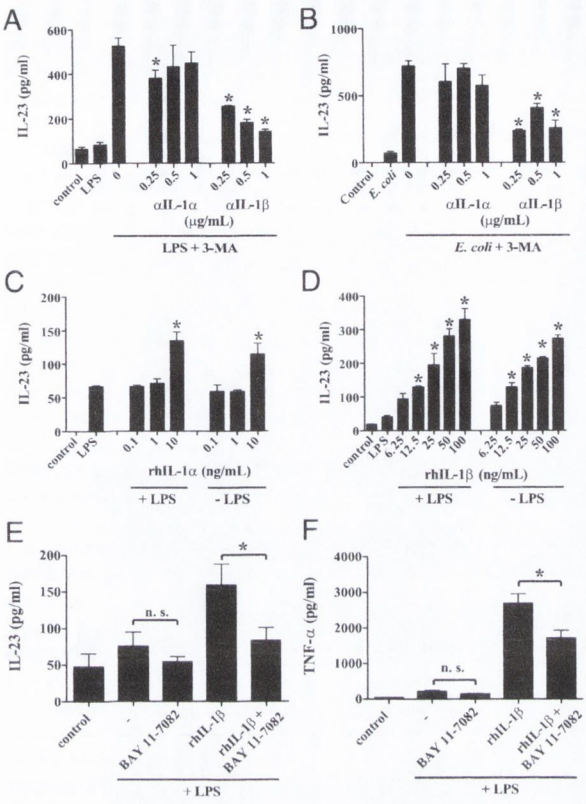

FIGURE 6. IL-23 secretion is driven by IL-1. PMA-differentiated THP-1 were treated with LPS (100 ng/ml) and 3-MA (5 mM) (**A**) or heat-killed *E. coli* (multiplicity of infection 10:1 bacteria:cells) and 3-MA (5 mM) (**B**) for 24 h with different concentrations of neutralizing Ab against IL-1α or IL-1β. Secretion of IL-23 into culture supernatants was measured by ELISA. Data represent mean values + SD ($n \geq 3$); $^*p < 0.05$ compared with LPS or bacteria alone, one-way ANOVA with Bonferroni's multiple comparison test. (**C** and **D**) PMA-differentiated THP-1 cells were treated with rhIL-1α (C) or rhIL-1β (D) in the presence or absence of LPS (100 ng/ml) for 24 h, and IL-23 secretion was measured by ELISA. Data represent mean values + SD ($n \geq 3$); $^*p < 0.05$ compared with unstimulated or LPS alone, one-way ANOVA with Bonferroni's multiple comparison test. (**E** and **F**) PMA-differentiated THP-1 cells were treated with rhIL-1b and LPS (100 ng/ml) in the presence or absence of the NF-KB inhibitor BAY 11-7082 for 24 h and IL-23 secretion (E) or TNF-α secretion (F) measured by ELISA. Data represent mean values + SD ($n \geq 3$); $^*p < 0.05$, one-way ANOVA with Bonferroni's multiple comparison test.

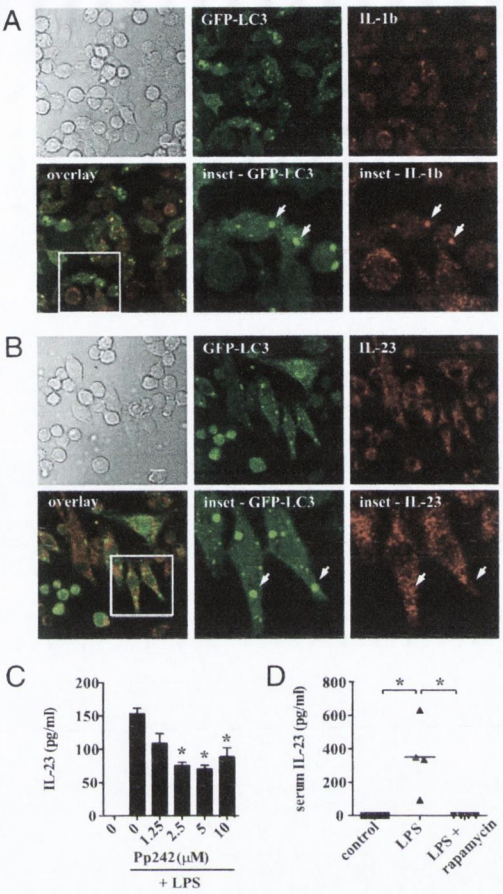

FIGURE 7. IL-23 is sequestered by autophagosomes. (**A** and **B**) Murine iBMM stably transfected with pEGFP-LC3 were treated with LPS for 24 h and stained with Ab against IL-1β (A) or IL-23 (B). Intracellular staining was visualized with Alexa 568 secondary Ab and analyzed by confocal microscopy. Arrows point to autophagosomes for comparisons between stains. Scale bar, 10 μm. (**C**) BMDC were treated with LPS (10 ng/ml), and different concentrations of the mTOR inhibitor PP242 for 24 h; IL-23 secretion into the culture supernatant was measured by ELISA. Data represent mean values + SD ($n \geq 3$); $^*p < 0.05$ compared with control, one-way ANOVA with Bonferroni's multiple comparison test. (**D**) Female C57BL/6 mice were injected i.p. with 200 μl PBS, LPS (10 μg/mouse, in PBS), or LPS + rapamycin (1.5 mg/kg in PBS), and serum levels of IL-23 were measured after 4 h by ELISA. Data represent actual and mean values from four mice; $^*p < 0.05$, Student *t* test.

TLR ligation via a type I PI3K-independent mechanism (35). In this study, we observed a similar effect, although in our system, LY294002 did enhance IL-23 secretion, as did both 3-MA and siRNA knockdown of the autophagy proteins beclin 1 and Atg7. This effect was specific to IL-23; IL-12p70 secretion was inhibited by 3-MA, whereas IL-12/23p40 levels were unaffected by autophagy inhibition.

Our data suggest that autophagy has a largely indirect effect on IL-23 through its regulation of IL-1β secretion. Previous studies have demonstrated that increased IL-1β secretion in autophagy-deficient cells is dependent on TRIF and ROS (10, 12). The present study suggests that increased IL-23 secretion in autophagy-deficient cells is similarly dependent on both ROS and TRIF. Interestingly, zymosan, which is not known to signal through TRIF but signals through TLR2/MyD88 and the β-glucans receptor Dectin-1 receptor (36), also acts synergistically with 3-MA to induce IL-23. However, Dectin-1 also signals through a Syk kinase-dependent pathway that occurs independently of TLR2 (37), and a previous study has demonstrated that β-glucans can induce IL-23 via an IL-1–dependent mechanism (33). Our previous study has demonstrated that pro–IL-1β colocalizes with GFP-LC3 in LPS-treated cells, and induction of autophagy, both in vitro and in vivo, has been shown to inhibit IL-1β secretion (10). In the current study, we have demonstrated that although IL-23 is not sequestered by autophagosomes, induction of autophagy in vitro and in vivo does inhibit IL-23 production, perhaps as a result of effects on IL-1β secretion.

Although neutralizing IL-1α had little or no effect on IL-23 secretion, IL-1α did itself enhance IL-23 secretion. This suggests that IL-1R signaling is important but perhaps that IL-1α release in response to 3-MA does not have consequences as significant as those of IL-1β. Interestingly, a recent study has suggested that IL-1α secretion may also depend on IL-1β (38), further implicating IL-1β as

Downloaded from http://www.jimmunol.org/ at IRIS - IReL Consortia on June 18, 2013

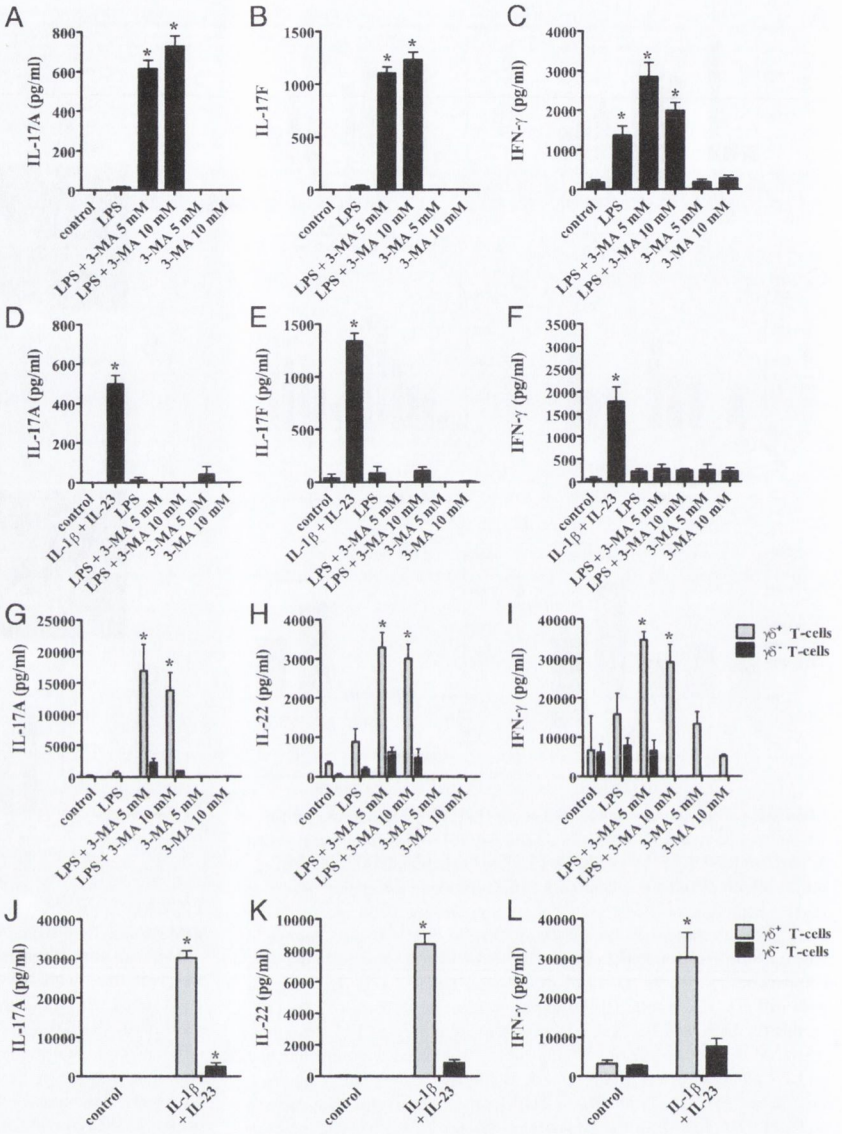

FIGURE 8. Autophagy-deficient DC stimulate γδ T cells. (**A–C**) $CD3^+$ T cells from spleens of female C57BL/6 mice were stimulated with supernatants from BMDC treated with LPS (10 ng/ml) and 3-MA (5 or 10 mM) or 3-MA alone for 72 h. Secretion of IL-17A (A), IL-17F (B), and IFN-γ (C) was measured by ELISA. Data represent mean values + SEM ($n = 6$); $^*p < 0.05$ compared with LPS only, one-way ANOVA with Bonferroni's multiple comparison test. (**D–F**) Splenic $CD3^+$ T cells from the same experiment were treated with recombinant murine IL-1β and IL-23, LPS (10 ng/ml), LPS + 3-MA (5 or 10 mM), or 3-MA alone. Secretion of IL-17A (D), IL-17F (E), and IFN-γ (F) was measured by ELISA. Data represent mean values + SEM ($n = 6$); $^*p < 0.05$ compared with control, one-way ANOVA with Bonferroni's multiple comparison test. (**G–I**) Lymph node T cells were separated into $\gamma\delta^+$ (10^4 cells/ml; light bars) and $\gamma\delta^-$ (10^5 cells/ml; dark bars) populations and treated with the same BMDC supernatants described above. Secretion of IL-17A (G), IL-22 (H), and IFN-γ (I) was measured by ELISA. Data represent mean values + SEM ($n = 3$); $^*p < 0.05$ compared with LPS only, one-way ANOVA with Bonferroni's multiple comparison test. (**J–L**) $\gamma\delta^+$ T cells from the same experiment were treated with recombinant murine IL-1β and IL-23 as a positive control. Secretion of IL-17A (J), IL-22F (K), and IFN-γ (L) was measured by ELISA. Data represent mean values + SEM ($n = 3$); $^*p < 0.05$ compared with control, one-way ANOVA with Bonferroni's multiple comparison test.

a key driver of inflammation. In agreement with our findings, IL-1β alone induced IL-23 secretion by human PBMC, and secretion of IL-23 in response to gliadin and β-glucans was also IL-1 dependent (33). Our data suggest that IL-1 drives IL-23 (and TNF-α) secretion through NF-κB signaling. Indeed, the IL-23 p19 promoter contains a κB site, which is required for the induction of p19 transcription (39), and IL-1R1 signaling activates NF-κB (40). Taken together, the data presented in this article, coupled with previous studies, suggests that in the absence of autophagy, TRIF- and ROS-dependent inflammasome activation, and IL-1β secretion drives IL-23 production and secretion in an NF-κB–dependent manner. It is notable that in some cases the effects of 3-MA on IL-23 are nonlinear, whereas those on IL-1β are linear at the dose range tested. This could be due to conflicting effects of 3-MA on autophagy and other PI3K-dependent processes, although further studies would be required to test this. Induction of autophagy, in contrast, leads to the sequestration and degradation of inflammasome components, pro–IL-1β, and other inflammatory stimuli, leading to reduced IL-1β secretion and thus reduced IL-23 production.

Intriguingly, IL-1β, IL-1α, and IL-23 can all induce autophagy, suggesting a potentially important negative feedback mechanism for the control of excessive inflammation. IL-23 is important in driving intestinal inflammation in various mouse models of inflammatory bowel disease (41–43). In humans, genome-wide association studies have identified the IL-23R as an important correlate in Crohn's disease (44). Moreover, polymorphisms in *ATG16L1*, which encodes a protein required for autophagy, have been associated with susceptibility to Crohn's disease (16, 45). In a murine model of dextran sodium sulfate-induced colitis, loss of the autophagy protein Atg16L1 results in more severe disease, with increased weight loss, enhanced colonic inflammation, and decreased survival (12). The same study also demonstrated greatly enhanced serum IL-1β levels in Atg16L1-deficient animals, although the effects on IL-23 were not examined. Thus, our data indicate that autophagy and IL-23 might be closely linked through the autophagic control of IL-1β secretion in this model.

γδ T cells are a rapid and potent innate source of cytokines, including IL-17, IL-22, and IFN-γ. Although IL-17 and IFN-γ are

thought to be key modulators of inflammation in disease models, such as dextran sodium sulfate-induced colitis, IL-22 acts on nonimmune cells, particularly in the skin, gut, liver, lungs, and kidneys, to induce production of antimicrobial peptides and to protect and maintain epithelial barriers. IL-1β drives—and IL-23 amplifies—such Th17-like cytokine responses, particularly from γδ T cells (19, 20, 26, 46, 47). Given that autophagy is a potent regulator of the inflammasome and IL-1 secretion, our data provide evidence that through the regulation of IL-1, autophagy is able to influence not only IL-23 secretion but also innate cytokine responses, characterized by robust secretion of IL-17, IL-22, and IFN-γ by γδ T cells independently of TCR stimulation.

Autophagy may thus represent a potent target for anti-inflammatory therapies that could impact on a number of autoimmune diseases, including multiple sclerosis and inflammatory bowel disease. Conversely, directed inhibition of autophagy might be useful to drive Th17-like cytokine responses against specific Ags. This could, in turn, increase the efficacy of some vaccines that require these cytokines, as has been suggested for subunit vaccines against *Streptococcus pneumonia* and *M. tuberculosis* (48, 49).

In summary, our data uncovers a novel role for autophagy in the regulation of IL-23 secretion by macrophages and dendritic cells and, as a result, IL-17, IFN-γ, and IL-22 production by γδ T cells. This is dependent on IL-1 secretion, which is regulated by autophagy through at least two separate mechanisms. These findings further highlight the potential of autophagy as a therapeutic target for inflammatory conditions mediated by IL-1.

Acknowledgments

We thank Gavin McManus and Barry Moran for technical assistance.

Disclosures

K.H.G.M. is a cofounder and shareholder in Opsona Therapeutics Ltd., involved in the development of anti-inflammatory therapeutics, and Trimod Therapeutics, involved in the development of cancer vaccines and therapeutics. The other authors have no financial conflicts of interest.

References

1. Levine, B., N. Mizushima, and H. W. Virgin. 2011. Autophagy in immunity and inflammation. *Nature* 469: 323–335.
2. Münz, C. 2010. Antigen processing via autophagy—not only for MHC class II presentation anymore? *Curr. Opin. Immunol.* 22: 89–93.
3. Gutierrez, M. G., S. S. Master, S. B. Singh, G. A. Taylor, M. I. Colombo, and V. Deretic. 2004. Autophagy is a defense mechanism inhibiting BCG and *Mycobacterium tuberculosis* survival in infected macrophages. *Cell* 119: 753–766.
4. Harris, J., and J. Keane. 2010. How tumour necrosis factor blockers interfere with tuberculosis immunity. *Clin. Exp. Immunol.* 161: 1–9.
5. Harris, J., S. A. De Haro, S. S. Master, J. Keane, E. A. Roberts, M. Delgado, and V. Deretic. 2007. T helper 2 cytokines inhibit autophagic control of intracellular *Mycobacterium tuberculosis*. *Immunity* 27: 505–517.
6. Ní Cheallaigh, C., J. Keane, E. C. Lavelle, J. C. Hope, and J. Harris. 2011. Autophagy in the immune response to tuberculosis: clinical perspectives. *Clin. Exp. Immunol.* 164: 291–300.
7. Park, H. J., S. J. Lee, S. H. Kim, J. Han, J. Bae, S. J. Kim, C. G. Park, and T. Chun. 2011. IL-10 inhibits the starvation induced autophagy in macrophages via class I phosphatidylinositol 3-kinase (PI3K) pathway. *Mol. Immunol.* 48: 720–727.
8. Van Grol, J., C. Subauste, R. M. Andrade, K. Fujinaga, J. Nelson, and C. S. Subauste. 2010. HIV-1 inhibits autophagy in bystander macrophage/monocytic cells through Src-Akt and STAT3. *PLoS ONE* 5: e11733.
9. Harris, J. 2011. Autophagy and cytokines. *Cytokine* 56: 140–144.
10. Harris, J., M. Hartman, C. Roche, S. G. Zeng, A. O'Shea, F. A. Sharp, E. M. Lambe, E. M. Creagh, D. T. Golenbock, J. Tschopp, et al. 2011. Autophagy controls IL-1β secretion by targeting pro-IL-1β for degradation. *J. Biol. Chem.* 286: 9587–9597.
11. Nakahira, K., J. A. Haspel, V. A. Rathinam, S. J. Lee, T. Dolinay, H. C. Lam, J. A. Englert, M. Rabinovitch, M. Cernadas, H. P. Kim, et al. 2011. Autophagy proteins regulate innate immune responses by inhibiting the release of mitochondrial DNA mediated by the NALP3 inflammasome. *Nat. Immunol.* 12: 222–230.
12. Saitoh, T., N. Fujita, M. H. Jang, S. Uematsu, B. G. Yang, T. Satoh, H. Omori, T. Noda, N. Yamamoto, M. Komatsu, et al. 2008. Loss of the autophagy protein Atg16L1 enhances endotoxin-induced IL-1β production. *Nature* 456: 264–268.
13. Zhou, R., A. S. Yazdi, P. Menu, and J. Tschopp. 2011. A role for mitochondria in NLRP3 inflammasome activation. *Nature* 469: 221–225.
14. Shi, C. S., K. Shenderov, N. N. Huang, J. Kabat, M. Abu-Asab, K. A. Fitzgerald, A. Sher, and J. H. Kehrl. 2012. Activation of autophagy by inflammatory signals limits IL-1β production by targeting ubiquitinated inflammasomes for destruction. *Nat. Immunol.* 13: 255–263.
15. Shi, C. S., and J. H. Kehrl. 2008. MyD88 and Trif target Beclin 1 to trigger autophagy in macrophages. *J. Biol. Chem.* 283: 33175–33182.
16. Hampe, J., A. Franke, P. Rosenstiel, A. Till, M. Teuber, K. Huse, M. Albrecht, G. Mayr, F. M. De La Vega, J. Briggs, et al. 2007. A genome-wide association scan of nonsynonymous SNPs identifies a susceptibility variant for Crohn disease in ATG16L1. *Nat. Genet.* 39: 207–211.
17. Rioux, J. D., R. J. Xavier, K. D. Taylor, M. S. Silverberg, P. Goyette, A. Huett, T. Green, P. Kuballa, M. M. Barmada, L. W. Datta, et al. 2007. Genome-wide association study identifies new susceptibility loci for Crohn disease and implicates autophagy in disease pathogenesis. *Nat. Genet.* 39: 596–604.
18. Brereton, C. F., C. E. Sutton, P. J. Ross, Y. Iwakura, M. Pizza, R. Rappuoli, E. C. Lavelle, and K. H. Mills. 2011. *Escherichia coli* heat-labile enterotoxin promotes protective Th17 responses against infection by driving innate IL-1 and IL-23 production. *J. Immunol.* 186: 5896–5906.
19. Sutton, C., C. Brereton, B. Keogh, K. H. Mills, and E. C. Lavelle. 2006. A crucial role for interleukin (IL)-1 in the induction of IL-17-producing T cells that mediate autoimmune encephalomyelitis. *J. Exp. Med.* 203: 1685–1691.
20. Sutton, C. E., S. J. Lalor, C. M. Sweeney, C. F. Brereton, E. C. Lavelle, and K. H. Mills. 2009. Interleukin-1 and IL-23 induce innate IL-17 production from γδ T cells, amplifying Th17 responses and autoimmunity. *Immunity* 31: 331–341.
21. Harrington, L. E., R. D. Hatton, P. R. Mangan, H. Turner, T. L. Murphy, K. M. Murphy, and C. T. Weaver. 2005. Interleukin 17-producing $CD4^+$ effector T cells develop via a lineage distinct from the T helper type 1 and 2 lineages. *Nat. Immunol.* 6: 1123–1132.
22. Koenders, M. I., E. Lubberts, B. Oppers-Walgreen, L. van den Bersselaar, M. M. Helsen, J. K. Kolls, L. A. Joosten, and W. B. van den Berg. 2005. Induction of cartilage damage by overexpression of T cell interleukin-17A in experimental arthritis in mice deficient in interleukin-1. *Arthritis Rheum.* 52: 975–983.
23. Langrish, C. L., Y. Chen, W. M. Blumenschein, J. Mattson, B. Basham, J. D. Sedgwick, T. McClanahan, R. A. Kastelein, and D. J. Cua. 2005. IL-23 drives a pathogenic T cell population that induces autoimmune inflammation. *J. Exp. Med.* 201: 233–240.
24. Park, H., Z. Li, X. O. Yang, S. H. Chang, R. Nurieva, Y. H. Wang, Y. Wang, L. Hood, Z. Zhu, Q. Tian, and C. Dong. 2005. A distinct lineage of CD4 T cells regulates tissue inflammation by producing interleukin 17. *Nat. Immunol.* 6: 1133–1141.
25. Higgins, S. C., A. G. Jarnicki, E. C. Lavelle, and K. H. Mills. 2006. TLR4 mediates vaccine-induced protective cellular immunity to *Bordetella pertussis*: role of IL-17-producing T cells. *J. Immunol.* 177: 7980–7989.
26. Veldhoen, M., R. J. Hocking, C. J. Atkins, R. M. Locksley, and B. Stockinger. 2006. TGFβ in the context of an inflammatory cytokine milieu supports de novo differentiation of IL-17-producing T cells. *Immunity* 24: 179–189.
27. Lutz, M. B., N. Kukutsch, A. L. Ogilvie, S. Rössner, F. Koch, N. Romani, and G. Schuler. 1999. An advanced culture method for generating large quantities of highly pure dendritic cells from mouse bone marrow. *J. Immunol. Methods* 223: 77–92.
28. Harris, J., O. Hanrahan, and S. A. De Haro. 2009. Measuring autophagy in macrophages. *Curr. Protoc. Immunol.* Chapter 14: Unit 14.14.
29. Seglen, P. O., and P. B. Gordon. 1982. 3-Methyladenine: specific inhibitor of autophagic/lysosomal protein degradation in isolated rat hepatocytes. *Proc. Natl. Acad. Sci. USA* 79: 1889–1892.
30. Klionsky, D. J., H. Abeliovich, P. Agostinis, D. K. Agrawal, G. Aliev, D. S. Askew, M. Baba, E. H. Baehrecke, B. A. Bahr, A. Ballabio, et al. 2008. Guidelines for the use and interpretation of assays for monitoring autophagy in higher eukaryotes. *Autophagy* 4: 151–175.
31. Kleinnijenhuis, J., M. Oosting, T. S. Plantinga, J. W. van der Meer, L. A. Joosten, R. V. Crevel, and M. G. Netea. 2011. Autophagy modulates the *Mycobacterium tuberculosis*-induced cytokine response. *Immunology* 134: 341–348.
32. Crişan, T. O., T. S. Plantinga, F. L. van de Veerdonk, M. F. Farcaş, M. Stoffels, B. J. Kullberg, J. W. van der Meer, L. A. Joosten, and M. G. Netea. 2011. Inflammasome-independent modulation of cytokine response by autophagy in human cells. *PLoS One* 6: e18666.
33. Harris, K. M., A. Fasano, and D. L. Mann. 2008. Cutting edge: IL-1 controls the IL-23 response induced by gliadin, the etiologic agent in celiac disease. *J. Immunol.* 181: 4457–4460.
34. Afonina, I. S., G. A. Tynan, S. E. Logue, S. P. Cullen, M. Bots, A. U. Lüthi, E. P. Reeves, N. G. McElvaney, J. P. Medema, E. C. Lavelle, and S. J. Martin. 2011. Granzyme B-dependent proteolysis acts as a switch to enhance the proinflammatory activity of IL-1α. *Mol. Cell* 44: 265–278.
35. Wang, Q., H. A. Franks, J. Porte, M. El Refaee, S. Shah, J. Crooks, P. M. Patel, and A. M. Jackson. 2011. Novel approach for interleukin-23 up-regulation in human dendritic cells and the impact on T helper type 17 generation. *Immunology* 134: 60–72.
36. Brown, G. D., J. Herre, D. L. Williams, J. A. Willment, A. S. Marshall, and S. Gordon. 2003. Dectin-1 mediates the biological effects of beta-glucans. *J. Exp. Med.* 197: 1119–1124.
37. Rogers, N. C., E. C. Slack, A. D. Edwards, M. A. Nolte, O. Schulz, E. Schweighoffer, D. L. Williams, S. Gordon, V. L. Tybulewicz, G. D. Brown, and C. Reis e Sousa. 2005. Syk-dependent cytokine induction by Dectin-1

Downloaded from http://www.jimmunol.org/ at IRIS - IReL Consortia on June 18, 2013

reveals a novel pattern recognition pathway for C type lectins. *Immunity* 22: 507–517.
38. Fettelschoss, A., M. Kistowska, S. LeibundGut-Landmann, H. D. Beer, P. Johansen, G. Senti, E. Contassot, M. F. Bachmann, L. E. French, A. Oxenius, and T. M. Kündig. 2011. Inflammasome activation and IL-1β target IL-1α for secretion as opposed to surface expression. *Proc. Natl. Acad. Sci. USA* 108: 18055–18060.
39. Mise-Omata, S., E. Kuroda, J. Niikura, U. Yamashita, Y. Obata, and T. S. Doi. 2007. A proximal κB site in the IL-23 p19 promoter is responsible for RelA- and c-Rel-dependent transcription. *J. Immunol.* 179: 6596–6603.
40. O'Neill, L. A. 2000. The interleukin-1 receptor/Toll-like receptor superfamily: signal transduction during inflammation and host defense. *Sci. STKE* 2000: re1.
41. Buonocore, S., P. P. Ahern, H. H. Uhlig, I. I. Ivanov, D. R. Littman, K. J. Maloy, and F. Powrie. 2010. Innate lymphoid cells drive interleukin-23-dependent innate intestinal pathology. *Nature* 464: 1371–1375.
42. Hue, S., P. Ahern, S. Buonocore, M. C. Kullberg, D. J. Cua, B. S. McKenzie, F. Powrie, and K. J. Maloy. 2006. Interleukin-23 drives innate and T cell-mediated intestinal inflammation. *J. Exp. Med.* 203: 2473–2483.
43. Kullberg, M. C., D. Jankovic, C. G. Feng, S. Hue, P. L. Gorelick, B. S. McKenzie, D. J. Cua, F. Powrie, A. W. Cheever, K. J. Maloy, and A. Sher. 2006. IL-23 plays a key role in *Helicobacter hepaticus*-induced T cell-dependent colitis. *J. Exp. Med.* 203: 2485–2494.
44. Duerr, R. H., K. D. Taylor, S. R. Brant, J. D. Rioux, M. S. Silverberg, M. J. Daly, A. H. Steinhart, C. Abraham, M. Regueiro, A. Griffiths, et al. 2006. A genome-wide association study identifies IL23R as an inflammatory bowel disease gene. *Science* 314: 1461–1463.
45. Prescott, N. J., S. A. Fisher, A. Franke, J. Hampe, C. M. Onnie, D. Soars, R. Bagnall, M. M. Mirza, J. Sanderson, A. Forbes, et al. 2007. A nonsynonymous SNP in ATG16L1 predisposes to ileal Crohn's disease and is independent of CARD15 and IBD5. *Gastroenterology* 132: 1665–1671.
46. Zielinski, C. E., F. Mele, D. Aschenbrenner, D. Jarrossay, F. Ronchi, M. Gattorno, S. Monticelli, A. Lanzavecchia, and F. Sallusto. 2012. Pathogen-induced human TH17 cells produce IFN-γ or IL-10 and are regulated by IL-1β. *Nature* 484: 514–518.
47. Chung, Y., S. H. Chang, G. J. Martinez, X. O. Yang, R. Nurieva, H. S. Kang, L. Ma, S. S. Watowich, A. M. Jetten, Q. Tian, and C. Dong. 2009. Critical regulation of early Th17 cell differentiation by interleukin-1 signaling. *Immunity* 30: 576–587.
48. Khader, S. A., G. K. Bell, J. E. Pearl, J. J. Fountain, J. Rangel-Moreno, G. E. Cilley, F. Shen, S. M. Eaton, S. L. Gaffen, S. L. Swain, et al. 2007. IL-23 and IL-17 in the establishment of protective pulmonary $CD4^+$ T cell responses after vaccination and during *Mycobacterium tuberculosis* challenge. *Nat. Immunol.* 8: 369–377.
49. Moffitt, K. L., T. M. Gierahn, Y. J. Lu, P. Gouveia, M. Alderson, J. B. Flechtner, D. E. Higgins, and R. Malley. 2011. T(H)17-based vaccine design for prevention of *Streptococcus pneumoniae* colonization. *Cell Host Microbe* 9: 158–165.

CHAPTER 21

Adjuvant Strategies for Vaccines

The Use of Adjuvants within the Cancer Vaccine Setting

Claire Hearnden, Ed C. Lavelle
Adjuvant Research Group, School of Biochemistry and Immunology, Trinity Biomedical Sciences Institute, Trinity College Dublin, Dublin 2, Ireland

I. INTRODUCTION

The immune system and tumor cells have a complex interplay whereby leukocytes and tumor cells are in a constant battle. The tumor microenvironment is dynamic and the immune system can determine whether premalignant lesions develop into aggressive cancers. It has been known since the 1940s that mice immunized with irradiated cancer cells show resistance to subsequent challenges with corresponding viable cancer cells [1]. This implies that cancers are immunogenic and that an optimal antitumor cell immune response can inhibit tumor growth.

Vaccination is a means by which the immune response can be "taught" how to respond to antigens. Indeed, vaccination has led to the eradication of smallpox and greatly reduced the incidence of many diseases including polio. In the context of cancer it has been suggested that people who are predisposed to tumor growth could be protected via therapeutic or prophylactic vaccine strategies [2]. The advantages of cancer vaccines over other therapies include increased specificity to tumor cells, reduced toxicity and more robust long-term effects [3].

II. WHY ADJUVANTS WORK

Vaccination aims to provide a stimulus that will generate an appropriate long-term protective immune response [4]. To generate such a response the host must be exposed to the antigen in a controlled way that will facilitate immune recognition, activation and memory generation. This process is dependent on antigen-presenting cells (APCs), particularly dendritic cells (DCs), which capture tumor antigens, process them and display the resulting peptide epitopes in an immunogenic context to stimulate T cells [5].

Most antigens do not induce a protective T-cell response when administered by themselves as a vaccine. Adjuvants are substances that can be incorporated into vaccines to enhance the magnitude, breadth and quality of the immune response to antigens. Adjuvants were first described by Ramon as "substances used in combination with a specific antigen that produce more immunity than the antigen alone" [6]. Despite extensive research, in most cases the precise mechanism of adjuvanticity remains unknown and it is because of this that Charles Janeway once referred to adjuvants as "the dirty little secret of immunologists."

Cancer Immunotherapy. http://dx.doi.org/10.1016/B978-0-12-394296-8.00021-X
Copyright © 2013 Elsevier Inc. All rights reserved.

Adjuvants comprise a diverse group of compounds whose proposed roles range from carriers/antigen depots to immunostimulatory/immunomodulatory molecules [7]. There are many advantages of using adjuvants in vaccine formulations including their ability to promote cell-mediated immunity, to serve as an antigen depot and reduce the amount of antigen necessary in vaccines for protection ("dose sparing") and also to reduce the number of vaccinations required to induce an effective immune response [8]. Ultimately, adjuvants are required to activate DCs and promote effective uptake, processing and presentation of antigen to T cells in secondary lymphoid organs, thereby stimulating powerful antigen-specific immune responses [9].

Pathogens are recognized by DCs through the range of pattern recognition receptors (PRR) that can be found on the cell surface as well as in the cytosol, and have evolved to recognize particular patterns on pathogens that are conserved across several species termed PAMPs (Pathogen Associated Molecular Patterns) [10]. These PAMPs can be purified or synthesized and used as adjuvants. Different PRR recognize specific types of PAMPs and are broadly grouped by structure. Prominent PRR include mannose-binding lectin, pulmonary surfactant protein, C-reactive protein, Toll-like receptors (TLRs), C-type lectin receptors (CLRs), Nod-like receptors (NLRs), Rig-I like receptors (RLRs) and MX proteins.

Charles Janeway demonstrated that the adaptive immune responses generated against infectious microorganisms are dependent on the initial innate immune responses upon exposure to the pathogen [11]. Upon recognition of PAMPs, DCs become activated, a process termed maturation, and begin to upregulate co-stimulatory molecules, process antigens and present these antigens to T cells, thus initiating adaptive immunity [11]. Thus, DCs bridge the divide between innate and adaptive immunity. This led to the rational design of adjuvants that can target specific receptors and generate adaptive immune responses, as well as adjuvants that are not immunostimulatory themselves, but are capable of modulating the immune system in a particular way.

III. TUMOR-ASSOCIATED ANTIGENS AND THE NEED FOR ADJUVANTS IN CANCER VACCINES

The rationale for therapeutic vaccines in cancer began in the 1950s when it was demonstrated that transformed tumor cells express antigens called tumor-associated antigens (TAAs) that are not found on normal cells [12–14]. Since these endogenous TAAs are not expressed by normal cells, they have potential as antigens that could be presented to DCs. For example, malignant melanomas, which are one of the most aggressive malignancies in humans, express many TAAs that can be recognized by T cells. These TAAs include gp100, Melan-A/Mart-1, tyrosinase, MAGE-A1, and NY-ESO [15]. However, tumors are capable of modulating the immune response to facilitate their own growth, most notably through their ability to downregulate the expression of TAAs, secrete inhibitory molecules and reduce the expression of co-stimulatory molecules, thus making tumor cells poorly immunogenic [12,16].

An important aspect of cancer immunotherapy is developing appropriate adjuvants for cancer vaccines to enable the immune system to mount an effective TAA-specific response. The nature of the adjuvant used can determine the type of immune response generated against the antigen. When a DC is activated, or matures, as well as upregulating co-stimulatory molecules it upregulates receptors that allow it to migrate to the lymph nodes and here the DC displays antigen complexes on its cell surface. The nature of the antigen and adjuvant can influence whether peptides are displayed on major histocompatibility complex (MHC) class I (MHCcI) or MHC class II (MHCcII) and the type of T-cell response that will be generated. MHCcI usually display peptides derived from proteins synthesized in the cytosol, such as those from viruses or endogenous TAAs. MHCcII bind peptides derived from intracellular vesicles, for example those containing pathogens internalized by phagocytosis. MHCcI complexes are recognized by T cells expressing CD8 molecules on their surface ($CD8^+$ cytotoxic T lymphocyte

(CTL)) and MHCcII complexes are recognized by T cells expressing CD4 molecules on their surface ($CD4^+$ T-helper cells). A process referred to as *cross-presentation* enables DCs to promote a CTL response against exogenous antigens by delivering them to MHCcI molecules, a process which is critical for immunity against tumor cells and virus-infected cells [17,18,19]. CD4 T-helper (Th) cells are categorized into various subsets including Th1, Th2 and Th17 cells. The cytokines that DCs secrete following maturation and subsequent T-cell activation polarize the different T-cell subsets; for example, IFN-γ is a Th1 polarizing cytokine and IL-4 a Th2 polarizing cytokine [20].

Regulatory T (Treg) cells represent approximately 5–10% of peripheral Th cells and are characterized by their ability to suppress components of the immune system including T-cell responses [12]. There are two types of Treg cells, those that are produced in the thymus and are functionally mature, and those that can be recruited from the periphery and induced to become Treg cells. Treg cells selectively recruited to the tumor site will be activated by mature DCs and since inducible Treg cells are highly specific for antigens, they have the ability to exert T-cell suppression in an antigen-dependent manner [21,22].

Efficient delivery of TAA to DCs requires an adjuvant so that the DC can mature and elicit effective antitumor immunity [23]. DCs' need to be activated by adjuvants as targeted antigen does not generate an effective antitumor immune response [24–26]. Antitumor activity is strongly dependent on CTL, which have been shown previously to secrete IFN-γ and also to possess cytolytic ability [25,27–29]. $CD4^+$ T cells with a Th1 phenotype also have a role in preventing tumor growth although the need for Th1 cells may be TAA specific [23]. Therefore, induction of a CTL response coupled with pro-inflammatory stimuli such as IFN-γ, IL-12p70 and TNF-α which can polarize a Th1 type response is critical for the development of an effective antitumor therapeutic vaccine (Figure 21.1) [8,30,31].

Although a cellular immune response is crucial for antitumor immunity, studies have also shown that humoral responses can provide protection. Vaccination of HER-2/neu mice, a mouse model of metastatic breast cancer using the oncogenic TAA HER-2, with IL-12 and allogeneic mammary carcinoma cells expressing p185(neu) prevented tumor onset independently of CTL by anti-p185(neu) antibodies [32]. Similarly, Park et al. found that in transgenic BALB-neuT HER-2 mice, a transgenic BALB/c mouse model for the *neu* oncogene, development of spontaneous HER-2 positive carcinomas was independent of $CD8^+$ T cells. Importantly $CD4^+$ T cells were required only early in the immediate post-vaccination period to induce anti-HER-2 Abs, which were both necessary and sufficient for protection [33].

A caveat with developing cancer vaccines is that TAAs are self antigens that are over-expressed. This means that there may be preexisting tolerance for these antigens within the immune

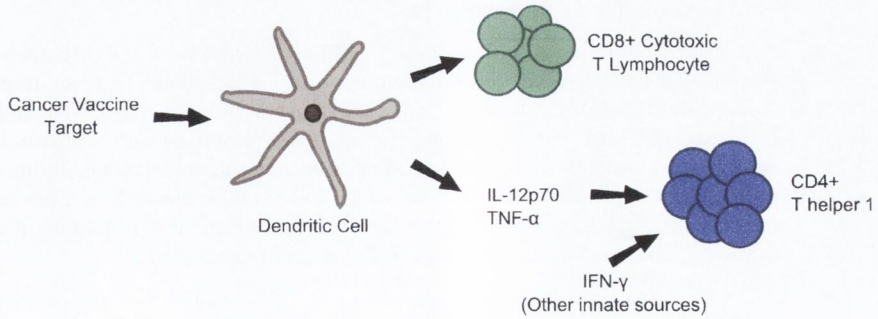

FIGURE 21.1
Cancer vaccines, as with most vaccines, target dendritic cells. The immunological correlate of protective immunity in cancer is a CD8+ cytotoxic T-lymphocyte response and a cytokine response made up of IFN-γ, IL-12p70 and TNF-α which promote a Th1 T-cell response.

system. In order to overcome the tolerance, both humoral and cellular immunity may be required. Reilly et al., using mice tolerant to the oncogene neu, found that neu-specific IgG alone was insufficient for protection against challenge and a combined cellular and humoral response was required for effective antitumor immunity [34].

IV. IMMUNOSTIMULATORY ADJUVANTS

It is critical that the adjuvants administered in vaccines are safe, well tolerated, biodegradable and can promote long-lasting protective immunity [35]. For this reason adjuvants must be very well characterized, both physically and chemically. Adjuvants can be roughly divided into immunostimulatory adjuvants, those that are capable of interacting directly with specific receptors on APCs, and particulate vaccine adjuvants, that are capable of delivering antigen to APCs, particularly DCs [36].

A. Pathogen derived immunostimulatory adjuvants

A primary aim of cancer vaccines is to induce DC maturation so that tumor antigens can be presented to T cells and break TAA tolerance [2,37]. DC activated via PRR have an enhanced capacity to present peptides to T cells and generate antigen-specific responses [38]. For example, CG-enriched oligodeoxynucleotides (CpG) engage TLR9 and induce DC maturation, a process characterized by increased surface expression of CD80, CD86 and MHCcII and also secretion of a range of pro-inflammatory cytokines [39,40]. Unmethylated CpG motifs are abundant in mycobacterial DNA and induce a Th1 immune response. Synthetic oligodeoxynucleotides containing CpG motifs have been used with a CTL peptide epitope from the RNEU (rat HER-2/*neu* gene product) sequence (p66) as a vaccine therapy in a mouse model for spontaneous breast tumors [41]. Vaccination with peptide in combination with CpG was effective in promoting CTL responses and subsequent antitumor activity. However, this was dependent on combined Treg-cell suppression and multiple booster vaccinations [41].

CpG motifs have also been used in other vaccine strategies, including exposure of tumor B cells to CpG *ex vivo* and injection into the host as a whole cell tumor vaccine. Intratumoral vaccination with CpG in combination with cytotoxic chemotherapy has also been used [42]. Interestingly, direct intratumoral immunization induced a CTL response whereas vaccination with CpG-loaded tumor B cells resulted in an antitumor response mediated by $CD4^+$ T cells [42].

Some studies have shown that encapsulation of CpG motifs in liposomes enhances the immunostimulatory activity of the ligand by targeting it directly to DCs for uptake and processing [43]. In models of thymoma and melanoma this approach generated adaptive immune responses against co-administered TAAs after subcutaneous immunization with liposomes containing CpG motifs [43].

3-O-desacyl-4′-monophosphoryl lipid A (MPL) is derived from the detoxified LPS of the Gram-negative bacterium *Salmonella Minnesota* and is recognized by TLR4. Importantly, MPL® is significantly less toxic then LPS so is safe for use in humans, but it also retains its adjuvant properties [44–46]. MPL® promotes cell-mediated immunity with a predominantly Th1 profile in addition to CTL responses and is currently the only TLR ligand in licensed human vaccines [8,46]. MPL® is used in combination with aluminum salt as Adjuvant System 04 (ASO4) and is included in two licensed vaccines, the human papillomavirus (HPV) vaccine Cervarix® and the Hepatitis B virus (HBV) vaccine Fendrix.®

Due to the success of MPL a new generation of TLR4 agonists is being developed, including aminoalkyl glucosamimide phosphates (AGPs) and a synthetic LPS mimetic RC-529.

The double-stranded RNA mimic and TLR3 ligand polyinosinic polycytidylic acid (poly(I:C)) has also been investigated as a potential cancer adjuvant [47]. As a synergistic strategy

for DC maturation, poly(I:C) has been combined with an agonistic anti-CD40 antibody which mimics CD40L functions [48–50]. Using these adjuvants with OVA as an antigen in prophylactic vaccination experiments induced both $CD8^+$ and $CD4^+$ responses, and in a challenge model 94% of animals immunized with poly(I:C) and anti-CD40 in combination with OVA were protected against tumor growth in an E.G7-OVA thymoma model [51].

The same group working on the B16-OVA melanoma model also found that the combination of poly(I:C) and anti-CD40 was ineffective. However, a combination approach relying on synergy between poly(I:C), anti-CD40 and the TLR7 ligand, Imiquimoid, with OVA coupled to the extra domain A of the TLR4 ligand, fibronectin (EDA), led to a complete block of tumor growth and protection against rechallenge with B16-OVA cells [37]. Interestingly, mice were also protected against challenge with B16.F10 tumor cells, which do not express OVA and 80% of mice remained tumor free for up to 80 days later, indicating that the adjuvant combination vaccine not only induces responses against the administered antigen, but also against other antigens expressed by tumor cells [37].

While TLRs are not the only PRR which are current cancer vaccine adjuvant targets, they are the best defined. CLRs are involved in the recognition of carbohydrate entities. For example, the CLR Mincle is a ligand for the mycobacterial cord factor/trehalose dimycolate which promotes Th1/Th17 responses [52,53]. Other PRR such as RLRs and intracellular DNA-sensing receptors are less well characterized and may have important roles in adjuvanticity that are being resolved.

Strategies to activate both cell surface and intracellular PRR simultaneously have also shown promise. Flagellin is the main component of the bacterial flagellum and is recognized by the immune system through TLR5 on the cell surface as well as cytosolic Nod-like receptors (NLRs). Expression of flagellin within tumor cells was shown to clear these cells through TLR5-mediated activation of macrophages in addition to TLR5 and NLRC4 (NOD-, LRR- and CARD-containing 4)/NAIP5 (neuronal apoptosis inhibitory protein 5) mediated priming of antitumor $CD4^+$ and $CD8^+$ T cells [54]. Although using flagellin as an adjuvant is still at an early stage, it is clear that this TLR agonist has potential as an effective antitumor vaccination strategy.

B. QS21

Saponins come from the bark, stem, roots and flowers of many plant species and are made up of sterol glycosides and triterpenoid glycosides and were named due to their detergent nature [55]. Saponin fractions from the South American tree *Quillaja saponaria* have been isolated and shown to have potent adjuvant properties [56]. Kensil et al. purified numerous fractions and found fraction 21 (QS21), a mixture of soluble triterpene glycosides, to have exceptional adjuvant properties for a range of antigens [55,57].

QS21 has been used as an adjuvant with various cell surface gangliosides whose expression is upregulated in the process of malignant transformation of cancers [58]. Immunization with gangliosides alone (including the monosialoganglioside GM2 and the disialo gangliosides GD2 and GD3) failed to induce production of antigen-specific antibodies [59]. Induction of IgG antibodies against carbohydrate antigens such as gangliosides requires a $CD4^+$ Th cell response so that isotype class switching of immunoglobulins occurs. The optimal approach for induction of antibodies against gangliosides requires covalent attachment of the tumor antigen to an immunogenic carrier molecule such as keyhole limpet hemocyanin (KLH), in addition to the use of a potent adjuvant. Helling et al. showed that the conjugate GM2-KLH in combination with QS-21 elicited significant $CD4^+$ Th-cell responses, higher antibody titers, a longer-lasting GM2-specific IgM antibody response, and also an IgG response (isotype IgG1 and IgG3) [58]. Kim et al. screened 19 different adjuvants including CpG ODN, Ginseng saponin and MPL, in combination with either the MUC1 peptide or GD3 ganglioside tumor antigens and found that QS-21 was the most effective adjuvant [60]. Interestingly, the authors did not detect strong T-cell responses to the TAA themselves but potent KLH-specific T-cell

responses appeared to lead to higher levels of antibody against the conjugated antigens [61]. Further studies determined that, although QS-21 is effective as an adjuvant when used alone, it is more effective when used in combination with other adjuvants such as CpG, MPL, Titermax and MoGM-CSF, highlighting the potential of adjuvant combinations in cancer vaccines [61].

C. Heat shock proteins

Heat Shock Proteins (HSP) are chaperones that bind a wide repertoire of peptides, including antigenic peptides. They are endogenous molecules that can be captured by DCs when released from a cell, and can present HSP-associated peptides on MHCcI by cross presentation [62–64]. Although the proteins are involved in numerous physiological processes and can bind various peptides, this approach typically promotes CTL and antibody responses, the specificity of which is dependent on the peptide being chaperoned [64,65]. If HSP are stripped of their associated peptides their ability to induce protection is lost [64,66]. Interestingly, HSPs were the first adjuvants of mammalian origin described [67].

Cancer-derived HSP-peptide complexes have been used to elicit regression and even cure of preexisting cancers in mice [1,68]. Since HSPs chaperone the antigenic repertoire of the cells from which they are purified, cancer-derived HSP preparations permit access to the antigenic fingerprint of a cancer cell and are capable of eliciting potent T-cell responses against the cells from which they are purified [68,69].

Prophylactic immunization experiments in mice with the HSPs GP96 and HSP70 showed specificity in treating established tumors [69]. Human HSP70-mediated T-cell activation was shown to occur *in vitro* via recognition by MHC molecules of the matched DCs pulsed with the melanoma-derived HSP70 and was strictly dependent on the presence of peptides chaperoned by HSP [65]. Clinical studies have generated mixed results.

Autologous, patient-derived gp96-peptide complexes elicited tumor-specific T-cell responses in HSP-vaccinated cancer patients [70]. However, a Phase III trial comparing autologous, tumor-derived gp96 peptide complexes (vitespen) with the current best treatment for stage IV melanoma found that only a subset of patients with early stage disease that received a large number of vitespen injections survived longer [71]. A separate Phase III trial focusing on renal cell carcinoma found that delivery of the gp96 peptide complex as an adjuvant to patients with high risk of recurrence was ineffective with regard to recurrence-free survival compared to patients who received no treatment [72].

Current strategies in adjuvant development of HSP involve extracting HSP-protein complexes from both patient-derived and established cancer cells and exposing them *ex vivo* to healthy donor DCs for 5 days. The enriched antigenic peptides, bound to HSP, from the DC-tumor cell mix are then extracted using an anti-HSP antibody and used to stimulate T cells [73]. DCs can be mixed with different types of cancer cells *ex vivo*. The DC loaded with HSP-bound peptides are capable of inducing polyclonal CTLs that kill tumor cells from which the HSP was extracted, as well as tumor cells with shared antigen and restriction elements [73].

V. PARTICULATE VACCINE ADJUVANTS

Particulate adjuvants do not generally contain specific agonists for PRR yet are still capable of promoting innate and subsequently adaptive immunity. How they accomplish this is not fully understood but proposed mechanisms include depot formation, release of danger signals, controlled antigen release, and/or inflammasome activation [74].

A. EMULSIONS

The first use of emulsions as adjuvants can be traced back to 1916 when LeMoignic Pinoy used a water and Vaseline emulsion containing inactivated *Salmonella typhimurium*. Since then

emulsion adjuvants have diversified slightly but still remain the same in essence. Emulsions make antigens particulate in nature through aggregate formation [75].

One of the most widely used adjuvants was developed by Freund in the 1930s. This adjuvant is a paraffin-oil based emulsion that can contain heat-killed *Mycobacteria*. Freund's adjuvant is an example of a water-in-oil (W/O) emulsion. W/O emulsions consist of water droplets containing antigen that are surrounded by a continuous oil phase and have been found to be very efficient in enhancing immune responses. However, Freund's adjuvants are too toxic for use in humans.

Alternative W/O emulsions with better safety profiles such as ISA 51 and ISA 720 have been developed using specific surfactants and refined oils. ISA 51 is a mineral-oil based emulsion while ISA 720 contains the animal or vegetable oil squalene [76,77]. Although both ISA 51 and ISA 720 can lead to the development of mild to moderate local reactions, where the benefit outweighs the risk these adjuvants have been used in both therapeutic and prophylactic vaccines [77].

The ability of Montanide ISA 51 to promote T-cell responses appears to be dependent on the surfactant composition. For example, a clinical trial for melanoma involved an ISA 51 formulation that included a surfactant containing the fatty acid, oleic acid, which comes from beef tallow. Due to the possible risk of prions in beef tallow, the use of beef oleic acid was discontinued in 2006 and was substituted with oleic acid of olive origin. However, when patients were immunized with the same peptide emulsified in the new vegetable oleic acid-based Montanide ISA 51 (ISA 51 VG) there appeared to be less adjuvanticity as measured by a reduction in peptide-specific T cells and local skin inflammation at the injection site [78]. O'Neill et al. have shown that ISA 51 VG is well tolerated in humans. Indeed, when immunized with six HLA-A2 antigens and KLH, KLH-specific $CD4^+$ T cells were generated which secreted the Th1 cytokines IFN-γ, TNF-α and IL-2. Hence the potential of this adjuvant in cancer vaccines should not be underestimated [79].

Oil-in-water (O/W) emulsions were developed as an alternative to W/O emulsion adjuvants, and are composed of antigen in a water phase with oil droplets. O/W emulsions have a far superior safety profile due to the reduced oil content. MF59™ is an O/W emulsion which is composed of squalene with Tween 80 and Span 85 as surfactants. It appears to work by acting as an antigen depot, which in turn causes an influx of granulocytes to the site of injection, as well as an increase in endocytosis and increased expression of markers indicative of DC maturation (MHCcII, CD86, CD83, CCR7) [35,80]. MF59™ has been used extensively as an adjuvant in vaccines against infectious diseases such as herpes simplex virus (HSV), HBV, and human immunodeficiency virus (HIV). However, its ability to induce a protective response in cancer has yet to be tested [8].

B. ISCOMs

Immunostimulating complexes or ISCOMs are spherical cage-like particles, approximately 40nm in diameter, and were first described in 1984 by Morein et al. [81]. They are capable of promoting long-lasting functional antibody responses as well as powerful T-cell responses, including enhanced cytokine secretion and CTL activation which, as mentioned earlier, is critical in controlling cancer [82,83]. Studies have shown that ISCOMs can be efficiently phagocytosed and activate DCs, leading to the development of an immune response [84–86].

ISCOMs can be composed of several different materials and tend to be subdivided into two main types, classical ISCOMs and the ISCOMATRIX.® Classical ISCOMs are made up of saponins from *Quillaia saponaria*, cholesterol, phospholipid and amphipathic protein, and were originally designed to incorporate viral components, thus making them extremely immunogenic [81]. The difference between ISCOMATRIX® and classical ISCOMs is that the protein component and antigen which are incorporated into ISCOMs can be mixed together with ISCOMATRIX.®

Since pancreatic carcinoma cells can be recognized by T cells, a method to overcome immunotolerance in patients with pancreatic cancer would be of huge benefit [87]. TAA require cross presentation on MHCcI by DC to activate CTL, a task which is effectively performed by ISCOMs. Studies using ISCOMs as adjuvants for pancreatic cancer vaccines have had varying degrees of success. Injection of NY-ESO-1 (a highly immunogenic antigen expressed in several malignancies) with ISCOMATRIX® in patients with resected malignant melanoma generated a broad cellular immune response with an excellent safety profile in an initial study [88]. However, in a follow-up study of patients with advanced malignant melanoma injected with NY-ESO-1 and ISCOMATRIX,® antibodies were present but a T-cell response capable of overcoming the tumor-induced immune suppression in patients was lacking [89]. In a mouse orthotopic model of pancreatic carcinoma, a similar antigen-specific immunosuppression rendered the ISCOM vaccine ineffective as a therapeutic strategy. However, when the TLR agonist CpG was added to the ISCOM vaccine, superior CTL priming was generated and tumor-induced immunosuppression was broken [90].

C. Mineral salts

Adjuvants containing aluminum have been used in numerous different types of vaccines for decades, yet their exact mechanism of action still remains elusive. Aluminum potassium phosphate (Alum-phos) and aluminum hydroxide (commonly called "alum") are the most common mineral salts currently being used and are licensed for use in several vaccines including Diptheria-Pertussis-Tetanus, *Haemophilus influenza* B and human papillomavirus (HPV) [91]. It has been proposed that alum principally works as an antigen "depot," thus allowing prolonged exposure of the antigen to the immune system [92–96]. However, since alum is a potent inducer of humoral immunity but is less effective in promoting cell-mediated immunity, its use in cancer vaccines is limited.

D. Biodegradable microparticles

Controlled release vaccine delivery can be effectively achieved by the use of biodegradable microparticles such as poly (lactide-co-glycolide) (PLGA) particles. PLGA is a Food and Drugs Administration (FDA) approved polymer that is degraded into lactic acid and glycolic acid, which are normal metabolites and well tolerated in the human body [17]. PLG microparticles are prime candidates for development of vaccine adjuvants as they are biodegradable *in vivo* and their half-life can range from days to years depending on their composition. Antigens, as well as other adjuvants, can be encapsulated within PLG particles and released into the processing pathways for presentation on MHC class I and II. These systems have been shown to effectively increase antibody titers compared to antigen/adjuvant alone [97–99].

The advantages of using PLGA particles include their ability to target DCs while protecting antigen from degradation and from entering the systemic circulation, their ability to efficiently facilitate antigen cross presentation and to facilitate co-delivery of various immunomodulators to DCs [17].

In the mouse B16 tumor model, tyrosine related protein-2 (TRP2) is over-expressed. Hamdy et al. encapsulated this antigen, along with 7-acyl lipid A (a synthetic derivative of lipid A from MPL which has comparable immunostimulatory effects to MPL) within PLGA microparticles and observed a TRP2-specific CTL response that correlated with a therapeutic antitumor response [100]. They also found that the immunosuppressive milieu of the tumor microenvironment was overcome, an event characterized by an increase in characteristic Th1 cytokines such as IFN-γ, IL-6, IL-12 and TNF-α and a decrease in the tumor-promoting factor vascular endothelial growth factor (VEGF) [100].

Schlosser et al. found that co-encapsulation of poly I:C and CpG oligonucleotides within the same PLGA microparticle was more effective for generating cross priming and a CTL response than encapsulation of either adjuvant alone [101]. Heit et al. also used the co-encapsulation

method for CpG ODNs and their antigen, OVA, in PLGA particles and found that the expansion of antigen-specific $CD4^+$ and $CD8^+$ T cells generated a protective and therapeutic effect towards mouse melanoma tumor cells [102].

E. Other particulate vaccine adjuvants

Based on the ability of viruses to efficiently penetrate cells, virus-like particles (VLP) and virosomes have been developed as adjuvant vectors to present and deliver antigens to immune cells. These particles range from 20–100nm in size (the average cell being 10μm), consist of self-assembling viral envelope proteins and lack the ability to replicate and infect cells as they do not contain any viral nucleic acids [103]. Importantly, they are capable of stimulating both cell-mediated and humoral immunity through their highly repetitive surfaces composed of viral proteins [104–106]. VLP can be manipulated in such a way that other PAMPs can be incorporated within them, making them capable of targeting specific PRR and hence dictating the type of immune response induced [107].

The role for infectious agents, particularly viruses, as causative agents of cancer is substantial [108,109]. The bacterium *Heliobacter pylori* colonizes the gastric epithelium and is a strong risk factor for noncardia gastric adenocarcinoma. Worldwide, 5.5% of cancers are attributed to *H. pylori* [109]. Viruses such as Hepatitis B and C and Epstein-Barr virus can cause liver cancer and Burkitt's lymphoma, respectively. In fact, Hepatitis B is responsible for half of all liver cancers and Hepatitis C causes 30% of liver cancers. Vaccines against such infectious agents implicated in the development of cancer are currently being developed, the most successful of which is the HPV cervical cancer vaccine. Developing vaccines and adjuvants for these types of cancers can involve different approaches as a prophylactic rather than a therapeutic approach is feasible and neutralizing antibodies are a key requirement. This type of cancer vaccine will target the pathogen that causes the cancer, rather than the cancer itself.

The human papillomaviruses (HPVs) are a group of viruses which can cause benign and malignant lesions of the skin and the mucosa. There are 12 types of HPV that are known to cause cervical cancer, and infection with at least one of these HPV types is required for cervical cancer to develop [110]. HPV-16 and HPV-18 are most virulent and account for approximately 70% of cervical neoplasms [111]. Gardasil® and Cervarix® are prophylactic vaccines against HPV that are currently licensed. Gardasil® is a VLP-based vaccine composed of LI (a major capsid protein) from several HPV serotypes (6,11,16,18) and uses aluminum hydroxyphosphate sulphate as its adjuvant (Table 21.1) [112]. Antibody responses are critical for immunity against these viruses and alum adjuvants are extremely effective at generating humoral immunity. Gardasil® vaccine has been shown to reduce HPV infection by 90% [112]. Cervarix® is a bivalent vaccine against HPV serotypes 16 and 18 and uses a GSK adjuvant system called AS04 which is composed of alum and MPL (Table 21.1). Further studies have shown that the vaccines are immunogenic 4 years after vaccination and that it confers cross-protection for other HPV types including HPV 45 and HPV 31 [110].

Other particulate vaccine adjuvants include liposomes, which are particulate structures composed of either natural or synthetic phospholipids. They were developed by Alec Bangham who extracted lipids from egg yolk and described the formation of a double-layered bubble the size of a cell when these lipids were added to an aqueous solution. Incorporating antigen into liposomes leads to increased antibody titers, and this is why so much work has gone into designing liposomes that are stable in the bloodstream and can target specific cells of the immune system to generate a particular immune response [113–115].

Stimuvax® is a liposome-based vaccine containing MPL which was developed for the treatment of non-small cell lung cancer, but has also been tested on breast cancers and multiple myelomas. MUC1 is a membrane protein of mucin-secreting epithelial cells and

TABLE 21.1 Currently Licensed Cancer Vaccines and their Adjuvant Components

Vaccine	Application	Adjuvant
Cervarix®	Prophylactic vaccine against cervical cancer caused by HPV virus strains 16 and 18	AS04 (GSK adjuvant system composed of Alum and MPL).
Gardasil®	Prophylactic recombinant vaccine composed of virus-like particles derived from the L1 capsid proteins of HPV virus strains 6, 11, 16 and 18.	Aluminum Hydroxyphosphate Sulfate.
Sipuleucel-T	Treatment vaccine for men with metastatic prostate cancer.	Leukapheresis involving stimulation with prostatic acid phosphatase (PAP) antigen and GM-CSF.

is over-expressed in 60% of lung cancers [116]. Stimuvax® targets this TAA using a lyophilized preparation of the 25-amino-acid BLP25 lipopeptide, MPL and three lipids (cholesterol, dimyristoyl phosphatidylglycerol and dipalmitoyl phosphatidylcholine) [117]. After a patient participating in a Phase II exploratory clinical trial with the therapeutic cancer vaccine developed encephalitis, clinical trials were halted. However, the study has been reintroduced and is currently recruiting for a Phase III trial with predicted completion in 2018 [117].

F. Combination vaccine adjuvants

The advances in biotechnology, molecular biology and immunology have enabled the rational development of well-defined, PAMP-based adjuvants. This, along with developments in synthetic chemistry and particulates which are capable of activating the immune system, has enabled the advancement of combination vaccine adjuvants.

Combining different adjuvants allows for a tailored immune response to be optimized. Advantages of these types of adjuvant strategies can include the ability to promote the development of heterologous antibodies that have increased cross reactivity among strains of pathogens, more effective T-cell responses and more potent functional antibodies. Although the process of combining adjuvants with other immunostimulatory components is not new, it is only recently that these types of adjuvants have been licensed [35].

GlaxoSmithKline (GSK) has been the front-runner in combination adjuvant development. Their adjuvant system (AS) portfolio is composed of various mixtures of classical adjuvants combined with other immunomodulators (Table 21.2) [118]. AS04 is a combination of MPL and alum and is used in the Fendrix® and Cervarix® vaccines that are currently on the market. Indeed there are several other AS combinations that are in clinical trials for infectious diseases such as malaria as well as some cancers.

As mentioned in Section D, biodegradable microparticles can enhance the immune response to associated antigens and adjuvants. It has been shown that PLG-encapsulated CpG promotes higher antibody titers and enhanced T-cell responses compared with soluble CpG [97,98].

VI. DC PRIMING *IN VIVO* VERSUS *EX VIVO*

Activation or priming of DCs is a key objective of the adjuvants mentioned above as these cells have a unique ability for antigen acquisition and display, leading to the generation of antigen-specific immune responses [17]. However, it should be recognized that in addition to *in vivo* methods of doing this, including injecting irradiated cytokine secreting whole tumor cells

TABLE 21.2 Combination Adjuvants that are Licensed or are Currently in Clinical Trials

Name	Company	Class	Indications	Stage
AS01	GSK	MPL + liposomes + QS21	Malaria	Phase III [118]
AS02	GSK	MPL + O/W emulsion + QS21	Malaria	Phase III [118]
AS03	GSK	α-tocopherol + O/W emulsion	Pandemic Influenza	Licensed (EU) [118]
AS04	GSK	MPL + Aluminum hydroxide	HBV (Fendrix), HPV (Cervarix)	Licensed (EU) [118]
AS15	GSK	ASO1 + CpG	Metastatic breast cancer	Phase I [118]
L-BLP25	Merck	Liposomes + MPL	Non-small cell lung cancer	Phase III [117]
IC31	Intercell	Anti-microbial peptide KLK & oligodeoxynocleotide ODN1a	Tuberculosis	Phase I*

*(http://www.intercell.com/main/forvaccperts/product-pipeline/)

which DCs can then phagocytose, and vaccinating with certain adjuvant combinations, there are also strategies being employed to prime DCs *ex vivo* [5]. One method involves isolating DCs from patients' blood, loading them with tumor antigens in culture medium, treating the cells with various stimuli to induce maturation and injecting them back into the patient [17,119]

Tumor cells already killed by chemotherapy or targeted therapies also have the potential to facilitate DC priming *in situ* [5]. Using patient-derived TAA and synthetic peptides derived from TAA, a DC focused immunotherapy can be achieved that induces antitumor effector cells [2,41]. As with *in vivo* targeting of DCs, adjuvants can be used in an *ex vivo* setting to optimize the type of DC-induced immune response generated against cancer. Advantages of *ex vivo* DC activation compared to *in vivo* activation is that the activation status can be determined before intratumoral injection [120].

Shibata and colleagues used an *ex vivo* method in mice to mature DCs by infecting them with recombinant Sendai virus (SeV) [120]. When these mature DCs were injected intratumorally to a B16F1 melanoma, the tumors were eliminated and the mice survived. The effect was enhanced by expressing IFN-β in DCs (SeV-murine IFN-β) and this approach could render the established low malignancy tumors dormant [120].

A recent study compared *in vivo* DC-targeting with priming *ex vivo* antigen-loaded DCs [28]. A vaccine composed of anti-DEC-205-OVA in the presence of CD40 monoclonal antibodies prevented B16 OVA tumor growth in a mouse model whereas *ex vivo* OVA-loaded mature DCs did not protect against tumor growth [28].

PROVENGE® (Sipuleucel-T) is an FDA-approved DC vaccine against metastatic, castration-resistant prostate cancer, designed to stimulate T cells specific for prostatic acid phosphatase (PAP) which is over-expressed in prostate carcinoma cells. This therapy involves the culture of a patient's own DCs with a fusion protein of PAP fused to granulocyte–macrophage colony-stimulating factor (GMCSF), a cytokine which can activate immune cells [121]. The DCs are then infused back into the patient and the hypothesis is that the primed DCs are capable of activating T cells that recognize the PAP antigen [122]. Patients showed increased survival with this therapy; however, the median improved survival was only 4 months and no effect on time to disease progression was observed [123]. The vaccine has come under some criticism due to the fact that there is a lack of direct antitumor responses to the treatment, the increased survival found was strongly related to the age of the patient and that the placebo was not directly

comparable to the treatment group. It is important that the exact mechanisms of action of the vaccine are determined [124].

Although these recent developments are encouraging, *ex vivo* targeting has encountered several issues. *Ex vivo* targeted DCs that have been re-infused do not migrate to the lymph nodes very efficiently, with only 3–5% able to present antigen to T cells [125]. Other limitations are that only certain subsets of DCs can be isolated and cultured *in vitro*. Furthermore, DCs that are used in this treatment must come from each individual patient and must be put back into the same patient, thus making the strategy time consuming and costly [17]. For these reasons, *in vivo* targeting of DCs through the development of cancer vaccines and adjuvants seems a more robust option [123].

VII. CONCLUSIONS

The importance of choosing the right adjuvant in vaccines cannot be overestimated. An adjuvant can determine the immunophenotype and consequently the efficacy of the vaccine [74]. In terms of adjuvant development, the acceptable tolerability profile for a therapeutic cancer vaccine may be different from a prophylactic vaccine to be used in infants. Currently this is not a consideration in safety procedures by both the FDA and the EMA, which will severely limit the development of adjuvants that have potential within a therapeutic vaccine setting [35]. In certain circumstances a degree of adjuvant-mediated toxicity may be acceptable if the overall result is effective antitumor immunity [123].

Tumors are known to interfere with DC function and hence designing a vaccine is not straightforward [126]. Correct adjuvant design involves selecting an appropriate stimulus to bring about DC maturation that generates strong helper and cytotoxic T-cell immunity [126]. In cancer vaccines, adjuvants that elicit CTL accompanied by a Th1 response will be the most effective and hence should be prioritized in current clinical research settings.

References

[1] Srivastava PK, Menoret A, Basu S, Binder RJ, McQuade KL. Heat Shock Proteins Come of Age: Primitive Functions Acquire New Roles in an Adaptive World. Immunity 1998;8:657–65.

[2] Palucka K, Ueno H, Banchereau J. Recent developments in cancer vaccines. J Immunol 2011;186:1325–31.

[3] Schuster M, Nechansky A, Kircheis R. Cancer immunotherapy. Biotechnol J 2006;1:138–47.

[4] Pulendran B, Ahmed R. Translating innate immunity into immunological memory: implications for vaccine development. Cell 2006;124:849–63.

[5] Vanneman M, Dranoff G. Combining immunotherapy and targeted therapies in cancer treatment. Nat Rev Cancer 2012;12:237–51.

[6] Ramon G. Sur la toxine et sur l'anatoxine diphtheriques. Annales de l'Institut Pasteur 1924;38:1–10.

[7] Guy B. The perfect mix: recent progress in adjuvant research. Nat Rev Microbiol 2007;5:505–17.

[8] Dubensky TW, Reed SG. Adjuvants for cancer vaccines. Semin Immunol 2010;22:155–61.

[9] Cluff CW. Monophosphoryl lipid A (MPL) as an adjuvant for anti-cancer vaccines: clinical results. Adv Exp Med Biol 2009;667:111–23.

[10] Takeuchi O, Akira S. Pattern recognition receptors and inflammation. Cell 2010;140:805–20.

[11] Janeway CA, Medzhitov R. Innate immune recognition. Annu Rev Immunol 2002;20:197–216.

[12] Pandolfi F, Cianci R, Pagliari D, et al. The Immune Response to Tumors as a Tool toward Immunotherapy. Clin Develop Immunol 2011;2011:894704.

[13] Foley EJ. Antigenic properties of methylcholanthrene-induced tumors in mice of the strain of origin. Cancer Resear 1953;13:835–7.

[14] Prehn RT, Main JM. Immunity to methylcholanthrene-induced sarcomas. J Natl Cancer Institute 1957;18:769–78.

[15] Dunn IS, Haggerty TJ, Kono M, et al. Enhancement of human melanoma antigen expression by IFN-beta. J Immunol 2007;179:2134–42.

[16] Smith MEF. Loss of HLA-A, B, C Allele Products and Lymphocyte Function-Associated Antigen 3 in Colorectal Neoplasia. Pro Natl Acad Sci 1989;86:5557–61.

[17] Hamdy S, Haddadi A, Hung RW, Lavasanifar A. Targeting dendritic cells with nano-particulate PLGA cancer vaccine formulations. Adv Drug Deliv Rev 2011;63:943–55.

[18] Norbury CC, Malide D, Gibbs JS, Bennink JR, Yewdell JW. Visualizing priming of virus-specific CD8+ T cells by infected dendritic cells in vivo. Nat Immunol 2002;3:265–71.

[19] Norbury CC, Basta S, Donohue KB, et al. CD8+ T cell cross-priming via transfer of proteasome substrates. Science (New York, NY) 2004;304:1318–21.

[20] Kaech SM, Wherry EJ, Ahmed R. Effector and memory T-cell differentiation: implications for vaccine development. Nat Rev Immunol 2002;2:251–62.

[21] Nishikawa H, Sakaguchi S. Regulatory T cells in tumor immunity. Int J Cancer 2010;127:759–67.

[22] Bonertz A, Weitz J, Pietsch D-HK, et al. Antigen-specific Tregs control T cell responses against a limited repertoire of tumor antigens in patients with colorectal carcinoma. J Clin Invest 2009;119:3311–21.

[23] Caminschi I, Maraskovsky E, Heath R. Targeting dendritic cells in vivo for cancer therapy. Frontiers in Immunology 2012;3:1–13.

[24] Van Broekhoven CL, Parish CR, Demangel C, Britton WJ, Altin JG. Targeting dendritic cells with antigen-containing liposomes: a highly effective procedure for induction of antitumor immunity and for tumor immunotherapy. Cancer Res 2004;64:4357–65.

[25] Mahnke K, Qian Y, Fondel S, Brueck J, Becker C, Enk AH. Targeting of antigens to activated dendritic cells in vivo cures metastatic melanoma in mice. Cancer Res 2005;65:7007–12.

[26] Dickgreber N, Stoitzner P, Bai Y, et al. Targeting antigen to MHC class II molecules promotes efficient cross-presentation and enhances immunotherapy. J Immunol (Baltimore, Md : 1950) 2009;182:1260–9.

[27] Wei H, Wang S, Zhang D, et al. Targeted delivery of tumor antigens to activated dendritic cells via CD11c molecules induces potent antitumor immunity in mice. Clin Cancer Res 2009;15:4612–21.

[28] Bonifaz LC, Bonnyay DP, Charalambous A, et al. In vivo targeting of antigens to maturing dendritic cells via the DEC-205 receptor improves T cell vaccination. J Exp Med 2004;199:815–24.

[29] Hishii M, Kurnick JT, Ramirez-Montagut T, Pandolfi F. Studies of the mechanism of cytolysis by tumour-infiltrating lymphocytes. Clin Exp Immunol 1999;116:388–94.

[30] Pulendran B. Modulating vaccine responses with dendritic cells and Toll-like receptors. Immunol Rev 2004;199:227–50.

[31] Kennedy R, Celis E. Multiple roles for CD4+ T cells in anti-tumor immune responses. Immunol Rev 2008;222:129–44.

[32] Nanni P, Landuzzi L, Nicoletti G, et al. Immunoprevention of mammary carcinoma in HER-2/neu transgenic mice is IFN-gamma and B cell dependent. J Immunol (Baltimore, Md : 1950) 2004;173:2288–96.

[33] Park JM, Terabe M, Sakai Y, et al. Early role of CD4+ Th1 cells and antibodies in HER-2 adenovirus vaccine protection against autochthonous mammary carcinomas. J Immunol 2005;174:4228–36.

[34] Reilly RT, Machiels JP, Emens LA, et al. The collaboration of both humoral and cellular HER-2/neu-targeted immune responses is required for the complete eradication of HER-2/neu-expressing tumors. Cancer Res 2001;61:880–3.

[35] O'Hagan DT, De Gregorio E. The path to a successful vaccine adjuvant–'the long and winding road'. Drug discovery today 2009;14:541–51.

[36] O'Hagan DT, Singh M. Microparticles as vaccine adjuvants and delivery systems. Expert Rev vaccines 2003;2:269–83.

[37] Aranda F, Llopiz D, Díaz-Valdés N, et al. Adjuvant combination and antigen targeting as a strategy to induce polyfunctional and high-avidity T-cell responses against poorly immunogenic tumors. Cancer Res 2011;71:3214–24.

[38] Kaisho T, Akira S. Toll-like receptors as adjuvant receptors. Biochim Biophys Acta 2002;1589:1–13.

[39] Haining WN, Davies J, Kanzler H, et al. CpG oligodeoxynucleotides alter lymphocyte and dendritic cell trafficking in humans. Clin Cancer Res 2008;14:5626–34.

[40] Jahrsdorfer B, Hartmann G, Racila E, et al. CpG DNA increases primary malignant B cell expression of costimulatory molecules and target antigens. J Leukoc Biol 2001;69:81–8.

[41] Nava-Parada P, Forni G, Knutson KL, Pease LR, Celis E. Peptide vaccine given with a Toll-like receptor agonist is effective for the treatment and prevention of spontaneous breast tumors. Cancer Res 2007;67:1326–34.

[42] Goldstein MJ, Varghese B, Brody JD, et al. A CpG-loaded tumor cell vaccine induces antitumor CD4+ T cells that are effective in adoptive therapy for large and established tumors. Blood 2011;117:118–27.

[43] de Jong S, Chikh G, Sekirov L, et al. Encapsulation in liposomal nanoparticles enhances the immunostimulatory, adjuvant and anti-tumor activity of subcutaneously administered CpG ODN. Cancer Immunol Immunother 2007;56:1251–64.

[44] Ulrich J, Myers K. Monophosphoryl lipid A as an adjuvant. Past experiences and new directions. In: Vaccine Design: the subunit and adjuvant approach; 1995. p. 495–524.

[45] Persing D, Coler R, Lacy M, et al. Taking toll: lipid A mimetics as adjuvants and immunomodulators. Trends Microbiol 2002;10:S32–7.

[46] Didierlaurent AM, Morel S, Lockman L, et al. AS04, an aluminum salt- and TLR4 agonist-based adjuvant system, induces a transient localized innate immune response leading to enhanced adaptive immunity. J Immunol 2009;183:6186–97.

[47] Alexopoulou L, Holt AC, Medzhitov R, Flavell RA. Recognition of double-stranded RNA and activation of NF-kappaB by Toll-like receptor 3. Nature 2001;413:732–8.

[48] Warger T, Osterloh P, Rechtsteiner G, et al. Synergistic activation of dendritic cells by combined Toll-like receptor ligation induces superior CTL responses in vivo. Blood 2006;108:544–50.

[49] Whitmore MM, DeVeer MJ, Edling A, et al. Synergistic activation of innate immunity by double-stranded RNA and CpG DNA promotes enhanced antitumor activity. Cancer Res 2004;64:5850–60.

[50] Ahonen CL, Doxsee CL, McGurran SM, et al. Combined TLR and CD40 triggering induces potent CD8+ T cell expansion with variable dependence on type I IFN. J Exp Med 2004;199:775–84.

[51] Llopiz D, Dotor J, Zabaleta A, et al. Combined immunization with adjuvant molecules poly(I: C) and anti-CD40 plus a tumor antigen has potent prophylactic and therapeutic antitumor effects. Cancer Immunol Immunother 2008;57:19–29.

[52] Schoenen H, Bodendorfer B, Hitchens K, et al. Cutting edge: Mincle is essential for recognition and adjuvanticity of the mycobacterial cord factor and its synthetic analog trehalose-dibehenate. J Immunol (Baltimore, Md : 1950) 2010;184:2756–60.

[53] Ishikawa E, Ishikawa T, Morita YS, et al. Direct recognition of the mycobacterial glycolipid, trehalose dimycolate, by C-type lectin Mincle. J Exp Med 2009;206:2879–88.

[54] Garaude J, Kent A, van Rooijen N, Blander JM. Simultaneous targeting of toll- and nod-like receptors induces effective tumor-specific immune responses. Sci Transl Med 2012;4:120. ra16.

[55] Kensil C, Patel U, Lennick M, Marciani D. Separation and characterization of saponins with adjuvant activity from Quillaja saponaria Molina cortex. J Immunol 1991;146:431–7.

[56] Sun H-X, Xie Y, Ye Y- P. Advances in saponin-based adjuvants. Vaccine 2009;27:1787–96.

[57] Ragupathi G, Gardner JR, Livingston PO, Gin DY. Natural and synthetic saponin adjuvant QS-21 for vaccines against cancer. Exp Rev Vaccin 2011;10:463–70.

[58] Helling F, Zhang S, Shang A, et al. GM2-KLH conjugate vaccine: increased immunogenicity in melanoma patients after administration with immunological adjuvant QS-21. Cancer Res 1995;55:2783–8.

[59] Livingston PO, Natoli E, Calves M, Stockert E, Oettgen HF, Old LJ. Vaccines containing purified GM2 ganglioside elicit GM2 antibodies in melanoma patients. Proc Natl Acad Sci 1987;84:2911–5.

[60] Kim SK, Ragupathi G, Musselli C, Choi S-J, Park YS, Livingston PO. Comparison of the effect of different immunological adjuvants on the antibody and T-cell response to immunization with MUC1-KLH and GD3-KLH conjugate cancer vaccines. Vaccine 1999;18:597–603.

[61] Kim SK, Ragupathi G, Cappello S, Kagan E, Livingston PO. Effect of immunological adjuvant combinations on the antibody and T-cell response to vaccination with MUC1–KLH and GD3–KLH conjugates. Vaccine 2000;19:530–7.

[62] Nencioni A, Grüenbach F, Patrone F, Brossart P. Anticancer vaccination strategies. Annals of oncology : official journal of the European Society for Medical Oncology / ESMO 2004;15(Suppl. 4). iv153–60.

[63] Arnold D, Faath S, Rammensee H, Schild H. Cross-priming of minor histocompatibility antigen-specific cytotoxic T cells upon immunization with the heat shock protein gp96. J Exp Med 1995;182:885–9.

[64] Suto R, Srivastava P. A mechanism for the specific immunogenicity of heat shock protein-chaperoned peptides. Science 1995;269:1585–8.

[65] Castelli C, Ciupitu A, Rini F, et al. Human heat shock protein 70 peptide complexes specifically activate antimelanoma T cells. Cancer Res 2001;61:222–7.

[66] Udono H. Cellular Requirements for Tumor-Specific Immunity Elicited by Heat Shock Proteins: Tumor Rejection Antigen gp96 Primes CD8+ T Cells in vivo. Proc Natl Acad Sci 1994;91:3077–81.

[67] Blachere N, Li Z, Chandawarkar R, et al. Heat shock protein-peptide complexes, reconstituted in vitro, elicit peptide-specific cytotoxic T lymphocyte response and tumor immunity. J Exp Med 1997;186: 1315–22.

[68] Srivastava PK. Immunotherapy for human cancer using heat shock protein-peptide complexes. Curr Oncol Rep 2005;7:104–8.

[69] Tamura Y, Peng P, Liu K, Daou M, Srivastava PK. Immunotherapy of tumors with autologous tumor-derived heat shock protein preparations. Science 1999;278:117–20.

[70] Rivoltini L, Castelli C, Carrabba M, et al. Human tumor-derived heat shock protein 96 mediates in vitro activation and in vivo expansion of melanoma- and colon carcinoma-specific T cells. J Immunol 2003;171: 3467–74.

[71] Testori A, Richards J, Whitman E, et al. Phase III comparison of vitespen, an autologous tumor-derived heat shock protein gp96 peptide complex vaccine, with physician's choice of treatment for stage IV melanoma: the C-100-21 Study Group. J Clin Oncol 2008;26:955–62.

[72] Wood C, Srivastava P, Bukowski R, et al. An adjuvant autologous therapeutic vaccine (HSPPC-96; vitespen) versus observation alone for patients at high risk of recurrence after nephrectomy for renal cell carcinoma: a multicentre, open-label, randomised phase III trial. Lancet 2008;372:145–54.

[73] Gong J, Zhang Y, Durfee J, et al. A Heat Shock Protein 70-Based Vaccine with Enhanced Immunogenicity for Clinical Use. J Immunol 2009;184:488–96.

[74] Schijns VEJC, Lavelle EC. Trends in vaccine adjuvants. Exp Rev Vaccin 2011;10:539–50.

[75] Morse MA, Clay TM, Lyerly HK. Handbook of cancer vaccines, Volume 1., 204AD.

[76] Aucouturier J, Dupuis L, Ganne V. Adjuvants designed for veterinary and human vaccines. Vaccine 2001;19:2666–72.

[77] Aucouturier J, Ascarateil S, Dupuis L. The use of oil adjuvants in therapeutic vaccines. Vaccine 2006;24:S44–5.

[78] Rosenberg SA, Yang JC, Kammula US, et al. Different adjuvanticity of incomplete freund's adjuvant derived from beef or vegetable components in melanoma patients immunized with a peptide vaccine. J Immunother; 33: 626–9

[79] O'Neill D, Adams S, Goldberg J, et al. Comparison of the immunogenicity of Montanide ISA 51 adjuvant and cytokine-matured dendritic cells in a randomized controlled clinical trial of melanoma vaccines. J Clin Oncol 2009;27:15s.

[80] Seubert A, Monaci E, Pizza M, O'Hagan DT, Wack A. The adjuvants aluminum hydroxide and MF59 induce monocyte and granulocyte chemoattractants and enhance monocyte differentiation toward dendritic cells. J Immunol 2008;180:5402–12.

[81] Morein B, Sundquist B, Höglund S, Dalsgaard K, Osterhaus A. Iscom, a novel structure for antigenic presentation of membrane proteins from enveloped viruses. Nature 1984;308:457–60.

[82] Barr IG, Mitchell GF. ISCOMs (immunostimulating complexes): the first decade. Immunol Cell Biol 1996;74:8–25.

[83] Claassen I, Osterhaus A. The iscom structure as an immune-enhancing moiety: experience with viral systems. Resear Immunol 1992;143:531–41.

[84] Villacres-Eriksson M, Bergström-Mollaoglu M, Kåberg H, Lövgren K, Morein B. The induction of cell-associated and secreted IL-1 by iscoms, matrix or micelles in murine splenic cells. Clin Exp Immunol 1993;93:120–5.

[85] Behboudi S, Morein B, Villacres-Eriksson M. In vivo and in vitro induction of IL-6 by Quillaja saponaria molina triterpenoid formulations. Cytokine 1997;9:682–7.

[86] Behboudi S, Morein B, Villacres-Eriksson M. In vitro activation of antigen-presenting cells (APC) by defined composition of Quillaja saponaria Molina triterpenoids. Clin Exp Immunol 1996;105:26–30.

[87] Schmitz-Winnenthal FH, Volk C, Z'graggen K, et al. High frequencies of functional tumor-reactive T cells in bone marrow and blood of pancreatic cancer patients. Cancer Res 2005;65:10079–87.

[88] Davis ID, Chen W, Jackson H, et al. Recombinant NY-ESO-1 protein with ISCOMATRIX adjuvant induces broad integrated antibody and CD4+ and CD8+ T cell responses in humans. Proc Natl Acad Sci USA 2004;101:10697–702.

[89] Nicholaou T, Ebert LM, Davis ID, et al. Regulatory T-cell-mediated attenuation of T-cell responses to the NY-ESO-1 ISCOMATRIX vaccine in patients with advanced malignant melanoma. Clin Cancer Res 2009;15:2166–73.

[90] Jacobs C, Duewell P, Heckelsmiller K, et al. An ISCOM vaccine combined with a TLR9 agonist breaks immune evasion mediated by regulatory T cells in an orthotopic model of pancreatic carcinoma. Int J Cancer 2011;128:897–907.

[91] Clements CJ, Griffiths E. The global impact of vaccines containing aluminium adjuvants. Vaccine 2002;20:S24–33.

[92] Jordan MB, Mills DM, Kappler J, Marrack P, Cambier JC. Promotion of B cell immune responses via an alum-induced myeloid cell population. Science 2004;304:1808–10.

[93] McKee AS, MacLeod M, White J, Crawford F, Kappler JW, Marrack P. Gr1+IL-4-producing innate cells are induced in response to Th2 stimuli and suppress Th1-dependent antibody responses. Int Immunol 2008;20:659–69.

[94] Wang H-B, Weller PF. Pivotal advance: eosinophils mediate early alum adjuvant-elicited B cell priming and IgM production. J Leukoc Biol 2008;83:817–21.

[95] Glenny A, Pope C. The antigenic effect of intravenous injection of diphtheria toxin. J Pathol Bacteriol 1925;28:273–8.

[96] Glenny A, Buttle G, Stevens M. Rate of disappearance of diptheria toxoid injected into rabbits and guinea pigs: toxoid precipitated with alum. J Pathol Bacteriol 1931;34:267–75.

[97] Malyala P, Chesko J, Ugozzoli M, et al. The potency of the adjuvant, CpG oligos, is enhanced by encapsulation in PLG microparticles. J Pharma Sci 2008;97:1155–64.

[98] Kazzaz J, Singh M, Ugozzoli M, Chesko J, Soenawan E, O'Hagan DT. Encapsulation of the immune potentiators MPL and RC529 in PLG microparticles enhances their potency. J Control Release 2006;110: 566–73.

[99] Waeckerle-Men Y, Allmen EU-von Gander B, et al. Encapsulation of proteins and peptides into biodegradable poly(D, L-lactide-co-glycolide) microspheres prolongs and enhances antigen presentation by human dendritic cells. Vaccine 2006;24:1847–57.

[100] Hamdy S, Molavi O, Ma Z, et al. Co-delivery of cancer-associated antigen and Toll-like receptor 4 ligand in PLGA nanoparticles induces potent CD8+ T cell-mediated anti-tumor immunity. Vaccine 2008;26: 5046–57.

[101] Schlosser E, Mueller M, Fischer S, et al. TLR ligands and antigen need to be coencapsulated into the same biodegradable microsphere for the generation of potent cytotoxic T lymphocyte responses. Vaccine 2008;26:1626–37.

[102] Heit A, Schmitz F, Haas T, Busch DH, Wagner H. Antigen co-encapsulated with adjuvants efficiently drive protective T cell immunity. Eur J Immunol 2007;37:2063–74.

[103] Scheerlinck J-PY, Greenwood DLV. Virus-sized vaccine delivery systems. Drug Discovery Today 2008;13:882–7.

[104] Glück R, Moser C, Metcalfe IC. Influenza virosomes as an efficient system for adjuvanted vaccine delivery. Expert Opin Biol Ther 2004;4:1139–45.

[105] Grgacic EVL, Anderson DA. Virus-like particles: passport to immune recognition. Methods 2006;40:60–5.

[106] Huckriede A, Bungener L, Stegmann T, et al. The virosome concept for influenza vaccines. Vaccine 2005;23(Suppl. 1):S26–38.

[107] Bachmann MF, Jennings GT. Vaccine delivery: a matter of size, geometry, kinetics and molecular patterns. Nat Rev Immunol 2010;10:787–96.

[108] de Martel C, Franceschi S. Infections and cancer: established associations and new hypotheses. Crit Rev Oncol/Hematol 2009;70:183–94.

[109] Parkin DM. The global health burden of infection-associated cancers in the year 2002. Int J Cancer 2006;118:3030–44.

[110] Harper DM, Franco EL, Wheeler CM, et al. Sustained efficacy up to 4.5 years of a bivalent L1 virus-like particle vaccine against human papillomavirus types 16 and 18: follow-up from a randomised control trial. Lancet 2006;367:1247–55.

[111] Smith JS, Lindsay L, Hoots B, et al. Human papillomavirus type distribution in invasive cervical cancer and high-grade cervical lesions: a meta-analysis update. Int J Cancer 2007;121:621–32.

[112] Villa LL, Costa RLR, Petta CA, et al. Prophylactic quadrivalent human papillomavirus (types 6, 11, 16, and 18) L1 virus-like particle vaccine in young women: a randomised double-blind placebo-controlled multicentre phase II efficacy trial. Lancet Oncol 2005;6:271–8.

[113] Maruyama K, Okuizumi S, Ishida O, Yamauchi H, Kikuchi H, Iwatsuru M. Phosphatidyl polyglycerols prolong liposome circulation in vivo. Inter J Pharma 1994;111:103–7.

[114] Foged C, Arigita C, Sundblad A, Jiskoot W, Storm G, Frokjaer S. Interaction of dendritic cells with antigen-containing liposomes: effect of bilayer composition. Vaccine 2004;22:1903–13.

[115] Allison A, Gregoriadis G. Liposomes as immunological adjuvants. Nature 1974;252. 252–252.

[116] Morgensztern D, Goodgame B, Govindan R. Vaccines and Immunotherapy for non-small cell lung cancer. J Thorac Oncol 2010;5:S463–5.

[117] Wu Y-L, Park K, Soo RA, et al. INSPIRE: A phase III study of the BLP25 liposome vaccine (L-BLP25) in Asian patients with unresectable stage III non-small cell lung cancer. BioMed Central Cancer 2011;11:430.

[118] Garçon N, Chomez P, Van Mechelen M. GlaxoSmithKline Adjuvant Systems in vaccines: concepts, achievements and perspectives. Exp Rev Vaccin 2007;6:723–39.

[119] Tacken PJ, de Vries IJM, Torensma R, Figdor CG. Dendritic-cell immunotherapy: from ex vivo loading to in vivo targeting. Nat Rev Immunol 2007;7:790–802.

[120] Shibata S, Okano S, Yonemitsu Y, et al. Induction of Efficient Antitumor Immunity Using Dendritic Cells Activated by Recombinant Sendai Virus and Its Modulation by Exogenous IFN-beta Gene. J Immunol 2006;177:3564–76.

[121] Kantoff P, Higano C, Shore N, et al. Sipuleucel-T Immunotherapy for castration-resistant prostate cancer. New Engl J Med 2010;363:411–22.

[122] Sonpavde G, Di Lorenzo G, Higano CS, Kantoff PW, Madan R, Shore ND. The role of sipuleucel-T in therapy for castration-resistant prostate cancer: a critical analysis of the literature. Eur Urol 2012;61:639–47.

[123] Madorsky-Rowdo FP, Lacreu ML, Mordoh J. Melanoma vaccines and modulation of the immune system in the clinical setting: building from new realities. Frontiers in immunology 2012;3:103.

[124] Huber ML, Haynes L, Parker C, Iversen P. Interdisciplinary critique of sipuleucel-T as immunotherapy in castration-resistant prostate cancer. J Nat Cancer Inst 2012;104:273–9.

[125] De Vries IJM, Lesterhuis WJ, Scharenborg NM, et al. Maturation of dendritic cells is a prerequisite for inducing immune responses in advanced melanoma patients. Clin Cancer Res 2003;9:5091–100.

[126] Steinman RM. Decisions About Dendritic Cells: Past, Present, and Future, http://www.annualreviews.org/doi/abs/10.1146/annurev-immunol-100311-102839, 2011. (accessed 26 Jan2012).